Anion-induced molecular motion within interlocked structures

Timothy A. Barendt

Pembroke College, University of Oxford



A thesis submitted for the degree of Doctor of Philosophy

Inorganic Chemistry Laboratory

University of Oxford

Trinity Term 2016

ABSTRACT

Anion-induced molecular motion within interlocked structures

Timothy A. Barendt, Pembroke College, University of Oxford.

Abstract of thesis submitted for the degree of D. Phil., Trinity Term 2016.

This thesis describes the construction and exploration of a variety of interlocked structures that exhibit anion-induced molecular motion of their constituent parts.

Chapter One provides a brief overview of the field of supramolecular chemistry; in particular anion recognition and the concept of mechanically interlocked molecules and their applications in the fields of nanotechnology.

Chapter Two describes the preparation of a series of bistable [2]rotaxanes followed by thorough investigation of their dynamic properties. Specifically, the success of an iodo-triazolium–naphthalene-diimide-based two-station axle component to facilitate halide-stimulated large-amplitude translational motion of the macrocyclic wheel in a [2]rotaxane is demonstrated.

Chapter Three expands on the design principles established in the previous chapter with the synthesis of exotic higher-order structures including the first halogen bonding [3]rotaxane. These systems are capable of the recognition and colorimetric sensing of oxoanions *via* a novel dynamic pincer-like motion of the macrocycle components.

Chapter Four further highlights the capabilities of controlled co-conformational switching in interlocked structures, resulting in a unique mechanism to accomplish anion sensing. The incorporation of C_{60} fullerene- and ferrocenyl-reporter groups into a four-station [3]rotaxane enables sensing of chloride to be realised by a dual fluorescence response.

Chapter Five presents the synthesis of novel interlocked structures containing a substituted perylene diimide motif that functions as a recognition site for macrocycles. Chloride binding stimulates translational motion in a [3]rotaxane and unprecedented rotary motion in a [3]catenane, with co-conformational changes in both systems resulting in a colorimetric response for this anion.

Chapter Six describes experimental procedures used throughout this work and details the characterisation of novel compounds.

Chapter Seven provides a summary of the major conclusions from the research described in this thesis.

Supplementary information relating to methodologies, experimental procedures and crystallographic data is provided in the Appendices.

ACKNOWLEDGEMENTS

According to the red half of the city of Liverpool "You'll never walk alone" and, since it has certainly felt this way throughout my time in Oxford as a D. Phil. Student in Chemistry, there are many people I wish to thank.

Firstly, I am extremely grateful to Prof. Paul Beer for the opportunity to carry out the projects under the title of this thesis. As he will always say, “it is what you wanted to do from the start”, but his patience and guidance throughout this degree have been invaluable and I am looking forward to continuing to work together in the future.

In the same vein, the support I have received from members of the Beer Group throughout both my undergraduate and graduate years has been fantastic. More than just colleagues, they have all been great friends, making labs S8 and S7 the best place to have a bad day in the office. In particular, I must thank Stuart Cornes, Sean Robinson, Alex Hess, Thomas Mole, Ben Mullaney, Jason Lim, Asha Brown, Ben Partridge and Thomas Lang for inspirational discussions on many of the aspects of the work in this thesis, and to Rémi Tirfoin for providing a (dodgy) soundtrack to most of them. I am also grateful to several of these people for proof-reading the chapters of this thesis, ensuring that there is still red ink left in some of Paul’s pens, and especially to Sean for his assistance with formatting and compiling this document.

If ever there was a “breakthrough moment” then it would be the first time the two-station naphthalimide axle component was isolated and for this credit must go to Dr. J. Pancholi who lent some superb advice on NI functionalisation to kick-start Chapter Two after our meeting in China. Since then, I have been fortunate to witness two students in Greg Carton and Andrew Docker also develop a love affair with molecular machines and subsequently both have made significant contributions to this thesis (Chapters Two and Three). More recently, collaboration links with Prof. K. Porfyrakis’ group in the Department of Materials have allowed me the privilege to work alongside Ilija Rašović and learn

about the chemistry of fullerenes (Chapter Four). I also acknowledge Dr. T. Claridge for providing some much-needed assistance interpreting the sub-optimal proton NMR spectra that feature in Chapter Five.

Away from the CRL I am lucky enough to have a wonderful group of family and friends who, although don't wish to discuss the positional integrities of rotaxanes, have been equally generous in their support throughout these last three and a half years. I would especially like to thank Jess for all her encouragement and kind words, (perhaps reading this will help you believe in atoms?!). In addition, my most recent flat mates Lucy, Marieke, Katie and Gareth have been a great group of people to share The Furnace with and very accommodating toward my recent antisocial working hours.

Finally, none of the fortunes I have had in Oxford would have been possible without the firm foundations of my loving parents and sisters. This thesis is dedicated to the four of you, thank you for *everything*. Would the real Dr. Barendt please stand up?!

Timothy Barendt

Oxford, 6th April 2016.

“Welcome my son, welcome to the machine.”

R. Waters, Pink Floyd, 1975.

PREVIOUSLY PUBLISHED WORK

Anion Sensing by Solution- and Surface-Assembled Osmium(II) Bipyridyl Rotaxanes

J. Lehr, T. Lang, O. A. Blackburn, T.A. Barendt, S. Faulkner, J. J. Davis and P. D. Beer, *Chem. Eur. J*. 2013, **19**, 15898-15906

Halogen bonding in supramolecular chemistry

L. C. Gilday, S. W. Robinson, T. A. Barendt, M. J. Langton, B. R. Mullaney and P. D. Beer, *Chem. Rev*., 2015**, 115**, 7118–7195.

Superior Anion-Induced Shuttling Behaviour Exhibited by a Halogen Bonding Two Station Rotaxane

T. A. Barendt, S. Robinson, P. D. Beer, *Chem. Sci*., 2016. DOI: 10.1039/C6SC00783J

Selective Nitrate Recognition by a Halogen Bonding [3]Rotaxane Molecular Shuttle

T. A. Barendt, A. Docker, I. Marques, V. Félix and P. D. Beer, *Angew. Chem. Int. Ed*., 2016. DOI: 10.1002/anie.201604327

Oral presentations

"Anion-Induced Molecular Motion Exhibited by Multi-station Rotaxanes"

UK Halogen Bonding Symposium

University of York, 2015

Poster presentations

"Anion-Induced Molecular Motion Exhibited by a Multi-Station Halogen Bonding Rotaxane"

International Symposium on Macrocyclic and Supramolecular Chemistry

Strasbourg, France, 2015

ABBREVIATIONS

δ	chemical shift
λ	wavelength
μ	micro, dipole moment
ν	frequency
Δ	change in (a measurement), heat
°	degree
°C	degrees Celsius
*	excited state
Å	Ångstrom
A	acceptor
A^-	anion
abs	absorption
aq.	aqueous
Ar	aromatic
Arg	arginine
Asp	aspartate
ATP	adenosine triphosphate
a.u.	arbitrary units
bipy	2,2'-bipyridine
Boc	di-*tert*-butyl dicarbonate
BODIPY	Boron-dipyrromethene
br	broad
Bu	butyl
cat.	catalytic
conc.	concentrated
COSY	homonuclear correlation spectroscopy
CuAAC	copper(I)-catalysed azide–alkyne cycloaddition
D	donor
d	doublet
DBU	1,8-diazabicycloundec-7-ene
dd	doublet of doublets
DEAD	diethyl azidocarboxylate
DIPEA	*N*,*N*-di-*iso*-propylethylamine
DMF	*N*,*N*-dimethylformamide
DMSO	dimethyl sulfoxide
DN	1,4-dialkoxynaphthalene
DNA	deoxyribonucleic acid
e.g.	*exempli gratia*
em	emission
eq., equiv.	equivalent

ESI	electrospray ionisation
ET	electron transfer
Et	ethyl
ex	excitation
ext.	external
Fc	ferrocene
g	gram
G	Gibbs free energy
Grubbs' I/II	Grubbs' first/second generation catalyst
h	Planck's constant
HB	hydrogen bonding
HOMO	highest occupied molecular orbital
hr.	hour
HSQC	heteronuclear single quantum coherence
Hz	hertz
I	intensity
int.	internal
i.e.	*id est*
ISC	intersystem crossing
iso.	isophthalamide
J	Joule
J	coupling constant
k	kilo
K	Kelvin
K_{Ass}	association constant
L	litre
LUMO	lowest occupied molecular orbital
M	molar
M	mega, molecular ion
m	milli, multiplet,
m	*meta*
m/z	mass-to-charge ratio
macro	macrocycle
max.	maximum
Me	methyl
Mes	1,3,5-trimethylbenzene
MIM	mechanically interlocked molecule
min	minute
MLCT	metal-to-ligand charge transfer
mol	mole
MS	mass spectrometry
Ms, mesyl	methanesulfonyl chloride
n	nano

NDI	naphthalene diimide
NI, nap	naphthalimide
NMR	nuclear magnetic resonance
OAc	acetate
o/n	overnight
p	*para*
PDI	perylene diimide
PET	photoinduced electron transfer
pH	$-\log_{10}[H^+]$
Ph	phenyl
pK_a	$-\log_{10}K_a$
ppm	parts per million
Pr	propyl
Py	pyridinium
q	quartet
quin.	quintet
R	chemical substituent
RCM	ring closing metathesis
R_f	Retention factor
ROESY	rotating-frame nuclear Overhauser effect correlation spectroscopy
rt	room temperature
s	second, singlet
SAM	self-assembled monolayer
sat.	saturated
sept.	septet
St	stopper
t	triplet
t, tert	tertiary
TBA	tetrabutyl ammonium
TBDMSCl	tert-butyldimethylsilyl chloride
TBTA	tris[(1-benzyl-1*H*-1,2,3-triazol-4-yl)methyl]amine
TLC	thin layer chromatography
trz/trz$^+$	triazolium
Ts, tosyl	*para*-toluenesulfuonyl chloride
UV	ultra-violet
V	volt
vis.	visible
vs.	*versus*
VT	variable temperature
v/v %	volume/volume percent
wt.	weight
X	halogen atom
XB	halogen bonding

TABLE OF CONTENTS

ABSTRACT iii
ACKNOWLEDGEMENTS v
PREVIOUSLY PUBLISHED WORK ix
ABBREVIATIONS xi
TABLE OF CONTENTS xv
Chapter One: Introduction 1
1. INTRODUCTION 3
1.1. Anion Supramolecular Chemistry 3
1.1.1. Introduction to Supramolecular Chemistry 3
1.1.2. The importance of anions 5
1.1.3. The challenges of anion coordination 5
1.1.4. Non-covalent interactions for anion recognition 7
1.1.5. Anion recognition 9
1.1.6. Anion Sensing 22
1.2. Mechanically Interlocked Molecules 28
1.2.1. Synthesis of MIMs 29
1.2.2. Templated assembly of MIMs 30
1.3. Applications of Mechanically Interlocked Molecules 40
1.3.1. Molecular machines 40
1.3.2. MIMs as Catalysts 45
1.3.3. MIMs for Recognition and Sensing 47
1.4. Objectives 48
1.5. References 49
Chapter Two: Anion-induced shuttling in bistable [2]rotaxanes 59
2. ANION-INDUCED SHUTTLING IN BISTABLE [2]ROTAXANES 61
2.1. Introduction 61
2.1.1. Anion-induced molecular motion in MIMs 61
2.1.2. Chapter Objectives 62
2.2. A two-station NI-triazolium [2]rotaxane 64
2.2.1. Synthesis of two-station NI-iodo-triazolium thread and macrocycle components 65
2.2.2. Pseudorotaxane Investigations 69
2.2.3. Synthesis of two-station NI-triazolium axle components 72
2.2.4. Synthesis of HB two station NI-proto-triazolium [2]rotaxane 74

2.2.5. ^{1}H NMR spectroscopic studies of anion-induced shuttling behaviour 76
2.2.6. ^{1}H NMR spectroscopic studies of solvent effects on anion-induced shuttling behaviour 82
2.2.7. Summary 86
2.3. Two-station NDI-iodo-/proto-triazolium [2]rotaxanes 87
2.3.1. Synthesis of two-station NDI-XB/HB-triazolium axle components 87
2.3.2. Synthesis of two-station NDI-XB/HB-triazolium [2]rotaxanes 92
2.3.3. ^{1}H NMR spectroscopic studies of anion-induced shuttling behaviour 93
2.3.4. X-ray crystallography 101
2.3.5. Optical responses from anion-induced shuttling behaviour 102
2.3.6. One-station NDI/triazolium [2]rotaxane syntheses 104
2.3.7. Quantitative estimations of macrocycle occupancies in two-station NDI-XB/HB-triazolium [2]rotaxane shuttles 107
2.3.8. Solvent effects on macrocycle occupancies within two-station NDI-XB/HB-triazolium [2]rotaxane shuttles 110
2.3.9. Summary 114
2.4. A two-station *N*-alkyl pyridinium-triazolium [2]rotaxane 115
2.4.1. Synthesis of a two-station *N*-alkyl pyridinium-triazolium axle component 115
2.4.2. Synthesis of a two-station *N*-alkyl pyridinium-triazolium [2]rotaxane 117
2.4.3. ^{1}H NMR spectroscopic studies of anion-induced shuttling behaviour 118
2.4.4. Summary 121
2.5. Conclusions and future work 121
2.6. References 123
Chapter Three: Oxoanion recognition and shuttling in four-station [3]rotaxanes 127
3. OXOANION RECOGNITION AND SHUTTLING IN FOUR-STATION [3]ROTAXANES 129
3.1 Introduction 129
3.1.1. Oxoanion recognition 129
3.1.2. Higher-order interlocked assemblies 130
3.1.3. Utilising molecular motion for anion sensing 135
3.1.4. Chapter objectives 137
3.2. Synthesis of four-station HB and XB axle components 138
3.3. Synthesis of four-station HB and XB [3]rotaxanes 142
3.4 ^{1}H NMR spectroscopic studies of chloride-induced shuttling behaviour 144
3.5 ^{1}H NMR spectroscopic studies of oxoanion-induced shuttling behaviour 153
3.6 ^{1}H NMR oxoanion binding and molecular motion studies of the four-station HB [3]rotaxane in DMSO-d_6 159
3.7 Optical oxoanion sensing by the four-station HB [3]rotaxane in DMSO 163

3.8 A comparison of the anion recognition properties of HB and XB [3]rotaxanes 165
3.9 Conclusions and future work 169
3.10 References 171
Chapter Four: Fluorescence anion sensing in C_{60} fullerene-containing multi-station rotaxanes 175
4. FLUORESCENCE ANION SENSING IN C_{60} FULLERENE-CONTAINING MULTI-STATION ROTAXANES 177
4.1. Introduction 177
4.1.1. Fullerenes and their applications in supramolecular chemistry 177
4.1.2. Fluorescence anion sensing using molecular motion 180
4.1.3. Chapter objectives 181
4.2. A ferrocene macrocycle-containing two-station [2]rotaxane 182
4.2.1. Synthesis 182
4.2.2. Chloride-induced shuttling in a ferrocene macrocycle-containing two-station [2]rotaxane 184
4.2.3. Photophysical studies of nitro- and ferrocene-containing two-station [2]rotaxanes 186
4.3. C_{60} fullerene-containing [3]rotaxanes 189
4.3.1. Exohedral functionalisation of a C_{60} fullerene 189
4.3.2. Synthesis of a C_{60} fullerene-containing four-station axle component 191
4.3.3. Photophysical properties of the four-station C_{60} fullerene-containing axle component 193
4.3.4. Synthesis of C_{60} fullerene-containing four-station [3]rotaxanes 194
4.3.5. Characterisation of chloride-induced shuttling in the C_{60} fullerene-containing four-station [3]rotaxanes 196
4.3.6. Preliminary photophysical studies of chloride-induced shuttling in the C_{60} fullerene-containing four-station [3]rotaxanes 206
4.4. Conclusions and future work 211
4.5. References 214
Chapter Five: Dynamic behaviour in a perylene diimide-containing [3]rotaxane and [3]catenane 217
5. DYNAMIC BEHAVIOUR IN A PERYLENE DIIMIDE-CONTAINING [3]ROTAXANE AND [3]CATENANE 219
5.1. Introduction 219
5.1.1. The chemistry of perylene diimides 219
5.1.2. PDI-containing MIMs 221
5.1.3. Chapter objectives 223
5.2. A PDI-containing [3] rotaxane 226
5.2.1. Synthesis of a four-station PDI-containing axle component 226
5.2.2. Synthesis of a four-station PDI-containing [3]rotaxane 228

5.2.3. ^{1}H NMR spectroscopic studies of anion-induced shuttling behaviour in $CDCl_3$ 230
5.2.4. ^{1}H NMR spectroscopic studies of solvent-induced shuttling behaviour 234
5.2.5. UV-Vis spectroscopic studies of solvent-induced shuttling behaviour 240
5.2.6. ^{1}H NMR spectroscopic studies of anion-induced shuttling behaviour in $CDCl_3$-CD_3OD solvent mixtures 242
5.2.7. UV-Vis spectroscopic studies of anion-induced shuttling behaviour in 3:1 $CHCl_3$:CH_3OH 248
5.3. A PDI-containing [3]catenane 249
5.3.1. Synthesis of a four-station PDI-containing macrocycle 249
5.3.2. Synthesis of a four-station PDI-containing [3]catenane 252
5.3.3. ^{1}H NMR spectroscopic studies of anion-induced shuttling behaviour in $CDCl_3$ 254
5.3.4. ^{1}H NMR spectroscopic studies of anion-induced shuttling behaviour in 3:1 $CDCl_3$:CD_3OD 258
5.3.5. UV-Vis spectroscopic studies of anion-induced shuttling behaviour in 3:1 $CDCl_3$:CD_3OD 262
5.4. Summary and future work 264
5.5. References 265
Chapter Six: Experimental 267
6. EXPERIMENTAL 269
6.1. General Considerations 269
6.1.1. Reactants and reagents 269
6.1.2. Characterisation and instrumentation 269
6.1.3. General procedure for anion exchange 270
6.2. Synthesis and characterisation of novel compounds 270
6.3. References 350
Chapter 7: Conclusions 351
7. CONCLUSIONS 353
Appendices 357
APPENDICES 359
1. ^{1}H NMR anion binding titration protocol 359
2. Fluorescence experiments 360
3. UV-Vis experiments 361
4. Estimations of station occupancies 362
5. Characterisation data for C_{60} fullerene bis-alkyne 369
6. Crystal structure data 370
X-ray diffraction 370
Discussion of structures 370

7. References 372

Chapter One
Introduction

1. INTRODUCTION

1.1. Anion Supramolecular Chemistry

1.1.1. Introduction to Supramolecular Chemistry

The foundations of supramolecular chemistry are expressed within the simplest of chemical processes: the reversible association of two or more species held together by non-covalent intermolecular forces.[1] These individual forces might be weak, however when used in concert, the strength of association can rival a traditional covalent bond between two molecular components. The inspiration for supramolecular chemistry comes from Nature where non-covalent interactions are employed in numerous biological processes including substrate recognition by enzymes, protein mediated cellular transport and the transcription and replication of DNA.[2] With clear origins in host–guest chemistry, the field of supramolecular chemistry has expanded enormously to include disciplines such as molecular self-assembly and in turn promises a variety of applications in the field of nanotechnology.[3]

The principles of molecular recognition were first hypothesised by Fischer in 1884 with the notion that biological enzyme–substrate interactions take the form of a “lock and key”. As such, host–guest chemistry is founded upon complementarity between the species involved; selective binding is achieved by a complementary shape, size and chemical functionality between the host (lock) and guest (key) species.[4,5]

Nearly a century later, this “lock and key” theory was elegantly demonstrated by Pedersen’s discovery of the selective group I metal cation binding ability of crown ethers, such as dibenzo-18-crown-6 (Figure 1.1a).[6] Further development of alkali metal cation hosts was achieved through Lehn’s three dimensional cryptands[7] (Figure 1.1b) and Cram’s rigid spherands (Figure 1.1c),[8] both of which exhibited enhanced group I metal cation recognition properties in comparison to the crown ethers. This seminal work was acknowledged as integral in launching the field of supramolecular chemistry when the trio were awarded the Nobel Prize for Chemistry in 1987.[9–11]

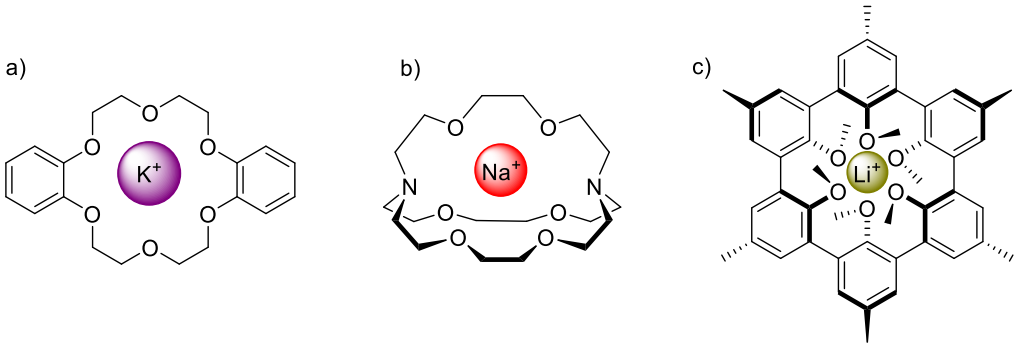


Figure 1.1. Macrocyclic alkali metal cation receptors a) Pedersen's crown ether[6] b) Lehn's cryptand[7] and c) Cram's spherand.[8]

Alongside these early advancements, anion coordination chemistry was beginning to be investigated independently. Park and Simmons' report in 1968 of a series of protonated macrobicyclic amine derivatives capable of the encapsulation of halide anions in water, with structures analogous to Lehn's cryptands, provided the first examples of synthetic anion receptors (Figure 1.2).[12] In spite of these early contributions however, the field of anion coordination chemistry remained relatively underdeveloped until the last two decades or so, which has seen the emergence of an ever increasing number of synthetic hosts capable of anion recognition. As a consequence, the field of anion supramolecular chemistry is now an established and fundamental area of chemical research.

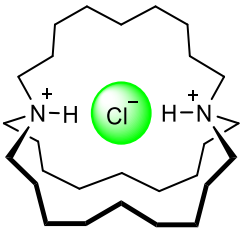


Figure 1.2. Park and Simmons' anion receptor [9.9.9]-'katapinate'.[12]

Of relevance to the theme of this thesis, this introductory chapter focuses on brief reviews of anion supramolecular chemistry followed by discussions on the construction of mechanically interlocked molecules for nanotechnological applications such as molecular machines, switches and sensors.

1.1.2. The importance of anions

The importance of anions is evident throughout biology. The majority of enzyme substrates and co-factors are negatively charged,[13] while the genetic instructions for forming these 'biological catalysts' are encoded within DNA, a doubly helical polyanionic phosphate polymer.[14] Nature's energy currency, ATP, is another phosphate-containing polyanion, and the binding, transport and hydrolysis of this molecule is crucial to the processes of cellular activity.[15]

Halide anions also have an important role *in vivo*, for example iodide is critical for hormone biosynthesis in the thyroid gland.[16] Of greater prevalence within the body is chloride, which is required to regulate blood pressure, metabolism and, alongside bicarbonate, maintain ionic strength and pH.[17] The misregulation of intercellular transportation of chloride by membrane channel proteins is known to cause cystic fibrosis,[18,19] whilst other diseases such as Alzheimers' have also been linked to anion imbalances, resulting from defects in anion exchange channels.[20]

In the environment, oxoanions such as nitrate and phosphates are pollutants resulting from the overuse of fertilisers causing algal blooms and eutrophication.[21,22] While nitrate and sulfate are both constituents of acid rain, an increased level of nitrate in drinking water is also associated with a range of diseases.[23] Pertechnetate, generated as a waste side product from nuclear fuel reprocessing, is another toxic anionic pollutant found in aquatic environments.[24]

Finally the pivotal role of anions as nucleophiles, bases and catalysts in a variety of chemical processes cannot be overplayed. In summary, the fundamental importance of anions has meant that the design and synthesis of artificial anion receptors, sensors and sequestering agents has become highly desirable.[25,26]

1.1.3. The challenges of anion coordination

The intrinsic properties of anions present specific challenges in the design of anion host systems for their selective recognition. The lower charge densities of anions relative to their isoelectronic cationic

analogues is a direct consequence of larger ionic radii and limits the effectiveness of electrostatic interactions for their coordination (Table 1.1).

Table 1.1. Effective ionic radii and free energies of hydration of selected isoelectronic cations and anions.

Anion	Ionic Radius (Å)[27]	$\Delta G_{hydration}$ (kJ mol^{-1})[1]	Cation	Ionic Radius (Å)[27]	$\Delta G_{hydration}$ (kJ mol^{-1})[1]
F^-	1.19	−465	Na^+	1.16	−365
Cl^-	1.67	−340	K^+	1.52	−295
Br^-	1.82	−315	Rb^+	1.66	-
I^-	2.06	−275	Cs^+	1.81	−250

Potential anion binding hosts must overcome the penalty of relatively high free energies of anion–guest solvation which are particularly evident in protic, polar solvents such as alcohols and water. The Hofmeister series classifies anions according to their degree of solvation (Figure 1.3).[28] In order to achieve anti-Hofmeister selectivity, an effective receptor must "out compete" with the solvent for the anion, whereas hydrophobic effects may be employed to bias selectivity for lipophilic anions of lower charge density (*vide infra*).[29]

$$HPO_4^{2-} < F^- \approx SO_4^{2-} < H_2PO_4^- < HCO_3^- < Cl^- < Br^- < NO_3^- < ClO_3^- < I^- < ClO_4^- < SCN^-$$

Figure 1.3. The Hofmeister Series.[28]

Anions adopt a range of distinct geometries which can be exploited as means for achieving selective recognition (Figure 1.4). Through the design of anion receptors with complementary three-dimensional binding cavities, discrimination between guests based on their shape is possible, although the synthesis of such systems is often non-trivial.

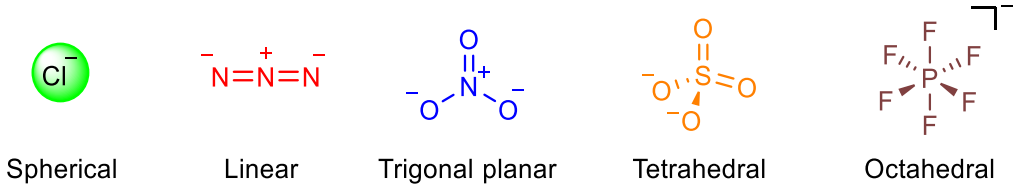


Figure 1.4. A selection of anion geometries.

Finally, all anions display some degree of pH dependence in aqueous solution due to their propensity to protonate under acidic conditions. Likewise, the pH sensitivity of the host must also be taken into consideration.[30]

1.1.4. Non-covalent interactions for anion recognition

Fundamental to anion supramolecular chemistry is the use of complementary non-covalent interactions between the host and the anionic guest.[31] These intermolecular forces are individually much weaker than conventional covalent bonds, but when acting in concert can produce strong and selective binding affinities. The following section summarises the primary non-covalent interactions employed in anion recognition.

Electrostatic interactions occur as a result of the Coulombic attraction between groups of opposing charge. Positive charge–anion (ion pair) interactions (Figure 1.5a) are the strongest electrostatic interaction making them ideal for anion receptors operating in highly competitive protic solvent media, with the caveat that they have no intrinsic directionality. By contrast, dipole–anion interactions are anisotropic and hence are of significant importance to receptors designed to exhibit selectivity for an anionic guest by means of its defined geometry (Figure 1.5b).[1]

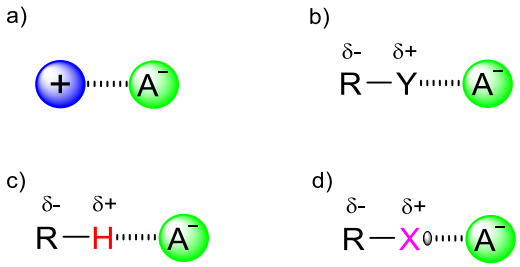


Figure 1.5. A selection of non-covalent interactions a) ion pair, b) dipole–anion, c) hydrogen bonding and d) halogen bonding. R = electron-withdrawing group, Y = not halogen or hydrogen, X = halogen and A^- = anion.

Hydrogen bonding is a special class of dipole–anion interaction[32] which is considered to be primarily electrostatic in character, with the strength of a single hydrogen bond varying greatly from 4–120 kJ mol^{-1} (Figure 1.5c).[33]

Analogous to the hydrogen bond, a halogen bond (Figure 1.5d), according to IUPAC, occurs when "there is evidence of a net attractive interaction between an electrophilic region associated with a halogen atom [known as the σ-hole] in a molecular entity and a nucleophilic region in another, or the same, molecular entity."[34] Halogen atoms have three lone pairs of electrons that form a belt of electron density surrounding the central σ-hole resulting in a repulsion of any Lewis basic species within their vicinity. In stark contrast to hydrogen bonds, this restricts halogen bonds to near linear geometries. The size and polarisation of the electrophilic σ-hole (the red region of the electrostatic surface potential - Figure 1.6) is maximised when inductively electron-withdrawing groups are connected to the halogen bond donor group and when larger, more polarisable halogen atoms such as bromine and iodine are used.[35]

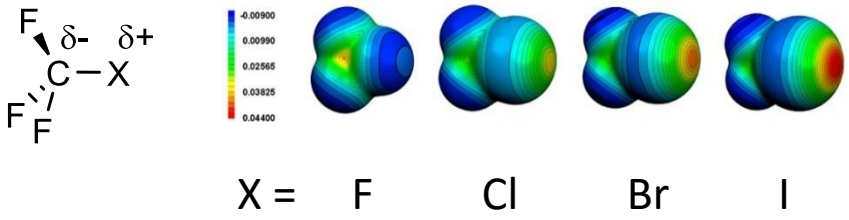


Figure 1.6. The molecular electrostatic surface potentials, in Hartrees, of CF_3X.[35] Reprinted with permission from ref 35. Copyright 2007 Springer.

The ability of halogen atoms to interact with neutral Lewis bases has been known for some time due to their observation in the solid state[36,37] and some biological systems.[38] However, the inherent negative charge and nucleophilicity of anionic species make them strong candidates as halogen bond acceptors.[39] Initial thermodynamic investigations of the association of iodine with I^- to form triiodide (I_3^-) revealed the XB interaction between the two species to be as strong as 126 kJ mol^{-1} in the gas phase[40] and 17 kJ mol^{-1} in water,[41] comparable in magnitude to hydrogen bonding.[33] More recently, the unique characteristics of halogen bonding (bond strength and interaction geometry) has been demonstrated in many cases to outperform hydrogen bonding in solution phase anion recognition (*vide infra*).[42]

Anion–π interactions are defined as the interaction between an electron-deficient aromatic surface and an anion, occurring as a consequence of an electrostatic attraction and anion-induced polarisation of the π system.[43–47] However, owing to their relative weakness compared to the aforementioned intermolecular forces, anion–π interactions are less common in anion receptor design, and when present, they appear to supplement other stronger anion–host interactions.[48,49] Theoretical calculations and ^{1}H NMR spectroscopy have revealed this to be the case for Johnson's acyclic receptor in which chloride binding to the sulfonamide motif was augmented by an anion–π interaction with the electron-deficient perfluorinated aryl ring in $CDCl_3$ (Figure 1.7).[50]

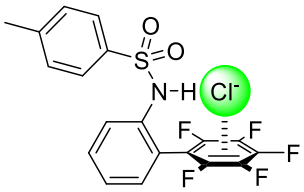


Figure 1.7. Hydrogen bonding and anion–π interactions occurring with chloride in Johnson's sulfonamide-based receptor.[50]

1.1.5. Anion recognition

This section highlights how the influence of naturally-occurring anion–host systems and the design principles from the cation recognition field have been employed in the design of positively-charged and neutral abiotic anion receptors that can function in polar organic and aqueous media.[51]

1.1.5.1. Anion recognition by nature

Nature demonstrates complementarity for anionic species in the sulfate- and phosphate-binding proteins found in bacteria (Figure 1.8).[52,53] In the former, the almost exclusive coordination of sulfate (K_a = 8.3 × 10^6 M^{-1}) occurs within a cleft between two globular domains of the polypeptide *via* the formation of seven specific hydrogen bonds with the surrounding amino acid residues. Similarly, the phosphate-binding protein achieves recognition through twelve hydrogen bonds and additional complementary electrostatic stabilisation from a guanidinium group present in the Arg-135 peptide residue (Figure 1.8b).[54]

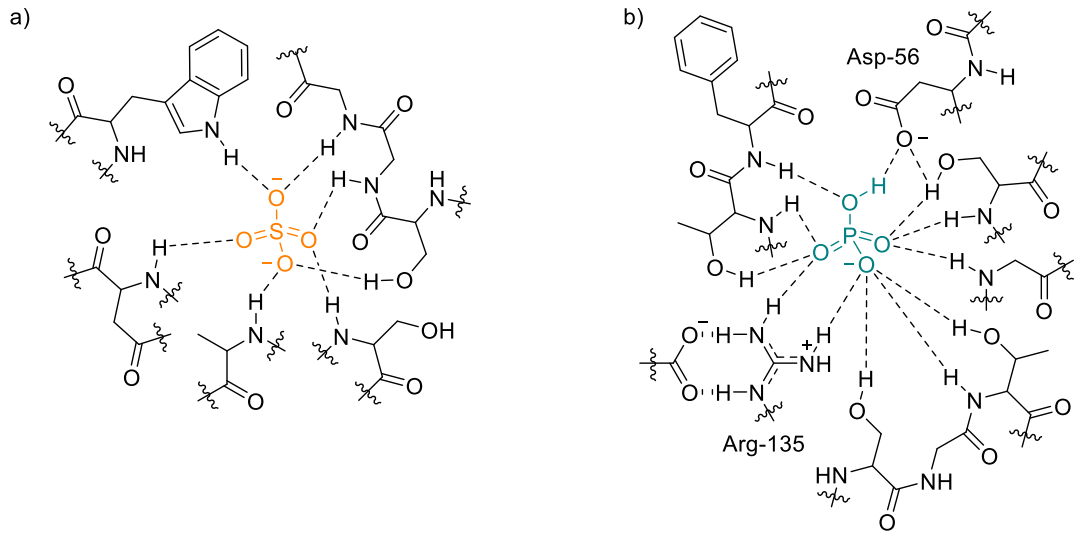


Figure 1.8. Schematic representations taken from X-ray crystal structures of a) the sulfate binding cleft of the sulfate-binding protein and b) the phosphate binding cleft of the phosphate-binding protein. Arg = Arginine and Asp = Aspartate.[52,53]

Taking inspiration from these neutral oxoanion protein host systems together with fundamental supramolecular design principles, such as preorganisation[8] and the chelate[55] and macrocyclic[56,57] effects the following section discusses examples of synthetic anion receptors.

1.1.5.2. Synthetic anion receptors

It is convenient to classify the enormous variety of anion receptors reported in the literature by the types of non-covalent interactions used to achieve anion recognition.

1.1.5.3. Protonated amine-, quaternary ammonium- and guanidinium-based receptors

Building on Park and Simmons' original anion receptor design (Figure 1.2),[12] Lehn and co-workers developed a range of macrocyclic and macrobicyclic polyammonium hosts capable of recognising anions in aqueous media. For example the receptor shown in Figure 1.9a, containing an ellipsoidal cavity, exhibited selectivity for azide anions ($\log K_a$ = 4.6 in H_2O)[58,59] whereas the smaller cavity of a hexaprotonated octaazacryptand host (Figure 1.9b) was selective for fluoride ($\log K_a$ = 10.6 in H_2O).[60–62] Sessler has demonstrated that the protonated forms of expanded porphyrins such as sapphyrin (Figure 1.9c) also have fluoride-binding properties.[63] More recently the same group have incorporated

protonated pyridine groups into similar porphyrin-based macrocycles to permit the binding of larger anions such as bromide, sulfate and dihydrogen phosphate in organic media.[64]

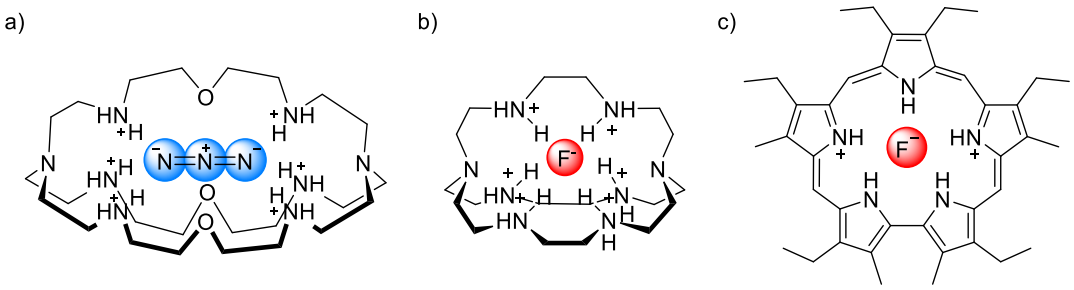


Figure 1.9. Lehn's hexaprotonated macrobicyclic polyammonium hosts a) azide-selective ellipsoidal receptor[58,59] b) fluoride-selective octaazacryptand receptor[60–62] and c) Sessler's diprotonated sapphyrin host for fluoride recognition.[63]

The strict requirement for secondary ammonium-based receptors to operate in low or moderate pH was overcome by Schmidtchen and co-workers with the syntheses of pH-independent quaternary ammonium macrotricyclic cage-like compounds capable of binding a range of halide and oxoanionic guests in water, driven predominantly by electrostatic and hydrophobic effects (Figure 1.10a).[65–67] The anion selectivity exhibited by these systems was tuned through size complementarity effects by varying the length of the alkyl spacers between the quaternary ammonium nitrogen heteroatoms. For example the smaller cage (R = $(CH_2)_6$) was found to bind bromide selectively whilst *p*-nitrophenolate was favoured by the larger host (R = $(CH_2)_8$). To overcome competition from the receptor's counter anions, a zwitterionic analogue (R' = $(CH_2)_6$) was also prepared, and this was demonstrated to enhance the halide binding in water (Figure 1.10b).[68]

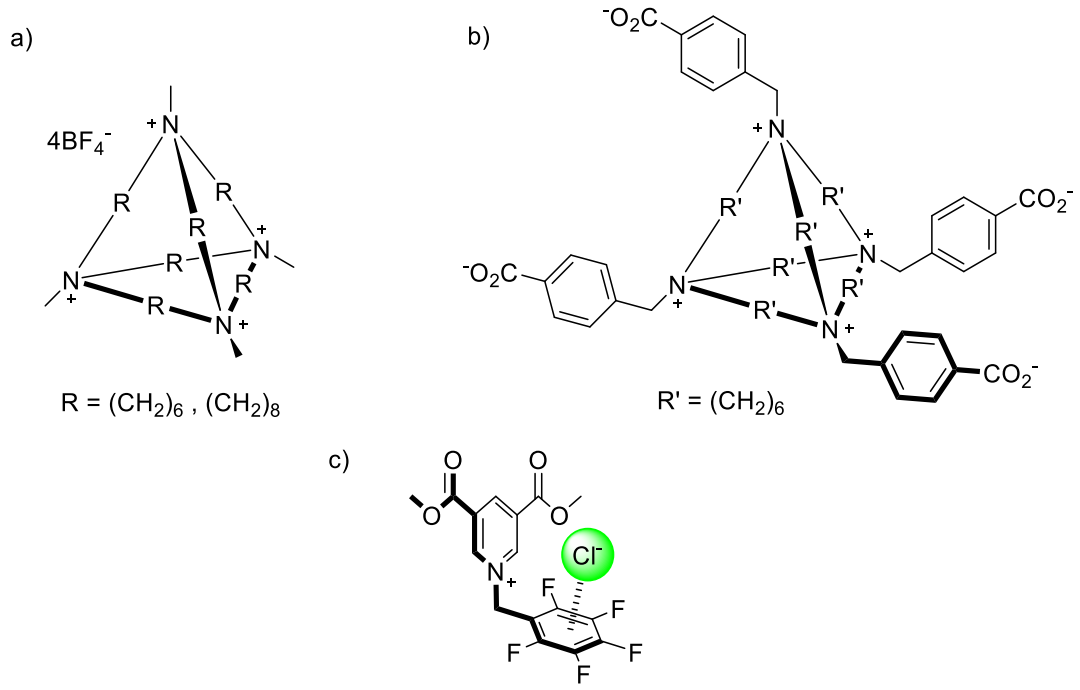


Figure 1.10. Quaternary ammonium cage receptors a) Schmidtchen's macrocyclic tetrahedral polyammonium cages,[65–67] b) a zwitterionic analogue[68] and c) Berkessel's quaternary pyridinium chloride receptor.[69]

Recent work by Berkessel has utilised Coulombic and anion–π interactions from a 3,5-di(carbomethoxy)pyridinium group functionalised with an electron-withdrawing pentafluorobenzyl substituent (Figure 1.10c) to achieve chloride binding in 9:1 THF:MeCN (K_a = 200 M^{-1}). Further to its coordination capabilities, this acyclic receptor functions as an anion binding organocatalyst for the C–C coupling reaction between 1-chloroisochroman and silyl ketene acetals.[69]

As a consequence of its high pK_a value[70] the guanidinium motif has been extensively used in biotic and synthetic anion–host systems.[71,72] The planar "Y" shaped geometry adopted by the bidentate guanidinium group provides an ideal spatial arrangement for association with complementary oxoanion species such as carboxylates, sulfates, phosphates and nitrates (Figure 1.11).[73,74]

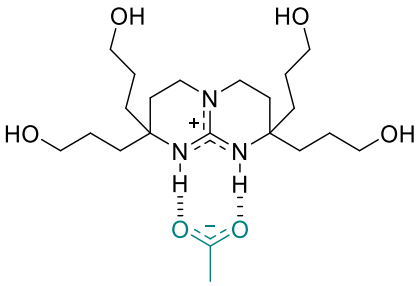


Figure 1.11. A guanidinium-based host for acetate.[73]

1.1.5.4. Receptors containing C–H donors

In contrast to amine-based receptors, those containing acidic C–H donor groups are insensitive to pH. In 1999, Sato[75] (Figure 1.12a) and Alcalde[76] (Figure 1.12b) reported the first use of convergent charge-assisted C–H hydrogen bond donation from imidazolium motifs for anion recognition.[77,78] Sato's acyclic tripodal receptor bound halide anions strongly in CD_3CN whereas Alcalde's family of preorganised imidazoliophane macrocycles recognised fluoride, dihydrogen phosphate and acetate in DMSO-d_6. Sessler and co-workers also incorporated C–H donor groups into a macrocyclic receptor by covalently attaching two pyridine bis-imidazolium sub-units together. Named the 'Texas-sized' molecular box, this tetracationic system was capable of forming 1:1 stoichiometric complexes with both mono- and di-terephthalate anions in DMSO-d_6 with association constants of $K_a = 2.1 \times 10^3$ M^{-1} and $K_a = 3.3 \times 10^3$ M^{-1} respectively (Figure 1.12c).[79] More recently, related systems such as Kim's benzimidazolium-based cyclophane can coordinate the biologically important anions guanosine-5′-15 triphosphate and iodide in aqueous solution at physiological pH (Figure 1.12d).[80]

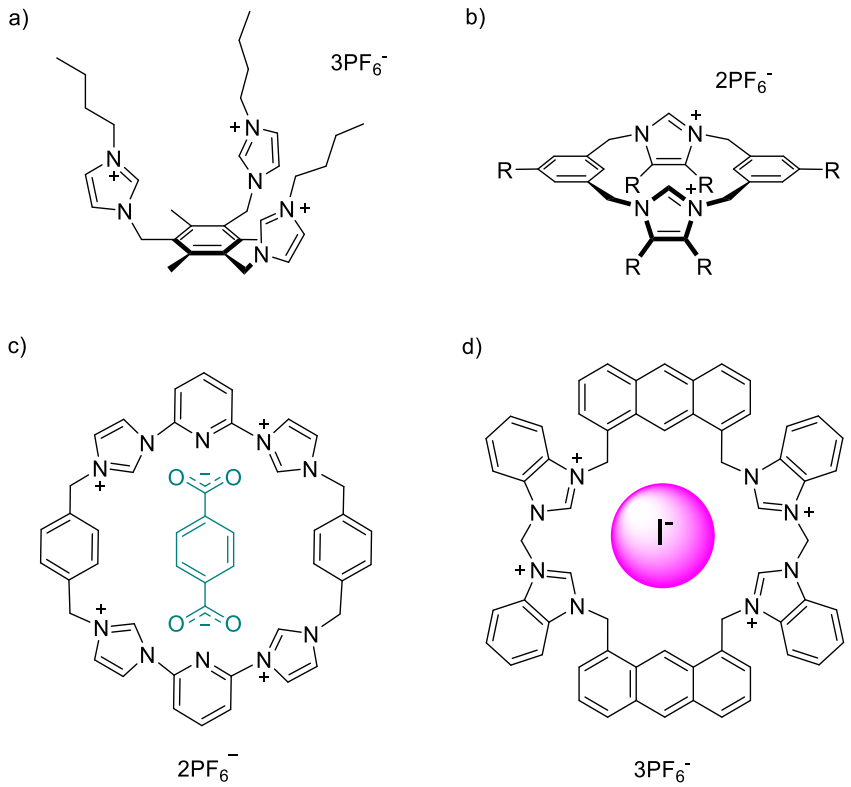


Figure 1.12. Imidazolium-based receptors a) Sato[75] and b) Alcade's[76] seminal hosts, c) Sessler's "Texas-sized" molecular box[79] and d) Kim's benzimidazolium-based cyclophane receptor capable of iodide-binding in water.[80] R = ^{t}Bu.

Since the first reports in 2008,[81,82] the 1,2,3-triazole motif has been demonstrated to coordinate anions effectively,[83–89] especially when integrated into cyclic host structures.[57,90] The anion-binding affinity of the triazole heterocycle may be further enhanced by alkylation of the triazole N^3 atom to produce the 1,2,3-triazolium motif which has been incorporated into a variety of acyclic and cyclic frameworks for anion binding *via* charge assisted C–H hydrogen bonding interactions.[91–96] By functionalisation of a steroidal framework Pandey *et al.* prepared the first triazolium-based receptor, which displayed selectivity for dihydrogen phosphate over chloride in $CDCl_3$ (Figure 1.13a).[97] More recently, the same group described a macrocyclic analogue with a reversed binding trend of chloride over dihydrogenphosphate in the same solvent (Figure 1.13b).[94]

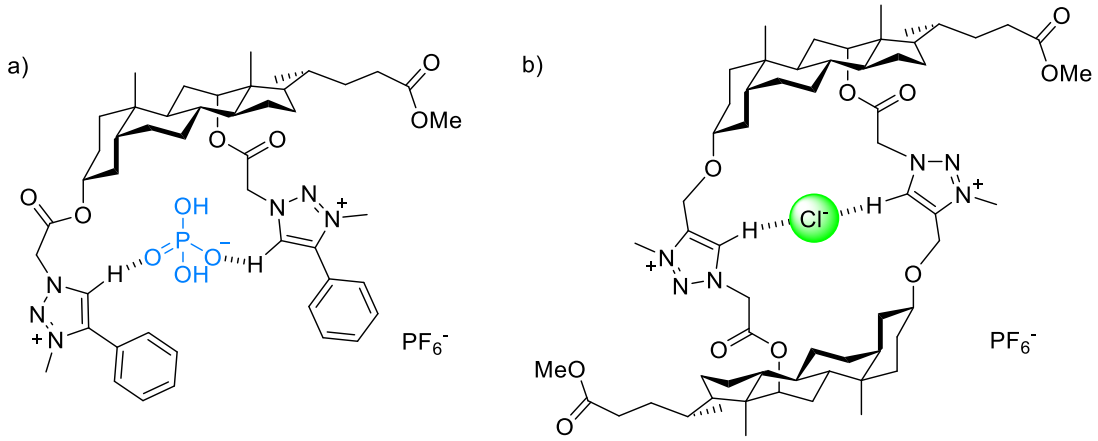


Figure 1.13. Pandey's a) acyclic[97] and b) cyclic bis-triazolium-containing receptors.[94]

Multiple triazolium groups have also been appended to water soluble cyclodextrin motifs to produce hosts capable of recognising biologically relevant polyanions such as inositol-1,4,5-trisphosphate and ATP in aqueous solution (Figure 1.14a).[98] Recent work by Molina and co-workers demonstrated the capability of the electron-deficient triazolium heterocycle to interact with anionic substrates through anion–π interactions, in combination with conventional intermolecular C–H hydrogen bonding.[99] The dual role of the triazolium motif permitted the receptor shown in Figure 1.14b to strongly bind the hydrogenpyrophosphate trianion in 9:1 CD_3CN:CD_3OD.

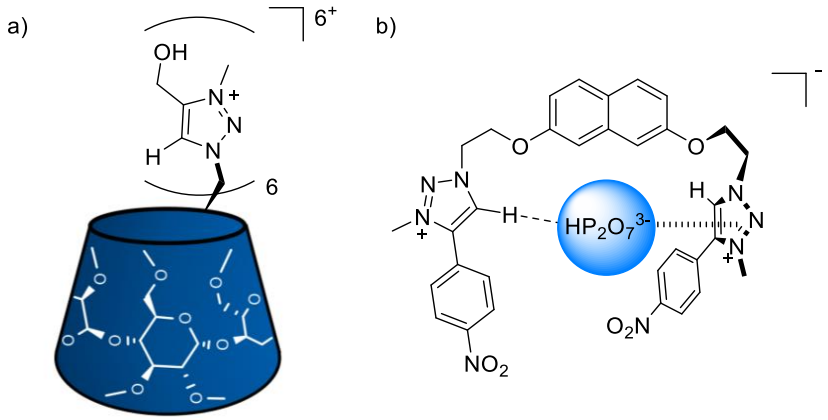


Figure 1.14. Triazolium-based receptors a) a water-soluble cyclodextrin-containing host for biological polyanions[98] and b) Molina's receptor exhibiting C–H hydrogen bonding and anion–π interactions to the anion guest.[99]

1.1.5.5. Neutral and negatively charged receptors

Nature's use of multiple amide motifs for the purpose of anion recognition has provided the inspiration for an extensive and diverse range of abiotic amide-containing anion receptors.[100,101] The seminal example of such a system was described by Pascal and co-workers in 1986.[102] However, arguably it was not until a decade or so later, when Crabtree reported a neutral, acyclic isophthalamide-based receptor capable of the strong binding of halide anions in CD_2Cl_2 that an expansion of research in this area began (Figure 1.15a).[103,104] Since then, isophthalamide and other related amide motifs have been incorporated into a variety of preorganised hosts such as macrocycles, cryptands[101] and mechanically bonded interlocked architectures (*vide infra*).

Kubik *et al.* integrated naturally occurring amino acids into a series of cyclic amide-based receptors,[105] including a bis-cyclopeptide "molecular oyster" which forms strong 1:1 stoichiometric sandwich complexes with sulfate and iodide anions ($K_a = 6.6 \times 10^6$ M^{-1} and $K_a = 5.6 \times 10^4$ M^{-1} respectively) in 2:1 CH_3CN:H_2O (Figure 1.15b).[106,107]

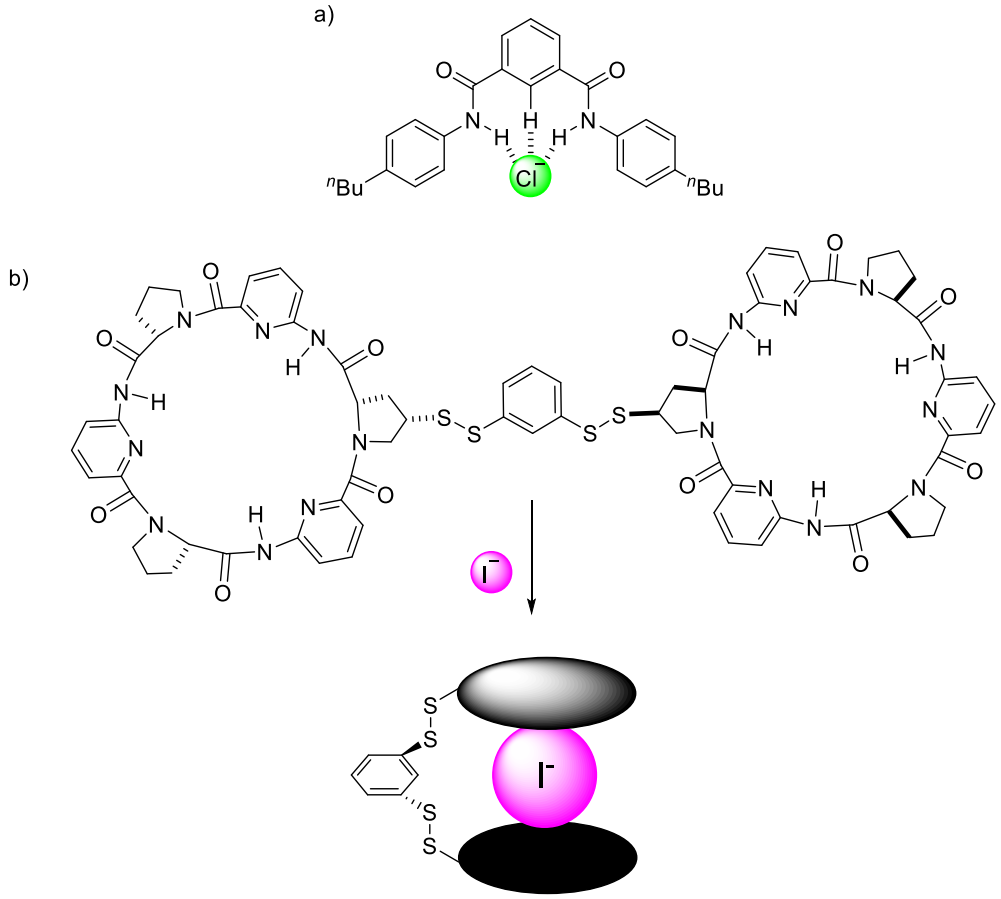


Figure 1.15. Amide-based receptors a) Crabtree's seminal isophthalamide-containing anion host[103,104] and b) Kubik's bis-cyclopeptide "molecular oyster" demonstrating the unique binding mode for iodide recognition.[106,107]

Ureas and thioureas are also powerful hydrogen bond donors and synthetic accessibility has resulted in their incorporation into a variety of anion receptor systems.[108,109] Gale's acyclic bis-urea host binds carboxylates up to three orders of magnitude more strongly than halides in DMSO containing 0.5% D_2O, as a consequence of the complementarity between the "Y-shaped" oxoanion and the two parallel hydrogen bond donor groups (Figure 1.16a).[110] Meanwhile a cyclic peptide scaffold triply functionalised with thioureas by Jolliffe, exhibits high affinity for sulfate in aqueous solution (Figure 1.16b).[111]

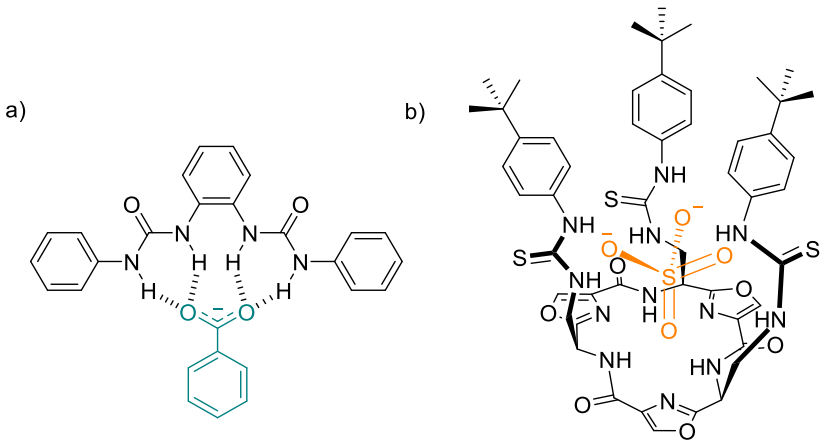


Figure 1.16. a) Gale's acyclic bis-urea host for benzoate[110] and b) Jolliffe's tripodal thiourea-based host selective for sulfate.[111]

Closely related to ureas, the squaramide derivative is a potent binding motif for halides on account of the strong hydrogen bond-donating abilities of its highly acidic N–H protons.[112,113] Gale and Davis have constructed powerful anion receptors by positioning squaramide groups in the axial positions of a preorganised steroidal framework. The halide anion association constants for the receptor in Figure 1.17 determined in water-saturated chloroform are four to five orders of magnitude larger than the corresponding urea-based analogue, and in particular the value of $K_a = 10^{14}\ M^{-1}$ reported for chloride is the highest known for coordination of this anion to any neutral receptor.[114]

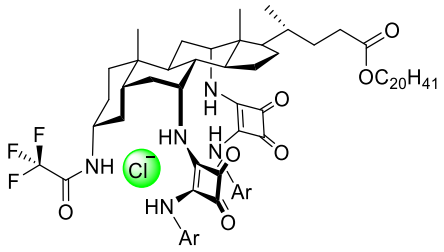


Figure 1.17. Gale and Davis' squaramide-containing receptor that exhibits a very strong affinity for chloride.[114]

Sessler and co-workers were the first to reveal the fluoride binding properties of the calix[4]pyrrole macrocycle in a range of polar organic solvents (Figure 1.18a),[115] and since then larger calix[*n*]pyrroles[116] and more complex "strapped" systems have been synthesised.[117,118] The receptor shown in Figure 1.18b was found to exhibit a marked affinity for sulfate relative to the parent calix[4]pyrrole in CD_2Cl_2.[119]

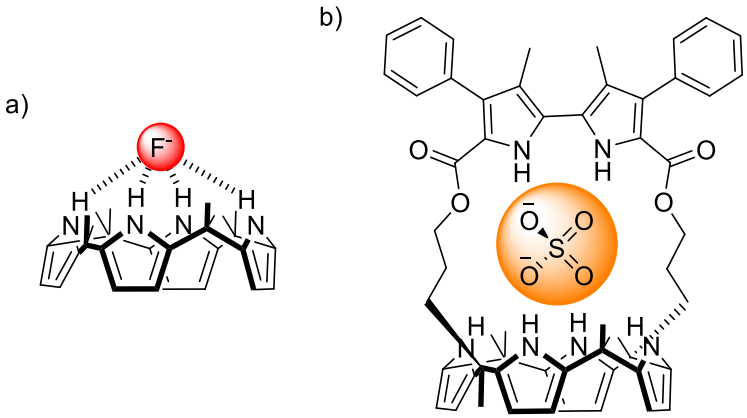


Figure 1.18. a) The parent calix[4]pyrrole macrocycle that exhibits strong fluoride recognition properties[115] and b) strapping of this motif to construct a sulfate-selective receptor.[119]

Current efforts to perform anion recognition in highly competitive aqueous environments has counter-intuitively resulted in the synthesis of negatively-charged hosts such as Sindelar's bambusuril-based macrocycle comprising a central hydrophobic cavity surrounded by carboxylate groups to facilitate water solubility (Figure 1.19).[120] The receptor exhibits Hofmeister-type selectivity where iodide and perchlorate are preferentially bound over other inorganic anions in phosphate-buffered water. Interestingly thermodynamic analysis revealed the binding to be an enthalpically-driven process, in conflict with the entropic origins of a classical hydrophobic effect.[105,121,122] The enthalpically-favoured association is attributed to energetically favourable CH–anion hydrogen-bonding interactions between host and guest.[123,124] The release of high-energy water molecules that form more numerous or stronger hydrogen bonding interactions in the bulk solution relative to when encapsulated in the binding pocket, is also likely to contribute to this nonclassical hydrophobic effect.[125,126]

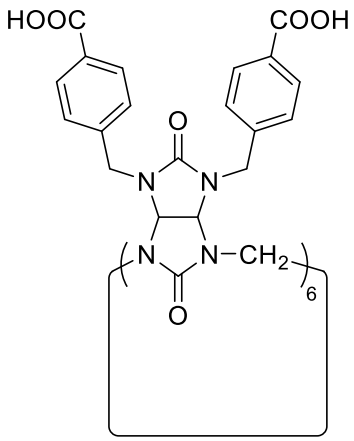


Figure 1.19. Sindelar's water soluble variant of the bambusuril macrocycle.[120]

1.1.5.6. Lewis acid and transition metal-based receptors

The integration of Lewis acidic elements into a host's molecular scaffold can facilitate anion binding by the formation of dative anion–Lewis acid bonds. A number of electron-deficient moieties have been used including three coordinate boron- (*vide infra* Figure 1.26),[127] tin-[128] and transition metal-[129–133] based receptors such as Nelson's metal–anion–metal cascade complex (Figure 1.20).[134] Transition metals can also stereochemically aid in the preorganisation of hydrogen bond donor groups for anion guest encapsulation.[135]

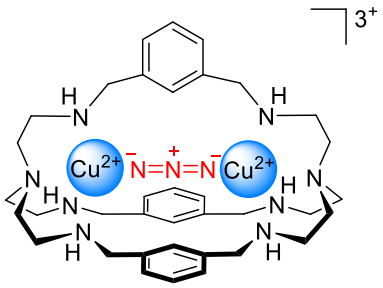


Figure 1.20. Recognition of azide via formation of a cascade complex with the Cu(II) complex of a bis-tren cryptand-based receptor.[134]

1.1.5.7. Halogen bonding receptors

In stark contrast to hydrogen bonds, the use of halogen bonds for the recognition of anions in solution is underdeveloped, in part because the first demonstration of halogen bonding for this purpose was only reported relatively recently by Resnati and Metrangolo.[136] Their heteroditopic receptor containing three halogen bond donor para-iodotetrafluorophenyl groups appended to a tris-ethyleneglycol amine

was capable of binding a separated alkali metal halide ion pair (Figure 1.21a). In particular, the formation of the adduct with NaI was found to be approximately 20 times stronger (K_a = 2.6 × 10^5 M^{-1}) than the non-halogen bonding perfluorinated analogue (K_a = 1.3 × 10^4 M^{-1}) in $CDCl_3$. Taylor *et al.* have also made significant contributions *via* the synthesis of neutral, acyclic receptors containing multidentate halogen bond donor groups.[137,138] For example the tripodal receptor shown in Figure 1.21b displays a preference for chloride over oxoanions in acetone.

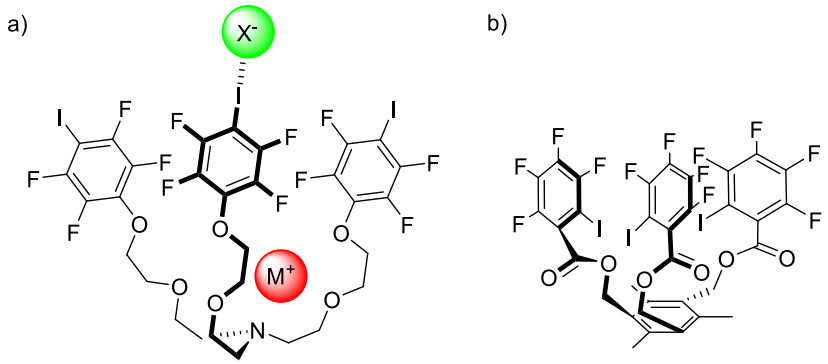


Figure 1.21. Tripodal halogen bonding receptors a) Resnati's alkali metal halide ion pair host[136] and b) Taylor's multidentate halide receptor.[137] MX = alkali metal halide.

The recognition of a greater variety of anionic guests in more competitive polar organic and polar organic–aqueous solvents has been achieved through the use of charge-assisted halogen bonds. Resnati and Metrangolo highlighted the potential of these non-covalent interactions with the synthesis of a monodentate, acyclic 2-iodo-imidazolium receptor (Figure 1.22a) that exhibited a strong affinity for oxoanions such as dihydrogen phosphate in DMSO (K_a = 10^3 M^{-1}).[139] Meanwhile, Beer and co-workers have used a family of bidentate haloimidazoliophane receptors to facilitate strong binding of halide anions in 9:1 CH_3OH:H_2O (Figure 1.22b).[140,141] Importantly the halogen bonding haloimidazoliophanes exhibited superior anion recognition properties in comparison to the hydrogen bonding analogues.

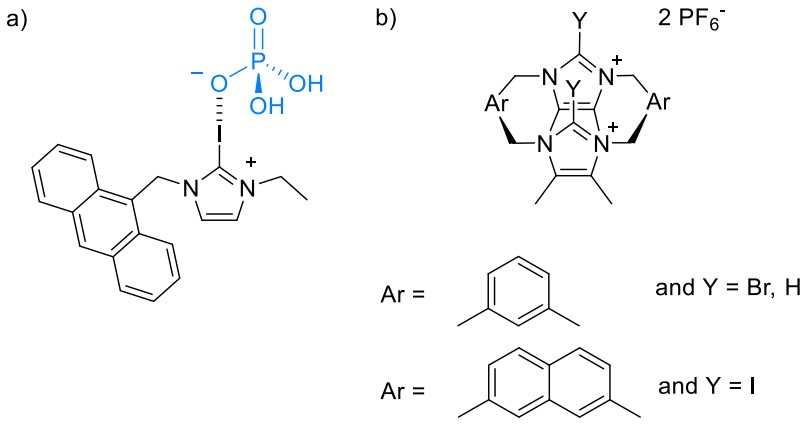


Figure 1.22. a) Resnati[139] and b) Beer's haloimidazolium-based[140,141] charge-assisted halogen bonding receptors.

1.1.6. Anion Sensing

Molecular anion sensors function *via* the production of a macroscopic detectable signal upon occurrence of the anion recognition event.[142] The most common sensor design involves the appendage of an optical or electrochemical reporter group to an anion receptor motif: guest binding then perturbs either the photo-physical or electrochemical properties of the reporter group, resulting in a measurable response (Figure 1.23a). It is also possible to use displacement assays in which sensing is achieved *via* the anion-induced displacement of a dye from a receptor, which in turn incurs a detectable change in the optical properties of the dye (Figure 1.23b).[143] An alternative strategy is to administer a reagent which is known to react with the target anion and in doing so produce a new compound with optical or redox properties differing from those of the starting material; this is known as the chemodosimeter approach (Figure 1.23c).[144]

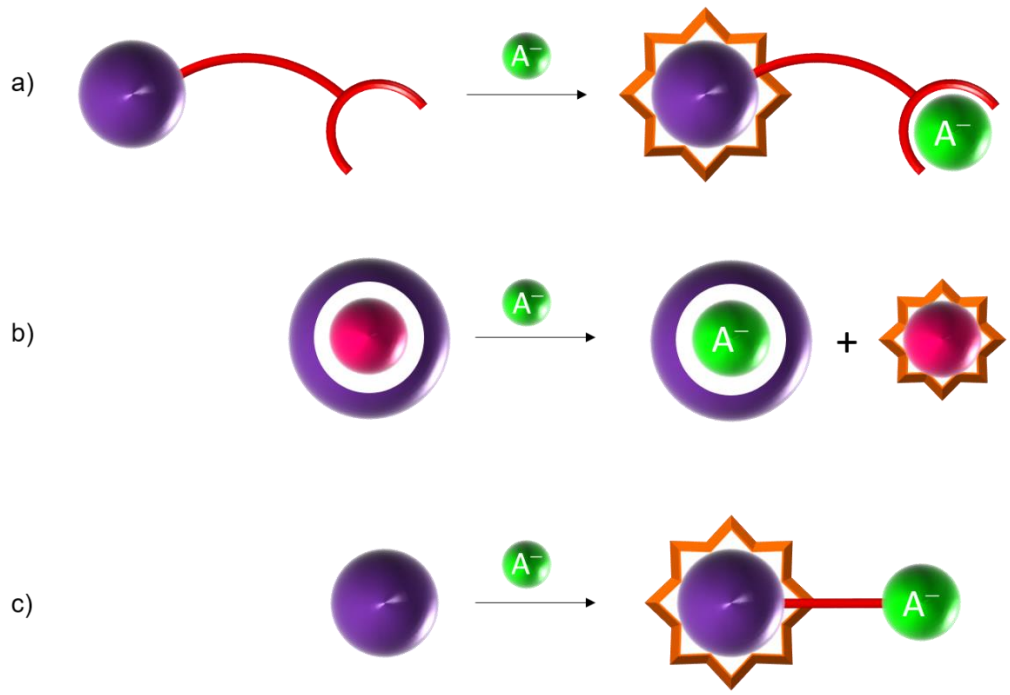


Figure 1.23. Schematic representations of general approaches to anion sensing a) a discrete molecular sensor incorporating an anion recognition site in close proximity to a reporter group,[142] b) a displacement-assay-based approach[143] and c) an anion chemodosimeter.[144] A^- = anion.

1.1.6.1. Fluorescent anion sensors

Depending on the mode of signalling, there are two classes of optical sensors: fluorescent sensors signal binding through changes in emission from the excited state, and colorimetric sensors which display ground state absorbance changes in the visible spectrum (*vide infra*). Fluorescence is a form of luminescence defined as photon emission from a singlet excited state[145] and so anion fluorescence sensing is achieved by modulating the wavelength and/or intensity of light emission upon anion coordination. Fluorescent anion sensors are widely applicable due to the inherent sensitivity of fluorescence spectroscopy allowing experiments to be performed on extremely low analyte concentrations.

Some of the methods of communication commonly employed by fluorescent sensors to signal anion recognition events include photoinduced electron transfer (PET), excimer formation and rigidity effects. Most relevant to this thesis is PET; a mechanism for fluorescence quenching in which a proximal orbital can facilitate through-space, non-radiative electron transfer to an excited fluorophore

(Figure 1.24a).[146,147] This excited state process results in the fluorophore being returned to the ground state without the emission of a photon. Any perturbations in the electronic potential of the donor orbital or its proximity to the fluorophore, for example by an anionic species, will alter the extent of quenching and hence the intensity of fluorescence emission.[148,149]

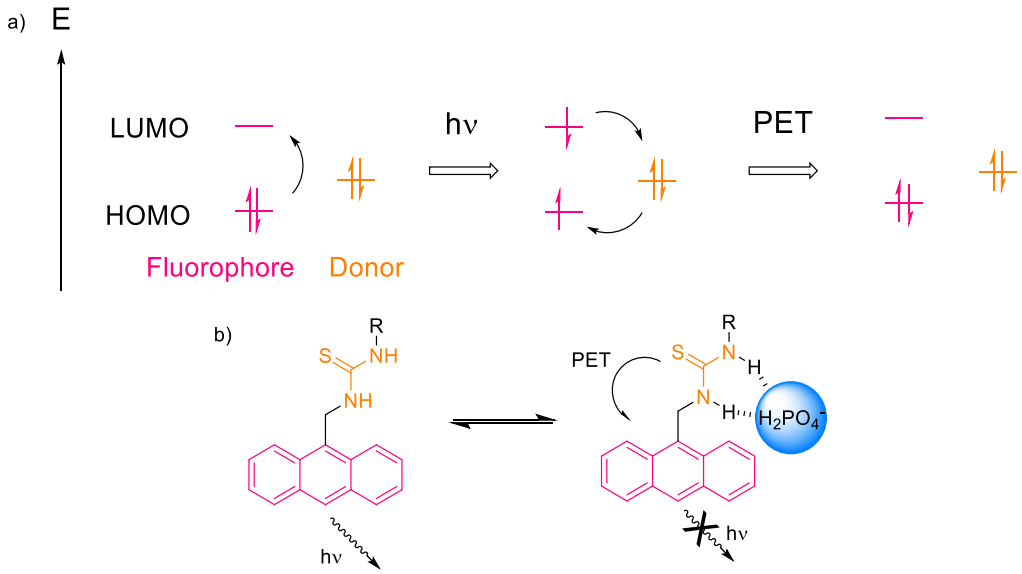


Figure 1.24. a) Mechanism for PET quenching of a fluorophore by a proximal donor group[150] and b) Gunnlaugsson's napthalene-based anion sensor that exhibits PET fluorescence quenching upon dihydrogen phosphate recognition.[151] R = alkyl, aryl.

Significant contributions to the collection of PET anion sensors have come from the group of Gunnlaugsson.[152,153] The covalent attachment of a thiourea binding motif to an anthracene fluorophore was the first of a family of anion sensors based upon the fluorophore–spacer–receptor model design (Figure 1.24b).[151] In these systems, the formation of an electron-rich anion–receptor complex results in a greater degree of PET quenching of the excited state. In DMSO, the binding of dihydrogen phosphate to the thiourea receptor results in a 70% decrease in fluorescence intensity of the diagnostic anthracene emission profile. More recently a probe containing a boron-dipyrromethene (BODIPY) reporter group and amidothiourea recognition site displayed fluoride selective PET fluorescence quenching in 1:1 DMSO:H_2O with an impressive sensitivity of 0.01 ppm (Figure 1.25).[154]

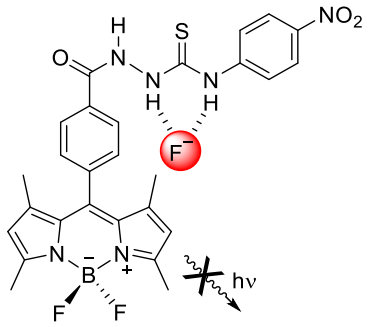


Figure 1.25. A fluoride selective fluorescent sensor based on a BODIPY chromophore covalently linked to an amidothiourea recognition site.[154]

1.1.6.2. Colorimetric anion sensors

The construction of synthetic sensors capable of a colorimetric response upon anion recognition is highly desirable because they generate signalling events that are detectable by the naked-eye, precluding the requirement for expensive instrumentation. The majority of examples incorporate conjugated organic chromophores into anion receptor frameworks in such a way that anion-binding perturbs the chromophore's visible light absorption sufficiently to produce an observable colour change.

Aldridge and co-workers have used ferrocene–indenyl chromophores, substituted with three-coordinate boron and phosphonium derivatives, to sense fluoride *via* a distinct colour change from green to maroon in THF (Figure 1.26).[155]

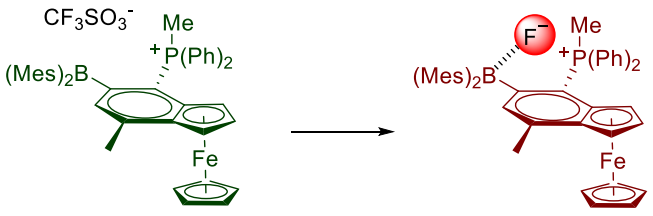


Figure 1.26. Aldridge's fluoride selective colorimetric sensor that employs the chemodosimeter approach to signal the target anion.[155] *Mes = 1,3,5-trimethylbenzene.*

Deprotonation events have also been used for the colorimetric detection of basic anions. Fabrizzi's symmetric bis-naphthalimide based receptor relies on the mono-deprotonation of a urea motif by

fluoride or dihydrogen phosphate to signal the presence of these anions in DMSO, which manifests in a colour change from yellow to red (Figure 1.27).[156]

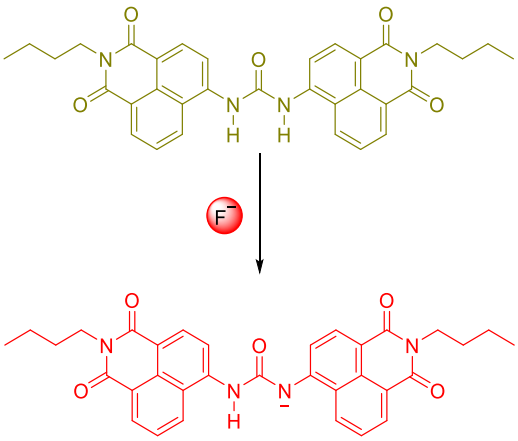


Figure 1.27. Fabrizzi's bis-naphthalimide-based sensor that produces a naked-eye colour change on exposure to fluoride in DMSO because of a deprotonation reaction.[156]

1.1.6.3. Electrochemical anion sensors

Electrochemical anion sensing can be achieved by the incorporation of redox-active groups, such as metallocenes into anion receptor frameworks. Anion binding causes a perturbation of the metallocene redox potential and the first example of a redox responsive anion receptor was reported by Beer and co-workers in 1989.[157] The recognition of bromide in the cavity of a bis-colbaltocenium cyclic ester in acetonitrile solution resulted in a 45 mV cathodic shift of the cobaltocenium/cobaltocene redox couple (Figure 1.28a). Since then the use of ferrocene reporter groups has become widespread where anion binding produces diagnostic cathodic shifts in the ferrocene/ferrocenium redox couple, as demonstrated in Molina's acyclic bis-ferrocenyl thiourea receptor on addition of fluoride, acetate or dihydrogen phosphate in DMF (Figure 1.28b).[158–162]

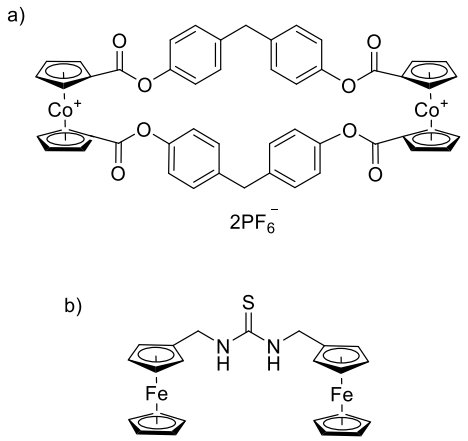


Figure 1.28. a) Beer's bis-colbaltocenium[157] and b) Molina's bis-ferrocenyl thiourea-based electrochemical anion sensors.[158]

1.1.6.4. Surface-attached anion sensors

The interfacing of chemical sensors with solid electroactive (e.g. gold) or optically transparent (e.g. glass) surfaces lies central to the construction of sensing molecular devices.[163–166]

The first ferrocene-containing self-assembled monolayer (SAM) was reported by Alonso *et al.*, which detected dihydrogen phosphate in CH_2Cl_2 solution *via* a 290 mV cathodic shift of the ferrocene/ferrocenium redox couple (Figure 1.29a).[167] Alongside SAMs, nanoparticles have been utilised as scaffolds for a variety of sensing applications.[168,169] Recently Sessler *et al.* decorated gold nanoparticles with calix[4]pyrrole-based anion recognition sites to produce materials that exhibit enhanced fluorogenic sensing behaviour, relative to the monomeric congener, while maintaining significant guest selectivity for fluoride in CH_2Cl_2 (Figure 1.29b).[170]

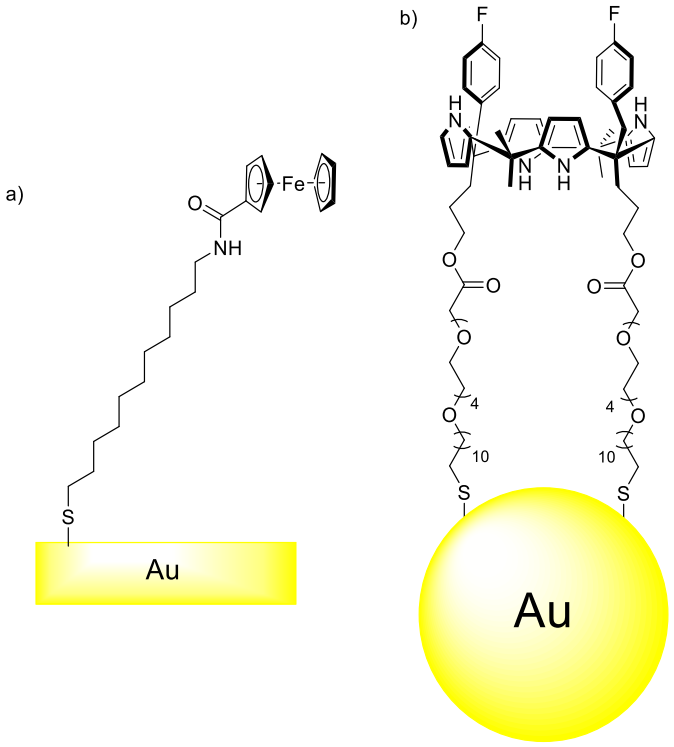


Figure 1.29. a) Alonso's ferrocene-containing SAM[167] and b) Sessler's gold nanoparticales decorated with calix[4]pyrrole fluoride recognition sites.[170]

1.2. Mechanically Interlocked Molecules

Mechanically interlocked molecules (MIMs) belong to a category of structures containing at least two molecular components that, despite not being linked covalently, are inextricably held together due to the inability of covalent bonds to pass through one another.[171] The desire for supramolecular chemists to synthesise such structures began as no more than chemical curiosity but has since expanded as the fascinating properties arising from the unique molecular topologies created by the mechanical bond have become apparent.[172] This has led to numerous applications of MIMs within the emerging fields of nanotechnology.[173–175]

Interlocked species such as [n]catenanes (from the Latin *catena* meaning chain) and [n]rotaxanes (from the Latin *rota* (wheel) and *axis* (axle)), are the two most prevalent classes of MIMs, where "n" refers to the number of interlocked molecular components. Catenanes consist of two or more macrocycles linked together in the manner of rings in a chain (Figure 1.30a). Likewise rotaxanes comprise of one or more macrocycles threaded by a dumbbell shaped molecule (an axle), in which the large terminal

stopper groups prevent the macrocycle(s) from slipping off (Figure 1.30b). A pseudorotaxane is an interpenetrated assembly formed by the threading of a macrocycle, with the threading component containing no peripheral stoppering groups allowing it to often function as a precursor to interlocked catenane and rotaxane species (Figure 1.30c). In addition to these "simpler" systems, a number of more complex interlocked molecular topologies have been constructed including knotted and higher-order linked architectures such as the Trefoil knot[176,177] (Figure 1.30d) and Solomon link.[178]

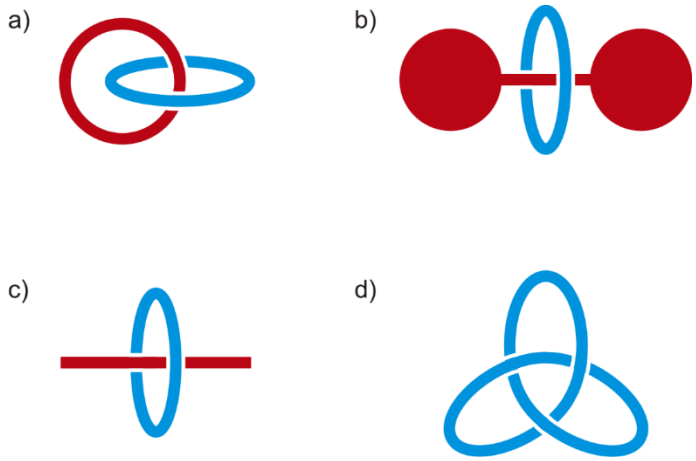


Figure 1.30. Schematic representation[179] of a) a catenane b) a rotaxane c) a pseudorotaxane and d) a trefoil knot.

1.2.1. Synthesis of MIMs

Rotaxanes may be synthesised by a variety of routes, with the most common being clipping and stoppering. The former methodology involves the ring closing of a macrocycle(s) around an axle (Figure 1.31a), while stoppering relies on formation of a pseudorotaxane assembly between a macrocyclic component and a molecular thread; this thread is subsequently appended with bulky stopper groups to form the rotaxane axle and in turn the mechanical bond (Figure 1.31b). More elaborate methods of slippage,[180,181] shrinkage[182,183] and swelling[184,185] have also been employed in the construction of [n]rotaxanes. Catenanes are frequently synthesised by a single clipping reaction of a macrocycle precursor threaded through a macrocycle (Figure 1.31c) or by a double cyclisation of two interwoven acyclic precursors (Figure 1.31d).

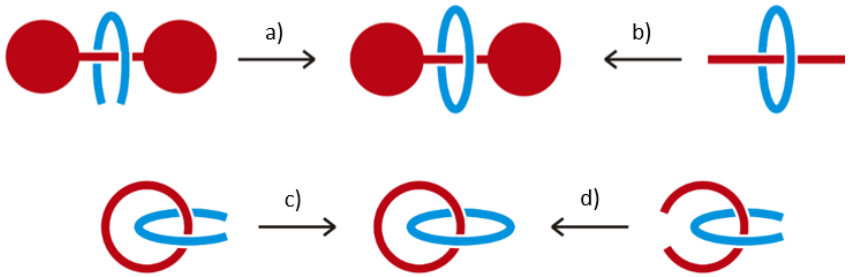


Figure 1.31. Schematic representations[179] of common synthetic routes towards interlocked structures a) clipping and b) stoppering for rotaxane synthesis and c) cyclisation and d) double-cyclisation for catenane synthesis.

1.2.2. Templated assembly of MIMs

The initial attempts to synthesise MIMs by Wasserman[186] and Harrison[187] relied on statistical approaches whereby macrocyclisation reactions occurred within serendipitously interpenetrated co-conformations of molecules and as such were plagued by low yields of the final catenane product (Figure 1.32a). Early directed syntheses were developed by Schill and co-workers, however the need for long synthetic routes lowered the efficiency of such methods and stunted further progress.[188] It was apparent that the challenge of synthesising MIMs arose from the difficulty in attempting to arrange two or more independent molecules to maximise the probability of forming a mechanical bond. Therefore the pioneering work of Sauvage and co-workers to utilise a Cu(I) template to organise two phenanthroline ligands in an orthogonal fashion, which upon covalent bond linkage formation, afforded a [2]catenane in high yield, was a vast improvement on the statistical approach (Figure 1.32b).[189,190] A plethora of examples of template-directed syntheses of interlocked systems now exist.[191–201] Importantly, the topology of the interweaving template, such as the stereochemical preference of a transition metal will define the topology of the product.

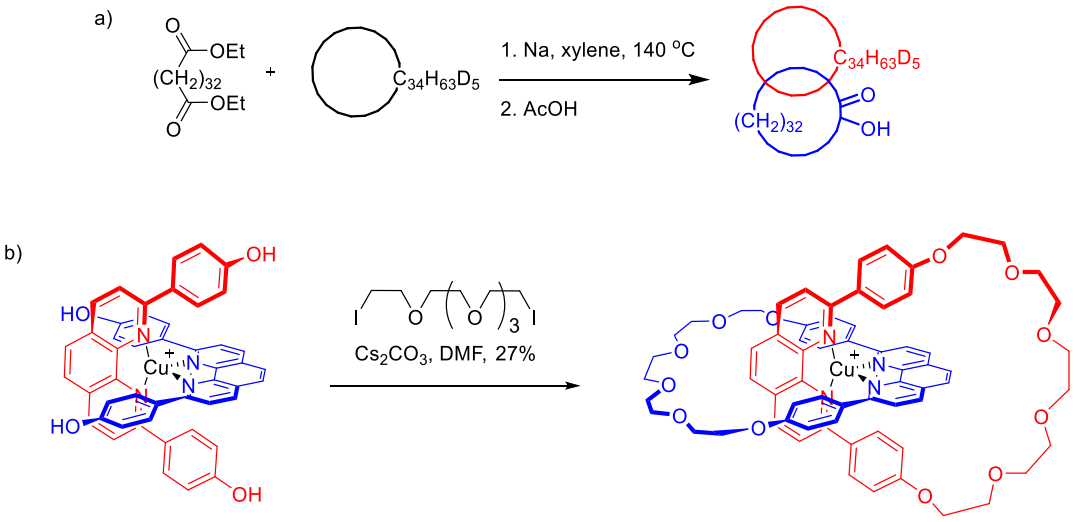


Figure 1.32. a) Wasserman's statistical [2]catenane synthesis[186] and b) Sauvage's pioneering Cu(I)-templated synthesis of a [2]catenane via a double-clipping methodology.[189,190]

Whilst the majority of templates are considered "passive" (they are responsible for the association of the components prior to a reaction), Leigh *et al.* have pioneered a new class of active metal templates.[202] Here the metal templating substrate also plays a role in promoting the crucial covalent bond formation used to form the mechanical bond of the interlocked molecule, for example *via* catalysis.

Examples of templation employed in the assembly of MIMs are discussed in the following sections; the templates have been divided into three classes: cationic, neutral and anionic.

1.2.2.1. Cation-templated assembly of MIMs

Furthering the seminal work of Sauvage[189,190] the coordination geometries of a variety of transition metal cations such as linear Au(I),[203] square planar Pd(II)[204,205] and octahedral Co(III)[206] have been employed in the synthesis of MIMs. Notably, preforming a tridentate macrocycle Co(III) complexed interpenetrated assembly enabled an interlocked [2]catenane to be obtained in high yield using a ring closing metathesis (RCM) clipping methodology (Figure 1.33).

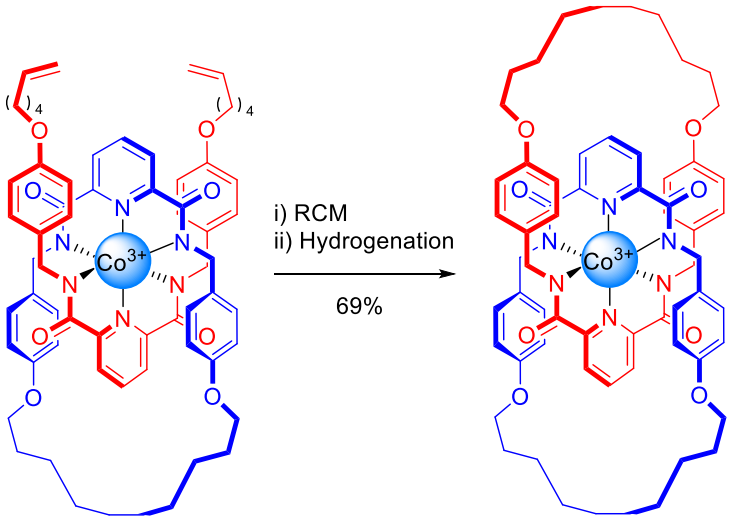


Figure 1.33. The synthesis of Leigh's [2]catenane in high yield from a preformed Co(III)-templated pseudorotaxane assembly.[206]

More recently the work of Chiu *et al*. has complemented the traditional transition metal cation templation approach by employing Na^+ to template rotaxane formation between a bis-*p*-xylyl[26]crown-6 macrocycle and an axle containing single urea or amide moieties (Figure 1.34).[207] The ion–dipole interaction formed between the carbonyl group of the axle and group I metal cation held within the binding pocket of the glycol chain of the macrocycle has been demonstrated to be the principle interaction for interpenetration and subsequent interlocked structure formation.

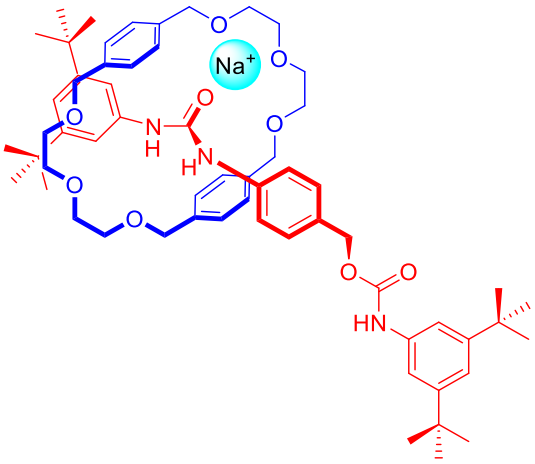


Figure 1.34. Chiu's [2]rotaxane, the formation of which is mediated by a Na^+ group I metal cation.[207]

In 2006 the CuAAC 'click' reaction was utilised by Leigh as a means of preparing rotaxanes by an active metal template mechanism.[202,208,209] In this method, the Cu(I) metal ion is bound within the

macrocycle's cavity, in the preferred tetrahedral coordination geometry, allowing it to template formation of the interpenetrated assembly and catalytically promote the synthesis of the covalent bond between the two axle precursors that captures the interlocked structure (Figure 1.35). Active metal-templated reactions such as Cu(I)-mediated Glaser coupling,[210] Pd(II)-catalysed oxidative Heck coupling[211] and Ni(II)-mediated alkyl homocoupling[212] have also been used as viable methods for MIM construction.

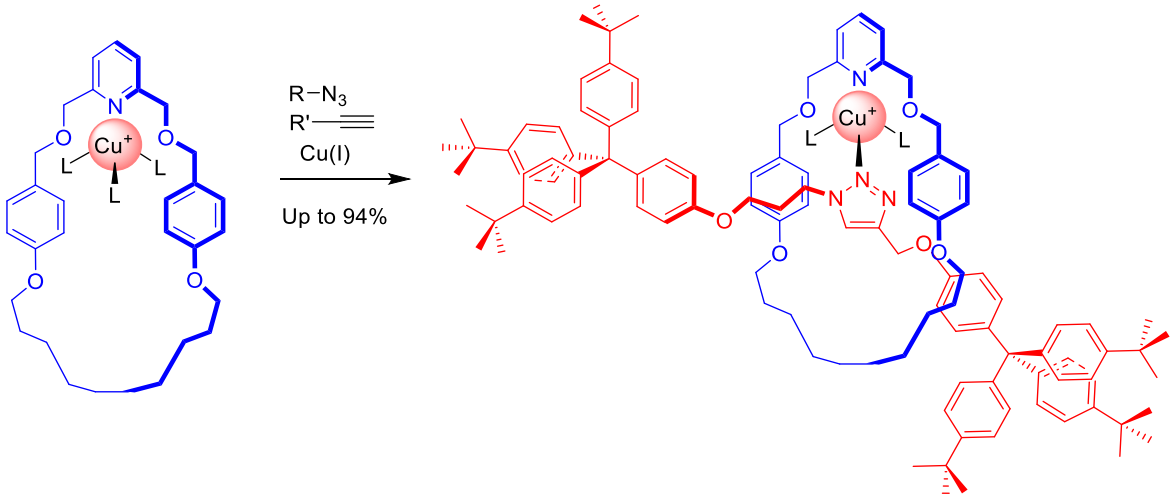


Figure 1.35. A demonstration of active metal templation for [2]rotaxane formation.[202,208,209] L = MeCN, H_2O, CH_2Cl_2, pyridine, alkyne or azide.

Organic cations may also function as effective templates for the formation of MIMs.[213–218] The strength of the donor–acceptor charge–transfer interactions formed between electron-donating dialkoxynaphthalene and electron-accepting positively charged bis(4,4'-bipyridinium) were elegantly exploited to their full potential in the synthesis of Stoddart's [5]catenane 'Olympiadane' (Figure 1.36).[219]

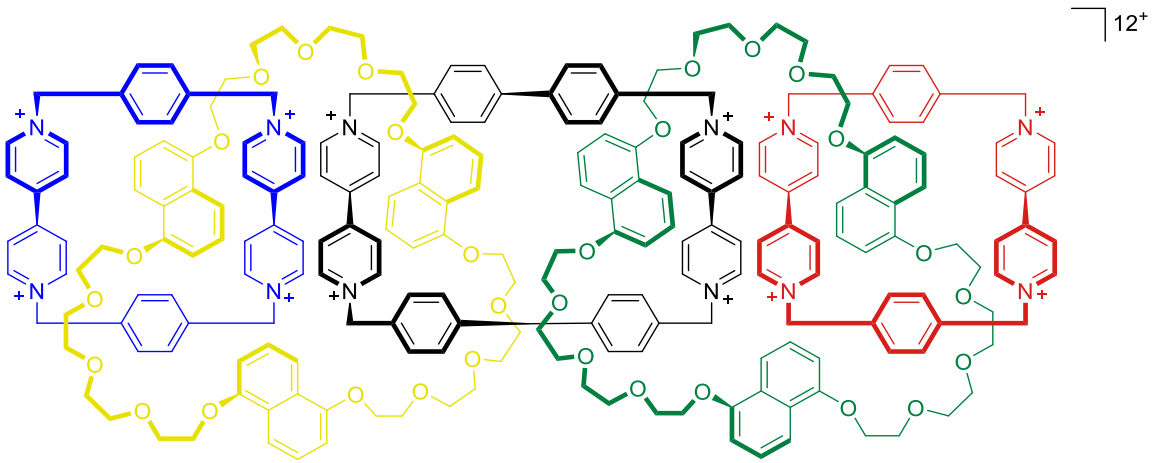


Figure 1.36. Stoddart's [5]catenane 'Olympiadane'.[219]

Loeb and Stoddart have used 1,2-bis(4,4'-bipyridinium)ethane and secondary ammonium organic cation templates respectively to construct a variety of catenanes and rotaxanes with dibenzo-24-crown-8 crown ether macrocycles (Figure 1.37a,b).[220–223]

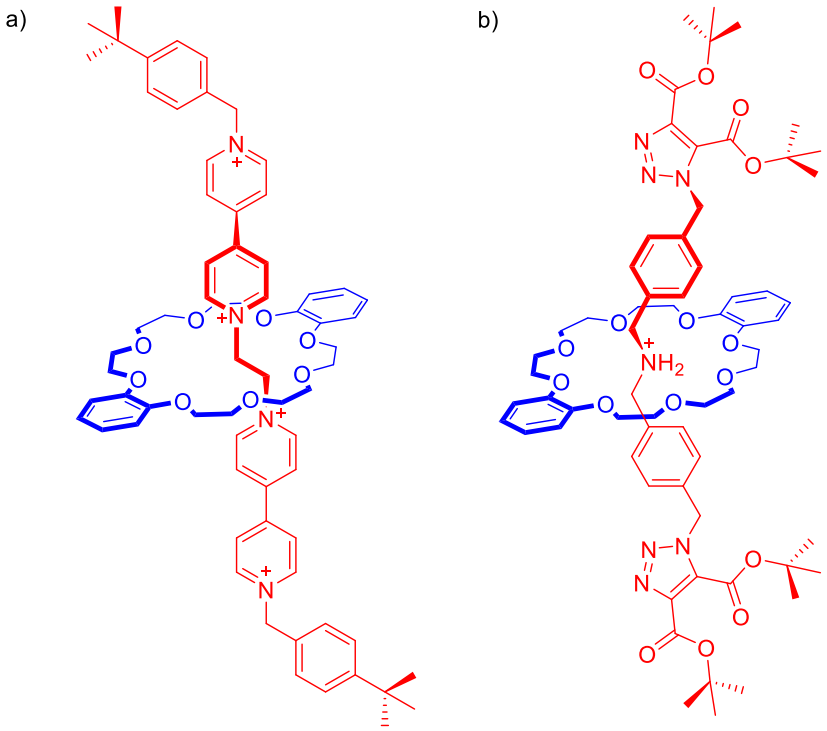


Figure 1.37. [2]Rotaxanes synthesised using templating interactions between a dibenzo-24-crown-8 macrocycle and a) 1,2-bis(4,4'-dipyridinium)ethane[220] *and b) dialkylammonium derivatives*[222] *in the axle component.*

1.2.2.2. Neutral-templated assembly of MIMs

The first example of a neutral recognition motif being utilised for templating the synthesis of a MIM was the serendipitous formation of an amide-based [2]catenane templated *via* intermolecular hydrogen bonding between the isophthalamide units, by Hunter in 1992 (Figure 1.38a).[224] Taking inspiration from this, inter-component hydrogen bonding templation in non-competitive solvent media has since been employed by other groups such as Leigh[225] and Schalley[226] (Figure 1.38b) in the synthesis of a variety of neutral rotaxanes.

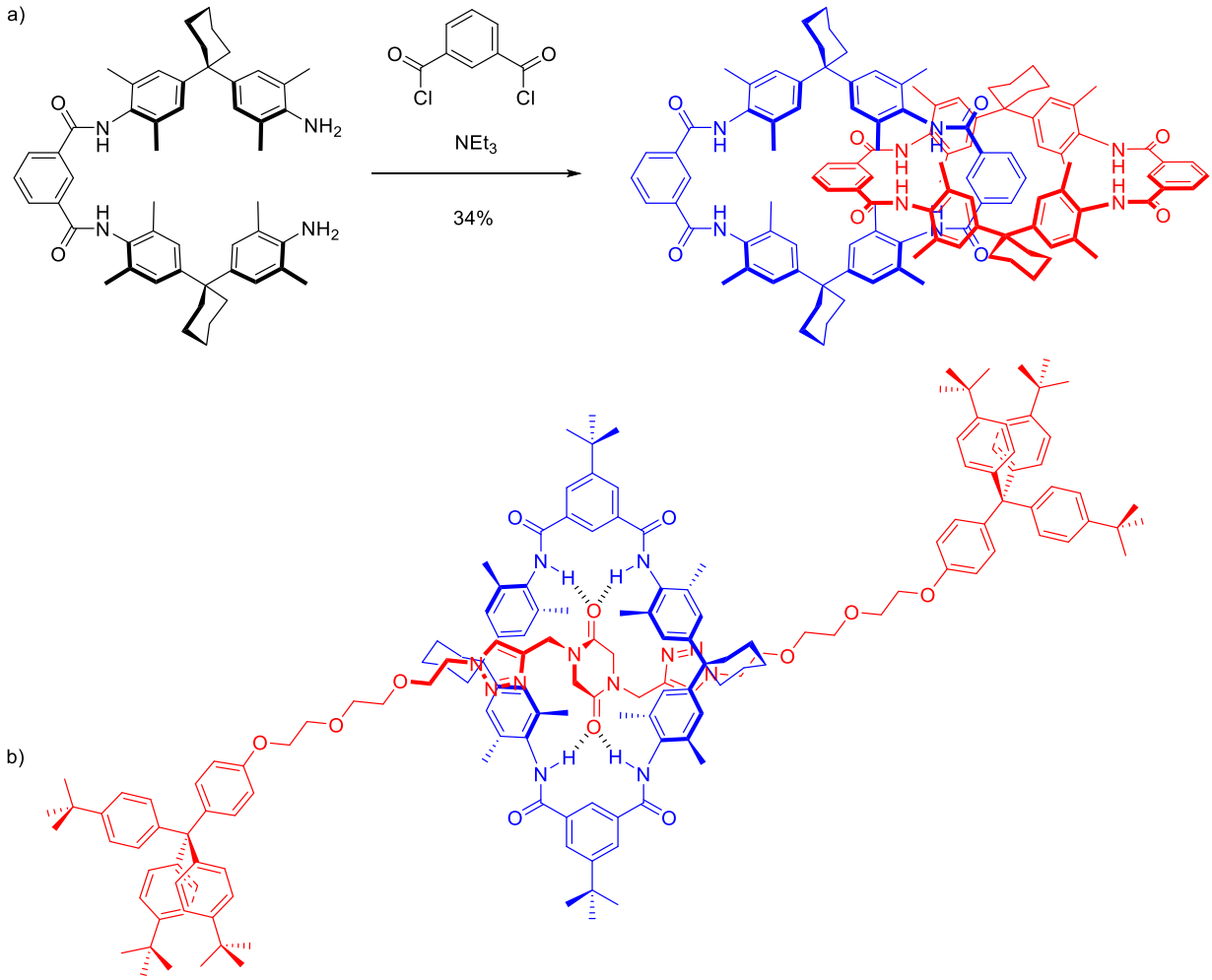


Figure 1.38. The synthesis of interlocked structures templated by neutral inter-component hydrogen bonding interactions a) Hunter's [2]catenane[224] and b) Schalley's [2]rotaxane.[226]

Sanders *et al.* have prepared neutral analogues to Stoddart's aforementioned 4,4'-bipyridinium interlocked structures, by utilising charge–transfer donor–acceptor templating interactions between molecules containing electron-rich dialkoxynaphthalene (DN) and electron-deficient naphthalene

diimide (NDI) motifs.[227] In solvents of low polarity the association of the components in a donor–acceptor–donor–acceptor (DADA) fashion is principally driven by electrostatic stacking interactions between the planar aromatic cores (Figure 1.39a).[228] However, when the assembly of similar systems was explored in aqueous media, a perturbation from the usual DADA pattern of stacking was observed, which is indicative of a strong hydrophobic contribution to the interlocked catenation process (*vide infra*).[229,230]

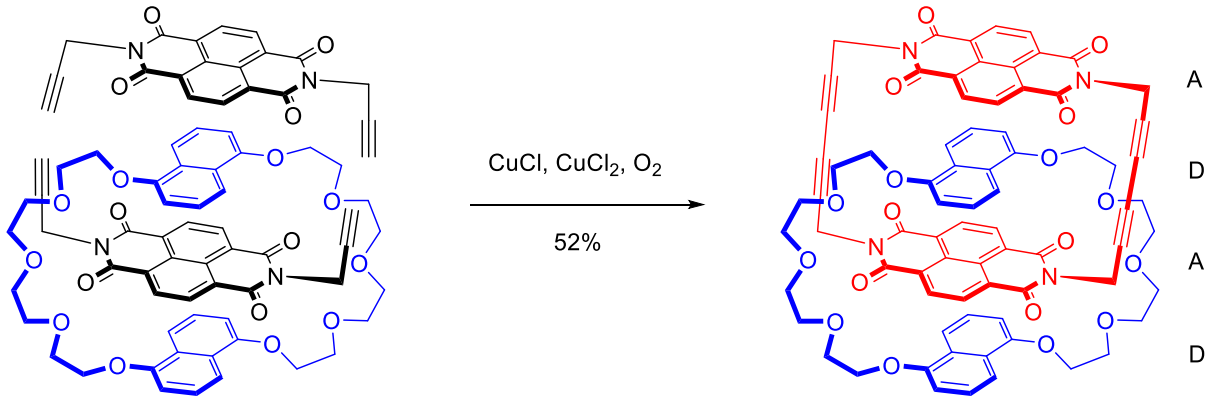


Figure 1.39. Sanders' synthesis of a [2]catenane templated by donor–acceptor charge–transfer aromatic stacking interactions.[228]

1.2.2.3. Anion-templated assembly of MIMs

Developed later than cationic and neutral templation, an anionic template was first used in the formation of an interlocked structure by Vögtle in 1999, where a sterically bulky phenoxide anion strongly bound within a tetralactam macrocycle *via* hydrogen bonding to an isophthalamide motif, upon reaction with an electrophilic stopper derivative produced a [2]rotaxane (Figure 1.40).[231]

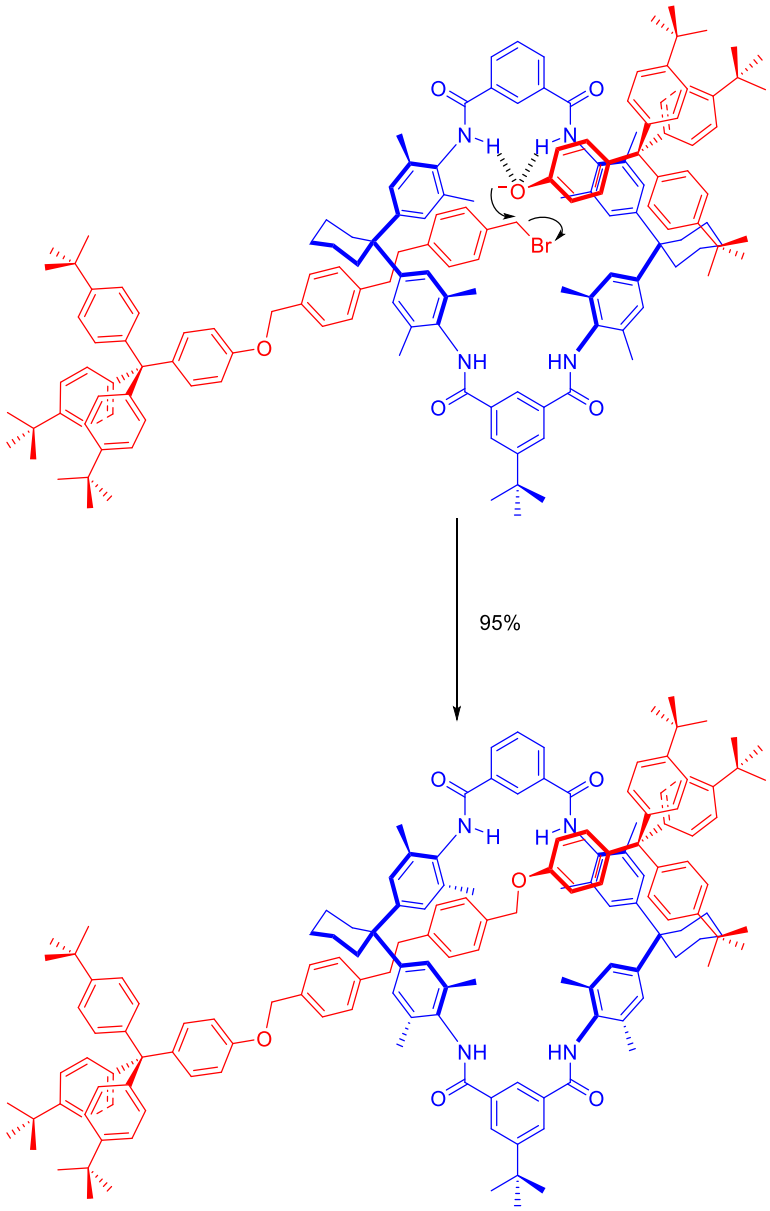


Figure 1.40. Synthesis of the first anion-templated interlocked structure by Vögtle et al.[231]

Taking inspiration from Sauvage's use of the Cu(I) metal cation to template the assembly of MIMs, Beer has used discrete anions to synthesise interpenetrated architectures and interlocked species.[232–234] In this work, the chloride anion of a tightly associated *N*-methyl pyridinium chloride ion-pair is coordinatively unsaturated, allowing a macrocycle containing an anion-binding isophthalamide motif to coordinate the halide's vacant meridian, resulting in an orthogonal interpenetrated pseudorotaxane assembly. Additional favourable charge–transfer donor–acceptor interactions between the electron-deficient pyridinium and electron-rich hydroquinone groups and hydrogen bonding between the *N*-

methyl pyridinium group of the threading component and the polyether cavity of the macrocycle stabilise the association of the two components. The success of this approach facilitated the synthesis of the first chloride-templated [2]rotaxane and [2]catenane by a single RCM clipping reaction (Figure 1.41).[235] Upon chloride template removal, a unique interlocked three-dimensional topological cavity is created which was demonstrated to exhibit a high degree of selectivity for chloride over oxoanions, providing an important benefit of this discrete anion templation approach (Figure 1.41).

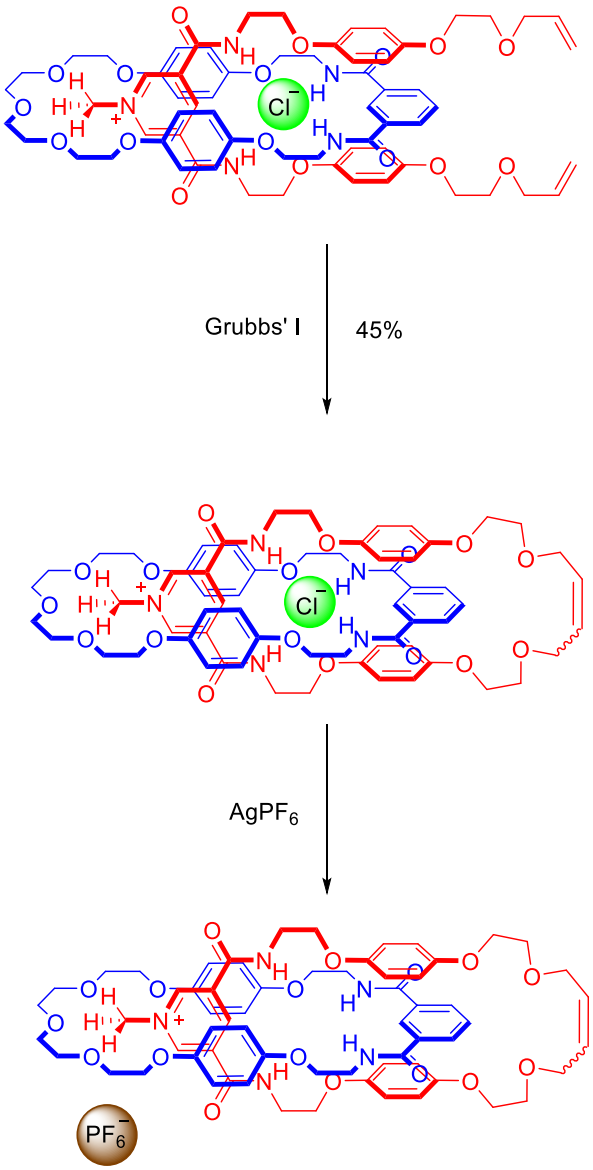


Figure 1.41. Beer's synthesis of a [2]catenane by discrete anion templation. Removal of the chloride template reveals a unique interlocked three-dimensional cavity for anion recognition.[235]

The scope of this methodology was extended to the synthesis of interlocked host structures that incorporate a variety of anion recognition motifs, enabling templation by anions other than chloride. Some recent examples include a nitrate-templated [2]catenane[236] (Figure 1.42a) and a [2]rotaxane (Figure 1.42b) containing a halogen bonding motif enabling mechanical bond formation to be mediated by a bromide anion.[237]

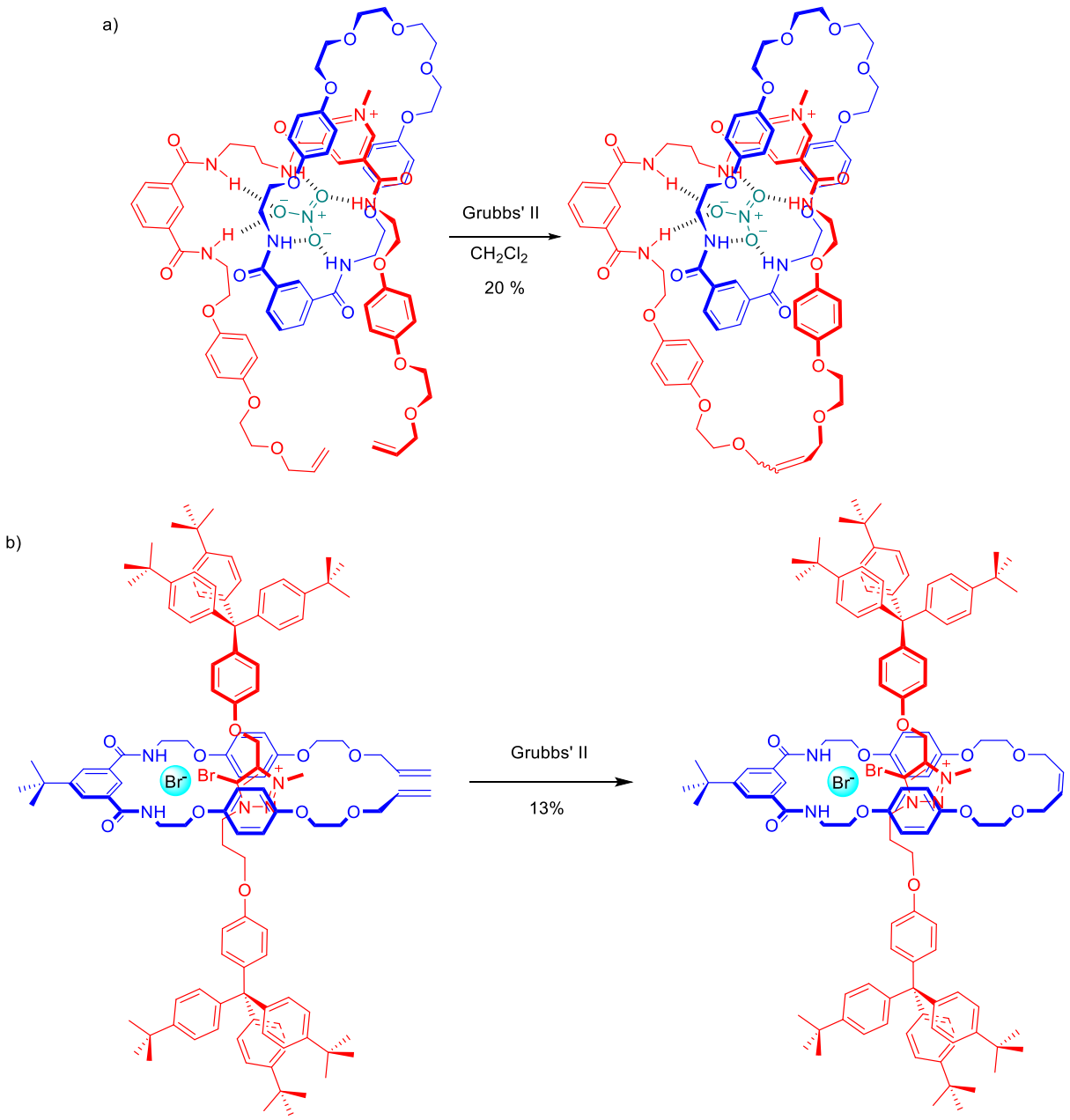


Figure 1.42. Beer's interlocked structures templated by discrete anions such as a) nitrate[236] and b) bromide.[237]

1.3. Applications of Mechanically Interlocked Molecules

The variety and wealth of MIMs continues to expand as a result of continuing advances in synthetic methods for their construction and the realisation of potential nanotechnological applications which are discussed in the following sections.[173,175,238,239]

1.3.1. Molecular machines

Molecular machines are systems in which the relative positioning of the molecular components of the structure may be switched, rotated or directionally driven to perform a task on the nanoscale.[175,240–242] Biological motor proteins convert chemical energy to effect stepwise linear or rotary motion[243] and may be found performing numerous biotic functions such as intracellular transport and molecular synthesis.[15] As a specific example, myosin filaments fuelled by ATP are operated in a ratchet-style mechanism to cause them to proceed over complementary actin filaments, to effect muscle contraction (Figure 1.43).[244] The construction of artificial molecular machines is motivated by the promise of their potential applications in nanotechnology, a notion promoted as early as 1959 by Richard Feynman.[245,246]

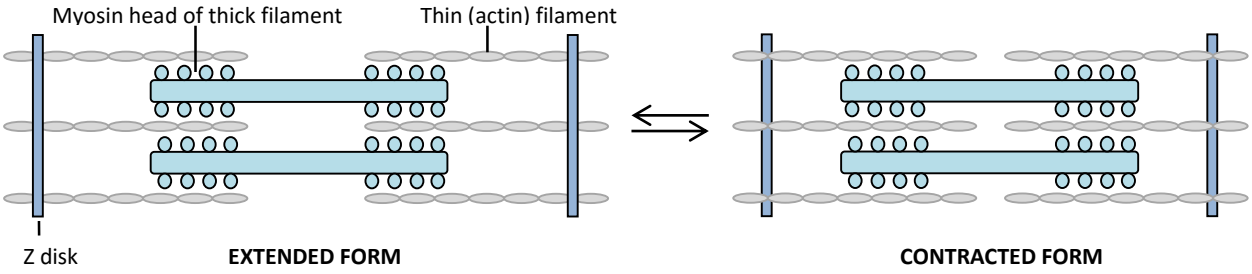


Figure 1.43. Schematic representation of muscle action in which contraction is caused via a ratchet mechanism.[244]

1.3.1.1. Artificial MIM molecular machines

MIMs such as rotaxanes provide ideal candidates as artificial molecular machines because the nature of the mechanical bond restricts motion of the macrocyclic wheel orthogonal to the axle component,

whilst translational shuttling or rotary motion of the macrocycle are readily permitted (Figure 1.44a). Catenanes may exhibit rotational, but not translational, motion as either macrocycle can freely circulate within the other (Figure 1.44b).

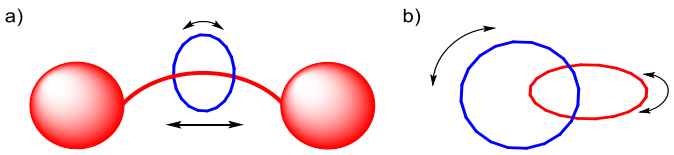


Figure 1.44. Molecular motion in interlocked structures a) rotation or translation of a macrocycle in a [2]rotaxane and b) rotation of macrocycles in a [2]catenane.

Artificial molecular machines may be broadly categorised into behaving as molecular switches or motors. Molecular switches are prototypes towards the latter and have applications in controlling chemical reactivity and in recognition and sensing. The templation methods employed in synthesising catenanes and rotaxanes almost inevitably result in residual interactions between components of the interlocked structures and these recognition sites are called stations (Figure 1.45). A degree of control over the dynamic switching behaviour of the macrocycle between these stations may be exerted through an external stimulus that modulates the non-covalent interactions between the components.



Figure 1.45. Schematic of the shuttling of a macrocycle between stations A and B in a bistable [2]rotaxane molecular switch.

A molecular switch, such as a rotaxane-based translational shuttle shown in Figure 1.45, cannot be used progressively to perform work since the change in position of a macrocycle on the axle influences the system only as a function of its state.[175] This means that when the components of the shuttle are returned to their original position, the work that has been performed will be undone. However the

opposite is true for a molecular motor. One of the simplest demonstrations of this concept may be seen in Leigh's [2]rotaxane that operates *via* a ratcheting mechanism that causes an irreversible change in the average position of the macrocycle, courtesy of a bulky silyl ether blocking group incorporated into the axle component (Figure 1.46). This allows it to perform useful work upon desilylation (Figure 1.46c).[247] A more elaborate [3]catenane rotary motor has been reported by the same group.[248]

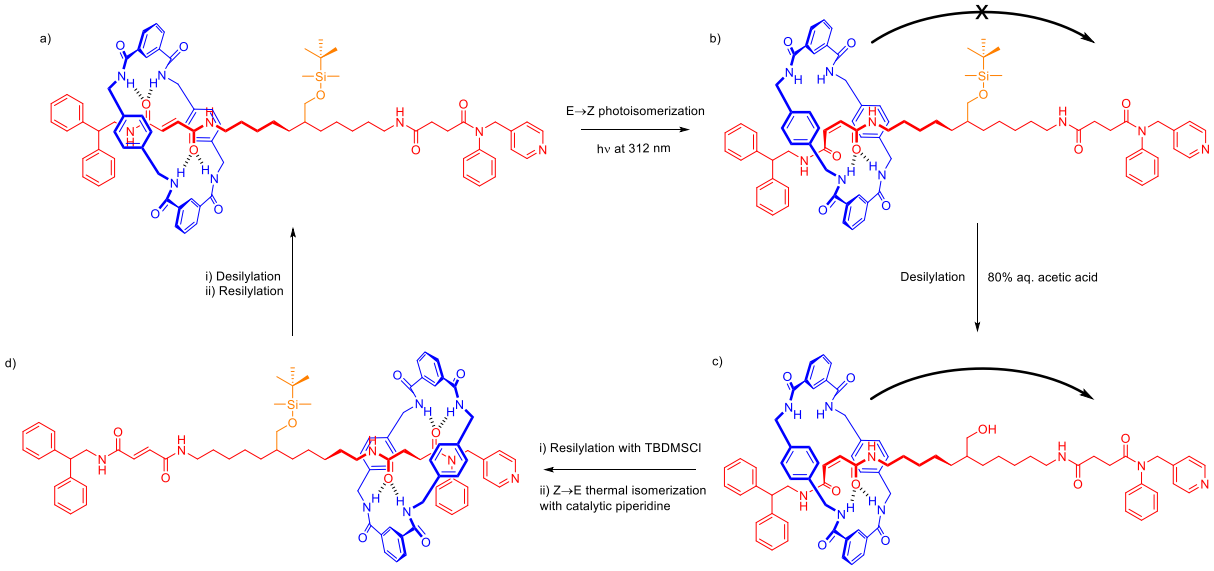


Figure 1.46. Leigh's irreversible [2]rotaxane ratchet[247] where a) the macrocycle originally resides at the fumaramide station, b) photoisomerization of the alkene destabilises the macrocycle's position but it cannot shuttle because of the blocking group, c) removal of the kinetic barrier allows macrocycle motion and the system performs work, d) the molecular motor has been reset so that upon a desilylation reaction the macrocycle can perform work again. TBDMSCl = tert-butyldimethylsilyl chloride.

1.3.1.2. Stimuli-responsive molecular shuttles

Stoddart and co-workers constructed the first molecular shuttle in 1991; a bistable [2]rotaxane that demonstrated translational molecular motion of a macrocyclic wheel along a symmetrical axle component (Figure 1.47).[217] Since both stations on the axle were identical, the macrocycle's position was shown to be equally distributed as a result of the rapid inherent Brownian motion that occurs at a rate faster than the NMR timescale.

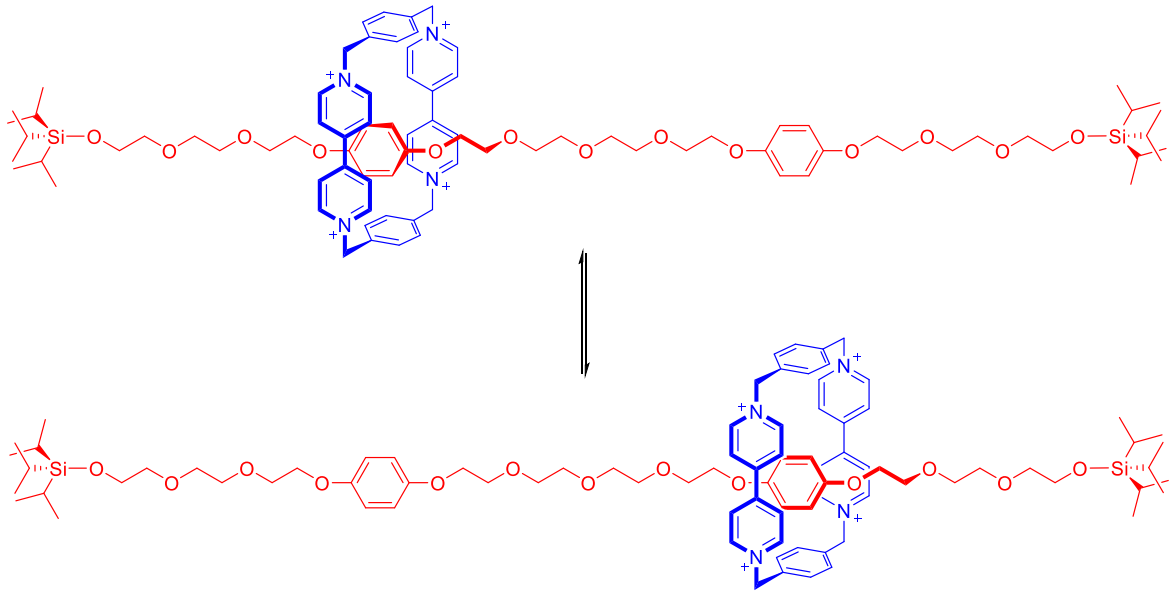


Figure 1.47. The first molecular shuttle synthesised by Stoddart et al.[217]

By expanding on this proof of principle, a variety of asymmetric molecular switches have been synthesised containing multiple binding sites with affinities for the macrocycle that vary under different conditions. Therefore by weakening an existing interaction, or increasing the affinity for a competing station by use of an external chemical-,[249–259] light-[260–263] or redox-based[264–268] stimulus, the macrocycle may be driven to shuttle along the axle and establish a new equilibrium position.

Examples of cation-induced co-conformational change within a multi-station rotaxane are now relatively common and may be controlled by stimuli such as lowering pH to induce protonation of a basic group[269–273] or by cation-coordination at a recognition site.[274,275] The groups of Stoddart and Sanders have collaboratively demonstrated the latter *via* a co-conformational change within a bistable [2]rotaxane facilitated by the addition of Li^+ cations (Figure 1.48).[276,277] In the initial state the macrocycle occupies the NDI station due to superior donor–acceptor charge–transfer interactions relative to an alternative pyromellitic diimide station. However upon addition of the alkali metal cation shuttling occurs to facilitate preferential coordination of Li^+ between the pyromellitic station and the macrocycle. Importantly this shuttling process is reversible as the addition of [18]crown-6 sequesters the alkali metal cation and in doing so returns the rotaxane to its original state. It was also revealed

that an identical switching process occurs upon a reversible one electron reduction of the NDI station hence allowing this rotaxane to operate as a dual redox- and cation-driven molecular shuttle.

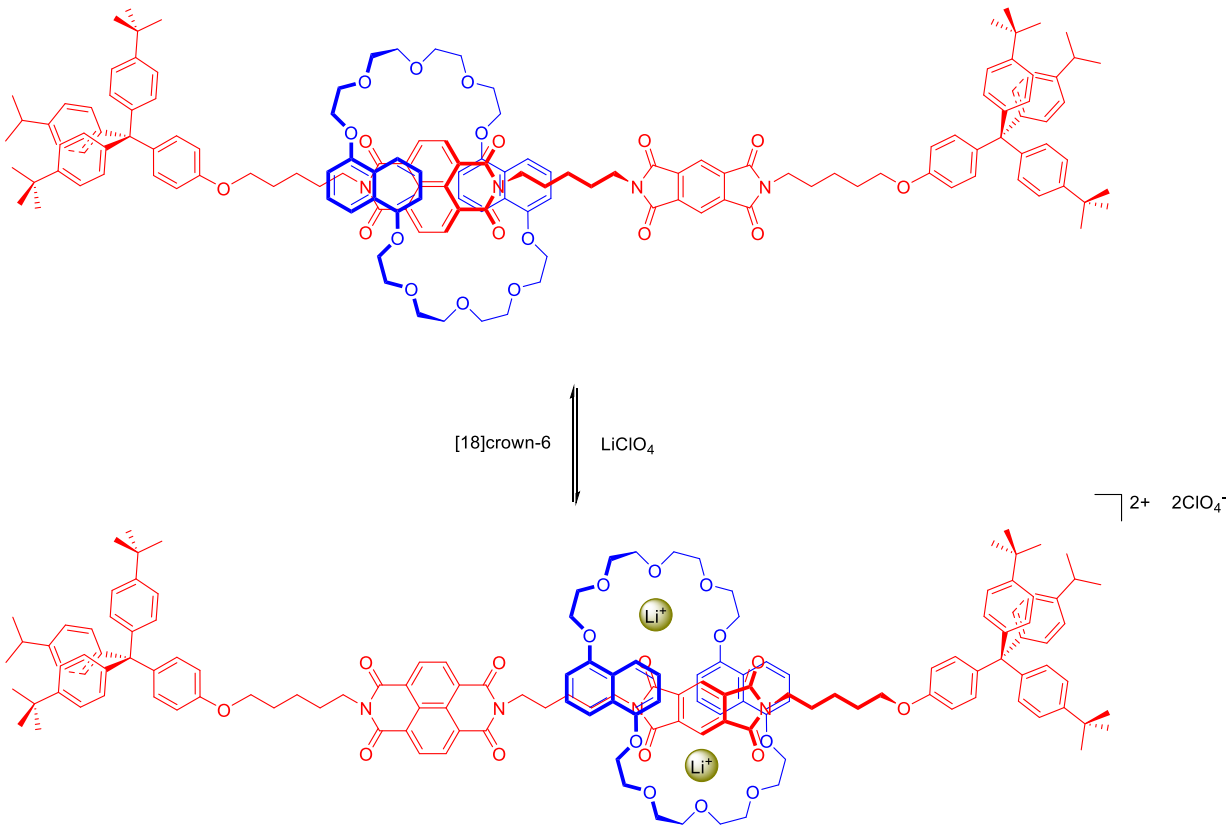


Figure 1.48. Alkali metal cation-induced shuttling based on complexation and decomplexation of Li^+ within a bistable [2]rotaxane molecular switch.[276,277]

Systems that use anions to promote molecular switching in MIMs are rare relative to their cation counterparts.[226,278–285] The majority employ chloride to induce changes in a rotaxane's co-conformation such as Leigh's serendipitous discovery that coordination of this halide anion by Pd(II) can be used as a basis for a rotaxane molecular shuttle (Figure 1.49).[285]

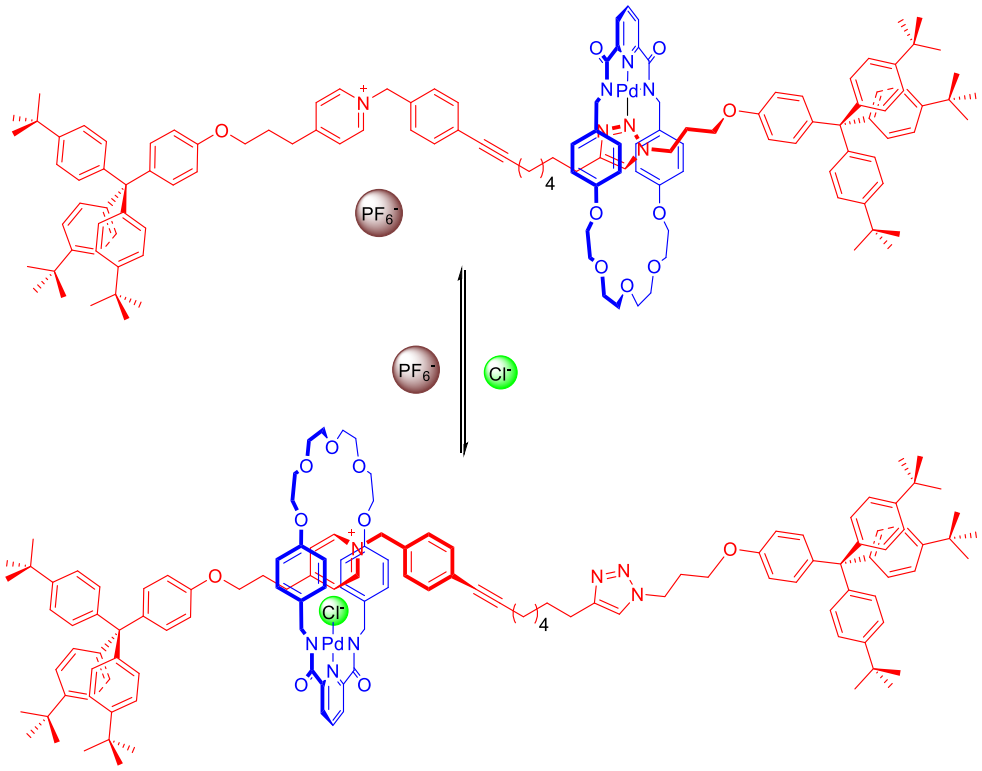


Figure 1.49. Chloride-induced molecular shuttling in Leigh's bistable [2]rotaxane.[285]

Recently more elaborate rotaxane based switches have been designed and synthesised including those that mimic the macroscale behaviour of cable cars,[255] elevators[286] and muscles.[287] In addition, it has been demonstrated that rotaxane shuttling is not limited to the solution phase. Loeb *et al.* have incorporated a bistable shuttle into a metal organic framework proving that the concept of translational motion of a molecular system can be organised, initiated and operated inside a crystalline, solid-state material.[288]

1.3.2. MIMs as Catalysts

The development of mechanically interlocked homogeneous catalysts has been achieved by exploiting residual catalytically active metals or organocatalytic functionality employed in the construction of rotaxanes and catenanes. Goldup and co-workers have recently demonstrated the former by realising the ability of a rotaxane scaffold to regulate both the catalytic activity and diastereoselectivity of a gold-catalysed reaction *via* provision of an unconventional and sterically crowded environment for the Au(I) centre.[289] Importantly this catalyst is the first example of a rotaxane-based metal complex with

stimuli-responsive catalytic activity. Cation guest binding 'switches on' the catalytic activity and, importantly, induces a change in the co-conformation of the Au(I)-containing rotaxane that allows it to affect selectivity of the reaction product in a mechanism that is similar to the allosteric modulation of enzymes (Figure 1.50a).[290] The most exotic example to date of an interlocked species acting as a processive catalyst within a chemical reaction is Leigh's peptide-synthesising [2]rotaxane (Figure 1.50b).[291] In this highly complex system a macrocycle bearing the active catalyst proceeds along a threading component cleaving multiple amino acid derivatives to produce a single, sequence-specific polypeptide-containing product and in doing so replicates the complex functionality of a protein-synthesising ribosome.

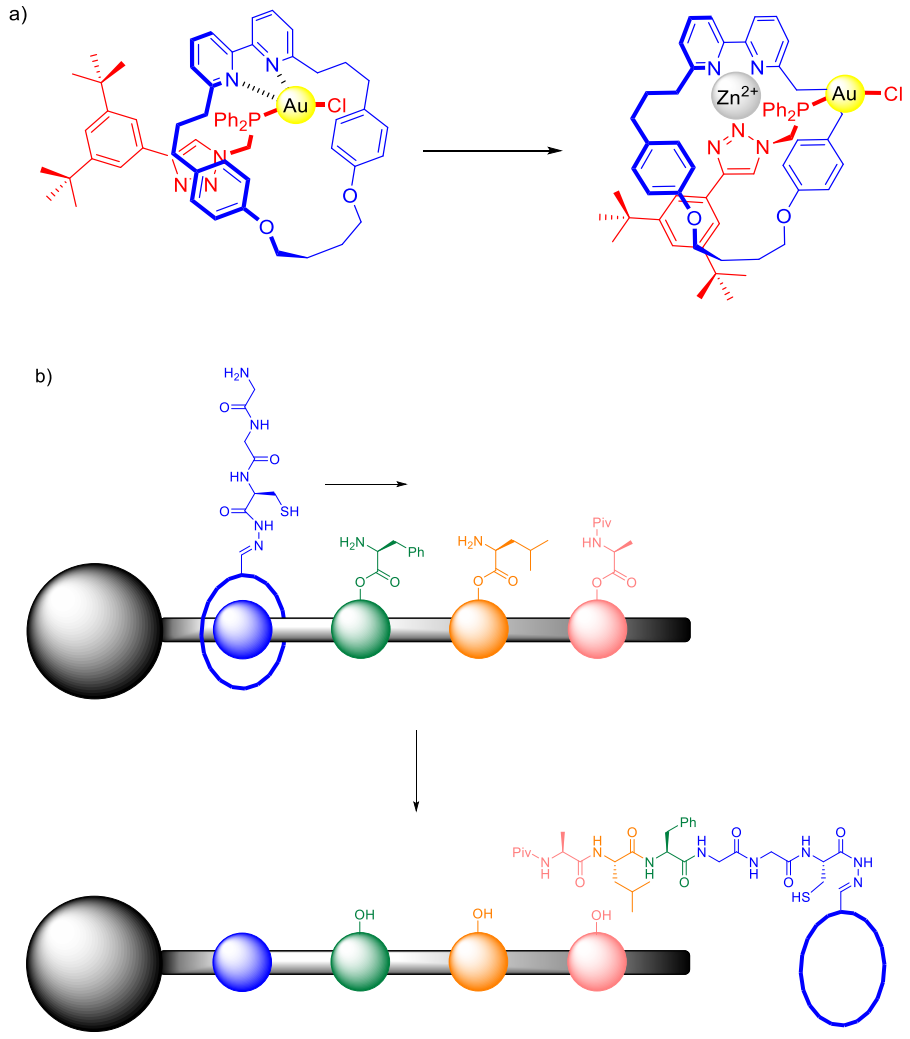


Figure 1.50. Functional MIM catalysts a) Goldup's Au(I)-containing [2]rotaxane in which the catalytic activity can be switched on by Zn(II) binding[289] and b) Leigh's peptide-synthesising [2]rotaxane.[291]

1.3.3. MIMs for Recognition and Sensing

The three-dimensional cavities created between the components of interlocked host molecules have been exploited in the construction of effective receptors and sensors for a variety of different target guest species. In particular, the appendage of electro- or photochemical reporter groups to interlocked systems allows them to function as effective anion sensing species.[292] For example, Beer's 1,2,3,4,5-pentaphenyl ferrocene-stoppered rotaxane[293] (Figure 1.51a) signals chloride binding *via* a cathodic shift in the ferrocene redox couple whilst Jeong's indolocarbazole-based catenane[294] (Figure 1.51b) produces a turn-on fluorescence response upon the recognition of anions such as dihydrogen phosphate.

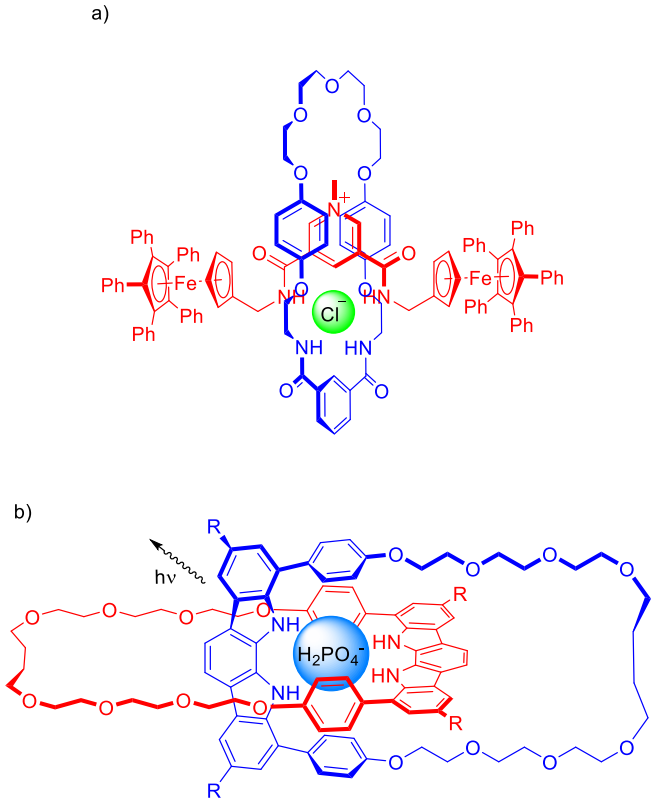


Figure 1.51. Anion sensing MIMs a) Beer's electrochemically-active 1,2,3,4,5-pentaphenyl ferrocene-stoppered [2]rotaxane[293] and b) Jeong's photochemically-active indolocarbazole-based [2]catenane.[294] R = $CO_2(CH_2)_7CH_3$.

1.4. Objectives

The theme of the research in this thesis is concerned with the synthesis of multi-station interlocked rotaxane and catenane host systems designed with the capability to bind and sense target anionic guest species *via* a dynamic mechanism involving molecular motion of their constituent parts.

Chapter two describes the development of bistable [2]rotaxane host systems incorporating a triazolium-based anion recognition site and a π-electron-deficient aromatic station. The capability of these systems to exhibit halide-induced molecular motion will be explored in depth with particular focus on the contrasting behaviour of hydrogen *versus* halogen bonding and solvent effects on the translational shuttling processes (Figure 1.52).

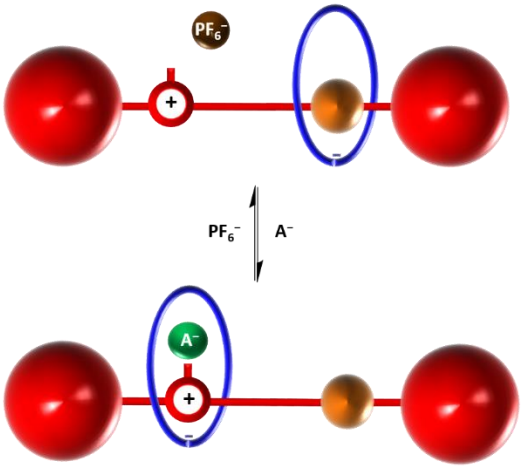


Figure 1.52. Schematic of the anion-induced translational molecular motion within a two-station [2]rotaxane. A^- = halide.

Chapter three expands on these principles, detailing the synthesis of multi-station [3]rotaxane host systems exploited for the purpose of recognition and sensing of oxoanion species *via* a novel dynamic pincer-like mechanism.

Chapter four investigates the integration of the photo- and redox-active C_{60} fullerene group and/or ferrocene motifs into the components of multi-station rotaxane-based anion host systems. The dual sensing properties of these unique dynamic receptors are thoroughly studied.

Chapter five details the syntheses of multi-station axle and macrocycle components containing triazolium recognition motifs and a perylene diimide recognition site. The incorporation of these components into rotaxane and catenane host systems produces novel interlocked systems exhibiting dynamic properties which are examined using a variety of spectroscopic techniques.

1.5. References

1 J. W. Steed and J. L. Atwood, *Supramolecular Chemistry*, Wiley-VCH, 2nd edition., 2009.
2 J.-M. Lehn, *Science*, 1985, **227**, 849–856.
3 U. Lüning, *Applications of Supramolecular Chemistry*, CRC Press, Boca Raton, 2012.
4 E. Fischer, *Berichte Dtsch. Chem. Ges.*, 1894, **27**, 2985–2993.
5 F. W. Lichtenthaler, *Angew. Chem. Int. Ed. Engl.*, 1995, **33**, 2364–2374.
6 C. J. Pedersen, *J. Am. Chem. Soc.*, 1967, **89**, 2495–2496.
7 J. M. Lehn, *Acc. Chem. Res.*, 1978, **11**, 49–57.
8 D. J. Cram, *Angew. Chem. Int. Ed. Engl.*, 1986, **25**, 1039–1057.
9 J.-M. Lehn, *Angew. Chem. Int. Ed. Engl.*, 1988, **27**, 89–112.
10 D. J. Cram, *Angew. Chem. Int. Ed. Engl.*, 1988, **27**, 1009–1020.
11 C. J. Pedersen, *Angew. Chem. Int. Ed. Engl.*, 1988, **27**, 1021–1027.
12 C. H. Park and H. E. Simmons, *J. Am. Chem. Soc.*, 1968, **90**, 2431–2432.
13 P. Chakrabarti, *J. Mol. Biol.*, 1993, **234**, 463–482.
14 J. D. Watson and F. H. C. Crick, *Nature*, 1953, **171**, 737–738.
15 J. M. Berg, J. L. Tymoczko and L. Stryer, *Biochemistry: International Edition*, W. H. Freeman, New York, 7th edition edition., 2011.
16 F. Delange, *Thyroid*, 1994, **4**, 107–128.
17 J. L. Sessler, P. A. Gale and W.-S. Cho, in *Anion Receptor Chemistry*, 2007.
18 A. L. Berger, C. O. Randak, L. S. Ostedgaard, P. H. Karp, D. W. Vermeer and M. J. Welsh, *J. Biol. Chem.*, 2005, **280**, 5221–5226.
19 M. P. Anderson, R. J. Gregory, S. Thompson, D. W. Souza, S. Paul, R. C. Mulligan, A. E. Smith and M. J. Welsh, *Science*, 1991, **253**, 202–205.
20 G. J. C. G. M. Bosman, K. Renkawek, V. Workum, I. G. P. Bartholomeus and D. Grip, *Gerontology*, 1997, **43**, 67–78.
21 B. Moss, *Philos. Trans. R. Soc. Lond. B Biol. Sci.*, 2008, **363**, 659–666.
22 V. H. Smith and D. W. Schindler, *Trends Ecol. Evol.*, 2009, **24**, 201–207.
23 J. L. Hatfield and R. F. Follett, *Nitrogen in the Environment*, Elsevier, 2008.
24 E. A. Katayev, G. V. Kolesnikov and J. L. Sessler, *Chem. Soc. Rev.*, 2009, **38**, 1572–1586.
25 A. Bianchi, K. Bowman-James and E. García-España, *Supramolecular chemistry of anions*, Wiley-VCH, 1st edition., 1997.
26 N. Busschaert, C. Caltagirone, W. Van Rossom and P. A. Gale, *Chem. Rev.*, 2015, **115**, 8038–8155.
27 R. D. Shannon, *Acta Crystallogr. Sect. A*, 1976, **32**, 751–767.
28 F. Hofmeister, *Arch. Für Exp. Pathol. Pharmakol.*, 1888, **24**, 247–260.
29 R. S. Carnegie, C. L. D. Gibb and B. C. Gibb, *Angew. Chem. Int. Ed.*, 2014, **53**, 11498–11500.
30 C. Caltagirone, G. W. Bates, P. A. Gale and M. E. Light, *Chem. Commun.*, 2007, 61–63.
31 H.-J. Schneider, *Angew. Chem. Int. Ed.*, 2009, **48**, 3924–3977.
32 E. Arunan, G. R. Desiraju, R. A. Klein, J. Sadlej, S. Scheiner, I. Alkorta, D. C. Clary, R. H. Crabtree, J. J. Dannenberg, P. Hobza, H. G. Kjaergaard, A. C. Legon, B. Mennucci and D. J. Nesbitt, *Pure Appl. Chem.*, 2011, **83**.

33 J. Emsley, *Chem. Soc. Rev.*, 1980, **9**, 91–124.
34 G. R. Desiraju, P. S. Ho, L. Kloo, A. C. Legon, R. Marquardt, P. Metrangolo, P. Politzer, G. Resnati and K. Rissanen, *Pure Appl. Chem.*, 2013, **85**.
35 T. Clark, M. Hennemann, J. S. Murray and P. Politzer, *J. Mol. Model.*, 2006, **13**, 291–296.
36 K. Rissanen, *CrystEngComm*, 2008, **10**, 1107–1113.
37 L. Brammer, G. M. Espallargas and S. Libri, *CrystEngComm*, 2008, **10**, 1712–1727.
38 R. Wilcken, M. O. Zimmermann, A. Lange, A. C. Joerger and F. M. Boeckler, *J. Med. Chem.*, 2013, **56**, 1363–1388.
39 T. M. Beale, M. G. Chudzinski, M. G. Sarwar and M. S. Taylor, *Chem. Soc. Rev.*, 2013, **42**, 1667–1680.
40 K. Do, T. P. Klein, C. A. Pommerening and L. S. Sunderlin, *J. Am. Soc. Mass Spectrom.*, 1997, **8**, 688–696.
41 D. A. Palmer, R. W. Ramette and R. E. Mesmer, *J. Solut. Chem.*, 1984, **13**, 673–683.
42 L. C. Gilday, S. W. Robinson, T. A. Barendt, M. J. Langton, B. R. Mullaney and P. D. Beer, *Chem. Rev.*, 2015, **115**, 7118–7195.
43 B. L. Schottel, H. T. Chifotides and K. R. Dunbar, *Chem. Soc. Rev.*, 2007, **37**, 68–83.
44 P. Arranz-Mascarós, C. Bazzicalupi, A. Bianchi, C. Giorgi, M.-L. Godino-Salido, M.-D. Gutiérrez-Valero, R. Lopez-Garzón and M. Savastano, *J. Am. Chem. Soc.*, 2013, **135**, 102–105.
45 M. Giese, M. Albrecht and K. Rissanen, *Chem. Rev.*, 2015, **115**, 8867–8895.
46 H. T. Chifotides and K. R. Dunbar, *Acc. Chem. Res.*, 2013, **46**, 894–906.
47 S. Guha, F. S. Goodson, L. J. Corson and S. Saha, *J. Am. Chem. Soc.*, 2012, **134**, 13679–13691.
48 A. Robertazzi, F. Krull, E.-W. Knapp and P. Gamez, *CrystEngComm*, 2011, **13**, 3293–3300.
49 Y. Zhao, N. Sakai and S. Matile, *Nat. Commun.*, 2014, **5**, 3911.
50 O. B. Berryman, F. Hof, M. J. Hynes and D. W. Johnson, *Chem. Commun.*, 2006, 506–508.
51 J.-M. Lehn, *Angew. Chem. Int. Ed. Engl.*, 1988, **27**, 89–112.
52 J. W. Pflugrath and F. A. Quiocho, *Nature*, 1985, **314**, 257–260.
53 J. W. Pflugrath and F. A. Quiocho, *J. Mol. Biol.*, 1988, **200**, 163–180.
54 H. Luecke and F. A. Quiocho, *Nature*, 1990, **347**, 402–406.
55 A. E. Martell, R. D. Hancock and R. J. Motekaitis, *Coord. Chem. Rev.*, 1994, **133**, 39–65.
56 D. K. Cabbiness and D. W. Margerum, *J. Am. Chem. Soc.*, 1969, **91**, 6540–6541.
57 Y. Li and A. H. Flood, *Angew. Chem. Int. Ed.*, 2008, **47**, 2649–2652.
58 J. M. Lehn, E. Sonveaux and A. K. Willard, *J. Am. Chem. Soc.*, 1978, **100**, 4914–4916.
59 B. Dietrich, J. Guilhem, J.-M. Lehn, C. Pascard and E. Sonveaux, *Helv. Chim. Acta*, 1984, **67**, 91–104.
60 B. Dietrich, J.-M. Lehn, J. Guilhem and C. Pascard, *Tetrahedron Lett.*, 1989, **30**, 4125–4128.
61 B. Dietrich, B. Dilworth, J.-M. Lehn, J.-P. Souchez, M. Cesario, J. Guilhem and C. Pascard, *Helv. Chim. Acta*, 1996, **79**, 569–587.
62 S. D. Reilly, G. R. K. Khalsa, D. K. Ford, J. R. Brainard, B. P. Hay and P. H. Smith, *Inorg. Chem.*, 1995, **34**, 569–575.
63 J. L. Sessler, M. J. Cyr, V. Lynch, E. McGhee and J. A. Ibers, *J. Am. Chem. Soc.*, 1990, **112**, 2810–2813.
64 Z. Zhang, D. S. Kim, C.-Y. Lin, H. Zhang, A. D. Lammer, V. M. Lynch, I. Popov, O. Š. Miljanić, E. V. Anslyn and J. L. Sessler, *J. Am. Chem. Soc.*, 2015, **137**, 7769–7774.
65 F. P. Schmidtchen, *Angew. Chem. Int. Ed. Engl.*, 1977, **16**, 720–721.
66 F. P. Schmidtchen, *Chem. Ber.*, 1981, **114**, 597–607.
67 F. P. Schmidtchen and G. Müller, *J. Chem. Soc. Chem. Commun.*, 1984, 1115–1116.
68 K. Worm and F. P. Schmidtchen, *Angew. Chem. Int. Ed. Engl.*, 1995, **34**, 65–66.
69 A. Berkessel, S. Das, D. Pekel and J.-M. Neudörfl, *Angew. Chem. Int. Ed.*, 2014, **53**, 11660–11664.
70 T. H. Wirth and N. Davidson, *J. Am. Chem. Soc.*, 1964, **86**, 4325–4329.
71 M. D. Best, S. L. Tobey and E. V. Anslyn, *Coord. Chem. Rev.*, 2003, **240**, 3–15.

72 P. Blondeau, M. Segura, R. Pérez-Fernández and J. de Mendoza, *Chem. Soc. Rev.*, 2007, **36**, 198–210.
73 G. Müller, J. Riede and F. P. Schmidtchen, *Angew. Chem. Int. Ed. Engl.*, 1988, **27**, 1516–1518.
74 R. A. Doyle, L. M. Daniels, R. J. Angelici and F. G. A. Stone, *J. Am. Chem. Soc.*, 1989, **111**, 4995–4997.
75 K. Sato, S. Arai and T. Yamagishi, *Tetrahedron Lett.*, 1999, **40**, 5219–5222.
76 E. Alcalde, N. Mesquida, L. Pérez-García, C. Alvarez-Rúa, S. García-Granda and E. García-Rodriguez, *Chem. Commun.*, 1999, 295–296.
77 J. Yoon, S. K. Kim, N. J. Singh and K. S. Kim, *Chem. Soc. Rev.*, 2006, **35**, 355–360.
78 Z. Xu, S. K. Kim and J. Yoon, *Chem. Soc. Rev.*, 2010, **39**, 1457–1466.
79 H.-Y. Gong, B. M. Rambo, E. Karnas, V. M. Lynch and J. L. Sessler, *Nat. Chem.*, 2010, **2**, 406–409.
80 N. Ahmed, B. Shirinfar, I. S. Youn, M. Yousuf and K. S. Kim, *Org. Biomol. Chem.*, 2013, **11**, 6407–6413.
81 H. Juwarker, J. M. Lenhardt, D. M. Pham and S. L. Craig, *Angew. Chem. Int. Ed.*, 2008, **47**, 3740–3743.
82 R. M. Meudtner and S. Hecht, *Angew. Chem. Int. Ed.*, 2008, **47**, 4926–4930.
83 Q.-Y. Cao, T. Pradhan, S. Kim and J. S. Kim, *Org. Lett.*, 2011, **13**, 4386–4389.
84 Y. Wang, J. Xiang and H. Jiang, *Chem. – Eur. J.*, 2011, **17**, 613–619.
85 Y. Wang, F. Bie and H. Jiang, *Org. Lett.*, 2010, **12**, 3630–3633.
86 V. Haridas, S. Sahu and P. Venugopalan, *Tetrahedron*, 2011, **67**, 727–733.
87 M. R. Krause, R. Goddard and S. Kubik, *J. Org. Chem.*, 2011, **76**, 7084–7095.
88 Y. H. Lau, P. J. Rutledge, M. Watkinson and M. H. Todd, *Chem. Soc. Rev.*, 2011, **40**, 2848–2866.
89 C.-H. Lee, S. Lee, H. Yoon and W.-D. Jang, *Chem. – Eur. J.*, 2011, **17**, 13898–13903.
90 Y. Li and A. H. Flood, *J. Am. Chem. Soc.*, 2008, **130**, 12111–12122.
91 L. C. Gilday, N. G. White and P. D. Beer, *Dalton Trans.*, 2012, **41**, 7092–7097.
92 B. Schulze, C. Friebe, M. D. Hager, W. Günther, U. Köhn, B. O. Jahn, H. Görls and U. S. Schubert, *Org. Lett.*, 2010, **12**, 2710–2713.
93 K. Ohmatsu, M. Kiyokawa and T. Ooi, *J. Am. Chem. Soc.*, 2011, **133**, 1307–1309.
94 R. K. Chhatra, A. Kumar and P. S. Pandey, *J. Org. Chem.*, 2011, **76**, 9086–9089.
95 J. M. Aizpurua, R. M. Fratila, Z. Monasterio, N. Pérez-Esnaola, E. Andreieff, A. Irastorza and M. Sagartzazu-Aizpurua, *New J. Chem.*, 2014, **38**, 474–480.
96 N. Mesquida, I. Dinarès, A. Ibáñez and E. Alcalde, *Org. Biomol. Chem.*, 2013, **11**, 6385–6396.
97 A. Kumar and P. S. Pandey, *Org. Lett.*, 2008, **10**, 165–168.
98 H. T. Le, S. C. Park, C. Kang, C. W. Lim and T. W. Kim, *Org. Biomol. Chem.*, 2015, **13**, 8291–8297.
99 F. Zapata, L. Gonzalez, A. Caballero, I. Alkorta, J. Elguero and P. Molina, *Chem. – Eur. J.*, 2015, **21**, 9797–9808.
100 C. R. Bondy and S. J. Loeb, *Coord. Chem. Rev.*, 2003, **240**, 77–99.
101 S. O. Kang, R. A. Begum and K. Bowman-James, *Angew. Chem. Int. Ed.*, 2006, **45**, 7882–7894.
102 R. A. Pascal Jr., J. Spergel and D. Van Engen, *Tetrahedron Lett.*, 1986, **27**, 4099–4102.
103 K. Kavallieratos, S. R. de Gala, D. J. Austin and R. H. Crabtree, *J. Am. Chem. Soc.*, 1997, **119**, 2325–2326.
104 K. Kavallieratos, C. M. Bertao and R. H. Crabtree, *J. Org. Chem.*, 1999, **64**, 1675–1683.
105 S. Kubik, *Chem. Soc. Rev.*, 2010, **39**, 3648–3663.
106 S. Otto and S. Kubik, *J. Am. Chem. Soc.*, 2003, **125**, 7804–7805.
107 Z. Rodriguez-Docampo, S. I. Pascu, S. Kubik and S. Otto, *J. Am. Chem. Soc.*, 2006, **128**, 11206–11210.
108 A.-F. Li, J.-H. Wang, F. Wang and Y.-B. Jiang, *Chem. Soc. Rev.*, 2010, **39**, 3729–3745.
109 V. Amendola, L. Fabbrizzi and L. Mosca, *Chem. Soc. Rev.*, 2010, **39**, 3889–3915.
110 S. J. Brooks, P. A. Gale and M. E. Light, *Chem. Commun.*, 2005, 4696–4698.
111 V. J. Dungan, H. T. Ngo, P. G. Young and K. A. Jolliffe, *Chem. Commun.*, 2012, **49**, 264–266.
112 R. B. P. Elmes and K. A. Jolliffe, *Supramol. Chem.*, 2015, **27**, 321–328.

113 V. Amendola, G. Bergamaschi, M. Boiocchi, L. Fabbrizzi and M. Milani, *Chem. – Eur. J.*, 2010, **16**, 4368–4380.
114 S. J. Edwards, H. Valkenier, N. Busschaert, P. A. Gale and A. P. Davis, *Angew. Chem. Int. Ed.*, 2015, **54**, 4592–4596.
115 P. A. Gale, J. L. Sessler, V. Král and V. Lynch, *J. Am. Chem. Soc.*, 1996, **118**, 5140–5141.
116 J. L. Sessler, J. A. Shriver, K. Jursíková, V. M. Lynch and M. Marquez, *J. Am. Chem. Soc.*, 2000, **122**, 12061–12062.
117 C.-H. Lee, J.-S. Lee, H.-K. Na, D.-W. Yoon, H. Miyaji, W.-S. Cho and J. L. Sessler, *J. Org. Chem.*, 2005, **70**, 2067–2074.
118 D.-W. Yoon, D. E. Gross, V. M. Lynch, C.-H. Lee, P. C. Bennett and J. L. Sessler, *Chem. Commun.*, 2009, 1109–1111.
119 S. K. Kim, J. Lee, N. J. Williams, V. M. Lynch, B. P. Hay, B. A. Moyer and J. L. Sessler, *J. Am. Chem. Soc.*, 2014, **136**, 15079–15085.
120 M. A. Yawer, V. Havel and V. Sindelar, *Angew. Chem. Int. Ed.*, 2015, **54**, 276–279.
121 P. W. Snyder, J. Mecinović, D. T. Moustakas, S. W. Thomas, M. Harder, E. T. Mack, M. R. Lockett, A. Héroux, W. Sherman and G. M. Whitesides, *Proc. Natl. Acad. Sci.*, 2011, **108**, 17889–17894.
122 M. J. Langton, C. J. Serpell and P. D. Beer, *Angew. Chem. Int. Ed.*, 2016, **55**, 1974–1987.
123 R. U. Lemieux, *Acc. Chem. Res.*, 1996, **29**, 373–380.
124 J. Mecinović, P. W. Snyder, K. A. Mirica, S. Bai, E. T. Mack, R. L. Kwant, D. T. Moustakas, A. Héroux and G. M. Whitesides, *J. Am. Chem. Soc.*, 2011, **133**, 14017–14026.
125 E. A. Meyer, R. K. Castellano and F. Diederich, *Angew. Chem. Int. Ed.*, 2003, **42**, 1210–1250.
126 L. M. Salonen, M. Ellermann and F. Diederich, *Angew. Chem. Int. Ed.*, 2011, **50**, 4808–4842.
127 T. W. Hudnall, C.-W. Chiu and F. P. Gabbaï, *Acc. Chem. Res.*, 2009, **42**, 388–397.
128 M. Newcomb, J. H. Horner and M. T. Blanda, *J. Am. Chem. Soc.*, 1987, **109**, 7878–7879.
129 T. J. Wedge and M. F. Hawthorne, *Coord. Chem. Rev.*, 2003, **240**, 111–128.
130 E. J. O'Neil and B. D. Smith, *Coord. Chem. Rev.*, 2006, **250**, 3068–3080.
131 R. Vilar, *Eur. J. Inorg. Chem.*, 2008, **2008**, 357–367.
132 K. J. Wallace, R. Daari, W. J. Belcher, L. O. Abouderbala, M. G. Boutelle and J. W. Steed, *J. Organomet. Chem.*, 2003, **666**, 63–74.
133 V. Amendola, L. Fabbrizzi, C. Mangano, P. Pallavicini, A. Poggi and A. Taglietti, *Coord. Chem. Rev.*, 2001, **219–221**, 821–837.
134 C. J. Harding, F. E. Mabbs, E. J. L. MacInnes, V. McKee and J. Nelson, *J. Chem. Soc. Dalton Trans.*, 1996, 3227–3230.
135 D. J. Mercer and S. J. Loeb, *Chem. Soc. Rev.*, 2010, **39**, 3612–3620.
136 A. Mele, P. Metrangolo, H. Neukirch, T. Pilati and G. Resnati, *J. Am. Chem. Soc.*, 2005, **127**, 14972–14973.
137 M. G. Sarwar, B. Dragisic, S. Sagoo and M. S. Taylor, *Angew. Chem. Int. Ed.*, 2010, **49**, 1674–1677.
138 M. G. Chudzinski, C. A. McClary and M. S. Taylor, *J. Am. Chem. Soc.*, 2011, **133**, 10559–10567.
139 M. Cametti, K. Raatikainen, P. Metrangolo, T. Pilati, G. Terraneo and G. Resnati, *Org. Biomol. Chem.*, 2012, **10**, 1329–1333.
140 A. Caballero, N. G. White and P. D. Beer, *Angew. Chem. Int. Ed.*, 2011, **50**, 1845–1848.
141 F. Zapata, A. Caballero, N. G. White, T. D. W. Claridge, P. J. Costa, V. Félix and P. D. Beer, *J. Am. Chem. Soc.*, 2012, **134**, 11533–11541.
142 A. Hulanicki, S. Glab and F. Ingman, *Pure Appl. Chem.*, 1991, **63**.
143 M. Comes, E. Aznar, M. Moragues, M. D. Marcos, R. Martínez-Máñez, F. Sancenón, J. Soto, L. A. Villaescusa, L. Gil and P. Amorós, *Chem. – Eur. J.*, 2009, **15**, 9024–9033.
144 D.-G. Cho, J. H. Kim and J. L. Sessler, *J. Am. Chem. Soc.*, 2008, **130**, 12163–12167.
145 J. R. Lakowicz, Ed., *Principles of Fluorescence Spectroscopy*, Springer US, Boston, MA, 2006.
146 A. P. de Silva, H. Q. N. Gunaratne, T. Gunnlaugsson, A. J. M. Huxley, C. P. McCoy, J. T. Rademacher and T. E. Rice, *Chem. Rev.*, 1997, **97**, 1515–1566.

147 J. F. Callan, A. P. de Silva and D. C. Magri, *Tetrahedron*, 2005, **61**, 8551–8588.
148 A. P. de Silva, T. S. Moody and G. D. Wright, *Analyst*, 2009, **134**, 2385–2393.
149 B. Daly, J. Ling and A. P. de Silva, *Chem. Soc. Rev.*, 2015, **44**, 4203–4211.
150 R. Martínez-Máñez and F. Sancenón, *Chem. Rev.*, 2003, **103**, 4419–4476.
151 T. Gunnlaugsson, H. D. P. Ali, M. Glynn, P. E. Kruger, G. M. Hussey, F. M. Pfeffer, C. M. G. dos Santos and J. Tierney, *J. Fluoresc.*, 2005, **15**, 287–299.
152 T. Gunnlaugsson, P. E. Kruger, T. C. Lee, R. Parkesh, F. M. Pfeffer and G. M. Hussey, *Tetrahedron Lett.*, 2003, **44**, 6575–6578.
153 T. Gunnlaugsson, A. P. Davis, J. E. O'Brien and M. Glynn, *Org. Biomol. Chem.*, 2005, **3**, 48–56.
154 P. Ashokkumar, H. Weißhoff, W. Kraus and K. Rurack, *Angew. Chem. Int. Ed.*, 2014, **53**, 2225–2229.
155 R. Tirfoin, J. A. B. Abdalla and S. Aldridge, *Chem. – Eur. J.*, 2015, **21**, 11813–11824.
156 D. Esteban-Gómez, L. Fabbrizzi and M. Licchelli, *J. Org. Chem.*, 2005, **70**, 5717–5720.
157 P. D. Beer and A. D. Keefe, *J. Organomet. Chem.*, 1989, **375**, C40–C42.
158 F. Otón, A. Espinosa, A. Tárraga, I. Ratera, K. Wurst, J. Veciana and P. Molina, *Inorg. Chem.*, 2009, **48**, 1566–1576.
159 A. E. J. Broomsgrove, D. A. Addy, C. Bresner, I. A. Fallis, A. L. Thompson and S. Aldridge, *Chem. – Eur. J.*, 2008, **14**, 7525–7529.
160 J. M. Lloris, R. Martínez-Máñez, M. E. Padilla-Tosta, T. Pardo, J. Soto, P. D. Beer, J. Cadman and D. K. Smith, *J. Chem. Soc. Dalton Trans.*, 1999, 2359–2370.
161 Y. Willener, K. M. Joly, C. J. Moody and J. H. R. Tucker, *J. Org. Chem.*, 2008, **73**, 1225–1233.
162 Á. Lorenzo, E. Aller and P. Molina, *Tetrahedron*, 2009, **65**, 1397–1401.
163 L. Basabe-Desmonts, D. N. Reinhoudt and M. Crego-Calama, *Chem. Soc. Rev.*, 2007, **36**, 993–1017.
164 N. H. Evans, H. Rahman, J. J. Davis and P. D. Beer, *Anal. Bioanal. Chem.*, 2011, **402**, 1739–1748.
165 S. Zhang, C. M. Cardona and L. Echegoyen, *Chem. Commun.*, 2006, 4461–4473.
166 L. G. Jensen, K. A. Nielsen, T. Breton, J. L. Sessler, J. O. Jeppesen, E. Levillain and L. Sanguinet, *Chem. – Eur. J.*, 2009, **15**, 8128–8133.
167 E. Alonso, A. Labande, L. Raehm, J.-M. Kern and D. Astruc, *Comptes Rendus Académie Sci. - Ser. IIC - Chem.*, 1999, **2**, 209–213.
168 M.-C. Daniel and D. Astruc, *Chem. Rev.*, 2004, **104**, 293–346.
169 K. Saha, S. S. Agasti, C. Kim, X. Li and V. M. Rotello, *Chem. Rev.*, 2012, **112**, 2739–2779.
170 P. Sokkalingam, S.-J. Hong, A. Aydogan, J. L. Sessler and C.-H. Lee, *Chem. – Eur. J.*, 2013, **19**, 5860–5867.
171 J.-P. Sauvage and C. Dietrich-Buchecker, Eds., in *Molecular Catenanes, Rotaxanes and Knots*, Wiley-VCH Verlag GmbH, 1999, pp. I–XIV.
172 G. A. Breault, C. A. Hunter and P. C. Mayers, *Tetrahedron*, 1999, **55**, 5265–5293.
173 M. J. Chmielewski, J. J. Davis and P. D. Beer, *Org. Biomol. Chem.*, 2009, **7**, 415–424.
174 R. Klajn, J. F. Stoddart and B. A. Grzybowski, *Chem. Soc. Rev.*, 2010, **39**, 2203–2237.
175 S. Erbas-Cakmak, D. A. Leigh, C. T. McTernan and A. L. Nussbaumer, *Chem. Rev.*, 2015, **115**, 10081–10206.
176 J.-F. Ayme, G. Gil-Ramírez, D. A. Leigh, J.-F. Lemonnier, A. Markevicius, C. A. Muryn and G. Zhang, *J. Am. Chem. Soc.*, 2014, **136**, 13142–13145.
177 T. Prakasam, M. Lusi, M. Elhabiri, C. Platas-Iglesias, J.-C. Olsen, Z. Asfari, S. Cianférani-Sanglier, F. Debaene, L. J. Charbonnière and A. Trabolsi, *Angew. Chem. Int. Ed.*, 2013, **52**, 9956–9960.
178 J. E. Beves, J. J. Danon, D. A. Leigh, J.-F. Lemonnier and I. J. Vitorica-Yrezabal, *Angew. Chem. Int. Ed.*, 2015, **54**, 7555–7559.
179 G. T. Spence, University of Oxford, 2012.
180 P. R. Ashton, M. Bělohradský, D. Philp and J. F. Stoddart, *J. Chem. Soc. Chem. Commun.*, 1993, 1269–1274.
181 M. Händel, M. Plevoets, S. Gestermann and F. Vögtle, *Angew. Chem. Int. Ed. Engl.*, 1997, **36**, 1199–1201.

182 I. Yoon, M. Narita, T. Shimizu and M. Asakawa, *J. Am. Chem. Soc.*, 2004, **126**, 16740–16741.
183 S.-Y. Hsueh, J.-L. Ko, C.-C. Lai, Y.-H. Liu, S.-M. Peng and S.-H. Chiu, *Angew. Chem. Int. Ed.*, 2011, **50**, 6643–6646.
184 J.-L. Ko, S.-H. Ueng, C.-W. Chiu, C.-C. Lai, Y.-H. Liu, S.-M. Peng and S.-H. Chiu, *Chem. – Eur. J.*, 2010, **16**, 6950–6960.
185 C.-W. Chiu, C.-C. Lai and S.-H. Chiu, *J. Am. Chem. Soc.*, 2007, **129**, 3500–3501.
186 E. Wasserman, *J. Am. Chem. Soc.*, 1960, **82**, 4433–4434.
187 I. T. Harrison and S. Harrison, *J. Am. Chem. Soc.*, 1967, **89**, 5723–5724.
188 G. Schill and A. Lüttringhaus, *Angew. Chem. Int. Ed. Engl.*, 1964, **3**, 546–547.
189 C. O. Dietrich-Buchecker, J. P. Sauvage and J. P. Kintzinger, *Tetrahedron Lett.*, 1983, **24**, 5095–5098.
190 C. O. Dietrich-Buchecker, J. P. Sauvage and J. M. Kern, *J. Am. Chem. Soc.*, 1984, **106**, 3043–3045.
191 W. R. Dichtel, O. Š. Miljanić, W. Zhang, J. M. Spruell, K. Patel, I. Aprahamian, J. R. Heath and J. F. Stoddart, *Acc. Chem. Res.*, 2008, **41**, 1750–1761.
192 J. F. Stoddart, *Chem. Soc. Rev.*, 2009, **38**, 1802–1820.
193 J. A. Faiz, V. Heitz and J.-P. Sauvage, *Chem. Soc. Rev.*, 2009, **38**, 422–442.
194 A. Harada, Y. Takashima and H. Yamaguchi, *Chem. Soc. Rev.*, 2009, **38**, 875–882.
195 K. D. Hänni and D. A. Leigh, *Chem. Soc. Rev.*, 2010, **39**, 1240–1251.
196 R. Klajn, J. F. Stoddart and B. A. Grzybowski, *Chem. Soc. Rev.*, 2010, **39**, 2203–2237.
197 J. E. Beves, B. A. Blight, C. J. Campbell, D. A. Leigh and R. T. McBurney, *Angew. Chem. Int. Ed.*, 2011, **50**, 9260–9327.
198 R. S. Forgan, J.-P. Sauvage and J. F. Stoddart, *Chem. Rev.*, 2011, **111**, 5434–5464.
199 A. Coskun, J. M. Spruell, G. Barin, W. R. Dichtel, A. H. Flood, Y. Y. Botros and J. F. Stoddart, *Chem. Soc. Rev.*, 2012, **41**, 4827–4859.
200 V. N. Vukotic and S. J. Loeb, *Chem. Soc. Rev.*, 2012, **41**, 5896–5906.
201 G. T. Spence and P. D. Beer, *Acc. Chem. Res.*, 2013, **46**, 571–586.
202 J. D. Crowley, S. M. Goldup, A.-L. Lee, D. A. Leigh and R. T. McBurney, *Chem. Soc. Rev.*, 2009, **38**, 1530–1541.
203 S. M. Goldup, D. A. Leigh, P. J. Lusby, R. T. McBurney and A. M. Z. Slawin, *Angew. Chem. Int. Ed.*, 2008, **47**, 6999–7003.
204 A.-M. L. Fuller, D. A. Leigh, P. J. Lusby, A. M. Z. Slawin and D. B. Walker, *J. Am. Chem. Soc.*, 2005, **127**, 12612–12619.
205 D. A. Leigh, P. J. Lusby, A. M. Z. Slawin and D. B. Walker, *Chem. Commun.*, 2005, 4919–4921.
206 D. A. Leigh, P. J. Lusby, R. T. McBurney, A. Morelli, A. M. Z. Slawin, A. R. Thomson and D. B. Walker, *J. Am. Chem. Soc.*, 2009, **131**, 3762–3771.
207 Y.-H. Lin, C.-C. Lai, Y.-H. Liu, S.-M. Peng and S.-H. Chiu, *Angew. Chem. Int. Ed.*, 2013, **52**, 10231–10236.
208 V. Aucagne, K. D. Hänni, D. A. Leigh, P. J. Lusby and D. B. Walker, *J. Am. Chem. Soc.*, 2006, **128**, 2186–2187.
209 V. Aucagne, J. Berná, J. D. Crowley, S. M. Goldup, K. D. Hänni, D. A. Leigh, P. J. Lusby, V. E. Ronaldson, A. M. Z. Slawin, A. Viterisi and D. B. Walker, *J. Am. Chem. Soc.*, 2007, **129**, 11950–11963.
210 S. Saito, E. Takahashi and K. Nakazono, *Org. Lett.*, 2006, **8**, 5133–5136.
211 J. D. Crowley, K. D. Hänni, A.-L. Lee and D. A. Leigh, *J. Am. Chem. Soc.*, 2007, **129**, 12092–12093.
212 S. M. Goldup, D. A. Leigh, R. T. McBurney, P. R. McGonigal and A. Plant, *Chem. Sci.*, 2010, **1**, 383–386.
213 B. L. Allwood, N. Spencer, H. Shahriari-Zavareh, J. F. Stoddart and D. J. Williams, *J. Chem. Soc. Chem. Commun.*, 1987, 1061–1064.
214 B. L. Allwood, N. Spencer, H. Shahriari-Zavareh, J. F. Stoddart and D. J. Williams, *J. Chem. Soc. Chem. Commun.*, 1987, 1064–1066.

215 B. Odell, M. V. Reddington, A. M. Z. Slawin, N. Spencer, J. F. Stoddart and D. J. Williams, *Angew. Chem. Int. Ed. Engl.*, 1988, **27**, 1547–1550.
216 P. R. Ashton, B. Odell, M. V. Reddington, A. M. Z. Slawin, J. F. Stoddart and D. J. Williams, *Angew. Chem. Int. Ed. Engl.*, 1988, **27**, 1550–1553.
217 P. L. Anelli, N. Spencer and J. F. Stoddart, *J. Am. Chem. Soc.*, 1991, **113**, 5131–5133.
218 P. R. Ashton, T. T. Goodnow, A. E. Kaifer, M. V. Reddington, A. M. Z. Slawin, N. Spencer, J. F. Stoddart, C. Vicent and D. J. Williams, *Angew. Chem. Int. Ed. Engl.*, 1989, **28**, 1396–1399.
219 D. B. Amabilino, P. R. Ashton, A. S. Reder, N. Spencer and J. F. Stoddart, *Angew. Chem. Int. Ed. Engl.*, 1994, **33**, 1286–1290.
220 S. J. Loeb and J. A. Wisner, *Angew. Chem. Int. Ed.*, 1998, **37**, 2838–2840.
221 S. J. Loeb and J. A. Wisner, *Chem. Commun.*, 1998, 2757–2758.
222 M.-V. Martínez-Díaz, N. Spencer and J. F. Stoddart, *Angew. Chem. Int. Ed. Engl.*, 1997, **36**, 1904–1907.
223 E. N. Guidry, S. J. Cantrill, J. F. Stoddart and R. H. Grubbs, *Org. Lett.*, 2005, **7**, 2129–2132.
224 C. A. Hunter, *J. Am. Chem. Soc.*, 1992, **114**, 5303–5311.
225 A. G. Johnston, D. A. Leigh, R. J. Pritchard and M. D. Deegan, *Angew. Chem. Int. Ed. Engl.*, 1995, **34**, 1209–1212.
226 E. V. Dzyuba, L. Kaufmann, N. L. Löw, A. K. Meyer, H. D. F. Winkler, K. Rissanen and C. A. Schalley, *Org. Lett.*, 2011, **13**, 4838–4841.
227 L. Raehm, D. G. Hamilton and J. K. Sanders, *Synlett*, 2002, **2002**, 1743–1761.
228 D. G. Hamilton, J. K. M. Sanders, J. E. Davies, W. Clegg and S. J. Teat, *Chem. Commun.*, 1997, 897–898.
229 F. B. L. Cougnon, H. Y. Au-Yeung, G. D. Pantoş and J. K. M. Sanders, *J. Am. Chem. Soc.*, 2011, **133**, 3198–3207.
230 H. Y. Au-Yeung, G. D. Pantoş and J. K. M. Sanders, *Proc. Natl. Acad. Sci.*, 2009, **106**, 10466–10470.
231 G. M. Hübner, J. Gläser, C. Seel and F. Vögtle, *Angew. Chem. Int. Ed.*, 1999, **38**, 383–386.
232 J. A. Wisner, P. D. Beer and M. G. B. Drew, *Angew. Chem. Int. Ed.*, 2001, **40**, 3606–3609.
233 J. A. Wisner, P. D. Beer, M. G. B. Drew and M. R. Sambrook, *J. Am. Chem. Soc.*, 2002, **124**, 12469–12476.
234 L. M. Hancock, L. C. Gilday, S. Carvalho, P. J. Costa, V. Félix, C. J. Serpell, N. L. Kilah and P. D. Beer, *Chem. – Eur. J.*, 2010, **16**, 13082–13094.
235 M. R. Sambrook, P. D. Beer, J. A. Wisner, R. L. Paul and A. R. Cowley, *J. Am. Chem. Soc.*, 2004, **126**, 15364–15365.
236 M. J. Langton and P. D. Beer, *Chem. Commun.*, 2014, **50**, 8124–8127.
237 J. M. Mercurio, R. C. Knighton, J. Cookson and P. D. Beer, *Chem. – Eur. J.*, 2014, **20**, 11740–11749.
238 E. A. Neal and S. M. Goldup, *Chem. Commun.*, 2014, **50**, 5128–5142.
239 M. J. Langton and P. D. Beer, *Acc. Chem. Res.*, 2014, **47**, 1935–1949.
240 V. Balzani, A. Credi and M. Venturi, in *Molecular Devices and Machines – A Journey into the Nano World*, Wiley-VCH Verlag GmbH & Co. KGaA, 2003, pp. i–ix.
241 W. R. Browne and B. L. Feringa, *Nat. Nanotechnol.*, 2006, **1**, 25–35.
242 K. Kinbara and T. Aida, *Chem. Rev.*, 2005, **105**, 1377–1400.
243 P. D. Boyer, *Nature*, 1999, **402**, 247–249.
244 K. Kitamura, M. Tokunaga, A. H. Iwane and T. Yanagida, *Nature*, 1999, **397**, 129–134.
245 F. Dyson and R. P. Feynman, *The Pleasure of Finding Things Out*, Penguin, London, 1st Edition, 2007.
246 R. P. . L. R. B.; Sands, M. The Feynman Lectures on Physics; Addison-Wesley: Reading, MA, 1963; Vol. 1, Chapter 46. Feynman, .
247 M. N. Chatterjee, E. R. Kay and D. A. Leigh, *J. Am. Chem. Soc.*, 2006, **128**, 4058–4073.
248 D. A. Leigh, J. K. Y. Wong, F. Dehez and F. Zerbetto, *Nature*, 2003, **424**, 174–179.

249 D. S. Marlin, D. González Cabrera, D. A. Leigh and A. M. Z. Slawin, *Angew. Chem. Int. Ed.*, 2006, **45**, 77–83.
250 J. Berná, M. Alajarín and R.-A. Orenes, *J. Am. Chem. Soc.*, 2010, **132**, 10741–10747.
251 Y.-C. You, M.-C. Tzeng, C.-C. Lai and S.-H. Chiu, *Org. Lett.*, 2012, **14**, 1046–1049.
252 R. A. Bissell, E. Córdova, A. E. Kaifer and J. F. Stoddart, *Nature*, 1994, **369**, 133–137.
253 O. Buyukcakir, F. T. Yasar, O. A. Bozdemir, B. Icli and E. U. Akkaya, *Org. Lett.*, 2013, **15**, 1012–1015.
254 C. J. Bruns and J. F. Stoddart, *Nat. Nanotechnol.*, 2013, **8**, 9–10.
255 Z. Meng, J.-F. Xiang and C.-F. Chen, *Chem. Sci.*, 2014, **5**, 1520–1525.
256 D. D. Günbaş, L. Zalewski and A. M. Brouwer, *Chem. Commun.*, 2011, **47**, 4977–4979.
257 A. Hanke and R. Metzler, *Chem. Phys. Lett.*, 2002, **359**, 22–26.
258 C. Gong and H. W. Gibson, *Angew. Chem. Int. Ed. Engl.*, 1997, **36**, 2331–2333.
259 T. Da Ros, D. M. Guldi, A. F. Morales, D. A. Leigh, M. Prato and R. Turco, *Org. Lett.*, 2003, **5**, 689–691.
260 V. Balzani, M. Clemente-León, A. Credi, B. Ferrer, M. Venturi, A. H. Flood and J. F. Stoddart, *Proc. Natl. Acad. Sci.*, 2006, **103**, 1178–1183.
261 Q.-C. Wang, D.-H. Qu, J. Ren, K. Chen and H. Tian, *Angew. Chem. Int. Ed.*, 2004, **43**, 2661–2665.
262 A. Altieri, G. Bottari, F. Dehez, D. A. Leigh, J. K. Y. Wong and F. Zerbetto, *Angew. Chem. Int. Ed.*, 2003, **42**, 2296–2300.
263 F. Vögtle, W. M. Müller, U. Müller, M. Bauer and K. Rissanen, *Angew. Chem. Int. Ed. Engl.*, 1993, **32**, 1295–1297.
264 A. M. Brouwer, C. Frochot, F. G. Gatti, D. A. Leigh, L. Mottier, F. Paolucci, S. Roffia and G. W. H. Wurpel, *Science*, 2001, **291**, 2124–2128.
265 A. Altieri, F. G. Gatti, E. R. Kay, D. A. Leigh, D. Martel, F. Paolucci, A. M. Z. Slawin and J. K. Y. Wong, *J. Am. Chem. Soc.*, 2003, **125**, 8644–8654.
266 P. Raiteri, G. Bussi, C. S. Cucinotta, A. Credi, J. F. Stoddart and M. Parrinello, *Angew. Chem. Int. Ed.*, 2008, **47**, 3536–3539.
267 P. R. Ashton, R. Ballardini, V. Balzani, A. Credi, K. R. Dress, E. Ishow, C. J. Kleverlaan, O. Kocian, J. A. Preece, N. Spencer, J. F. Stoddart, M. Venturi and S. Wenger, *Chem. – Eur. J.*, 2000, **6**, 3558–3574.
268 N. Kihara, M. Hashimoto and T. Takata, *Org. Lett.*, 2004, **6**, 1693–1696.
269 F. Coutrot and E. Busseron, *Chem. – Eur. J.*, 2009, **15**, 5186–5190.
270 H. Zhang, B. Zhou, H. Li, D.-H. Qu and H. Tian, *J. Org. Chem.*, 2012.
271 Y. Koyama, T. Matsumura, T. Yui, O. Ishitani and T. Takata, *Org. Lett.*, 2013, **15**, 4686–4689.
272 L. Liu, Y. Liu, P. Liu, J. Wu, Y. Guan, X. Hu, C. Lin, Y. Yang, X. Sun, J. Ma and L. Wang, *Chem. Sci.*, 2013, **4**, 1701–1706.
273 A. Martinez-Cuezva, A. Pastor, G. Cioncoloni, R.-A. Orenes, M. Alajarin, M. D. Symes and J. Berna, *Chem. Sci.*, 2015.
274 E. R. Kay, D. A. Leigh and F. Zerbetto, *Angew. Chem. Int. Ed.*, 2007, **46**, 72–191.
275 S. Erbas-Cakmak, D. A. Leigh, C. T. McTernan and A. L. Nussbaumer, *Chem. Rev.*, 2015, **115**, 10081–10206.
276 S. A. Vignon, T. Jarrosson, T. Iijima, H.-R. Tseng, J. K. M. Sanders and J. F. Stoddart, *J. Am. Chem. Soc.*, 2004, **126**, 9884–9885.
277 T. Iijima, S. A. Vignon, H.-R. Tseng, T. Jarrosson, J. K. M. Sanders, F. Marchioni, M. Venturi, E. Apostoli, V. Balzani and J. F. Stoddart, *Chem. – Eur. J.*, 2004, **10**, 6375–6392.
278 J. Berná, C. Franco-Pujante and M. Alajarín, *Org. Biomol. Chem.*, 2013, **12**, 474–478.
279 G. T. Spence, M. B. Pitak and P. D. Beer, *Chem. – Eur. J.*, 2012, **18**, 7100–7108.
280 N. H. Evans, C. J. Serpell and P. D. Beer, *Chem. – Eur. J.*, 2011, **17**, 7734–7738.
281 C. J. Serpell, R. Chall, A. L. Thompson and P. D. Beer, *Dalton Trans.*, 2011, **40**, 12052–12055.
282 J. J. Gassensmith, S. Matthys, J.-J. Lee, A. Wojcik, P. V. Kamat and B. D. Smith, *Chem. – Eur. J.*, 2010, **16**, 2916–2921.
283 H. Zheng, W. Zhou, J. Lv, X. Yin, Y. Li, H. Liu and Y. Li, *Chem. – Eur. J.*, 2009, **15**, 13253–13262.

284 T.-C. Lin, C.-C. Lai and S.-H. Chiu, *Org. Lett.*, 2009, **11**, 613–616.
285 M. J. Barrell, D. A. Leigh, P. J. Lusby and A. M. Z. Slawin, *Angew. Chem. Int. Ed.*, 2008, **47**, 8036–8039.
286 Z.-J. Zhang, M. Han, H.-Y. Zhang and Y. Liu, *Org. Lett.*, 2013, **15**, 1698–1701.
287 L. S. Witus, K. J. Hartlieb, Y. Wang, A. Prokofjevs, M. Frasconi, J. C. Barnes, E. J. Dale, A. C. Fahrenbach and J. F. Stoddart, *Org. Biomol. Chem.*, 2014, **12**, 6089–6093.
288 K. Zhu, C. A. O'Keefe, V. N. Vukotic, R. W. Schurko and S. J. Loeb, *Nat. Chem.*, 2015, **7**, 514–519.
289 M. Galli, J. E. M. Lewis and S. M. Goldup, *Angew. Chem. Int. Ed.*, 2015, **54**, 13545–13549.
290 A.-L. Lee, *Nat. Chem.*, 2016, **8**, 8–9.
291 B. Lewandowski, G. D. Bo, J. W. Ward, M. Papmeyer, S. Kuschel, M. J. Aldegunde, P. M. E. Gramlich, D. Heckmann, S. M. Goldup, D. M. D'Souza, A. E. Fernandes and D. A. Leigh, *Science*, 2013, **339**, 189–193.
292 M. D. Lankshear and P. D. Beer, *Acc. Chem. Res.*, 2007, **40**, 657–668.
293 N. H. Evans, C. J. Serpell, N. G. White and P. D. Beer, *Chem. – Eur. J.*, 2011, **17**, 12347–12354.
294 M. K. Chae, J. Suk and K.-S. Jeong, *Tetrahedron Lett.*, 2010, **51**, 4240–4242.

Chapter Two
Anion-induced shuttling in bistable [2]rotaxanes

2. ANION-INDUCED SHUTTLING IN BISTABLE [2]ROTAXANES

2.1. Introduction

2.1.1. Anion-induced molecular motion in MIMs

As outlined in Section 1.3 the potential for MIMs to act as molecular-scale switchable devices, even machines, arises from their ability to undergo reversible molecular motion through changes in the relative positions of their constituent parts,[1–6] driven by a variety of light-, chemical- and redox-based stimuli.[3,6–10] Whilst examples of cation-induced co-conformational change[3,6] within a rotaxane or catenane are prevalent in the literature, systems that use anions as an external stimulus to produce molecular motion are relatively rare.[11–26]

A recent example of the latter is Beer's bistable [2]rotaxane that incorporates a naphthalimide–triazolium motif in the axle component where shuttling of the macrocyclic wheel is facilitated by halide anion recognition in $CDCl_3$ (Figure 2.1).[12] In the absence of a coordinating anion the macrocycle resides at the electron-deficient naphthalimide station because of favourable donor–acceptor charge–transfer aromatic stacking interactions between the components. However, the addition of chloride causes macrocycle translocation towards the proto-triazolium anion recognition site as evidenced by ^{1}H NMR and UV-Vis spectroscopy.

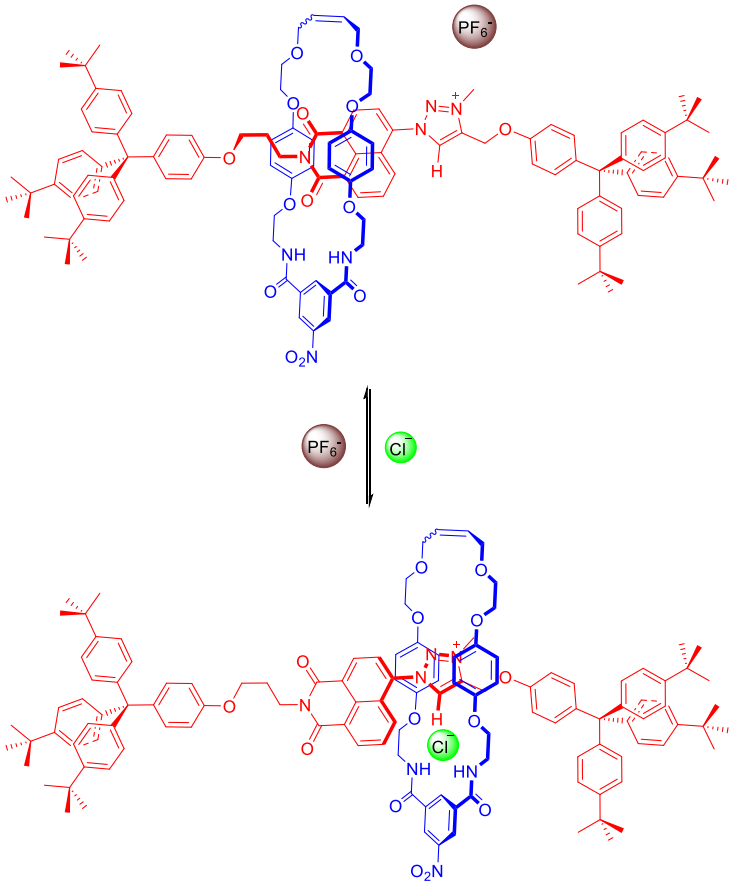


Figure 2.1. Chloride-induced molecular shuttling exhibited by a bistable NI–proto-triazolium [2]rotaxane.12

2.1.2. Chapter Objectives

This chapter describes efforts to build upon the principles of utilising anion recognition and aromatic stacking interactions to control co-conformational changes in mechanically interlocked molecules. The general design of a bistable [2]rotaxane with the potential to exhibit such dynamic behaviour is shown in Figure 2.2, where the distance between the stations, nature of the anion recognition site (red sphere) and electron-deficient station (yellow sphere) can be varied.

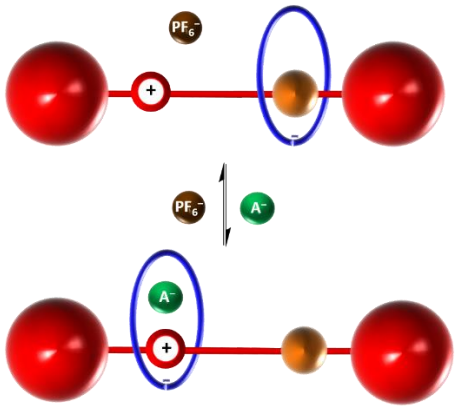


Figure 2.2. Schematic of the anion-induced translational molecular motion within a bistable [2]rotaxane. Yellow sphere = electron-deficient aromatic motif e.g. NI, NDI or N-alkyl pyridinium, red sphere = anion recognition site and A^- = halide anion.

In light of the contrasting anion recognition behaviour of XB- and HB-based anion receptors, [27–29] the axle component will incorporate either an XB iodo- or HB proto-triazolium group (Figure 2.3a) whilst the macrocycle component will contain an amide cleft allowing it to provide cooperative hydrogen bonding to a coordinating anion at this recognition site (Figure 2.3b,c).

A range of electron-deficient aromatic motifs such as naphthalimide (NI), naphthalene diimide (NDI) and *N*-alkyl pyridinium will be examined as candidates for the second station (Figure 2.3a). The electron-deficient aromatic surfaces of these derivatives are expected to interact strongly with the electron-rich hydroquinone groups of the macrocyclic wheel (Figure 2.3b,d). Importantly these donor–acceptor charge–transfer interactions are expected to be superior to aromatic stacking interactions experienced with the XB/HB-triazolium site on account of their larger aromatic surfaces.

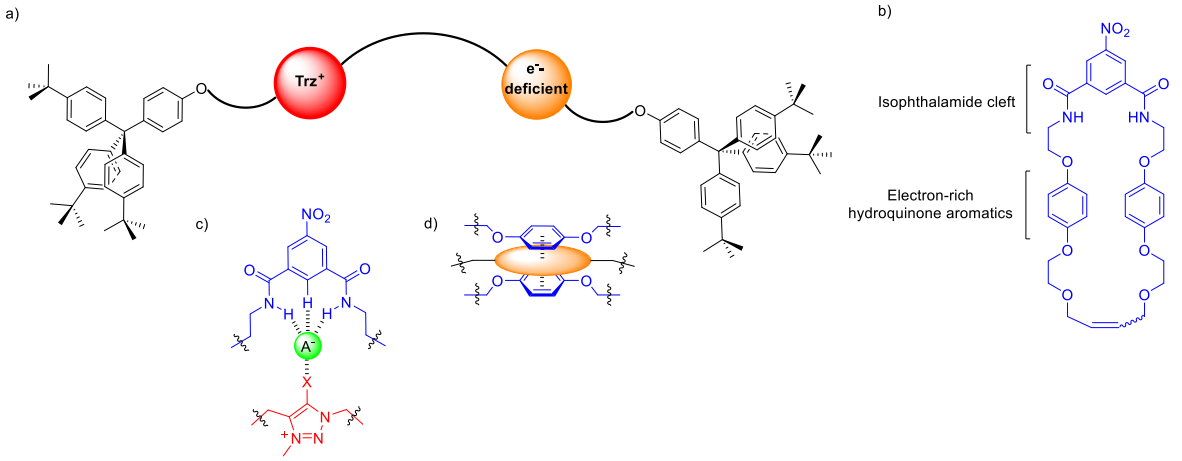


Figure 2.3. Designs of the target a) two station axle, b) isophthalamide-based macrocycle components. Potential non-covalent interactions between macrocycle and stations of the axle c) convergent hydrogen (X = H) or halogen (X = I) bonding towards an anion (A^-) and d) aromatic stacking. Trz^+ = HB/XB-triazolium

Various spectroscopic techniques will be used to thoroughly investigate the dynamic behaviour of these bistable [2]rotaxanes upon changing the counter anion(s) or the solvent. A particular focus of the study will be to uncover how differences in anion binding by either HB or XB affects the macrocycle switching process.

2.2. A two-station NI-triazolium [2]rotaxane

As demonstrated by the [2]rotaxane in Figure 2.1, there is precedent for the NI–triazolium motif to interact with an isophthalamide- and hydroquinone-containing macrocycle. It was hoped that the introduction of a rigid biphenyl spacer between these stations would increase the amplitude of the translational macrocycle motion. Therefore, prior to construction of a two-station [2]rotaxane containing an axle component of this design, novel mono-stoppered NI-HB/XB-triazolium-based threads were synthesised to investigate their capability to form interpenetrated assemblies with an isophthalamide-based macrocycle upon variation of the counter anion (Figure 2.4).

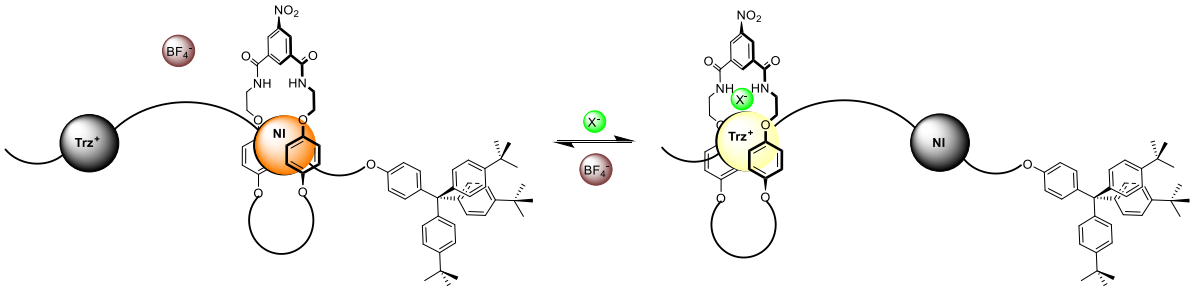
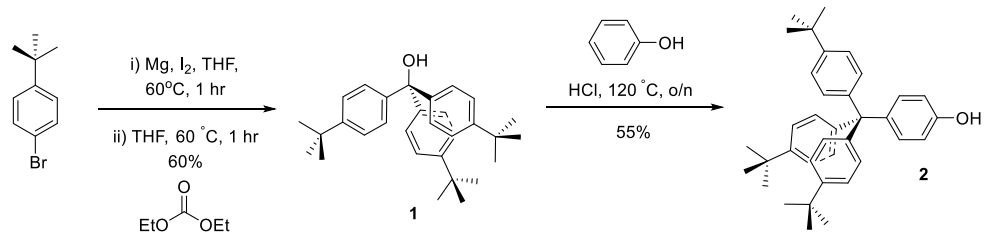


Figure 2.4. Schematic of the potential interpenetrated assemblies formed between a macrocycle and a two-station XB/HB-triazolium-NI threading component. The co-conformation of these [2]pseudorotaxanes may be modulated by changing the nature of the counter anion. X^- = halide. Trz^+ = XB/HB-triazolium.

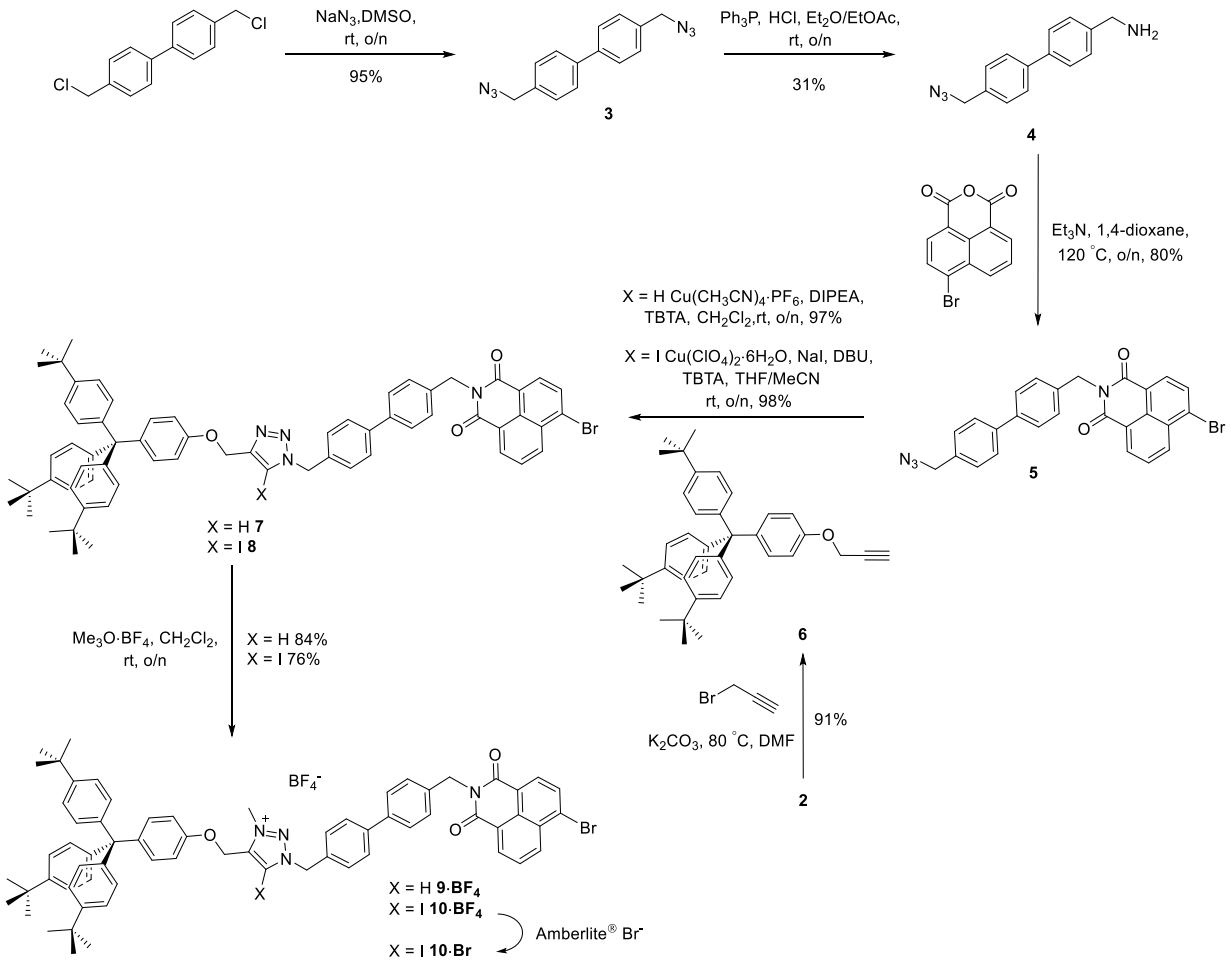
2.2.1. Synthesis of two-station NI-iodo-triazolium thread and macrocycle components

A bulky phenyl trityl stopper precursor for appendage to one terminus of the thread was prepared by a literature procedure (Scheme 2.1).[30,31] Commercially-available 1-bromo-4-*tert*-butylbenzene was heated under reflux in dry THF with Mg filings and a catalytic amount of I_2 to form a phenyl Grignard reagent. This intermediate was reacted *in situ* with diethyl carbonate to give trityl-alcohol **1**.[32] Upon heating this compound in an excess of molten phenol and concentrated $HCl_{(aq.)}$, the phenyl trityl alcohol **2** was generated, and purified by recrystallisation in 55% yield.[32] This compound was appended with a variety of functional groups *via* the phenol position to give a number of stopper-containing derivatives used throughout this thesis.



*Scheme 2.1. Synthesis of the phenyl trityl stopper alcohol derivative **4**.[30,31]*

The synthesis of the target mono-stoppered threads containing a proto- or iodo-triazolium group and an NI motif was achieved *via* a multi-step pathway shown in Scheme 2.2.



Scheme 2.2. Synthesis of mono-stoppered two-station XB/HB triazolium-NI threading components ***9·BF₄ , 10·BF₄*** *and* ***10·Br.***

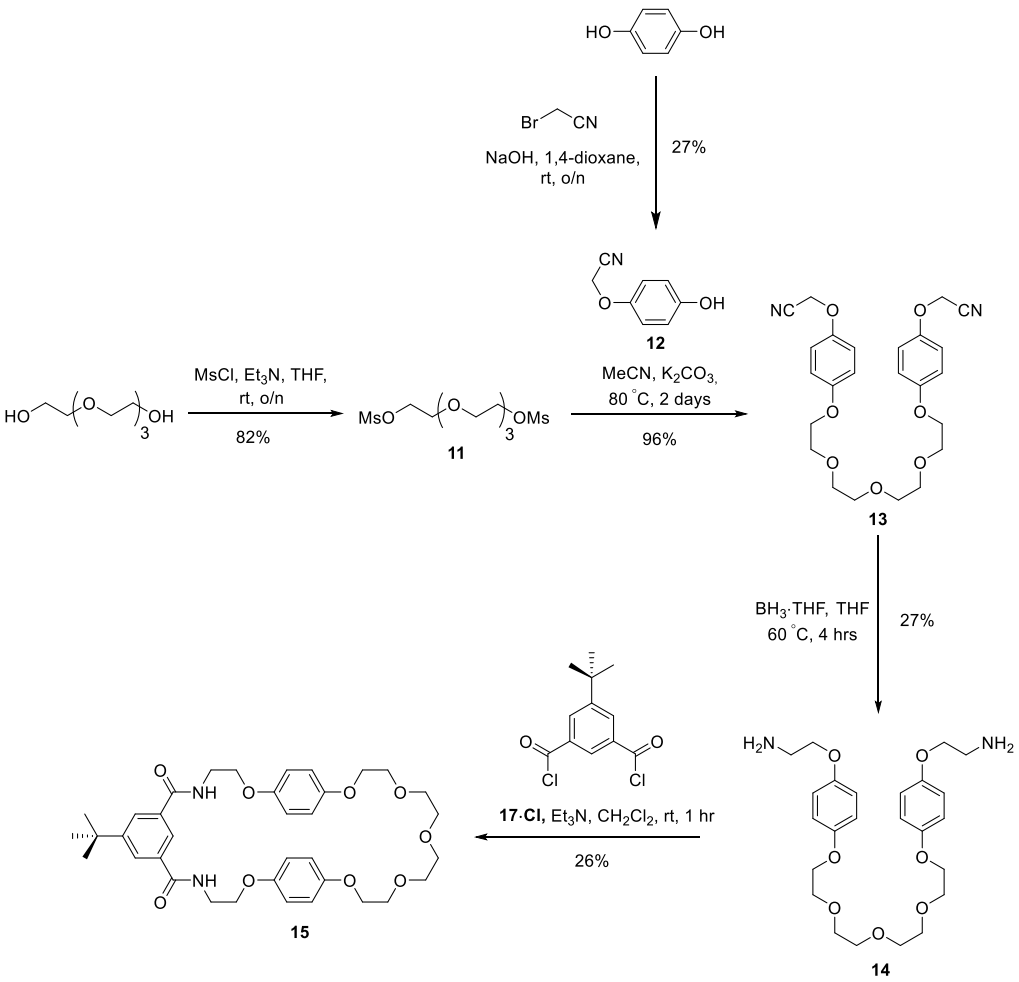
Commercially available bis-chloromethane biphenyl was converted to the bis-azido compound **3** by stirring with NaN_3 in DMSO at room temperature (Scheme 2.2).[33] Mono reduction of **3** was carried out using a Staudinger reaction with one equivalent of PPh_3 under acidic conditions which, after basic work-up, gave the free-base mono-amine **4** in 31% yield.[33] Commercial 4-bromo-1,8-naphthalic anhydride was heated under reflux overnight with amine **4** and Et_3N in dry 1,4-dioxane to form azido compound **5** in 80% yield. Phenyl trityl stopper alkyne compound **6** was synthesised by the reaction of **2** with propargyl bromide in DMF under basic conditions.[34]

This alkyne was stirred with azide **5** to prepare the proto-triazole mono-stoppered thread **7** using catalytic $Cu(CH_3CN)_4{\cdot}PF_6$, TBTA and DIPEA, in dry CH_2Cl_2. The versatility of this copper(I) catalysed azide-alkyne cycloaddition (CuAAC) 'proto-click' reaction[35–37] has recently been adapted for the formation of

5-iodo-1,2,3-triazole groups from a variety of alkyne- and azide-containing starting materials in a similar "one-pot" procedure.[38] The reaction relies upon the initial mixing of copper(II) perchlorate with a NaI solution and a Lewis base to generate a catalytically-active Cu(I) species and an electrophilic source of iodide *via* the formation of I_3^-.[39]

The iodo-triazole-containing analogue was therefore prepared under these conditions to give **8** in a yield of 98%. The cationic threads **9·BF$_4$** and **10·BF$_4$** were isolated in good yield following methylation of the proto/iodo-triazole groups using $Me_3O{\cdot}BF_4$ in dry CH_2Cl_2 and purification using silica gel column chromatography. The bromide salt of the XB thread **10·Br** was prepared by an Amberlite® anion-exchange procedure (Scheme 2.2).

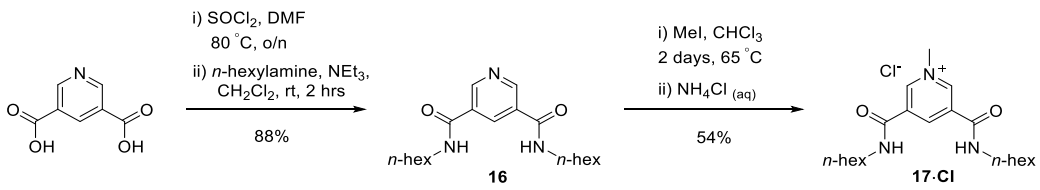
The synthesis of the isophthalamide-containing macrocycle **15** was performed according to an established literature procedure (Scheme 2.3).[40]



*Scheme 2.3. Synthesis of isophthalamide macrocycle **15**.*[40]

Mesylation of tetraethylene glycol under basic conditions gave bis-mesylate **11**[41] in 82% yield whilst commercially-available hydroquinone was mono-functionalised using bromoacetonitrile in 1,4-dioxane to give nitrile **12**.[42] Two equivalents of **12** were reacted with **11** and K_2CO_3 in CH_3CN to give bis-nitrile **13** in near quantitative yield.[43] Reduction with an excess of BH_3·THF gave the polyether-hydroquinone bis-amine derivative **14**.[43]

The *N*-methyl pyridinium chloride compound **17·Cl** was required as a template for the macrocyclisation and was prepared according to a standard literature procedure outlined in Scheme 2.4.[44]



*Scheme 2.4. Synthesis of N-methyl pyridinium chloride template **17·Cl**.*

The synthesis of macrocycle **15** was realised by amide condensation of equimolar equivalents of bis-amine **14** and 5-*tert*-butyl-isophthaloyl acid chloride in the presence of the *N*-methyl pyridinium chloride template **17·Cl** (Scheme 2.3).[40] The cyclic product was isolated in a 26% yield, after purification by silica gel column chromatography.

2.2.2. Pseudorotaxane Investigations

To probe the potential of the iodo-triazolium and NI motifs to facilitate co-conformational change mediated by the counter anion, solution phase pseudorotaxane studies were performed using threads **10·BF$_4$** and **10·Br** and the isophthalamide macrocycle component **15** (Figure 2.5).

It was anticipated that in the absence of a coordinating anion, thread **10·BF$_4$** and macrocycle **15** would undergo interpenetrative assembly due to strong donor–acceptor aromatic stacking interactions between electron-rich hydroquinone groups and the electron-deficient NI motif. In the case of **10·Br**, binding of bromide *via* simultaneous XB from the iodo-triazolium recognition site and HB from the macrocycle's isophthalamide motif would facilitate formation of an interpenetrated assembly.

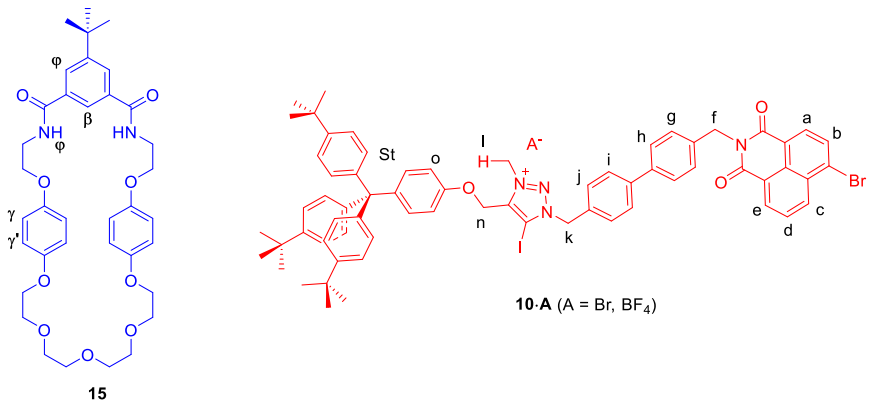


*Figure 2.5. Isophthalamide macrocycle **15** and two station iodo-triazolium-NI thread **10·A** components to be used in the pseudorotaxane investigations.*

Equimolar acetone-d_6 solutions of macrocycle **15** and thread **10·A** (A = BF_4, Br) were prepared and the resulting ^{1}H NMR spectra were recorded and examined (Figure 2.6 and Figure 2.7).

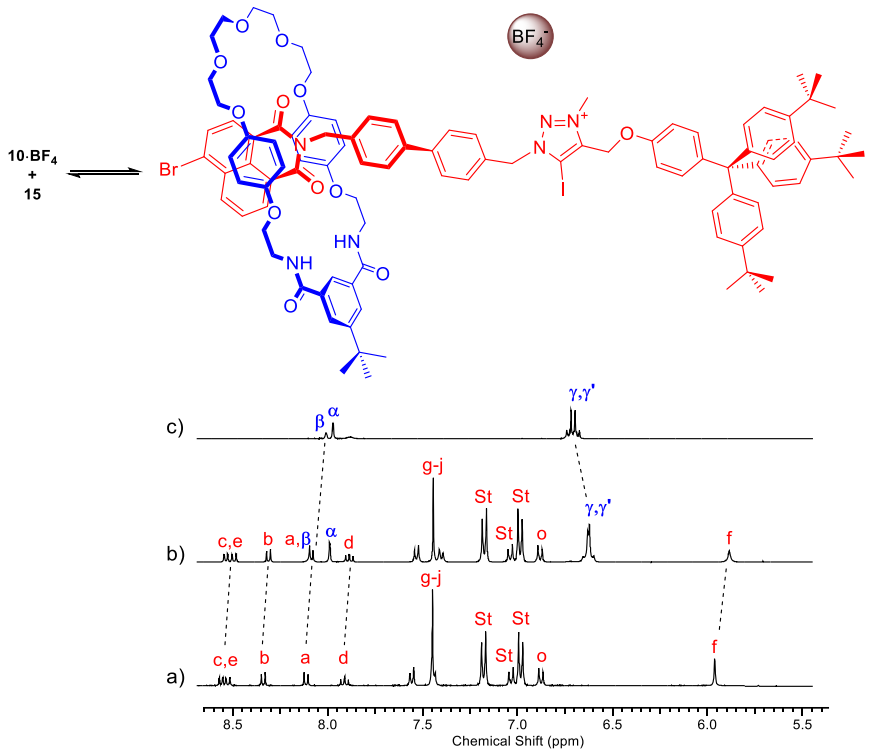


*Figure 2.6. Truncated ^{1}H NMR spectra of a) thread **10·BF$_4$**, b) 1.0 equivalent of thread **10·BF$_4$** and 1.0 equivalent of macrocycle **15** mixture and c) macrocycle **15** (acetone-d_6, 298 K, 500 MHz). The co-conformation of the interpenetrated [2]pseudorotaxane assembly formed in b) is also depicted.*

Comparing the aromatic region of the ^{1}H NMR spectra of **15** and the mixture **15** + **10·BF$_4$**, revealed upfield shifts of the macrocycle hydroquinone protons $H_{\gamma,\gamma'}$ ($\Delta\delta$ = 0.2 ppm) and the aromatic NI protons $H_{a\text{-}e}$. These perturbations indicate the formation of an interpenetrated assembly at the NI station as depicted in Figure 2.6. An upfield shift of the methylene proton (H_f) resonance is also presumed to be caused by ring current effects from proximal macrocycle hydroquinone protons.

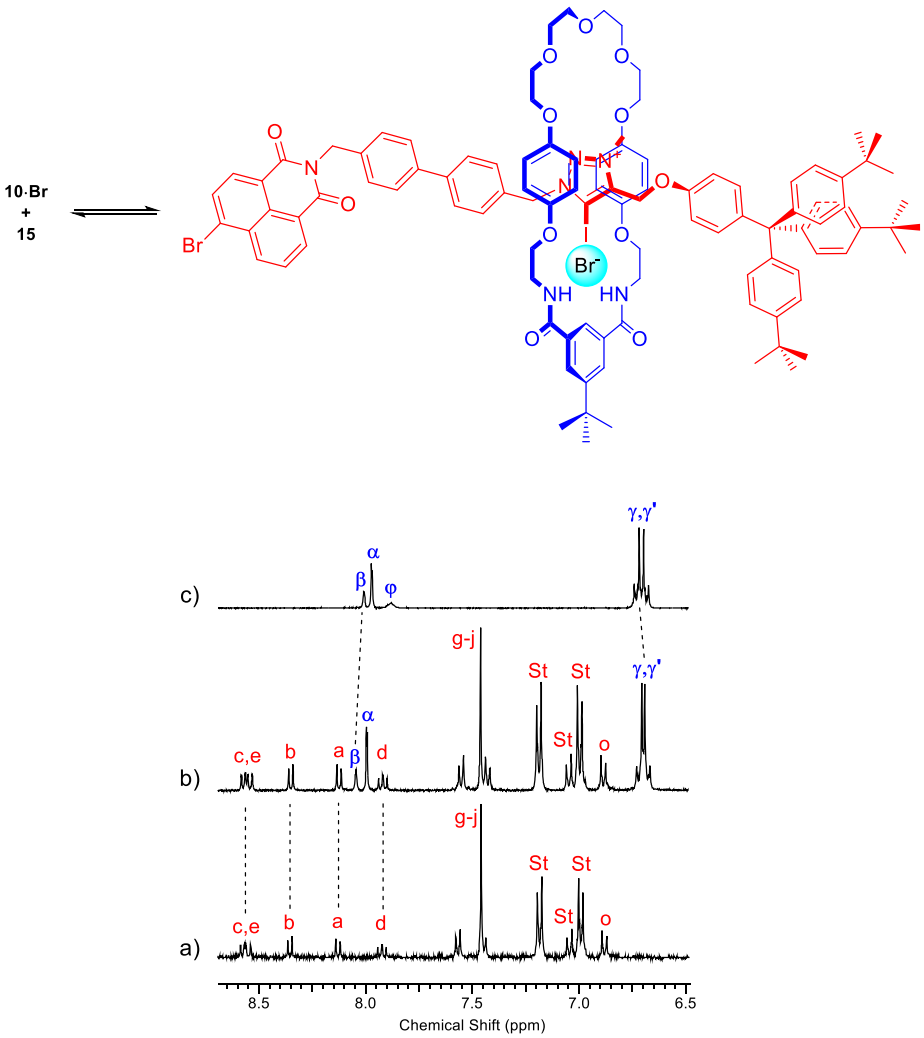


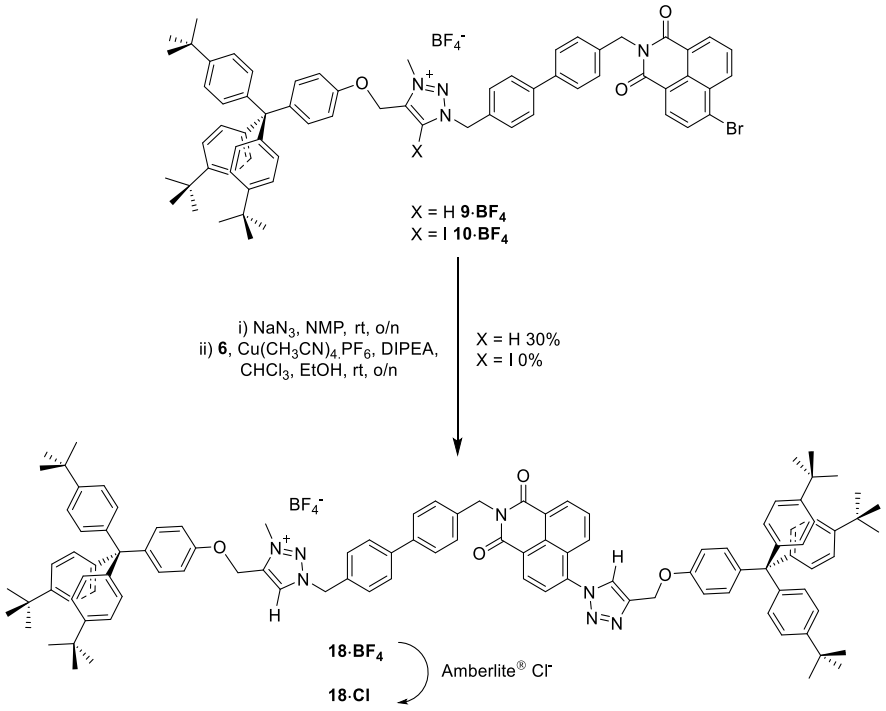
*Figure 2.7. Truncated ^{1}H NMR spectra of a) thread **10·Br**, b) 1.0 equivalent of thread **10·Br** and 1.0 equivalent of macrocycle **15** mixture and c) macrocycle **15** (acetone-d_6, 298 K, 500 MHz). The co-conformation of the interpenetrated [2]pseudorotaxane assembly formed in b) is also depicted.*

The analogous pseudorotaxane titration experiment with **15** and **10·Br** revealed a less pronounced upfield shift of the hydroquinone protons $H_{\gamma,\gamma'}$ ($\Delta\delta$ = 0.05 ppm) as might be expected because of the relatively smaller aromatic surface area of the iodo-triazolium motif in comparison to NI (Figure 2.7). Additionally, the NI protons $H_{a\text{-}e}$ are not perturbed giving further indication that the macrocycle does not interact with the NI terminus of the thread under these conditions. Instead the macrocycle most likely forms an interpenetrated assembly *via* the iodo-triazolium group because of convergent hydrogen bond formation from the isophthalamide cavity to the bromide counter anion, evidenced by the downfield shift of the internal macrocycle aromatic proton H_{β} (Figure 2.7).

The results of the ^{1}H NMR pseudorotaxane titration experiments indicated there was a marked difference in macrocycle affinity for each station of the thread which could be modulated by the nature of the counter anion, therefore providing the basis for a two-state molecular switch. Similar results were achieved when these experiments were repeated with the HB proto-triazolium-containing thread.

2.2.3. Synthesis of two-station NI-triazolium axle components

Encouraged by the results of the pseudorotaxane experiments, the stoppering of the mono-cationic threads **9·BF$_4$** and **10·BF$_4$** to form the respective XB and HB two-station target axles was attempted *via* the adaptation of a recent literature procedure (Scheme 2.5).[45] In this procedure the bromine atom of the NI group is replaced with an azide functionality and immediately reacted *in situ* with one equivalent of an alkyne derivative under conventional CuAAC 'proto-click' conditions. This 'one-pot' method was adopted following several unsuccessful attempts to isolate the azide intermediate, which was found to be unstable to decomposition *via* loss of $N_{2(g)}$, as evidenced by ESI mass spectrometry and thin layer chromatography (TLC) analysis.



*Scheme 2.5. Synthesis of two-station proto triazolium-NI axle **18·A** using a 'one-pot' procedure[45] and the attempted synthesis of an XB analogue via the same route.*

Compounds **9·BF$_4$** and **10·BF$_4$** were individually stirred with an excess of NaN_3 in 1-methyl-2-pyrrolidinone (NMP) in the absence of light and the substitution reaction was monitored by mass spectrometry to confirm formation of the desired azide intermediate. One equivalent of phenyl trityl alkyne stopper **6**, catalytic $Cu(CH_3CN)_4{\cdot}PF_6$ and DIPEA were added in 1:1 $CHCl_3$:EtOH and purification of the target axles was attempted using silica gel column chromatography (Scheme 2.5).

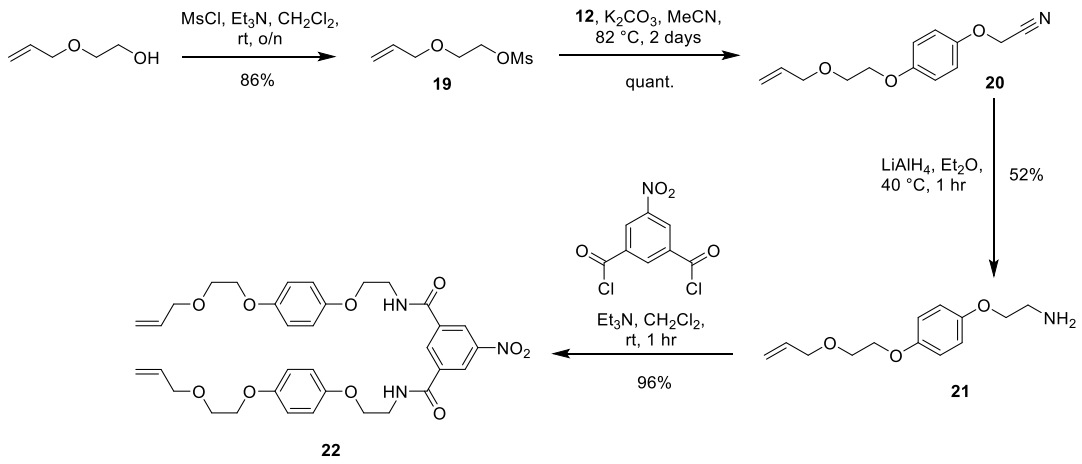
However, only the proto-triazolium-containing axle **18·BF$_4$** was isolated from either reaction flask (in a maximum yield of 30%) because in the procedure involving the XB thread (**10·BF$_4$**) the loss of the iodine atom from the iodo-triazolium motif was always observed by analysis of the crude reaction mixture using mass spectrometry. Therefore it was postulated that the polarised iodine atom was highly susceptible to cleavage and subsequent formation of a proto-triazolium heterocycle under the basic conditions of the CuAAC reaction step. Attempts were made to prevent this by repeating the procedure with **10·BF$_4$** in the absence of base or using $CuSO_4{\cdot}5H_2O$ with sodium ascorbate as a reducing agent but only starting materials were ever isolated. The possibility of performing the 'click' reaction

on the neutral XB compound **8** (in which the iodine might be less labile) was precluded due to the low probability of achieving the selective methylation of an iodo-triazole group in the presence of a proto-triazole.

Anion exchange of **18·BF$_4$** to the chloride salt **18·Cl** was achieved using an Amberlite® anion-exchange resin, in preparation for the attempted synthesis of a [2]rotaxane (Scheme 2.5).

2.2.4. Synthesis of HB two station NI-proto-triazolium [2]rotaxane

The macrocyclic wheel precursor compound **22** was prepared according to Scheme 2.6.[46]

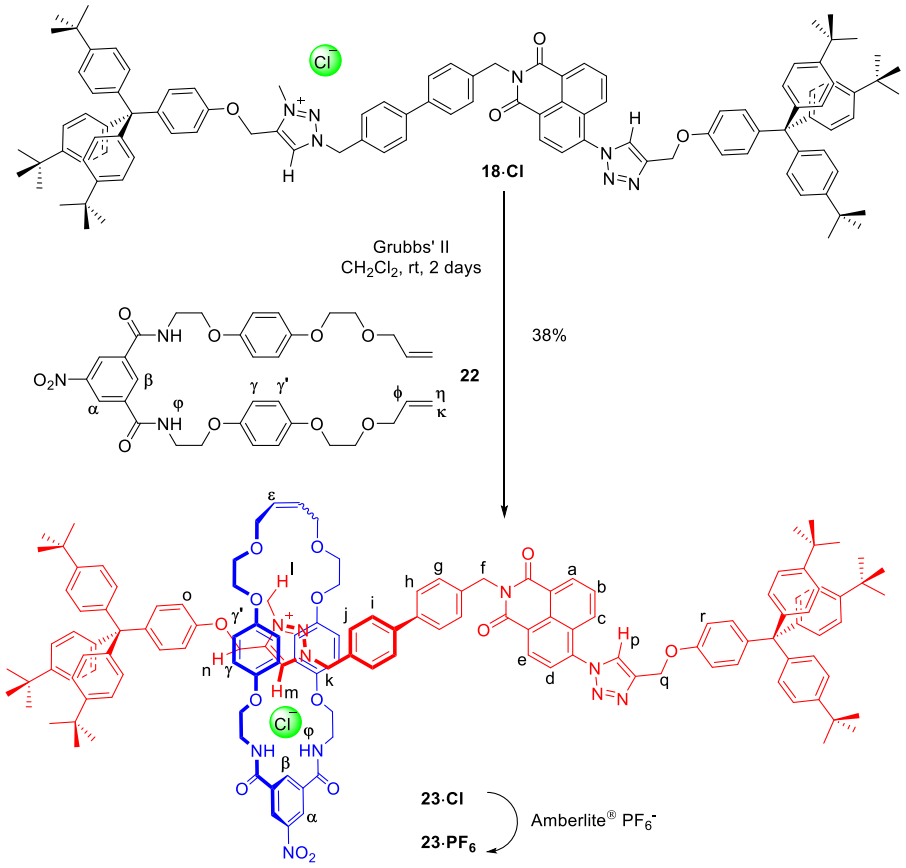


*Scheme 2.6. Synthesis of bis-vinyl-appended isophthalamide macrocycle precursor **22**.*[46]

The reaction of **12** with 2-(allyloxy)ethyl methanesulfonate (**19**),[47] prepared from the mesylation of 2-allyloxyethanol, afforded the vinyl-functionalised nitrile derivative **20**.[48] An excess of $LiAlH_4$ was used to reduce the nitrile functionality of **20** to form amine **21**,[48] which upon condensation with 5-nitroisophthaloyl dichloride gave macrocyclic precursor compound **22** in 96% yield following purification on silica gel.[46]

Chloride anion-templation was used to facilitate ring closing metathesis (RCM) of bis-vinyl-functionalised macrocyclic precursor **22** around the HB two-station axle component **18·Cl** using Grubbs' II catalyst in dry CH_2Cl_2 (Scheme 2.7). Purification using preparative silica thin-layer chromatography afforded the mono-cationic HB triazolium-NI [2]rotaxane **23·Cl** in 38% yield and this

was anion-exchanged to the hexafluorophosphate salt, **23·PF$_6$**. Both rotaxane salts were characterised by ^{1}H, ^{13}C and two-dimensional ^{1}H ROESY NMR spectroscopy and by mass spectrometry.



*Scheme 2.7. Synthesis of the two-station proto-triazolium-NI [2]rotaxane **23·A**.*

Truncated ^{1}H NMR spectra of rotaxane **23·Cl**, and macrocycle precursor **22**, in $CDCl_3$, are shown in Figure 2.8. The disappearance of the vinylic multiplet H_η and H_κ and the convergence of multiplet H_ϕ into a pseudo-singlet H_ε in the rotaxane spectrum are characteristic of successful cyclisation of the acyclic precursor.

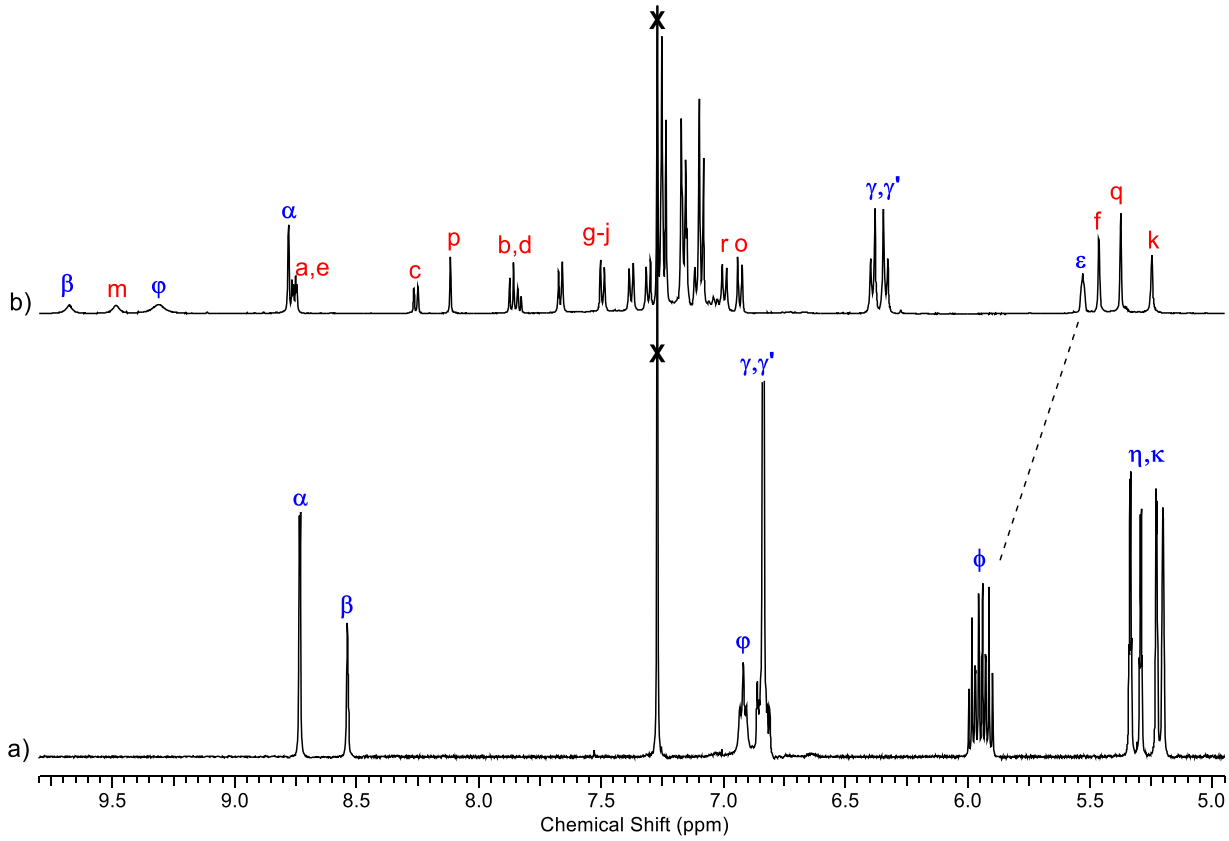


*Figure 2.8. Truncated ^{1}H NMR spectra of a) bis-vinyl-appended macrocycle precursor **22** and b) [2]rotaxane **23·Cl** ($CDCl_3$, 298 K, 400 MHz).*

2.2.5. ^{1}H NMR spectroscopic studies of anion-induced shuttling behaviour

In light of the successful isolation of the two-station HB triazolium-NI-containing [2]rotaxane, its ability to exhibit anion-induced shuttling, *via* changes in the relative position of the macrocycle component, was investigated using one- and two-dimensional ^{1}H NMR spectroscopy techniques.

To begin with, the predominant co-conformation of the HB triazolium-NI [2]rotaxane as the non-coordinating hexafluorophosphate salt **23·PF$_6$** in $CDCl_3$ was determined by comparison of the ^{1}H NMR spectrum with that of the axle component **18·PF$_6$** (Figure 2.9).

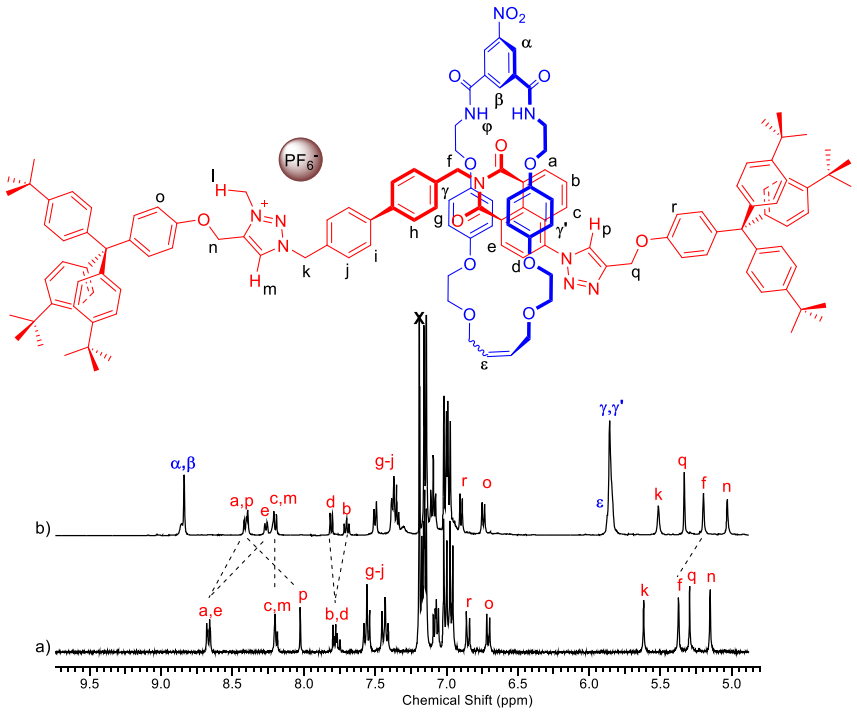


*Figure 2.9. Truncated ^{1}H NMR spectra of a) axle component **18·PF$_6$** and b) [2]rotaxane **23·PF$_6$** (CDCl$_3$, 298 K, 400 MHz). The predominant co-conformation of the [2]rotaxane is also depicted.*

The NI proton resonances H_a and H_e for the [2]rotaxane were found upfield relative to the axle component. This was indicative of strong aromatic donor–acceptor charge–transfer stacking interactions between the electron-rich macrocycle hydroquinone groups and the axle's electron-deficient NI motif. The same upfield shift was also seen for the NI station's neighbouring methylene group H_f, which was likely to be caused by the hydroquinone aromatic ring currents. By contrast, smaller shifts were observed for the proton resonances proximal to the proto-triazolium station, such as H_m and H_k.

The changes that occurred bore a strong resemblance to those observed from the pseudorotaxane study performed with thread **10·BF$_4$**. Therefore, the predominant co-conformation of [2]rotaxane **23·PF$_6$** is the one in which the macrocycle resides at the NI recognition site of the two-station axle as shown in Figure 2.9. This co-conformation assignment was strongly supported by a two-dimensional ^{1}H ROESY NMR spectrum of **23·PF$_6$** in CDCl$_3$ that revealed strong coupling between macrocycle protons

$H_{\gamma,\gamma'}$ or H_{ε} with the axle NI protons $H_{a\text{-}e}$, the adjacent methylene group H_f and triazole group H_p (Figure 2.10).

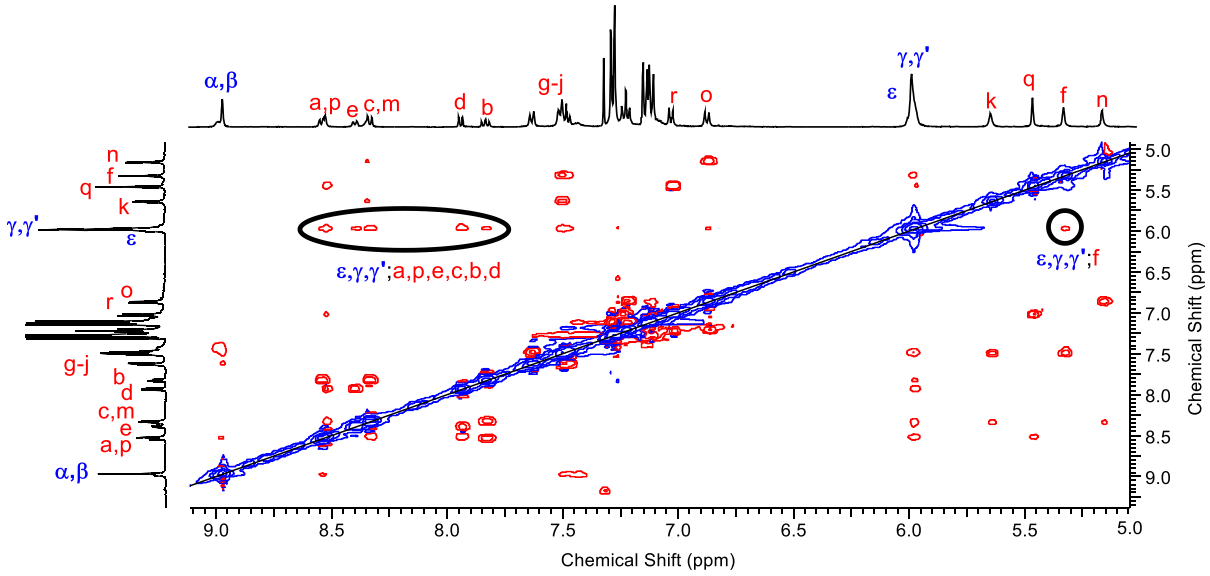


*Figure 2.10. Truncated ^1H–^1H ROESY NMR spectrum of [2]rotaxane **23·PF₆** with selected coupling interactions highlighted ($CDCl_3$, 298 K, 500 MHz).*

Comparisons between the ^1H NMR spectra of [2]rotaxane **23·Cl**, axle **18·Cl** and macrocycle precursor **22** in $CDCl_3$, were used to assign the chloride-induced co-conformational change (Figure 2.11).

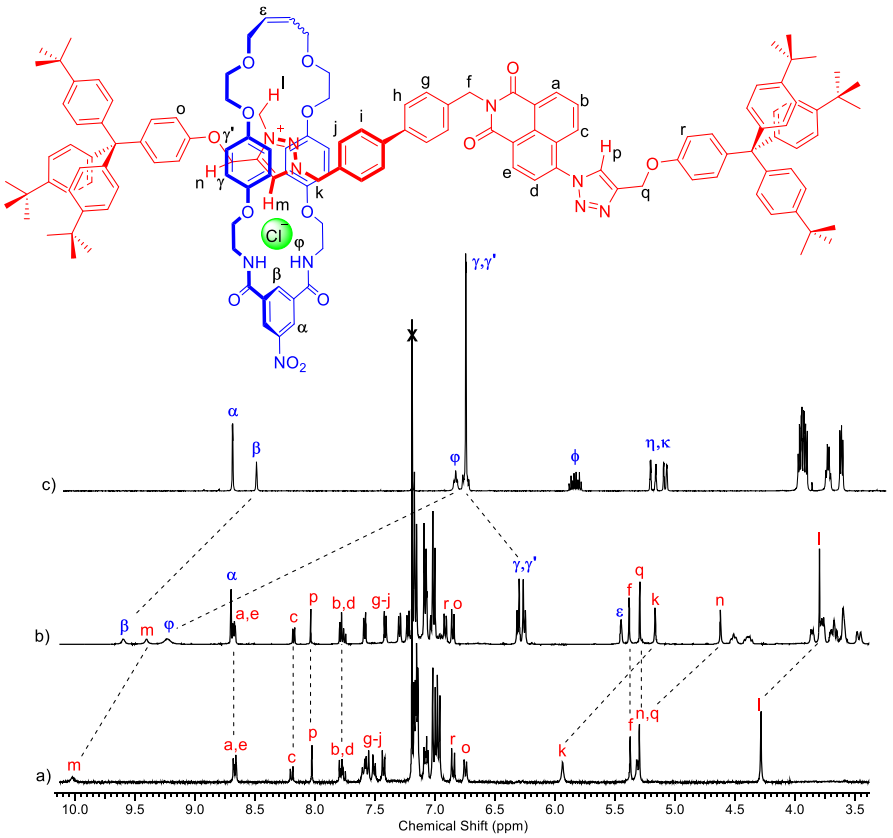


*Figure 2.11. Truncated ^{1}H NMR spectra of a) axle component **18·Cl**, b) [2]rotaxane **23·Cl** and c) macrocycle precursor **22** ($CDCl_3$, 298 K, 400 MHz). The dominant co-conformation of the [2]rotaxane is also depicted.*

Upon [2]rotaxane formation a significant upfield shift of the proto-triazolium proton H_m, and downfield shifts of the acidic protons H_β and H_φ corresponded to polarisation of the chloride anion away from the triazolium group of the axle and towards the hydrogen bond donors of the isophthalamide macrocycle. Shielding by hydroquinone aromatic ring currents also caused large upfield shifts of the *N*-methyl proto-triazolium group H_l and the methylene groups H_k and H_n proximal to the anion recognition site.

These chemical shift changes were indicative of macrocycle occupancy of the proto-triazolium station, facilitated by cooperative hydrogen bond donation from the triazolium and isophthalamide groups to the bound chloride anion from the orthogonal axle and macrocycle components. By contrast, no change in the NI protons $H_{a\text{-}e}$ or the station's proximal methylene groups H_f and H_q were observed, giving further evidence that the macrocycle resides almost exclusively at the proto-triazolium station

under these conditions as shown in Figure 2.11. This new co-conformation was supported by a two-dimensional ^{1}H ROESY NMR experiment in $CDCl_3$ that revealed, amongst other evidence, exclusive coupling interactions between axle protons H_l, H_n and H_k with macrocycle hydroquinone protons $H_{\gamma,\gamma'}$ (Figure 2.12). No interactions between $H_{\gamma,\gamma'}$ and the NI protons $H_{a\text{-}e}$ were observed.

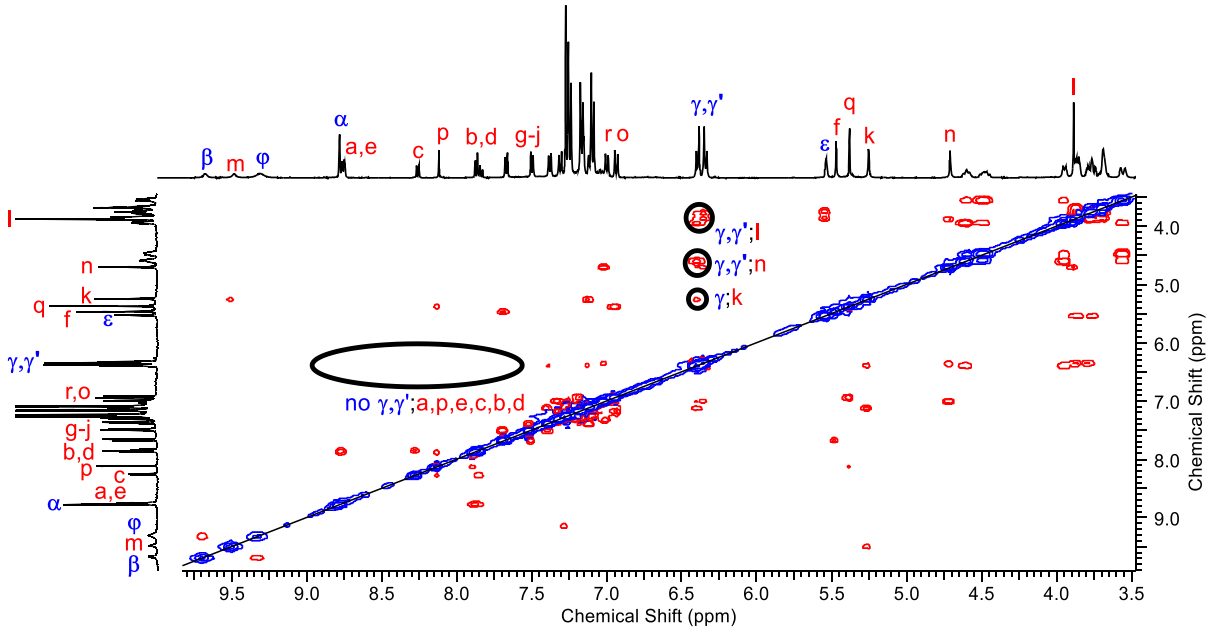


*Figure 2.12. Truncated ^{1}H–^{1}H ROESY NMR spectrum of [2]rotaxane **23·Cl** with selected coupling interactions highlighted ($CDCl_3$, 298 K, 500 MHz).*

Finally, a comparison of the ^{1}H NMR spectra of **23·Cl** with **23·PF$_6$** in $CDCl_3$ also supported anion-induced changes to the [2]rotaxane co-conformation (Figure 2.13). Upon exchange to the coordinating salt, large downfield shifts of the macrocycle hydroquinone protons $H_{\gamma,\gamma'}$ were revealed. These were indicative of weaker aromatic donor–acceptor charge–transfer interactions between the axle's proto-triazolium and macrocycle hydroquinone groups, relative to the previous aromatic stacking with the NI station. Likewise, downfield shifts of the NI station protons $H_{a\text{-}e}$ were also evident, leading to the conclusion that translational shuttling of the macrocyclic component from the NI station to the proto-triazolium site takes place, driven by anion recognition between the two components. Importantly, repeated Amberlite® exchanges between coordinating chloride and non-coordinating hexafluorphosphate salts produced the same ^{1}H NMR spectroscopic results indicating that the anion-induced shuttling process is fully reversible.

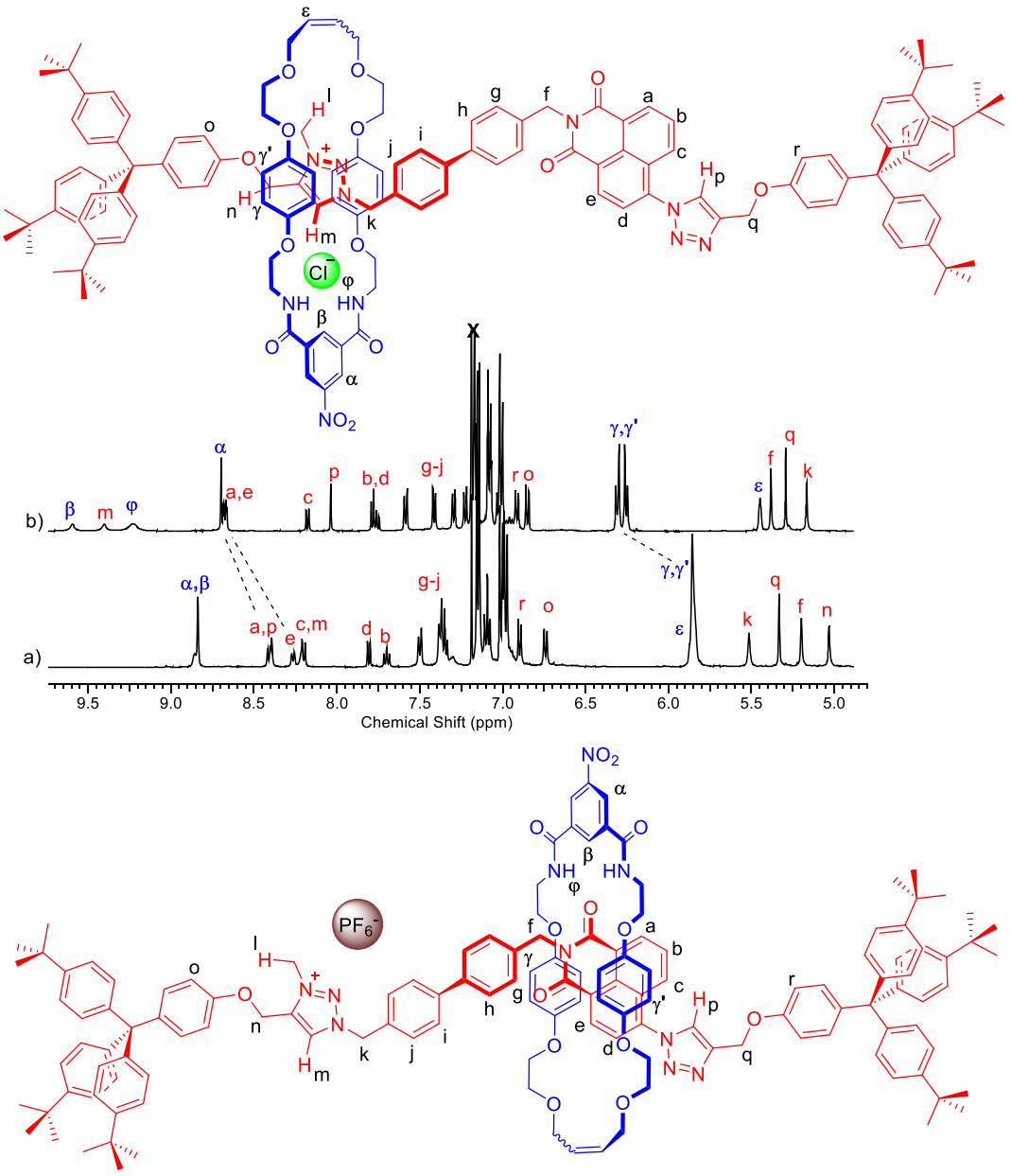


*Figure 2.13. Truncated ^{1}H NMR spectra of a) [2]rotaxane **23·PF$_6$** and b) [2]rotaxane **23·Cl** ($CDCl_3$, 298 K, 400 MHz). The dominant co-conformations of the [2]rotaxanes **23·PF$_6$** and **23·Cl** are also depicted.*

The degree of anion-induced switching was quantified by estimating the percentage of macrocycle occupancy at each station in the presence of either counter anion (Figure 2.14). This was achieved using ^{1}H NMR spectroscopic experiments that monitored changes in the chemical shift of the [2]rotaxane's *N*-methyl proto-triazolium protons, H_l. Full details of the method used to perform these calculations are described in Section 2.3.7 and in the Appendix.

As expected from previous one- and two-dimensional ^{1}H NMR experiments, a 100% occupancy of the triazolium station by the macrocycle was estimated for [2]rotaxane **23·Cl** in $CDCl_3$ solution. Upon exchange to the non-coordinating hexafluorophosphate salt, macrocycle occupancy of the NI station was estimated to be 78%, affording this bistable [2]rotaxane system a significant positional integrity between the stations in each state. Therefore, it was concluded that the bistable NI triazolium [2]rotaxane **23·PF$_6$** operates as a highly effective translational switch, stimulated by the recognition of chloride in $CDCl_3$ solution.

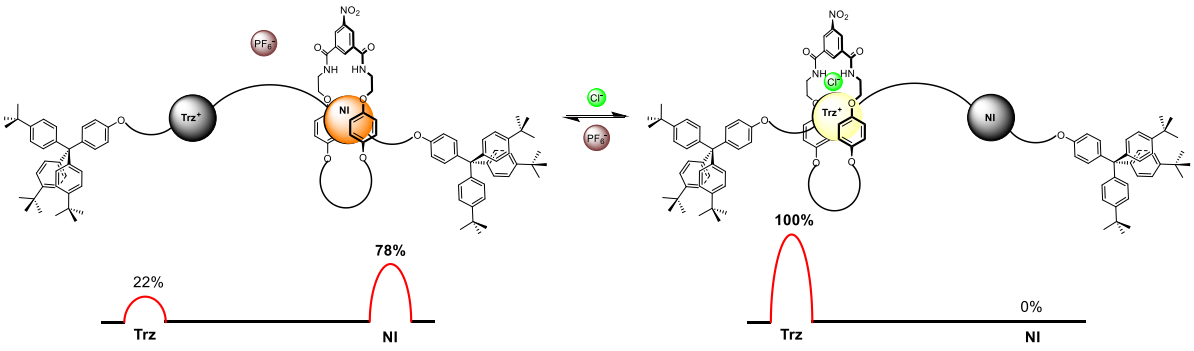


*Figure 2.14. The estimated macrocycle-station occupancies of the bistable [2]rotaxane **23·PF$_6$** and **23·Cl** as determined by ^{1}H NMR spectroscopy in $CDCl_3$ solution. Trz$^+$ = proto-triazolium.*

2.2.6. ^{1}H NMR spectroscopic studies of solvent effects on anion-induced shuttling behaviour

The work of Cubberley and Iverson on the solvent dependence of aromatic stacking in the dimeric 1,5-dialkoxynaphthalene–naphthalene diimide system shown in Figure 2.15 revealed that the association between components in polar, protic solvents is primarily driven by solvophobic interactions, and so the interactions become stronger with increasing solvent polarity.[49] It was hoped that this phenomenon could be exploited to increase macrocycle occupancy of the NI station in the hexafluorophosphate salt of [2]rotaxane **23·PF$_6$**, thereby increasing the positional integrity between stations in the absence of a coordinating anion and enhancing the effectiveness of the molecular switch.

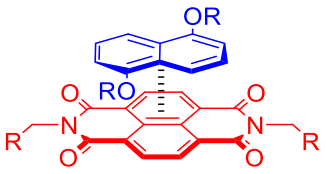


Figure 2.15. Aromatic stacking occurring in the dimeric 1,5-dialkoxynaphthalene–naphthalene diimide system studied by Cubberley and Iverson, R = polyethylene glycol chain.[49]

The ^{1}H NMR spectra of [2]rotaxane **23·PF$_6$** and axle component **18·PF$_6$** were recorded in the polar, protic solvent mixture 1:1 $CDCl_3$:CD_3OD (Figure 2.16).

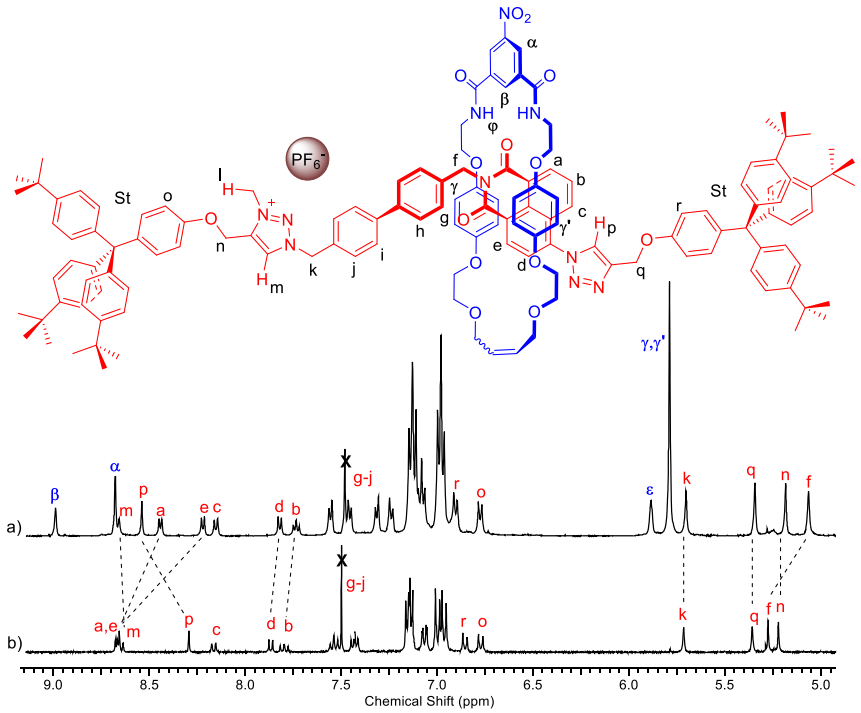


*Figure 2.16. Truncated ^{1}H NMR spectra of a) axle component **18·PF$_6$** and b) [2]rotaxane **23·PF$_6$** (1:1 $CDCl_3$:CD_3OD, 298 K, 400 MHz). The dominant co-conformation of the [2]rotaxane is also depicted.*

Interestingly, only signals corresponding to protons of the NI station $H_{a\text{-}e}$ were shifted in the [2]rotaxane relative to the axle, implying that in this solvent the macrocycle almost exclusively occupies the NI recognition site. A two-dimensional ^{1}H ROESY NMR spectrum of **23·PF$_6$** in these solvent conditions revealed strong through-space coupling interactions between protons diagnostic of the NI station $H_{a\text{-}e}$ and macrocycle hydroquinone protons $H_{\gamma,\gamma'}$ that strongly supported this as the predominant co-conformation (Figure 2.17).

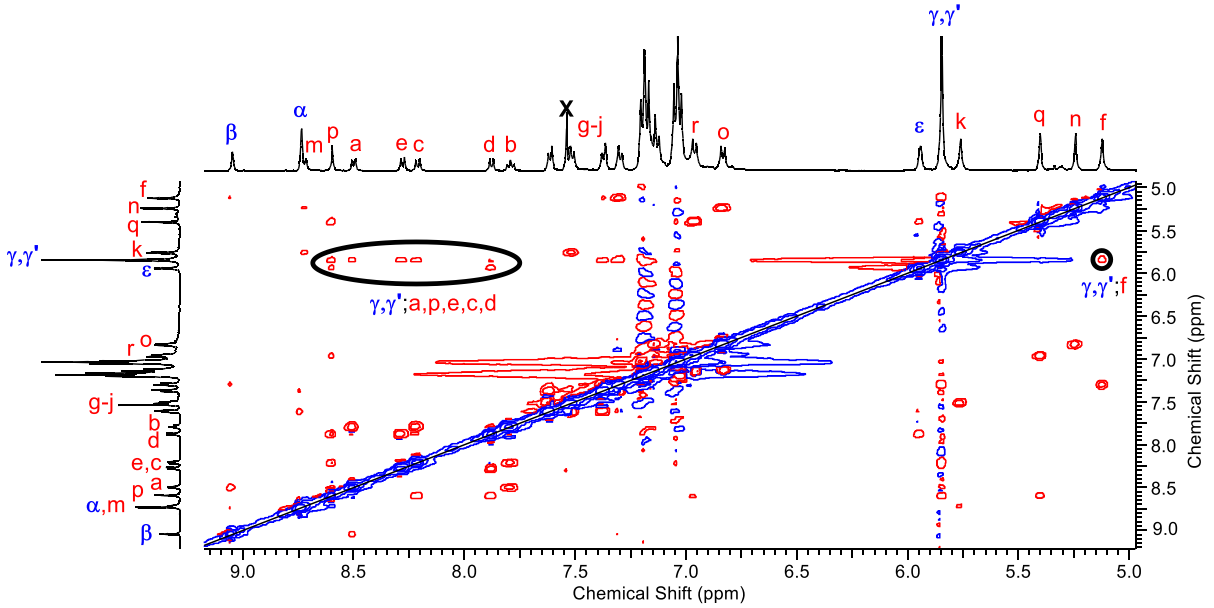


*Figure 2.17. Truncated ^{1}H–^{1}H ROESY NMR spectrum of [2]rotaxane **23·PF$_6$** with selected coupling interactions highlighted (1:1 $CDCl_3$:CD_3OD, 298 K, 500 MHz).*

Analogous comparisons between the ^{1}H NMR spectra of [2]rotaxane **23·Cl** with axle **18·Cl** in 1:1 $CDCl_3$:CD_3OD revealed only small changes in the chemical shift of protons associated with the proto-triazolium station (H_l and H_m). Likewise, contrasting the ^{1}H NMR spectra of **23·PF$_6$** and **23·Cl** in this solvent mixture also revealed slight shifts in the aromatic protons of the hydroquinone ($H_{\gamma,\gamma'}$) and NI functionalities, $H_{a\text{-}e}$ (Figure 2.18). This was in stark contrast to the large shifts observed in $CDCl_3$ (Figure 2.13).

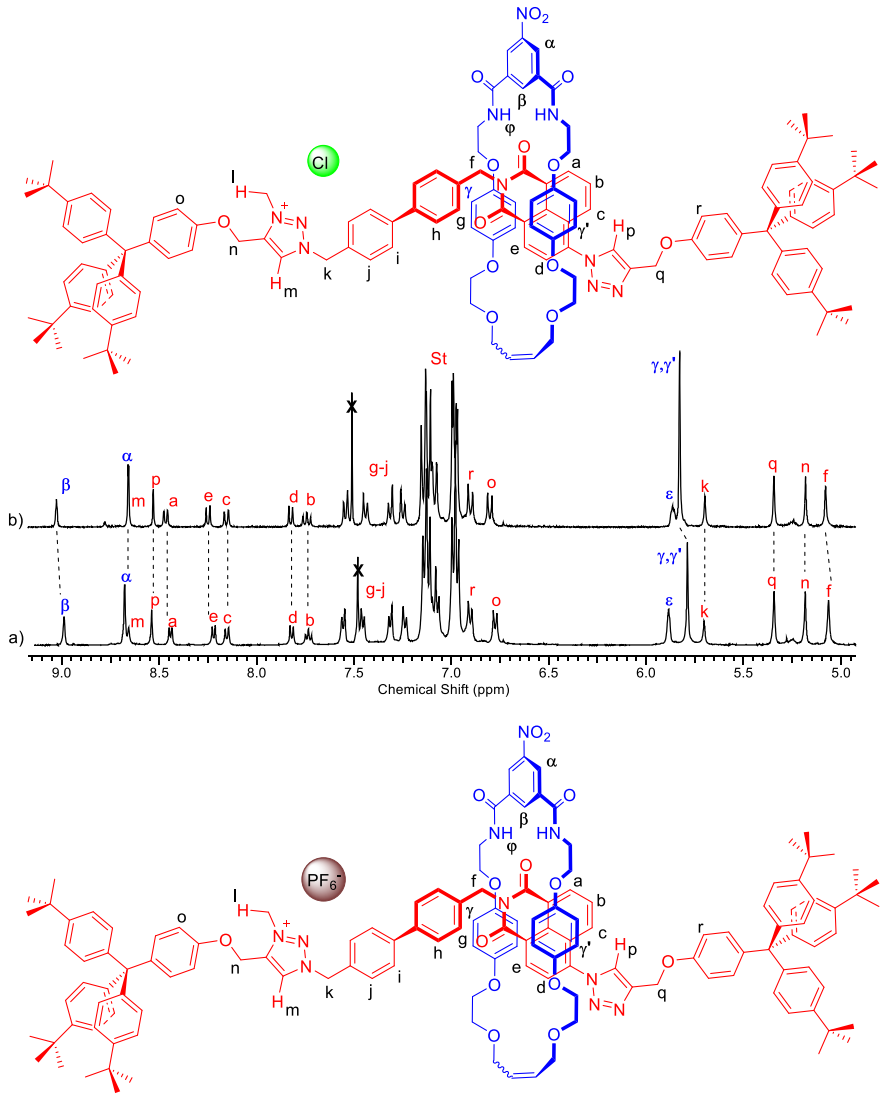


*Figure 2.18. Truncated ^{1}H NMR spectra of a) [2]rotaxane **23·PF$_6$** and b) [2]rotaxane **23·Cl** (1:1 $CDCl_3$:CD_3OD, 298 K, 400 MHz). The dominant co-conformations of the [2]rotaxanes **23·PF$_6$** and **23·Cl** are also depicted.*

This suggested that the co-conformation of the [2]rotaxane was almost identical for each counter anion; namely a large occupation of the NI station (Figure 2.18). A quantification of the degree of switching in this solvent mixture estimated that triazolium station occupancy only increases by 7% upon anion-exchange from hexafluorophosphate to the chloride salt (Figure 2.19).

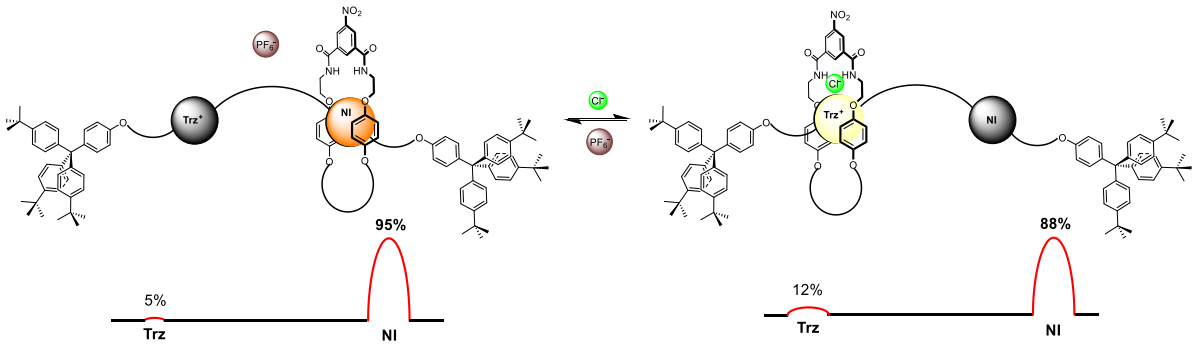


Figure 2.19. The estimated macrocycle-station occupancies of the bistable [2]rotaxanes ***23·PF$_6$*** *and* ***23·Cl*** *as determined by ^{1}H NMR spectroscopy in 1:1 $CDCl_3$:CD_3OD solution. Trz^+ = proto-triazolium.*

The low occupancy of the anion recognition site in **23·Cl** is partly attributed to the weak halide binding exhibited by the [2]rotaxane in the highly competitive polar, protic solvent mixture. The stimulus of anion recognition therefore failed to provide a thermodynamic driving force strong enough to facilitate macrocycle shuttling from NI to the proto-triazolium station. Furthermore, under these solvent conditions, stronger aromatic stacking interactions between macrocycle and NI may occur because of an increased solvophobic contribution to their association. Therefore, a larger enthalpic and/or entropic penalty must be overcome to enable translational motion of the macrocycle to occur.

2.2.7. Summary

A bistable [2]rotaxane containing an HB proto-triazolium anion recognition site and an electron-deficient NI station was synthesised by chloride-templation. The ability of this [2]rotaxane to undergo large amplitude anion-induced molecular motion in $CDCl_3$ solution was demonstrated using one- and two-dimensional ^{1}H NMR spectroscopy and quantified *via* estimations of the percentage occupancy of each station in each state. As the hexafluorophosphate salt, NI was the predominant station occupied by the macrocycle. By contrast, the complete association of the macrocycle at the proto-triazolium station in the chloride salt was driven by cooperative HB donation between the orthogonal axle and macrocycle components to the chloride species. Interestingly, in the more competitive solvent mixture of 1:1 $CDCl_3$:CD_3OD the strength of these anion–receptor interactions were significantly weakened to

the point that they could not outcompete the strong solvophobic-driven aromatic stacking interactions occurring between macrocycle and NI station preventing anion-induced co-conformational change.

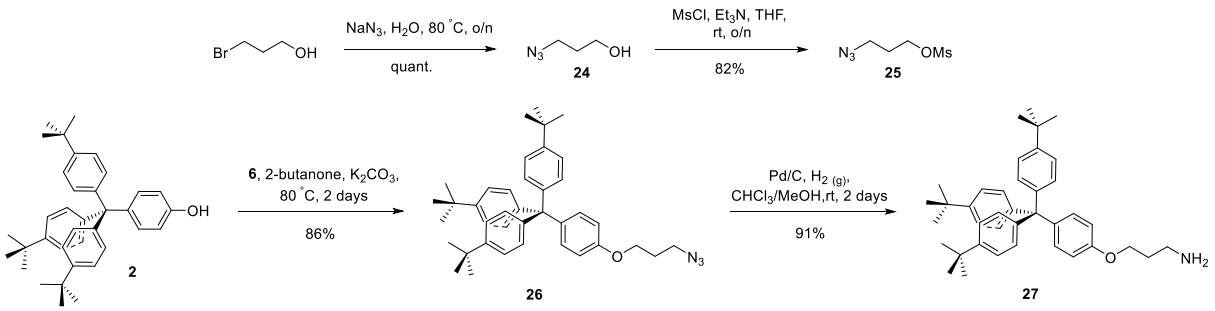
This suggested the anion binding strength of the proto-triazolium station needed to be increased if a two-station rotaxane switch of this design was to operate effectively in a competitive solvent medium. Attempts to achieve this *via* the incorporation of an XB donor group as an anion recognition motif are discussed in the next section.

2.3. Two-station NDI-iodo-/proto-triazolium [2]rotaxanes*

The previous unsuccessful attempts to synthesise an XB analogue of rotaxane **23·A** (A = anion), necessitated modifications to the two-station axle design, in which the NI station was replaced with a comparable electron-deficient aromatic motif, NDI. This section begins by describing the preparation of a two station XB iodo-triazolium–NDI axle component, a HB proto-triazolium-containing analogue and the incorporation of these axles into bistable [2]rotaxane interlocked host structures. This is followed by investigations into the dynamic behaviour of these systems upon changing the nature of the counter anion and the solvent.

2.3.1. Synthesis of two-station NDI-XB/HB-triazolium axle components

The synthesis of the novel NDI-based two-station axle components required a phenyl trityl stopper derivative appended with a propyl amine functionality.

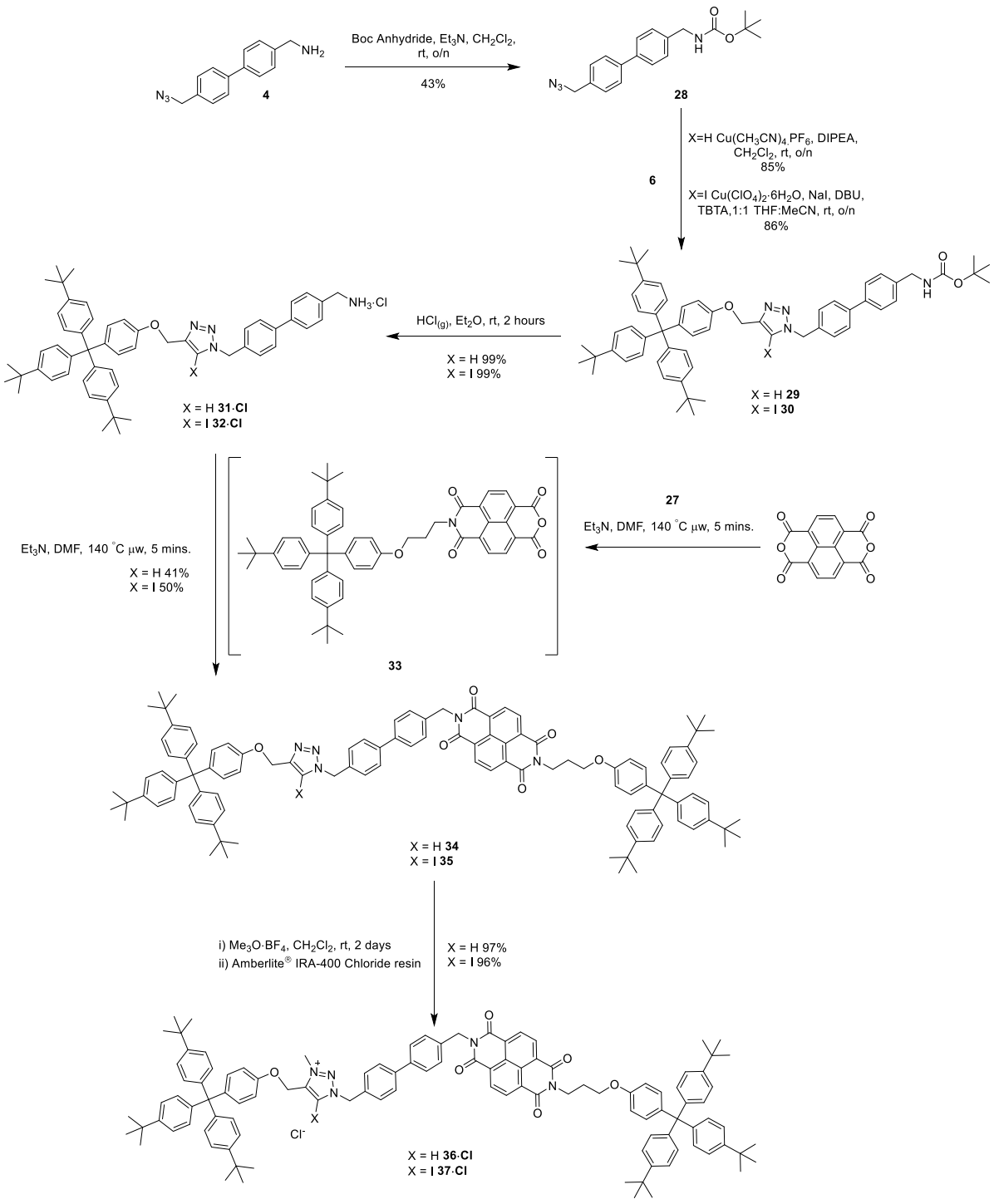


*Scheme 2.8. Syntheses of azide- and amine-functionalised phenyl trityl stopper derivatives **26** and **27**.*[30,50]

* The work in the following section was published as an edge article in the journal Chemical Science: T. A. Barendt, S. Robinson, P. D. Beer, *Chem. Sci.*, 2016. DOI: 10.1039/C6SC00783J

Azido propylmesylate **25**[30] was prepared from 3-bromo-1-propanol in two steps from reactions with NaN_3 and methanesulfonyl chloride. The synthesis of phenyl trityl propyl azide **26** was then achieved by the alkylation of **2** with **25** by heating overnight in 2-butanone with K_2CO_3 whilst stopper-amine **27**,[50] was prepared by the hydrogenation of **26** with catalytic Pd/C (Scheme 2.8).

In light of the apparent instability of the iodo-triazolium motif under CuAAC reaction conditions the synthetic route chosen for the axles required that methylation of the XB triazole group be left until the final step. Therefore the preparation of the two-station HB/XB-triazolium and NDI-containing axle components **36·Cl** and **37·Cl** was achieved *via* the pathways outlined in Scheme 2.9. This began with the construction of two mono-stoppered amine-appended derivatives, containing HB or XB triazole groups which were subsequently coupled to the anhydride terminus of a mono-stoppered anhydride intermediate.



*Scheme 2.9. Synthesis of the two-station HB/XB triazolium-NDI axles **36·Cl** and **37·Cl**.*

Initially, Boc protection[51] of mono amine **4** was performed to inhibit interference from this functional group in the subsequent CuAAC 'click' reaction. The reaction of Boc azide **28** and a small excess of alkyne-functionalised phenyl trityl stopper **6** under appropriate CuAAC conditions resulted in formation of either the proto- or iodo-triazole-containing derivatives, **29** and **30** respectively, in high

yields. Removal of the Boc protecting group was achieved by bubbling $HCl_{(g)}$ through a solution of **29** or **30** in dry Et_2O giving the HB and XB amine-containing axle precursors as their hydrochloride salts **31·Cl** and **32·Cl**.[51]

Synthesis of the XB/HB-triazole-containing axle required the condensation of one equivalent of each mono-stoppered amine (**27** and **31·Cl**/**32·Cl**) with 1,4,5,8-naphthalenetetracarboxylic dianhydride. Traditionally the asymmetric-functionalisation of 1,4,5,8-naphthalenetetracarboxylic dianhydride involves multiple steps because of the necessity for protection and deprotection of the anhydride termini,[52] whilst a statistical approach typically results in low yields of the desired NDI product.[53] However, Sanders and Pantoş have reported a method in which asymmetrical NDI derivatives may be prepared in high yields *via* a one-pot stepwise process using microwave dielectric heating.[54] The authors proposed that the success of this procedure is a consequence of the short exposures to high reaction temperatures that favour formation of the mono-substituted NDI products. An adaptation of this literature procedure was used for the XB/HB-triazole axle syntheses.

An equimolar mixture of amine **27**, 1,4,5,8-naphthalenetetracarboxylic dianhydride and Et_3N were heated at 140 ˚C under microwave irradiation for five minutes in dry DMF. Formation of the mono substituted anhydride intermediate **33** was assumed to be quantitative and after the subsequent addition of amine **31·Cl** or **32·Cl** and base to the same pot, the reaction was heated under microwave irradiation for a further five minutes at 140 ˚C. Following purification of the crude mixture by silica gel column chromatography, the asymmetric bis-stoppered NDI HB proto- and XB iodo-triazole-containing axles **34** and **35** were isolated in reasonable yields. Methylation of axles **34** and **35** with $Me_3O{\cdot}BF_4$ in dry CH_2Cl_2 afforded the cationic two-station axle components **36·BF$_4$** and **37·BF$_4$**. Both axles were exchanged to their chloride salts by the use of Amberlite® chloride-loaded resin in preparation for anion-templated [2]rotaxane syntheses.

Interestingly the ^{1}H NMR spectrum of **37·Cl** (and to a lesser extent **35**) suggested that this XB axle exhibits two conformations in solution that are in slow exchange on the NMR timescale, producing two

sets of peaks for the iodo-triazolium group's diagnostic protons; namely the methylene groups H_k and H_m, the methyl group H_l and aromatic stopper protons H_n (Figure 2.20). Since this was not found for the HB proto-triazolium analogue **36·Cl**, it is plausible that the large iodine atom restricts rotation around the neighbouring methylene groups H_k and H_m resulting in conformational locking. Strong association between the iodo-triazolium group and the counter anion by XB was discounted because the ^{1}H NMR spectrum was not simplified in the more competitive solvent mixture of 1:1 $CDCl_3$:CD_3OD.

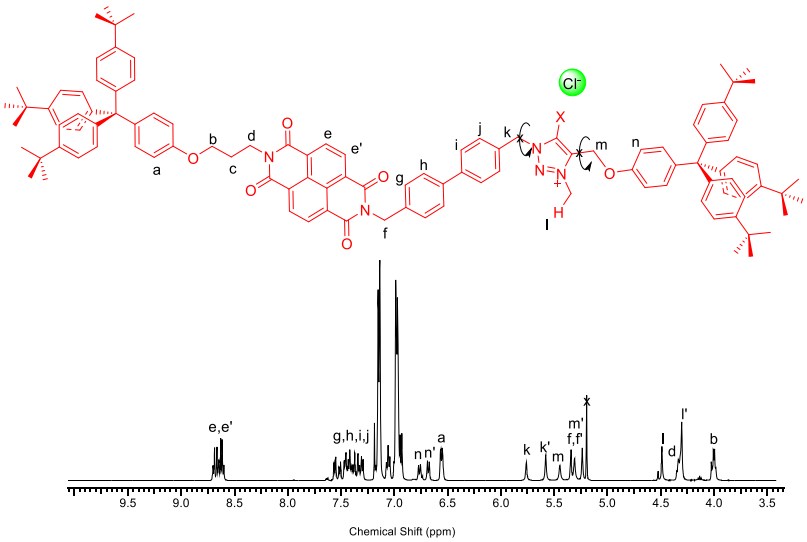
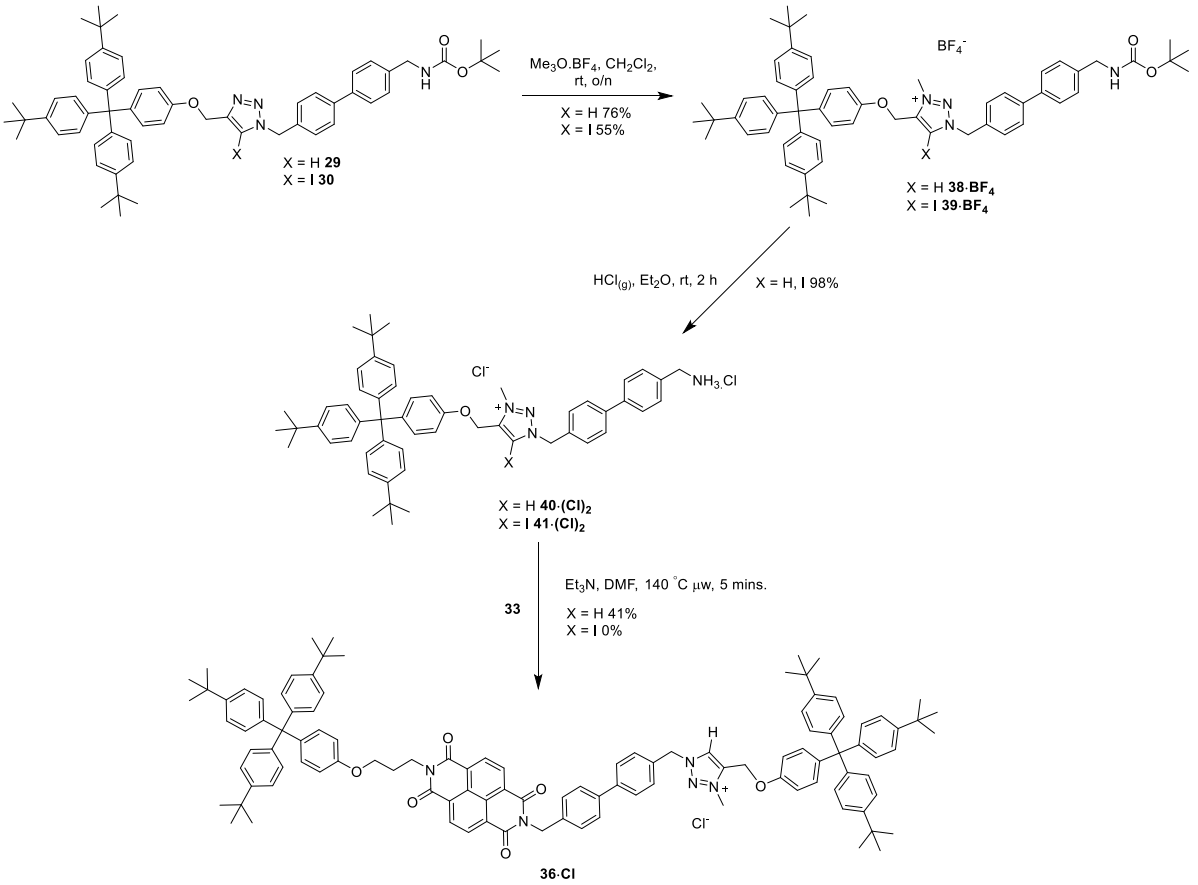


*Figure 2.20. Truncated ^{1}H NMR spectrum of the XB two-station axle **37·Cl** ($CDCl_3$, 298 K, 400 MHz). Potential restricted rotations around the iodo-triazolium's neighbouring methylene groups H_k and H_m are indicated on the structure.*

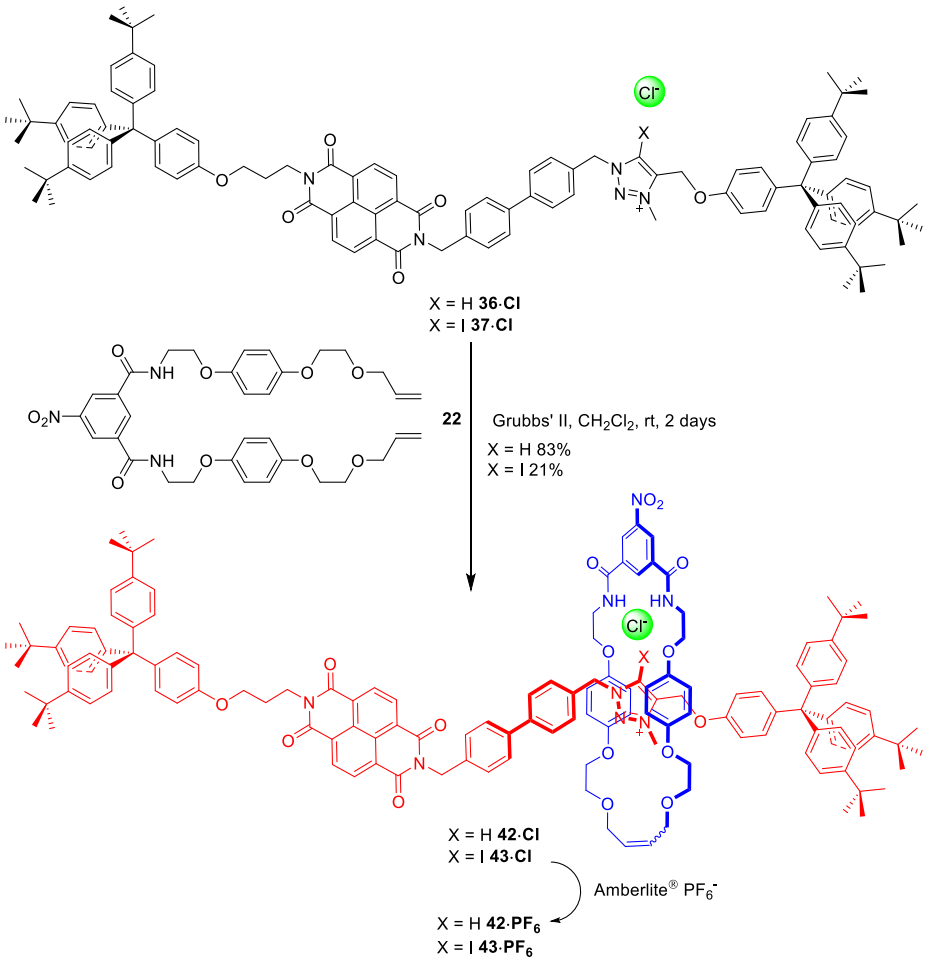
As a final point, Scheme 2.10 demonstrates how it was possible to synthesise the HB axle **36·Cl** directly from a proto-triazolium-containing amine **40·(Cl)$_2$** upon coupling of this species to the mono-stoppered NDI intermediate **33** under microwave irradiation. However, this synthetic route resulted in a lower overall yield of the HB axle. Interestingly, this procedure also gave **36·Cl** when the analogous XB iodo-triazolium-containing amine, **41·(Cl)$_2$**, was used. This was ascribed to the same intolerance of the iodo-triazolium group to high temperatures and basic conditions, observed in previous XB iodo-triazolium-NI axle synthetic attempts.



*Scheme 2.10. Synthesis of two-station proto-triazolium-NI axle **36·Cl** via an alternative route. This procedure was not successful for the XB analogue **37·Cl**.*

2.3.2. Synthesis of two-station NDI-XB/HB-triazolium [2]rotaxanes

The preparation of the two-station HB/XB-triazolium-NDI [2]rotaxanes **42·Cl** and **43·Cl** was achieved *via* clipping of the bis-vinyl-appended macrocycle precursor **22** in the presence of Grubbs' II catalyst around the chloride salt of the corresponding axle (Scheme 2.11). Preparative silica thin-layer chromatography purification afforded the desired HB and XB [2]rotaxanes **42·Cl** and **43·Cl** in yields of 83% and 21% respectively. The [2]rotaxanes were characterised as their chloride salts by ^{1}H, ^{13}C and two-dimensional ^{1}H ROESY NMR spectroscopy and by high resolution mass spectrometry and further characterised as their hexafluorophosphate salts after anion exchange using an Amberlite® exchange resin (Scheme 2.11).



*Scheme 2.11. Synthesis of the two-station HB/XB triazolium-NDI [2]rotaxanes **42·A** and **43·A**.*

2.3.3. ^{1}H NMR spectroscopic studies of anion-induced shuttling behaviour

The successful synthesis of two-station HB/XB-triazolium-NDI [2]rotaxanes **42·A** and **43·A** allowed detailed investigations into their dynamic behaviour to be performed, importantly including an in-depth analysis of how the contrasting recognition properties of the HB and XB [2]rotaxanes would influence their ability to exhibit anion-induced shuttling of the macrocyclic wheel.

The predominant co-conformations of the HB- and XB-triazolium NDI [2]rotaxanes as their non-coordinating hexafluorophosphate salts **42·PF$_6$** and **43·PF$_6$** in $CDCl_3$ were determined by a comparison of their ^{1}H NMR spectra with those of their respective axle components **36·PF$_6$** and **37·PF$_6$** (Figure 2.21).

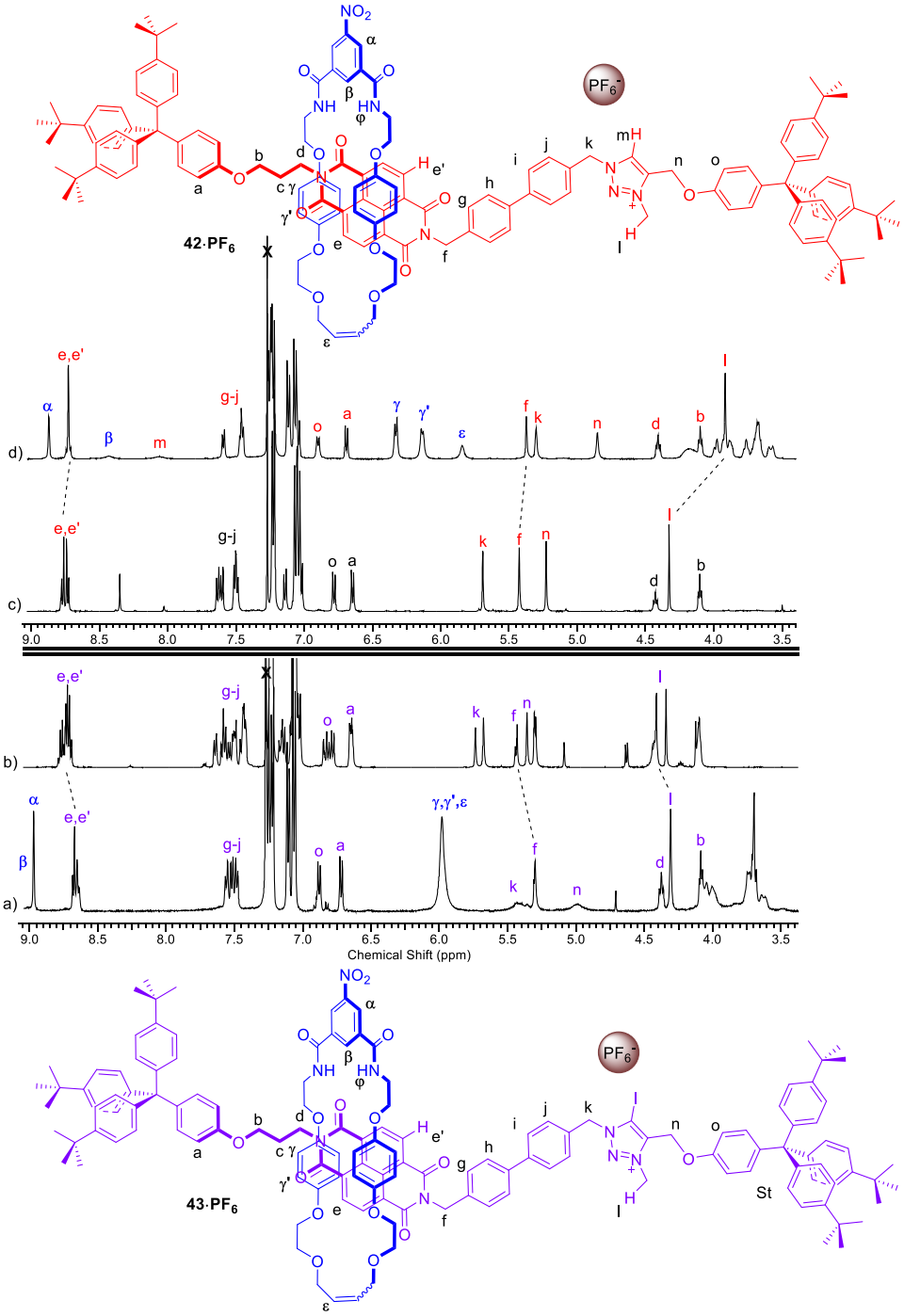


*Figure 2.21. Truncated ^{1}H NMR spectra of a) XB [2]rotaxane **43·PF$_6$**, b) XB axle component **37·PF$_6$**, c) HB axle component **36·PF$_6$** and d) HB [2]rotaxane **42·PF$_6$** ($CDCl_3$, 298 K, 400 MHz). The predicted co-conformations of these HB and XB [2]rotaxanes as their hexafluorophosphate salts are also shown.*

This revealed that in both [2]rotaxanes, the resonances associated with the NDI protons ($H_{e,e'}$) were shifted upfield relative to their position in the axle component which is diagnostic of strong aromatic donor–acceptor charge–transfer aromatic stacking interactions between the axle's electron-deficient

NDI motif and the macrocycle hydroquinone groups. A similar change in chemical shift of the NDI's neighbouring methylene group H_f was also observed, providing further indication of an interaction between the macrocycle and this station in the absence of a coordinating anion, as shown in Figure 2.21. The ^{1}H NMR spectroscopic evidence is similar to that observed with the NI-containing rotaxane **23·PF$_6$** described in the previous section. However, unlike the NI rotaxane, the ^{1}H NMR spectra in Figure 2.21 also showed that the protons associated with the XB/HB-triazolium stations (H_l, H_k and H_n) are significantly shifted, suggesting relatively poorer positional integrity in [2]rotaxanes **42·PF$_6$** and **43·PF$_6$**. A two-dimensional ^{1}H ROESY NMR spectrum of each system confirmed that in addition to strong coupling interactions between macrocycle hydroquinone protons $H_{\gamma,\gamma'}$ and NDI protons $H_{e,e'}$, there were also interactions between $H_{\gamma,\gamma'}$ and the *N*-methyl triazolium protons H_l (Figure 2.22 and Figure 2.23). Therefore it was predicted that the macrocycle occupancy of the NDI station in **42·PF$_6$** and **43·PF$_6$** would not be as high as that found for the NI rotaxane in $CDCl_3$.

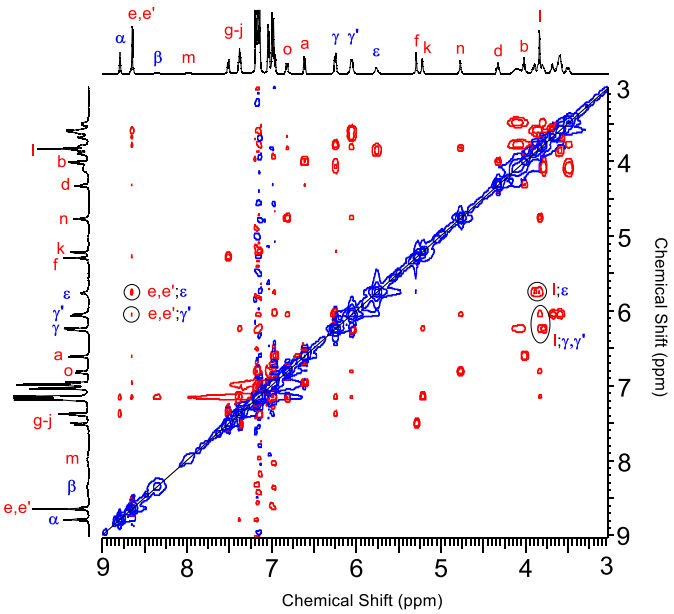


*Figure 2.22. Truncated ^{1}H–^{1}H ROESY NMR spectrum of HB [2]rotaxane **42·PF$_6$** with selected coupling interactions highlighted ($CDCl_3$, 298 K, 500 MHz).*

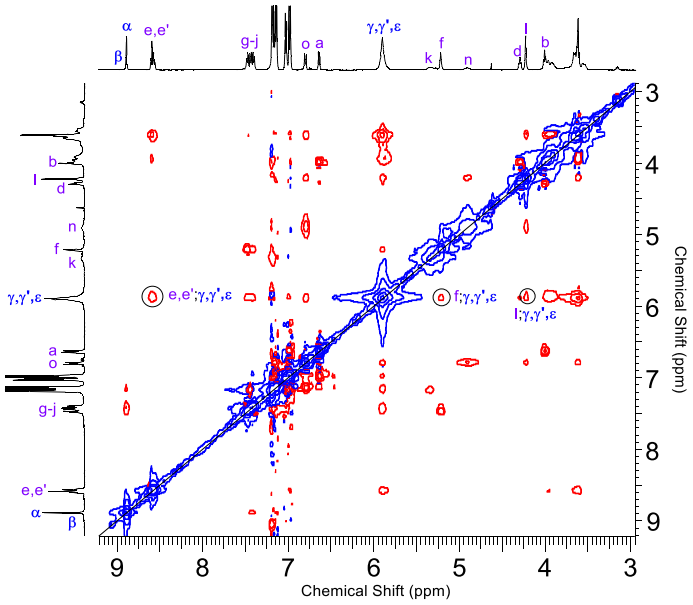


*Figure 2.23. Truncated ^{1}H–^{1}H ROESY NMR spectrum of XB [2]rotaxane **43·PF$_6$** with selected coupling interactions highlighted ($CDCl_3$, 298 K, 500 MHz).*

A comparison of the ^{1}H NMR spectra of the axle components **36·Cl** and **37·Cl** with their respective [2]rotaxanes **42·Cl** and **43·Cl**, in $CDCl_3$, was used to determine the dominant co-conformation of these interlocked structures as their chloride salts (Figure 2.24).

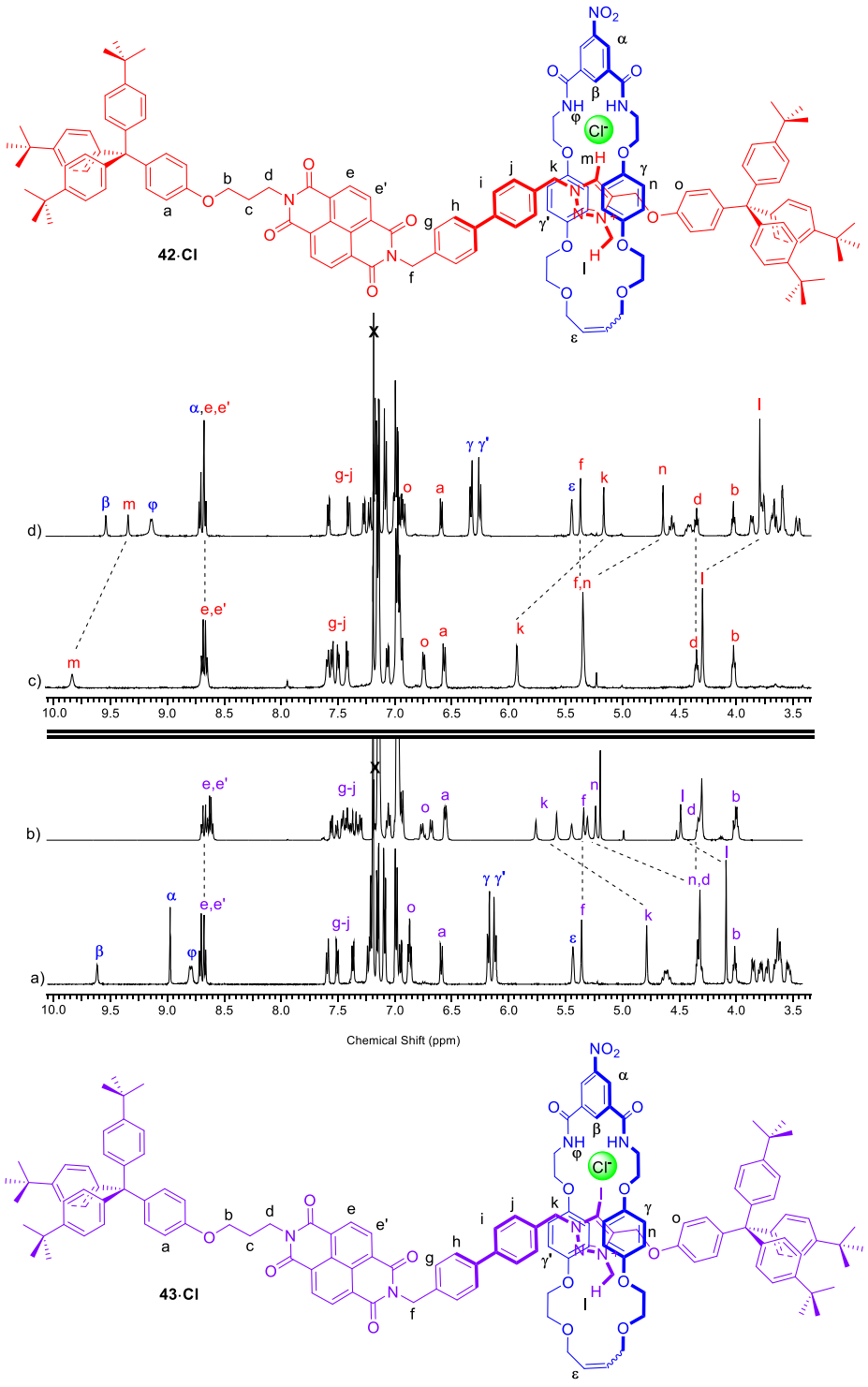


*Figure 2.24. Truncated ^{1}H NMR spectra of a) XB [2]rotaxane **43·Cl**, b) XB axle component **37·Cl**, c) HB axle component **36·Cl** and d) HB [2]rotaxane **42·Cl** ($CDCl_3$, 298 K, 400 MHz). The predicted co-conformations of these HB and XB [2]rotaxanes as their chloride salts are also shown.*

Large upfield shifts of proton resonances associated with the *N*-methyl triazolium group (H_l) and methylene groups neighbouring the HB/XB-triazolium station (H_k and H_n) were observed on comparing

the ^{1}H NMR spectra of both sets of axle and rotaxane. These are indicative of macrocycle occupation at the HB/XB-triazolium station, with the chemical shift changes of these protons due to the presence of hydroquinone ring currents upon [2]rotaxane formation (Figure 2.24). In the case of HB rotaxane **42·Cl**, an upfield shift of the proto-triazolium proton H_m corresponds to halide recognition by multiple HB interactions within the cavity created between the orthogonal axle and macrocycle components, resulting in partial polarisation of the halide anion away from the axle triazolium group. The aforementioned shifts of proton resonances $H_{l,k,n}$ indicate the macrocycle of [2]rotaxane **43·Cl** behaves in the same way, with the only difference being the chloride anion is shared with the axle component by XB to the iodo-triazolium group, in addition to HB with the isophthalamide cleft. Therefore chloride recognition from the orthogonal components of XB and HB [2]rotaxanes facilitates the change in co-conformation, which is achieved by macrocycle translational shuttling from NDI to the XB/HB-triazolium station upon anion-exchange (Figure 2.24).

Further comparisons indicated there was no change in the chemical shift of the NDI aromatic protons $H_{e,e'}$ or this station's proximal alkyl protons H_f and H_d, which suggested that under these conditions the macrocycle resided almost exclusively at the XB/HB-triazolium recognition site in both [2]rotaxanes. These co-conformations were confirmed by two-dimensional ^{1}H ROESY NMR experiments of **42·Cl** and **43·Cl** in $CDCl_3$ that showed, amongst other evidence, only coupling between hydroquinone protons of the macrocycle $H_{\gamma,\gamma'}$ and *N*-methyl triazolium protons H_l, with no interaction between $H_{\gamma,\gamma'}$ and the NDI protons $H_{e,e'}$ (Figure 2.25 and Figure 2.26).

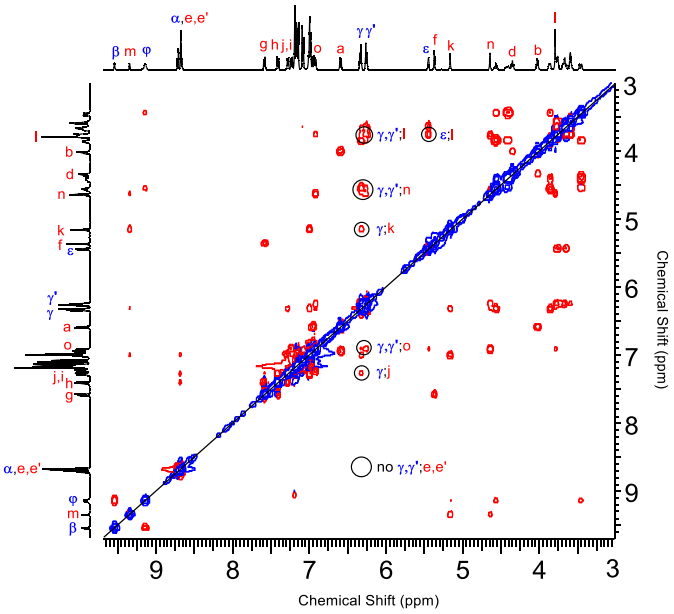


*Figure 2.25. Truncated ^{1}H–^{1}H ROESY NMR spectrum of HB [2]rotaxane **42·Cl** with selected coupling interactions highlighted ($CDCl_3$, 298 K, 500 MHz).*

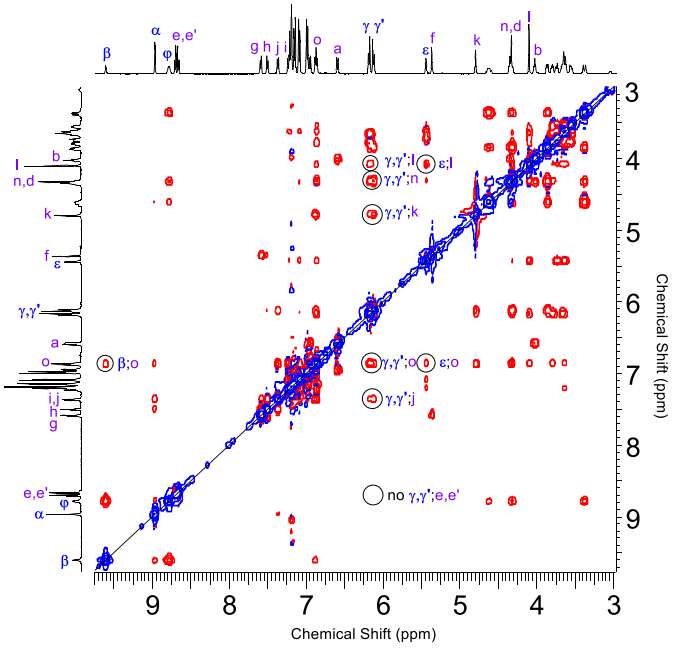


*Figure 2.26. Truncated ^{1}H–^{1}H ROESY NMR spectrum of XB [2]rotaxane **43·Cl** with selected coupling interactions highlighted ($CDCl_3$, 298 K, 500 MHz).*

A final comparison of the ^{1}H NMR spectra of [2]rotaxanes **42·PF$_6$** and **43·PF$_6$** with their respective [2]rotaxane chloride salts **42·Cl** and **43·Cl** in $CDCl_3$ also gave evidence for anion mediated co-conformational change (Figure 2.27).

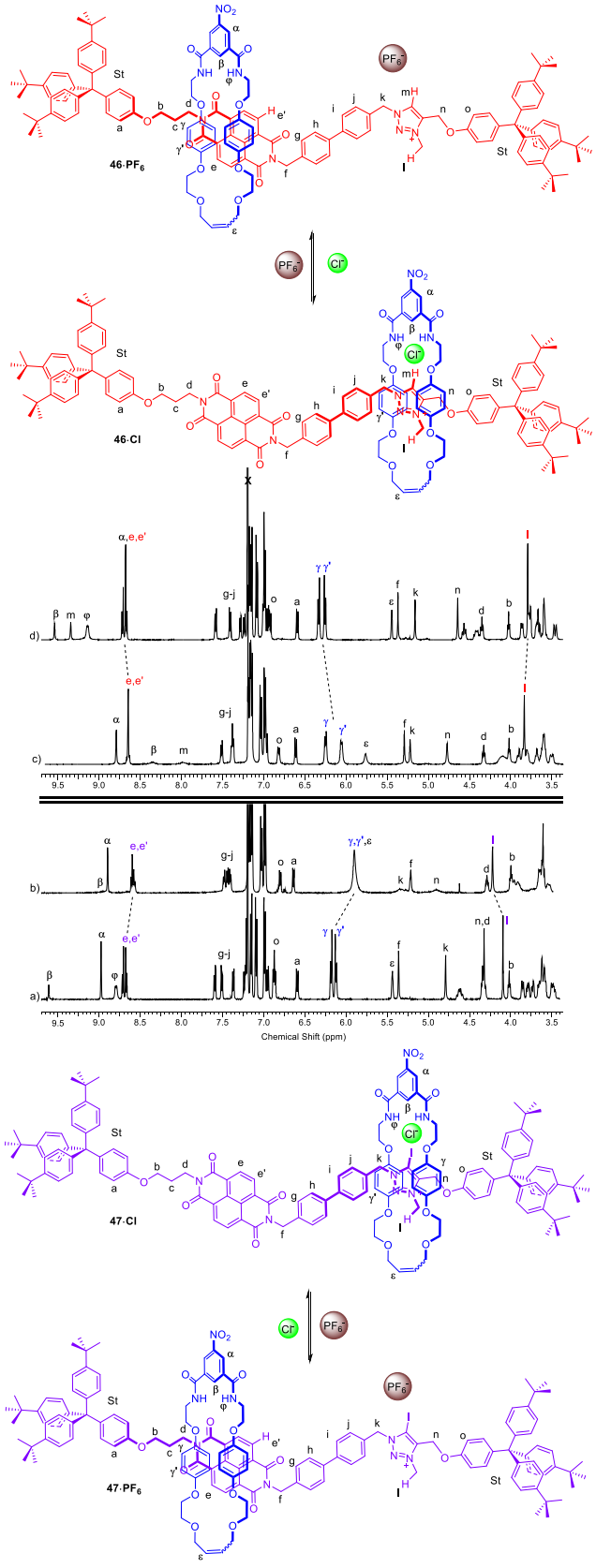


*Figure 2.27. Truncated ^{1}H NMR spectra of a) XB [2]rotaxane **43·Cl**, b) XB [2]rotaxane **43·PF$_6$**, c) HB [2]rotaxane **42·PF$_6$** and d) [2]rotaxane **42·Cl** ($CDCl_3$, 298 K, 400 MHz). The predicted co-conformations of these HB and XB [2]rotaxanes as their chloride and hexafluorophosphate salts are also shown.*

Translational switching of the macrocycle's position was inferred in both systems by significant downfield shifts of the hydroquinone proton resonances $H_{\gamma,\gamma'}$ upon addition of the chloride anion. These are indicative of weaker aromatic donor–acceptor charge–transfer interactions between the axle's HB/XB-triazolium and macrocycle hydroquinone groups, relative to those originally occurring with the NDI station. Furthermore, downfield shifts of the aromatic NDI proton resonances $H_{e,e'}$, in contrast to an upfield shift of the *N*-methyl triazolium protons H_I, resulting from changes in exposure to hydroquinone ring currents, also suggests shuttling of the macrocyclic component to the XB/HB-triazolium station as shown in Figure 2.27. Interestingly, anion-exchange gave the largest proton shifts in the bistable XB rotaxane **43·Cl** (e.g. $\Delta\delta$ H_I = 0.13 ppm), indicating a greater degree of macrocycle switching in this system relative to the HB analogue **42·Cl** ($\Delta\delta$ H_I = 0.05 ppm).

2.3.4. X-ray crystallography

Crystals suitable for single crystal X-ray diffraction structural analysis were obtained for the chloride salt of XB rotaxane **43·Cl** by slow evaporation of a solution of the rotaxane in 1:1 $CDCl_3$:CD_3OD. The interlocked [2]rotaxane host crystallises as a 1:1 stoichiometric complex with chloride, as well as one molecule each of chloroform and water (Figure 2.28). Notably, the solid-state structure showed the macrocycle interacting exclusively with the iodo-triazolium station, in the presence of the chloride template ($D_{I\cdots Cl^-}$ = 2.987(6) Å). This chloride anion···iodo-triazolium halogen bond is much shorter than the sum of the van der Waals radii (80%), indicating a very strong interaction. The solid state data corroborated the aforementioned one- and two-dimensional ^{1}H NMR evidence for the favoured co-conformation of the molecular shuttle in the presence of a coordinating counter anion in solution.

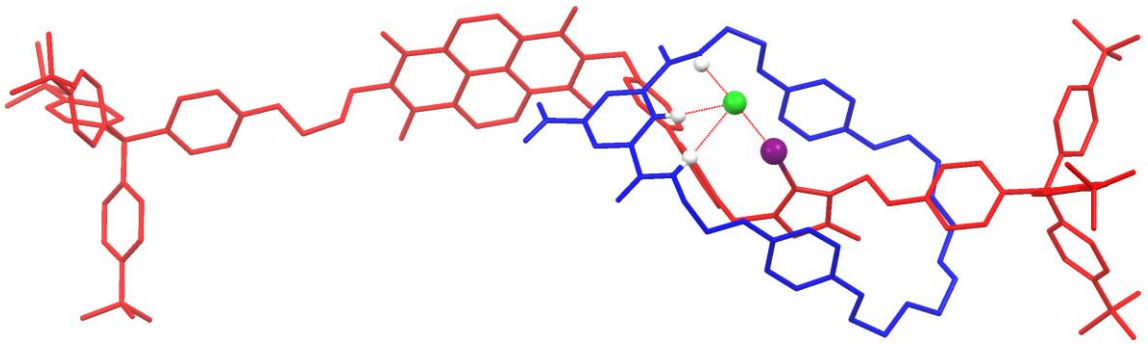


*Figure 2.28. X-ray crystal structure of **43·Cl** showing the macrocycle (blue) situated at the iodo-triazolium station on the axle (red), templated by the coordinating chloride anion (green). Notable hydrogen and halogen bonding interactions are shown as dotted red lines with the atoms involved shown as spheres. Non-coordinating hydrogens and the co-crystallised chloroform and water molecules are omitted for clarity.*

2.3.5. Optical responses from anion-induced shuttling behaviour

In addition to the ^{1}H NMR spectroscopic investigations, it was also possible to probe the counter anion-dependent changes in co-conformation of **42·A** and **43·A** using UV-Vis spectroscopy.

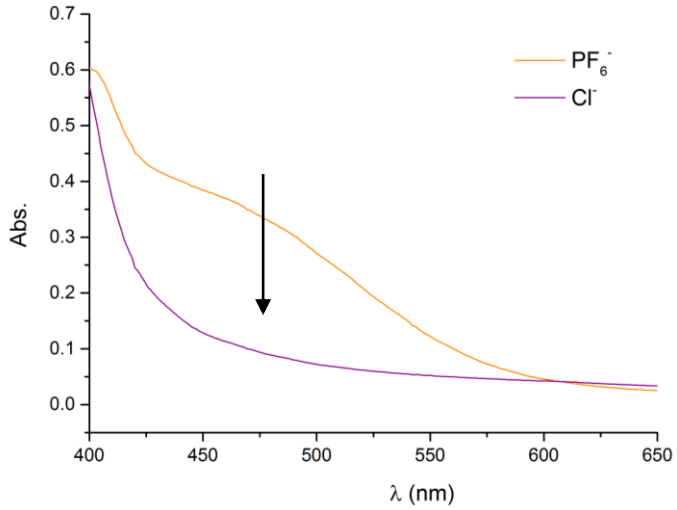


*Figure 2.29. Superimposed UV-Vis spectra of solutions of the [2]rotaxane **42·PF$_6$** in $CHCl_3$ (3.3×10^{-3} mol L^{-1}) in the absence and presence of one equivalent of tetrabutylammonium chloride. The addition of chloride leads to a decrease in intensity of the charge–transfer absorbance band.*

The donor–acceptor stacking interactions between the macrocycle hydroquinone motifs and the large aromatic surface of the NDI station gave rise to a charge–transfer absorbance band at $\lambda_{abs,max}$ ~ 450 nm in the UV-Vis spectra of rotaxanes **42·PF$_6$** and **43·PF$_6$** in $CHCl_3$ (Figure 2.29). This was manifested in these compounds possessing a vivid orange colour at concentrations above 1×10^{-3} mol L^{-1}. Upon the addition of chloride, the intensity of this charge–transfer band was shown to decrease, on account of a loss of the aromatic stacking interactions with NDI, triggered by translational motion of the macrocycle to partake in anion recognition at the HB/XB-triazolium station (Figure 2.29). As a consequence of the loss of this absorption band in the visible region of the spectrum, solutions of **42·Cl** and **43·Cl** in $CHCl_3$ were colourless. Therefore the anion-induced switching occurring within these bistable [2]rotaxanes could be detected by a naked-eye colour change, allowing them to behave as rare examples of colorimetric anion sensors that act *via* a signalling mechanism that involves co-conformational changes of their interlocked molecular components (Figure 2.30).



*Figure 2.30. Schematic of the anion-induced molecular shuttling exhibited by rotaxanes **42·A** and **43·A** and photographs showing the resulting colour of their co-conformations in $CDCl_3$ solution. Trz = XB/HB-triazolium*

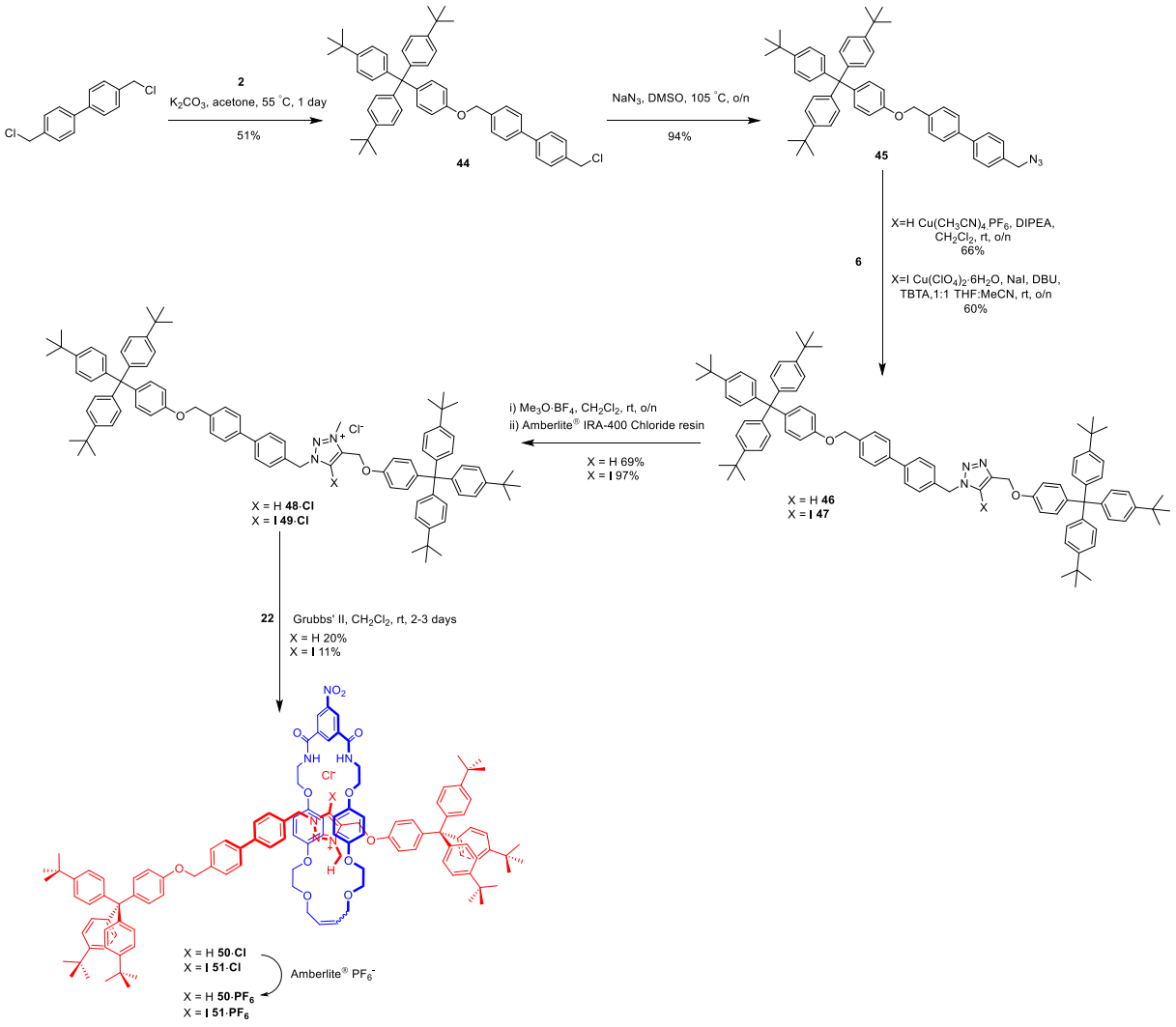
Interestingly, the addition of small amounts of MeOH (a minimum of 10% v/v) to colourless solutions of **42·Cl** and **43·Cl** in $CHCl_3$ resulted in a colour change to orange, at concentrations above 1×10^{-3} mol L^{-1}. This was caused by a weakening in the halide binding by the rotaxane host at the XB/HB-triazolium station in this polar, protic solvent mixture, in combination with a probable enhancement in the strength of the donor–acceptor aromatic stacking interactions between the hydroquinone and NDI groups.

2.3.6. One-station NDI/triazolium [2]rotaxane syntheses

In order to quantify how varying the nature of the counter anion and the solvent influences the co-conformation of the HB and XB molecular shuttles, three new one-station rotaxanes containing either a proto-triazolium, iodo-triazolium or NDI motif were prepared. These rotaxanes were designed to model the environment for each station in the bistable [2]rotaxane shuttles, and in doing so allow estimations of macrocycle–station occupancies under a variety of conditions.

2.3.6.1. One-station XB/HB-triazolium [2]rotaxanes

Two [2]rotaxanes containing either a HB- or XB-triazolium anion recognition site in the axle component were prepared by synthetic pathways outlined in Scheme 2.12 and fully characterised.

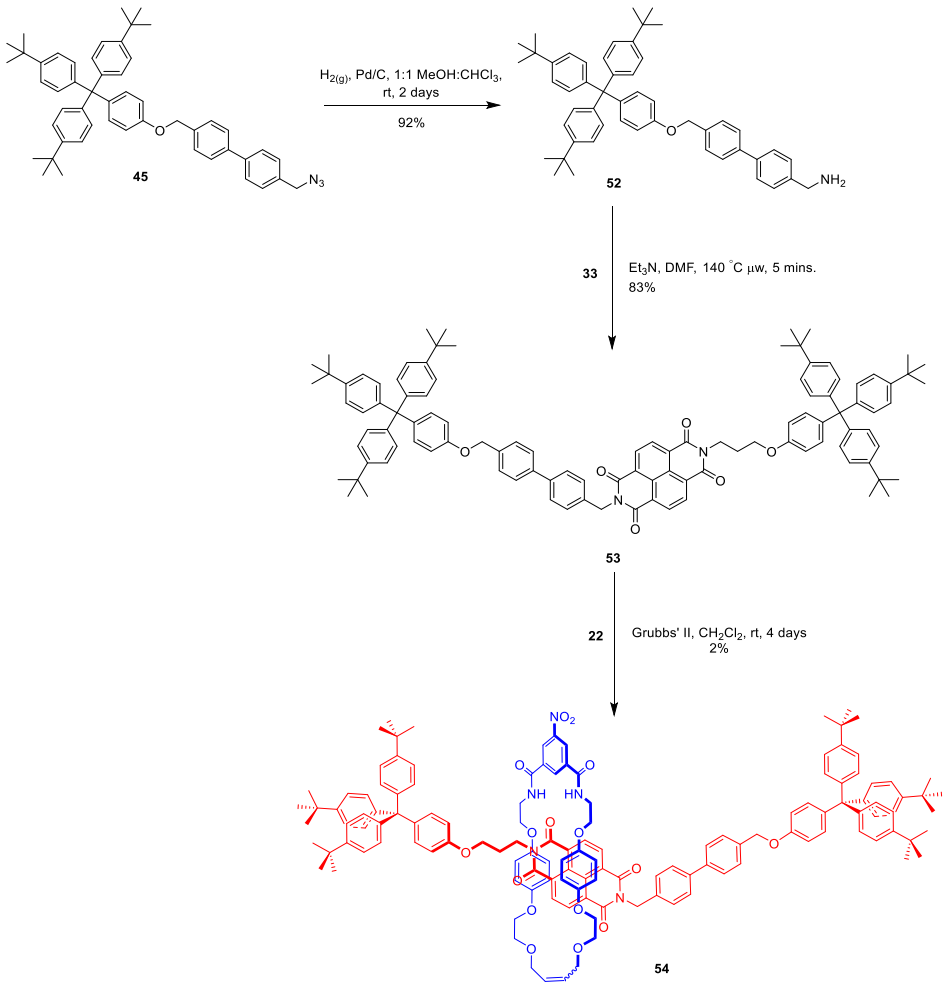


*Scheme 2.12. Synthesis of the one-station HB/XB triazolium [2]rotaxanes **50·A** and **51·A.***

Phenyl trityl alcohol stopper compound **2** was reacted with an excess of bis-chloromethane biphenyl under basic conditions to favour formation of the mono-substituted product **44** isolated in 51% yield following purification using silica gel column chromatography. This was converted to the corresponding azide **45** by heating in DMSO with NaN_3. Proto- or iodo- CuAAC 'click' reactions were performed using azide **45** and phenyl trityl stopper alkyne **6** to produce HB- or XB-triazole-containing bis-stoppered axles **46** and **47** respectively in good yields. Methylation to form cationic axles **48·Cl** and **49·Cl** was achieved by treatment with $Me_3O{\cdot}BF_4$, followed by anion exchange. Finally the one-station HB/XB-triazolium-containing [2]rotaxanes **50·Cl** and **51·Cl** were synthesised using chloride anion-templation *via* RCM of the bis-vinyl-functionalised macrocycle precursor **22** around the appropriate axle component using Grubbs' II catalyst in dry CH_2Cl_2. The XB and HB [2]rotaxanes were isolated in moderate yields of 20% and 11% respectively following purification by preparative silica thin-layer chromatography (Scheme 2.12).

2.3.6.2. One-station NDI [2]rotaxane

A one-station [2]rotaxane, containing an NDI recognition site within the axle component was also prepared (Scheme 2.13).



*Scheme 2.13. Synthesis of the one-station NDI [2]rotaxane **54.***

Mono-stoppered azide derivative **45** was reduced to the amine using a catalytic amount of Pd/C under a pressurised atmosphere of $H_{2\,(g)}$. The condensation of amine **52** with the mono-stoppered anhydride intermediate **33** was performed under microwave irradiation conditions, and, following purification on silica gel, one-station NDI axle **53** was isolated in 83% yield. An equimolar mixture of axle **53** and macrocycle precursor **22** in dry $CH_2Cl_2$was stirred for four days with a catalytic amount of Grubbs' II RCM catalyst. Unfortunately following purification by preparative silica thin-layer chromatography the target [2]rotaxane **54** could not be isolated in a yield greater than 2%, with the predominant product found to be cyclised macrocycle and axle starting material. This was ascribed to weak donor–acceptor charge–transfer interactions between the components under these conditions. An identical rotaxanation procedure was performed in the more polar solvent mixture of 2:1 CH_2Cl_2:$MeNO_2$ in the

hope that solvophobic effects would enhance the templation effect *via* stronger intermolecular aromatic stacking. Unfortunately, the lipophilic axle **53** precipitated after several hours, resulting in negligible yield of **54**.

2.3.7. Quantitative estimations of macrocycle occupancies in two-station NDI-XB/HB-triazolium [2]rotaxane shuttles

The one-station rotaxanes **50·A**, **51·A** and **54** were found to be appropriate models for the HB and XB two-station rotaxanes **42·A** and **43·A**. This was because the ^{1}H NMR chemical shift values of each station's diagnostic protons, specifically the *N*-methyl triazolium group H_I and NDI aromatics $H_{e,e'}$, in the model one-station axles (**48·PF$_6$**, **49·PF$_6$** and **53**) were observed to be very similar to those of their corresponding two-station axles (**36·PF$_6$** and **37·PF$_6$**) (Figure 2.31).[†]

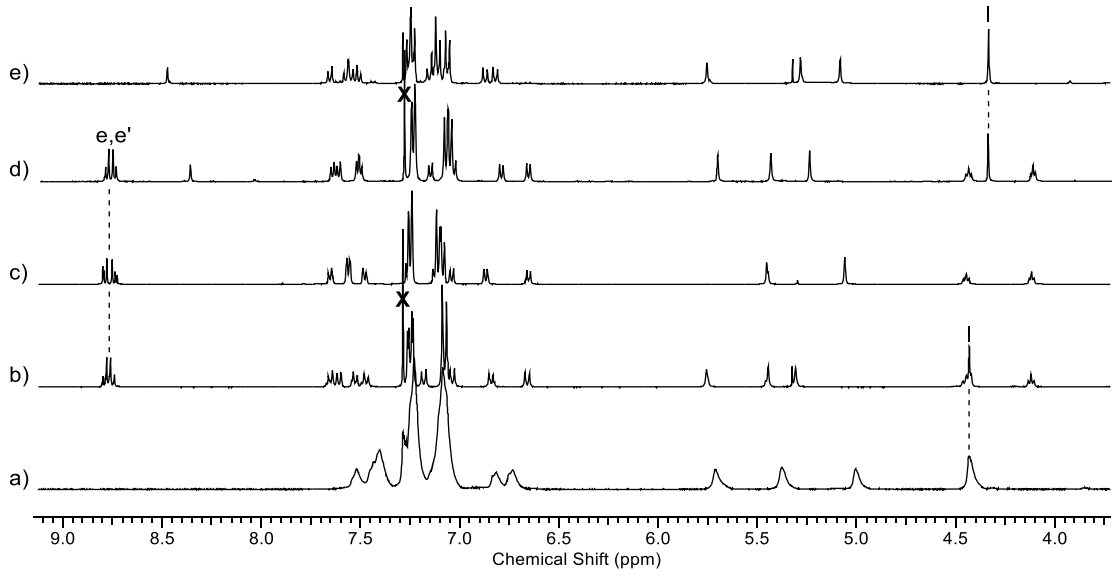


*Figure 2.31. ^{1}H NMR spectra of a) one-station XB triazolium axle **49·PF$_6$**, b) two-station XB triazolium-NDI axle **37·PF$_6$**, c) one-station NDI axle **53**, d) two-station HB triazolium-NDI axle **36·PF$_6$** and e) one-station HB triazolium axle **48·PF$_6$** showing the similarities in chemical shifts of diagnostic protons $H_{e,e'}$ and H_I ($CDCl_3$, 298 K, 400 MHz).*

Therefore it was assumed that the ^{1}H NMR spectra of the model one-station [2]rotaxanes **50·Cl**, **51·Cl** and **54** gave representative and precise ^{1}H NMR chemical shift values of each station's diagnostic protons (H_I and $H_{e,e'}$) when there was 100% occupancy by the macrocycle. The chemical shift values for

[†] This was also true for δH_I in the naphthalimide axle **18·PF$_6$** and the one-station proto-triazolium axle **48·PF$_6$**, therefore enabling **50·PF$_6$** to be used for the station occupancy estimations detailed in Sections 2.2.5 and 2.2.6.

the same protons at 0% occupancy were obtained from the ^{1}H NMR spectra in $CDCl_3$ of the two-station axles **36·PF$_6$** and **37·PF$_6$**. Using these data, chemical shift scales were determined with respect to each station, in the presence of each anion, to characterise the two extremes of macrocycle occupation (see Appendix for further details).

The complete occupation of the triazolium station by the macrocycle in the HB two-station [2]rotaxane system as the chloride salt (**42·Cl**) was confirmed by comparison of the chemical shift of the *N*-methyl triazolium protons in **42·Cl** ($\delta(H_l)$ = 3.88 ppm) with the HB *N*-methyl triazolium chloride chemical shift scale (Figure 2.32). This was supported *via* comparison of the chemical shift of the NDI protons, $\delta(H_e)$ in **42·Cl** with the NDI chemical shift scale which indicated 0% occupancy of the NDI station (see Appendix). This method was used to determine the macrocycle occupancies of both HB and XB [2]rotaxanes **42·A** and **43·A** as their chloride, iodide[‡] and hexafluorophosphate salts in $CDCl_3$ using the appropriate *N*-methyl triazolium chemical shift scale (Figure 2.32). These figures were reinforced using the chemical shift of the NDI protons (see Appendix).

[‡] The iodide salts were prepared by the standard procedure of Amberlite® anion exchange.

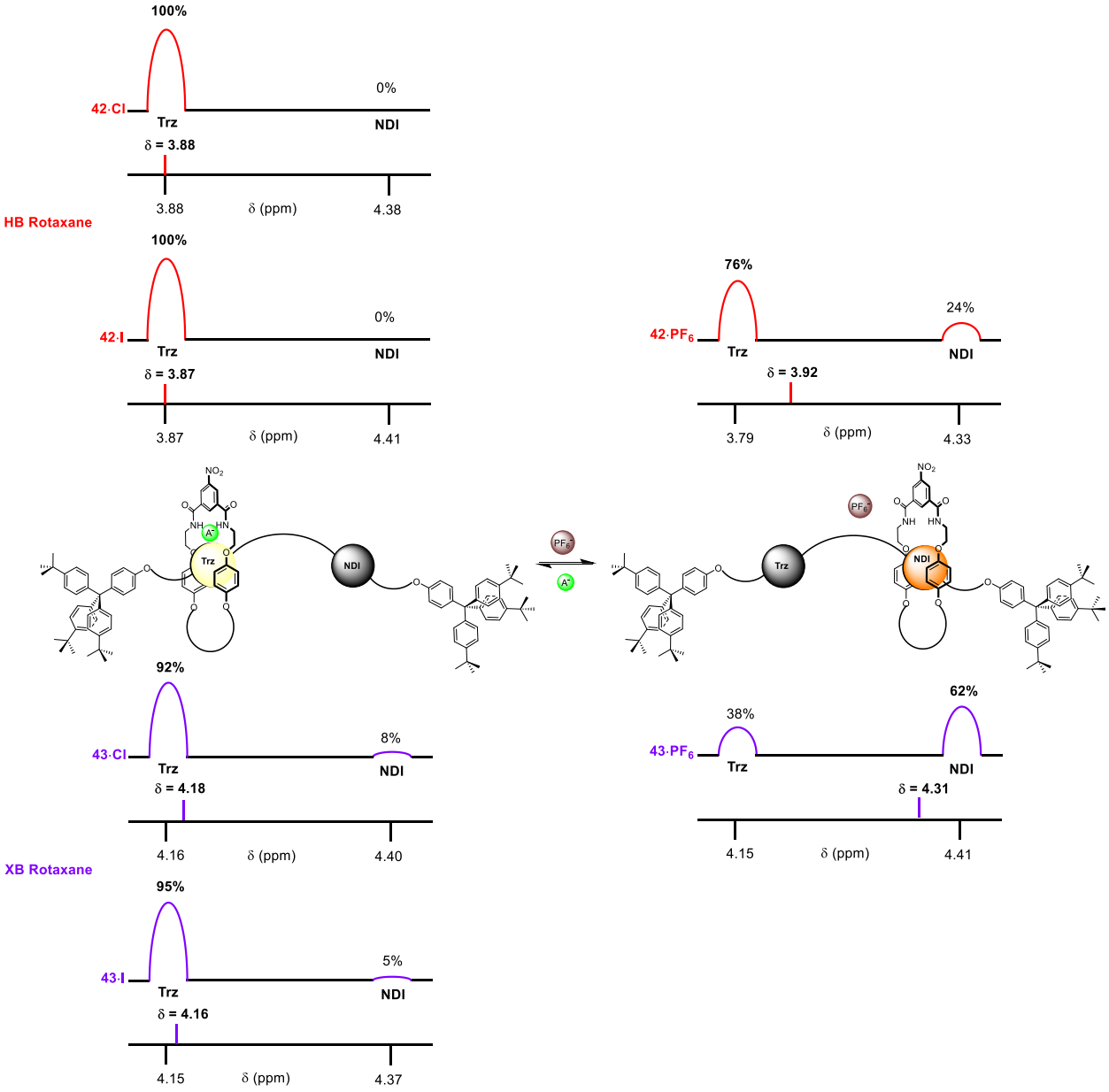


*Figure 2.32. The estimated macrocycle station occupancies (based upon the chemical shift of H_I protons) of the HB and XB rotaxanes **42·A** and **43·A** as hexafluorphosphate, iodide and chloride salts as determined by ^{1}H NMR spectroscopy in $CDCl_3$ solution. Trz = XB/HB triazolium.*

These results unequivocally confirmed that both two-station rotaxanes exhibited anion-induced molecular motion in $CDCl_3$ (Figure 2.32). The preference for the proto- or iodo-triazolium station in the chloride salts (**42·Cl** and **43·Cl**) was evident for both HB (100% occupancy of the triazolium station) and XB (92%) rotaxane switches, giving excellent positional integrity within this state. The same was true for the iodide salts (**42·I** and **43·I**), with HB and XB rotaxanes estimated to have 100% and 95% occupancies of their triazolium stations respectively.

Upon exchange to the non-coordinating hexafluorophosphate salt, both systems demonstrated an increase in occupancy of the NDI station (Figure 2.32), which was in line with the one- and two-dimensional ^{1}H NMR spectroscopy data discussed earlier. The largest occupation of the NDI station was found to occur with the XB rotaxane **43·PF$_6$** (62%) relative to the HB rotaxane **42·PF$_6$** (24%). This indicated the XB rotaxane behaved as a superior molecular shuttle to the HB analogue on account of the larger swing in percentage occupancy of the stations upon exchange between non-coordinating and coordinating anions (Cl^-/I^- = 54/57% for the XB rotaxane *vs.* 24% for the HB rotaxane). The difference in behaviour of the two systems may be rationalised by the greater degree of steric or electronic repulsion between the macrocycle and the iodo-triazolium group relative to that experienced with the smaller proto-triazolium station in the HB system. This is in light of the fact the iodo-triazolium group was perhaps responsible for restricted rotation in the XB axle component **37·A** described earlier (Figure 2.20).

2.3.8. Solvent effects on macrocycle occupancies within two-station NDI-XB/HB-triazolium [2]rotaxane shuttles

The propensity for anion receptors containing XB donor groups to exhibit enhanced halide, in particular iodide, recognition properties over their HB analogues in protic, organic and aqueous, organic solvent mixtures provided the impetus for investigating the dynamic behaviour of the HB and XB [2]rotaxanes in more competitive solvent mixtures.[55,56] The percentage occupancies of **42·A** and **43·A** as their hexafluorophosphate, chloride and iodide salts were estimated in the competitive solvent mixture of 4:1 $CDCl_3$:CD_3OD *via* analogous ^{1}H NMR spectroscopic experiments that monitored changes in the chemical shift of each [2]rotaxane's *N*-methyl triazolium protons, H_I (Figure 2.33).

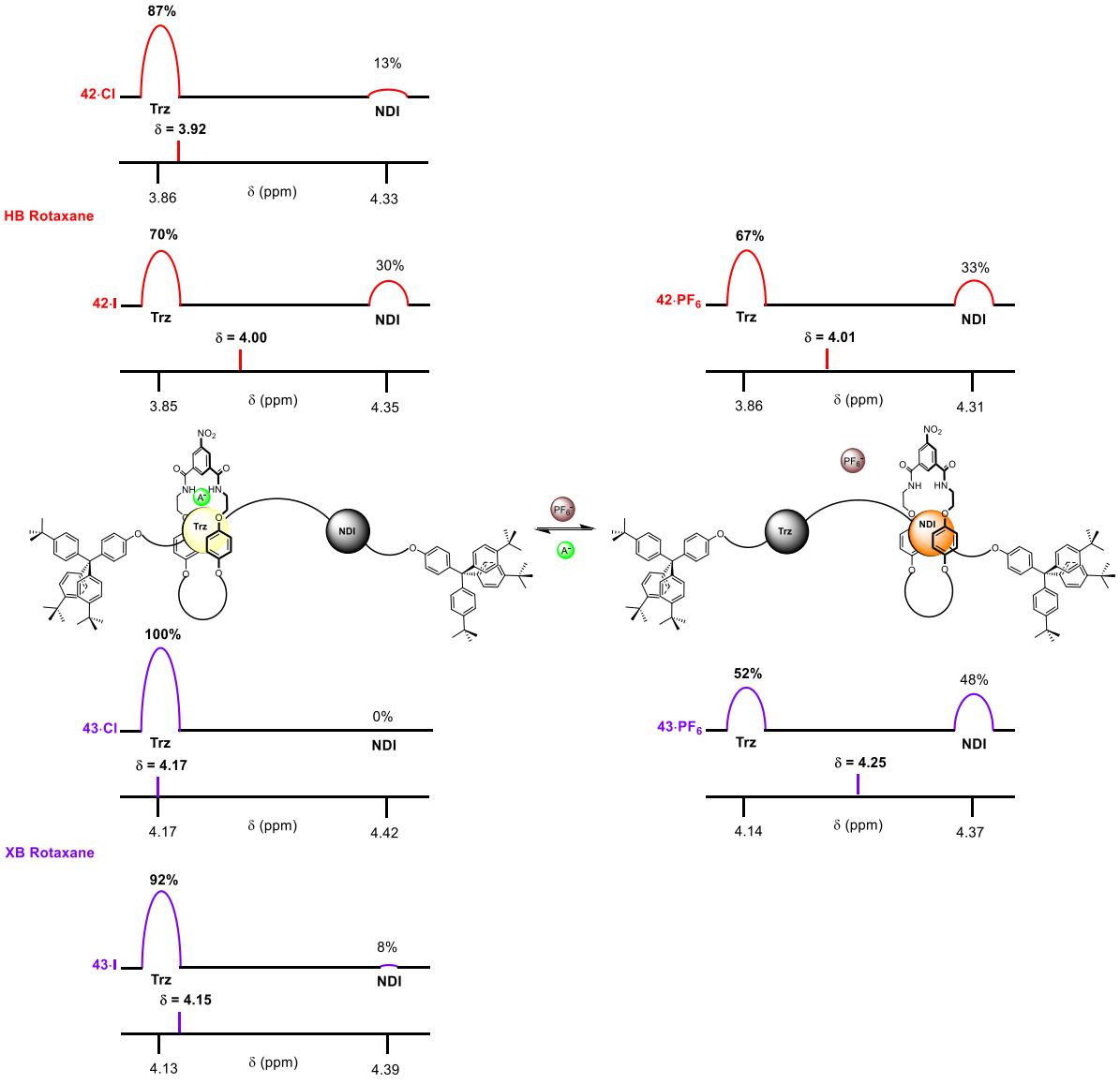


*Figure 2.33. The estimated macrocycle station occupancies (based upon the chemical shift of H_I protons) of the HB and XB rotaxanes **42·A** and **43·A** as hexafluorophosphate, iodide and chloride salts as determined by ^1H NMR spectroscopy in 4:1 $CDCl_3$:CD_3OD solution. Trz = XB/HB triazolium.*

Under these conditions, the difference in behaviour between HB and XB [2]rotaxanes was most strongly manifested within the iodide salt of the rotaxanes. XB rotaxane **43·I** exhibited a 92% occupancy of the triazolium station whereas the HB analogue **42·I** was estimated at 70% (Figure 2.33). The differences between the chloride salt occupancies of the triazolium stations of the two rotaxanes were, by contrast, smaller: XB rotaxane **43·Cl** was 100% *vs*. 87% for the HB rotaxane **42·Cl** (Figure 2.33). These differences were attributed to superior halide affinity afforded by strong XB formation from the

iodo-triazolium anion recognition site in comparison to the weaker proto-triazolium HB donor motif which is less effectively able to compete with the polar, protic solvent medium.

Upon exchange to their respective hexafluorophosphate salts, an enhanced positional integrity in favour of the NDI station was observed in the XB system **43·PF$_6$** (48% occupancy of the NDI station), relative to the HB rotaxane **42·PF$_6$** (33%); the same trend that was found in $CDCl_3$ solution. Overall, the swing in macrocycle-station occupancies upon exchange between non-coordinating and coordinating anions was larger for the XB rotaxane **43·A** (48 or 40%) than the HB analogue **42·A** (20 or 3%) making it a superior molecular shuttle under these solvent conditions. However, unlike in $CDCl_3$, the cause for the large co-conformational change was now predominantly a consequence of stronger halide anion recognition, due to XB donation from the iodo-triazolium motif, which resulted in almost complete occupation of the macrocycle at this station in the presence of a halide anion.

Finally, the percentage occupancies of both rotaxane systems were estimated as their iodide and hexafluorophosphate salts in the highly competitive solvent medium of 1:1 $CDCl_3$:CD_3OD using ^{1}H NMR spectroscopy experiments, based upon the H_I protons (Figure 2.34).

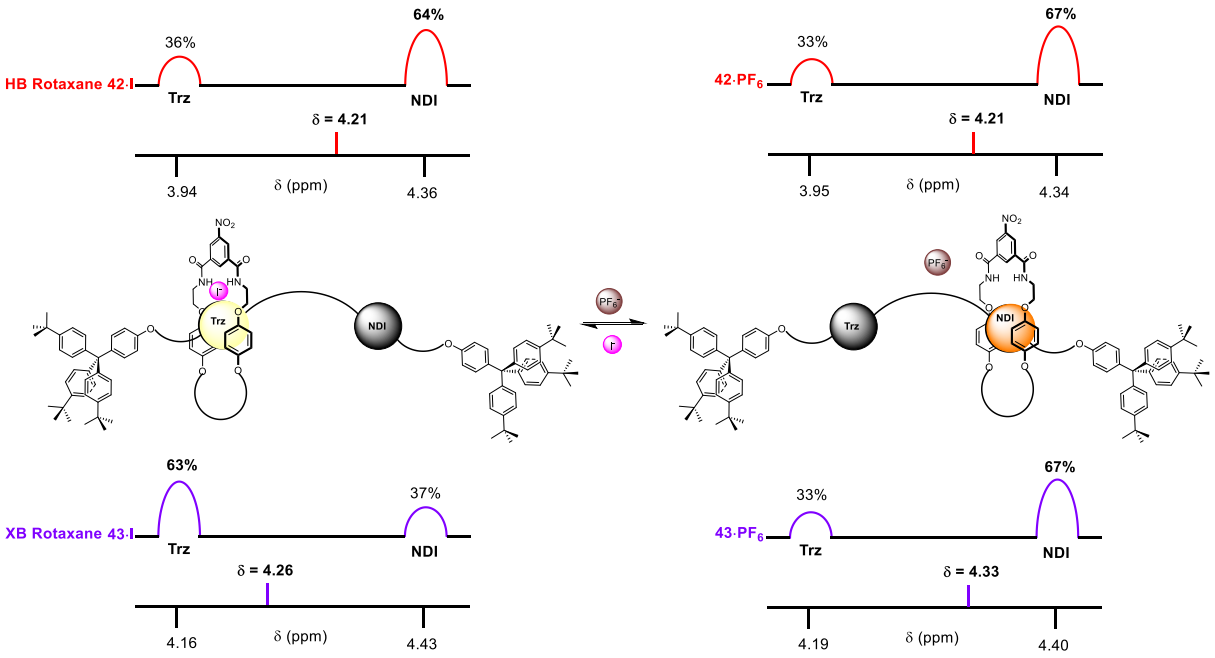


*Figure 2.34. The estimated macrocycle station occupancies (based upon the chemical shift of H_I protons) of the HB and XB rotaxanes **42·A** and **43·A** as hexafluorophosphate and iodide salts as determined by ^{1}H NMR spectroscopy in 1:1 CD_3OD:$CDCl_3$ solution. Trz = HB/XB triazolium.*

Under these solvent conditions, the hexafluorophosphate salts of HB and XB rotaxanes (**42·PF$_6$** and **43·PF$_6$**) were estimated to have the same occupancy of the NDI station (67%). Importantly though, a change in the nature of the counter anion revealed a significantly larger preference for the XB-triazolium station was exhibited by the XB system **43·I** (63% occupancy of the iodo-triazolium), over the weaker HB system **42·I** (36%). The large difference in these solvent conditions was caused by stronger iodide binding within the XB [2]rotaxane host in comparison to the HB analogue. This superior recognition enabled the XB shuttle to produce effective anion-induced switching in 1:1 $CDCl_3$:CD_3OD, with an overall change in macrocycle-station occupancy of 30%. By contrast, the HB system afforded only negligible changes in station occupancies (3%), so like the previous HB triazolium NI [2]rotaxane, it was much less accomplished as a two-station shuttle within this competitive solvent mixture.

These experiments demonstrated that within this family of XB/HB-triazolium-NDI bistable [2]rotaxanes, positional integrity in favour of the triazolium station is achievable upon increasing the competitive nature of the solvent system, but only when it is facilitated by strong XB formation to iodide. Therefore, the XB rotaxane switch, incorporating an iodo-triazolium anion recognition station,

was shown to be a superior example of an anion-driven molecular shuttle, relative to an HB analogue, in both $CDCl_3$ and competitive $CDCl_3$-CD_3OD solvent mixtures.

2.3.9. Summary

This section describes the preparation of five novel rotaxanes, including two bistable [2]rotaxanes and three one-station [2]rotaxane interlocked structures. In depth one- and two-dimensional ^{1}H NMR spectroscopic studies and an X-ray crystal structure revealed the XB and HB two-station [2]rotaxanes to be capable of anion-induced molecular switching of their co-conformations in $CDCl_3$ solution. This shuttling behaviour resulted in a distinct colour change of the solution that could be monitored by UV-Vis spectroscopy, and also gave a naked-eye response, allowing these systems to act as a prototype colorimetric anion sensor. Estimations of the macrocycle occupancies of the stations using ^{1}H NMR spectroscopic techniques based upon chemical shift scales clearly demonstrated superior molecular shuttling in the XB two-station rotaxane **43·A** over the HB analogue rotaxane **42·A** in $CDCl_3$ solution.

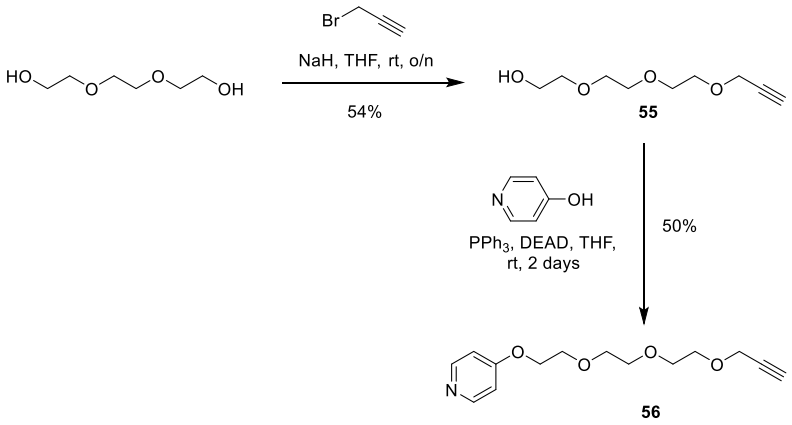
Upon increasing the competitive nature of the solvent mixture to 4:1 $CDCl_3$:CD_3OD, the XB two-station rotaxane again demonstrated superior molecular shuttling, reflected in estimations of the macrocycle occupancies of the stations in the various states. This was primarily caused by XB–halide binding from the unique XB iodo-triazolium donor site within the axle component that facilitated macrocycle translocation. Halide recognition in the HB [2]rotaxane was, by comparison, weaker. The differences in anion-induced switching were most prevalent in the highly competitive solvent mixture of 1:1 $CDCl_3$:CD_3OD, because under these solvent conditions the superior strength of iodide binding by the XB [2]rotaxane over the HB analogue was maximised. The XB [2]rotaxane therefore displayed significant co-conformational changes upon anion exchange whereas those of the HB [2]rotaxane were negligible. This is the first example of using XB in concert with donor–acceptor charge–transfer aromatic stacking interactions to exert significant control over solution phase molecular motion within an interlocked supramolecular system.

2.4. A two-station *N*-alkyl pyridinium-triazolium [2]rotaxane

The design of the axle component was varied further by preparation of a two-station axle containing an electron-deficient *N*-alkyl pyridinium motif separated from an XB/HB-triazolium group by a polyether spacer. This was incorporated into a [2]rotaxane and the dynamic behaviour of the system investigated using ^{1}H NMR spectroscopy.

2.4.1. Synthesis of a two-station *N*-alkyl pyridinium-triazolium axle component

Synthesis of the XB and HB two-station axles was undertaken using multistep synthetic pathways outlined in Scheme 2.14, Scheme 2.15 and Scheme 2.16.

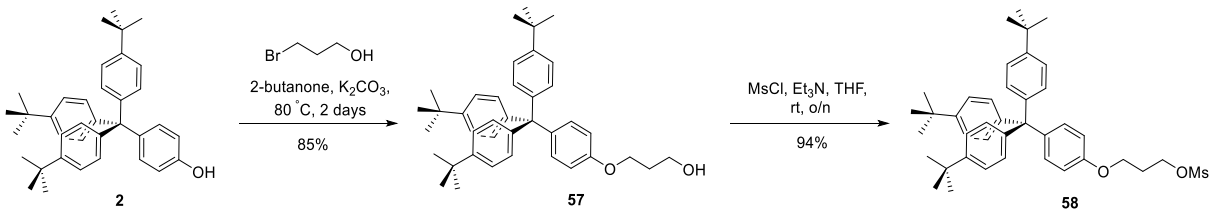


*Scheme 2.14. Synthesis of the pyridine–alkyne-functionalised polyether axle precursor **56**.*

The first stage was a statistical reaction between equimolar amounts of triethylene glycol and NaH in dry THF, followed by the addition of one equivalent of propargyl bromide to form mono-functionalised polyether alkyne **55** in 54% yield.[57] A procedure based on the Mitsunobu reaction was then used to functionalise the other alcohol terminus of **55** with 4-hydroxypyridine to give polyether derivative **56** (Scheme 2.14).[58]

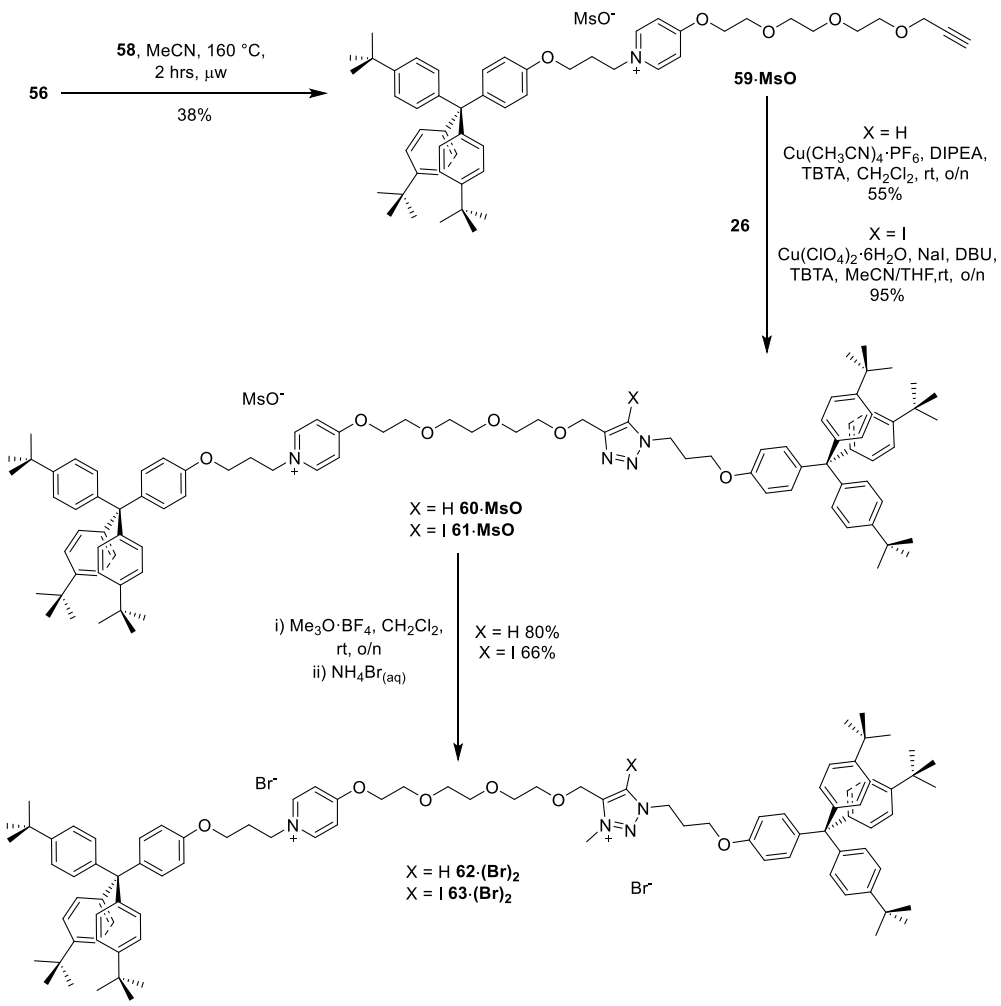
The bulky phenyl trityl stopper group to be appended to the pyridine functionality of **56** was prepared by an adapted literature procedure in accordance with Scheme 2.15.[31,34] The reaction of **2** with an excess of 3-bromo-1-propanol in refluxing 2-butanone with K_2CO_3 (Scheme 2.15) afforded **57**[34] which

on reaction with methanesulfonyl chloride and Et_3N in dry THF gave the mesylate stopper derivative **58**.[31]



*Scheme 2.15. Syntheses of mesylate-functionalised phenyl trityl stopper derivative **58**.*

Alkylation of pyridyl derivative **56** with **58** proved to be problematic. The reaction was found to require relatively forcing conditions; with heating under microwave irradiation at 160 °C for two hours providing the largest yield of the mono-stoppered thread **59·MsO** (Scheme 2.16).



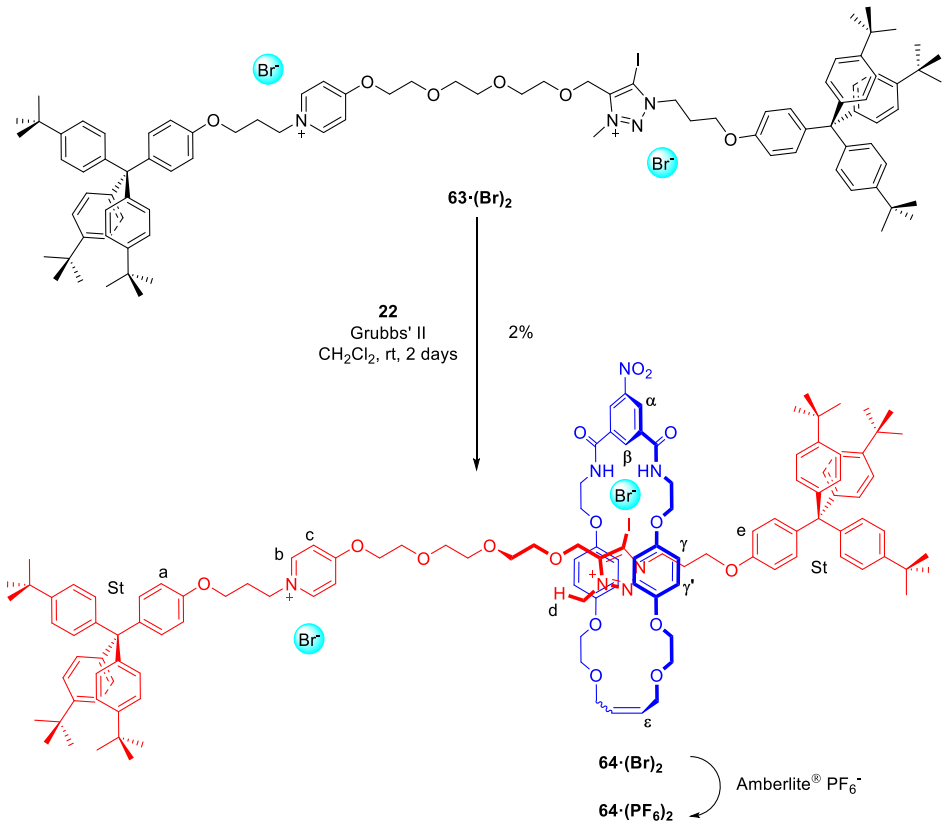
Scheme 2.16. Synthesis of two-station HB/XB-triazolium-N-alkyl pyridinium axle components ***62·(Br)₂*** *and* ***63·(Br)₂****.*

An appropriate CuAAC 'click' reaction, between alkyne **59·MsO** and the azide **26** gave HB and XB axles **60·MsO** and **61·MsO** respectively (Scheme 2.16). Exposure of **60·MsO** or **61·MsO** to a small excess of $Me_3O{\cdot}BF_4$ in dry CH_2Cl_2 resulted in near-quantitative methylation of the proto- or iodo-triazole groups which upon anion exchange afforded the bromide salts, **62·(Br)₂** and **63·(Br)₂**.

2.4.2. Synthesis of a two-station *N*-alkyl pyridinium-triazolium [2]rotaxane

[2]Rotaxane synthesis was attempted *via* the bromide anion templated Grubbs' II catalysed RCM of bis-vinyl-functionalised macrocyclic precursor **22** around the dicationic XB iodo-triazolium-containing axle **63·(Br)₂** (Scheme 2.17). Although ESI MS analysis of the crude reaction mixture indicated significant formation of the interlocked product, [2]rotaxane **64·(Br)₂** was isolated in only 2% yield.

This was attributed to the difficulty in separating the interlocked product from the unreacted axle and ring closed macrocycle, which required the use of several preparative silica TLC purifications. Anion exchange using Amberlite® resin produced the bis-hexafluorophosphate salt **64·(PF$_6$)$_2$** which was characterised by two-dimensional ^{1}H ROESY NMR spectroscopy that showed, amongst other evidence, coupling interactions between the hydroquinone protons of the macrocycle and the *N*-alkyl pyridinium protons of the axle component (Figure 2.37).



*Scheme 2.17. Synthesis of two-station iodo-triazolium-N-alkyl pyridinium [2]rotaxane **64·(A)$_2$**.*

2.4.3. ^{1}H NMR spectroscopic studies of anion-induced shuttling behaviour

Having synthesised the desired two-station iodo-triazolium *N*-alkyl pyridinium [2]rotaxane **64·(A)$_2$**, ^{1}H NMR spectroscopy was employed to determine the capability of the macrocycle to undergo translational shuttling between the stations mediated by the nature of the counter anion. Therefore initial attempts to determine the predominant co-conformation of the XB [2]rotaxane as the bromide

salt in $CDCl_3$ were made by comparisons between the ^1H NMR spectra of **64·(Br)$_2$** with that of the axle component **63·(Br)$_2$** (Figure 2.35).

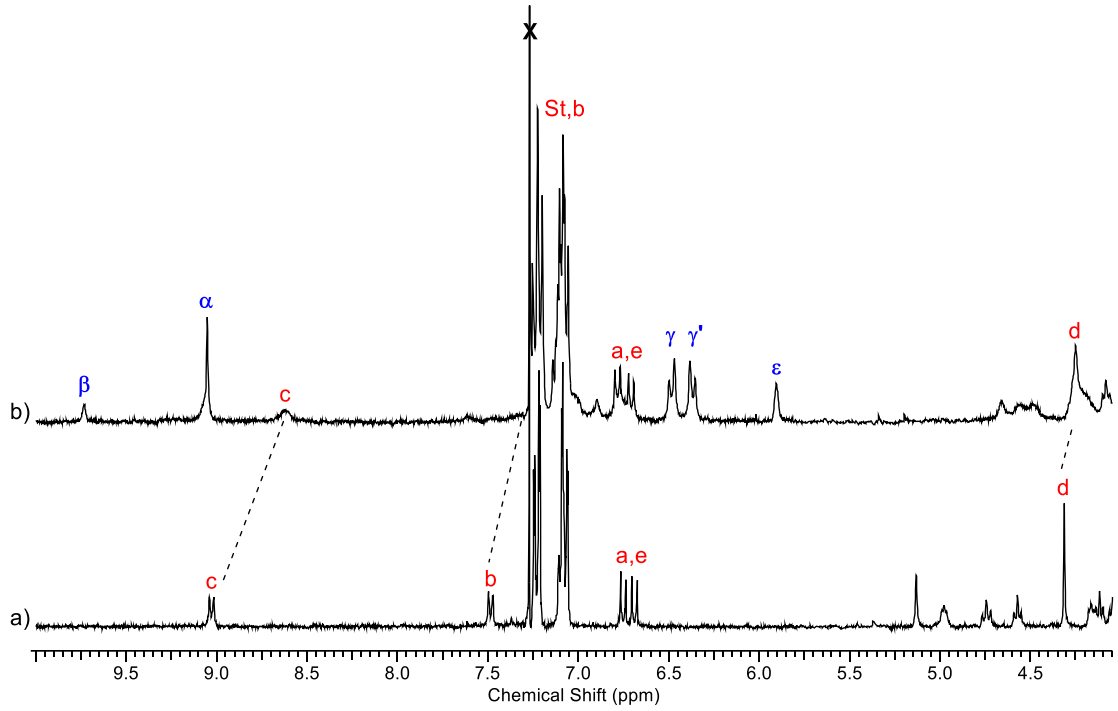


*Figure 2.35. Truncated ^1H NMR spectra of a) two-station axle component **63·(Br)$_2$** and b) [2]rotaxane **64·(Br)$_2$** ($CDCl_3$, 298 K, 300 MHz).*

Formation of the [2]rotaxane resulted in significant upfield shifts of *N*-alkyl pyridinium and *N*-methyl iodo-triazolium group protons ($H_{c/b}$ and H_d), most likely due to ring current effects from the macrocycle hydroquinone protons $H_{\gamma,\gamma'}$. This provided strong evidence that the macrocycle was interacting with both stations under these conditions. This dynamic behaviour was explained by the fact each station was capable of bromide recognition; the iodo-triazolium *via* charge assisted XB, and the *N*-alkyl pyridinium through a combination of electrostatics and C–H hydrogen bonding. Although the latter was expected to be the weaker of the two interactions, it was apparent that anion recognition at both cationic sites was inhibiting the system from exhibiting one dominant co-conformation in the presence of bromide (Figure 2.36).

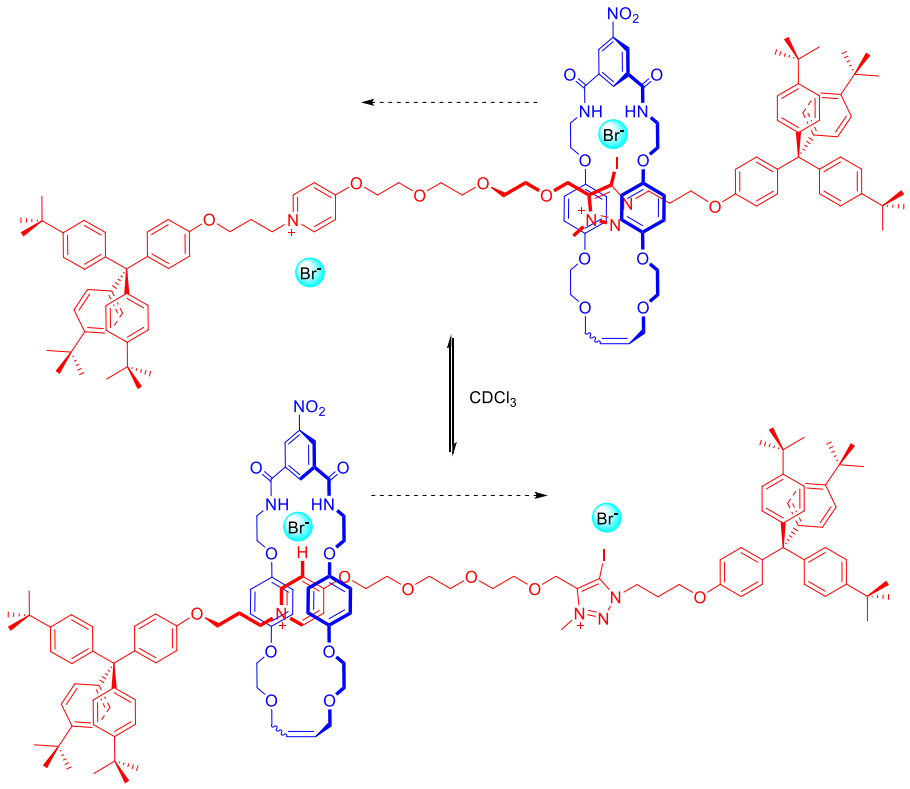


Figure 2.36. The proposed dynamic behaviour of two-station [2]rotaxane ***64·(Br)₂*** *in* $CDCl_3$.

To elucidate any changes to the co-conformation of the XB [2]rotaxane as the hexafluorophosphate salt, a two-dimensional ^{1}H ROESY NMR spectrum of **64·(PF$_6$)$_2$** was recorded in 1:1 $CDCl_3$:CD_3OD (Figure 2.37). The change in solvent system was enforced by the low solubility of **64·(PF$_6$)$_2$** in $CDCl_3$. The spectrum revealed coupling between the macrocycle protons $H_{\gamma,\gamma'}$ and H_ε and the *N*-methyl group of the iodo-triazolium (H_d) indicating that in the absence of coordinating anions, there were still residual interactions with this station. However, some of the strongest couplings were those observed between the macrocycle hydroquinone protons ($H_{\gamma,\gamma'}$) and the axle's *N*-alkyl pyridinium protons H_c (Figure 2.37). This suggested that the macrocycle favoured this station, driven by strong donor–acceptor charge–transfer interactions between the electron-rich and electron-deficient aromatic rings.

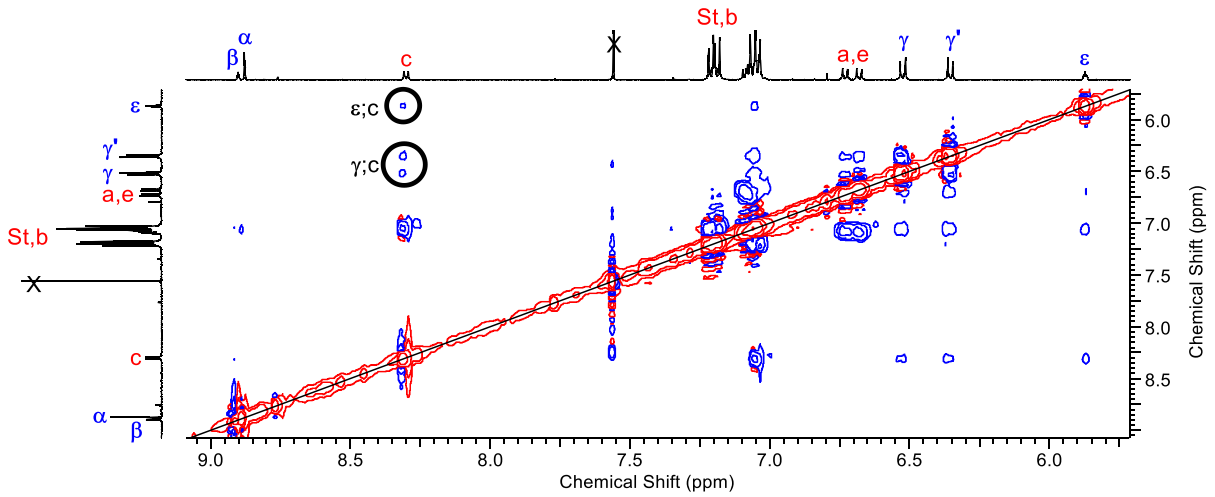


*Figure 2.37. Truncated ^{1}H–^{1}H ROESY NMR spectrum of [2]rotaxane **64·(PF$_6$)$_2$** with selected coupling interactions highlighted (1:1 $CDCl_3$:CD_3OD, 298 K, 500 MHz).*

Unfortunately, further investigations into the dynamic behaviour of XB [2]rotaxane in the presence of alternative anions were prevented due to repeated decomposition of the compound upon exchange from the non-coordinating bis-hexafluorophosphate salt. ^{1}H NMR and MS evidence suggested this occurred by elimination of the stopper species from the *N*-alkyl pyridinium group and so no additional attempts to synthesise interlocked molecules incorporating this motif were performed.

2.4.4. Summary

The synthesis of a novel bistable [2]rotaxane containing an iodo-triazolium and an *N*-alkyl pyridinium station was achieved and encouraging ^{1}H NMR spectroscopy evidence indicated both sites were capable of macrocycle recognition. However, the dynamic nature of the [2]rotaxane in the presence of coordinating and, to a lesser extent, non-coordinating anions, inhibited discrete anion-induced molecular motion. In order to operate as an effective shuttle it must be possible to exert control between the co-conformations of the [2]rotaxane, and since the stations of **64·(A)$_2$** acted as simultaneous macrocycle recognition sites, this could not be achieved.

2.5. Conclusions and future work

This chapter detailed the construction of a variety of novel bistable [2]rotaxanes and demonstrated their capability to exhibit anion-induced shuttling of the macrocyclic wheel. These systems incorporate

either an XB iodo- or HB proto-triazolium group capable of anion coordination whilst electron-deficient NI, NDI and *N*-alkyl pyridinium aromatic motifs were investigated as potential second stations. In $CDCl_3$ the NI- and NDI-containing [2]rotaxanes **23·A**, **42·A** and **43·A** exhibited significant halide anion mediated co-conformational changes, whilst the macrocycle of the *N*-alkyl pyridinium-based [2]rotaxane (**64·(A)$_2$**) was shown to interact with both stations regardless of the counter anion.

Increasing the competitive nature of the solvent medium reduced station bias and therefore the degree of translational shuttling in HB [2]rotaxanes **23·A** and **42·A** because of a combination of stronger aromatic stacking interactions and a weakening of the halide binding ability of the host. However, quantitative estimations of the station occupancies demonstrated that the XB [2]rotaxane **43·A** produced superior iodide-mediated switching in competitive $CDCl_3$:CD_3OD solvent mixtures courtesy of strong halide coordination between orthogonal macrocycle and axle components.

Taking inspiration from these results, it would be desirable to utilise the power of halogen bonding anion recognition to construct bistable [2]rotaxanes capable of anion-induced molecular motion in highly competitive aqueous solvent environments. This would require the incorporation of water-solubilising motifs, such as cyclodextrin-based stopper groups in the axle component, whilst the inclusion of cooperative bidentate XB donors in the macrocycle might enhance the anion recognition properties of the interlocked host.

Finally, based on precedent from the literarure,[59–61] preliminary work has been carried out to investigate the possibility of utilising Li^+ metal cations to stimulate co-conformational change in [2]rotaxane **43·A**. Initial ^{1}H NMR spectroscopic studies suggested that the Lewis basic carbonyl groups of the NDI station and polyether cavity of the macrocycle were capable of coordinating Li^+, resulting in an increase in macrocycle occupation at this site (Figure 2.38). The ability of NDI to act as a recognition site for group I metal cations or even anionic species (by means of anion–π interactions) would be an intriguing avenue for future work into the construction of chemically stimulated molecular machines.

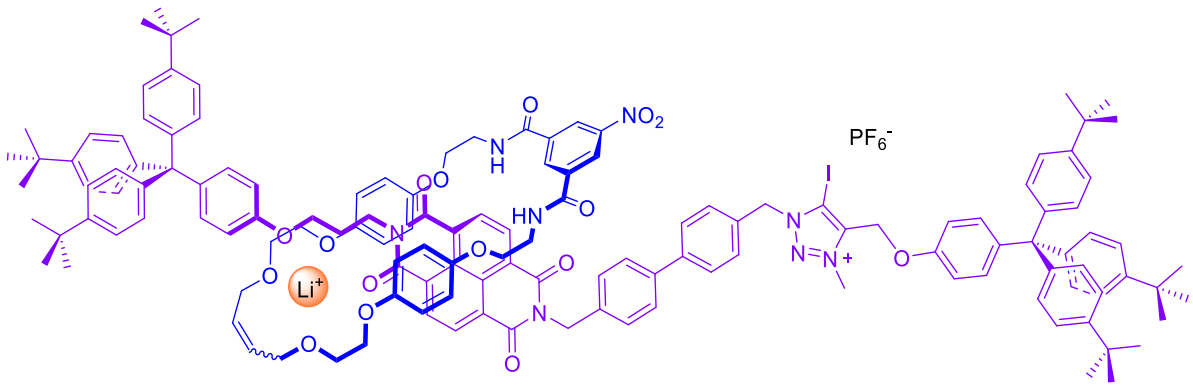


*Figure 2.38. Occupation of the NDI station in **43·PF6** facilitated by coordination of Li^+ between macrocycle and axle components.*

2.6. References

1 J. F. Stoddart, *Acc. Chem. Res.*, 2001, **34**, 410–411.
2 R. Ballardini, V. Balzani, A. Credi, M. T. Gandolfi and M. Venturi, *Acc. Chem. Res.*, 2001, **34**, 445–455.
3 E. R. Kay, D. A. Leigh and F. Zerbetto, *Angew. Chem. Int. Ed.*, 2007, **46**, 72–191.
4 A. Coskun, M. Banaszak, R. D. Astumian, J. F. Stoddart and B. A. Grzybowski, *Chem. Soc. Rev.*, 2011, **41**, 19–30.
5 E. A. Neal and S. M. Goldup, *Chem. Commun.*, 2014, **50**, 5128–5142.
6 S. Erbas-Cakmak, D. A. Leigh, C. T. McTernan and A. L. Nussbaumer, *Chem. Rev.*, 2015, **115**, 10081–10206.
7 F. Vögtle, W. M. Müller, U. Müller, M. Bauer and K. Rissanen, *Angew. Chem. Int. Ed. Engl.*, 1993, **32**, 1295–1297.
8 V. Balzani, A. Credi and M. Venturi, *Chem. Soc. Rev.*, 2009, **38**, 1542–1550.
9 R. A. Bissell, E. Córdova, A. E. Kaifer and J. F. Stoddart, *Nature*, 1994, **369**, 133–137.
10 A. Livoreil, C. O. Dietrich-Buchecker and J.-P. Sauvage, *J. Am. Chem. Soc.*, 1994, **116**, 9399–9400.
11 J. Berná, C. Franco-Pujante and M. Alajarín, *Org. Biomol. Chem.*, 2013, **12**, 474–478.
12 G. T. Spence, M. B. Pitak and P. D. Beer, *Chem. – Eur. J.*, 2012, **18**, 7100–7108.
13 N. H. Evans, C. J. Serpell and P. D. Beer, *Chem. – Eur. J.*, 2011, **17**, 7734–7738.
14 C. J. Serpell, R. Chall, A. L. Thompson and P. D. Beer, *Dalton Trans.*, 2011, **40**, 12052–12055.
15 E. V. Dzyuba, L. Kaufmann, N. L. Löw, A. K. Meyer, H. D. F. Winkler, K. Rissanen and C. A. Schalley, *Org. Lett.*, 2011, **13**, 4838–4841.
16 J. J. Gassensmith, S. Matthys, J.-J. Lee, A. Wojcik, P. V. Kamat and B. D. Smith, *Chem. – Eur. J.*, 2010, **16**, 2916–2921.
17 H. Zheng, W. Zhou, J. Lv, X. Yin, Y. Li, H. Liu and Y. Li, *Chem. – Eur. J.*, 2009, **15**, 13253–13262.
18 T.-C. Lin, C.-C. Lai and S.-H. Chiu, *Org. Lett.*, 2009, **11**, 613–616.
19 M. J. Barrell, D. A. Leigh, P. J. Lusby and A. M. Z. Slawin, *Angew. Chem. Int. Ed.*, 2008, **47**, 8036–8039.
20 C. M. Keaveney and D. A. Leigh, *Angew. Chem. Int. Ed.*, 2004, **43**, 1222–1224.
21 C.-F. Lin, C.-C. Lai, Y.-H. Liu, S.-M. Peng and S.-H. Chiu, *Chem. – Eur. J.*, 2007, **13**, 4350–4355.
22 Y.-L. Huang, W.-C. Hung, C.-C. Lai, Y.-H. Liu, S.-M. Peng and S.-H. Chiu, *Angew. Chem. Int. Ed.*, 2007, **46**, 6629–6633.
23 T.-C. Lin, C.-C. Lai and S.-H. Chiu, *Org. Lett.*, 2009, **11**, 613–616.

24 L. Liu, Y. Liu, P. Liu, J. Wu, Y. Guan, X. Hu, C. Lin, Y. Yang, X. Sun, J. Ma and L. Wang, *Chem. Sci.*, 2013, **4**, 1701–1706.
25 M. V. R. Raju and H.-C. Lin, *Org. Lett.*, 2013, **15**, 1274–1277.
26 H. Zhang, J. Hu and D.-H. Qu, *Org. Lett.*, 2012, **14**, 2334–2337.
27 M. J. Langton, S. W. Robinson, I. Marques, V. Félix and P. D. Beer, *Nat. Chem.*, 2014, **6**, 1039–1043.
28 L. C. Gilday, S. W. Robinson, T. A. Barendt, M. J. Langton, B. R. Mullaney and P. D. Beer, *Chem. Rev.*, 2015, **115**, 7118–7195.
29 B. R. Mullaney, A. L. Thompson and P. D. Beer, *Angew. Chem. Int. Ed.*, 2014, **53**, 11458–11462.
30 V. Aucagne, K. D. Hänni, D. A. Leigh, P. J. Lusby and D. B. Walker, *J. Am. Chem. Soc.*, 2006, **128**, 2186–2187.
31 J.-C. Chambron, J.-P. Sauvage, K. Mislow, A. De Cian and J. Fischer, *Chem. – Eur. J.*, 2001, **7**, 4085–4096.
32 H. W. Gibson, S. H. Lee, P. T. Engen, P. Lecavalier, J. Sze, Y. X. Shen and M. Bheda, *J. Org. Chem.*, 1993, **58**, 3748–3756.
33 L. M. Hancock and P. D. Beer, *Chem. Commun.*, 2011, **47**, 6012–6014.
34 J. D. Crowley, K. D. Hänni, A.-L. Lee and D. A. Leigh, *J. Am. Chem. Soc.*, 2007, **129**, 12092–12093.
35 H. C. Kolb, M. G. Finn and K. B. Sharpless, *Angew. Chem. Int. Ed.*, 2001, **40**, 2004–2021.
36 V. V. Rostovtsev, L. G. Green, V. V. Fokin and K. B. Sharpless, *Angew. Chem. Int. Ed.*, 2002, **41**, 2596–2599.
37 C. W. Tornøe, C. Christensen and M. Meldal, *J. Org. Chem.*, 2002, **67**, 3057–3064.
38 W. S. Brotherton, R. J. Clark and L. Zhu, *J. Org. Chem.*, 2012, **77**, 6443–6455.
39 D. N. Barsoum, N. Okashah, X. Zhang and L. Zhu, *J. Org. Chem.*, 2015, **80**, 9542–9551.
40 M. R. Sambrook, P. D. Beer, J. A. Wisner, R. L. Paul, A. R. Cowley, F. Szemes and M. G. B. Drew, *J. Am. Chem. Soc.*, 2005, **127**, 2292–2302.
41 L. M. Hancock, L. C. Gilday, S. Carvalho, P. J. Costa, V. Félix, C. J. Serpell, N. L. Kilah and P. D. Beer, *Chem. – Eur. J.*, 2010, **16**, 13082–13094.
42 M. E. Bakleh, V. Sol, K. Estieu-Gionnet, R. Granet, G. Déléris and P. Krausz, *Tetrahedron*, 2009, **65**, 7385–7392.
43 K.-Y. Ng, V. Felix, S. M. Santos, N. H. Rees and P. D. Beer, *Chem. Commun.*, 2008, 1281–1283.
44 J. A. Wisner, P. D. Beer and M. G. B. Drew, *Angew. Chem. Int. Ed.*, 2001, **40**, 3606–3609.
45 J. Pancholi, D. J. Hodson, K. Jobe, G. A. Rutter, S. M. Goldup and M. Watkinson, *Chem. Sci.*, 2014, **5**, 3528–3535.
46 M. R. Sambrook, P. D. Beer, M. D. Lankshear, R. F. Ludlow and J. A. Wisner, *Org. Biomol. Chem.*, 2006, **4**, 1529–1538.
47 K. Bala and H. C. Hailes, *Synthesis*, 2005, 3423–3427.
48 M. D. Lankshear, N. H. Evans, S. R. Bayly and P. D. Beer, *Chem. – Eur. J.*, 2007, **13**, 3861–3870.
49 M. S. Cubberley and B. L. Iverson, *J. Am. Chem. Soc.*, 2001, **123**, 7560–7563.
50 H. Zheng, W. Zhou, J. Lv, X. Yin, Y. Li, H. Liu and Y. Li, *Chem. – Eur. J.*, 2009, **15**, 13253–13262.
51 *Wiley: Greene's Protective Groups in Organic Synthesis, 4th Edition - Peter G. M. Wuts, Theodora W. Greene*, .
52 W. S. Horne, N. Ashkenasy and M. R. Ghadiri, *Chem. – Eur. J.*, 2005, **11**, 1137–1144.
53 S. V. Bhosale, C. H. Jani and S. J. Langford, *Chem. Soc. Rev.*, 2008, **37**, 331–342.
54 P. Pengo, G. D. Pantoş, S. Otto and J. K. M. Sanders, *J. Org. Chem.*, 2006, **71**, 7063–7066.
55 L. C. Gilday, S. W. Robinson, T. A. Barendt, M. J. Langton, B. R. Mullaney and P. D. Beer, *Chem. Rev.*, 2015, **115**, 7118–7195.
56 M. J. Langton, S. W. Robinson, I. Marques, V. Félix and P. D. Beer, *Nat. Chem.*, 2014, **6**, 1039–1043.
57 G. Lu, S. Lam and K. Burgess, *Chem. Commun.*, 2006, 1652–1654.
58 O. Mitsunobu and M. Yamada, *Bull. Chem. Soc. Jpn.*, 1967, **40**, 2380–2382.

59 G. Kaiser, T. Jarrosson, S. Otto, Y.-F. Ng, A. D. Bond and J. K. M. Sanders, *Angew. Chem. Int. Ed.*, 2004, **43**, 1959–1962.
60 S. A. Vignon, T. Jarrosson, T. Iijima, H.-R. Tseng, J. K. M. Sanders and J. F. Stoddart, *J. Am. Chem. Soc.*, 2004, **126**, 9884–9885.
61 T. Iijima, S. A. Vignon, H.-R. Tseng, T. Jarrosson, J. K. M. Sanders, F. Marchioni, M. Venturi, E. Apostoli, V. Balzani and J. F. Stoddart, *Chem. – Eur. J.*, 2004, **10**, 6375–6392.

Chapter Three
Oxoanion recognition and shuttling in four-station [3]rotaxanes

3. OXOANION RECOGNITION AND SHUTTLING IN FOUR-STATION [3]ROTAXANES

3.1 Introduction

3.1.1. Oxoanion recognition

As previously discussed in Section 1.1, oxoanions such as ATP are essential to biological processes within living organisms,[1] and anthropogenic pollutants rich in phosphate, sulfates and nitrates are linked with environmental degredation.[2,3] In particular, over-exposure to nitrate *via* contaminated drinking water is associated with the formation of carcinogenic nitrosamines and a range of diseases such as methemoglobinemia (blue baby syndrome) in infants.[4] This provides the impetus for chemists to design and construct synthetic receptors capable of binding oxoanions. However, the selective recognition of nitrate presents a specific challenge owing to the anion's inherent low affinity for hydrogen bonds and high energy of solvation.[5]

The small number of nitrate-selective acyclic and macrocyclic host systems reporting nitrate selectivity, e.g. Ghosh's tripodal receptor[6] (Figure 3.1a), has motivated Beer and co-workers to synthesise interlocked molecules capable of nitrate recognition in competitive solvent media.[7,8] Most recently the unique three-dimensional cavity created between a bis-triazolium-acridine-containing axle and isophthalamide macrocycle components of a [2]rotaxane was demonstrated to selectively recognise nitrate over a range of more basic oxoanion guests in an aqueous, organic solvent mixture (Figure 3.1b).[9] However, in similar fashion to previous nitrate-designed [2]rotaxane and [2]catenane interlocked hosts[7,8] a comparable affinity for chloride was also observed.

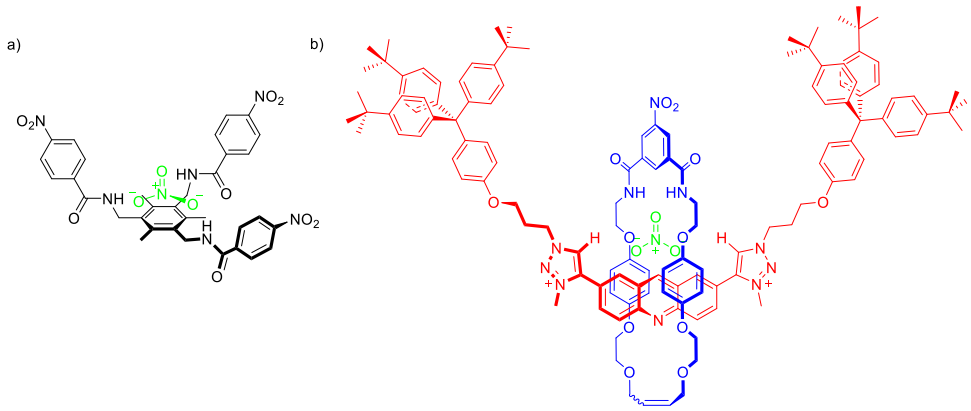


Figure 3.1. a) Ghosh's tripodal nitrate receptor[6] and b) Beer's bis-triazolium-acridine [2]rotaxane that exhibits selectivity for nitrate over other oxoanions.[9]

The difficulties associated with using conventional non-covalent interactions such as hydrogen bonding for selective nitrate recognition provide the motivation for utilising halogen bond donor groups in anion receptor design. Resnati, Metrangolo and co-workers have reported an acyclic 2-iodo-imidazolium receptor that exhibited a strong affinity for oxoanions over an HB analogue in DMSO-d_6 (Figure 1.22a).[10] Beer *et al.* have also reported a bidentate bis-iodo-triazolium-based receptor that displays enhanced perrhenate recognition in water compared to the proto-triazolium-containing analogue (Figure 3.2).[11] However, the use of strong and highly directional charge-assisted halogen bonding has not yet been exploited in the design of interlocked host molecules containing three-dimensional cavities to target oxoanion guest recognition.

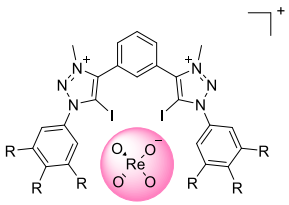


Figure 3.2. Beer's acyclic bis-iodo-triazolium-based receptor that utilises charge-assisted XB for perrhenate recognition in water.[11] R = $(OCH_2CH_2)_4OMe$.

3.1.2. Higher-order interlocked assemblies

Over half a century since the synthesis of the first mechanically interlocked molecular assemblies (Section 2.1.1),[12,13] increasingly creative synthetic methodologies have allowed the construction of

higher-order interlocked architectures exhibiting startling complexities.[14–16] A growing number of intricate topologies formed from rings linked *via* mechanical bonds have been reported including knots,[17–21] Borromean rings[22] and a Star of David catenane (Figure 3.3a).[23] The latter consists of two triply entwined 114-membered rings (two rings, six crossings) expanding on previous work that saw the development of a pentafoil knot[24] (one ring, five crossings) adapted from Lehn's original pentanuclear Fe(II)-helicate (Figure 1.33).[25] The vast majority of this work has been made possible by the extensive use of metal-template-directed syntheses.[26] This is also evident in the construction of a variety of higher-order rotaxane-based structures such as Leigh's [4]rotaxane in which three macrocycles are assembled onto an axle component by an iterative procedure through the repeated use of a single Pd(II) template site (Figure 3.3b).[27]

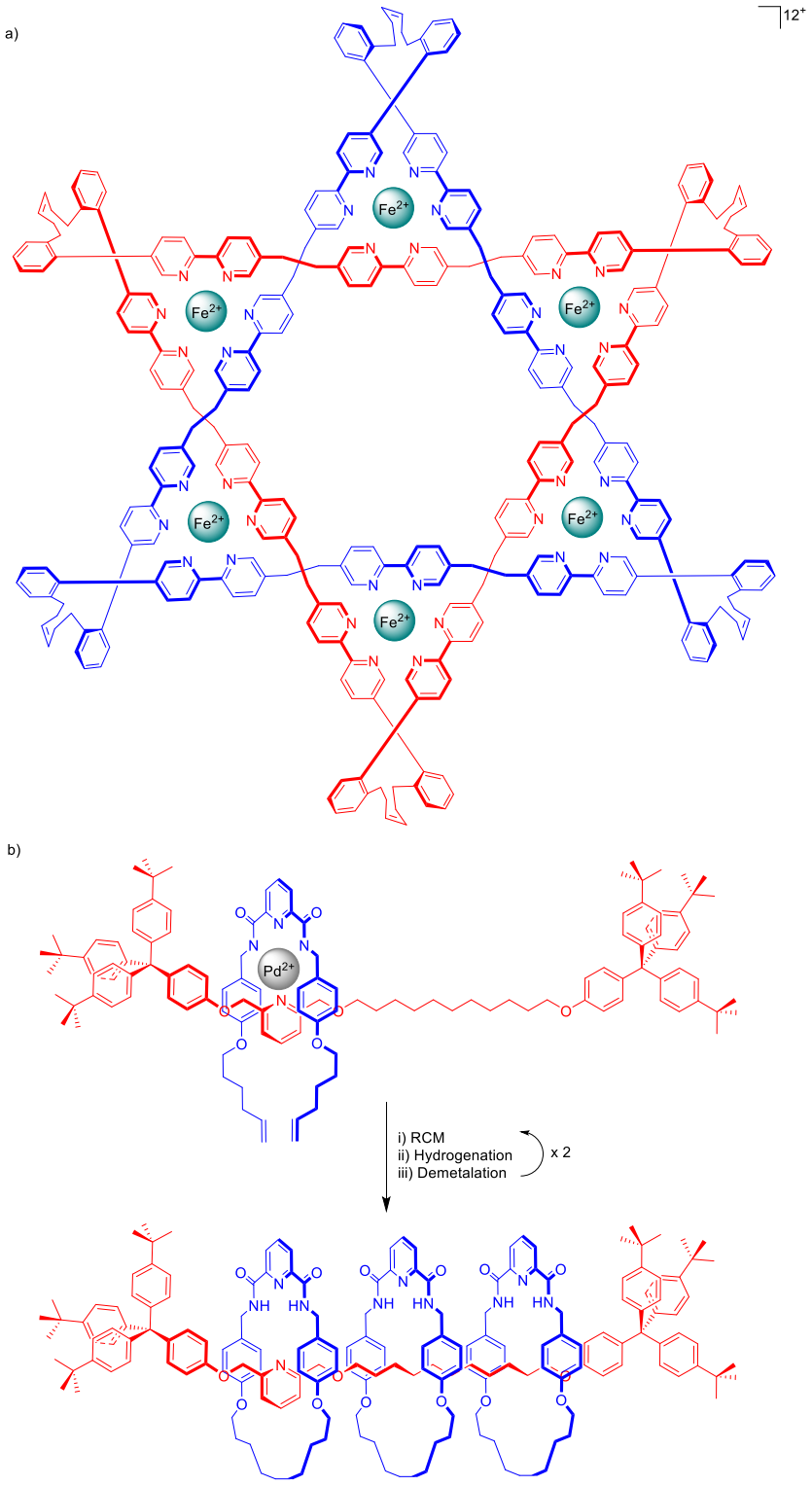


Figure 3.3. Complex interlocked molecular topologies constructed by metal-directed syntheses such as a) a Star of David [2]catenane[23]and b) a [4]rotaxane.[27]

Beyond the challenge presented in the construction of interlocked architectures, chemists also seek to harness the properties of mechanical bonding, particularly their large amplitude motions for

exploitation in artificial molecular machinery.[28–31] Sauvage's cyclic [4]rotaxane neatly demonstrates this principle since it can be switched from an elongated co-conformation to one in which the structure is collapsed, producing compressor-like motion, upon removal of the templating Cu(I) cations (Figure 3.4).[32,33]

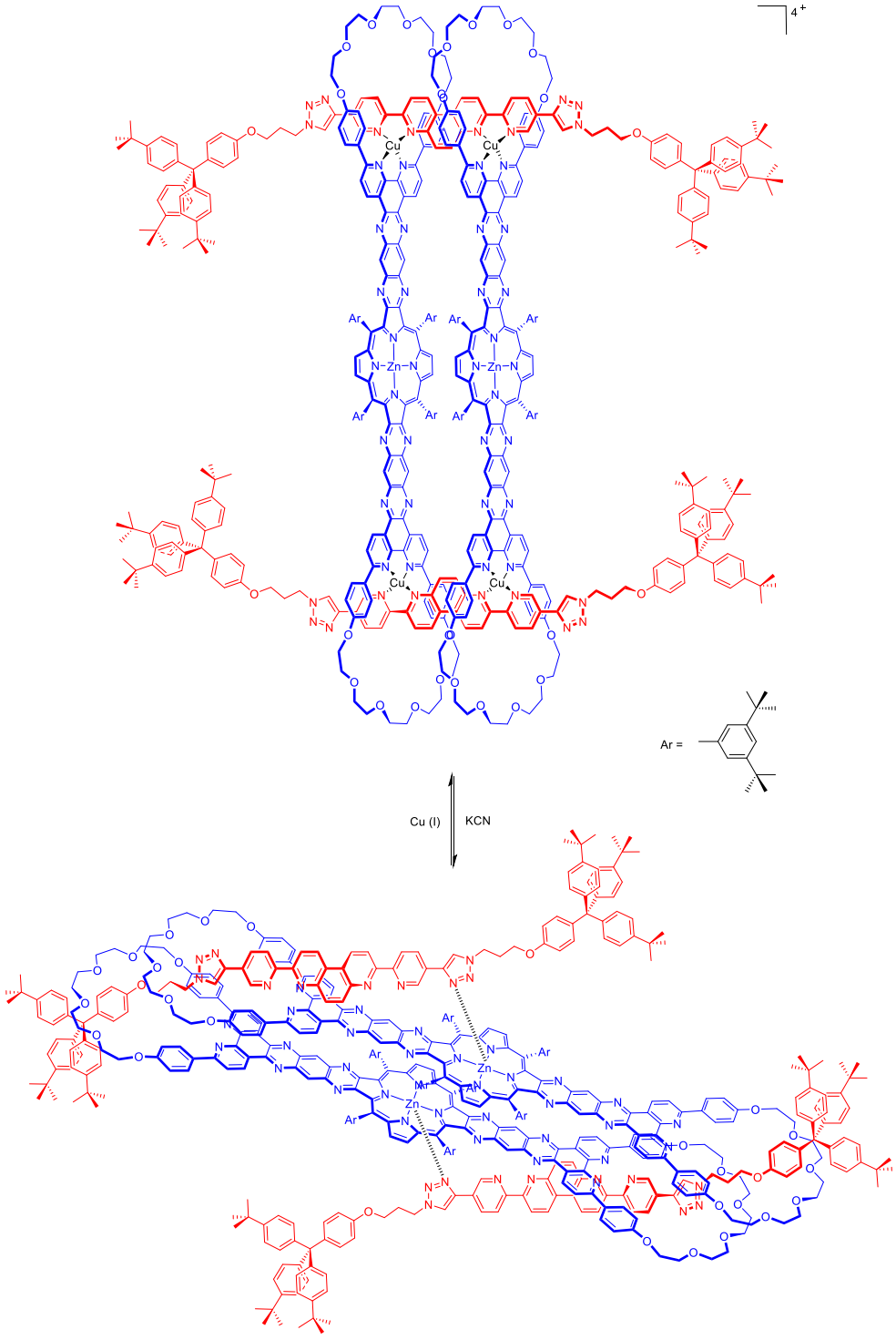


Figure 3.4. Sauvage's [4]rotaxane molecular press.[32,33]

In contrast to cation templation, anion templation has been relatively underexploited in the construction of mechanically interlocked molecules and as such, the synthesis of complex higher-order architectures directed by negatively-charged species are rare. Of the most impressive, the serendipitous formation of a chloride-templated [3]catenane[34] by Beer and co-workers inspired the design and synthesis of a "handcuff" catenane.[35] This unique molecular topology was realised by a double Grubbs'-catalysed RCM clipping reaction of a chloride-templated [3]pseudorotaxane assembly (Figure 3.5).

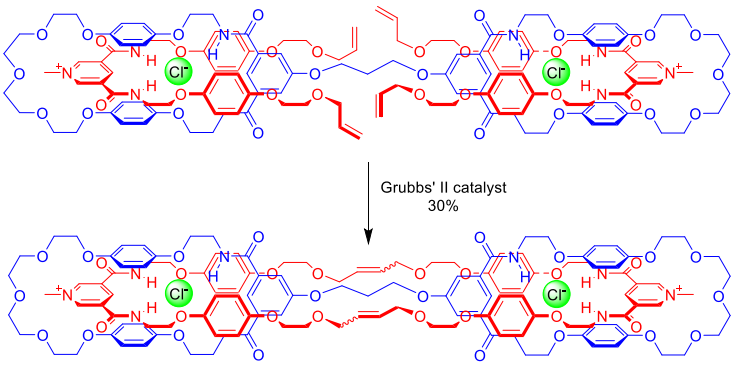


Figure 3.5. The synthesis of Beer's handcuff catenane via a double RCM clipping methodology.[35]

Meanwhile, Flood utilised an organophosphate group covalently integrated into an axle component to enable the synthesis of a [3]rotaxane by a stoppering methodology in good yield (Figure 3.6a).[36] Furthermore, Beer *et al.* have assembled [3]rotaxanes and exploited these systems for the purpose of anion sensing. This family of rotaxanes incorporate a ferrocene[37] or naphthalene[38] reporter group at the recognition sites allowing respective electro- or photo-chemical sensing of sulfate upon formation of a 1:1 stoichiometric sandwich-type complex with the anion (Figure 3.6b). A [3]rotaxane that coordinates a Cs^+ metal cation between two crownophane macrocycles has also been reported.[39]

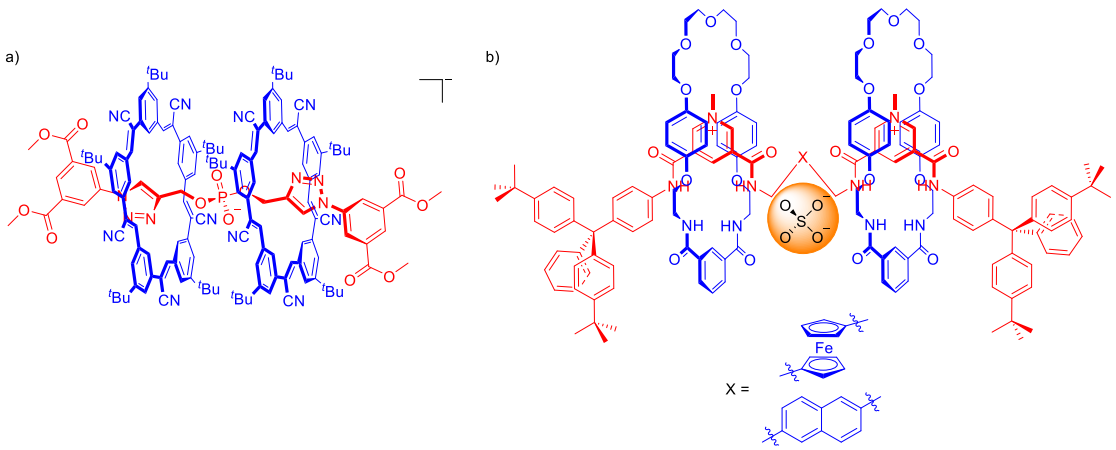


Figure 3.6. Higher-order interlocked structures formed via anion-templation a) Flood's bis-cyanostar [3]rotaxane[36] and b) Beer's sulfate-sensing [3]rotaxane host systems.[37,38]

3.1.3. Utilising molecular motion for anion sensing

Beyond the taming of molecular dynamics, the development of artificial molecular machines has also been motivated by their potential to process a selective input and use this to perform a specific task in the form of an output.[40] To this end, stimuli-responsive MIMs provide scaffolds for the construction of functioning molecular machines, switches, logic gates and drug-delivery systems.[30,41–43] As previously discussed in Section 2.1.3, stimuli based upon a molecular recognition event with an ionic species to trigger co-conformational change within an interlocked structure are relatively rare.[44–59] Among these, systems that use molecular motion induced by anion complexation to promote an output are even rarer.[44,45,49,58,59] However, by appropriate design, the unusual dynamic properties of interlocked host molecules can be exploited as a sophisticated means of achieving a selective and functional sensor response towards a target guest species, *via* the detection of co-conformational changes through photo- or electrochemical signalling (Figure 3.7).

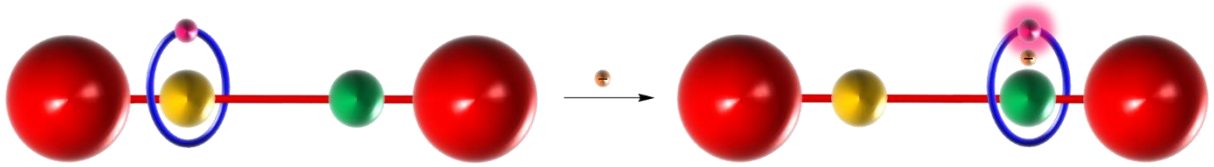


Figure 3.7. Schematic of anion sensing via a mechanism involving dynamic behaviour of a [2]rotaxane molecular shuttle.

Smith's [2]rotaxane is one example of a molecular shuttle that demonstrates this concept (Figure 3.8).[49] In the absence of an anion, the rotaxane fluorescence is partially quenched by the presence of the macrocycle over the squaraine unit. However, addition of chloride facilitates a change in rotaxane co-conformation *via* translocation of the macrocycle to either one of the two triazole anion recognition sites and a turn on fluorescence response is observed.

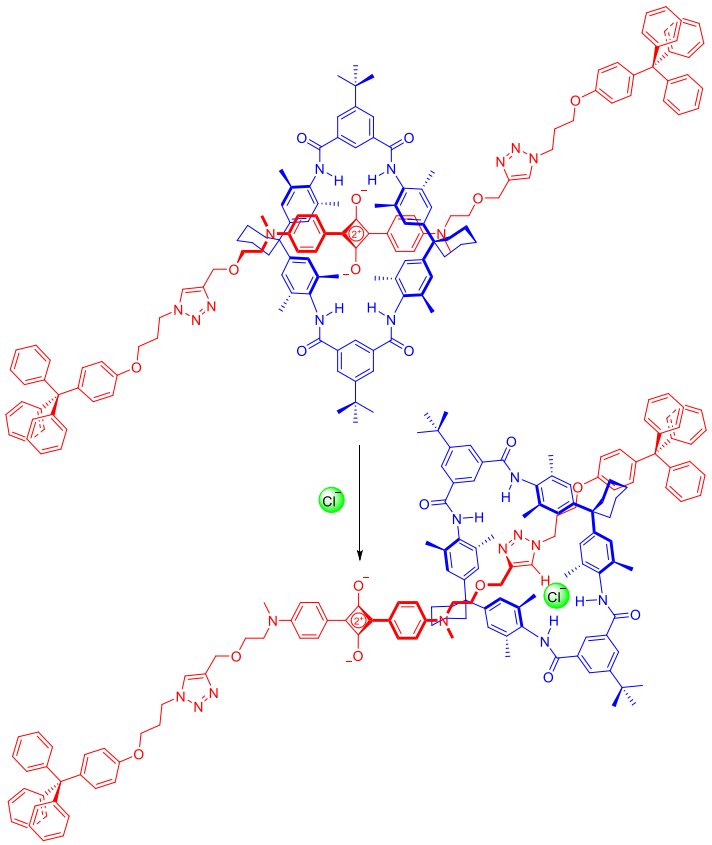


Figure 3.8. The chloride-induced shuttling exhibited by Smith's squaraine-based [2]rotaxane is accompanied by an increase in fluorescence emission intensity allowing it to optically sense this species via co-conformational change.[49]

Although the inherent flexibility of mechanically bound components in rotaxanes and catenanes contradicts Cram's preorganisation requirement for strong guest binding,[60] the penalty of reducing intramolecular dynamics upon recognition has been estimated to be small.[61] In addition, the mechanism of signal transduction based upon anion co-conformational change is particularly effective because it produces significant, well-defined responses. This is often in contrast to conventional anion-sensing systems, in which the reporter group is rigidly positioned proximal to the recognition site (see Figure 1.26).[62,63]

3.1.4. Chapter objectives

The work described in this chapter expands the principles outlined in Chapter Two of using anion recognition in concert with donor–acceptor charge–transfer interactions to exert control over solution phase molecular shuttling in a rotaxane host system. Motivated by the desire for the translational motion to be stimulated by binding of environmentally relevant oxoanionic species, a novel [3]rotaxane interlocked host is designed containing a symmetric four-station axle component and two isophthalamide-based macrocycles.

Specifically, two NDI stations are covalently integrated into the extremities of the axle, whilst the central section will comprise a HB/XB bis-triazolium motif to target oxoanion recognition *via* multiple HB and/or XB interactions. The clipping of two macrocyclic precursors around this axle using chloride-templation will produce an exotic interlocked anion receptor that employs a dynamic pincer-like mechanism in which both macrocycles can shuttle from the periphery of the axle component towards the core HB/XB bis-triazolium recognition sites to form a unique 1:1 stoichiometric oxoanion–rotaxane sandwich complex (Figure 3.9).

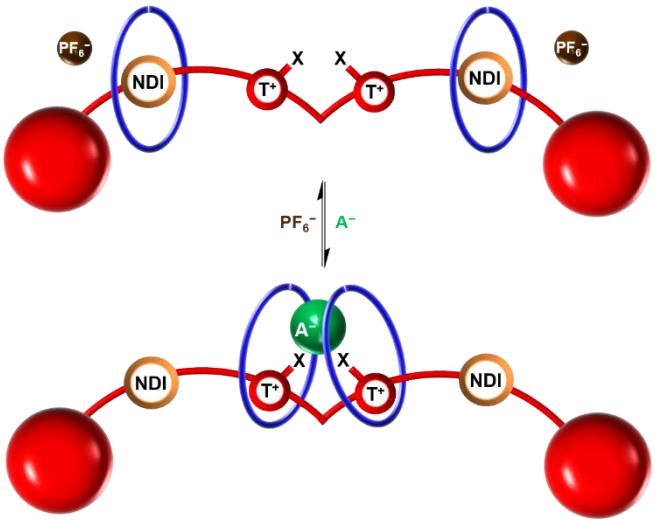


Figure 3.9. Schematic of a [3]rotaxane host design for the recognition of oxoanions (A^-) via a dynamic shuttling mechanism upon anion recognition. NDI = naphthalene diimide, T^+ = triazolium and X = I or H.

The inclusion of two NDI motifs into the target higher-order interlocked structures provides the potential for optical sensing of the macrocycle's position on the axle. Since this response is expected to be modulated by the nature of the counter anion, detailed investigations will be made into the anion sensing capabilities of these [3]rotaxanes.

3.2. Synthesis of four-station HB and XB axle components*

The synthesis of HB and XB four-station axle components containing two NDI motifs proximally positioned to phenyl trityl stopper termini, and each designed to be separated from a central bis-proto/iodo-triazolium anion recognition site by a rigid biphenyl spacer, was initially undertaken. The two HB/XB-triazolium stations were separated by a hydroquinone spacer to provide a bidentate binding cleft for anion recognition *via* the formation of complementary HB/XB interactions to oxygen atoms of an oxoanion such as nitrate (Figure 3.10).

* The work in the following section was published as a communication in the journal Angewandte Chemie: T. A. Barendt, A. Docker, I. Marques, V. Félix and P. D. Beer, *Angew. Chem. Int. Ed.*, 2016. DOI: 10.1002/anie.201604327

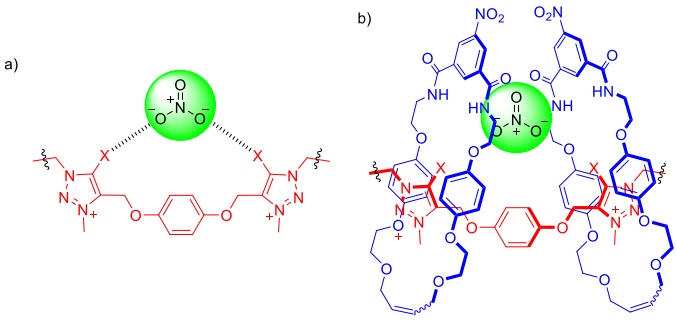
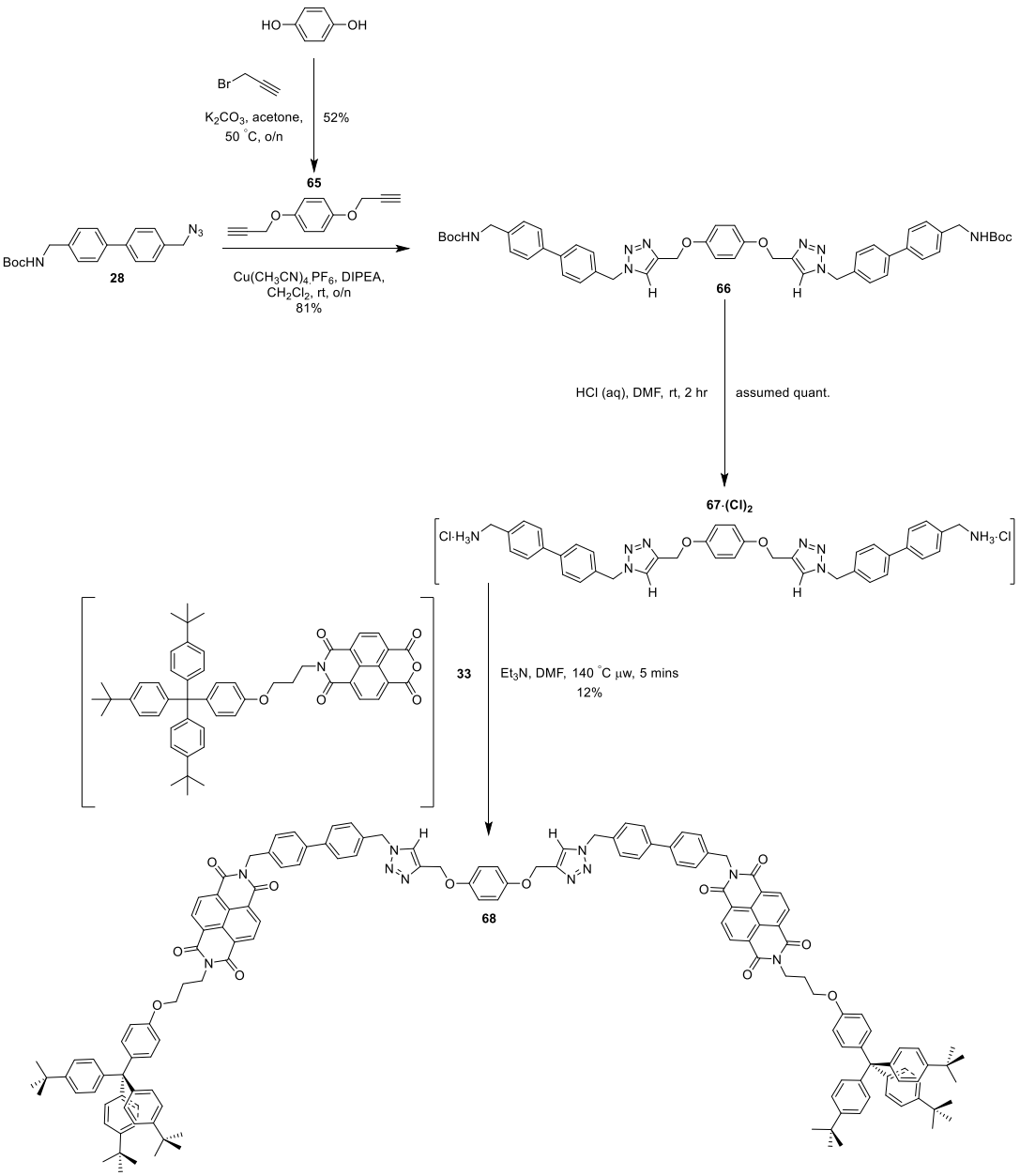


Figure 3.10. The XB/HB bis-triazolium recognition sites showing the potential coordination mode of an oxoanion guest to a) the bidentate axle and b) the [3]rotaxane. X = H, I

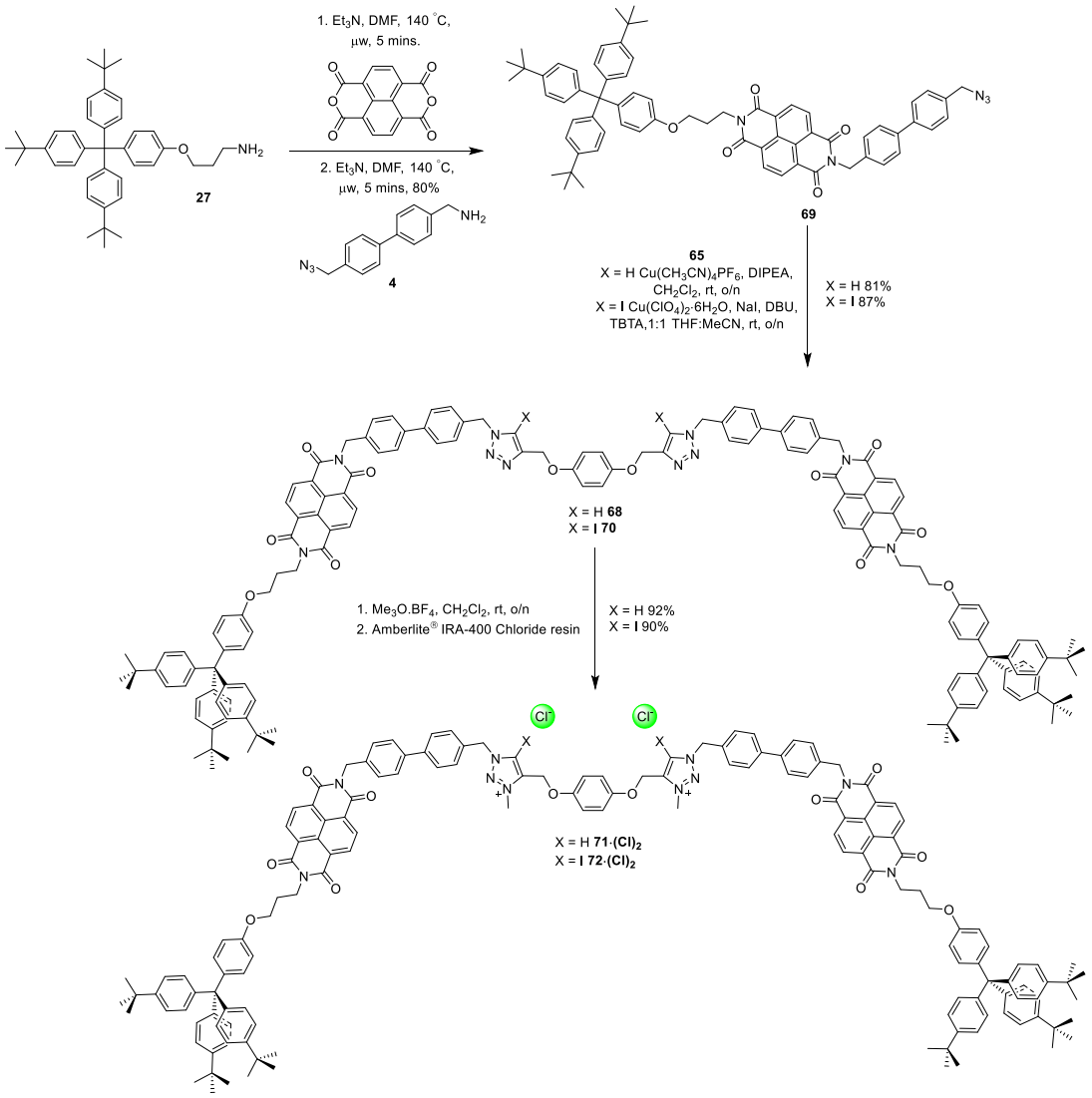
The neutral bis-proto-triazole-containing axle **68** was originally synthesised *via* the route shown in Scheme 3.1. Initially, bis-alkyne-functionalised hydroquinone **65** was prepared from a literature procedure[64] by heating commercial hydroquinone in acetone under basic conditions with a small excess of propargyl bromide. This alkyne was reacted with two equivalents of biphenyl azide **31** to afford the bis-triazole-containing derivative **66** in good yield. Cleavage of the Boc protecting groups was attempted by stirring **66** in DMF under acidic conditions. TLC analysis of the reaction indicated formation of the hydrochloride salt of the bis-amine, however, the insolubility of **67·(Cl)$_2$** in deuterated solvents precluded characterisation using ^{1}H NMR spectroscopy.

Unfortunately, this synthetic pathway was further hampered by the low yield of the condensation reaction between bis-amine **67·(Cl)$_2$** and two equivalents of anhydride intermediate **37** under the standard microwave conditions. Therefore further modification of the 'one pot' microwave procedure is required if it is to be utilised for couplings that are not simple bimolecular reactions between an amine and the mono-functionalised intermediate **33**.



*Scheme 3.1. Initial synthetic route to the HB four-station axle **68**.*

An alternative synthetic route towards the target four-station HB and XB axle components was adopted as shown in Scheme 3.2.



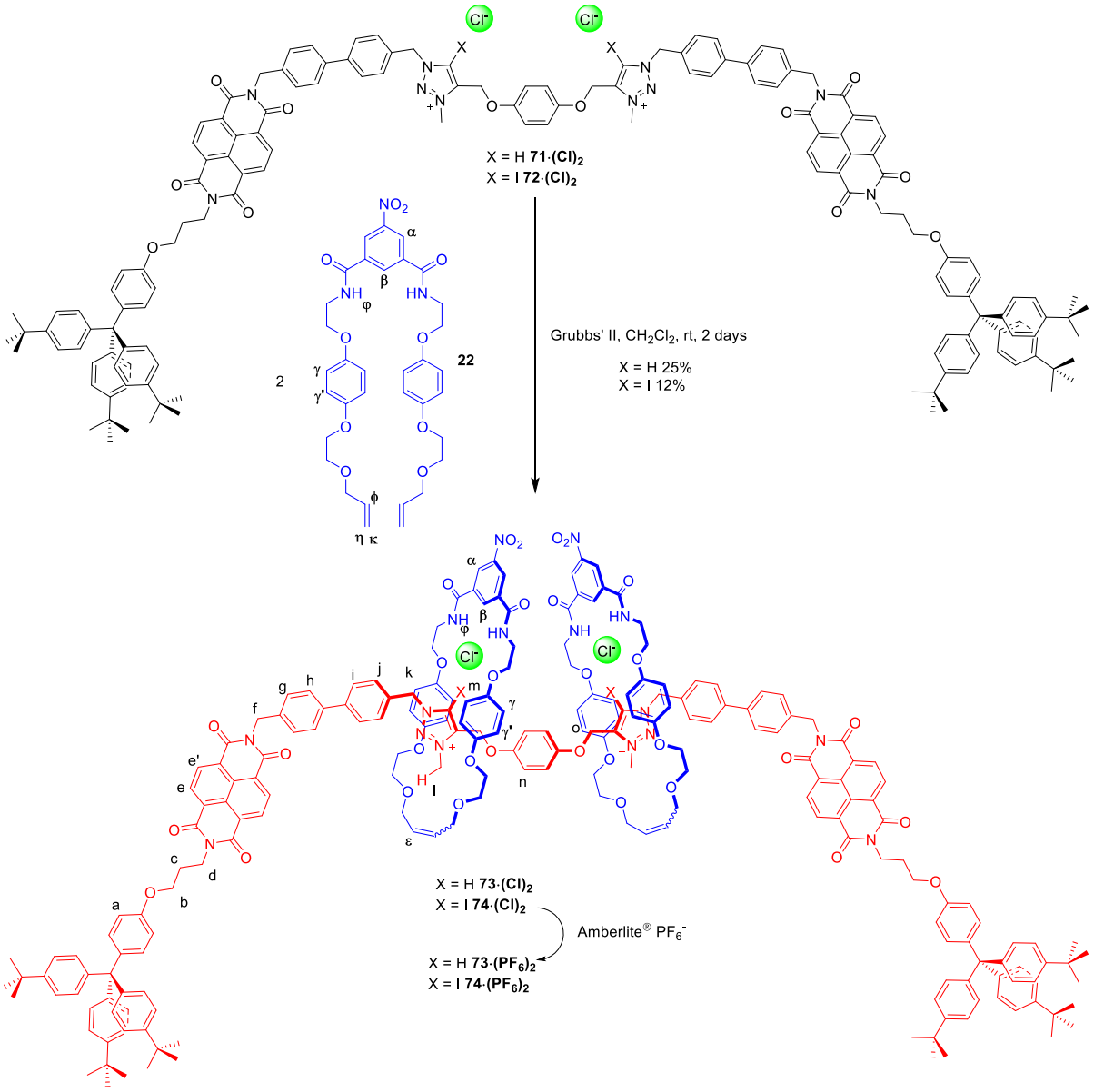
Scheme 3.2. Final synthetic route to the HB and XB four-station axles ***71·(Cl)₂*** *and* ***72·(Cl)₂****..*

The first stage was the functionalisation of 1,4,5,8-naphthalenetetracarboxylic dianhydride with amines **4** and **27**, using the established stepwise procedure under microwave conditions. This gave the desired mono-stoppered NDI biphenyl azide derivative **69** in a significantly larger yield than any symmetric side products. The bis-proto-triazole-containing axle **68** was then synthesised by a 'click' reaction between bis-alkyne **65** and two equivalents of azide **69** in dry CH_2Cl_2 under standard base-accelerated CuAAC conditions. The bis-iodo-triazole analogue **70** was prepared in similar fashion under CuAAC one-pot 'iodo-click' conditions in 87% yield. The axle precursors were subsequently reacted with $Me_3O{\cdot}BF_4$ to generate the bis-HB/XB-triazolium-containing axle components **71·(BF₄)₂** and **72·(BF₄)₂** in good yield. These dicationic axles were anion exchanged to the bis-chloride salts **71·(Cl)₂**

and **72·(Cl)$_2$** using chloride-loaded Amberlite® resin in preparation for anion-templated [3]rotaxane syntheses.

3.3. Synthesis of four-station HB and XB [3]rotaxanes

The HB and XB four-station [3]rotaxanes were prepared by a chloride-templated double-clipping procedure adapted from the [2]rotaxane syntheses previously described in Chapter Two (Scheme 3.3).



*Scheme 3.3. Synthesis of the HB and XB four-station [3]rotaxanes **73·(A)$_2$** and **74·(A)$_2$**.*

Axles **71·(Cl)$_2$** and **72·(Cl)$_2$** were individually stirred with three equivalents of bis-vinyl-appended isophthalamide macrocycle precursor **22** in dry CH_2Cl_2 for 30 minutes to allow association of the

components in solution. Following this, a catalytic amount of Grubbs' II catalyst was added to effect RCM of **22** and subsequent [3]rotaxane formation was observed in both cases by ESI mass spectrometry of the crude reaction mixture. Interestingly, this technique revealed that the reaction proceeded best under more dilute conditions of 1.5 mM (with respect to **71·(Cl)$_2$** or **72·(Cl)$_2$**) than the previous rotaxane systems described in Chapter 2 (5 mM with respect to the axle component), otherwise the predominant interlocked product was the [2]rotaxane. The target HB and XB interlocked structures **73·(Cl)$_2$** and **74·(Cl)$_2$** were isolated from crude reaction mixtures that also contained analogous [2]rotaxanes, ring closed macrocycle and starting materials using preparative silica thin-layer chromatography and anion exchanged to the bis-hexafluorophosphate salts **73·(PF$_6$)$_2$** and **74·(PF$_6$)$_2$** using an Amberlite® anion-exchange resin. All [3]rotaxane salts were fully characterised.

The truncated ^{1}H NMR spectra of [3]rotaxanes **73·(Cl)$_2$** and **74·(Cl)$_2$** alongside bis-vinyl macrocyclic precursor **22**, in $CDCl_3$, are shown in Figure 3.11. The $H_{\gamma,\gamma'}$ resonances each integrate for eight hydrogen nuclei, relative to the four axle phenyl trityl stopper aromatic protons H_a, indicating the presence of two macrocycle components in both interlocked systems. Furthermore, convergence of multiplet H_ϕ into a pseudo-singlet, integrating for four protons, and the disappearance of the vinylic multiplet H_η and H_κ in each [3]rotaxane spectrum, are characteristic of successful cyclisation of two equivalents of acyclic precursor around the HB/XB four-station axle.

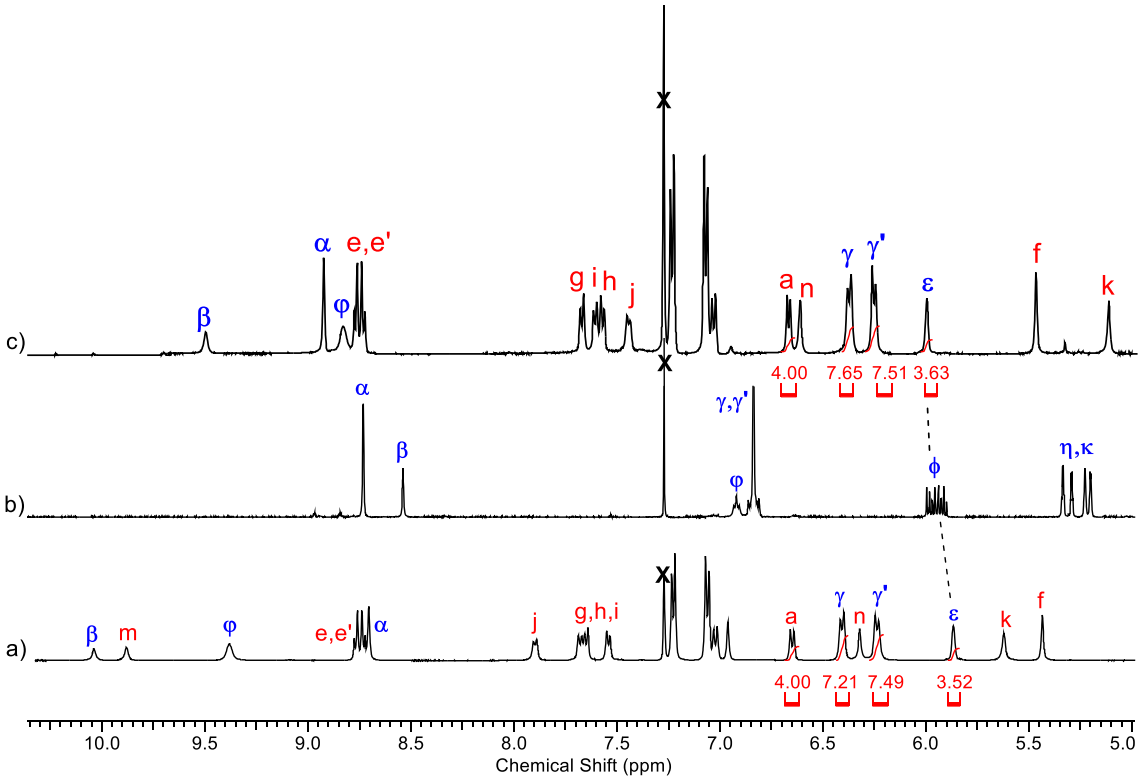


*Figure 3.11. Truncated ^{1}H NMR spectra of a) HB [3]rotaxane **73·(Cl)$_2$**, b) bis-vinyl-appended macrocycle precursor **22** and c) XB [3]rotaxane **74·(Cl)$_2$**. The integrals of selected proton resonances are referenced to H_a. ($CDCl_3$, 298 K, 400 MHz).*

3.4 ^{1}H NMR spectroscopic studies of chloride-induced shuttling behaviour

Following the successful isolation of the target HB and XB four-station [3]rotaxanes, one- and two-dimensional ^{1}H NMR spectroscopy were used to determine the dominant co-conformations of the bis-chloride and bis-hexafluorophosphate salts in $CDCl_3$. In turn, this would reveal if the [3]rotaxanes exhibited halide-induced shuttling. Comparisons of the ^{1}H NMR spectra of HB and XB [3]rotaxanes in the absence and presence of coordinating anions can be seen in Figure 3.12 and Figure 3.13.

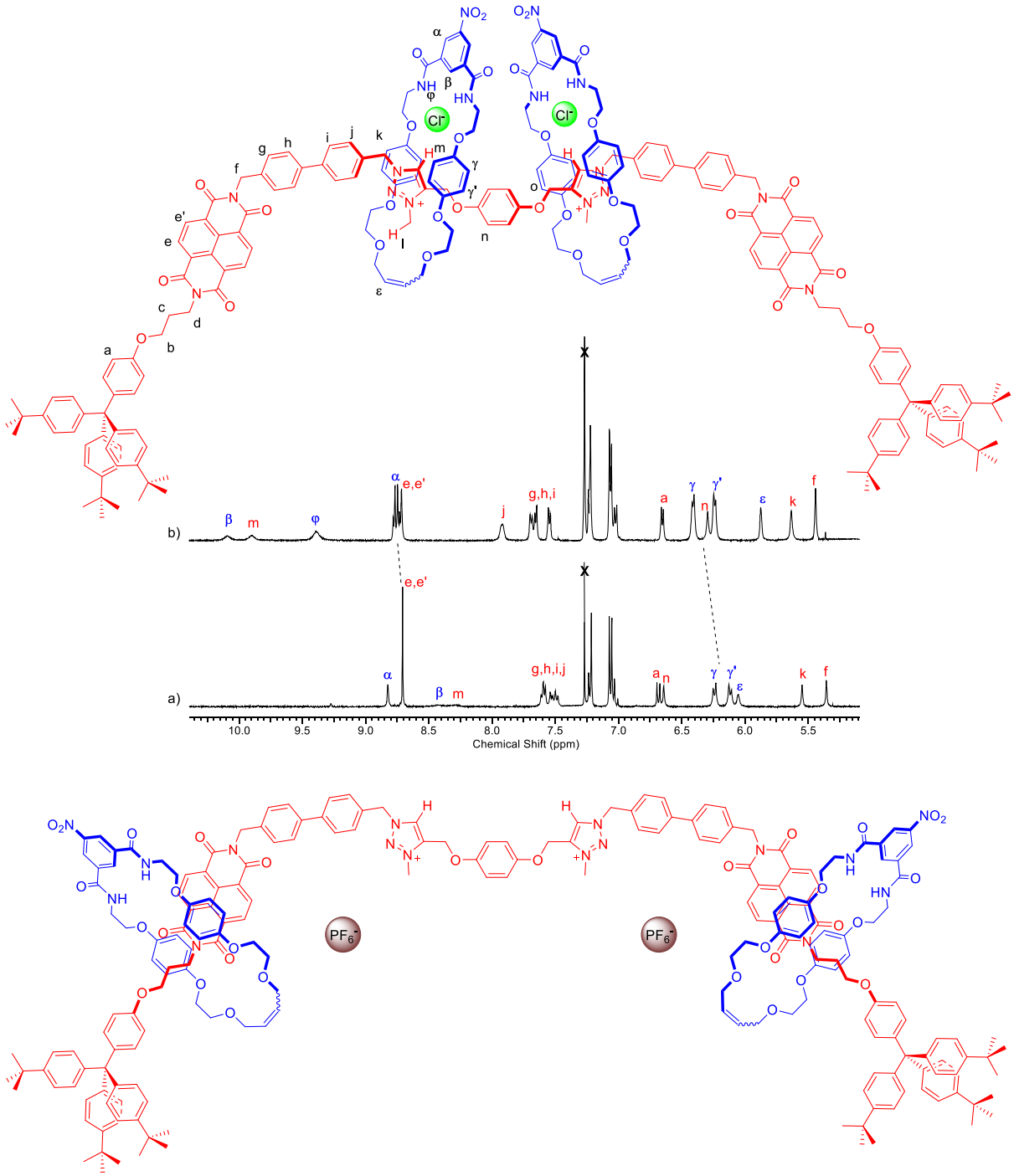


*Figure 3.12. Truncated ^{1}H NMR spectra of the HB [3]rotaxane **73·(A)$_2$** as its a) bis-hexafluorophosphate and b) bis-chloride salt ($CDCl_3$, 298 K, 400 MHz). The dominant co-conformations of the [3]rotaxane predicted from these spectra are also depicted.*

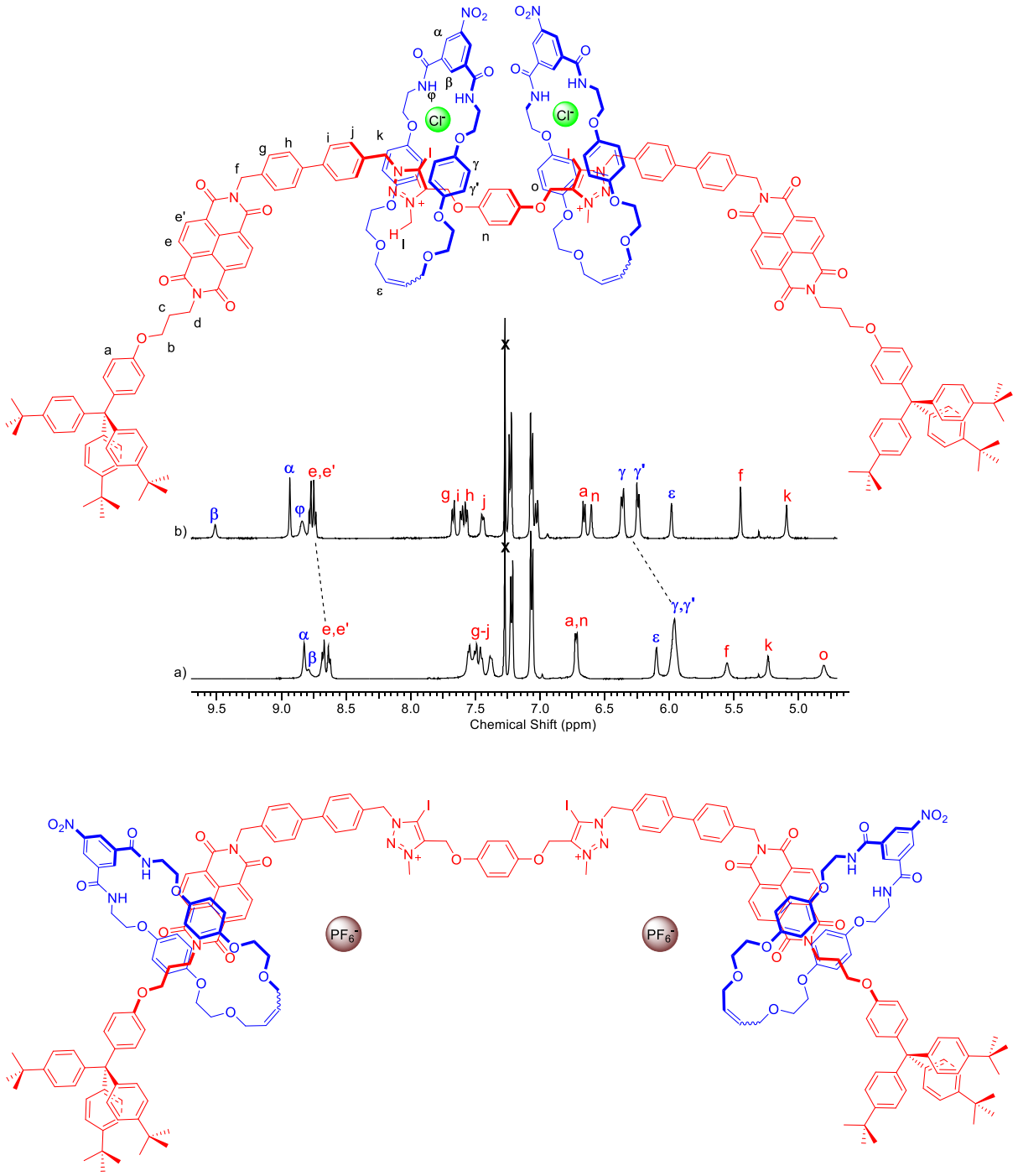


*Figure 3.13. Truncated ^{1}H NMR spectra of the XB [3]rotaxane **74·(A)$_2$** as its a) bis-hexafluorophosphate and b) bis-chloride salt (CDCl$_3$, 298 K, 400 MHz). The dominant co-conformations of the [3]rotaxane predicted from these spectra are also depicted.*

In both cases the resonances associated with the aromatic protons of the NDI and macrocycle hydroquinone protons ($H_{e,e'}$ and $H_{\gamma,\gamma'}$ respectively) are significantly downfield shifted in the ^{1}H NMR spectrum of the bis-chloride salt relative to the bis-hexafluorphosphate salt. This is diagnostic of a loss of strong donor–acceptor charge–transfer interactions, which would originally have occurred between

the peripheral NDI stations and macrocycle components in the absence of coordinating halide counter anions.

Furthermore, the downfield shifts of the acidic protons H_β and, in the case of the HB [3]rotaxane H_m, are indicative of halide recognition by multiple HB/XB interactions within the cavity created between the orthogonal bis-proto/iodo-triazolium axle and isophthalamide-containing macrocycle components (Figure 3.12 and Figure 3.13). This implies that upon exchange from hexafluorophosphate to chloride, translational motion of both macrocycles occurs from the two NDI stations at the extremities of the axle to the central anion recognition sites *via* a pincer-like shuttling mechanism (Figure 3.14). Importantly the symmetric nature of the ^{1}H NMR spectra of both [3]rotaxane salts suggests that the macrocycles occupy each set of stations equally meaning a macrocycle will only undergo switching on its own half of axle track.

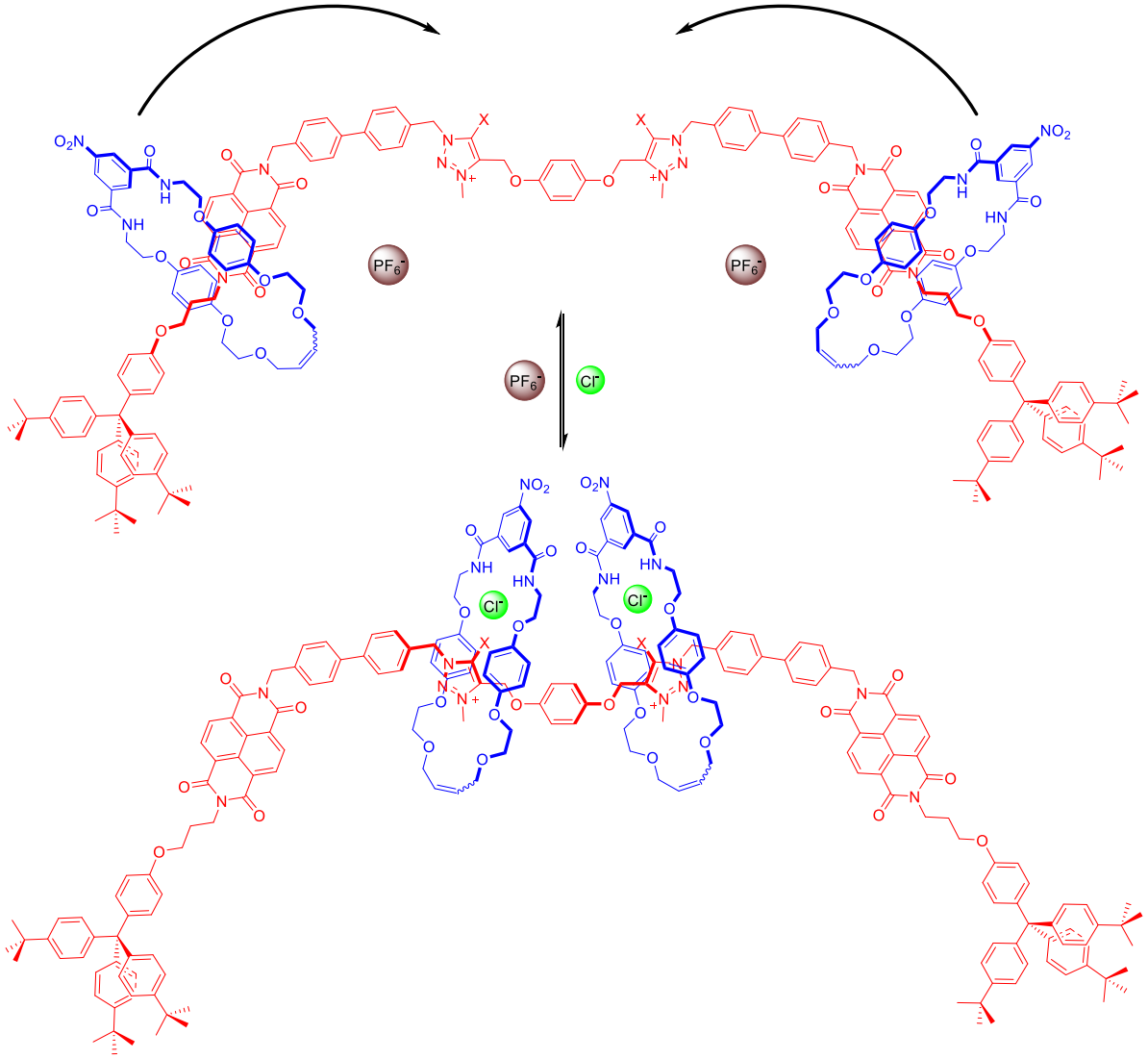


Figure 3.14. The chloride-induced pincer-like molecular motion exhibited by HB and XB [3]rotaxanes ***73·(PF$_6$)$_2$*** *and* ***74·(PF$_6$)$_2$****. X = H, I.*

The two co-conformations of the HB and XB [3]rotaxanes in the absence and presence of coordinating chloride counter-anions were confirmed using two-dimensional ^{1}H ROESY NMR experiments in $CDCl_3$ (Figure 3.15 and Figure 3.16).

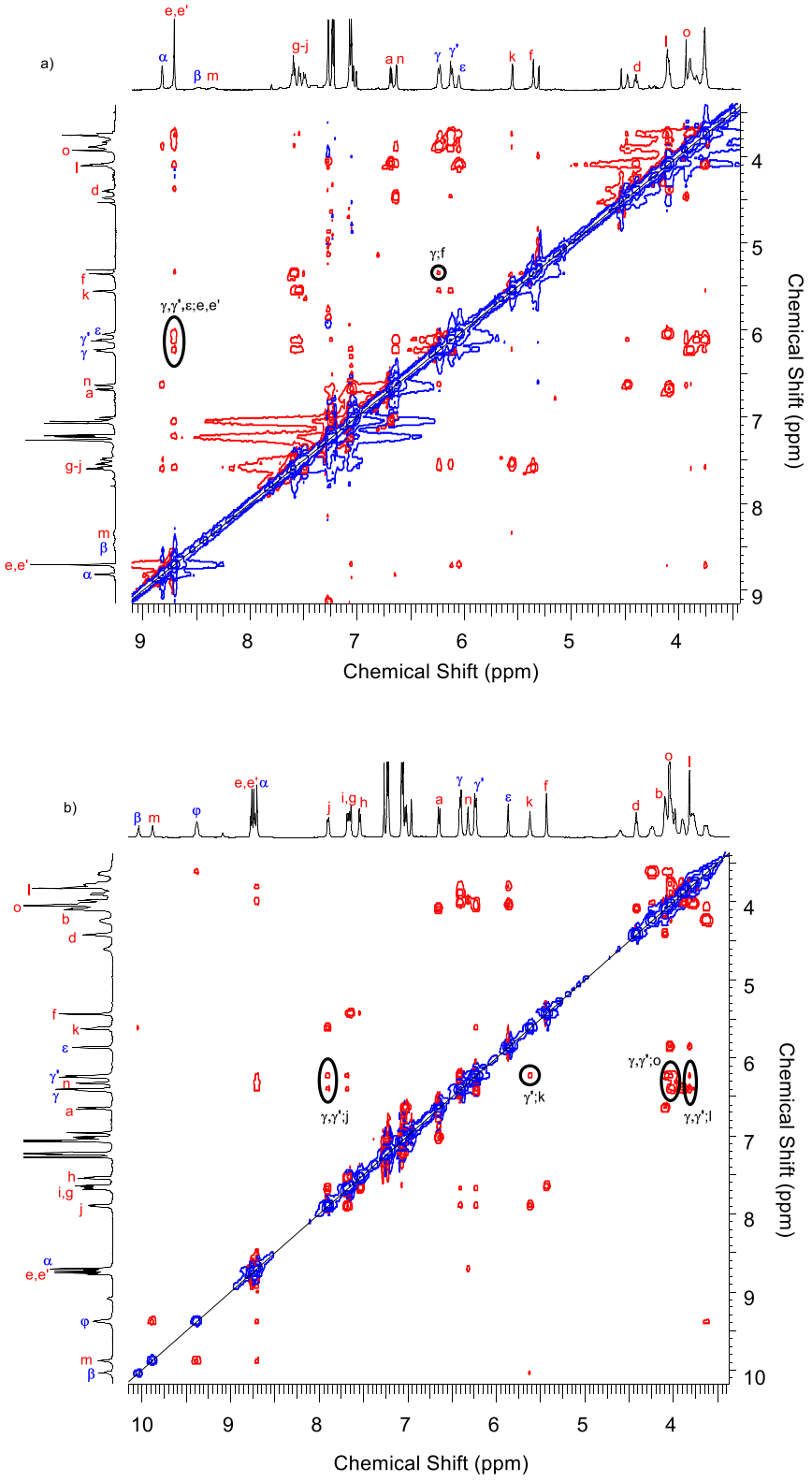


*Figure 3.15. Truncated ^{1}H–^{1}H ROESY NMR spectra of HB [3]rotaxane **73·(A)$_2$** as its a) bis-hexafluorophosphate and b) bis-chloride salt with selected coupling interactions highlighted ($CDCl_3$, 298 K, 500 MHz).*

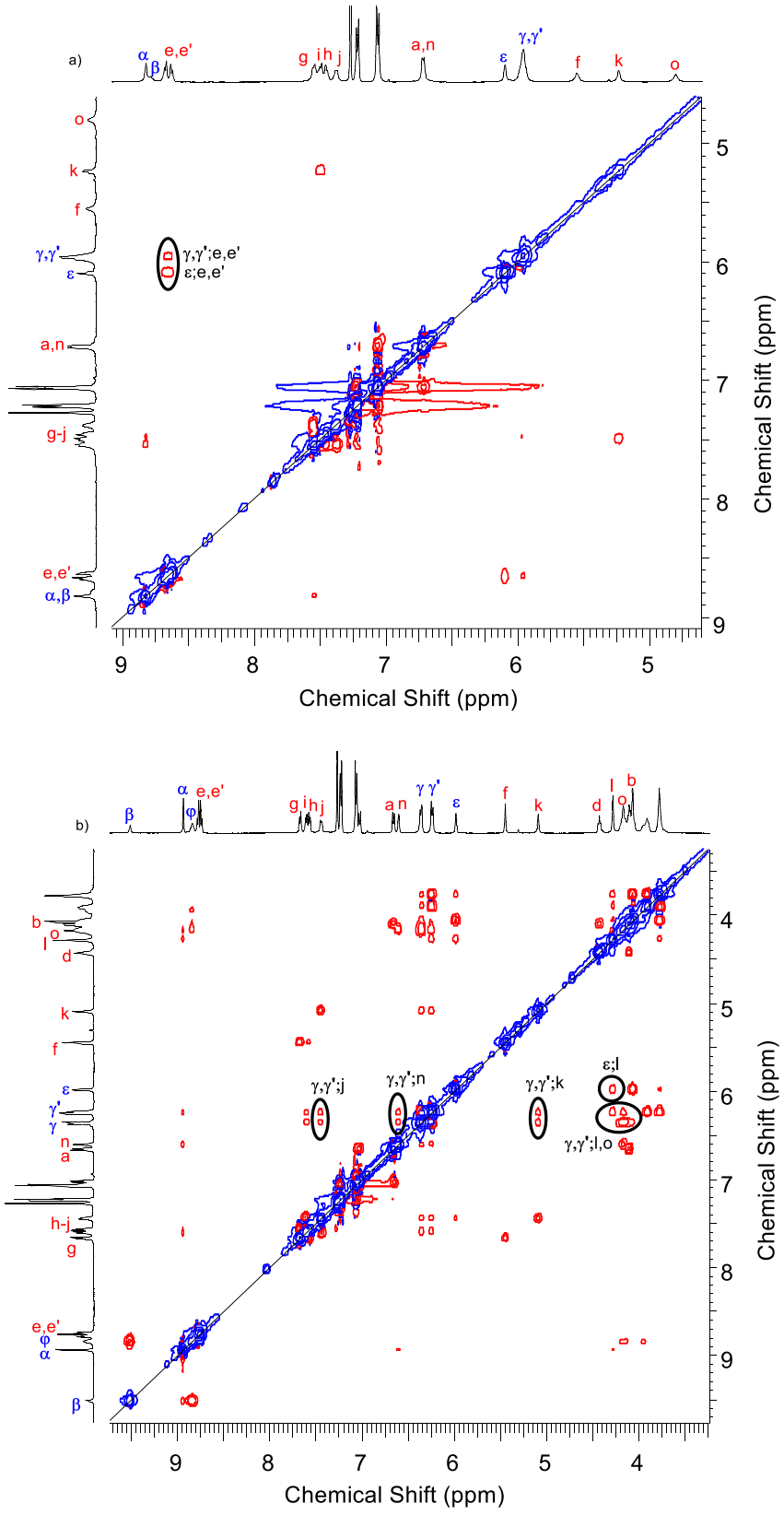


*Figure 3.16. Truncated ^{1}H–^{1}H ROESY NMR spectra of XB [3]rotaxane **74·(A)$_2$** as its a) bis-hexafluorophosphate and b) bis-chloride salt with selected coupling interactions highlighted ($CDCl_3$, 298 K, 500 MHz).*

The spectra of **73·(PF$_6$)$_2$** and **74·(PF$_6$)$_2$** show the expected coupling interactions between macrocycle proton resonances $H_{\gamma,\gamma'}$ and H_ε with the NDI aromatic protons $H_{e,e'}$, and for the HB [3]rotaxane a proximity between $H_{\gamma,\gamma'}$ and the methylene protons H_f (Figure 3.15a and Figure 3.16a). By contrast, the ^{1}H–^{1}H ROESY NMR spectra of the bis-chloride salts revealed none of these interactions and instead only through-space couplings between $H_{\gamma,\gamma'}$ and H_j, H_k, H_l and H_o, indicating that the macrocycles exclusively reside at the bis-triazolium recognition sites at the centre of the axle (Figure 3.15b and Figure 3.16b).

The one-station NDI [2]rotaxane **54** described in Section 2.3.6.2 was an appropriate model for the NDI stations of the [3]rotaxanes **73·(A)$_2$** and **74·(A)$_2$** because of identical chemical environments of this functional group.[†] Consequently, changes in the chemical shift of the NDI protons $H_{e,e'}$ could be used to estimate the macrocycle occupancies of each station in the bis-chloride and bis-hexafluorophosphate HB and XB [3]rotaxane salts **73·(Cl)$_2$**, **73·(PF$_6$)$_2$**, **74·(Cl)$_2$** and **74·(PF$_6$)$_2$** in $CDCl_3$ (Figure 3.17).

[†] Additionally the aromatic NDI protons $H_{e,e'}$ of the one-station model axle **53** were at an identical chemical shift in $CDCl_3$ (δ = 8.76 ppm) to those in the ^{1}H NMR spectra of the HB [3]rotaxane **73·SO$_4$** and the XB rotaxane **74·(NO$_3$)·(PF$_6$)**. In these salts the macrocycles underwent no interactions with the NDI motifs as conclusively demonstrated using ^{1}H–^{1}H ROESY NMR (*vide infra*). Unfortunately, the differing chemical environment of the diagnostic *N*-methyl triazolium protons H_l prevented the use of the triazolium-based models to estimate station occupancies.

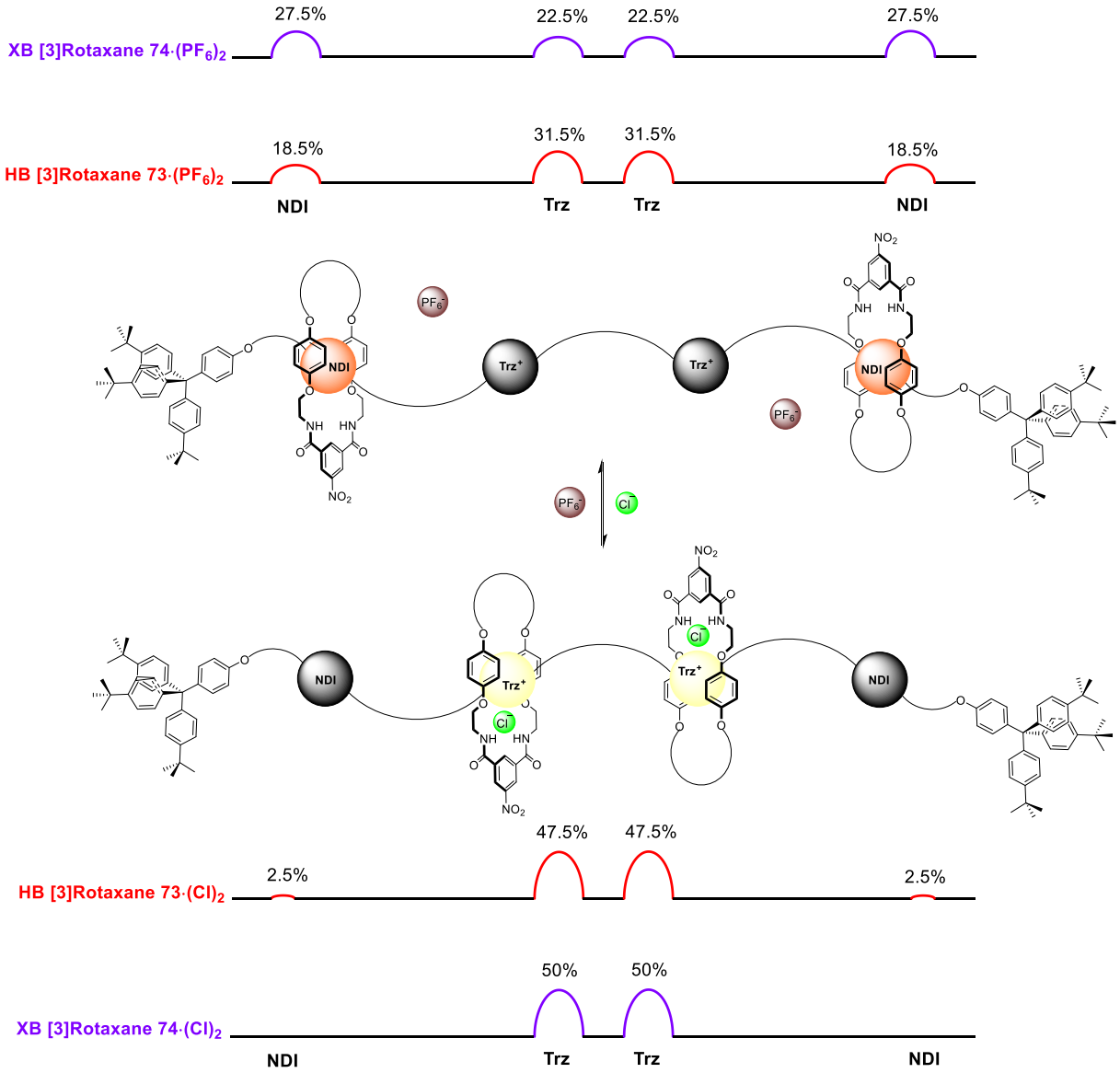


*Figure 3.17. The estimated macrocycle station occupancies (based upon $\Delta\delta H_{e,e'}$ protons) of the HB and XB [3]rotaxanes **73·(A)$_2$** and **74·(A)$_2$** as their bis-hexafluorphosphate and bis-chloride salts as determined by ^{1}H NMR spectroscopy in $CDCl_3$ solution. Trz$^+$ = proto/iodo-triazolium.*

For the HB [3]rotaxane, this revealed an occupancy of 37% for the NDI stations in the absence of coordinating anions, whereas the recognition of chloride results in a 95% occupancy of the central bis-proto-triazolium sites by the macrocycles. A similar trend was found for the XB [3]rotaxane, but interestingly the degree of chloride-induced macrocycle switching in $CDCl_3$ was 23% larger, because of an enhanced occupation of the NDI stations in the bis-hexafluorophosphate salt. The same result had also been observed on comparison of the HB and XB NDI-based [2]rotaxanes **42·A** and **43·A** in Section 2.3.7.

Importantly, conclusive evidence was provided that both **73·$(PF_6)_2$** and **74·$(PF_6)_2$** produce halide-induced co-conformational changes in a similar fashion to the to the structurally related bistable [2]rotaxanes described in Chapter Two. However, overall, these [3]rotaxanes exhibit more complex, pincer-like translational motion of the macrocycles courtesy of molecular scaffolds of higher interlocked order.

3.5 ^{1}H NMR spectroscopic studies of oxoanion-induced shuttling behaviour

The bidentate nature of the bis-HB/XB-triazolium recognition sites warranted an investigation into the capability of these four-station [3]rotaxanes to exhibit translational shuttling stimulated by oxoanion binding. A preliminary examination was conducted in which one equivalent of sulfate anion was added as its tetrabutylammonium salt to a solution of HB rotaxane host **73·$(PF_6)_2$** in $CDCl_3$. The ^{1}H NMR spectrum of the resultant species is shown in Figure 3.18 alongside that of the [3]rotaxane as the bis-hexafluorophosphate and bis-chloride salts for comparison.

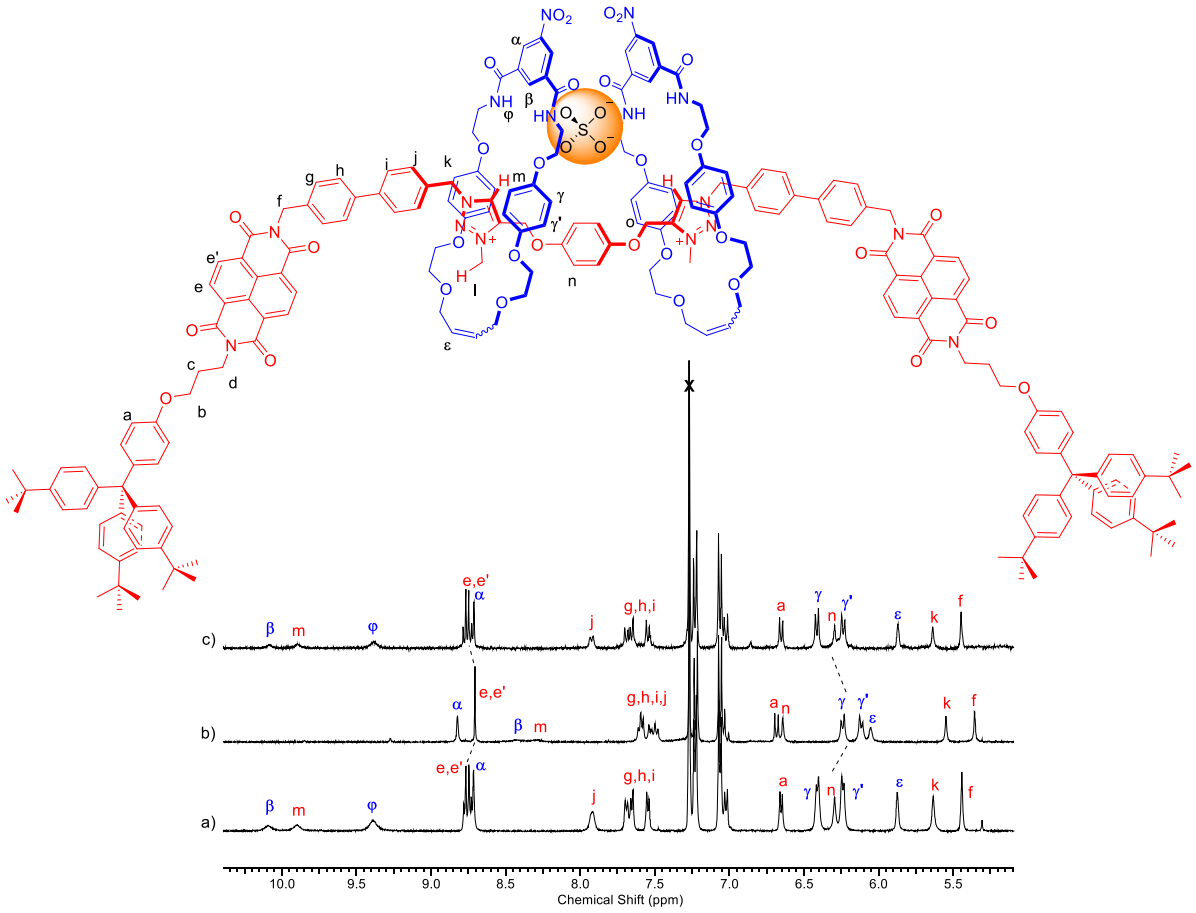


*Figure 3.18. Truncated ^{1}H NMR spectra of the HB [3]rotaxane **73·(A)$_2$** as the a) bis-chloride and b) bis-hexafluorophosphate salts and c) after addition of one equivalent of TBA·SO$_4$ to **73·(PF$_6$)$_2$** (CDCl$_3$, 298 K, 400 MHz). The co-conformation of the [3]rotaxane as the sulfate salt **73·SO$_4$** is also depicted.*

Significant downfield shifts of proton resonances associated with $H_{e,e'}$ and $H_{\gamma,\gamma'}$ are observed upon the addition of sulfate to **73·(PF$_6$)$_2$**. These chemical shift perturbations are analogous to those seen in the ^{1}H NMR spectrum of the [3]rotaxane upon exchange to the chloride salt **73·(Cl)$_2$** demonstrating that the four-station [3]rotaxane exhibits sulfate anion-mediated pincer-like shuttling motion (Figure 3.19). The similarity to **73·(Cl)$_2$** also reveals the capability of a single tetrahedral sulphate anion to bridge the bis-proto-triazolium recognition site whilst the remaining oxygen atoms of the anion simultaneously interact with both isophthalamide-containing macrocycles. Therefore the addition of sulfate to **73·(PF$_6$)$_2$** leads to the formation of a 1:1 stoichiometric host–oxoanion sandwich complex.

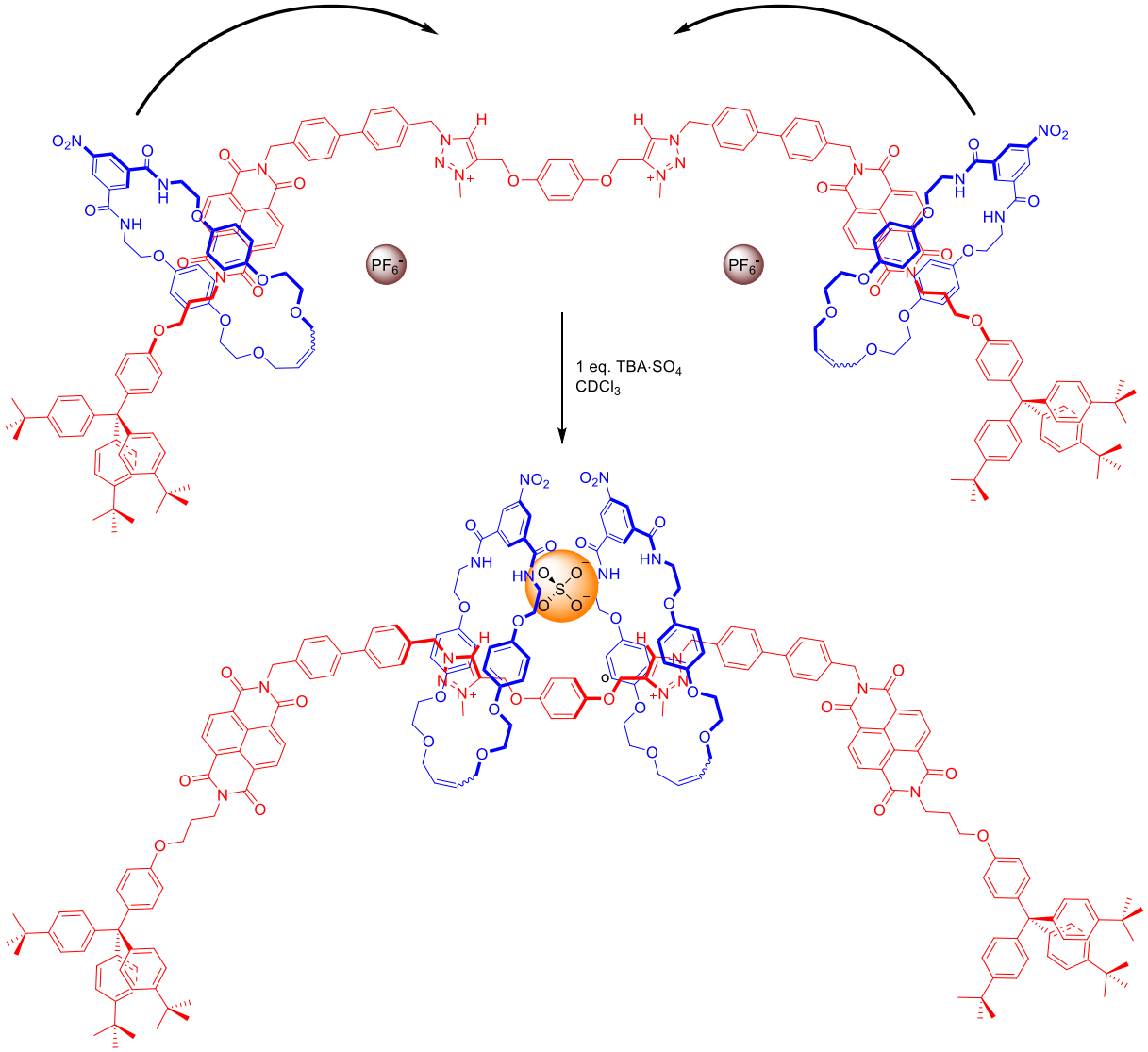


Figure 3.19. The sulfate-induced pincer-like molecular motion exhibited by HB [3]rotaxane ***73·(PF$_6$)$_2$*** *resulting in a 1:1 stoichiometric sandwich complex.*

Two-dimensional ^{1}H ROESY NMR spectroscopy of **73·SO$_4$** in $CDCl_3$ was also used to demonstrate this (Figure 3.20). The spectrum showed exclusive coupling interactions between $H_{\gamma,\gamma'}$ and H_j, H_k, H_l and H_o but none with $H_{e,e'}$ and so the anion-induced shuttling exhibited by [3]rotaxane **73·(PF$_6$)$_2$** results in 100% macrocycle occupancy of the bis-proto-triazolium sites following sulfate recognition.

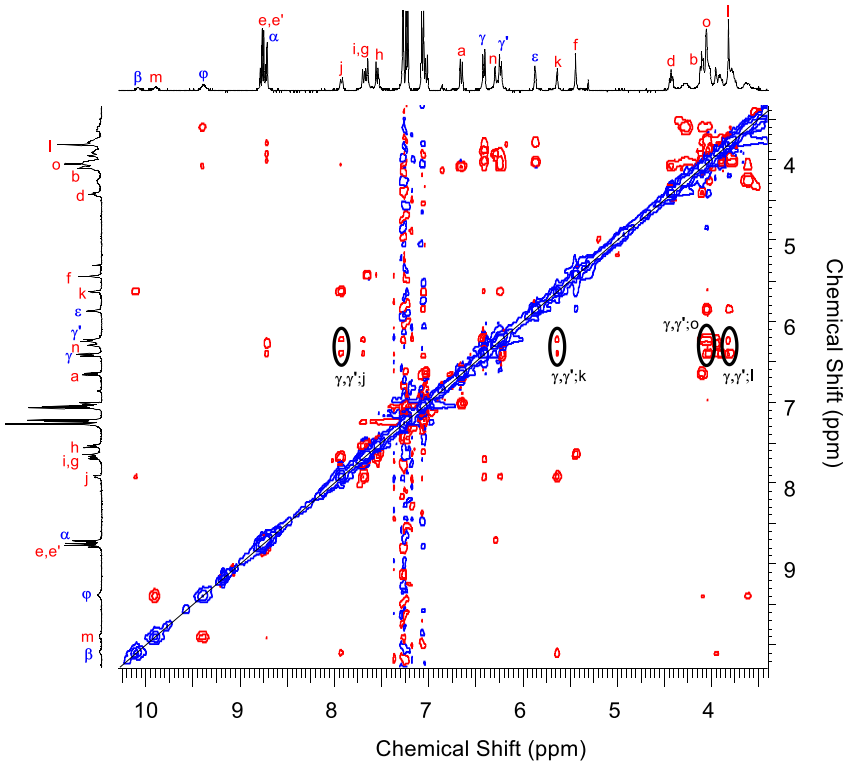


*Figure 3.20. Truncated ^{1}H–^{1}H ROESY NMR spectrum of HB [3]rotaxane **73·(PF$_6$)$_2$** after addition of one equivalent of TBA·SO$_4$ with selected coupling interactions highlighted (CDCl$_3$, 298 K, 500 MHz).*

The ability of the XB [3]rotaxane to undergo translational molecular motion of the macrocycle components facilitated by oxoanion recognition was also investigated by the addition of one equivalent of nitrate (as its tetrabutylammonium salt) to **74·(PF$_6$)$_2$** in $CDCl_3$. The resulting ^{1}H NMR spectrum was compared to the bis-hexafluorophosphate and bis-chloride salts (Figure 3.21).

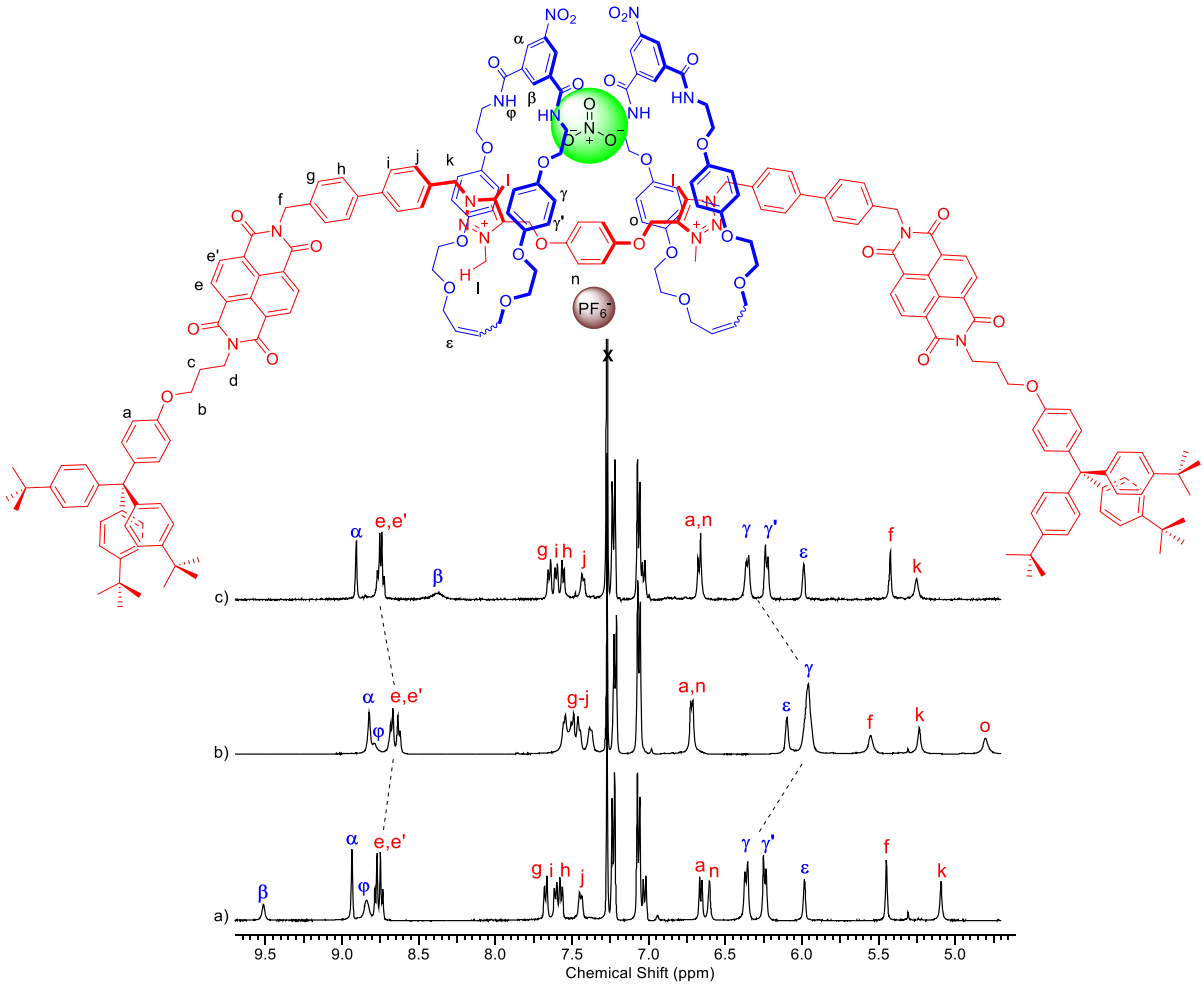


*Figure 3.21. Truncated ^{1}H NMR spectra of the XB [3]rotaxane **74·(A)$_2$** as the a) bis-chloride salt, b) bis-hexafluorophosphate salt and c) after addition of one equivalent of TBA·NO_3 to **74·(PF$_6$)$_2$** ($CDCl_3$, 298 K, 400 MHz). The dominant co-conformation of the [3]rotaxane as the mononitrate-salt **74·(PF$_6$)(NO$_3$)** is also depicted.*

The upfield shifts of the hydroquinone and NDI proton resonances $H_{\gamma,\gamma'}$ and $H_{e,e'}$ indicate that, in identical fashion to the HB [3]rotaxane, the macrocycle components of **74·(PF$_6$)$_2$** undergo concerted pincer-like motion from the peripheral NDI stations into the centre of the axle to participate in binding of the nitrate anion at the bis-iodo-triazolium stations *via* formation of a 1:1 stoichiometric sandwich complex (Figure 3.22).

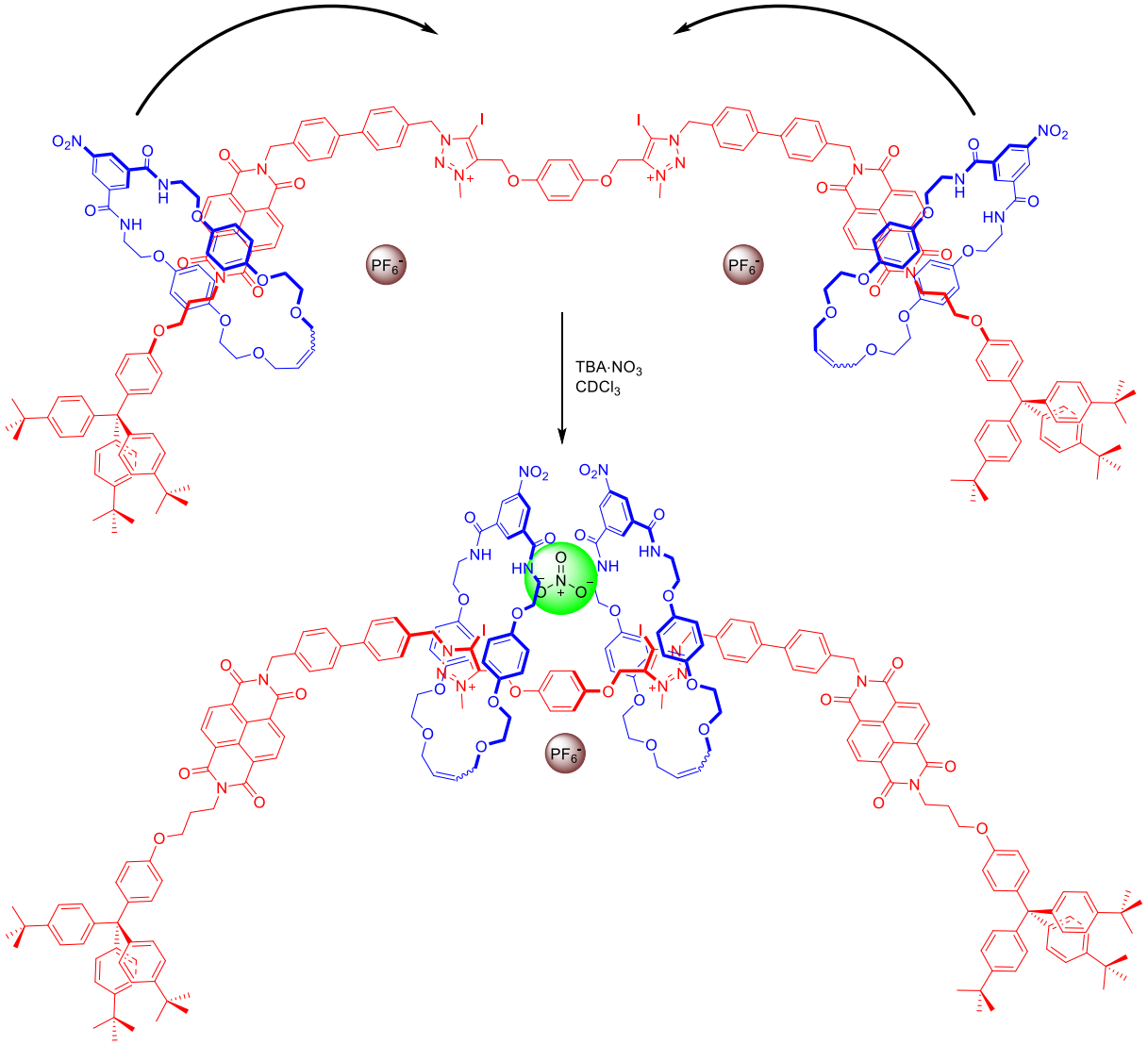


Figure 3.22. The nitrate-induced pincer-like molecular motion exhibited by XB [3]rotaxane ***74·(PF$_6$)$_2$*** *resulting in a 1:1 stoichiometric host–guest complex.*

A two-dimensional ^{1}H ROESY NMR spectrum of the sample **74·(PF$_6$)(NO$_3$)** in $CDCl_3$ (Figure 3.23) displayed the same coupling interactions as that of the bis-chloride salt, namely those between the macrocycle protons $H_{\gamma,\gamma'}$ and H_ε and the axle protons associated with the bis-iodo-triazolium station (H_I, H_o). Importantly, the absence of through-space interactions between the macrocycle hydroquinone protons $H_{\gamma,\gamma'}$ and the NDI aromatic protons $H_{e,e'}$ imply that any interactions with this station prior to nitrate addition are lost. Finally, the change in chemical shift of these latter protons revealed that 100% of the macrocycles occupy the bis-iodo-triazolium sites following nitrate addition in $CDCl_3$.

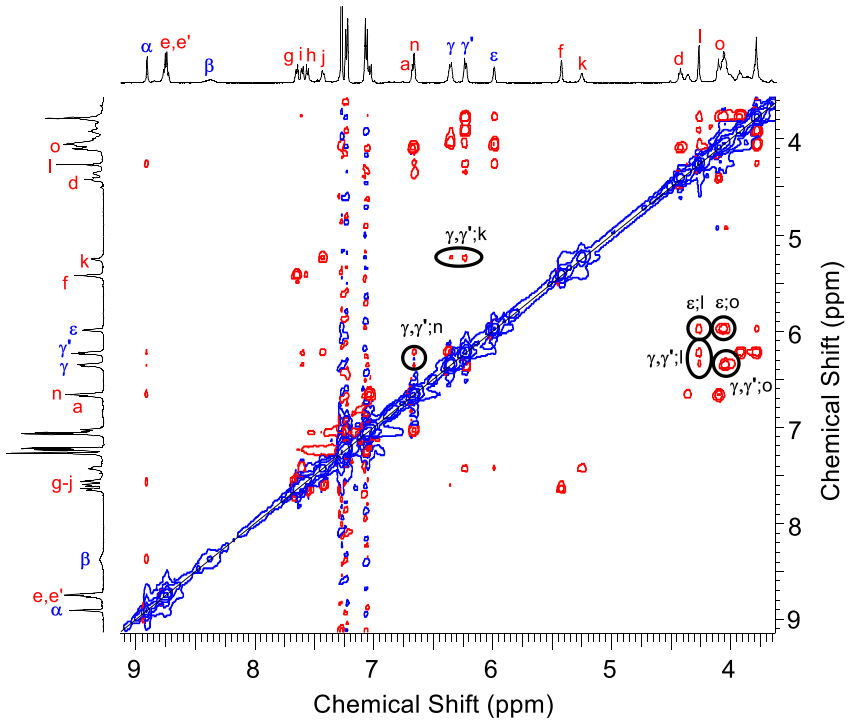


*Figure 3.23. Truncated ^{1}H–^{1}H ROESY NMR spectra of XB [3]rotaxane **74·(PF$_6$)$_2$** after addition of one equivalent of TBA·NO$_3$ with selected coupling interactions highlighted (CDCl$_3$, 298 K, 500 MHz).*

3.6 ^{1}H NMR oxoanion binding and molecular motion studies of the four-station HB [3]rotaxane in DMSO-d_6

Further investigations into the oxoanion binding ability of these higher-order interlocked hosts in DMSO-d_6 focused on the HB [3]rotaxane because of the limited supply of the corresponding XB [3]rotaxane.

Association constants for **73·(PF$_6$)$_2$** with sulfate, dihydrogen phosphate and oxalate anions (added as their respective TBA salts) were determined in DMSO-d_6 by conducting a series of ^{1}H NMR spectroscopic anion titration experiments. This solvent was chosen because an initial titration had demonstrated that sulfate binding was too strong to be quantified in CDCl$_3$. The addition of anion guests to **73·(PF$_6$)$_2$** resulted in significant downfield chemical shift perturbations of the bis-proto-triazolium protons H$_m$, and similar changes to the macrocycles' acidic internal isophthalamide protons H$_\beta$ (Figure 3.24). These were diagnostic of anion binding in the three-dimensional cavity of the [3]rotaxane in the same fashion as previously discussed in CDCl$_3$. Downfield shifts of the methylene

protons H_k adjacent to the proto-triazolium recognition sites were also informative of oxoanion recognition.

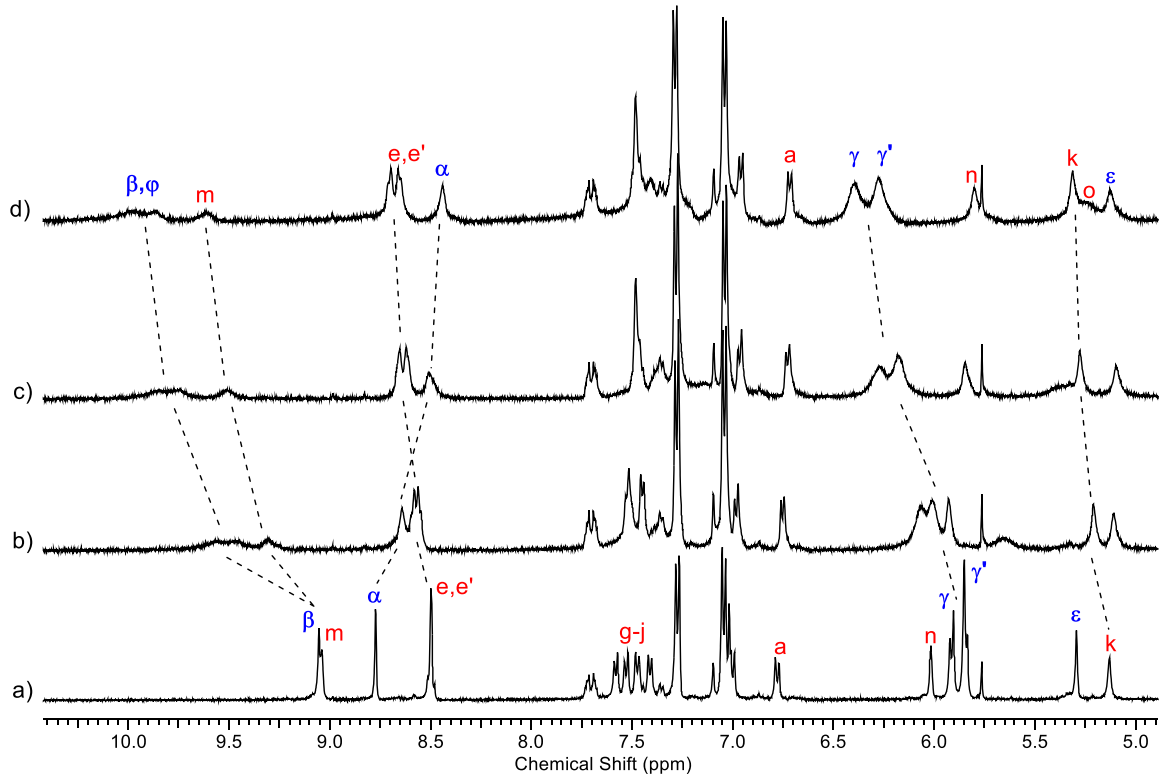


*Figure 3.24. Truncated ^{1}H NMR spectra of a) HB [3]rotaxane **73·(PF$_6$)$_2$** and after the addition of b) one c) two and d) three equivalents of TBA·H$_2$PO$_4$ (DMSO-d$_6$, 298 K, 500 MHz).*

WinEQNMR2[65] analysis of the titration data, monitoring proton H_k or H_α (Figure 3.25), enabled the determination of the anion association constants shown in Table 3.1. A 1:1 stoichiometric host–guest binding model was used because of the propensity for oxoanions to bridge the bis-proto-triazolium recognition site and form a sandwich complex *via* favourable HB interactions between the axle and macrocycle components (*vide supra*).[‡]

[‡] In spite of the smaller fitting errors obtained with a 1:1 stoichiometric host-guest model, 1:2 host-guest binding cannot be ruled out on the basis of the titration data shown here.

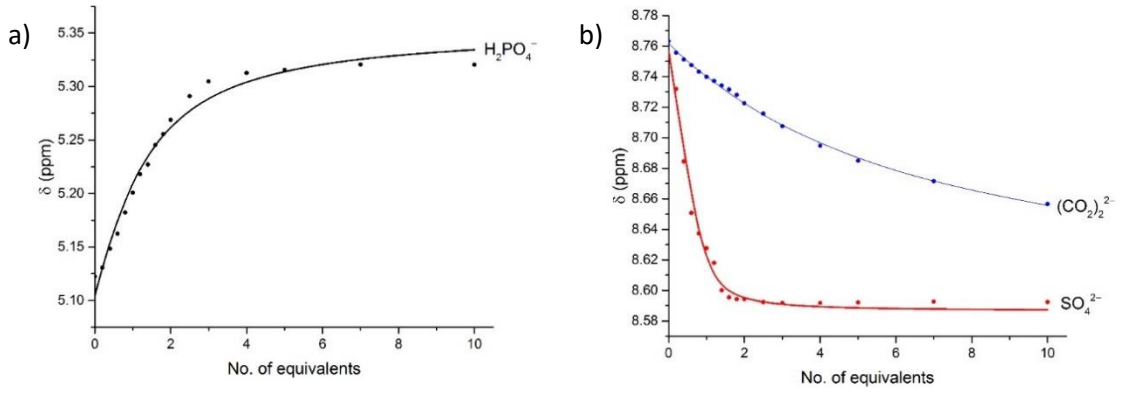


*Figure 3.25. Changes in the chemical shift of a) proton H_k upon addition of $H_2PO_4^-$ anions and b) proton H_α upon addition of SO_4^{2-} or $(CO_2)_2^{2-}$ anions to HB rotaxane **73·(PF$_6$)$_2$** (DMSO-d_6, 298 K, 500 MHz). Dots represent experimental data points; lines represent calculated titration curves.*

*Table 3.1. Anion association constants K_{Ass} (M^{-1}) for HB [3]rotaxane **73·(PF$_6$)$_2$** determined by ^{1}H NMR spectroscopy in DMSO-d_6 using chemical shift data of H_α unless otherwise stated (298 K, 500 MHz). Anions added as tetrabutylammonium (TBA) salts. Errors < 20%. pK_a values of the acids corresponding to the anion are given in water.*

Anion	pK_a[66–68]	HB [3]rotaxane K_{Ass}
SO_4^{2-}	2.0[a]	> 10^4
$H_2PO_4^-$	2.1	1211[c]
$(CO_2)_2^{2-}$	4.2[b]	141

[a] pK_a of HSO_4^- [b] pK_a of $C_2O_4H^-$ [c] Chemical shift of H_k used.

The [3]rotaxane's ability to distinguish between the tetrahedral oxoanions sulfate and dihydrogen phosphate is attributed to the differing charges of the guests. Interestingly, the association between **73·(PF$_6$)$_2$** and sulfate was found to be two orders of magnitude larger than that with oxalate, in spite of the dicarboxylate's higher basicity. This indicates that the size of the unique three-dimensional cavity of the [3]rotaxane, created between the bis-proto-triazolium axle and the two isophthalamide-containing macrocycles, imparts a strong influence on the selectivity of the receptor to the extent that

binding of larger tetradentate oxoanions[§68,69] is not as favoured. Complementarity also explains why association for smaller tetrahedral dihydrogen phosphate is ten times that of oxalate.

The oxoanion ^{1}H NMR spectroscopic titration results also revealed significant downfield shifts of the macrocycle hydroquinone and axle NDI proton resonances, $H_{v,v'}$ and $H_{e,e'}$, indicating that anion binding facilitated molecular motion (Figure 3.24). The change in chemical shift of $H_{e,e'}$ was used to estimate the occupancies of the NDI stations throughout the course of the titration (Figure 3.26).

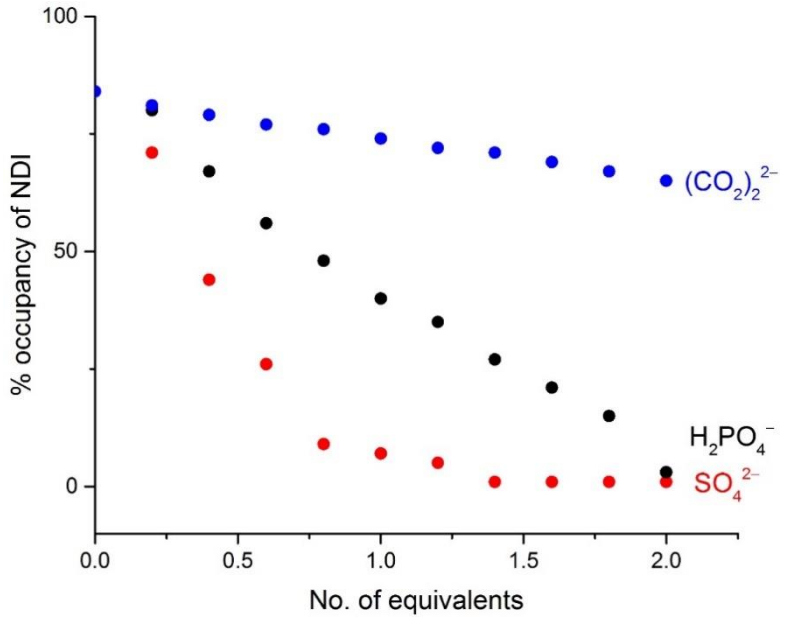


Figure 3.26. Changes in NDI station occupancy of HB [3]rotaxane ***73·(PF$_6$)$_2$*** *over the course of the titrations with $H_2PO_4^-$, SO_4^{2-} and $(CO_2)_2^{2-}$anions in DMSO-d_6.*

As the bis-hexafluorophosphate salt **73·(PF$_6$)$_2$** in DMSO-d_6, there is an 84% macrocycle occupancy of the NDI stations[**] and, upon the addition of oxoanions, it is clear that the stronger association of the [3]rotaxane host with sulfate imparts a greater degree of anion-induced translational shuttling per anion equivalent. After one equivalent of sulfate, macrocycle occupancy of the bis-proto-triazolium

[§] The effective radius of oxalate has been estimated to be 3-4 Å, whilst sulfate and dihydrogen phosphate are 2.3 Å and 2.0 Å.

[**] This is larger than the macrocycle occupancy of the NDI station exhibited by **73·PF$_6$** in $CDCl_3$ and is possibly due to the fact DMSO is a more polar solvent.

recognition sites is 93%, whilst two equivalents of phosphate are required to achieve the same degree of co-conformational change. Unsurprisingly, the weak binding of oxalate is manifested in only small changes (< 20%) of the station occupancies over the course of the titration.

3.7 Optical oxoanion sensing by the four-station HB [3]rotaxane in DMSO

Having demonstrated the four-station HB [3]rotaxane **73·$(PF_6)_2$** was capable of recognition of various oxoanions *via* pincer-like motion of the macrocycle components, it was decided to exploit this unique mechanism for the purpose of optical anion sensing. UV-Vis spectroscopy was used to monitor the charge–transfer band ($\lambda_{abs,max}$ ~ 470 nm) resulting from the donor–acceptor aromatic stacking interactions occurring between the macrocycle hydroquinone groups and the NDI recognition sites of **73·$(PF_6)_2$** in DMSO (Figure 3.27). Decreases in the intensity of this band to various degrees were observed upon the titration of sulfate, dihydrogen phosphate or oxalate (as their TBA salts) into equimolar solutions of the [3]rotaxane host at a concentration of 1.4 mM.

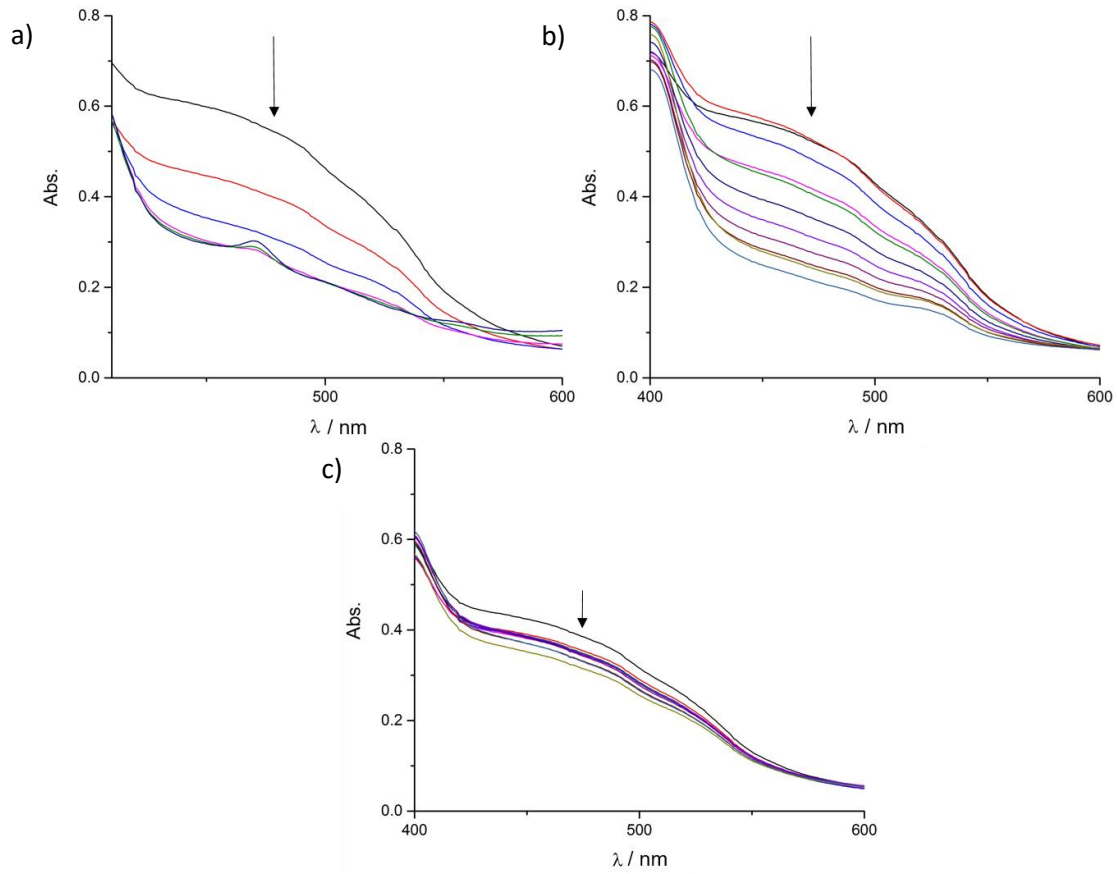


Figure 3.27. UV-Vis spectra showing the effect of the addition of a) one equivalent of TBA·SO_4 and two equivalents of b) TBA·H_2PO_4 and c) TBA·$(CO_2)_2$ into a solution of [3]rotaxane ***73·$(PF_6)_2$*** *in DMSO (1.4×10^{-3} mol L^{-1}). The addition of sulfate and dihydrogen phosphate leads to a decrease in intensity of the charge–transfer band, but oxalate incurs little change.*

It is clear that the strong affinity between **73·$(PF_6)_2$** and sulfate results in a decrease in intensity of the charge–transfer band, so that, in agreement with occupancy calculations, after the addition of one equivalent of oxoanion the aromatic stacking interactions with the NDI stations are negligible. The same intensity change required the addition of two equivalents of dihydrogen phosphate because binding of this anion with the host was weaker than sulfate. Finally, only small changes in the UV-Vis spectrum were revealed with oxalate.

Since the charge–transfer band appears in the visible region of the spectrum the addition of sulfate and dihydrogen phosphate to the [3]rotaxane bis-hexafluorophosphate salt **73·$(PF_6)_2$** produced a naked-eye colour change from orange to colourless (Figure 3.28). By contrast no significant colour change was observed for oxalate. Therefore the [3]rotaxane is capable of optically sensing tetrahedral

oxoanionic species whereby a discrete colorimetric response is produced courtesy of significant co-conformational change upon anion recognition.

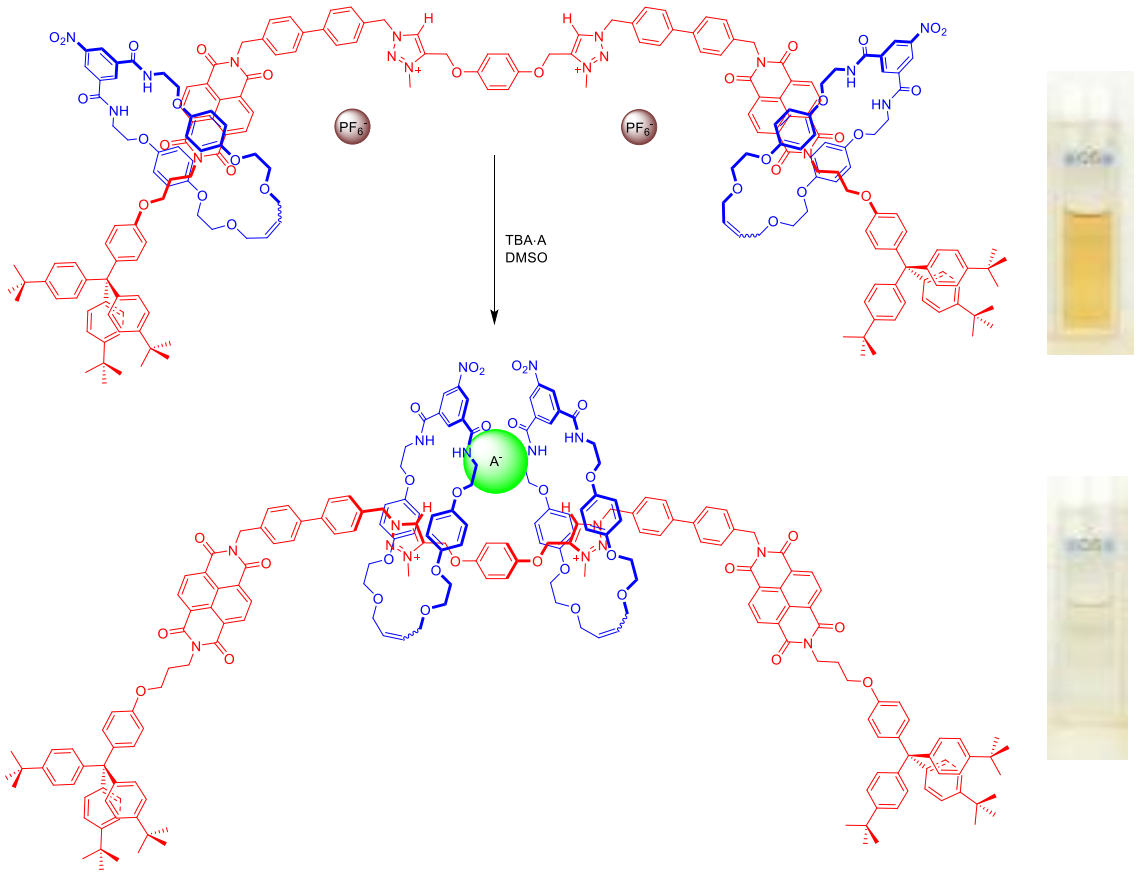


Figure 3.28. Co-conformations of HB [3]rotaxanes ***73·(PF$_6$)$_2$*** *and* ***73·(A)$_2$*** *in DMSO and photographs showing the naked-eye colour changes observable upon sulfate or dihydrogen phosphate addition in the same solvent. A^- = $H_2PO_4^-$, SO_4^{2-}.*

3.8 A comparison of the anion recognition properties of HB and XB [3]rotaxanes

The outcome of the research detailed in Chapter Two indicated that the incorporation of XB donor groups into anion-mediated molecular shuttles can enhance their recognition properties and, in turn, the degree of co-conformational switching they exhibit. Therefore, it was decided to quantify and compare the binding properties of both HB and XB interlocked hosts with a selection of oxoanions in the competitive polar, protic solvent mixture of 1:1 $CDCl_3$:CD_3OD.

The addition of anions to the [3]rotaxane bis-hexafluorophosphate salts **73·(PF$_6$)$_2$** and **74·(PF$_6$)$_2$** resulted in significant downfield chemical shift perturbations of the methylene protons H_o adjacent to

the triazolium recognition sites, as well as changes to the macrocycle's acidic internal isophthalamide proton resonance H_β, in both systems (Figure 3.29).

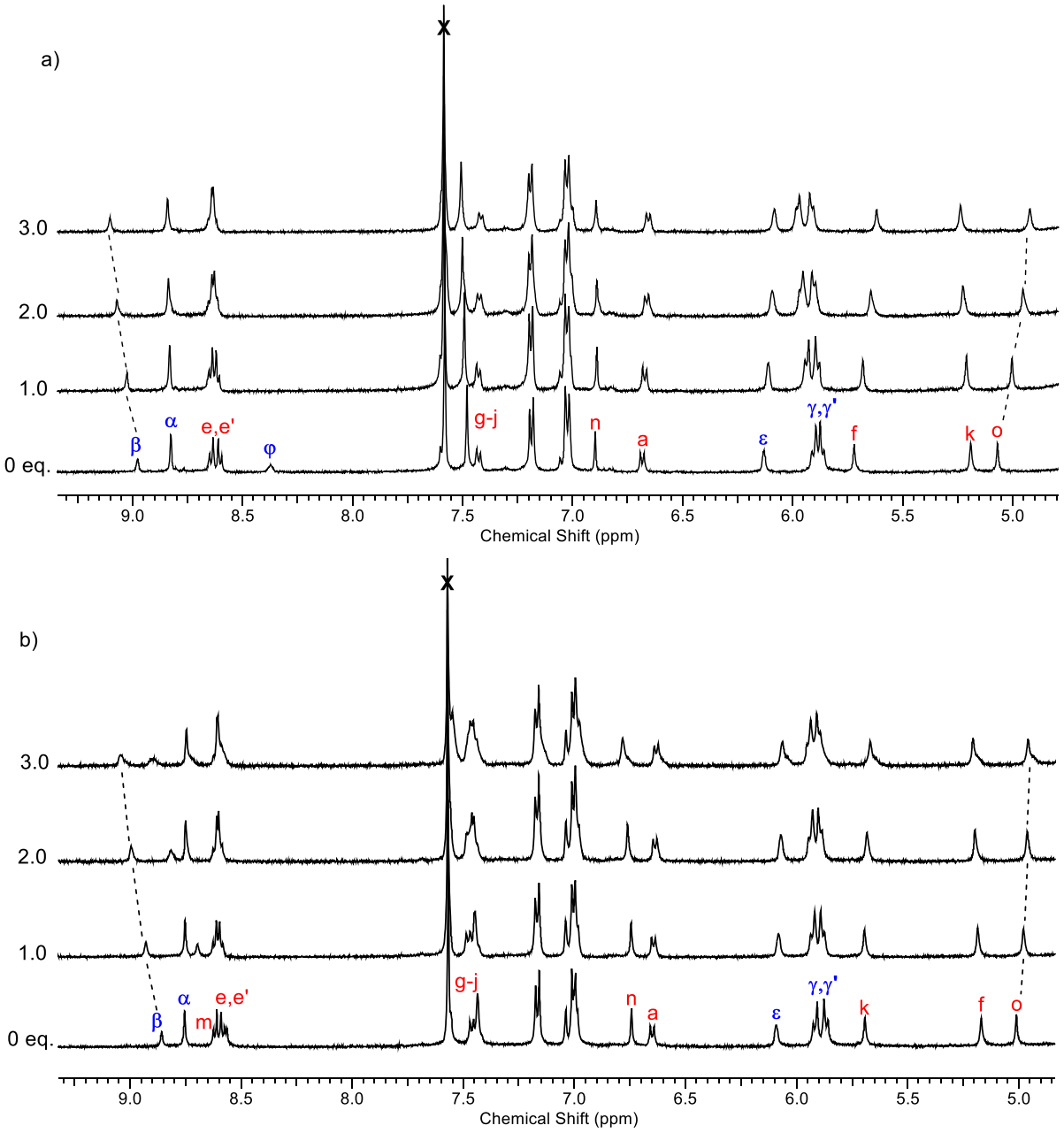


*Figure 3.29. Truncated ^{1}H NMR spectra of a) XB [3]rotaxane **74·(PF$_6$)$_2$** and b) HB [3]rotaxane **73·(PF$_6$)$_2$** after the addition of one, two and three equivalents of TBA·H$_2$PO$_4$ (1:1 CDCl$_3$:CD$_3$OD, 298 K, 500 MHz).*

In a similar fashion to the previous studies in DMSO-d_6, this indicated anion binding at the bis-triazolium groups, with recognition also aided by hydrogen bond interactions from the isophthalamide clefts of the two macrocycle components. WinEQNMR2[65] analysis of the titration data, monitoring either protons H_o or H_β (Figure 3.30), determined the anion association constants shown in Table 3.2.

Interestingly, the chemical shift perturbations were most accurately fitted using a 1:1 binding model, apart from chloride (1:2 host:guest model), assumingly because of the propensity for the larger oxoanions to bridge the bis-triazolium recognition site forming the sandwich complex (*vide supra*).[††]

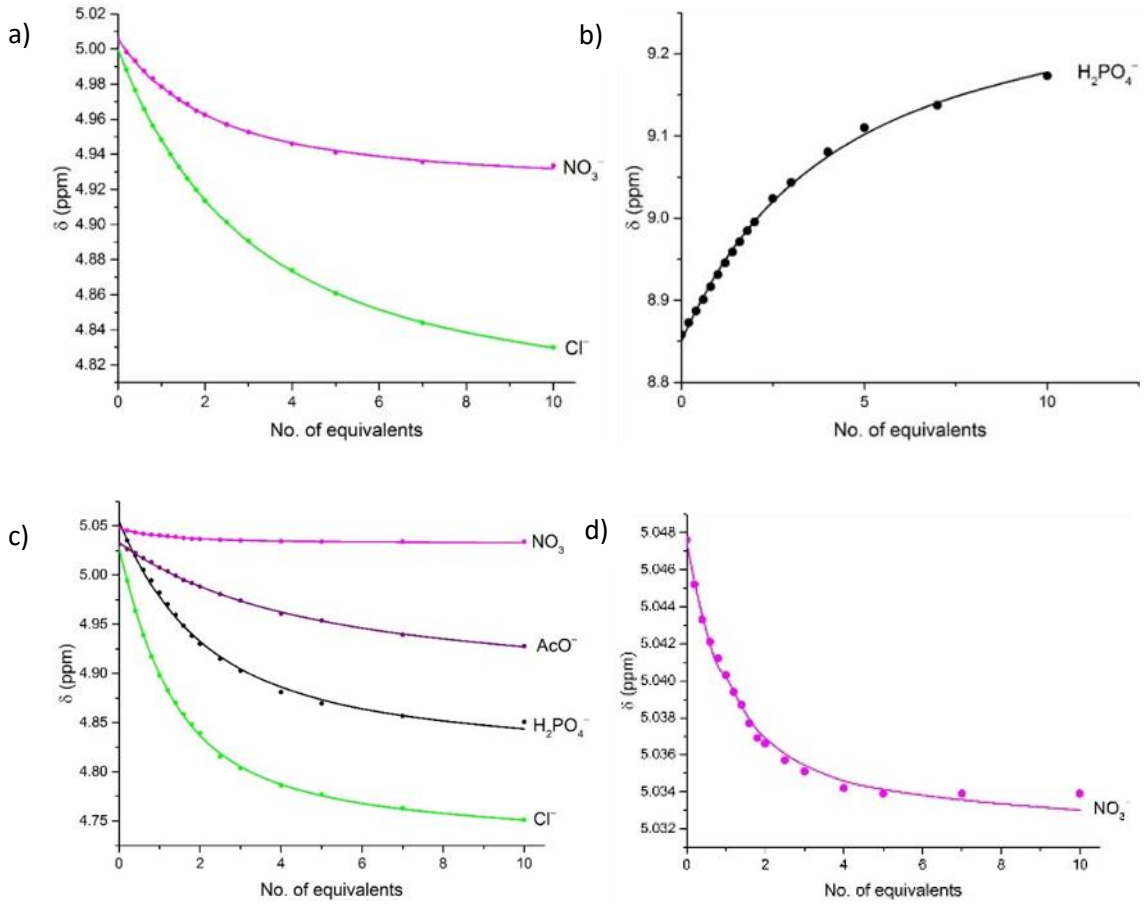


*Figure 3.30. Changes in the chemical shift of a) proton H_o upon addition of NO_3^- and Cl^- anions and b) proton H_β upon addition of $H_2PO_4^-$ anions to HB [3]rotaxane **73·(PF$_6$)$_2$**. Also, c) changes in the chemical shift of proton H_o upon addition of anions to XB [3]rotaxane **74·(PF$_6$)$_2$** and d) a close-up of the NO_3^- titration curve (1:1 $CDCl_3$:CD_3OD, 298 K, 500 MHz). Dots represent experimental data points; lines represent calculated titration curves.*

[††] In spite of the smaller fitting errors obtained for oxoanions with a 1:1 stoichiometric host-guest model, 1:2 host-guest binding cannot be ruled out on the basis of the titration data shown here.

*Table 3.2. Anion association constants K_{Ass} (M^{-1}) for HB and XB [3]rotaxanes **73·$(PF_6)_2$** and **74·$(PF_6)_2$** determined by ^{1}H NMR spectroscopy in 1:1 $CDCl_3$:CD_3OD using chemical shift data of H_o unless otherwise stated (298 K, 500 MHz). Anions added as tetrabutylammonium (TBA) salts. Errors < 10%. pK_a values of the acids corresponding to the anion are given in water.*

Anion	pK_a[67,68,71,72]	HB Rotaxane K_{Ass}	XB Rotaxane K_{Ass}
Cl^-	− 8.0	507[a]	1357[a]
NO_3^-	− 1.3	653	1782
$H_2PO_4^-$	2.1	256[b]	630
AcO^-	4.8	-[c]	221
SO_4^{2-}	2.0[e]	-[d]	-[d]

*[a] K_1 value. K_2 = 20 M^{-1} and 7 M^{-1} for **73·$(PF_6)_2$** and **74·$(PF_6)_2$** respectively. [b] Chemical shift of H_β used. [c] Small upfield shift perturbation so binding was too weak to be quantified. [d] Large downfield shifts of H_o gave evidence of strong sulfate binding but precipitation after one equivalent prevented calculation of $K_{Ass.}$ [e] pK_a of HSO_4^-.*

The HB and XB [3]rotaxanes **73·$(PF_6)_2$** and **74·$(PF_6)_2$** both exhibit a selectivity for binding nitrate over the oxoanions dihydrogen phosphate and acetate, in spite of the fact these latter anions are more basic (as indicated by the pK_a values of their respective acids in Table 3.2). The HB and XB receptors also display superior recognition of nitrate over chloride. This is a critical result because it is the first time that discrimination between these two species has been achieved within an interlocked host molecule. Previous nitrate-designed [2]rotaxane[7,9] and [2]catenane[8] systems have, by contrast, displayed comparable affinities for chloride. Therefore, it is the complementarity of the three-dimensional cavity resulting from the bidentate bis-triazolium site of the axle component and two hydrogen bond-donating isophthalamide macrocycles that delivers the nitrate selectivity of this next generation of higher-order [3]rotaxane hosts. These results are also in agreement with the findings from the ^{1}H NMR oxoanion titrations performed with HB [3]rotaxane **73·$(PF_6)_2$** in DMSO-d_6 (Section 3.2.5), that demonstrated the importance of a geometric match between the [3]rotaxane's cavity and the anionic guest.

Comparison of the association constants of **73·$(PF_6)_2$** and **74·$(PF_6)_2$** reveals the XB system exhibits superior recognition of all anionic species, relative to the HB analogue, courtesy of strong halogen

bond formation to the anionic guest. Importantly, this is the first time an XB interlocked host has displayed enhanced association for oxoanion guests over a comparable HB only system. In part, its success is attributed to the strength of the halogen bond interactions inherent to the XB [3]rotaxane host but also to the stricter preference for a linear bond geometry between an XB-donating iodo-triazolium group and the anion. In comparison to a hydrogen bond, this latter effect produces a more geometrically defined recognition site which may specifically aid in the binding of multidentate oxoanions. Finally, the superior recognition of the spherical chloride anion by the XB [3]rotaxane over the HB analogue matches the trend of enhanced halide binding exhibited by several previously reported XB interlocked hosts in polar, protic organic solvents.[73,74]

3.9 Conclusions and future work

In summary, two novel XB/HB [3]rotaxanes were synthesised, each containing a four-station bis-triazolium-bis-naphthalene diimide axle and two isophthalamide macrocycle components. One- and two- dimensional ^{1}H NMR experiments were used to demonstrate that these higher-order interlocked host molecules were capable of recognising oxoanions *via* a novel dynamic shuttling mechanism in which the HB-donating macrocycle components move from the peripheral NDI stations to the core bis-triazolium recognition sites in a pincer-like motion to form a unique 1:1 stoichiometric sandwich complex.

Interestingly, quantification of the binding of oxoanions to the HB [3]rotaxane in DMSO-d_6 revealed a preference for smaller tetrahedral species such as sulfate and dihydrogen phosphate over more basic oxalate, indicating the importance of complementarity between the guest and the three-dimensional cavity created between the rotaxane host's three components. The weaker binding of oxalate was also observed in smaller macrocycle occupancies of the bis-proto-triazolium anion recognition sites. The differences in the degree of anion-induced molecular motion exhibited by the HB [3]rotaxane were therefore used as a novel mechanism of optically sensing oxoanionic species by UV-Vis spectroscopy. A naked eye colour change was apparent for sulfate and dihydrogen phosphate upon titration of these

species into a solution of the receptor in DMSO courtesy of translational shuttling of the macrocycle components away from the NDI stations. However, there was no colorimetric response for oxalate. This neatly demonstrates the benefits of using interlocked host molecules for anion sensing purposes; the unique cavities provide strong guest recognition whilst exploitation of the inherent dynamics of these systems can produce functional sensor responses.

In order to probe the effectiveness of XB interactions for oxoanion recognition, ^{1}H NMR spectroscopy titration experiments were performed using the XB [3]rotaxane in the competitive solvent mixture of 1:1 $CDCl_3$:CD_3OD. These revealed that this interlocked host exhibited selectivity for the environmentally relevant nitrate anion over more basic acetate and dihydrogen phosphate oxoanions, and importantly, chloride. Analogous titration experiments with the HB [3]rotaxane revealed that the XB analogue is a superior anion host. These effects are attributed to the strength of XB interactions and a more geometrically defined recognition site that specifically assists in the recognition of multidentate oxoanions.

An avenue of further research would be to further exploit the superior recognition of oxoanions, in particular nitrate, by XB-based hosts containing the bis-iodo-triazolium motif, that has been established within this work. The incorporation of these XB donors into a number of preorganised cyclic and interlocked receptors may enable the recognition of these biologically and environmentally relevant species in more competitive solvent media, with the ultimate goal of achieving selective binding of nitrate in water. The latter may be possible by synthesising an all-XB version of the [3]rotaxane reported in this chapter (Figure 3.31). The introduction of cyclodextrin units as stoppering motifs would also be required to impart water solubility on the system. The benefit of using a dynamic rotaxane-based host such as this comes from the potential to perform optical sensing of nitrate in aqueous solution *via* anion-mediated molecular motion of the interlocked molecule's constituent parts.

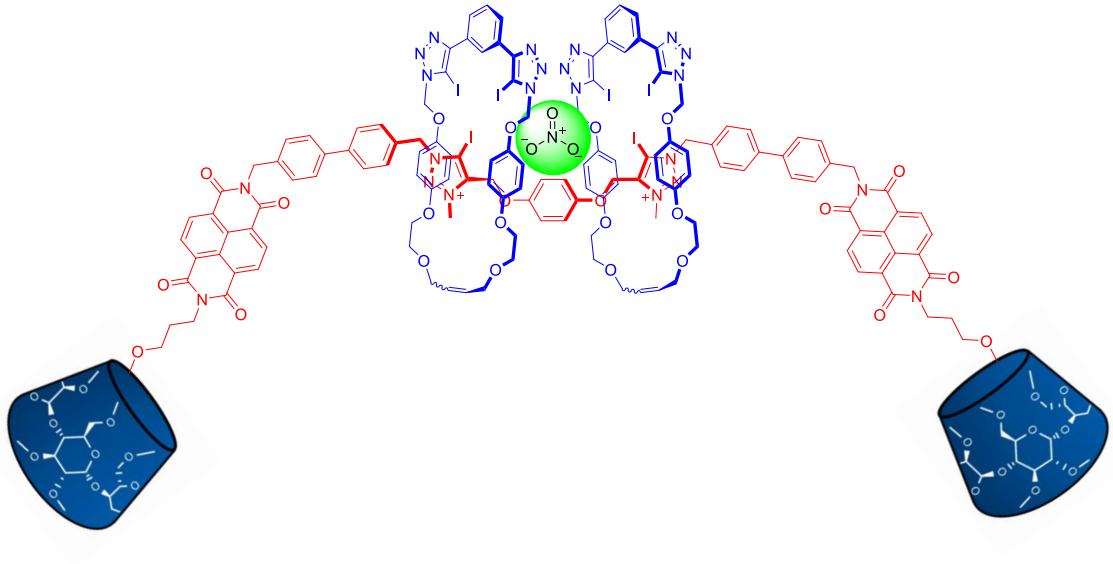


Figure 3.31. A proposed all-XB four-station [3]rotaxane capable of nitrate-sensing in water.

3.10 References

1 J. M. Berg, J. L. Tymoczko and L. Stryer, *Biochemistry: International Edition*, W. H. Freeman, New York, 7th edition edition., 2011.

2 B. Moss, *Philos. Trans. R. Soc. Lond. B Biol. Sci.*, 2008, **363**, 659–666.

3 V. H. Smith and D. W. Schindler, *Trends Ecol. Evol.*, 2009, **24**, 201–207.

4 J. L. Hatfield and R. F. Follett, *Nitrogen in the Environment*, Elsevier, 2008.

5 *Wiley: Supramolecular Chemistry, 2nd Edition - Jonathan W. Steed, Jerry L. Atwood*, Wiley, 2009.

6 M. Arunachalam and P. Ghosh, *Inorg. Chem.*, 2010, **49**, 943–951.

7 M. J. Langton, L. C. Duckworth and P. D. Beer, *Chem. Commun.*, 2013, **49**, 8608–8610.

8 M. J. Langton and P. D. Beer, *Chem. Commun.*, 2014, **50**, 8124–8127.

9 V. Martí-Centelles and P. D. Beer, *Chem. – Eur. J.*, 2015, **21**, 9397–9404.

10 M. Cametti, K. Raatikainen, P. Metrangolo, T. Pilati, G. Terraneo and G. Resnati, *Org. Biomol. Chem.*, 2012, **10**, 1329–1333.

11 J. Y. C. Lim and P. D. Beer, *Chem. Commun.*, 2015, **51**, 3686–3688.

12 E. Wasserman, *J. Am. Chem. Soc.*, 1960, **82**, 4433–4434.

13 I. T. Harrison and S. Harrison, *J. Am. Chem. Soc.*, 1967, **89**, 5723–5724.

14 R. S. Forgan, J.-P. Sauvage and J. F. Stoddart, *Chem. Rev.*, 2011, **111**, 5434–5464.

15 J.-C. Chambron and J.-P. Sauvage, *New J. Chem.*, 2012.

16 G. Gil-Ramírez, D. A. Leigh and A. J. Stephens, *Angew. Chem. Int. Ed.*, 2015, **54**, 6110–6150.

17 J.-F. Ayme, G. Gil-Ramírez, D. A. Leigh, J.-F. Lemonnier, A. Markevicius, C. A. Muryn and G. Zhang, *J. Am. Chem. Soc.*, 2014, **136**, 13142–13145.

18 C. Schouwey, J. J. Holstein, R. Scopelliti, K. O. Zhurov, K. O. Nagornov, Y. O. Tsybin, O. S. Smart, G. Bricogne and K. Severin, *Angew. Chem. Int. Ed.*, 2014, **53**, 11261–11265.

19 J. E. Beves, J. J. Danon, D. A. Leigh, J.-F. Lemonnier and I. J. Vitorica-Yrezabal, *Angew. Chem. Int. Ed.*, 2015, **54**, 7555–7559.

20 T. Prakasam, M. Lusi, M. Elhabiri, C. Platas-Iglesias, J.-C. Olsen, Z. Asfari, S. Cianférani-Sanglier, F. Debaene, L. J. Charbonnière and A. Trabolsi, *Angew. Chem. Int. Ed.*, 2013, **52**, 9956–9960.

21 G. Zhang, G. Gil-Ramírez, A. Markevicius, C. Browne, I. J. Vitorica-Yrezabal and D. A. Leigh, *J. Am. Chem. Soc.*, 2015.

22 K. S. Chichak, S. J. Cantrill, A. R. Pease, S.-H. Chiu, G. W. V. Cave, J. L. Atwood and J. F. Stoddart, *Science*, 2004, **304**, 1308–1312.
23 D. A. Leigh, R. G. Pritchard and A. J. Stephens, *Nat. Chem.*, 2014, **6**, 978–982.
24 J.-F. Ayme, J. E. Beves, D. A. Leigh, R. T. McBurney, K. Rissanen and D. Schultz, *Nat. Chem.*, 2012, **4**, 15–20.
25 B. Hasenknopf, J.-M. Lehn, B. O. Kneisel, G. Baum and D. Fenske, *Angew. Chem. Int. Ed. Engl.*, 1996, **35**, 1838–1840.
26 J. E. Beves, B. A. Blight, C. J. Campbell, D. A. Leigh and R. T. McBurney, *Angew. Chem. Int. Ed.*, 2011, **50**, 9260–9327.
27 A.-M. L. Fuller, D. A. Leigh and P. J. Lusby, *Angew. Chem. Int. Ed.*, 2007, **46**, 5015–5019.
28 E. A. Neal and S. M. Goldup, *Chem. Commun.*, 2014, **50**, 5128–5142.
29 E. R. Kay, D. A. Leigh and F. Zerbetto, *Angew. Chem. Int. Ed.*, 2007, **46**, 72–191.
30 S. Erbas-Cakmak, D. A. Leigh, C. T. McTernan and A. L. Nussbaumer, *Chem. Rev.*, 2015, **115**, 10081–10206.
31 K. Kinbara and T. Aida, *Chem. Rev.*, 2005, **105**, 1377–1400.
32 J.-P. Collin, F. Durola, J. Frey, V. Heitz, F. Reviriego, J.-P. Sauvage, Y. Trolez and K. Rissanen, *J. Am. Chem. Soc.*, 2010, **132**, 6840–6850.
33 J.-P. Collin, F. Durola, V. Heitz, F. Reviriego, J.-P. Sauvage and Y. Trolez, *Angew. Chem. Int. Ed.*, 2010, **49**, 10172–10175.
34 N. H. Evans, Ph.D., University of Oxford, 2011.
35 N. H. Evans, C. J. Serpell and P. D. Beer, *Angew. Chem. Int. Ed.*, 2011, **50**, 2507–2510.
36 S. Lee, C.-H. Chen and A. H. Flood, *Nat. Chem.*, 2013, **5**, 704–710.
37 N. H. Evans, C. J. Serpell and P. D. Beer, *Chem. Commun.*, 2011, **47**, 8775–8777.
38 M. J. Langton and P. D. Beer, *Chem. – Eur. J.*, 2012, **18**, 14406–14412.
39 Y. Nagawa, J. Suga, K. Hiratani, E. Koyama and M. Kanesato, *Chem. Commun.*, 2005, 749–751.
40 W. R. Browne and B. L. Feringa, *Nat. Nanotechnol.*, 2006, **1**, 25–35.
41 X. Ma and H. Tian, *Chem. Soc. Rev.*, 2009, **39**, 70–80.
42 M. M. Boyle, R. A. Smaldone, A. C. Whalley, M. W. Ambrogio, Y. Y. Botros and J. F. Stoddart, *Chem. Sci.*, 2011, **2**, 204–210.
43 V. Balzani, A. Credi, S. Silvi and M. Venturi, *Chem. Soc. Rev.*, 2006, **35**, 1135–1149.
44 J. Berná, C. Franco-Pujante and M. Alajarín, *Org. Biomol. Chem.*, 2013, **12**, 474–478.
45 G. T. Spence, M. B. Pitak and P. D. Beer, *Chem. – Eur. J.*, 2012, **18**, 7100–7108.
46 N. H. Evans, C. J. Serpell and P. D. Beer, *Chem. – Eur. J.*, 2011, **17**, 7734–7738.
47 C. J. Serpell, R. Chall, A. L. Thompson and P. D. Beer, *Dalton Trans.*, 2011, **40**, 12052–12055.
48 E. V. Dzyuba, L. Kaufmann, N. L. Löw, A. K. Meyer, H. D. F. Winkler, K. Rissanen and C. A. Schalley, *Org. Lett.*, 2011, **13**, 4838–4841.
49 J. J. Gassensmith, S. Matthys, J.-J. Lee, A. Wojcik, P. V. Kamat and B. D. Smith, *Chem. – Eur. J.*, 2010, **16**, 2916–2921.
50 H. Zheng, W. Zhou, J. Lv, X. Yin, Y. Li, H. Liu and Y. Li, *Chem. – Eur. J.*, 2009, **15**, 13253–13262.
51 T.-C. Lin, C.-C. Lai and S.-H. Chiu, *Org. Lett.*, 2009, **11**, 613–616.
52 M. J. Barrell, D. A. Leigh, P. J. Lusby and A. M. Z. Slawin, *Angew. Chem. Int. Ed.*, 2008, **47**, 8036–8039.
53 C. M. Keaveney and D. A. Leigh, *Angew. Chem. Int. Ed.*, 2004, **43**, 1222–1224.
54 C.-F. Lin, C.-C. Lai, Y.-H. Liu, S.-M. Peng and S.-H. Chiu, *Chem. – Eur. J.*, 2007, **13**, 4350–4355.
55 Y.-L. Huang, W.-C. Hung, C.-C. Lai, Y.-H. Liu, S.-M. Peng and S.-H. Chiu, *Angew. Chem. Int. Ed.*, 2007, **46**, 6629–6633.
56 T.-C. Lin, C.-C. Lai and S.-H. Chiu, *Org. Lett.*, 2009, **11**, 613–616.
57 L. Liu, Y. Liu, P. Liu, J. Wu, Y. Guan, X. Hu, C. Lin, Y. Yang, X. Sun, J. Ma and L. Wang, *Chem. Sci.*, 2013, **4**, 1701–1706.
58 M. V. R. Raju and H.-C. Lin, *Org. Lett.*, 2013, **15**, 1274–1277.
59 H. Zhang, J. Hu and D.-H. Qu, *Org. Lett.*, 2012, **14**, 2334–2337.
60 D. J. Cram, *Angew. Chem. Int. Ed. Engl.*, 1986, **25**, 1039–1057.

61 F. Eblinger and H.-J. Schneider, *Angew. Chem. Int. Ed.*, 1998, **37**, 826–829.
62 M. J. Chmielewski, J. J. Davis and P. D. Beer, *Org. Biomol. Chem.*, 2009, **7**, 415–424.
63 M. J. Langton and P. D. Beer, *Acc. Chem. Res.*, 2014, **47**, 1935–1949.
64 S. Erbas-Cakmak and E. U. Akkaya, *Angew. Chem. Int. Ed.*, 2013, **52**, 11364–11368.
65 M. J. Hynes, *J. Chem. Soc. Dalton Trans.*, 1993, 311–312.
66 H. C. Brown, D. H. McDaniel and O. Häfliger, in *Determination of Organic Structures by Physical Methods*, Academic Press, 1955, pp. 567–662.
67 W. D. Kumler and J. J. Eiler, *J. Am. Chem. Soc.*, 1943, **65**, 2355–2361.
68 J. Bjerrum, *Stability Constants: Part 1*, The Chemical Society, 1957.
69 Y. Marcus, *J. Chem. Soc. Faraday Trans.*, 1991, **87**, 2995–2999.
70 C. F. Verkoelen and J. C. Romijn, *Urol. Res.*, 1996, **24**, 183–191.
71 I. M. Kolthoff and P. J. Elving, *Treatise on Analytical Chemistry*, Interscience Encyclopedia, 1959.
72 J. F. J. Dippy, S. R. C. Hughes and A. Rozanski, *J. Chem. Soc. Resumed*, 1959, 2492–2498.
73 J. M. Mercurio, R. C. Knighton, J. Cookson and P. D. Beer, *Chem. – Eur. J.*, 2014, **20**, 11740–11749.
74 L. C. Gilday and P. D. Beer, *Chem. – Eur. J.*, 2014, **20**, 8379–8385.

Chapter Four
Fluorescence anion sensing in C_{60} fullerene-containing multi-station rotaxanes

4. FLUORESCENCE ANION SENSING IN C_{60} FULLERENE-CONTAINING MULTI-STATION ROTAXANES

4.1. Introduction

4.1.1. Fullerenes and their applications in supramolecular chemistry

Fullerenes are an allotrope of carbon in which the atoms are arranged in a network of hexagons and pentagons to form spherical cage-like structures.[1] Thirty years since the discovery of the first fullerene, C_{60} (Figure 4.1),[2] this family of carbon nanomaterials have been successfully employed for a variety of applications, for example as organic photovoltaics,[3,4] and more recently in the field of supramolecular chemistry.[5] Fullerenes of various cage sizes may be prepared (C_{2n}, n = 30, 35, 40, 48), most commonly *via* electrical discharge from a graphite rod in a helium atmosphere.[6,7]

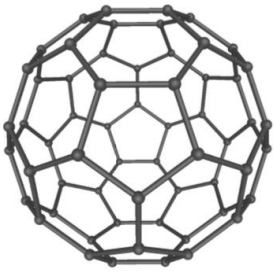


Figure 4.1. C_{60} fullerene.[2]

The chemical behaviour of the fullerene species generated is likened to that of electron-deficient alkenes; the average hybridisation of each carbon atom is between that of sp^2 (graphite) and sp^3 (diamond), causing the π orbitals to protrude outwards from the structure.[8,9] Consequently, fullerenes are excellent electron-acceptors.[10] The exterior of the cages can be decorated with a range of moieties (exohedral functionalisation, Figure 4.2a) and the relative inertness of the interior may be utilised for incarcerating a variety of ionic, atomic and small molecular species (endohedral functionalisation, Figure 4.2b).

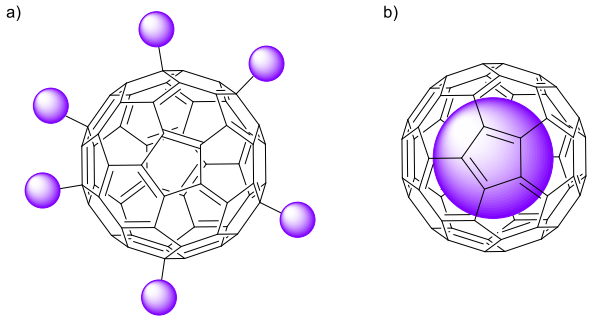


Figure 4.2. Schematic of a) exohedral and b) endohedral functionalisation of C_{60} fullerene.

The controlled exohedral functionalisation of fullerenes with a single chemical motif is commonly achieved *via* Prato[11] or Bingel[12] reactions, since direct amination or hydroxylation processes readily form multi-adduct products in a variety of regioisomers. Of these, Bingel is often preferred on the basis of milder reaction conditions, higher yields and accessibility of a wider range of chemically functionalised fullerene derivatives. The procedure requires the preparation of an alpha-halo ester/ketone which under basic conditions can undergo a cyclopropanation reaction to form a methanofullerene (Figure 4.3).

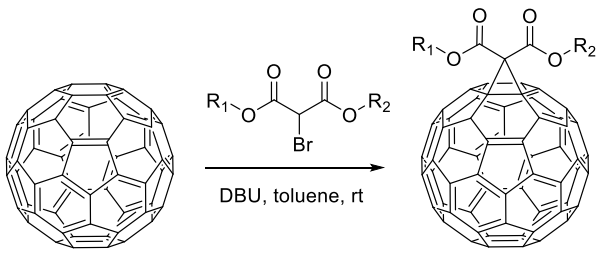


Figure 4.3. The Bingel reaction for the exohedral functionalisation of a C_{60} fullerene.[12]

Of the fullerene family, the electro- and photo-chemical properties of C_{60} and C_{60} derivatives have been most widely studied due to its high abundance. The electronic spectrum of C_{60} reveals absorptions throughout the UV-Vis spectral region[13] and it has been demonstrated to be fluorescent from the excited singlet state ($^1C_{60}$*), albeit with a lower quantum yield than common organic chromophores.[14] This low quantum yield is attributed to the efficient deactivation pathway *via* intersystem crossing (ISC) to the triplet excited state ($^3C_{60}$*) which is rapidly quenched by $^3O_{2(g)}$ (Figure 4.4). Functionalised C_{60} derivatives are highly coloured and often more strongly fluorescent than pristine C_{60} on account of ISC

being less favoured, with emission typically occurring at similar energies (λ_{em} ~ 700 nm) upon excitation.[14]

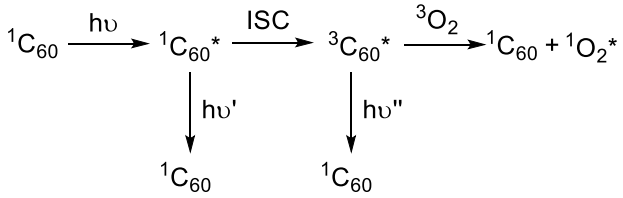


Figure 4.4. The deactivation pathway for fluorescence emission from excited C_{60} fullerene. ISC = intersystem crossing.[14]

Electrochemically, C_{60} exhibits up to six reversible reduction processes on account of its rigid, spherical geometry and electron-deficient nature.[15–17] The photochemical and photophysical properties of fullerenes therefore allow them to participate in photoinduced electron transfer (PET) processes with electron-donors, such as ferrocene, generating long-lived charge-separated states that are highly desirable for the development of artificial photosynthetic devices (Figure 4.5).[18–21]

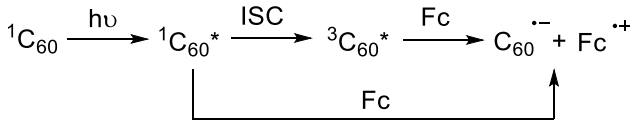


Figure 4.5. Excitation of C_{60} in the presence of a ferrocene electron-donor (Fc) can generate a fullerene radical anion as part of a charge-separated radical pair. For pristine C_{60} this occurs from $^3C_{60}$ while for functionalised derivatives this typically occurs from $^1C_{60}$* ISC = intersystem crossing.[21]*

The generation of long-lived charge-separated states in a manner akin to naturally occurring photosynthetic centres has been facilitated *via* the incorporation of fullerenes into interlocked systems; the mechanical bonding of rotaxanes and catenanes provides an ideal basis for fine-tuning the electronic communication between donor and fullerene acceptor chemical moieties.[22,23] Furthermore, dynamic donor–acceptor interlocked systems offer the potential of controlling the intramolecular processes of photoinduced charge separation or charge recombination *via* stimulated motion of their molecular components.[18,24]

For example, photophysical and electrochemical studies of a bistable [2]rotaxane containing a ferrocene-functionalised macrocycle (electron donor) and C_{60} stoppered axle component (electron acceptor) revealed that irradiation of the fullerene unit caused electron transfer from ferrocene to C_{60} (PET) generating a charge-separated radical pair state.[25] The lifetime of this state was shown to be reduced when the macrocycle was in closer proximity to the C_{60} stopper motif, whereas by increasing the distance between the ferrocene and fullerene groups *via* solvent variation, a longer-lived charge-separated state was observed (Figure 4.6).

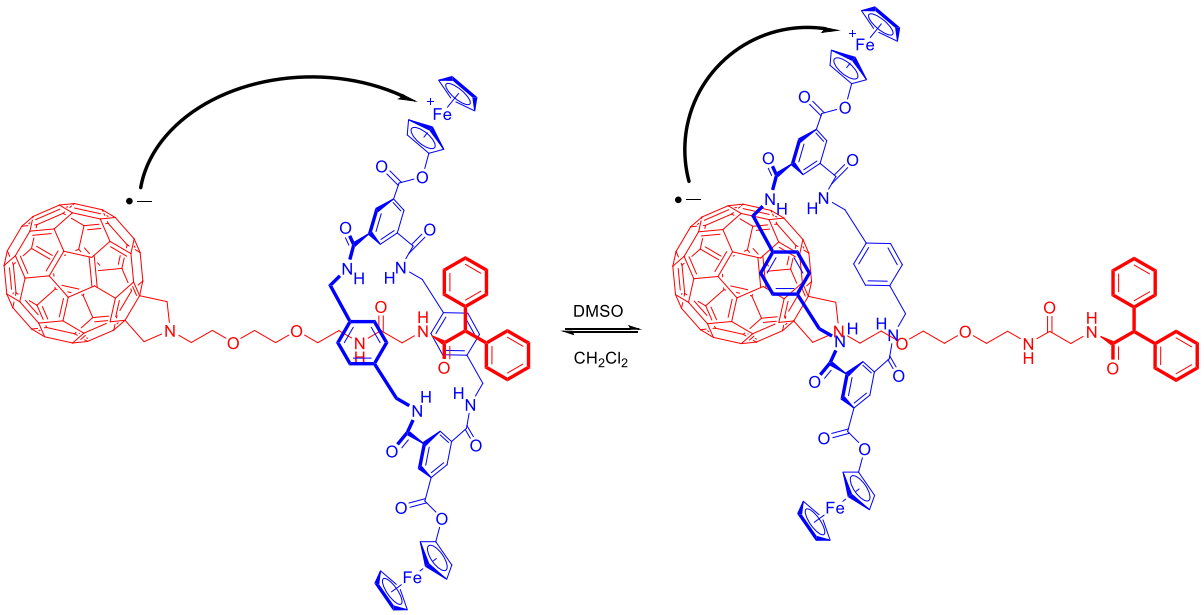


Figure 4.6. Prato's bistable [2]rotaxane that exhibits tuneable PET via macrocycle shuttling.[25]

4.1.2. Fluorescence anion sensing using molecular motion

The potential of dynamic interlocked molecules, such as bistable rotaxanes, to act as chemical sensors *via* photo- or electro-chemical signalling of co-conformational changes was introduced in Section 3.1.3. In these systems a fluorescence response is commonly achieved by modulating the rate of intramolecular energy transfer[26–29] or electron transfer[25,30–32] occurring between interlocked components. However, there are very few examples of this mechanism being successfully recruited to perform fluorescence anion sensing.[33–36]

Tian and co-workers have utilised the distant-dependency of PET quenching of fluorescence emission in the construction of a bistable [2]rotaxane that exhibits dual fluorescence signal outputs, stimulated by variation in pH (Figure 4.7).[37] Shuttling of the ferrocene-appended dibenzo-24-crown-8 macrocycle towards a dialkylammonium or proto-triazolium recognition site produces a simultaneous enhancement or quenching of the fluorescence emission from a fluorophore-based stopper. At the time of writing, no examples of interlocked systems capable of anion sensing *via* such a dual optical response exist.

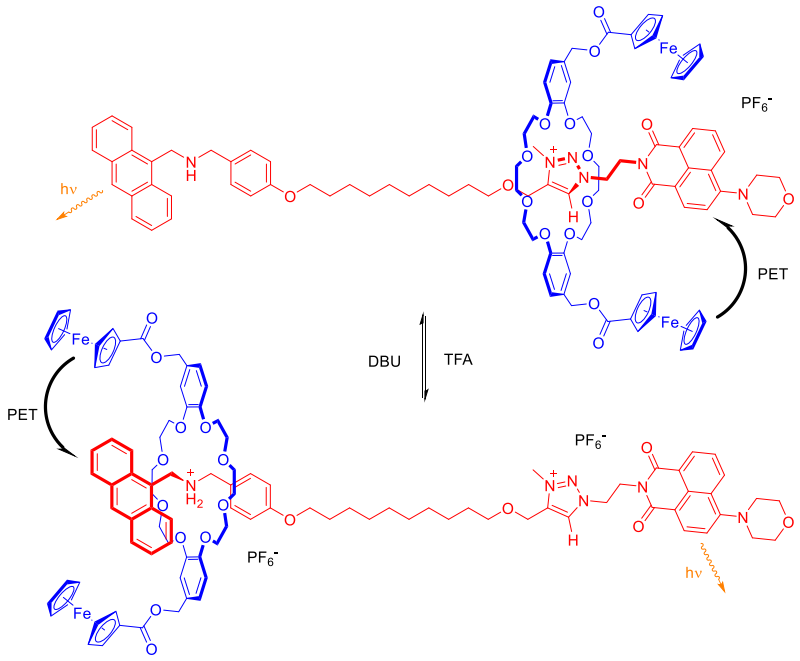


Figure 4.7. The pH-induced shuttling of a ferrocene-appended macrocycle in Tian's bistable [2]rotaxane is manifested in a dual fluorescence signal output courtesy of distant-dependent PET quenching to two fluorophores.[37]

4.1.3. Chapter objectives

Whilst previous work in this thesis has described efforts towards the colorimetric sensing of anions, the focus of this chapter is on the design and synthesis of multi-station rotaxane host systems that can sense negatively charged species *via* co-conformational changes which produce a fluorescence response.

Initially, the ability of a ferrocenyl-appended macrocycle to exhibit anion recognition-induced distance-dependent quenching of NDI fluorescence emission within a bistable NDI-proto-triazolium [2]rotaxane will be investigated and compared to an analogous nitro-functionalised macrocycle.

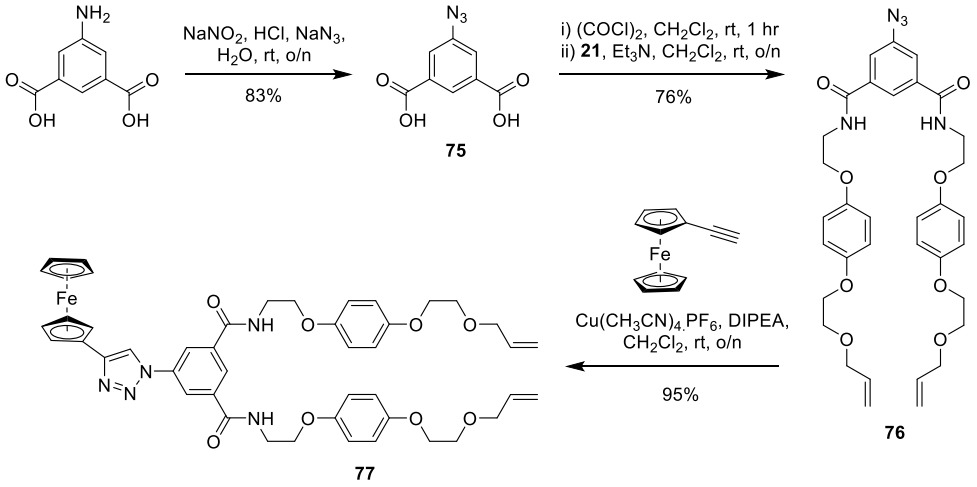
Following this, a mono-functionalised C_{60} fullerene will be incorporated into a bis-naphthalene diimide, bis-proto-triazolium axle component, and the anion-induced dynamic behaviour of [3]rotaxanes containing ferrocene- or nitro-appended macrocycles will be examined using ^{1}H NMR and fluorescence spectroscopy.

4.2. A ferrocene macrocycle-containing two-station [2]rotaxane

4.2.1. Synthesis

Initial work began with the challenge of integrating a ferrocene reporter group into a bis vinyl-appended macrocycle precursor followed by cyclisation using the established chloride anion templated clipping protocol around a NDI–proto-triazolium-based two-station axle component to produce a bistable [2]rotaxane.

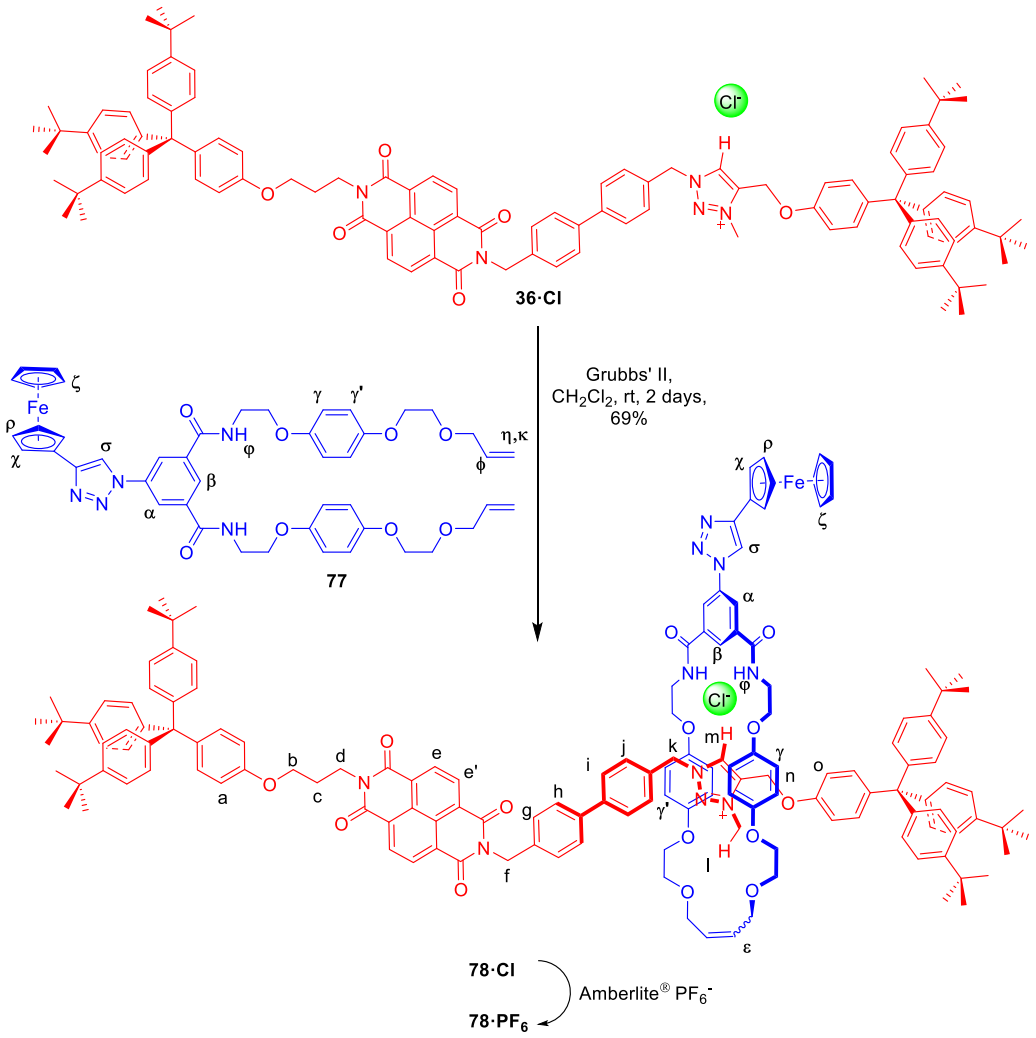
A triazole-ferrocene-appended bis-vinyl-functionalised isophthalamide macrocycle precursor was synthesised according to Scheme 4.1.



*Scheme 4.1. Synthesis of ferrocene triazole-containing bis-vinyl-appended macrocycle precursor **77**.*

5-Azidoisophthalic acid was prepared *via* a diazonium intermediate following a literature procedure,[38] and the corresponding bis-acid chloride (generated *in situ*) condensed with two equivalents of amine **21** to give the bis-vinyl isophthalamide derivative **76** in 76% yield following chromatographic purification on silica gel. This was followed by a facile CuAAC 'click' reaction between azide **76** and ethynyl ferrocene (provided by Mr J. Lim) to form the target ferrocene-functionalised isophthalamide macrocycle precursor **77** in 95% yield.

The incorporation of a ferrocene-appended macrocycle into a bistable [2]rotaxane was then realised by chloride anion-templated RCM clipping of the ferrocene bis-vinyl-containing macrocyclic precursor **77** around the NDI-proto-triazolium two-station axle component **36·Cl** (Scheme 4.2). Two equivalents of **77** were stirred with axle **36·Cl** in dry CH_2Cl_2 before Grubbs' II catalyst was added to effect RCM. The target ferrocene-containing two-station [2]rotaxane **78·Cl** was isolated in 69% yield using preparative silica thin-layer chromatography, and fully characterised as both chloride and hexafluorophosphate salts.



*Scheme 4.2. Synthesis of ferrocene-macrocycle-containing two-station [2]rotaxane **78·A**.*

4.2.2. Chloride-induced shuttling in a ferrocene macrocycle-containing two-station [2]rotaxane

The capability of ferrocene-containing [2]rotaxane **78·A** to exhibit chloride-induced shuttling in $CDCl_3$ was assessed using ^1H NMR spectroscopy (Figure 4.8).

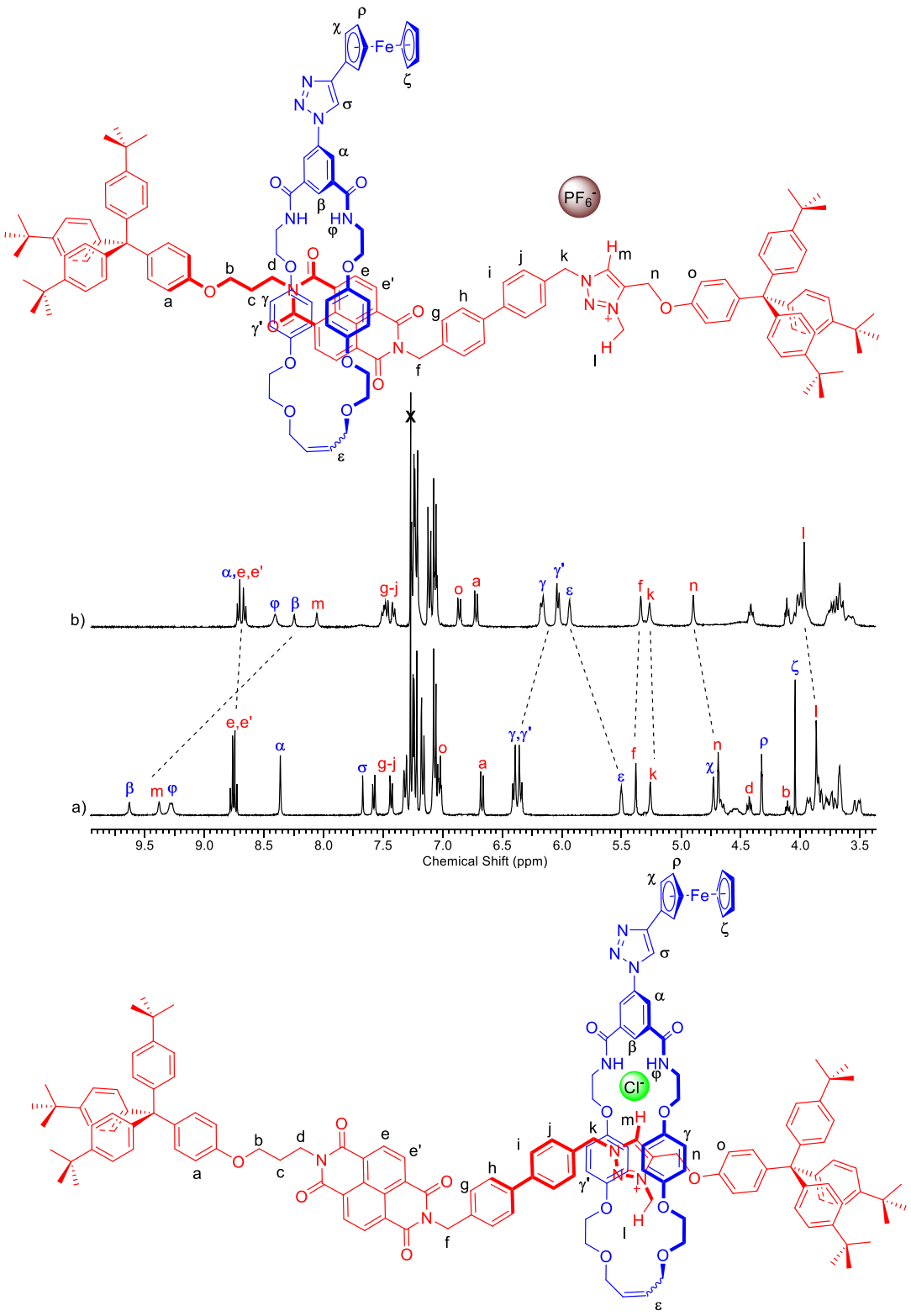


*Figure 4.8. Truncated ^{1}H NMR spectra of the ferrocene-containing [2]rotaxane **78·(A)$_2$** as the a) chloride and b) hexafluorophosphate salt ($CDCl_3$, 298 K, 400 MHz). The dominant co-conformations of the [2]rotaxane predicted from these spectra are also depicted.*

Comparison of the ^{1}H NMR spectra of the chloride and hexafluorophosphate salts **78·Cl** and **78·PF$_6$** revealed chemical shift changes diagnostic of anion-mediated co-conformational switching. Perturbation of the axle signal for the *N*-methyl triazolium protons H_I was used to estimate that occupancy of the proto-triazolium station increased by 33% upon chloride recognition in **78·Cl**, which is the same degree of shuttling achieved in the analogous nitro-macrocycle-containing bistable [2]rotaxane **42·A** reported in Section 2.3.3.

4.2.3. Photophysical studies of nitro- and ferrocene-containing two-station [2]rotaxanes

Rotaxane **78·A** was used to examine how the position of a ferrocene-based macrocyclic wheel on a two-station axle affected the photophysical properties of the NDI chromophore. UV-Vis and fluorescence emission experiments were also performed with the nitro-macrocycle-containing analogue of this [2]rotaxane (**42·A**) to demonstrate the suitability of ferrocene as an efficient and distance-dependent PET quenching motif.

Characteristic energies of absorption and emission bands for the NDI chromophore were observed in the UV-Vis and fluorescence spectra of [2]rotaxanes **78·PF$_6$** and **42·PF$_6$** in $CHCl_3$ (Table 4.1).[39]

*Table 4.1. Photophysical properties of the nitro- and ferrocene-macrocycle-containing [2]rotaxanes **42·PF$_6$** and **78·PF$_6$** in $CHCl_3$ (1×10^{-4} mol L^{-1}). λ_{ex} = 382 nm.*

	λ_{abs} / nm		λ_{em} / nm	
42·PF$_6$	363	382	411	431
78·PF$_6$	363	382	408	430
NDI[39,*]	360	380	400	420

[*] Values taken from a literature NDI derivative with alkyl groups substituted at the imide positions. λ_{ex} = 348 nm.

Fluorescence titrations (λ_{ex} = 382 nm) were performed by the addition of up to 50 equivalents of TBA·Cl to solutions of ferrocene- and nitro-macrocycle-containing [2]rotaxanes **78·PF$_6$** and **42·PF$_6$** in $CHCl_3$ (Figure 4.9).

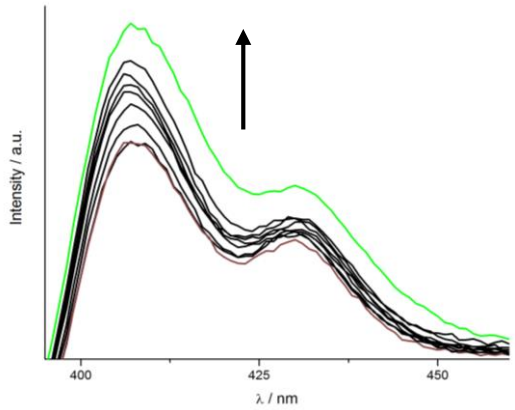


*Figure 4.9. Changes in the emission spectra of [2]rotaxane **78·PF$_6$** in $CHCl_3$ (1×10^{-4} mol L^{-1}) upon addition of 50 equivalents of TBA·Cl. λ_{ex} = 382 nm.*

Integration of the fluorescence spectra revealed a 30% increase in the intensity of the NDI fluorescence of ferrocene-containing [2]rotaxane **78·PF$_6$**. However, the analogous experiment with the nitro-macrocycle-containing system **42·PF$_6$** revealed no significant change in the fluorescence emission intensity (within experimental error i.e. < 10%).[†] This can be rationalised by chloride anion-induced translational motion of the macrocycle component from the NDI station to the proto-triazolium site, increasing the distance between macrocycle and fluorophore. When the macrocycle component is functionalised with an electron-donating ferrocenyl moiety **78·PF$_6$**, shuttling reduces the efficiency of PET fluorescence quenching, which is manifested in a turn-on emission response. By contrast the electron-deficient nitro-containing macrocycle does not exhibit PET quenching and so a negligible change in the fluorescence intensity is observed upon macrocycle translocation in **42·PF$_6$**. Hence, this demonstrates the potential of using distant-dependent PET fluorescence quenching[40] from a

[†] Emission intensity changes were calculated *via* integration of appropriate fluorescence spectra between λ_{em} = 400-450 nm. Error = ±10%. See Appendix for more details.

ferrocene-appended macrocycle as a mechanism for signalling anion-induced co-conformational changes within bistable rotaxane host systems.

In contrast to the fluorescence titration results, no significant change (< 1%[‡]) in the UV-Vis spectrum of the NDI chromophore in ferrocene-containing [2]rotaxane **78·PF$_6$** was observed upon the addition of chloride (Figure 4.10), indicating ground state absorption is not dependent upon macrocycle translocation and/or anion binding. This provides further evidence that the predominant change in NDI fluorescence emission is due to a through-space distant-dependent electron transfer mechanism between the ferrocene donor and fluorophore acceptor.[41]

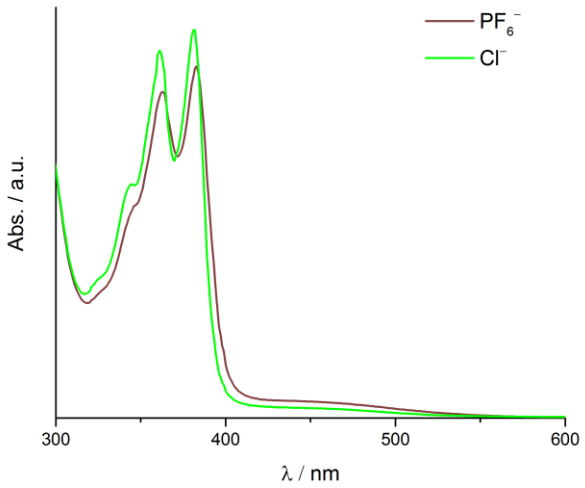


*Figure 4.10. Superimposed UV-Vis spectra of the hexafluorophosphate and chloride salts of ferrocene-containing [2]rotaxane **78·PF$_6$** and **78·Cl** in $CHCl_3$ (1×10^{-4} mol L^{-1}).*

Ferrocene has been shown to act as an electron-donor and hence to relax excited states of electron-deficient fluorophores *via* a PET mechanism[35,37,42,43] (Figure 4.11a), whilst the electron-withdrawing nature of the nitro group typically induces PET acceptor-functionality[33,44] making the nitro-functionalised macrocycle analogue less suited as a quenching synthon in a system of this design (Figure 4.11b). This provides further rationalisation for the experimental data observed above.

[‡] Absorption intensity changes were calculated *via* integration of appropriate UV-Vis spectra between λ_{em} = 300-600 nm. See Appendix for more details.

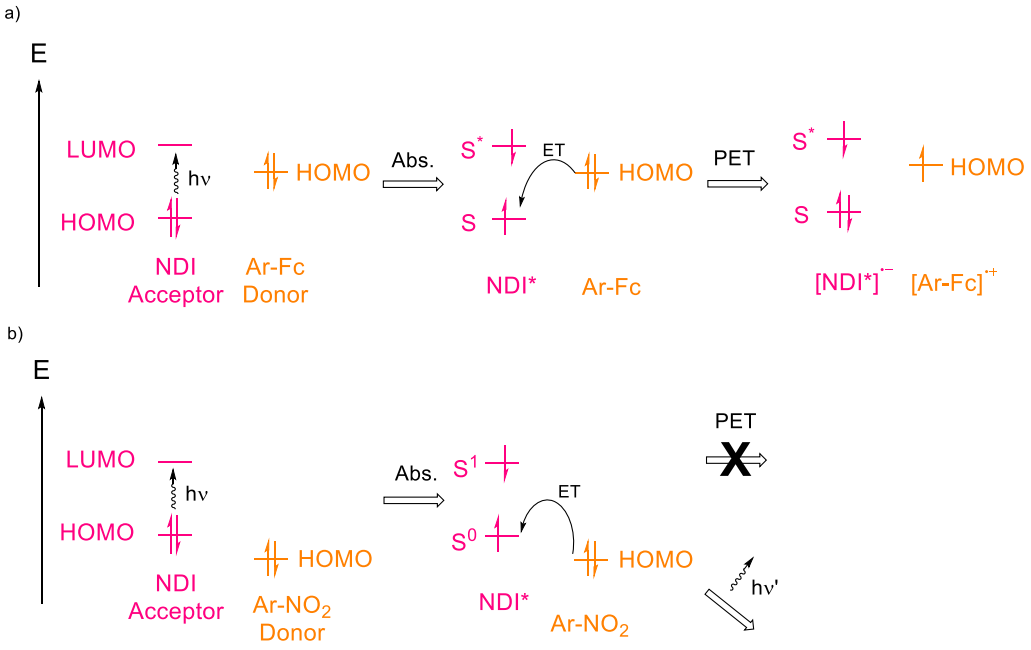


Figure 4.11. The redox potential of an electron donor influences the rate of electron transfer (ET) to an electron-deficient fluorophore (acceptor) such as NDI. Therefore PET quenching is exhibited by a) a ferrocenyl-appended macrocycle donor (Ar–Fc) but to a lesser extent by b) a nitro-functionalised macrocycle (Ar–NO_2) i.e. $k_{ET,NO2} << k_{ET,Fc}$. S = singlet state.

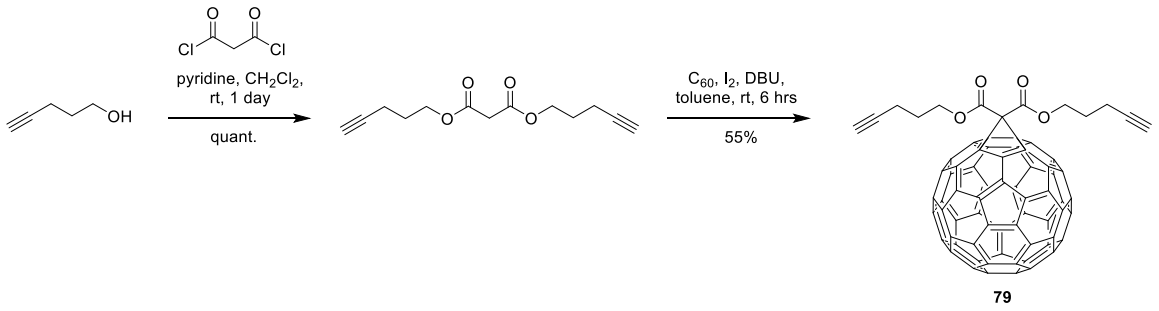
4.3. C_{60} fullerene-containing [3]rotaxanes

The synthesis of two fullerene-based [3]rotaxanes containing either ferrocene- or nitro-appended macrocycles began with the exohedral functionalisation of C_{60} and its subsequent incorporation into a four-station axle component. Detailed spectroscopic studies were used to investigate the dynamic behaviour of the [3]rotaxane systems and the effect of anion-induced molecular motion on the photophysical properties of the chromophores that decorate the interlocked architectures.

4.3.1. Exohedral functionalisation of a C_{60} fullerene

In collaboration with the research group of Prof. K. Porfyrakis from the Department of Materials, University of Oxford, the exohedral functionalisation of C_{60} fullerene with a bis-alkyne malonate using a Bingel reaction was performed by Mr I. Rasovic (Scheme 4.3). Initially, the bis-alkyne malonate was prepared using a literature procedure[45] and subsequently stirred with DBU, I_2 and C_{60} in toluene for six hours at room temperature. Deprotonation by DBU produces a nucleophilic malonate anion which attaches across a [6,6] bond of the fullerene *via* cyclopropanation. The desired bis-alkyne C_{60} mono-

adduct **79** was separated from multi-adduct and iodo-alkyne-containing side products using recycling HPLC in 55% yield and fully characterised (see Appendix).



*Scheme 4.3. Synthesis of C_{60} fullerene bis-alkyne **79**.*

C_{60} derivative **79** was also characterised using UV-Vis absorption and fluorescence emission spectroscopies (Figure 4.12).

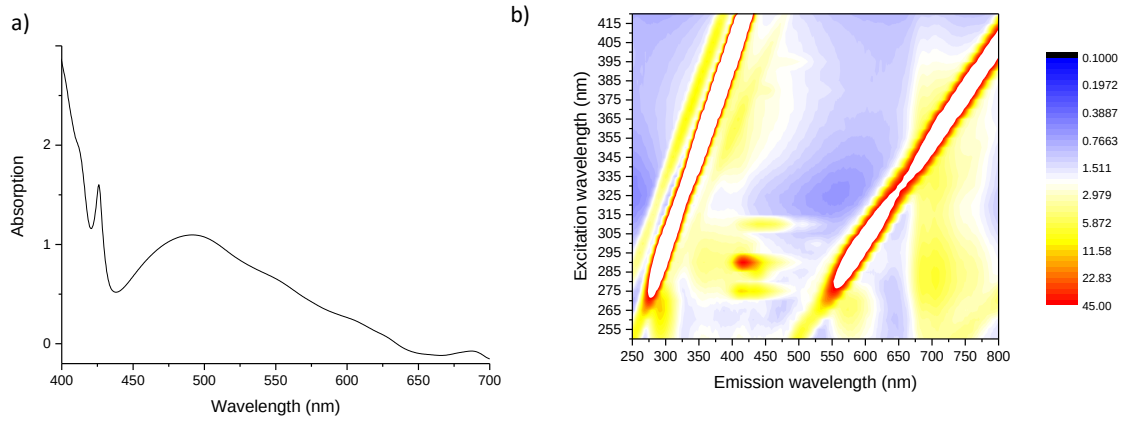


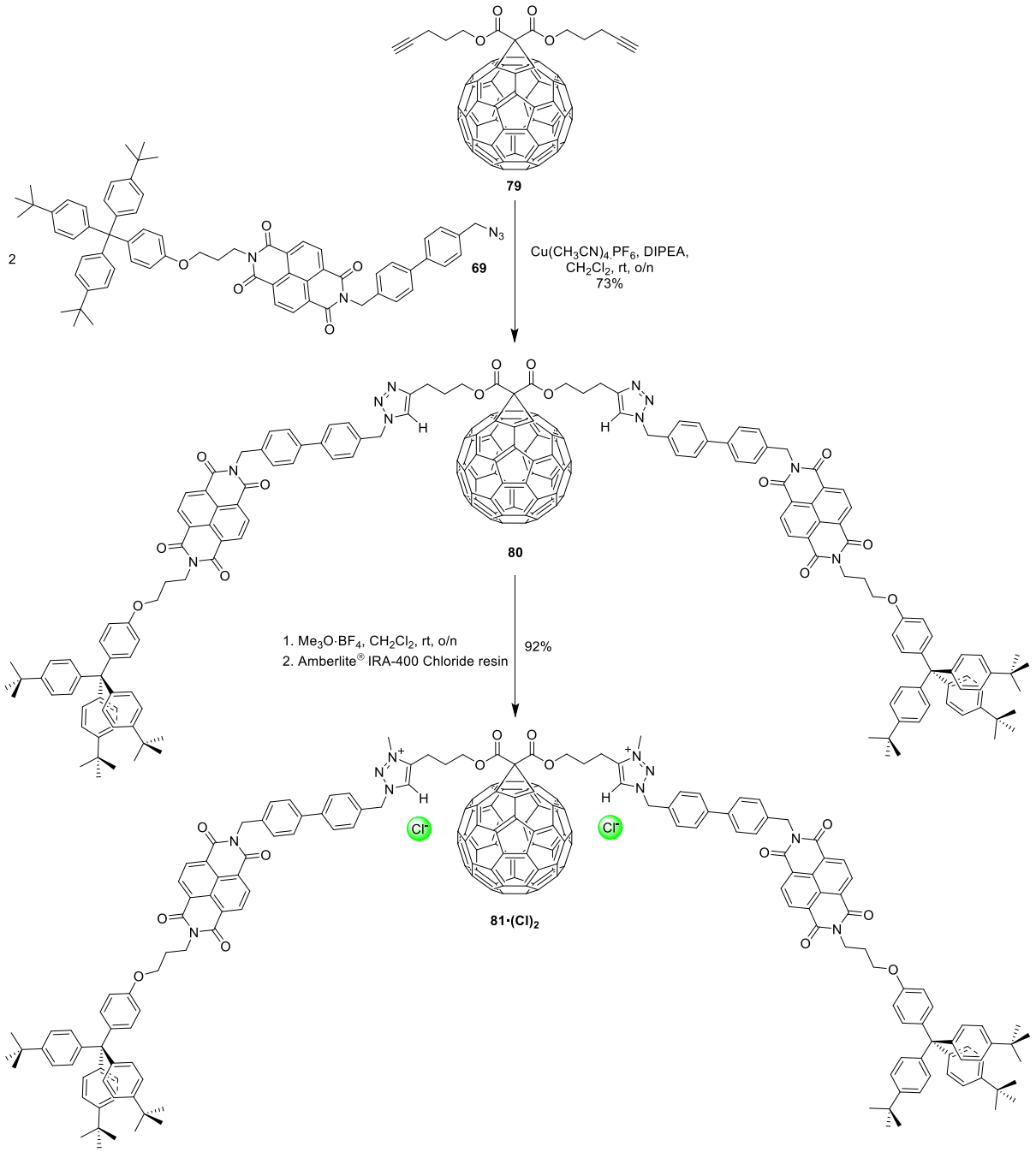
*Figure 4.12. Characterisation of C_{60} fullerene bis-alkyne **79** by a) UV-Vis and b) fluorescence spectroscopies. The three-dimensional fluorescence contour plot is created by collecting emission responses over a range of excitation wavelengths. Red and yellow regions indicate fluorescence peaks (intensity is in a.u.).*

Within the visible region, the UV-Vis spectrum of **79** displays a characteristic shoulder at λ_{abs} = 425 nm, indicating exohedral functionalisation of the fullerene cage.[46] Furthermore, diagnostic emission peaks of Bingle methanofullerene C_{60} derivatives are observed at λ_{em} = 700 nm and λ_{em} = 400–450 nm in the fluorescence contour map of **79**.[46]

4.3.2. Synthesis of a C_{60} fullerene-containing four-station axle component

The C_{60} bis-alkyne was incorporated into a four-station axle component, *via* an analogous multistep synthetic pathway used to prepare axle **71·(A)$_2$** described in Chapter Three (Scheme 4.4).

A base-accelerated CuAAC 'click' reaction between C_{60} bis-alkyne **79** and two equivalents of the mono stoppered NDI-containing biphenyl azide derivative **69** afforded bis-triazole axle **80** in high yield following purification using silica gel column chromatography. The triazole groups were methylated using a small excess of $Me_3O{\cdot}BF_4$ in dry CH_2Cl_2 giving the dicationic axle as the tetrafluoroborate salt **81·(BF$_4$)$_2$**. The bis-chloride salt **81·(Cl)$_2$** was obtained following anion exchange using chloride-loaded Amberlite® resin in preparation for anion-templated [3]rotaxane synthesis.



Scheme 4.4. Synthesis of a four-station C_{60} fullerene-containing axle component ***81·(Cl)$_2$***.

4.3.3. Photophysical properties of the four-station C_{60} fullerene-containing axle component

The UV-Vis spectra of axle **81·(A)$_2$** reveal no significant change (< 1%[§]) in the characteristic NDI (λ_{abs} = 361, 380 nm) and C_{60} fullerene absorptions (λ_{abs} = 400–600 nm) upon anion exchange from bis-tetrafluoroborate to bis-chloride salts (Figure 4.13).

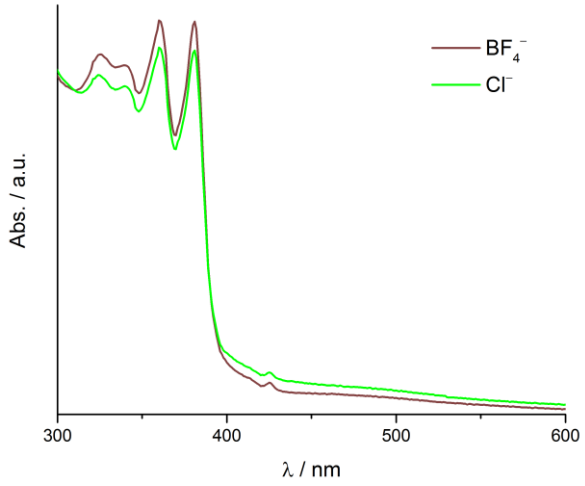


Figure 4.13. Superimposed UV-Vis spectra of the bis-tetrafluoroborate and bis-chloride salts of four-station axle component ***81·(BF$_4$)$_2$*** *and* ***81·(Cl)$_2$*** *in $CHCl_3$ (1×10^{-5} mol L^{-1}).*

Excitation of axle **81·(BF$_4$)$_2$** at λ_{ex} = 300 nm and λ_{ex} = 495 nm stimulated fluorescence emission at λ_{em} = 415 nm and λ_{em} = 710 nm from the respective NDI and C_{60} fullerene fluorophores (Figure 4.14). On excitation of the bis-chloride salt **81·(Cl)$_2$** at the same energies, the NDI fluorescence response was found to have decreased in intensity and undergone a small hypsochromic shift ($\Delta\lambda_{em}$ = 5 nm) whilst the intensity of the fullerene increased with no change in λ_{em} (Table 4.2). A possible explanation for the turning-off of the NDI emission is the occurrence of collisional quenching *via* electron transfer from chloride anions,[40] however the C_{60} fullerene fluorescence response is harder to rationalise without further experimentation.

[§] Absorption intensity changes were calculated *via* integration of appropriate UV-Vis spectra between λ_{em} = 300-600 nm. See Appendix for more details.

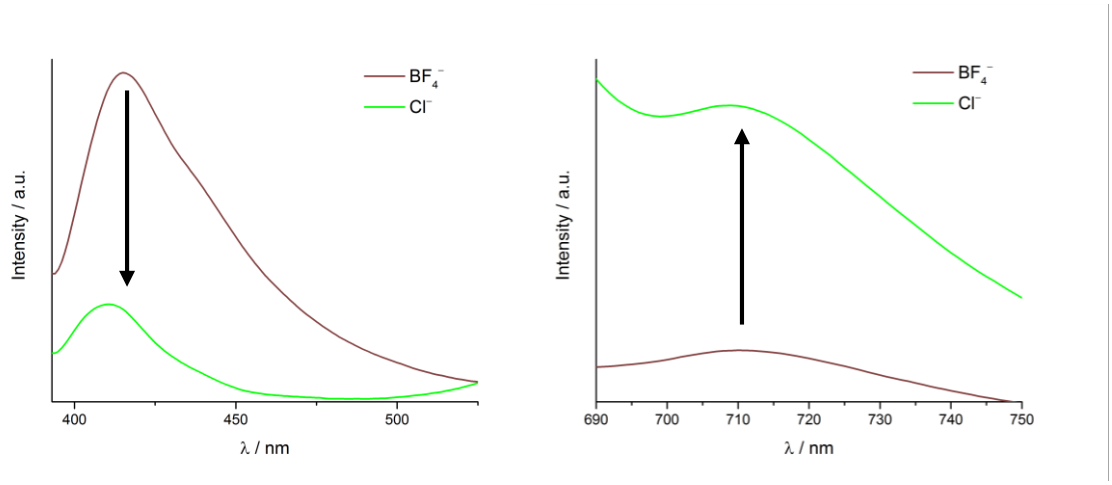


Figure 4.14. The fluorescence spectra of bis-tetrafluoroborate and bis-chloride salts of the four-station axle component ***81·(A)₂*** *in $CHCl_3$ (1×10^{-5} mol L^{-1}) showing emission upon excitation at a) λ_{ex} = 300 nm (NDI) and b) λ_{ex} = 475 nm (C_{60} fullerene).*

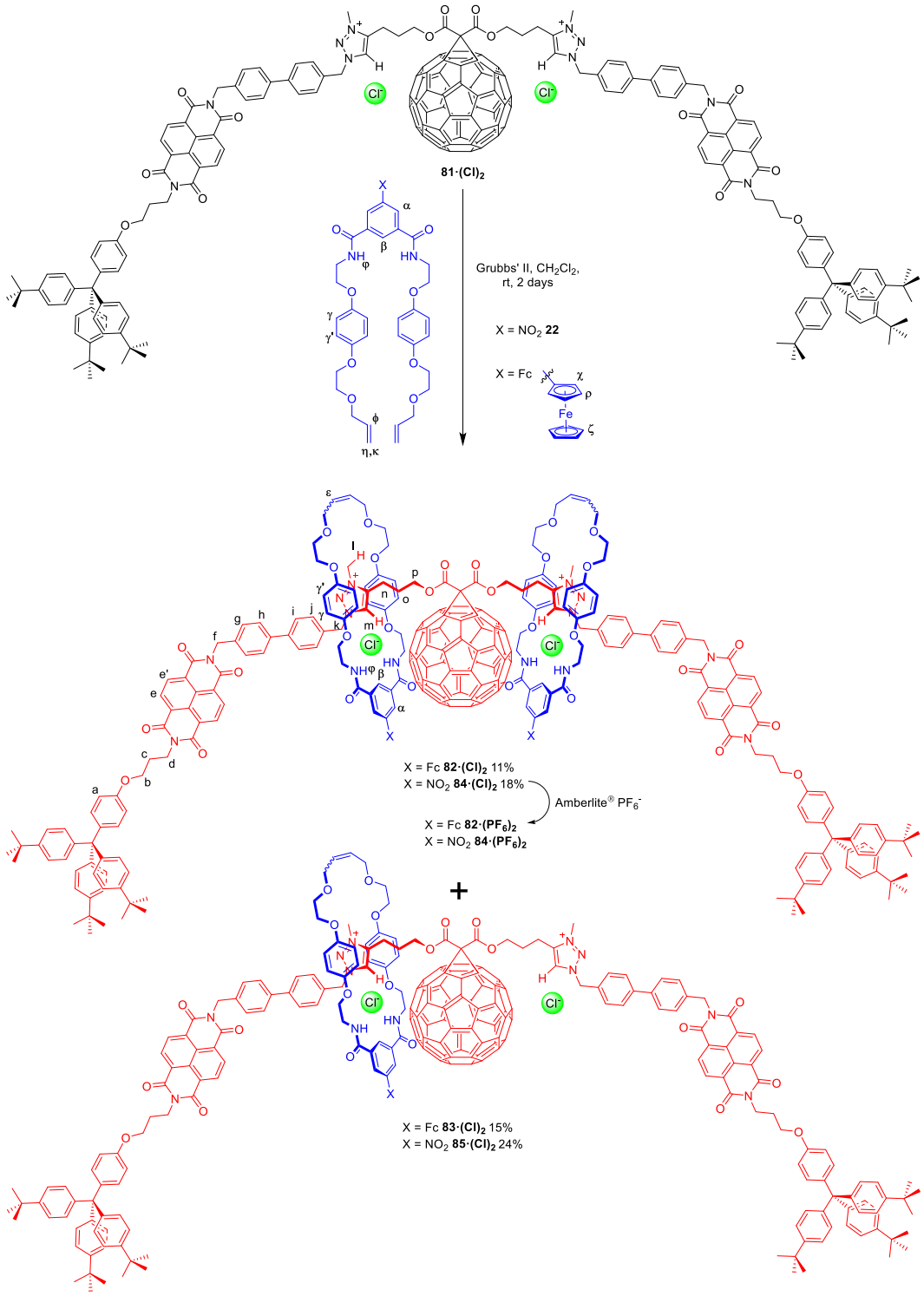
Table 4.2. Percentage changes in a) NDI and b) C_{60} fullerene emission intensity, ΔI (%), upon anion exchange of the four-station axle component from ***81·(BF₄)₂*** *to* ***81·(Cl)₂*** *in $CHCl_3$ (1×10^{-5} mol L^{-1}).*

Fluorophore	λ_{ex} / nm	ΔI (%)
NDI	300	−60[a]
C_{60}	475	+132[b]

Emission intensity changes were calculated via integration of appropriate fluorescence spectra between [a] λ_{em} = 390-525 nm and [b] λ_{em} = 700-750 nm. Error = ±10%. See Appendix for more details.

4.3.4. Synthesis of C_{60} fullerene-containing four-station [3]rotaxanes

The synthesis of two [3]rotaxanes containing a four-station bis-NDI, bis-proto-triazolium and C_{60} fullerene axle and either ferrocene- or nitro-functionalised macrocyclic components was performed by a chloride-templated clipping procedure (Scheme 4.5). A macrocycle precursor containing a ferrocenyl group directly attached to the isophthalamide motif was used to avoid the possibility of anion binding at the triazole group of derivative **77**. This ferrocene-functionalised isophthalamide-based macrocycle precursor was prepared by Mr J. Lim.



*Scheme 4.5. Synthesis of the C_{60} fullerene-containing four-station [3]rotaxanes **82·(A)₂** and **84·(A)₂** containing either ferrocene- or nitro-appended macrocycle components respectively. The [2]rotaxane analogues **83·(A)₂** and **85·(A)₂** were also isolated as side products.*

Axle **81·(Cl)₂** was stirred with three equivalents of either the ferrocene- or nitro-containing bis-vinyl-appended macrocycle precursor in dry CH_2Cl_2 before a catalytic amount of Grubbs' II catalyst was

added to effect RCM. Preparative silica thin-layer chromatography was used to separate the target ferrocene- or nitro-containing [3]rotaxanes as their bis-chloride salts **82·(Cl)$_2$** and **84·(Cl)$_2$** from [2]rotaxane side products which were also isolated. Anion exchange to the [3]rotaxane bis-hexafluorophosphate salts was performed using Amberlite® resin and all rotaxanes were fully characterised.

4.3.5. Characterisation of chloride-induced shuttling in the C_{60} fullerene-containing four-station [3]rotaxanes

The ^{1}H NMR spectra of nitro- and ferrocene-containing [3]rotaxanes **82·(Cl)$_2$** and **84·(Cl)$_2$** in $CDCl_3$ are compared to those of the axle component **81·(Cl)$_2$** and their respective isophthalamide-based macrocycle precursors in Figure 4.15 and Figure 4.16.

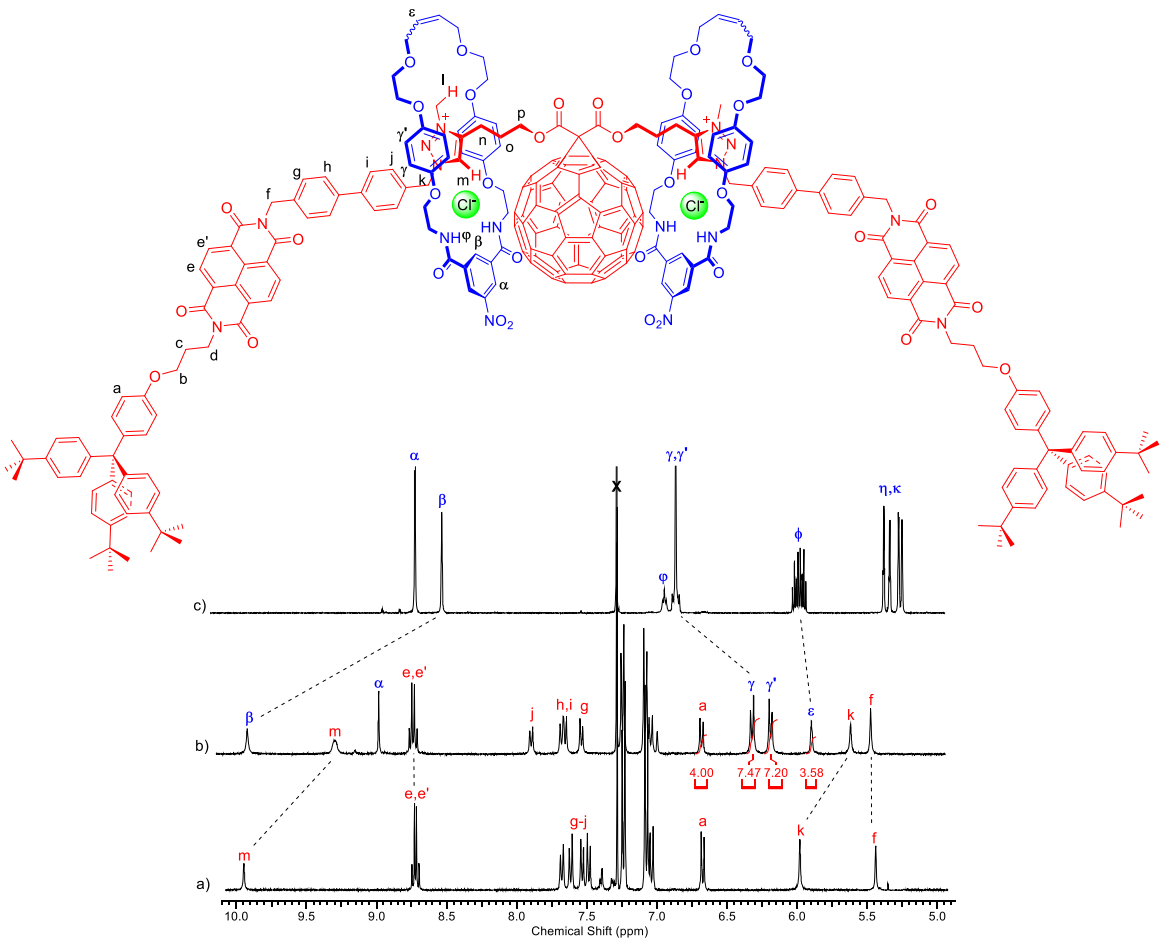


*Figure 4.15. Truncated ^{1}H NMR spectra of a) axle component **81·(Cl)$_2$**, b) nitro-macrocycle-containing [3]rotaxane **84·(Cl)$_2$** and c) nitro-isophthalamide macrocycle precursor **22** ($CDCl_3$, 298 K, 400 MHz). The dominant co-conformation of the [3]rotaxane **84·(Cl)$_2$** is also depicted.*

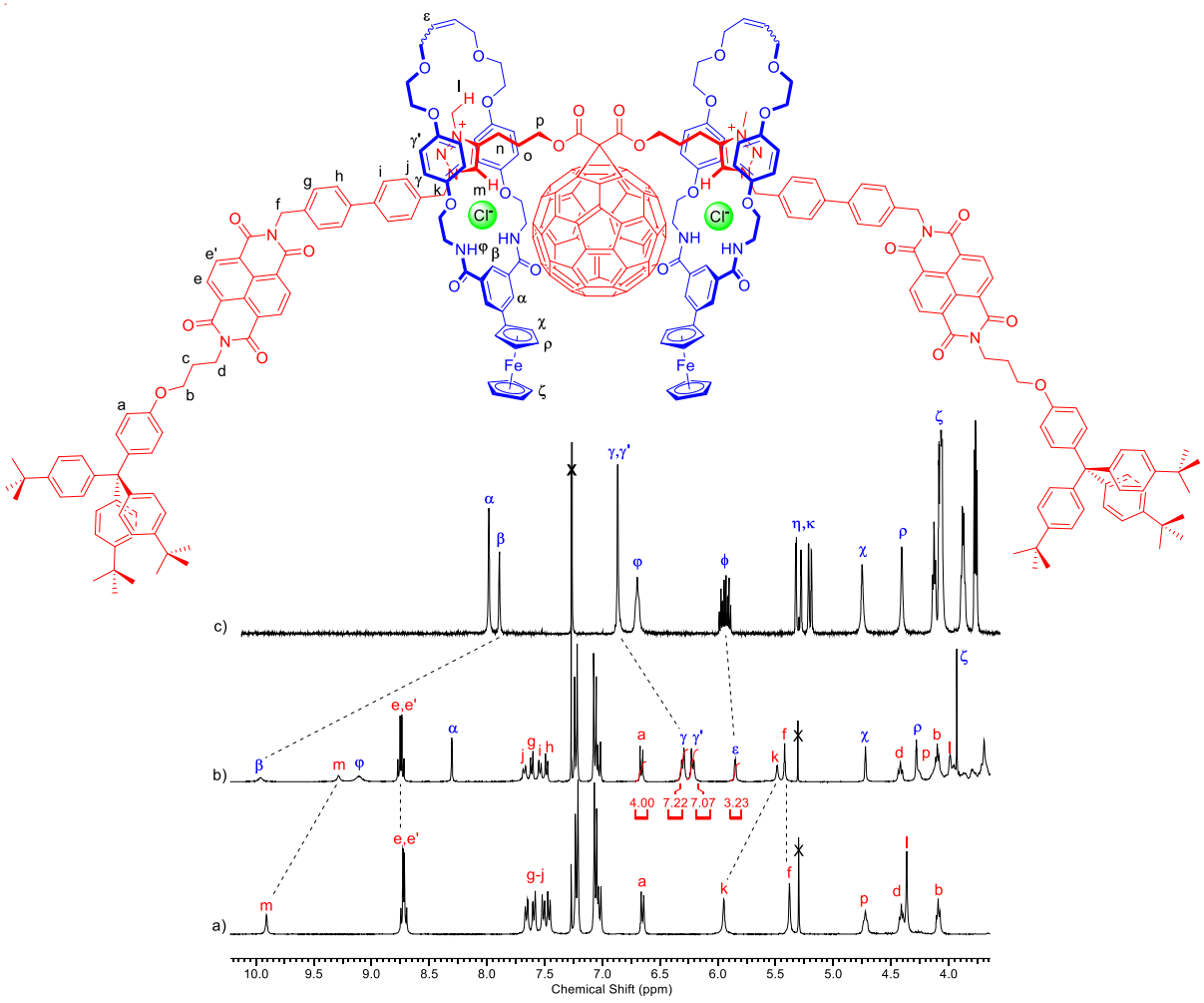


*Figure 4.16. Truncated ^{1}H NMR spectra of a) axle component **81·(Cl)$_2$**, b) ferrocene-macrocycle-containing [3]rotaxane **82·(Cl)$_2$** and c) ferrocene-isophthalamide macrocycle precursor ($CDCl_3$, 298 K, 400 MHz). The dominant co-conformation of the [3]rotaxane **82·(Cl)$_2$** is also depicted.*

For both [3]rotaxanes the two sets of hydroquinone proton resonances $H_{\gamma,\gamma'}$ integrate for 16 hydrogen nuclei, relative to the four axle phenyl trityl stopper aromatic protons H_a, indicating that two macrocyclic rings are clipped around the axle component. Further evidence that the [3]rotaxanes have been successfully isolated comes from the symmetric nature of the ^{1}H NMR spectra, in contrast to the more complex spectra of the [2]rotaxane analogues (*vide infra*).

In both interlocked systems the resonance of H_β is strongly downfield shifted, whilst the signal for H_m is shifted upfield, indicating polarisation of chloride anions toward the hydrogen bond donors of the isophthalamide binding cleft of the macrocycles. As expected from previous work, the signals associated with the macrocycle hydroquinone environments $H_{\gamma,\gamma'}$ have split and moved upfield due to

aromatic charge–transfer donor–acceptor interactions with the proto-triazolium motifs. Interestingly these protons are found 0.11–0.15 ppm further upfield than in the two station proto-triazolium-NDI [2]rotaxane **42·(A)** described in Chapter Two (Section 2.3.2). This is likely to be caused by ring current effects from the proximal fullerene cage. Additional evidence for macrocycle occupancy at the proto-triazolium stations comes from an upfield shift of the methylene group H_k in the [3]rotaxane relative to the axle, whilst signals H_f and $H_{e,e'}$ are unchanged. The two-dimensional ^{1}H ROESY NMR spectra of **82·(Cl)$_2$** and **84·(Cl)$_2$** in $CDCl_3$ further illustrate this is the predominant co-conformation because of strong through-space coupling interactions between the proto-triazolium station's diagnostic protons ($H_{\gamma,\gamma'}$, H_ε, H_β) and those of the macrocycle (H_k, H_j, H_i, H_l) (Figure 4.18).

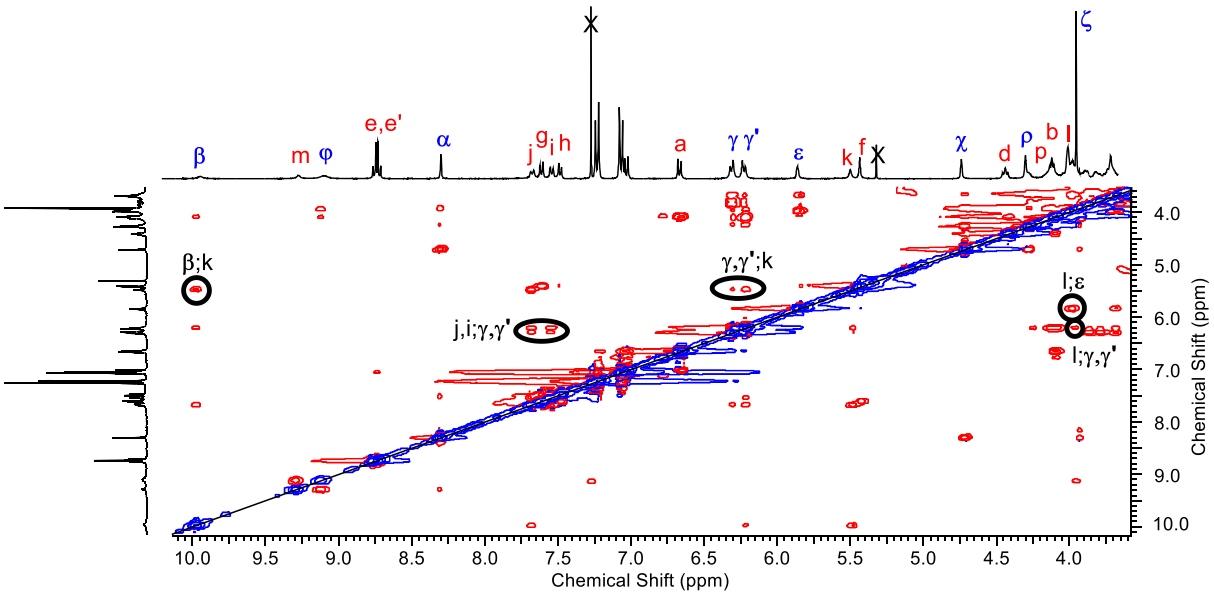


*Figure 4.17. Truncated ^{1}H–^{1}H ROESY NMR spectra of ferrocene-containing [3]rotaxane **82·(Cl)$_2$** with selected coupling interactions highlighted ($CDCl_3$, 298 K, 500 MHz).*

Unlike the [3]rotaxane systems synthesised in Chapter Three, the size of the fullerene cage prevents macrocycles from fully translocating across the axle component. Therefore desymmetrisation of the four-station axle results in a more complex ^{1}H NMR spectrum of the [2]rotaxane relative to the [3]rotaxane (e.g. **85·(Cl)$_2$** in Figure 4.18). Specifically, the methylene group adjacent to the proto-triazolium motifs produces discrete signals for H_k and $H_{k'}$, indicating two different environments arising from the presence or absence of a macrocycle. However, because the macrocycle resides at the proto-

triazolium site as the bis-chloride salt, the methylene group proximal to the NDI station, H_f, produces a single peak indicating the proton environments at this position of the axle are essentially identical. Therefore, the ^{1}H NMR spectra of [3]rotaxanes **82·(Cl)$_2$** and **84·(Cl)$_2$** are a true representation of a co-conformation in which both macrocycles reside at the proto-triazolium anion recognition sites either side of the fullerene cage to partake in chloride binding.

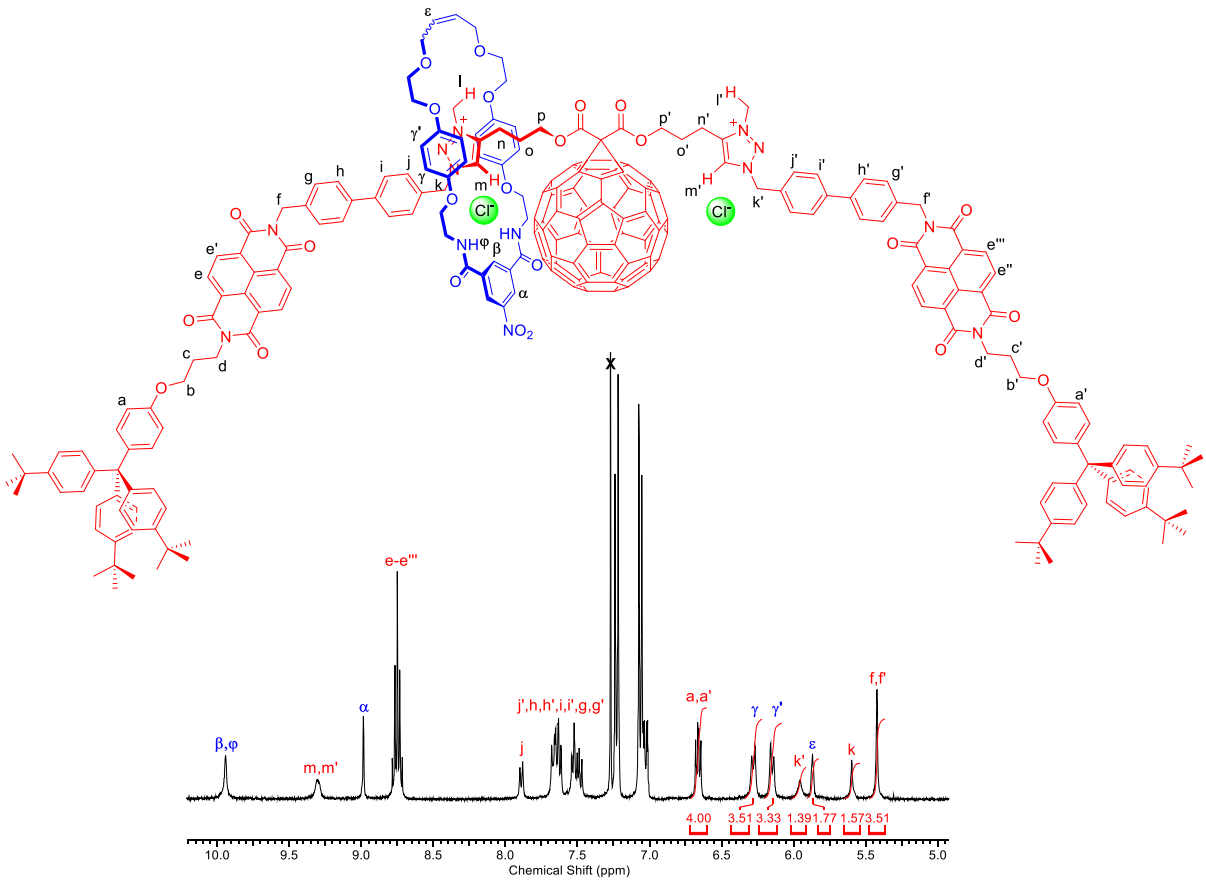


*Figure 4.18. Truncated ^{1}H NMR spectrum of nitro-macrocycle-containing [2]rotaxane **85·(Cl)$_2$** ($CDCl_3$, 298 K, 400 MHz). The dominant co-conformation of the [2]rotaxane **85·(Cl)$_2$** is also depicted.*

A comparison of the ^{1}H NMR spectra of the bis-chloride and bis-hexafluorophosphate salts of the nitro- and ferrocene-containing [3]rotaxanes indicate significant co-conformational change upon removal of the coordinating counter anions (Figure 4.19 and Figure 4.20).

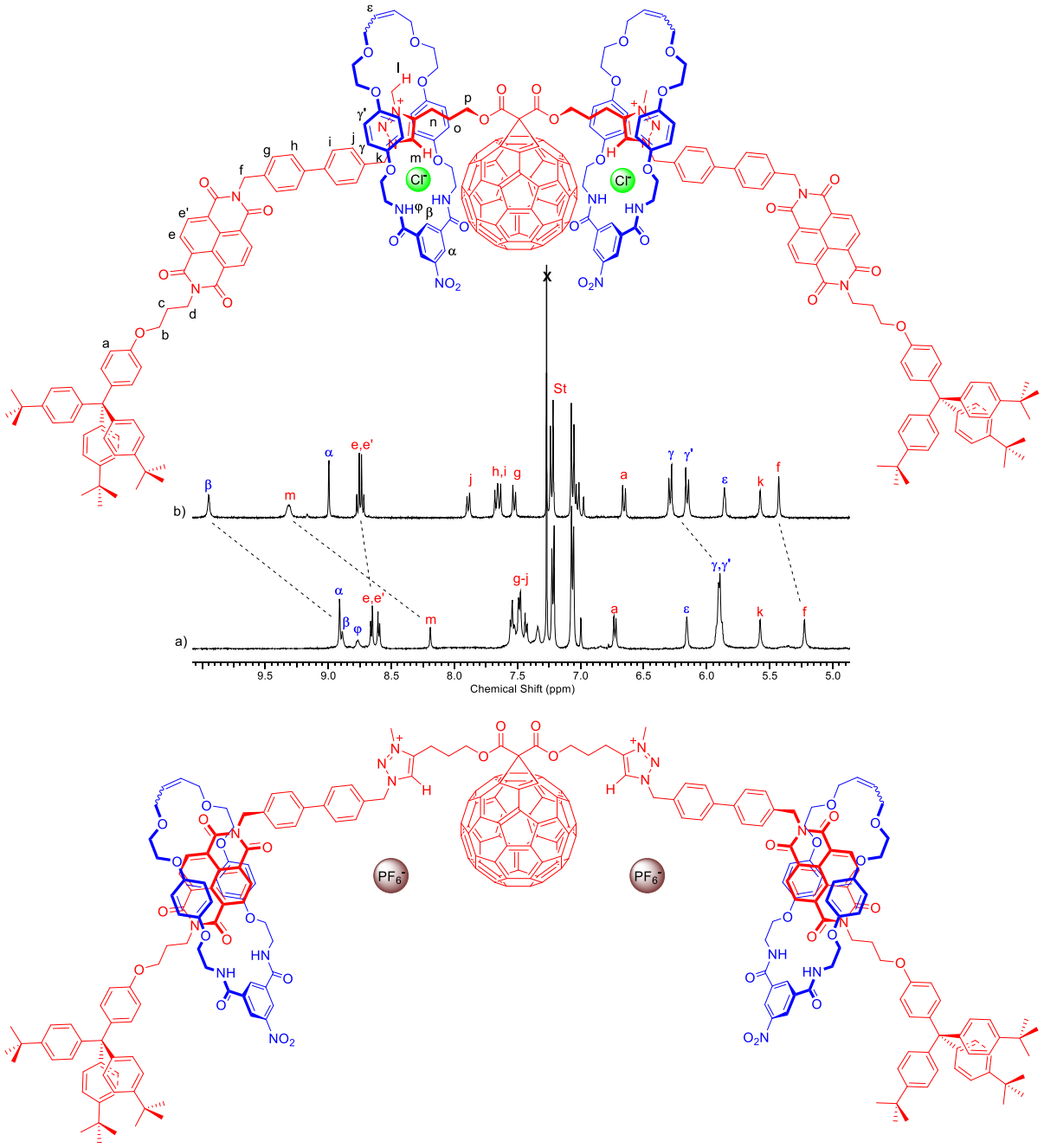


*Figure 4.19. Truncated ^{1}H NMR spectra of the nitro-containing [3]rotaxane **84·(A)$_2$** as the a) bis-hexafluorophosphate and b) bis-chloride salt ($CDCl_3$, 298 K, 400 MHz). The dominant co-conformations of the [3]rotaxane predicted from these spectra are also depicted.*

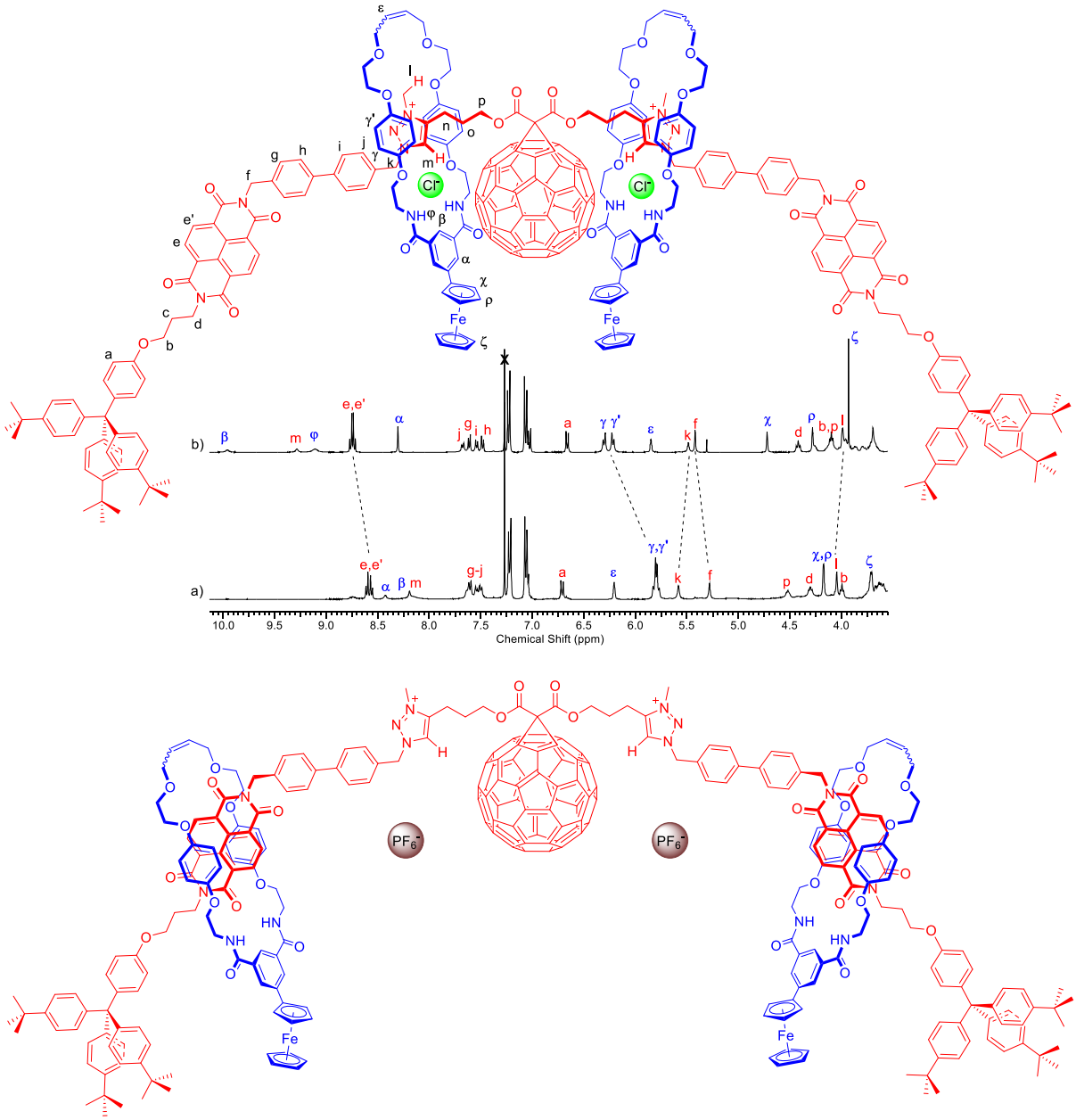


*Figure 4.20. Truncated ^{1}H NMR spectra of the ferrocene-containing [3]rotaxane **82·(A)$_2$** as the a) bis-hexafluorophosphate and b) bis-chloride salt (CDCl$_3$, 298 K, 400 MHz). The dominant co-conformations of the [3]rotaxane predicted from these spectra are also depicted.*

Anion exchange to the non-coordinating anion salts produces large downfield shifts of acidic protons H_m and H_β. In both [3]rotaxane systems significant upfield shifts of the macrocycle hydroquinone resonances are also observed due to formation of aromatic charge–transfer donor–acceptor interactions between macrocycles and the NDI stations. These aromatic stacking interactions predominantly occur with NDI and not the electron-deficient fullerene cage because protons $H_{e,e'}$ are

also significantly shifted. Upfield perturbations of the methylene signals H_f, further support macrocycle shuttling toward the peripheral NDI stations of the axle component. Two-dimensional ^{1}H ROESY NMR spectra of **82·(PF$_6$)$_2$** and **84·(PF$_6$)$_2$** confirmed the proximity of protons $H_{e,e'}$ and $H_{\varepsilon,\gamma,\gamma'}$, as well as $H_{\gamma,\gamma'}$ and H_a within this co-conformation (Figure 4.21).

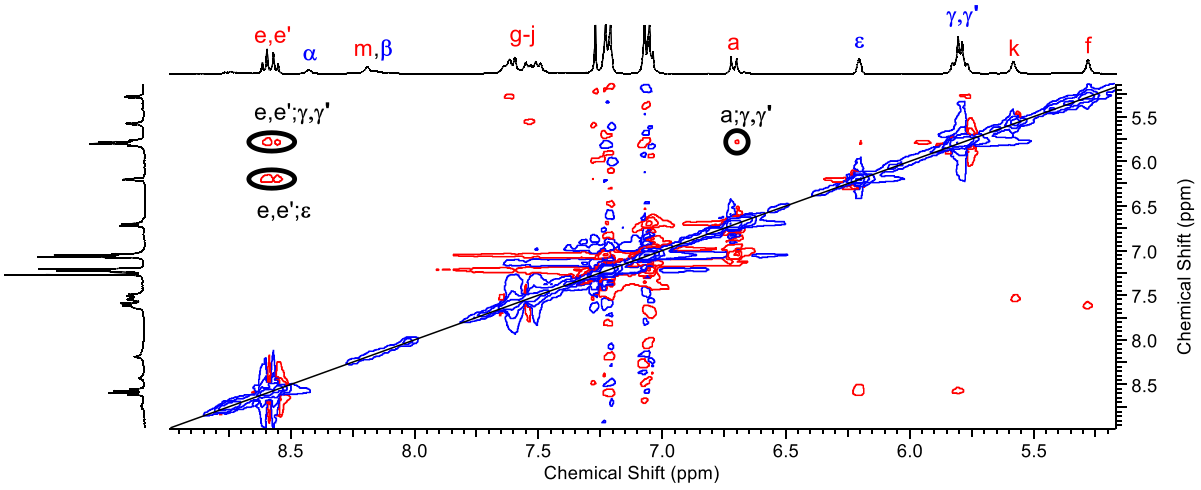


*Figure 4.21. Truncated ^{1}H–^{1}H ROESY NMR spectra of ferrocene-containing [3]rotaxane **82·(PF$_6$)$_2$** with selected coupling interactions highlighted (CDCl$_3$, 298 K, 500 MHz).*

Taken together, this evidence suggests changing the nature of the counter anions produces identical pincer-like translational motion of the macrocycle components in both [3]rotaxanes **82·(A)$_2$** and **84·(A)$_2$** (Figure 4.22).

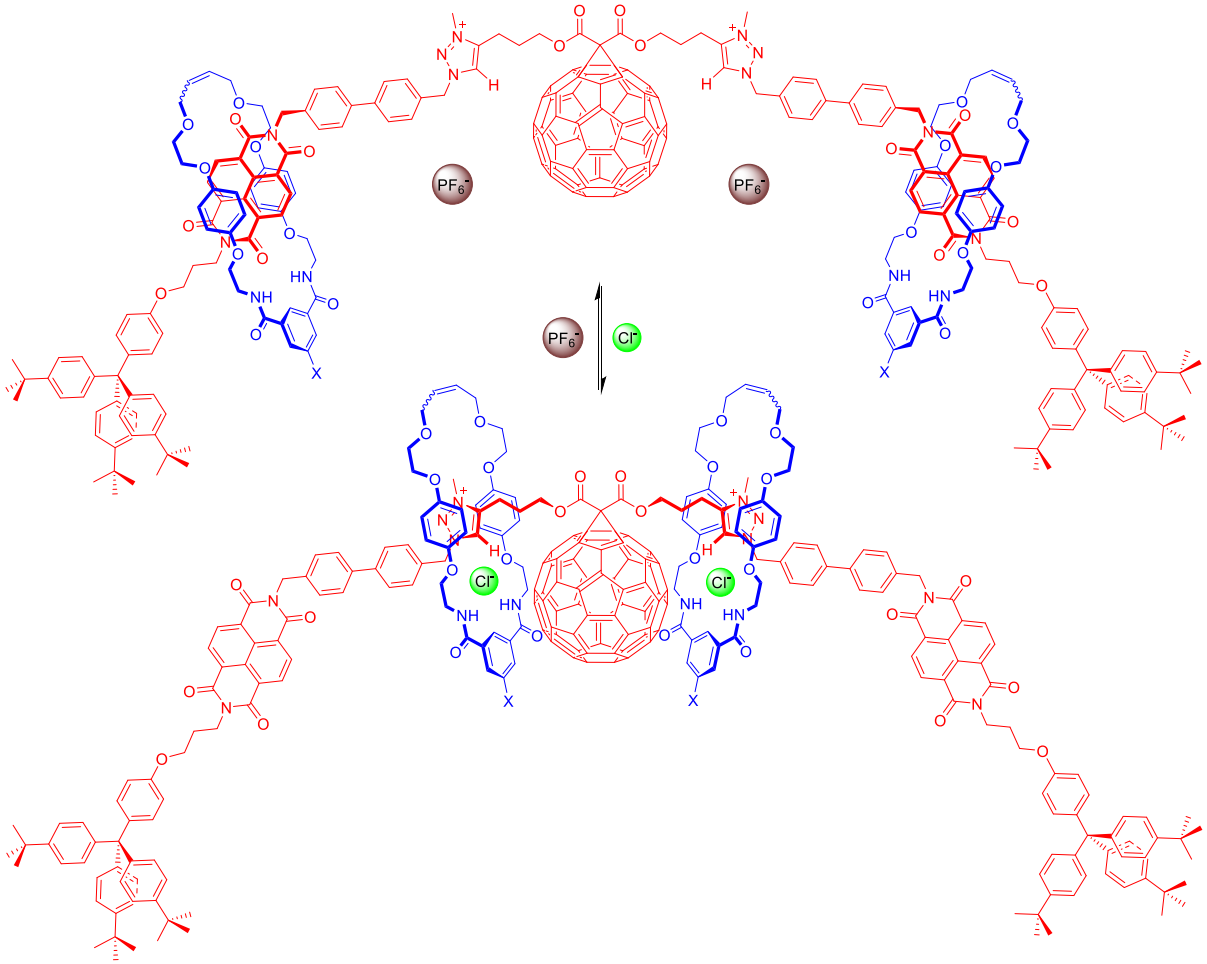


Figure 4.22. The anion-induced pincer-like translational motion exhibited by ferrocene- and nitro-containing [3]rotaxanes ***82·(A)₂*** *and* ***84·(A)₂****. X = Fc, NO_2.*

The particularly large perturbations of the ^{1}H NMR signals of the NDI protons $H_{e,e'}$ observed on anion exchange (Δδ = 0.13–0.18 ppm) indicate excellent positional integrity between NDI and proto-triazolium stations in both salts of these [3]rotaxanes in $CDCl_3$. To quantify the degree of co-conformational change, it was proposed that macrocycle station occupancies could be estimated using the change in ^{1}H NMR chemical shift of $H_{e,e'}$ relative to the model one-station NDI [2]rotaxane **54**. This was possible because of the similar chemical environments of the NDI groups in the one-station axle **53** and the C_{60} four-station axle component **81·(Cl)₂** resulting in signals of $H_{e,e'}$ having identical chemical shifts δ = 8.76 ppm in their ^{1}H NMR spectra (Figure 4.23).

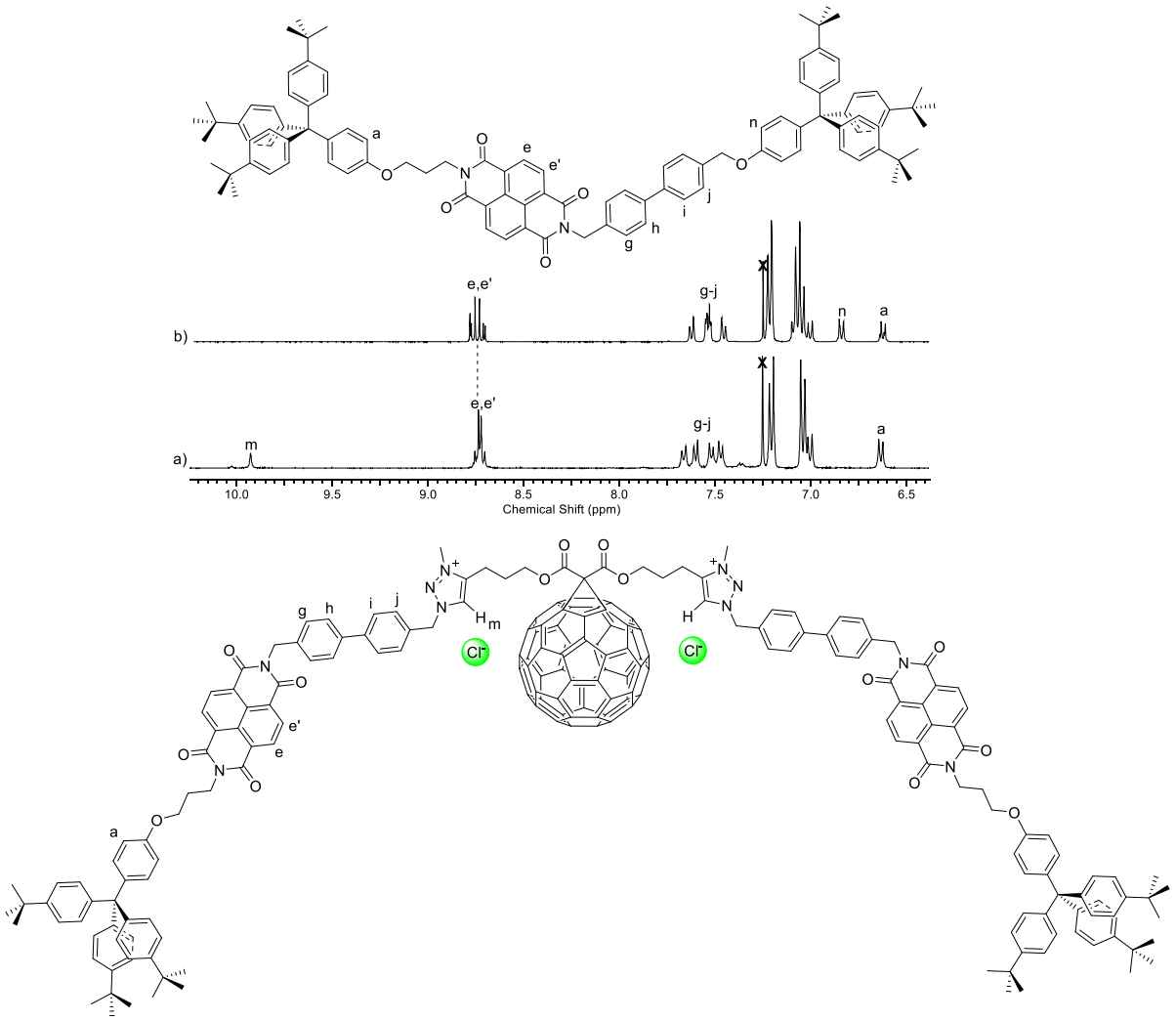


*Figure 4.23. Truncated ^{1}H NMR spectra of a) four station C_{60} fullerene-containing axle **81·(Cl)$_2$** and b) NDI model one-station axle **53** showing that the NDI proton signals $H_{e,e'}$ appear at the same chemical shift δ = 8.76 ppm ($CDCl_3$, 298 K, 400 MHz).*

The macrocycle station occupancies estimated for the bis-hexafluorphosphate and bis-chloride salts of [3]rotaxanes **82·(A)$_2$** and **84·(A)$_2$** in $CDCl_3$ are shown in Figure 4.24.

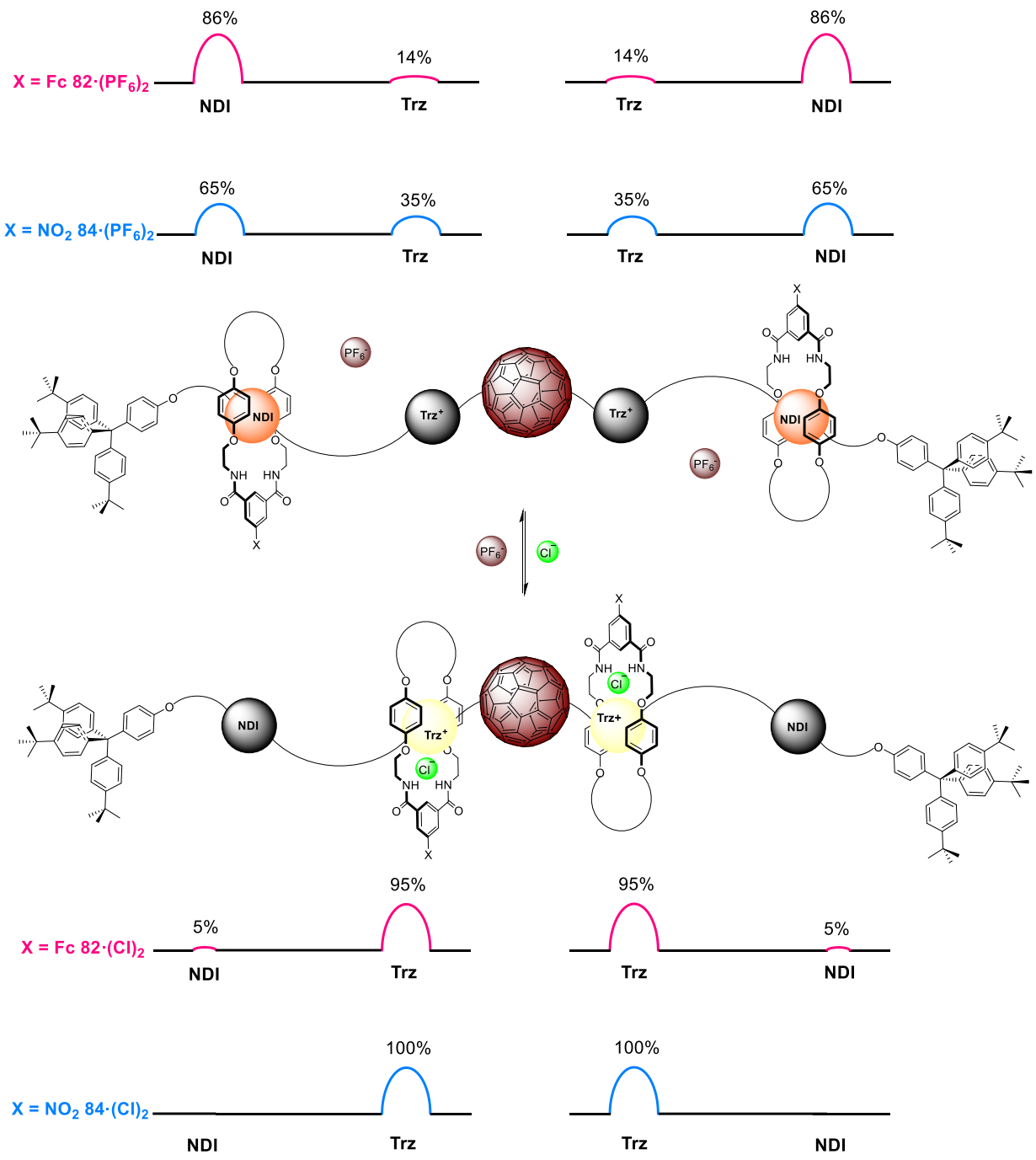


*Figure 4.24. The estimated macrocycle station occupancies (based upon $\Delta\delta H_{e,e'}$ protons) of the ferrocene- and nitro-macrocycle-containing [3]rotaxanes **82·(A)₂** and **84·(A)₂** as the bis-hexafluorphosphate and bis-chloride salt as determined by ^1H NMR spectroscopy in $CDCl_3$ solution. Trz^+ = proto-triazolium.*

Upon anion exchange, these calculations revealed station occupancy changes of 65% and 80% for the nitro- and ferrocene-containing [3]rotaxanes respectively. In particular the occupancy swing in the ferrocene-containing [3]rotaxane **82·(A)₂** is superior to any of the multi-station NDI-based rotaxane shuttles reported in $CDCl_3$ so far in this thesis (24–55% occupancy changes). It was therefore hoped

that this large-amplitude chloride-induced shuttling of the ferrocenyl macrocycle components in this [3]rotaxane would significantly modulate the photochemical responses from the NDI and C_{60} fluorophores in the axle.

In 1:1 $CDCl_3$:CD_3OD the occupancy of the NDI stations in the bis-chloride salt of the [3]rotaxanes was found to be 63%, therefore further studies were conducted in chloroform to ensure definitive anion-induced molecular shuttling.

4.3.6. Preliminary photophysical studies of chloride-induced shuttling in the C_{60} fullerene-containing four-station [3]rotaxanes

The fluorescence properties of the bis-chloride and bis-hexafluorophosphate salts of the ferrocene-containing [3]rotaxane **82·(A)$_2$** were investigated in $CHCl_3$ (Figure 4.25).

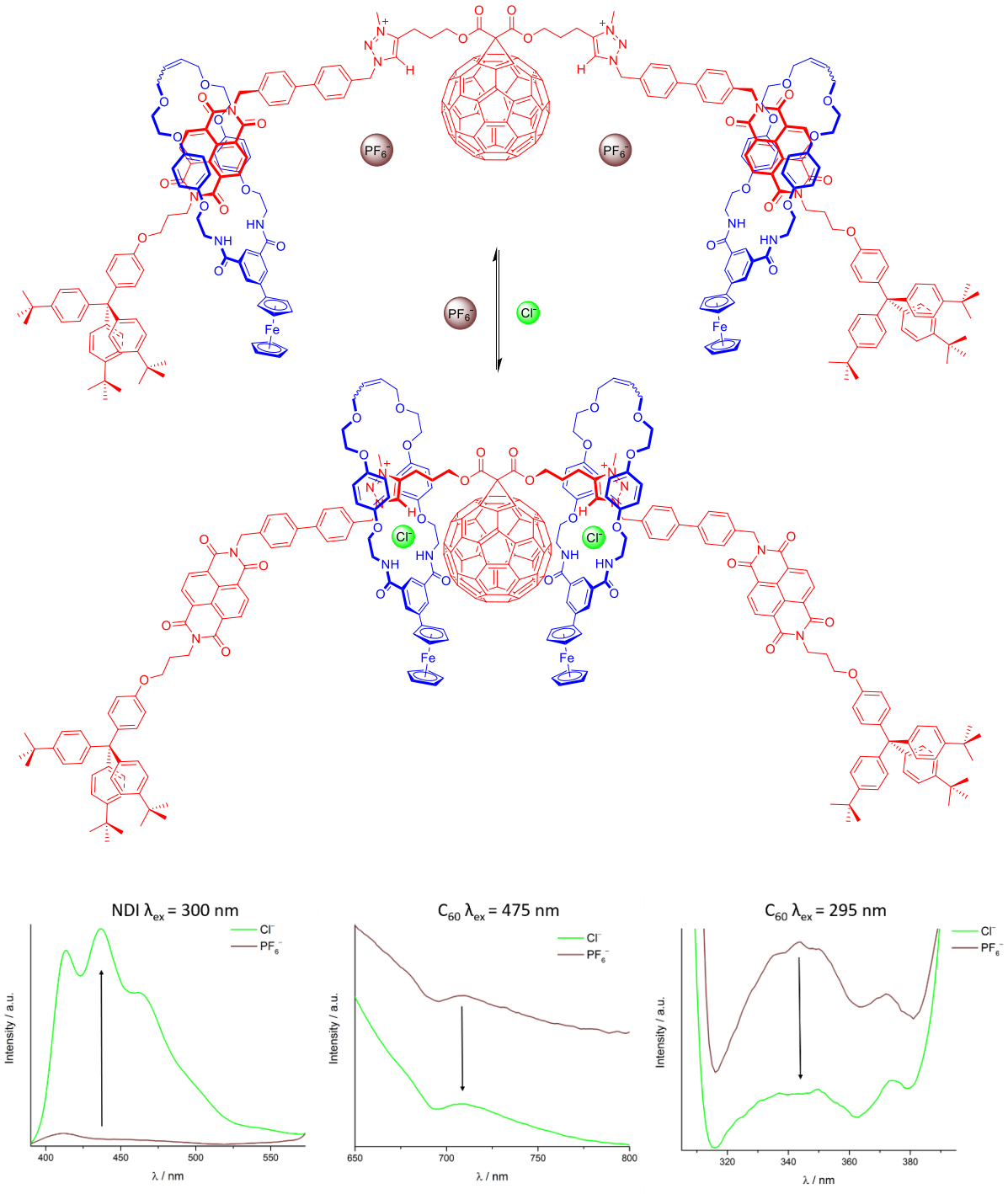


Figure 4.25. The fluorescence spectra of bis-hexafluorophosphate and bis-chloride salts of the ferrocene-macrocycle-containing [3]rotaxane ***82·(A)₂*** *in $CHCl_3$ (1×10^{-5} mol L^{-1}) showing emission upon excitation at a) λ_{ex} = 300 nm (NDI), b) λ_{ex} = 475 nm (C_{60} fullerene) and λ_{ex} = 295 nm (C_{60} fullerene).*

*Table 4.3. Percentage changes in NDI and C_{60} fullerene emission intensity, ΔI (%), upon anion exchange of the ferrocene-macrocycle-containing [3]rotaxane from **82·(PF$_6$)$_2$** to **82·(Cl)$_2$** in $CHCl_3$ (1×10^{-5} mol L^{-1}).*

Fluorophore	λ_{ex} / nm	ΔI (%)
NDI	300	+526[a]
C_{60}	475	−71[b]
C_{60}	295	−43[c]

Emission intensity changes were calculated via integration of appropriate fluorescence spectra between [a] λ_{em} = 390-570 nm, [b] λ_{em} = 694-800 nm and [c] λ_{em} = 315-363 nm. Error = ±10%. See Appendix for more details.

In identical fashion to the ferrocene-macrocycle-containing [2]rotaxane **78·(A)**, the addition of chloride to **82·(PF$_6$)$_2$** produces a large increase in the intensity of the NDI fluorescence emission (Table 4.3). This occurs because chloride recognition facilitates translational motion of the ferrocene-appended macrocycles away from the NDI stations thus reducing the degree of PET quenching of the excited state of the fluorophore. The degree of anion-induced co-conformational change is significant enough to elicit a turn-on fluorescence response for the halide that, under irradiation at λ_{ex} = 405 nm, is visible to the naked-eye (Figure 4.26).

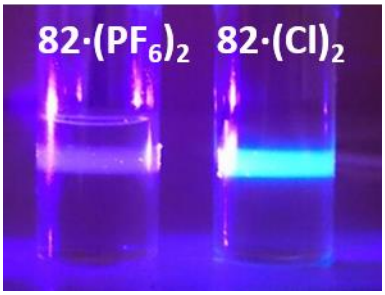


*Figure 4.26. Photograph showing the turn-on fluorescence response for chloride produced by ferrocene-containing [3]rotaxane **82·(PF$_6$)$_2$**. λ_{ex} = 405 nm with a laser.*

Chloride-induced shuttling in the [3]rotaxane is concomitantly manifested in a quenching of the characteristic C_{60} fluorescence emission peaks (Table 4.3) because of the closer proximity of the

ferrocenyl-appended macrocycle components to the fullerene cage.[**] By contrast the addition of chloride to the axle component **81·(PF$_6$)$_2$** produced an increase in the C_{60} fluorescence intensity.

For both NDI and C_{60} fullerene electron-deficient fluorophores, modulation of the fluorescence signal is attributed to a distant-dependent through-space quenching mechanism involving photoinduced electron transfer from the ferrocene-appended macrocycles. Analogous to earlier studies with the simpler two-station [2]rotaxane, this is supported by the lack of perturbation (< 1%[††]) in the absorption spectrum of **82·(PF$_6$)$_2$** upon anion exchange to **82·(Cl)$_2$** (Figure 4.27).

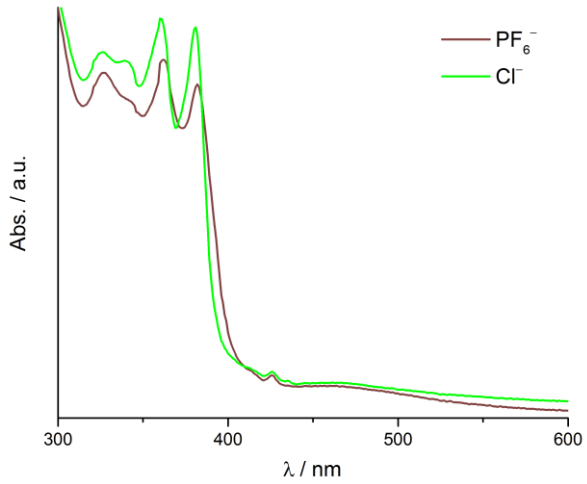


*Figure 4.27. Superimposed UV-Vis spectra of the bis-hexafluorophosphate and bis-chloride salts of ferrocene-containing [3]rotaxane **82·(A)$_2$** in $CHCl_3$ (1×10^{-5} mol L^{-1}).*

Following this, fluorescence emission spectroscopy was used to examine these same emission bands in the bis-hexafluorophosphate and bis-chloride salts of the nitro-containing [3]rotaxane **84·(A)$_2$** (Figure 4.28).

[**] The fullerene emission peaks are less defined than those of NDI because the fluorescence response is almost an order of magnitude lower on account of the accessible non-radiative pathways described in Section 4.1.1.
[††] Absorption intensity changes were calculated *via* integration of appropriate UV-Vis spectra between λ_{em} = 300-600 nm. See Appendix for more details.

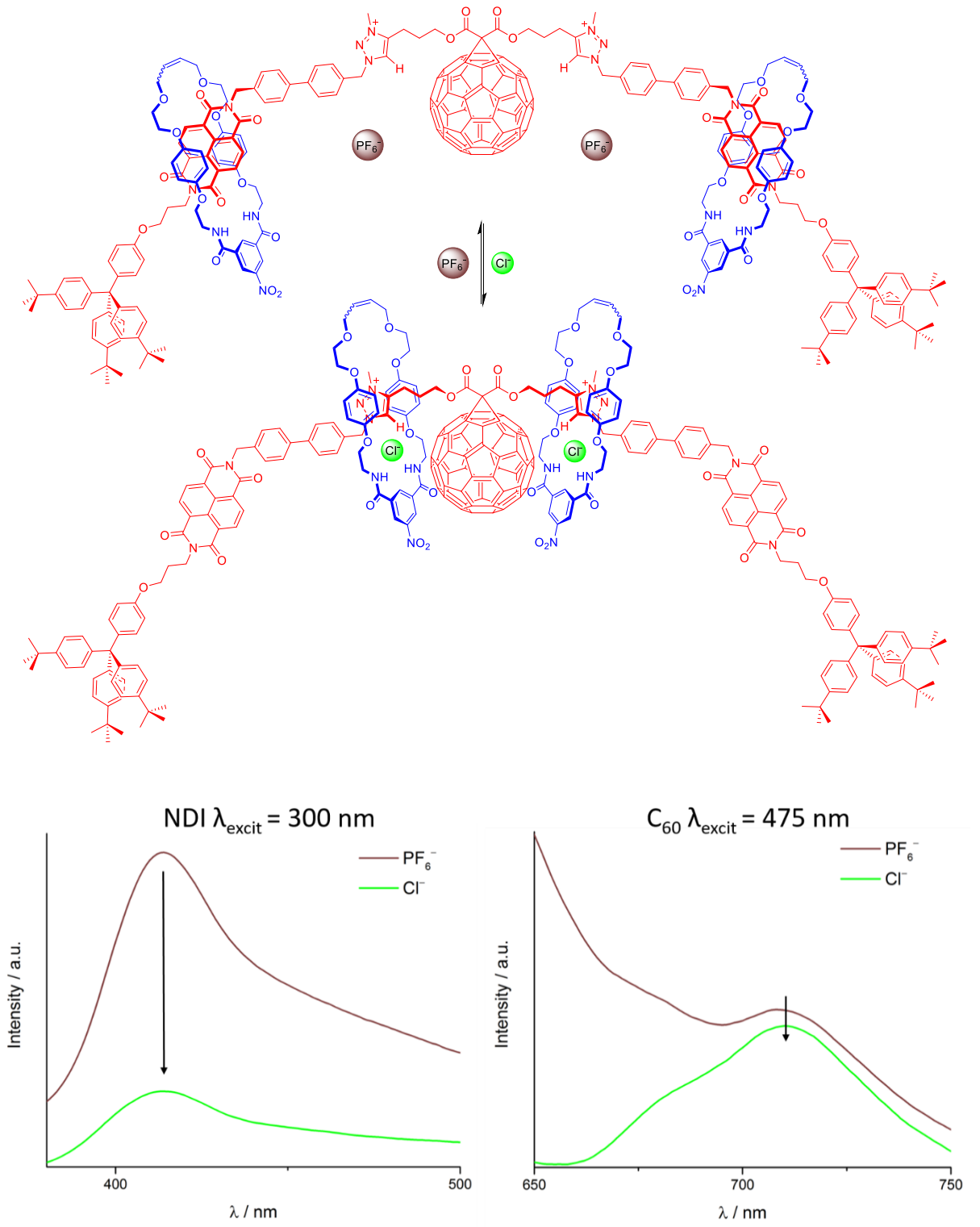


Figure 4.28. The fluorescence spectra of bis-hexafluorophosphate and bis-chloride salts of the nitro-macrocycle-containing [3]rotaxane ***84·(A)₂*** *in $CHCl_3$ (1×10^{-5} mol L^{-1}) showing emission upon excitation at a) λ_{ex} = 300 nm (NDI) and b) λ_{ex} = 475 nm (C_{60} fullerene).*

*Table 4.4. Percentage changes in NDI and C_{60} fullerene emission intensity, ΔI (%), upon anion exchange of the nitro-macrocycle-containing [3]rotaxane from **84·(PF$_6$)$_2$** to **84·(Cl)$_2$** in $CHCl_3$ (1×10^{-5} mol L^{-1}).*

Fluorophore	λ_{ex} / nm	ΔI (%)
NDI	300	−72[a]
C_{60}	475	−5[b]

Emission intensity changes were calculated via integration of appropriate fluorescence spectra between [a] λ_{em} = 380-500 nm and [b] λ_{em} = 694-750 nm. Error = ±10%. See Appendix for more details.

The addition of chloride to **84·(PF$_6$)$_2$** causes a 72% *decrease* in the intensity of NDI fluorescence emission (Table 4.4), possibly because of the same collisional quenching observed on anion exchange of the four-station axle component **81·(A)$_2$**. Importantly, this response is in stark contrast to the increase in NDI emission of ferrocene-containing [3]rotaxane, providing further evidence for the role of the shuttling ferrocenyl macrocycle as an efficient and distant dependent PET quenching motif.

A decrease in the intensity of the fullerene emission also occurs on anion exchange to the bis-chloride salt of nitro-containing [3]rotaxane **84·(Cl)$_2$**. However, this change is an order of magnitude smaller than the C_{60} fluorescence quenching observed in the ferrocene analogue **82·(Cl)$_2$** (Table 4.4).

4.4. Conclusions and future work

The work described in this chapter has demonstrated the capability of carefully-designed rotaxane-based switches to produce effective chemical sensing by means of their inherent dynamic properties.

Work began with the incorporation of a ferrocene-appended macrocycle into a novel NDI axle-containing bistable [2]rotaxane in order to furnish this dynamic interlocked system with an efficient and mobile distant-dependent PET quencher. This [2]rotaxane was used as a proof of principle for chloride-induced translational motion of the ferrocenyl macrocycle away from the NDI station reducing the degree of PET quenching and in turn producing a turning-on of fluorescence emission. Analogous titration studies with the nitro-macrocycle-functionalised analogue produced small changes

in the emission spectrum, providing evidence that modulation of the NDI photochemical response was a direct result of PET quenching by the ferrocene moiety.

In collaboration with the research group of Prof. K. Porfyrakis from the Department of Materials, University of Oxford, a four-station bis-proto-triazolium bis-NDI axle component was constructed around a mono-functionalised, photoactive C_{60} fullerene derivative. This axle was used in the assembly of two novel [3]rotaxanes containing either ferrocene- or nitro-appended macrocycles, which were shown to exhibit pincer-like translational motion stimulated by chloride recognition. In the ferrocene-containing [3]rotaxane, the positions of the macrocyclic wheels on the four-station axle produced a dual fluorescence response, courtesy of the photoactive reporter groups incorporated into the rotaxane. Subsequently, fluorescence chloride sensing was achieved through halide-induced molecular shuttling, which resulted in the simultaneous enhancement of the NDI fluorescence emission with concurrent quenching of the C_{60} fullerene emission (Figure 4.29). The importance of ferrocenyl groups as manipulable PET quenchers in the dynamic signalling mechanism of this [3]rotaxane was demonstrated by the lack of such a photophysical response in the nitro-appended analogue and axle component.

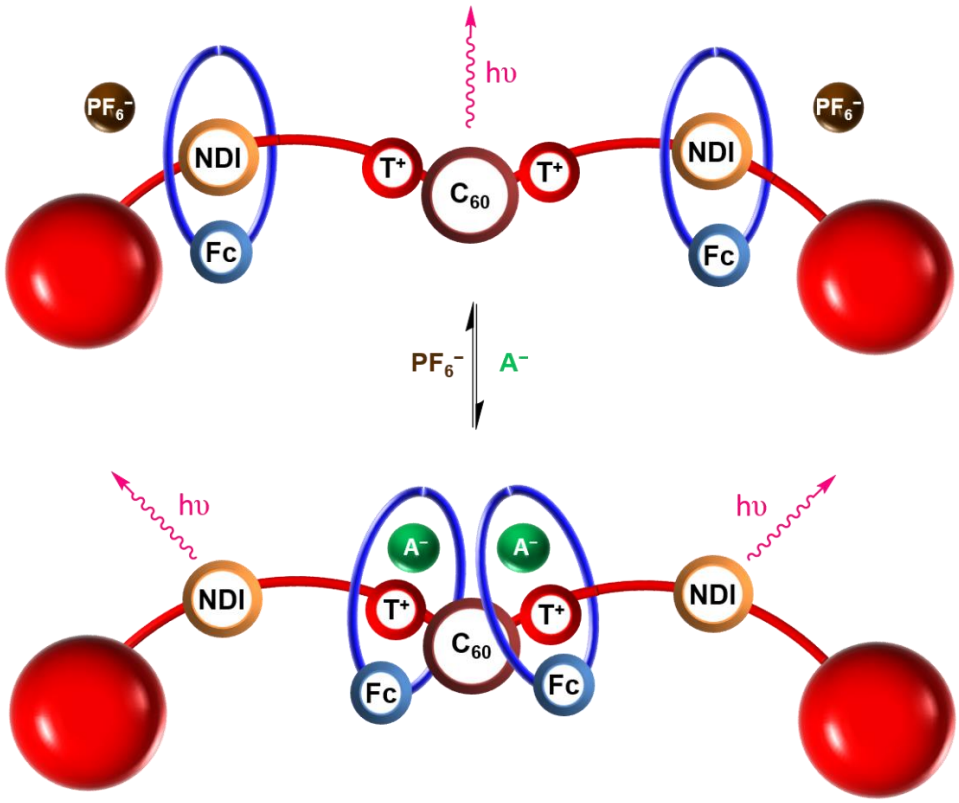


Figure 4.29. Schematic of the four-station C_{60} fullerene-containing [3]rotaxane capable of anion (A^-) sensing via a dual fluorescence response. NDI = naphthalene diimide, T^+ = proto-triazolium and Fc = ferrocene.

Ongoing work on this project is focused on further in depth photophysical investigations of the ferrocene-containing [3]rotaxane shuttle. These include time-resolved transient absorption measurements to provide additional insights into the electron transfer processes between the donor and acceptor moieties, specifically if the lifetime of radical ion-pair states is altered by the position of the macrocyclic wheels on the axle. In the longer term, the principles outlined in this work will be extended towards the design of new anion—host rotaxane-based switches containing multiple reporter groups, and in particular fullerenes, for the purpose of chemical sensing and controlling communication pathways of molecular dyads.

4.5. References

1 R. Taylor and D. R. M. Walton, *Nature*, 1993, **363**, 685–693.
2 H. W. Kroto, J. R. Heath, S. C. O'Brien, R. F. Curl and R. E. Smalley, *Nature*, 1985, **318**, 162–163.
3 T. Liu and A. Troisi, *Adv. Mater.*, 2013, **25**, 1038–1041.
4 R. Nakanishi, A. Nogimura, R. Eguchi and K. Kanai, *Org. Electron.*, 2014, **15**, 2912–2921.
5 Nazariortín and J.-F. Nierengarten, Eds., in *Supramolecular Chemistry of Fullerenes and Carbon Nanotubes*, Wiley-VCH Verlag GmbH & Co. KGaA, 2012, pp. I–XVI.
6 H. Murayama, S. Tomonoh, J. M. Alford and M. E. Karpuk, *Fuller. Nanotub. Carbon Nanostructures*, 2005, **12**, 1–9.
7 N. S. Goroff, *Acc. Chem. Res.*, 1996, **29**, 77–83.
8 R. C. Haddon, R. E. Palmer, H. W. Kroto and P. A. Sermon, *Philos. Trans. R. Soc. Lond. Math. Phys. Eng. Sci.*, 1993, **343**, 53–62.
9 P. W. Fowler and D. E. Manolopoulos, *An Atlas of Fullerenes*, Courier Corporation, 2006.
10 Q. Xie, E. Perez-Cordero and L. Echegoyen, *J. Am. Chem. Soc.*, 1992, **114**, 3978–3980.
11 M. Maggini, G. Scorrano and M. Prato, *J. Am. Chem. Soc.*, 1993, **115**, 9798–9799.
12 C. Bingel, *Chem. Ber.*, 1993, **126**, 1957–1959.
13 V. S. Pavlovich and E. M. Shpilevsky, *J. Appl. Spectrosc.*, 2010, **77**, 335–342.
14 N. Armaroli and G. Accorsi, in *Fullerenes*, eds. F. Langa De La Puente and J.-F. Nierengarten, Royal Society of Chemistry, Cambridge, 2007, pp. 79–126.
15 L. Echegoyen and L. E. Echegoyen, *Acc. Chem. Res.*, 1998, **31**, 593–601.
16 D. Dubois, K. M. Kadish, S. Flanagan, R. E. Haufler, L. P. F. Chibante and L. J. Wilson, *J. Am. Chem. Soc.*, 1991, **113**, 4364–4366.
17 D. Dubois, K. M. Kadish, S. Flanagan and L. J. Wilson, *J. Am. Chem. Soc.*, 1991, **113**, 7773–7774.
18 J. Jackson D. Megiatto and D. I. Schuster, in *RSC Nanoscience & Nanotechnology*, eds. F. Langa De La Puente and J.-F. Nierengarten, Royal Society of Chemistry, Cambridge, 2nd edn., 2011, pp. 354–385.
19 D. M. Guldi, *Chem. Soc. Rev.*, 2002, **31**, 22–36.
20 D. I. Schuster, P. Cheng, P. D. Jarowski, D. M. Guldi, C. Luo, L. Echegoyen, S. Pyo, A. R. Holzwarth, S. E. Braslavsky, R. M. Williams and G. Klihm, *J. Am. Chem. Soc.*, 2004, **126**, 7257–7270.
21 K. M. Kadish and R. S. Ruoff, *Fullerenes: Chemistry, Physics, and Technology*, John Wiley & Sons, 2000.
22 A. Mateo-Alonso, in *Supramolecular Chemistry of Fullerenes and Carbon Nanotubes*, eds. Nazariortín and J.-F. Nierengarten, Wiley-VCH Verlag GmbH & Co. KGaA, 2012, pp. 107–126.
23 F. Diederich, C. Dietrich-Buchecker, J.-F. Nierengarten and J.-P. Sauvage, *J. Chem. Soc. Chem. Commun.*, 1995, 781–782.
24 A. Mateo-Alonso, *Chem. Commun.*, 2010, **46**, 9089–9099.
25 A. Mateo-Alonso, C. Ehli, G. M. A. Rahman, D. M. Guldi, G. Fioravanti, M. Marcaccio, F. Paolucci and M. Prato, *Angew. Chem. Int. Ed.*, 2007, **46**, 3521–3525.
26 H. Onagi and J. Julius Rebek, *Chem. Commun.*, 2005, 4604–4606.
27 Y. Li, H. Li, Y. Li, H. Liu, S. Wang, X. He, N. Wang and D. Zhu, *Org. Lett.*, 2005, **7**, 4835–4838.
28 K. Sakamoto, Y. Takashima, N. Hamada, H. Ichida, H. Yamaguchi, H. Yamamoto and A. Harada, *Org. Lett.*, 2011, **13**, 672–675.
29 J.-S. Marois, K. Cantin, A. Desmarais and J.-F. Morin, *Org. Lett.*, 2008, **10**, 33–36.
30 E. M. Pérez, D. T. F. Dryden, D. A. Leigh, G. Teobaldi and F. Zerbetto, *J. Am. Chem. Soc.*, 2004, **126**, 12210–12211.
31 A. Mateo-Alonso, D. M. Guldi, F. Paolucci and M. Prato, *Angew. Chem. Int. Ed.*, 2007, **46**, 8120–8126.
32 W. Zhou, S. Zhang, G. Li, Y. Zhao, Z. Shi, H. Liu and Y. Li, *ChemPhysChem*, 2009, **10**, 2066–2072.
33 J. Berná, C. Franco-Pujante and M. Alajarín, *Org. Biomol. Chem.*, 2013, **12**, 474–478.

34 J. J. Gassensmith, S. Matthys, J.-J. Lee, A. Wojcik, P. V. Kamat and B. D. Smith, *Chem. – Eur. J.*, 2010, **16**, 2916–2921.
35 H. Zhang, J. Hu and D.-H. Qu, *Org. Lett.*, 2012, **14**, 2334–2337.
36 M. V. R. Raju and H.-C. Lin, *Org. Lett.*, 2013, **15**, 1274–1277.
37 H. Zhang, B. Zhou, H. Li, D.-H. Qu and H. Tian, *J. Org. Chem.*, 2012.
38 S. Ganguly, P. Pachfule, S. Bala, A. Goswami, S. Bhattacharya and R. Mondal, *Inorg. Chem.*, 2013, **52**, 3588–3590.
39 S. V. Bhosale, C. H. Jani and S. J. Langford, *Chem. Soc. Rev.*, 2008, **37**, 331–342.
40 J. R. Lakowicz, Ed., *Principles of Fluorescence Spectroscopy*, Springer US, Boston, MA, 2006.
41 T. Gunnlaugsson, H. D. P. Ali, M. Glynn, P. E. Kruger, G. M. Hussey, F. M. Pfeffer, C. M. G. dos Santos and J. Tierney, *J. Fluoresc.*, 2005, **15**, 287–299.
42 X. Wu, W. Wu, X. Cui, J. Zhao and M. Wu, *J. Mater. Chem. C*, 2015.
43 J. P. Sauvage, J. P. Collin, J. C. Chambron, S. Guillerez, C. Coudret, V. Balzani, F. Barigelletti, L. De Cola and L. Flamigni, *Chem. Rev.*, 1994, **94**, 993–1019.
44 Y. Tang, D. Lee, J. Wang, G. Li, J. Yu, W. Lin and J. Yoon, *Chem. Soc. Rev.*, 2015, **44**, 5003–5015.
45 R. Pereira de Freitas, J. Iehl, B. Delavaux-Nicot and J.-F. Nierengarten, *Tetrahedron*, 2008, **64**, 11409–11419.
46 M. J. Brites, C. Santos, S. Nascimento, B. Gigante, H. Luftmann, A. Fedorov and M. N. Berberan-Santos, *New J. Chem.*, 2006, **30**, 1036–1045.

Chapter Five
Dynamic behaviour in a perylene diimide-containing [3]rotaxane and [3]catenane

5. DYNAMIC BEHAVIOUR IN A PERYLENE DIIMIDE-CONTAINING [3]ROTAXANE AND [3]CATENANE

5.1. Introduction

5.1.1. The chemistry of perylene diimides

Traditionally used as dyes, perylene-3,4,9,10-tetracarboxylic acid diimide (PDI) derivatives (Figure 5.1) have more recently been employed in the field of supramolecular chemistry, finding a broad variety of applications in areas such as chemical sensing and self-assembly.[1,2] PDI is well-suited to this because, as a larger analogue of NDI, it also exhibits favourable optical and redox properties. Specifically, the PDI UV-Vis absorption band appears in the visible region of the spectrum making its compounds highly coloured, whilst fluorescent quantum yields are often close to unity.[3] The electron-deficient nature of the motif is exemplified by the high stability of the PDI dianion, revealed by spectro-electrochemical studies.[4–6]

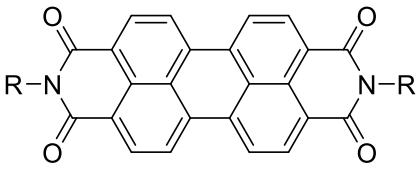


Figure 5.1. Perylene-3,4:9,10-tetracarboxylic acid diimide (PDI). R = functional groups of the imide termini.

The electron-deficient character of PDI is also demonstrated by the cyclophane shown in Figure 5.2.[7] This host is capable of encapsulating electron-rich aromatic compounds within the rigid cavity created between the two PDI units in $CHCl_3$, and sensing these guests *via* quenching of the fluorescence emission, owing to the formation of donor–acceptor charge–transfer complexes detectable by UV-Vis spectroscopy.

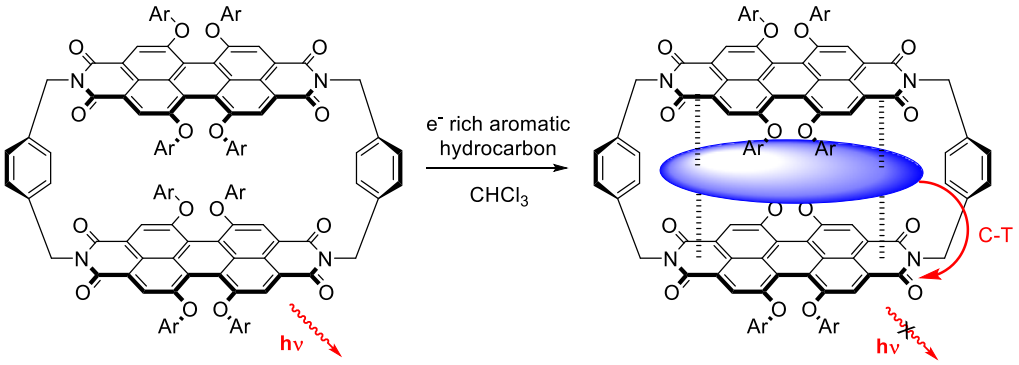


Figure 5.2. A PDI cyclophane that produces a turn-off fluorescence response upon the encapsulation of electron-rich aromatic hydrocarbons (blue spheroid) such as carbazole, anthracene and pyrene. C-T = charge–transfer.[7]

The localised electron-deficient (imide groups) and electron-rich (perylene core) regions of the PDI structure also produce a strong tendency towards solution aggregation *via* intermolecular aromatic stacking (Figure 5.3).[8] Würthner and co-workers' extensive studies showed this phenomenon is highly-dependent upon solvent polarity.[9] Analogous to Cubberley and Iverson's dimeric NDI–DN system,[10] they found that aggregation association constants became stronger in polar (e.g. acetone, MeCN) and protic (e.g. MeOH) solvents due to solvophobic effects, whilst chlorinated solvents provided the best solvation of PDI units.



Figure 5.3. Model of the columnar PDI aggregates in solution.[8] *Reproduced from Ref. 8 with permission from The Royal Society of Chemistry.*

In order to minimise aromatic stacking in solution, PDI can be substituted at the bay ($C^{1,6,7,12}$) positions to impart a propeller-type contortion of the aromatic scaffold away from planarity, effectively forming two naphthalimide subunits (Figure 5.4).[11] This significantly reduces the ability of PDI-containing compounds to form self-assembled stacks, therefore increasing solubility in organic solvents.

Tetrachlorination of PDI produces one of the largest core twists (θ = 35–37°) with a high energetic inversion barrier, whilst the introduction of four halogen groups also makes the species a stronger oxidant.[12] Importantly, this distortion imparts conformational chirality to the motif and the resulting stereoisomers are often referred to as atropisomers despite exhibiting planar and not axial chirality.[11,13]

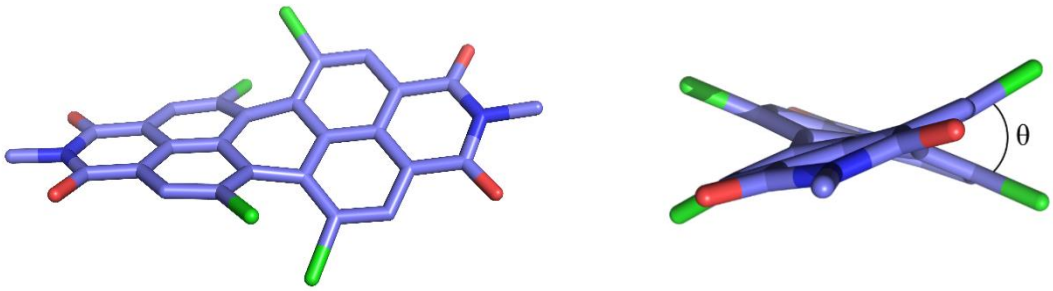


Figure 5.4. Fragment of the solid state structure of a peptide-appended 1,6,7,12-tetrachloroperylene diimide derivative illustrating the core-twisting effect of the bay substituents.[14] For clarity, hydrogen atoms and the peptide functionalities at the imide termini have been omitted, and only one of the two crystallographically independent molecules contained within the asymmetric unit is shown. The twisting angle ϑ = 35–37°.

5.1.2. PDI-containing MIMs

In spite of the useful photo- and electro-chemical properties of PDI only a small number of interlocked structures incorporating this motif have been reported in the literature.[15–19] An early example was a [3]rotaxane constructed from two bis-isophthalamide-based macrocycles and an axle component containing a twisted tetraphenoxy PDI core (Figure 5.5).[15] The positioning of the macrocyclic wheels could be sensed *via* a variety of spectroscopic techniques but specifically, a bathochromic shift in the absorption spectrum was attributed to formation of hydrogen bond interactions between the imide carbonyl groups of the PDI and the bis-isophthalamide motifs of the macrocycles.

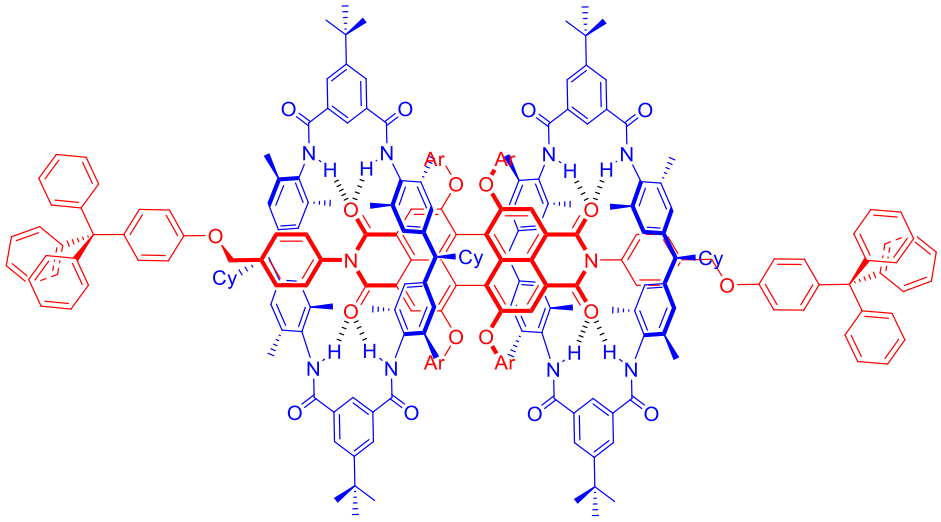


Figure 5.5. A [3]rotaxane in which a twisted tetraphenoxy PDI unit acts as a recognition site for bis-isophthalamide macrocycles via hydrogen bonding to the imide carbonyl groups. Ar = tert-butyl benzene.[15]

Champness *et al.* demonstrated that a PDI chromophore without core substituents could be incorporated into an axle component to facilitate formation of a [2]rotaxane with a dialkoxynaphthalene-based macrocycle courtesy of aromatic stacking between the electron-poor and electron-rich aryl species (Figure 5.6).[17] The importance of these interactions towards its stability was demonstrated when de-threading of the macrocycle occurred upon electrochemical reduction of the PDI moiety.

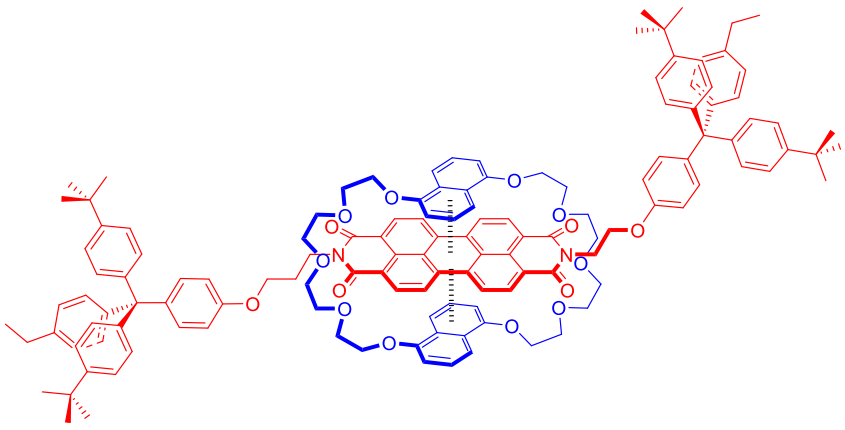


Figure 5.6. Champness' PDI [2]rotaxane, the synthesis of which is templated by donor–acceptor charge–transfer interactions between the electron-rich and electron-deficient aromatic motifs of macrocycle and axle components.[17]

Meanwhile, Li and co-workers have investigated the self-assembly of [2]catenanes comprised of two unsubstituted bis-PDI macrocycles formed *via* the reversible disulfide coupling of PDI monomers (Figure 5.7).[18] In contrast, since the catenation process is governed by aromatic stacking between the PDI units, steric hindrance between the twisted cores of tetrachlorinated PDI monomers inhibits the formation of any interlocked products.[20]

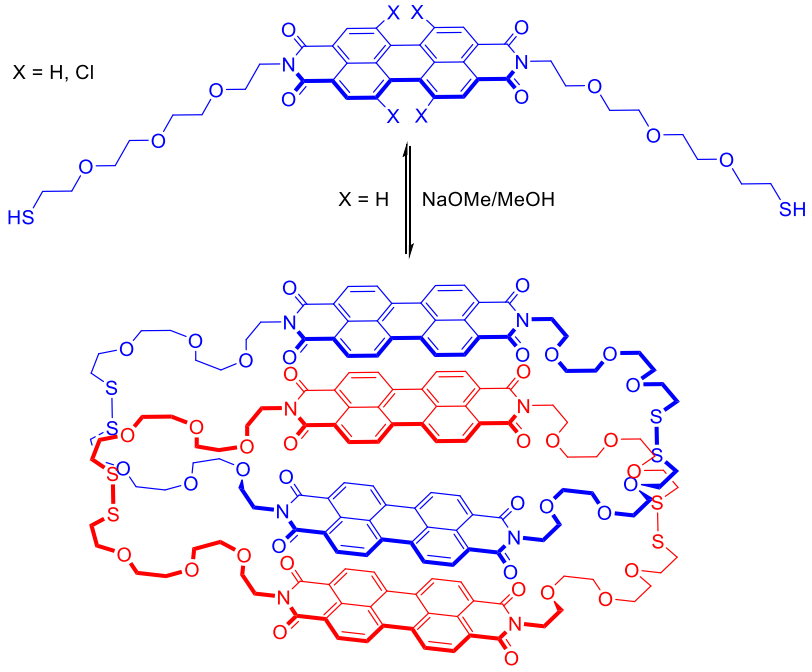


Figure 5.7. The formation of Li's PDI-containing homo [2]catenane only occurs when X = H. When X = Cl the twisted PDI units prevent self-assembly of an interlocked structure.[18,20]

5.1.3. Chapter objectives

On account of the small number of PDI-based MIMs reported in the literature, no systems currently exist in which this motif is used as a macrocycle recognition site to direct large-amplitude molecular motion. One of the aims of the work in this chapter is to realise this dynamic behaviour in a rotaxane-based architecture. This will begin with the construction of an axle component containing an electron-deficient PDI core, separated from two proto-triazolium stations by rigid biphenyl spacer units (Figure 5.8a). A tetrachlorinated PDI derivative will be used as the halogen substituents will increase both the solubility in organic solvents and the electron-deficient nature of the PDI, whilst generating two naphthalimide sub-units courtesy of the twisted perylene core. Consequently, these "NI stations"

should be capable of acting as recognition sites for macrocycles containing electron-rich hydroquinone groups (Figure 5.8b).

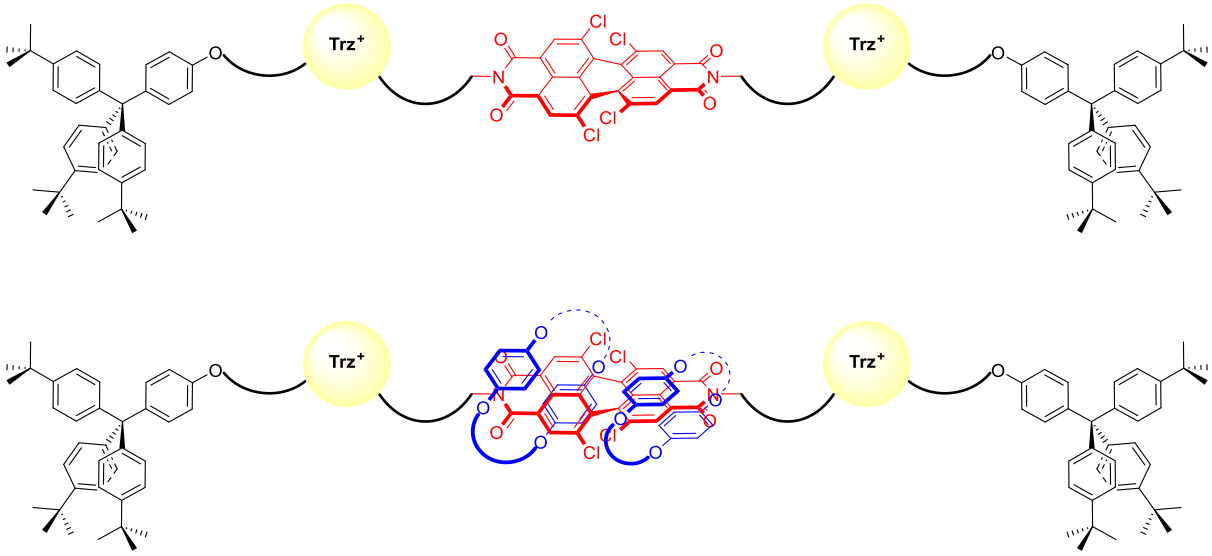


Figure 5.8. Schematic showing a) a multi-station tetrachloro PDI-bis-proto-triazolium axle component and b) the potential aromatic stacking mode of the NI sub-units of the PDI with two hydroquinone-containing macrocycles in a [3]rotaxane. Trz^+ = proto-triazolium.

It was hoped that the incorporation of this multi-station axle into a [3]rotaxane could produce a dynamic system in which shuttling of two isophthalamide–hydroquinone-based macrocycles from the central electron-deficient PDI stations to the peripheral proto-triazolium sites may be induced by halide anion binding (Figure 5.9).

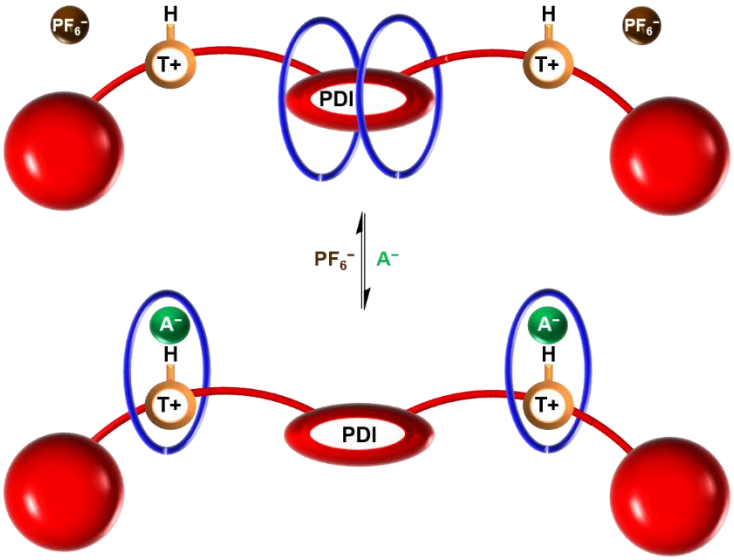


Figure 5.9. Schematic of the anion-induced translational molecular motion within a four-station PDI-bis-proto-triazolium [3]rotaxane. PDI = perylene diimide, T^+ = triazolium, A^- = halide anion.

Stimulus-induced changes in catenanes may be used to control the *rotational* motion of macrocycle components.[21] However, whilst pirouetting of macrocycles facilitated by anion recognition has only been reported in a small number of [2]catenane structures,[22,23] anion-induced rotary motion in higher-order catenane architectures has not yet been realised. Nonetheless, this dynamic process might be achieved *via* the construction of a [3]catenane with tetrachloro PDI and proto-triazolium stations integrated into the central macrocycle which would facilitate the halide anion mediated rotary motion of the peripheral isophthalamide- and hydroquinone-containing macrocycles as shown in Figure 5.10.

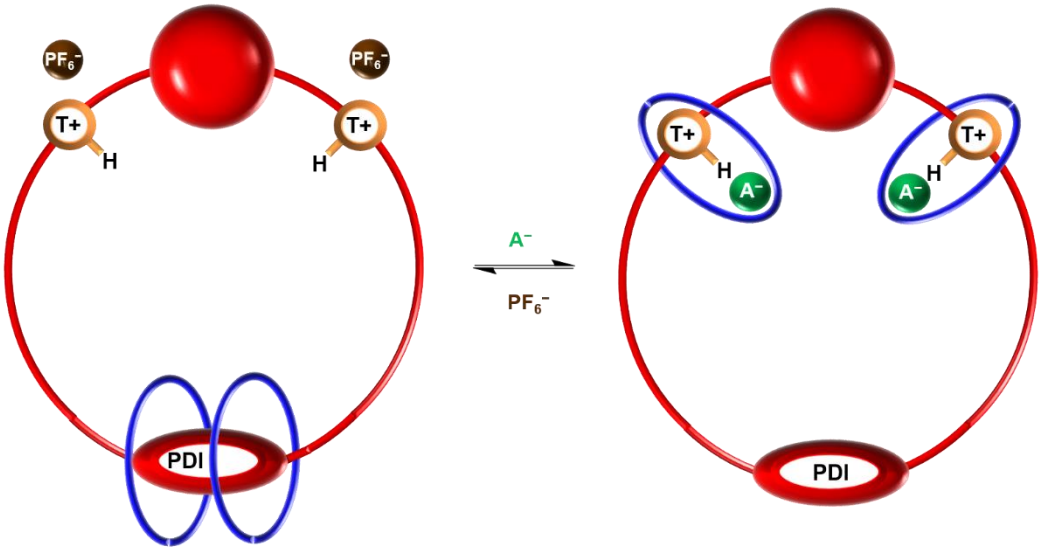
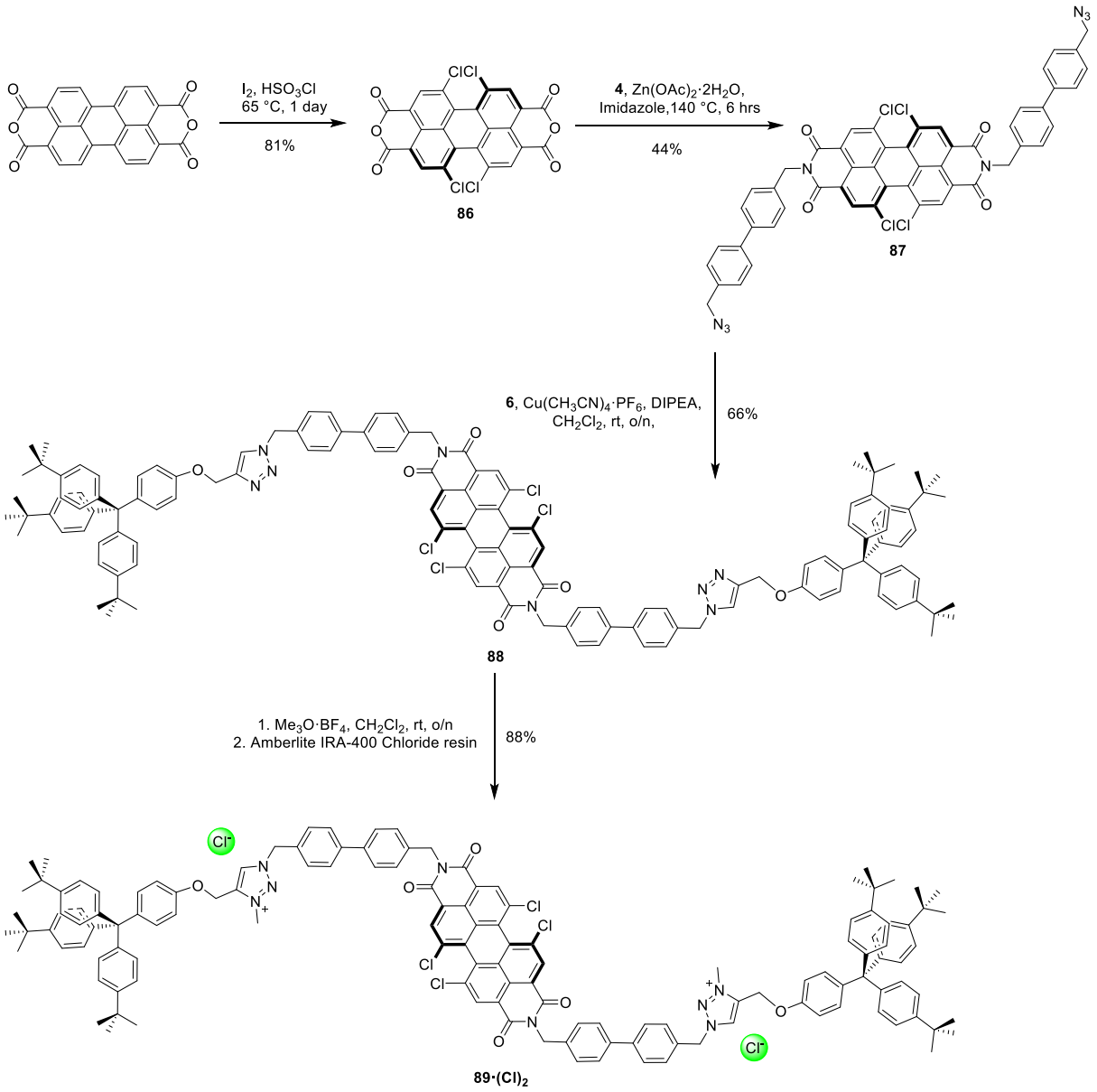


Figure 5.10. Schematic of the anion-induced rotary molecular motion within a four-station PDI-bis-proto-triazolium [3]catenane. PDI = perylene diimide, T^+ = triazolium, A^- = halide anion.

5.2. A PDI-containing [3] rotaxane

5.2.1. Synthesis of a four-station PDI-containing axle component

Initially a four-station bis-proto-triazolium axle component containing a central tetrachloro PDI motif was prepared as outlined in Scheme 5.1.



Scheme 5.1. Synthesis of four-station tetrachloro PDI-bis-proto-triazolium axle ***89·(Cl)₂***.

Synthesis of tetrachloro perylene dianhydride derivative **86** was performed in high yield *via* a literature procedure[24] that involved heating perylene-3,4,9,10-tetracarboxylic dianhydride in chlorosulfonic acid with a catalytic amount of I_2 for one day followed by aqueous work up. Further heating in molten imidazole with a Zn(II) Lewis acid catalyst[25] was required to functionalise the anhydride termini of **86** with two equivalents of biphenyl amine **4** to give bis-azide **87**. A standard CuAAC reaction between **87** and two equivalents of phenyl trityl stopper alkyne **6** was then used to prepare the bis-proto-triazole-containing axle **88** in 66% yield. Methylation of the proto-triazole heterocycles with $Me_3O{\cdot}BF_4$ in dry

CH_2Cl_2 gave the bis-triazolium axle **89·$(BF_4)_2$** which was exchanged to the bis-chloride salt using Amberlite® resin in preparation for the anion templated synthesis of an interlocked structure.

The ^{1}H NMR spectrum of the axle component **89·$(Cl)_2$** in $CDCl_3$ is shown in Figure 5.11.

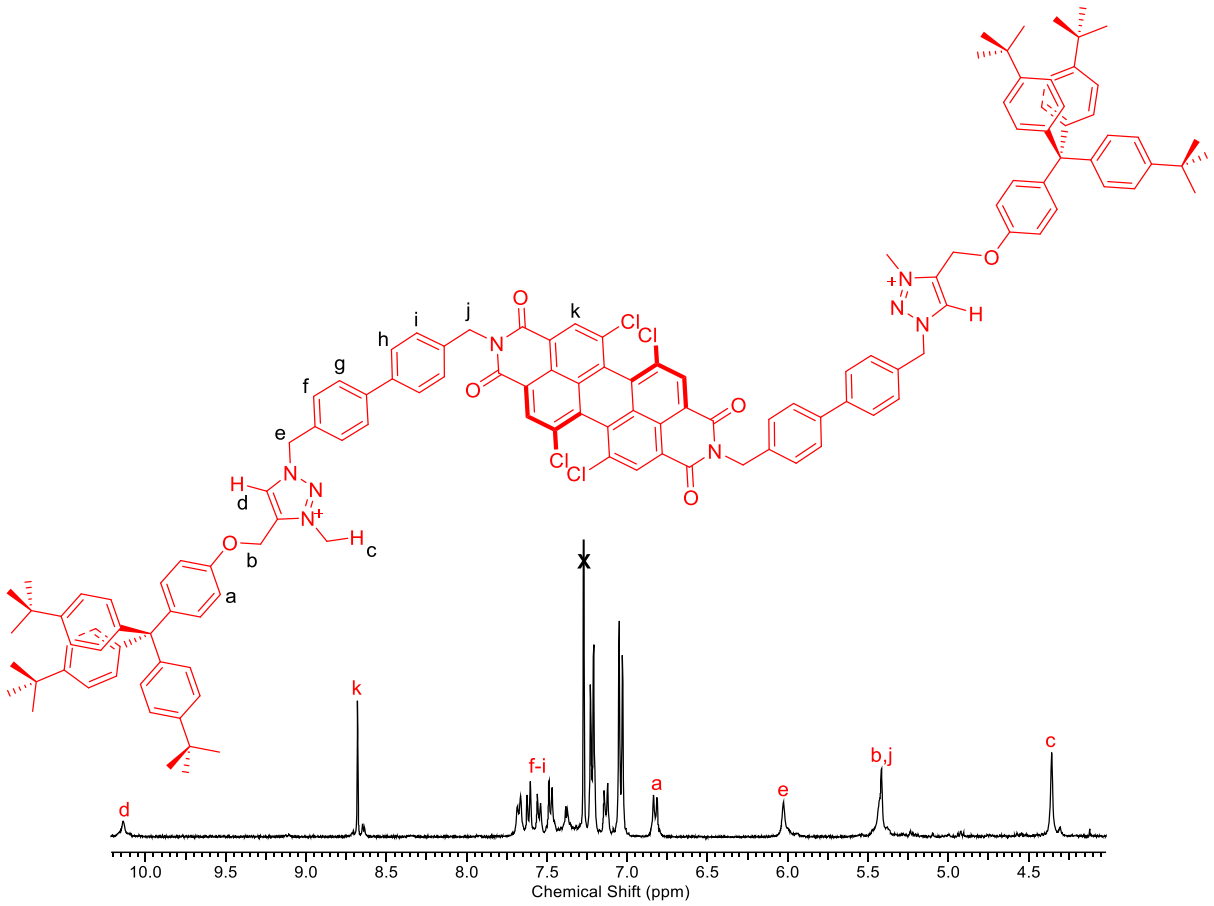
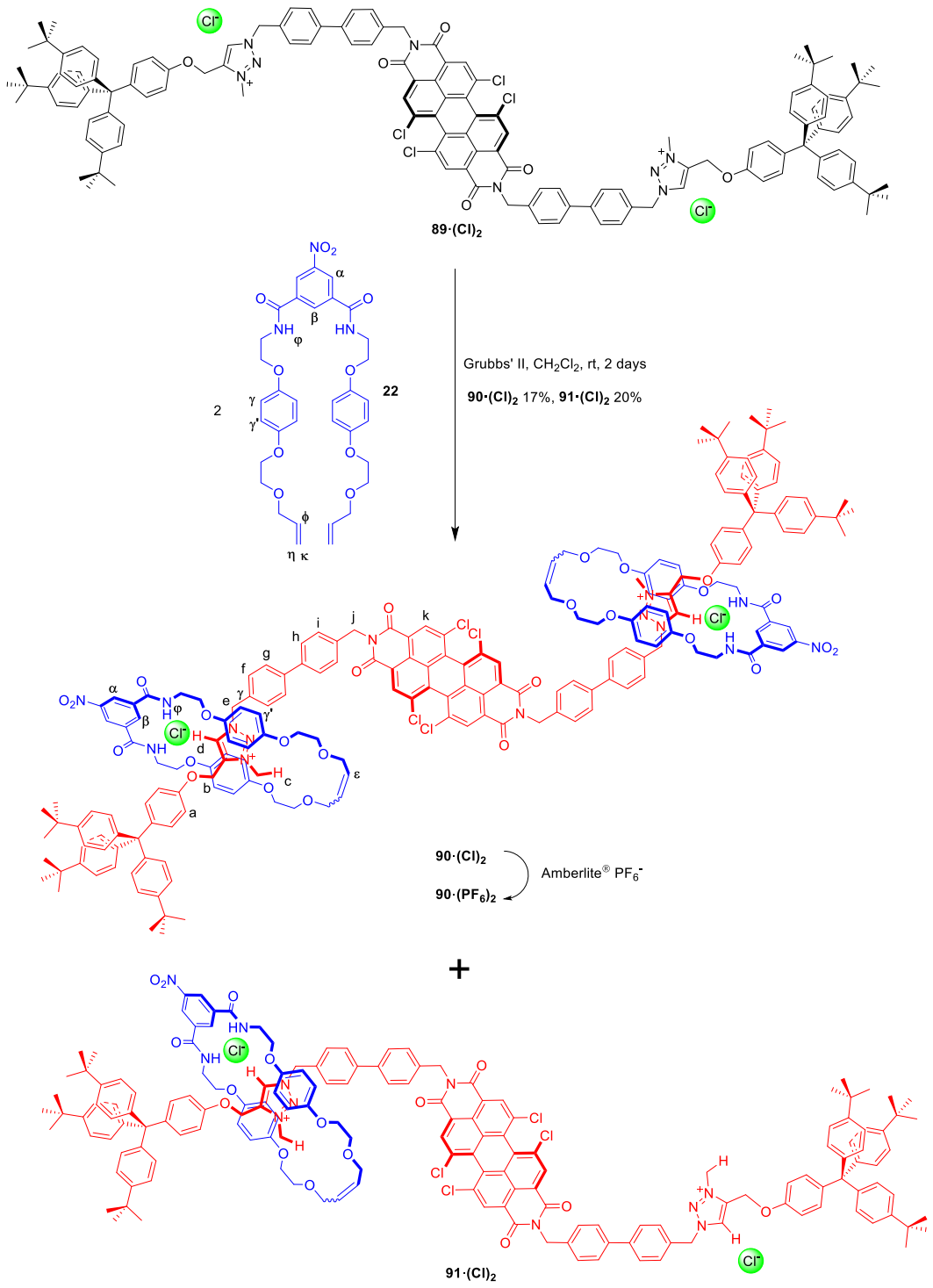


*Figure 5.11. Truncated ^{1}H NMR spectrum of axle **89·$(Cl)_2$** ($CDCl_3$, 298 K, 400 MHz).*

As discussed earlier, the twist of the tetrachloro substituted PDI imparts conformational chirality and thus, axle **89·$(Cl)_2$** exists as a racemic mixture of two atropisomers that slowly interconvert at room temperature. The protons H_k are therefore enantiotopic, producing a single, readily assignable peak in the ^{1}H NMR spectrum.

5.2.2. Synthesis of a four-station PDI-containing [3]rotaxane

This four-station PDI-containing axle component was incorporated into a [3]rotaxane *via* the chloride templated clipping of two bis-vinyl-appended macrocycle precursors around **89·$(Cl)_2$** using Grubbs' II-catalysed RCM (Scheme 5.2).



Scheme 5.2. Synthesis of four-station PDI [3]rotaxane ***90·(Cl)₂.***

Initially, axle component **89·(Cl)₂** and three equivalents of bis-vinyl-appended macrocycle precursor **22** were dissolved in dry CH_2Cl_2 and stirred for 30 minutes before Grubbs' II catalyst was added to facilitate the RCM reaction. The target [3]rotaxane **90·(Cl)₂** was isolated in 17% yield using preparative silica thin-layer chromatography and fully characterised as the bis-chloride and bis-hexafluorophosphate

salts. The analogous [2]rotaxane **91·(Cl)$_2$** was also isolated as a side product in 20% yield. In similar fashion to the axle, these rotaxanes exist as a racemic mixture of atropisomers.

5.2.3. ^{1}H NMR spectroscopic studies of anion-induced shuttling behaviour in $CDCl_3$

The co-conformation of the [3]rotaxane as the bis-chloride salt in $CDCl_3$ was elucidated by comparing its ^{1}H NMR spectrum to that of axle **89·(Cl)$_2$** and the macrocycle precursor **22** (Figure 5.12).

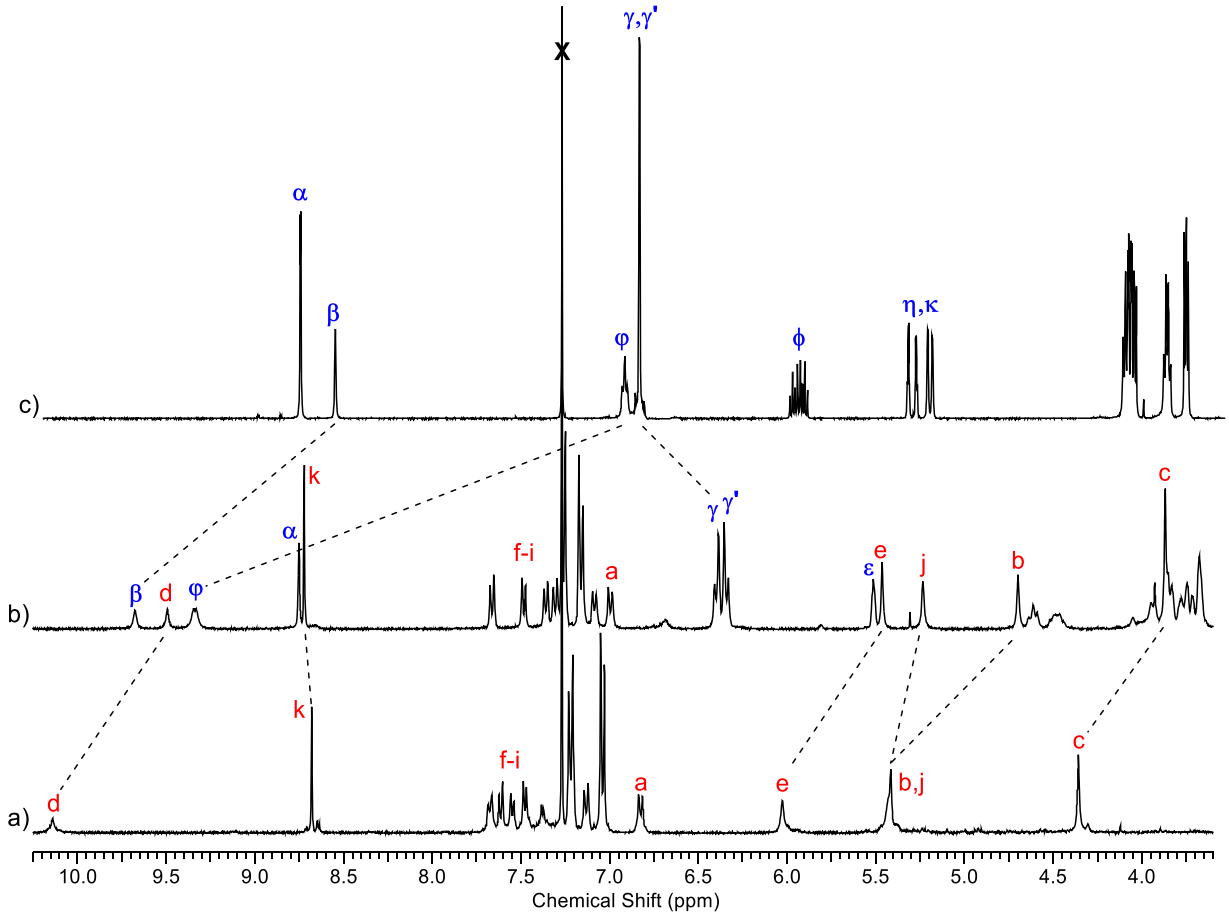


*Figure 5.12. Truncated ^{1}H NMR spectra of a) PDI axle **89·(Cl)$_2$**, b) PDI [3]rotaxane **90·(Cl)$_2$** and c) bis-vinyl-appended macrocycle precursor **22** ($CDCl_3$, 298 K, 400 MHz).*

An upfield shift of triazolium proton resonance H_d and downfield shifts of H_β and H_φ occur upon [3]rotaxane formation due to polarisation of the chloride anion towards the hydrogen bond donors of the macrocycle. Occupancy of the proto-triazolium stations was further evidenced by the larger upfield shifts of H_e, H_b and H_c ($\Delta\delta$ = 0.6 - 0.7 ppm) relative to H_j ($\Delta\delta$ = 0.2 ppm) on [3]rotaxane formation because these protons are in closer proximity to the macrocycle hydroquinone ring currents. By

comparison, the PDI protons H_k undergo a negligible shift ($\Delta\delta$ = 0.04 ppm) indicating the macrocycles do not significantly interact with this station.

It was hoped that removal of the coordinating chloride anions would enable the PDI motif to act as a recognition site for the macrocycles *via* the formation of aromatic stacking interactions with the hydroquinone groups. Therefore, the ^{1}H NMR spectra of **90·(Cl)$_2$** and **90·(PF$_6$)$_2$** were compared in $CDCl_3$ in order to determine if anion exchange to the non-coordinating hexafluorophosphate salt caused a co-conformational change in the [3]rotaxane (Figure 5.13).

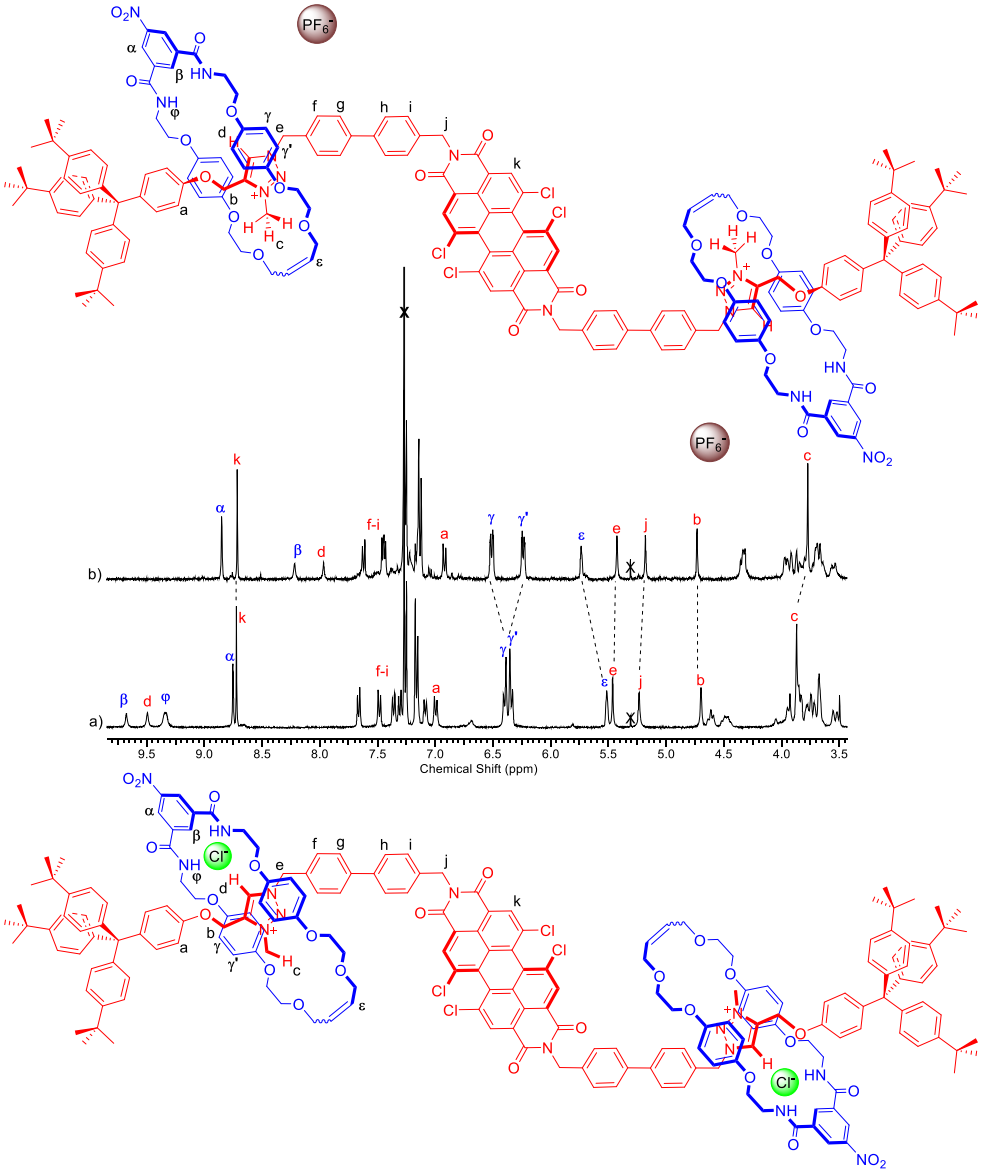


Figure 5.13. Truncated ^{1}H NMR spectra of a) bis-chloride and b) bis-hexafluorophosphate salts of [3]rotaxane ***90·(A)$_2$*** *($CDCl_3$, 298 K, 400 MHz). The predominant co-conformations of these [3]rotaxane salts are also depicted.*

Surprisingly, anion exchange from the bis-chloride to the bis-hexafluorophosphate salt causes very small changes in the chemical shift of methylene proton resonances H_e, H_j and H_b indicating negligible translational motion of the macrocycles along the axle. Furthermore, shuttling to the PDI motif was excluded because the resonances for H_k are not perturbed.

In previously described multi-station triazolium-containing rotaxane shuttles (Chapters Two, Three and Four), the *N*-methyl triazolium resonance shifts downfield upon removal of the coordinating halide anion, because these protons are less exposed to hydroquinone ring currents as the macrocycle moves

away from this station. However, within this [3]rotaxane system, an upfield shift of the *N*-methyl proto-triazolium peak (H_c) suggests that the macrocycles remain at these stations and instead undergo small co-conformational changes, possibly to maximise hydrogen bonding between this group and the polyether cavity, concurrent with the downfield shift of H_ε. This also explains why the $H_{\gamma,\gamma'}$ proton signals are not shifted upon anion exchange but the degree of splitting changes.

The similarity of the proto-triazolium environments in the PDI axle **89·(Cl)$_2$** and the axle component of the model proto-triazolium-containing [2]rotaxane **48·Cl** (Section 2.3.6.1) results in identical ^{1}H NMR chemical shifts of their *N*-methyl group resonances (δ = 4.38 ppm). Therefore, the chemical shift of H_c in [3]rotaxane **90·(Cl)$_2$** was used to show 100% macrocycle occupancy of the proto-triazolium stations in the bis-chloride salt (Figure 5.14). This 100% occupancy is maintained in the bis-hexafluorophosphate salt because the same perturbation of H_c is observed in the model [2]rotaxane **50·A** and the [3]rotaxane **90·(A)$_2$** upon anion exchange.

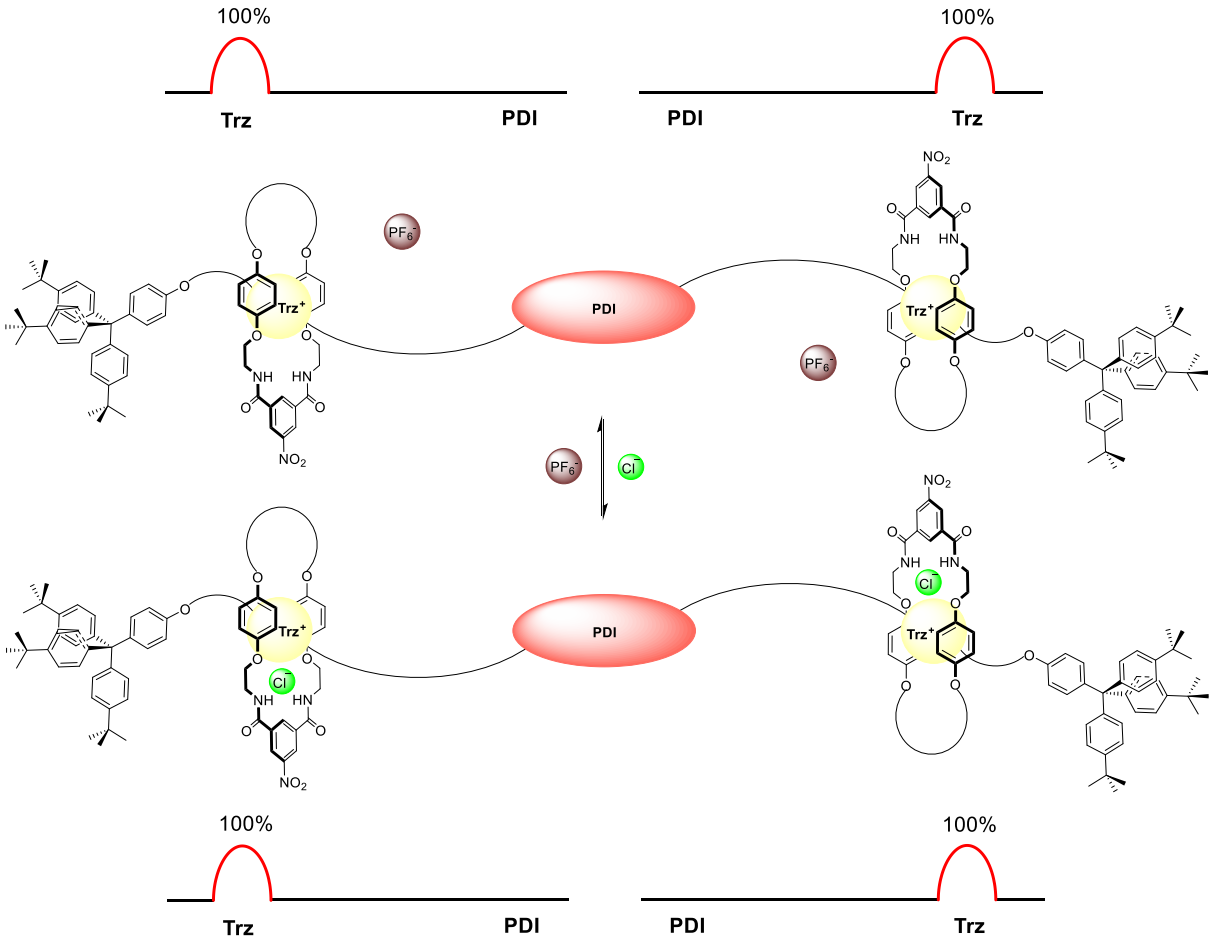


Figure 5.14. The estimated macrocycle-station occupancies of the PDI [3]rotaxanes ***90·(PF$_6$)$_2$*** *and* ***90·(Cl)$_2$*** *as determined by ^{1}H NMR spectroscopy in $CDCl_3$ solution. Trz$^+$ = proto-triazolium.*

5.2.4. ^{1}H NMR spectroscopic studies of solvent-induced shuttling behaviour

Motivated by the comprehensive work of Würthner on the solvent dependency of PDI self-aggregation[9] it was decided to investigate the effect of increasing the polarity of the solvent medium on the co-conformation of the PDI [3]rotaxane. This was achieved by monitoring the titration of CD_3OD into a solution of **90·(PF$_6$)$_2$** in $CDCl_3$ using ^{1}H NMR spectroscopy (Figure 5.15).

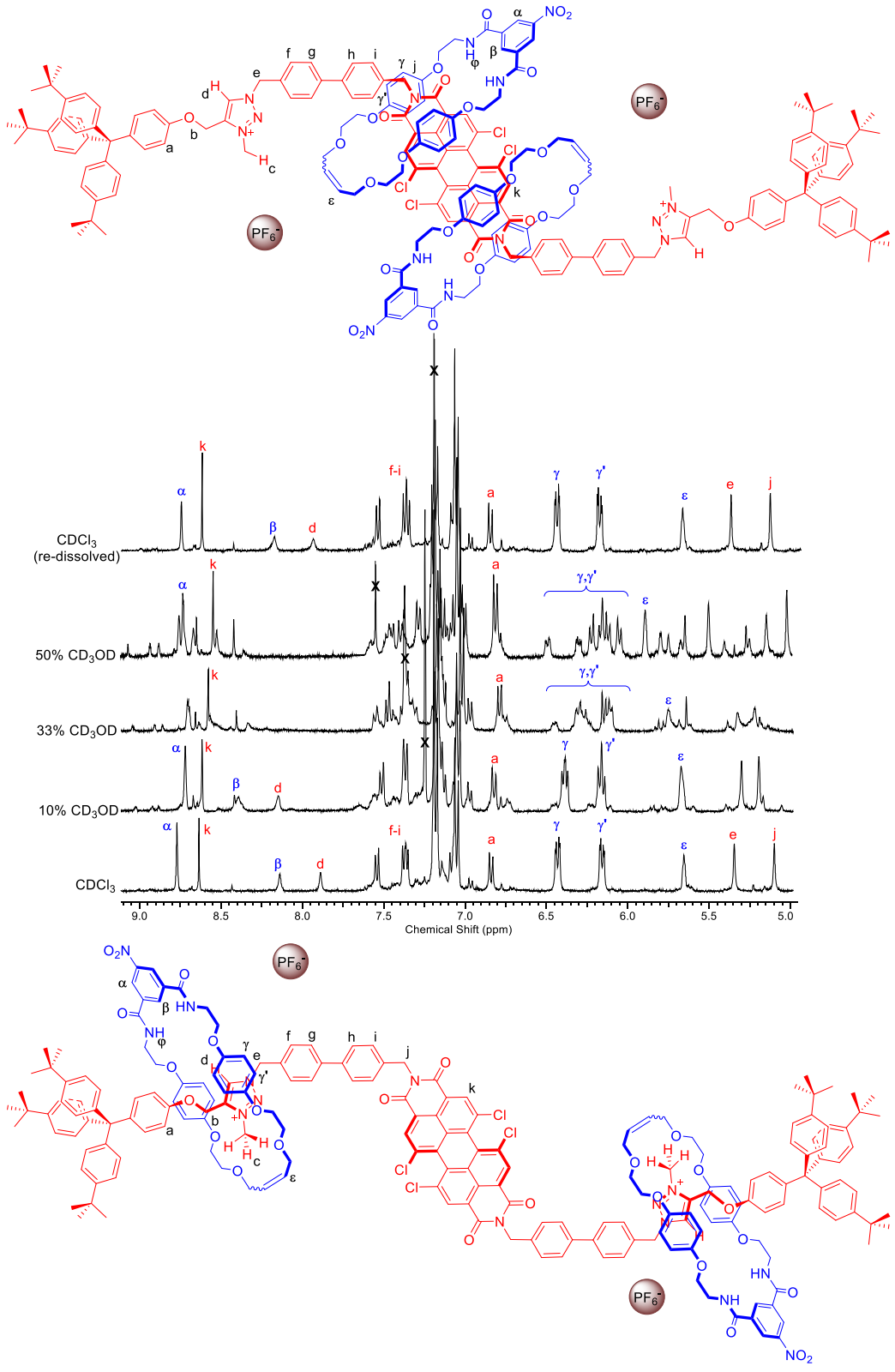


*Figure 5.15. Truncated ^{1}H NMR spectra of PDI [3]rotaxane **90·(PF$_6$)$_2$** dissolved in various $CDCl_3$–CD_3OD solvent mixtures (298 K, 500 MHz). The signals in the spectra containing CD_3OD have been assigned by comparison with the $CDCl_3$ spectrum. The predominant co-conformation of **90·(PF$_6$)$_2$** in $CDCl_3$ (bottom) and 1:1 $CDCl_3$:CD_3OD (top) are also depicted.*

Interestingly, the addition of CD_3OD significantly increased the complexity of the ^1H NMR spectrum of **90·$(PF_6)_2$** *via* the appearance of a large number of additional signals. For example, the macrocycle hydroquinone resonances $H_{y,y'}$ that are resolved as two doublets in $CDCl_3$ appear to form a set of complex multiplets in 1:1 $CDCl_3$:CD_3OD.

This indicates that the addition of CD_3OD promotes solvophobic-driven facial aromatic stacking interactions between the electron-rich hydroquinone groups of the macrocycles and the electron-deficient PDI motif. Presumably, owing to the size of the tetrachloro-substituted PDI unit, the [3]rotaxane is forced to adopt multiple co-conformations that appear to exist in slow exchange on the NMR time scale. Further complexity of the spectrum is likely to be caused by restricted rotary motion of macrocycles at the PDI stations causing de-symmetrisation of the rotaxane components. The notion that aromatic stacking interactions become stronger with increasing solvent polarity,[9,10] explains the increasing number and intensity of these new signals as the CD_3OD concentration is raised.

When the same sample of **90·$(PF_6)_2$** was re-dissolved in $CDCl_3$ the original ^1H NMR spectrum was reproduced demonstrating that additional resonance peaks are not caused by decomposition of the [3]rotaxane (Figure 5.15). This spectrum in $CDCl_3$ is simpler because it depicts a predominant co-conformation in which the isophthalamide-based macrocycles are positioned at the peripheral proto-triazolium stations and do not interact with the PDI unit.

The ^1H NMR spectrum of [2]rotaxane **91·$(Cl)_2$** in $CDCl_3$ is considerably more complicated than that of the [3]rotaxane in the same solvent because the isophthalamide macrocycle is too small to pass over the central tetrachloro PDI unit which leads to de-symmetrisation of the axle component (Figure 5.16). For example, separate resonances are observed for $H_a/H_{a'}$, $H_c/H_{c'}$ and the methylene groups $H_b/H_{b'}$, $H_e/H_{e'}$ and $H_j/H_{j'}$. The PDI protons also become inequivalent giving rise to multiple signals. This provides further evidence that interactions between the isophthalamide macrocycles and the PDI motif in the [3]rotaxane are susceptible to considerable steric constraints.

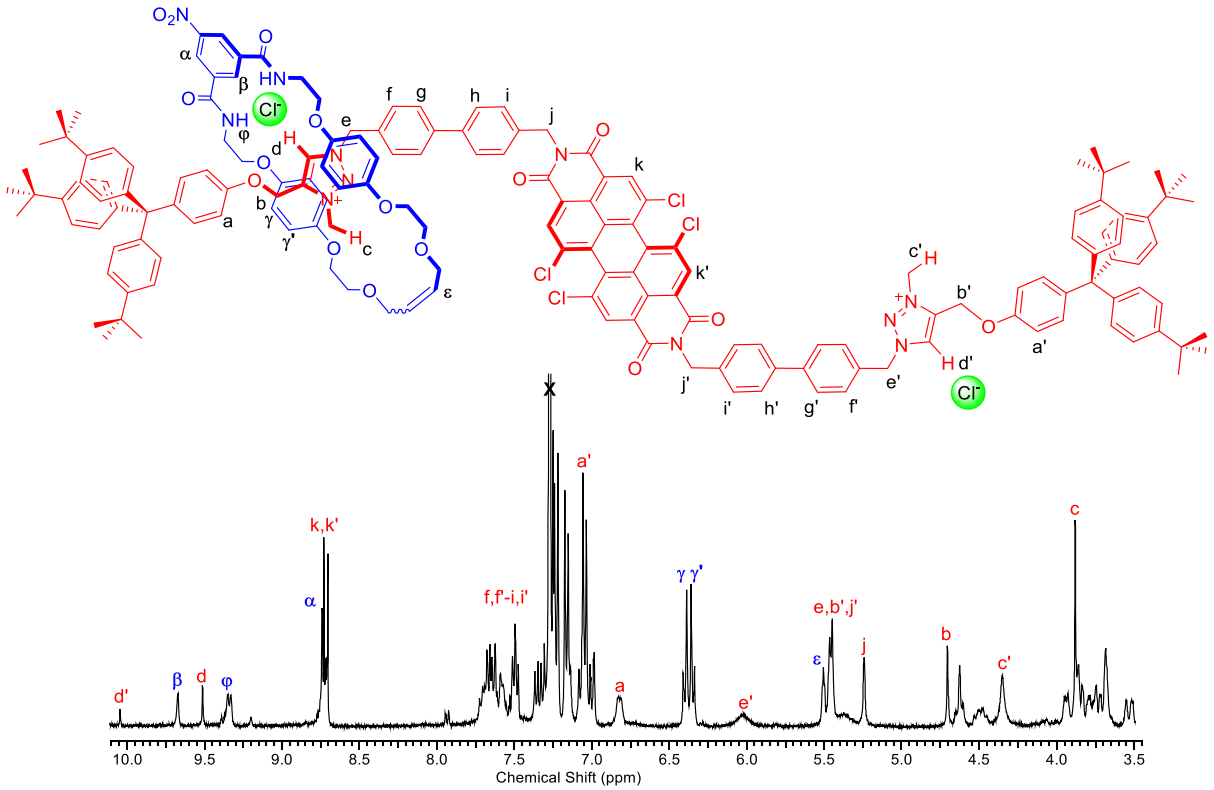


*Figure 5.16. Truncated ^{1}H NMR spectra of PDI [2]rotaxane **91·(Cl)$_2$** ($CDCl_3$, 298 K, 400 MHz).*

Finally, the addition of CD_3OD to a solution of the PDI-containing axle **89·(Cl)$_2$** in $CDCl_3$ did not produce additional signals in the ^{1}H NMR spectrum (Figure 5.17). This implies that the complexity of the ^{1}H NMR spectrum of the [3]rotaxane is not due to intermolecular aromatic stacking interactions of PDI groups (aggregation effects), but occurs due to discrete intramolecular interactions between the PDI axle and macrocycle components.*

* Within this chapter the exact assignment of peaks in the ^{1}H NMR spectra of the PDI [3]rotaxane **90·(A)$_2$** in CD_3OD:$CDCl_3$ solutions is a non-trivial task. Their complexity is most likely to be a combination of desymmetrisation and restricted motions of the macrocycle components, the latter causing co-conformations to exist in slow exchange on the NMR timescale.

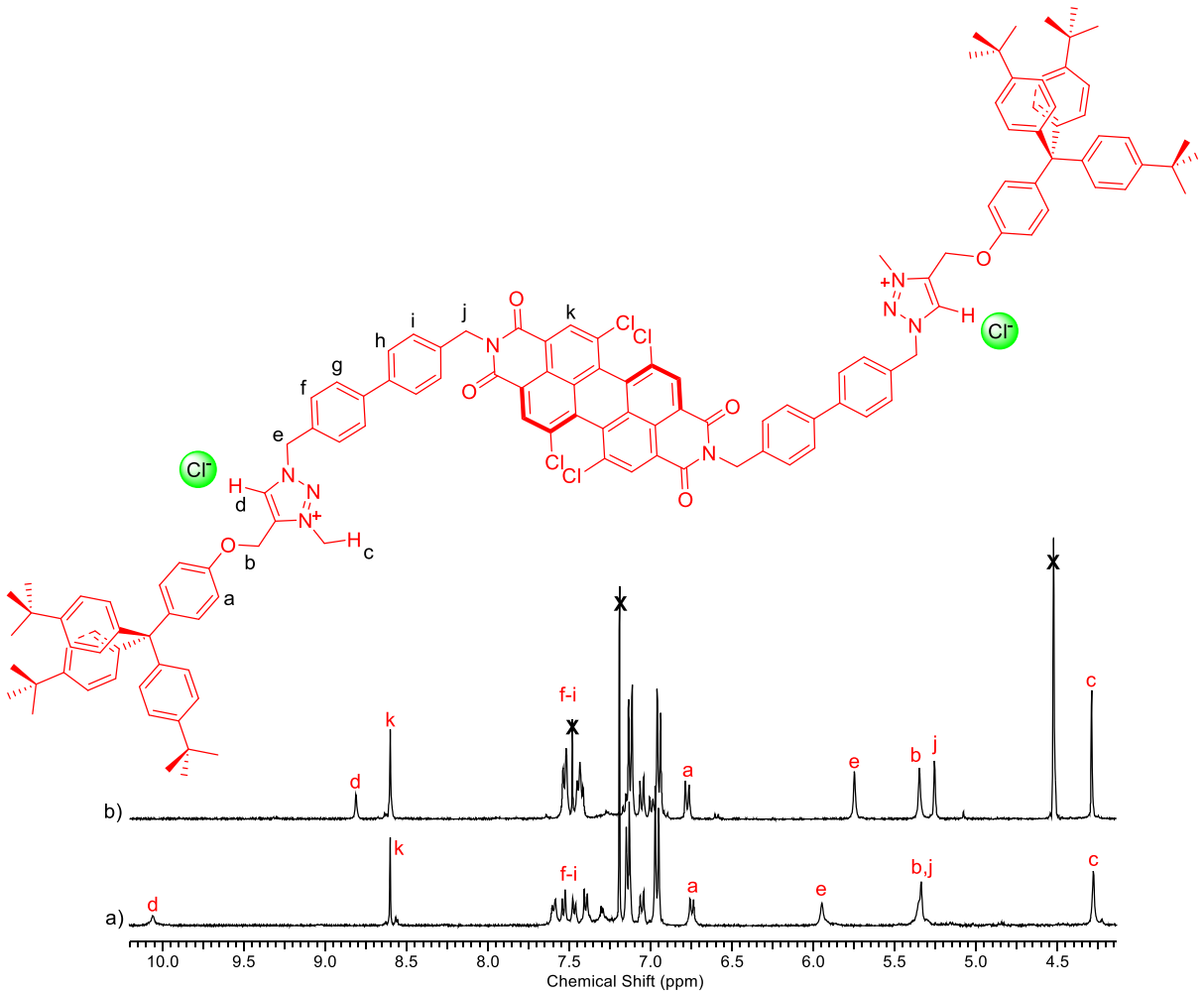


*Figure 5.17. Truncated ^{1}H NMR spectrum of PDI axle **89·(Cl)$_2$** in a) $CDCl_3$ and b) 1:1 $CDCl_3$:CD_3OD (298 K, 400 MHz).*

Analogous CD_3OD titration experiments with the bis-chloride salt of the [3]rotaxane also produced more complex ^{1}H NMR spectra. However, relative to **90·(PF$_6$)$_2$**, a smaller number of new signals with lower intensity were observed in the spectrum of **90·(Cl)$_2$** in 1:1 $CDCl_3$:CD_3OD. This is presumed to be a consequence of weaker macrocycle–PDI interactions because occupancy of the proto-triazolium stations is favoured due to halide recognition (Figure 5.18).

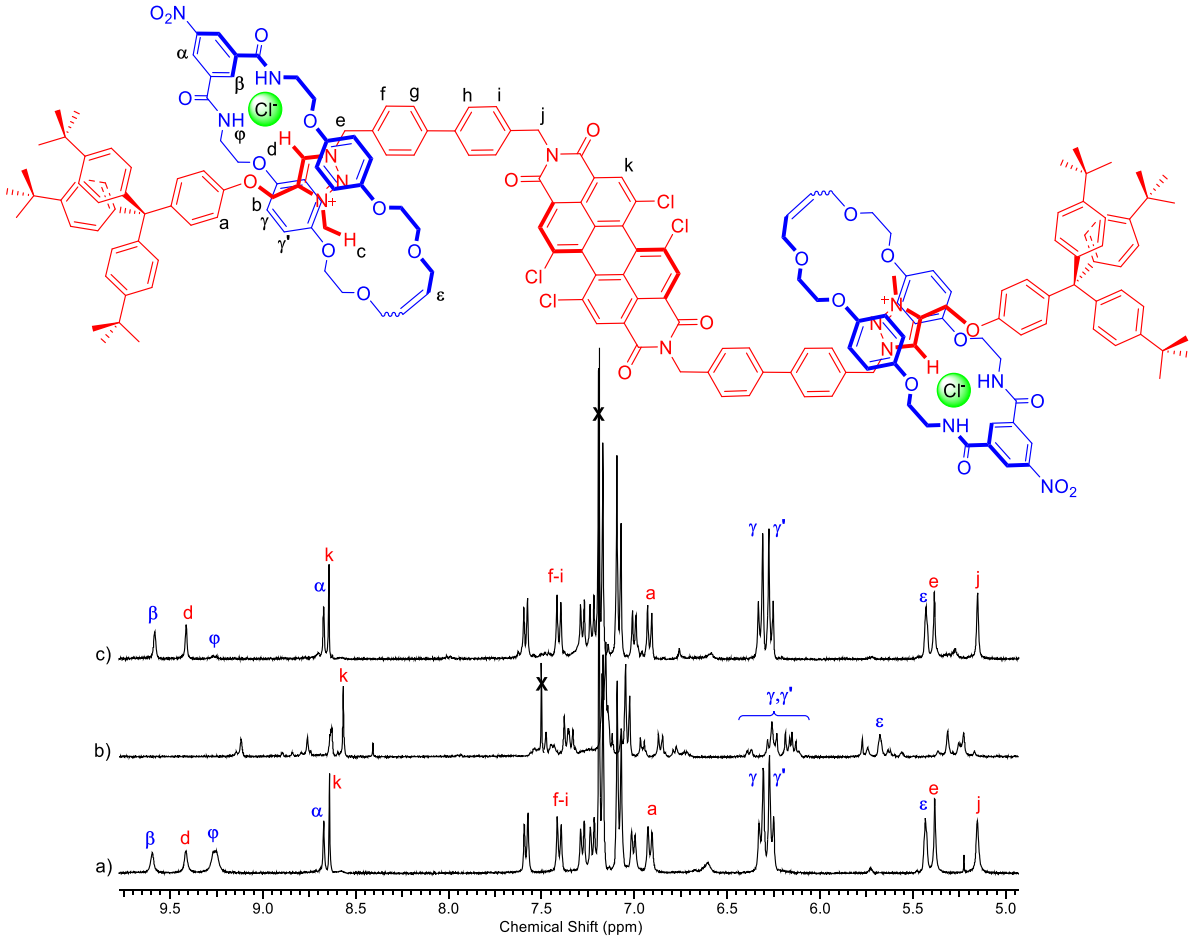


*Figure 5.18. Truncated ^{1}H NMR spectra of PDI [3]rotaxane **90·(Cl)$_2$** dissolved in a) $CDCl_3$, b) 1:1 $CDCl_3$:CD_3OD and c) re-dissolved in $CDCl_3$ (298 K, 400 MHz). The predominant co-conformation of **90·(Cl)$_2$** in these solvents is also depicted.*

It was hoped that the ^{1}H NMR spectrum of **90·(Cl)$_2$** in 1:1 $CDCl_3$:CD_3OD might be simplified upon heating because this would increase the rate of interchange between co-conformations, potentially into the fast exchange regime on the NMR timescale. However, almost no coalescence of signals was observed upon heating to 50 °C. Switching the solvent system to DMSO-d_6 allowed variable temperature ^{1}H NMR experiments to be performed up to 130 °C (Figure 5.19). Importantly, the macrocycles were shown to interact with the PDI stations in this polar solvent, because the ^{1}H NMR spectrum of **90·(Cl)$_2$** at 25 °C exhibited a similar level of complexity[†] as that in 1:1 $CDCl_3$:CD_3OD. Close proximity of $H_{\gamma,\gamma'}$ and H_k was also observed in the two-dimensional ^{1}H ROESY NMR spectrum of **90·(Cl)$_2$** in DMSO-d_6.

[†] Again, this is most likely to be a combination of desymmetrisation and restricted motions of the macrocycle components, the latter causing co-conformations to exist in slow exchange on the NMR timescale.

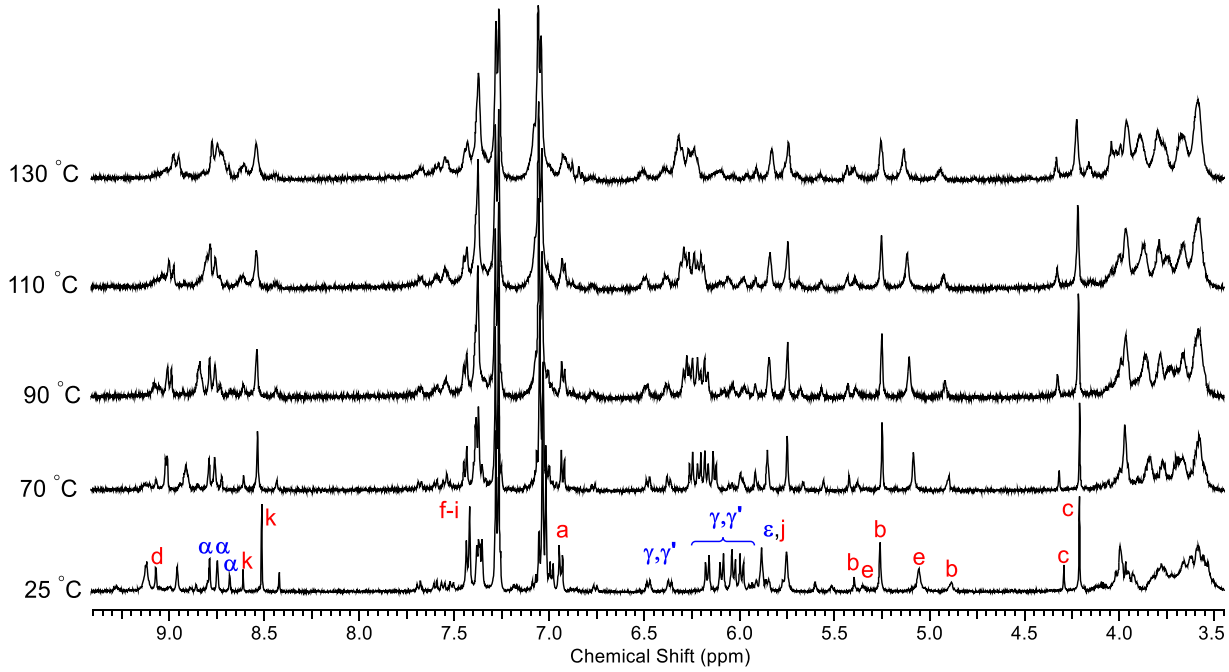


Figure 5.19. Variable-temperature ^{1}H NMR spectra of ***90·(Cl)$_2$*** *(DMSO-d_6, 500 MHz).*

Significant broadening of the ^{1}H NMR signals is observed upon heating making interpretation more challenging. However, even at 130 °C there was little evidence of coalescence of resonances. This suggests that the energetic barrier to permit free rotary motion of the macrocycles at the PDI stations is relatively large. The coalescence of interconverting atropisomers of tetrachloro PDI (leading to effective planarity of this motif on the NMR timescale) has been reported to occur at 103 °C in dichloroethane but interestingly no significant changes were observed in the ^{1}H NMR spectra of **90·(Cl)$_2$** in this temperature region.

5.2.5. UV-Vis spectroscopic studies of solvent-induced shuttling behaviour

Further to ^{1}H NMR studies, UV-Vis spectroscopy was utilised to monitor the effect of MeOH concentration on the absorption spectra of [3]rotaxane **90·(PF$_6$)$_2$** (Figure 5.20a) and axle component **89·(BF$_4$)$_2$** (Figure 5.20b).

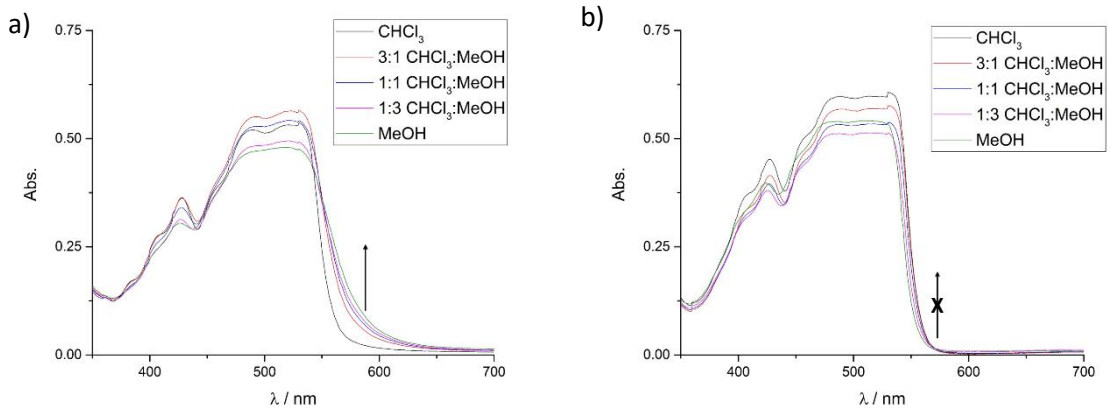


Figure 5.20. UV-Vis spectra of a) [3]rotaxane ***90·(PF$_6$)$_2$*** *and b) axle* ***89·(BF$_4$)$_2$*** *recorded at the same concentration (1 × 10^{-4} mol L^{-1}) in various CHCl$_3$–MeOH solvent mixtures.*

The addition of MeOH to a $CHCl_3$ solution of the [3]rotaxane produced new bathochromically-shifted absorptions at higher wavelengths (λ_{abs} > 575 nm), beside the maximum PDI band at λ_{abs} ~ 525 nm. Based upon similar observations by Würthner *et al.* in the UV-Vis spectra of charge–transfer complexes formed by the cyclophane in Figure 5.2,[7] these features are attributed to charge–transfer bands arising from donor–acceptor aromatic stacking interactions between the electron-rich hydroquinone groups of the macrocycles and the electron-deficient PDI motif. This explains why no significant changes in the UV-Vis spectrum of the axle component **89·(BF$_4$)$_2$** at λ_{abs} > 575 nm are observed.

It should be noted that interactions between a hydrogen-bond donating macrocycle and PDI imide carbonyl groups have been attributed to producing a red shift of the PDI absorption of Vögtle's [3]rotaxane in Figure 5.5.[15] However, since the addition of MeOH will reduce the strength of intramolecular hydrogen bonding, this is unlikely to be the sole cause of the observed spectral response in [3]rotaxane **90·(PF$_6$)$_2$**.

The bathochromic shift in the absorption spectrum of the [3]rotaxane caused by the addition of MeOH is manifested in a naked-eye colour change of the solution from orange to red (Figure 5.21a). However, no red shift is observed for the axle, which remains orange throughout the course of the titration experiment (Figure 5.21b).

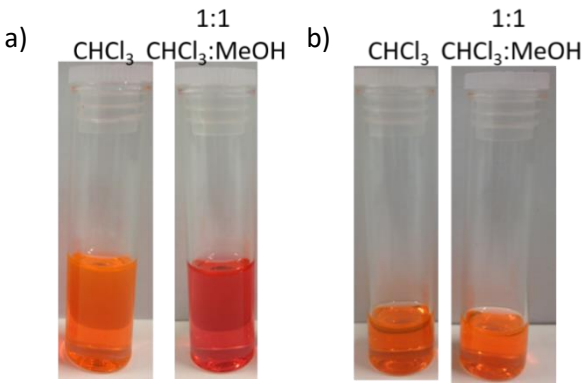


Figure 5.21. Photographs of solutions of a) [3]rotaxane ***90·(PF$_6$)$_2$*** *and b) axle* ***89·(BF$_4$)$_2$*** *in $CHCl_3$ and 1:1 $CHCl_3$:MeOH. The addition of MeOH to a $CHCl_3$ solution of the [3]rotaxane produces a naked-eye colour change from orange to red.*

5.2.6. ^{1}H NMR spectroscopic studies of anion-induced shuttling behaviour in $CDCl_3$-CD_3OD solvent mixtures

The solvent-dependency experiments have demonstrated that interactions between the macrocycles and the PDI stations are only switched on when the solvent polarity is increased. Therefore, by enabling the PDI stations to act as macrocycle recognition sites, it was proposed that co-conformational switching between the stations could also be mediated by anions in $CDCl_3$–CD_3OD solvent mixtures.

The station occupancies for the [3]rotaxane bis-chloride and bis-hexafluorophosphate salts **90·(Cl)$_2$** and **90·(PF$_6$)$_2$**, respectively, were estimated in 1:1 $CDCl_3$:CD_3OD using the change in chemical shift of the *N*-methyl triazolium proton H_c (Figure 5.22).[‡] As expected, the occupancy of the proto-triazolium station was no longer 100% (as found in $CDCl_3$) implying that macrocycles interact with the central PDI recognition site. The occupancy of PDI was larger in the absence of coordinating chloride anions (41% *vs.* 12%), suggesting that translational switching between the stations is modulated by the nature of the anion in the same fashion seen in dynamic multi-station rotaxane host systems described in previous chapters.

[‡] This peak was well resolved in the ^{1}H NMR spectrum.

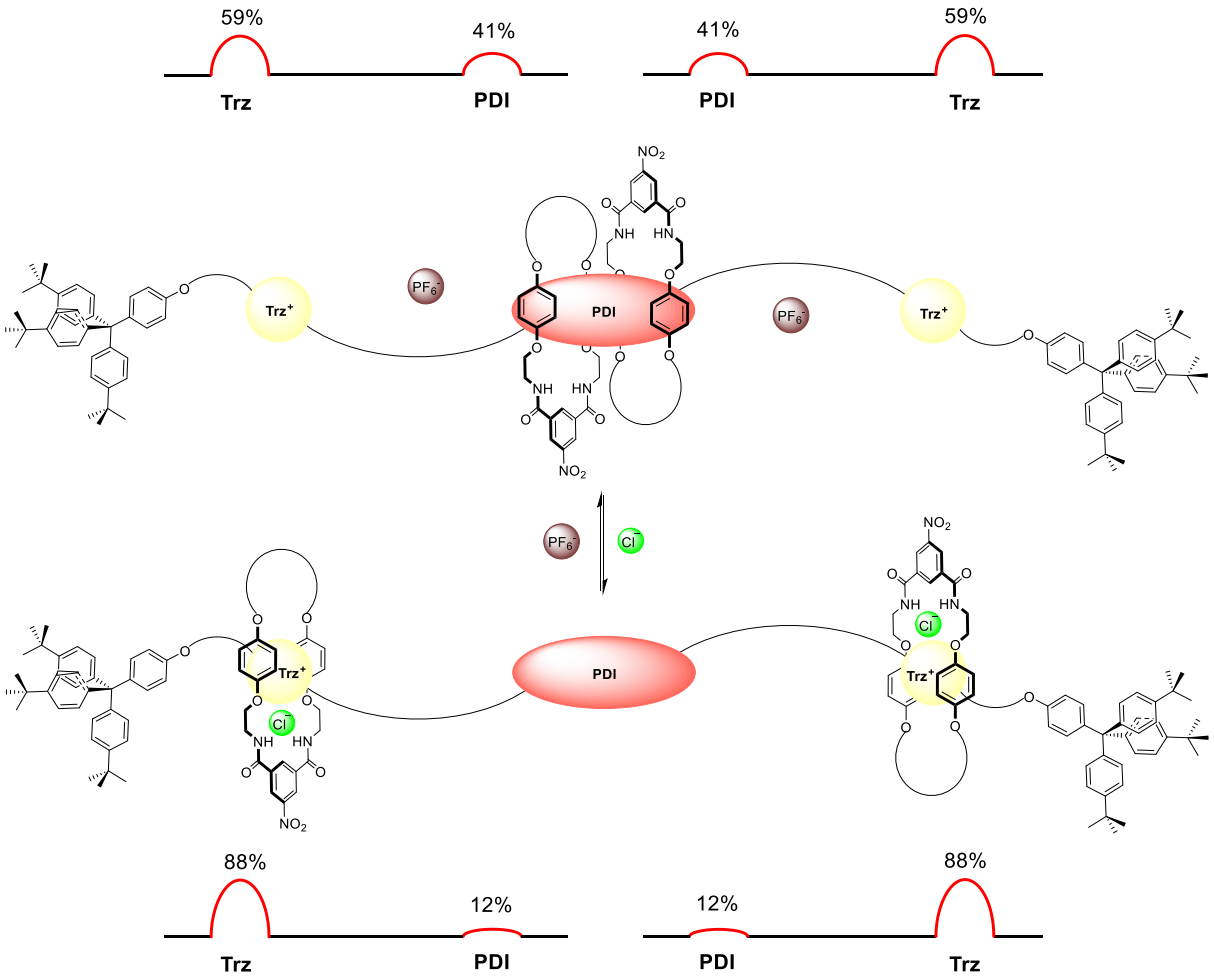


Figure 5.22. The estimated macrocycle-station occupancies of the PDI [3]rotaxanes ***90·(PF$_6$)$_2$*** *and* ***90·(Cl)$_2$*** *as determined by ^{1}H NMR spectroscopy in 1:1 $CDCl_3$:CD_3OD solution. Trz^+ = proto-triazolium.*

In order to further characterise this anion-meditated shuttling using two-dimensional ^{1}H NMR spectroscopy, attempts were made to assign the one-dimensional ^{1}H NMR spectra of **90·(PF$_6$)$_2$** and **90·(Cl)$_2$** in 3:1 $CDCl_3$:CD_3OD. This lower polarity solvent mixture was chosen because it provided ^{1}H NMR spectra that were relatively simpler than those in 1:1 $CDCl_3$:CD_3OD while still facilitating dynamic behaviour of the [3]rotaxane.

Initially, ^{1}H–^{13}C HSQC NMR spectra of [3]rotaxane **90·(A)$_2$** were run in $CDCl_3$ to assign the ^{13}C NMR chemical shifts of a selection of axle and macrocycle carbon nuclei. Following this, these chemical shifts were used in combination with ^{1}H–^{13}C HSQC NMR spectra in 3:1 $CDCl_3$:CD_3OD to assign proton resonances in the complex one-dimensional ^{1}H NMR spectra of **90·(PF$_6$)$_2$** and **90·(Cl)$_2$** in this solvent mixture (Figure 5.23). This technique was possible because the NMR solvent has a much smaller effect

on the chemical shift of ^{13}C nuclei than those of protons, and particularly when the volume fraction of CD_3OD in $CDCl_3$ is only increased by 25%.

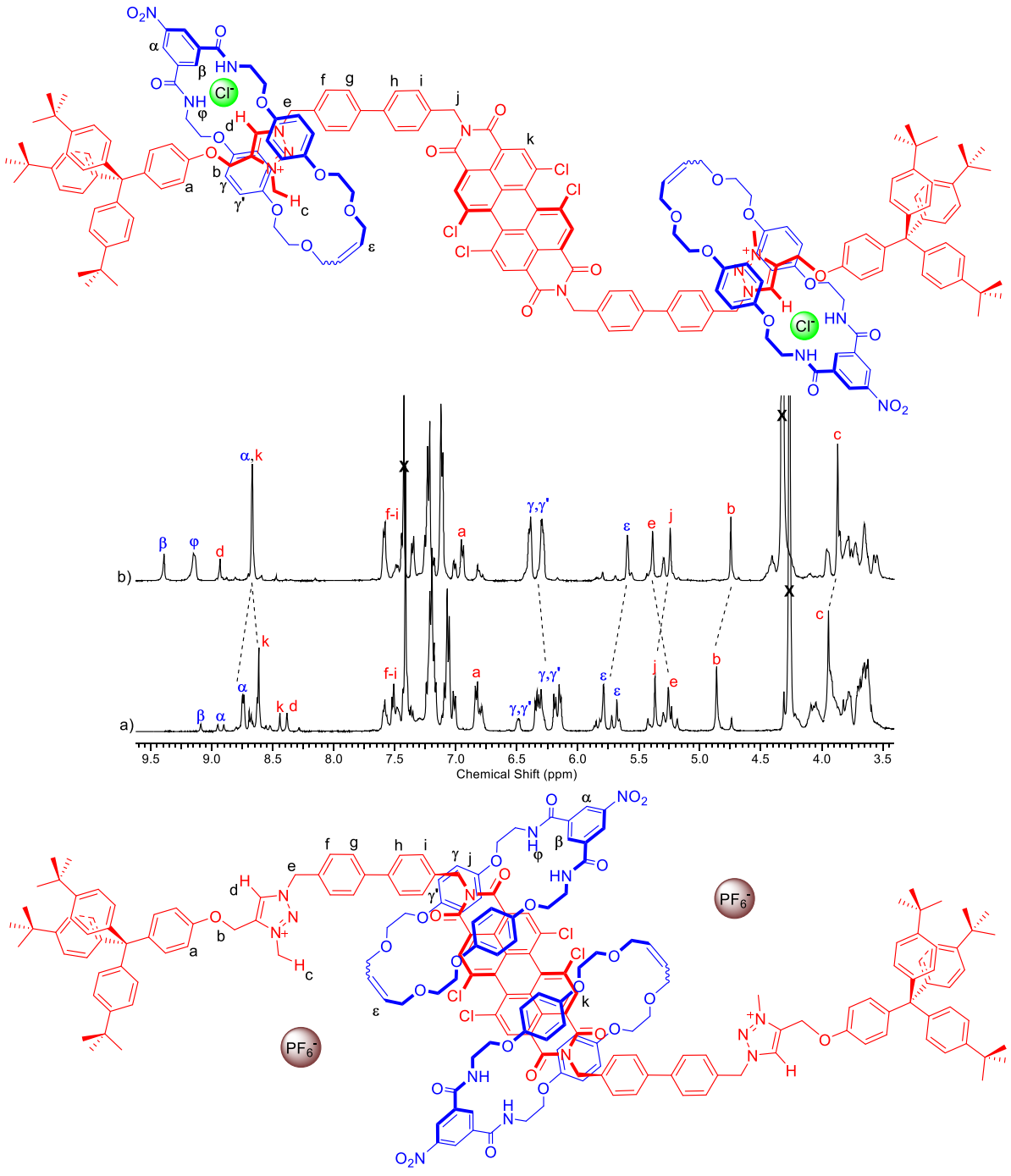


Figure 5.23. Truncated ^1H NMR spectra of a) bis-hexafluorophosphate and b) bis-chloride salts of [3]rotaxane ***90·(A)₂*** *(3:1 $CDCl_3$:CD_3OD, 298 K, 400 MHz). The predominant co-conformations of these [3]rotaxane salts are also depicted.*

The ^{1}H NMR spectrum of **90·(Cl)$_2$** is relatively simpler than that of **90·(PF$_6$)$_2$** suggesting interactions between the macrocycles and the PDI stations are weaker. On exchange to the bis-chloride salt, resonances associated with the hydroquinone and PDI protons ($H_{\gamma,\gamma'}$ and H_k) undergo a downfield shift, which also implies the macrocycles shuttle from the central PDI unit to the peripheral proto-triazolium stations of the axle component. These perturbations are significant because they were not observed in $CDCl_3$. Finally, addition of halide anions cause a diagnostic upfield shift of the *N*-methyl triazolium resonances H_c because of an increased exposure to the macrocycle's hydroquinone ring currents, whilst a downfield shift was previously seen in $CDCl_3$.

Two-dimensional ^{1}H ROESY NMR spectra were then recorded for **90·(PF$_6$)$_2$** and **90·(Cl)$_2$** in 3:1 $CDCl_3$:CD_3OD (Figure 5.24).

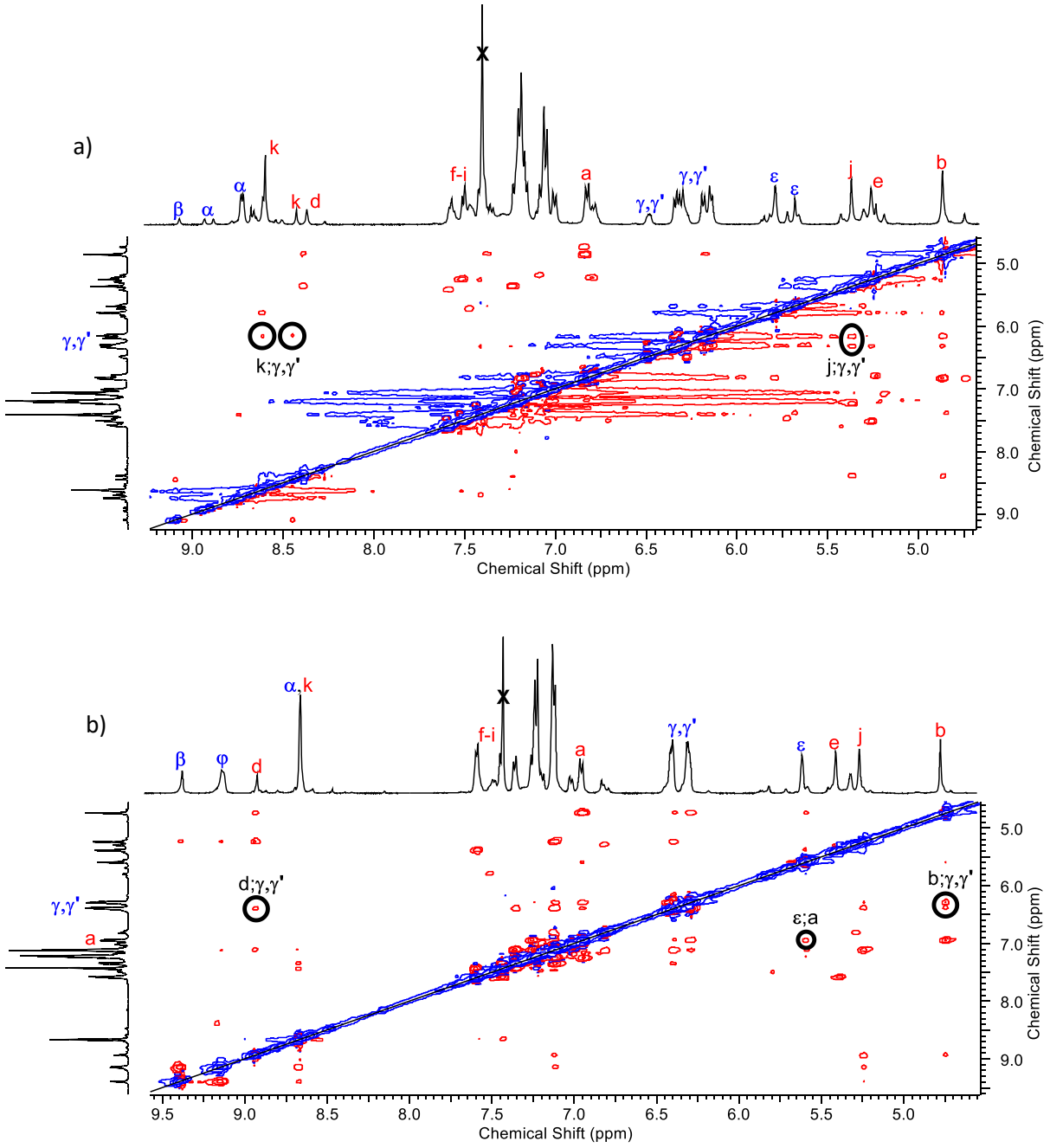


*Figure 5.24. Truncated ^{1}H–^{1}H ROESY NMR spectrum of PDI [3]rotaxane **90·(A)$_2$** as the a) bis-hexafluorophosphate salt and b) bis-chloride salt with selected coupling interactions highlighted (3:1 $CDCl_3$:CD_3OD, 298 K, 500 MHz).*

The proximity of the macrocycles to the PDI stations in **90·(PF$_6$)$_2$** produces through-space coupling interactions between the macrocycle hydroquinone resonances $H_{\gamma,\gamma'}$ and axle protons H_k and H_j. For the bis-chloride salt **90·(Cl)$_2$**, these peaks disappear, leaving instead strong coupling between macrocycle protons ($H_{\gamma,\gamma'}$ and H_ε) and those associated with the proto-triazolium stations, namely H_a, H_d and H_b.

The degree of anion-induced co-conformational switching in 3:1 $CDCl_3$:CD_3OD was then quantified using the chemical shift of the *N*-methyl triazolium resonance peak (H_c)[§] for each [3]rotaxane salt (Figure 5.25).

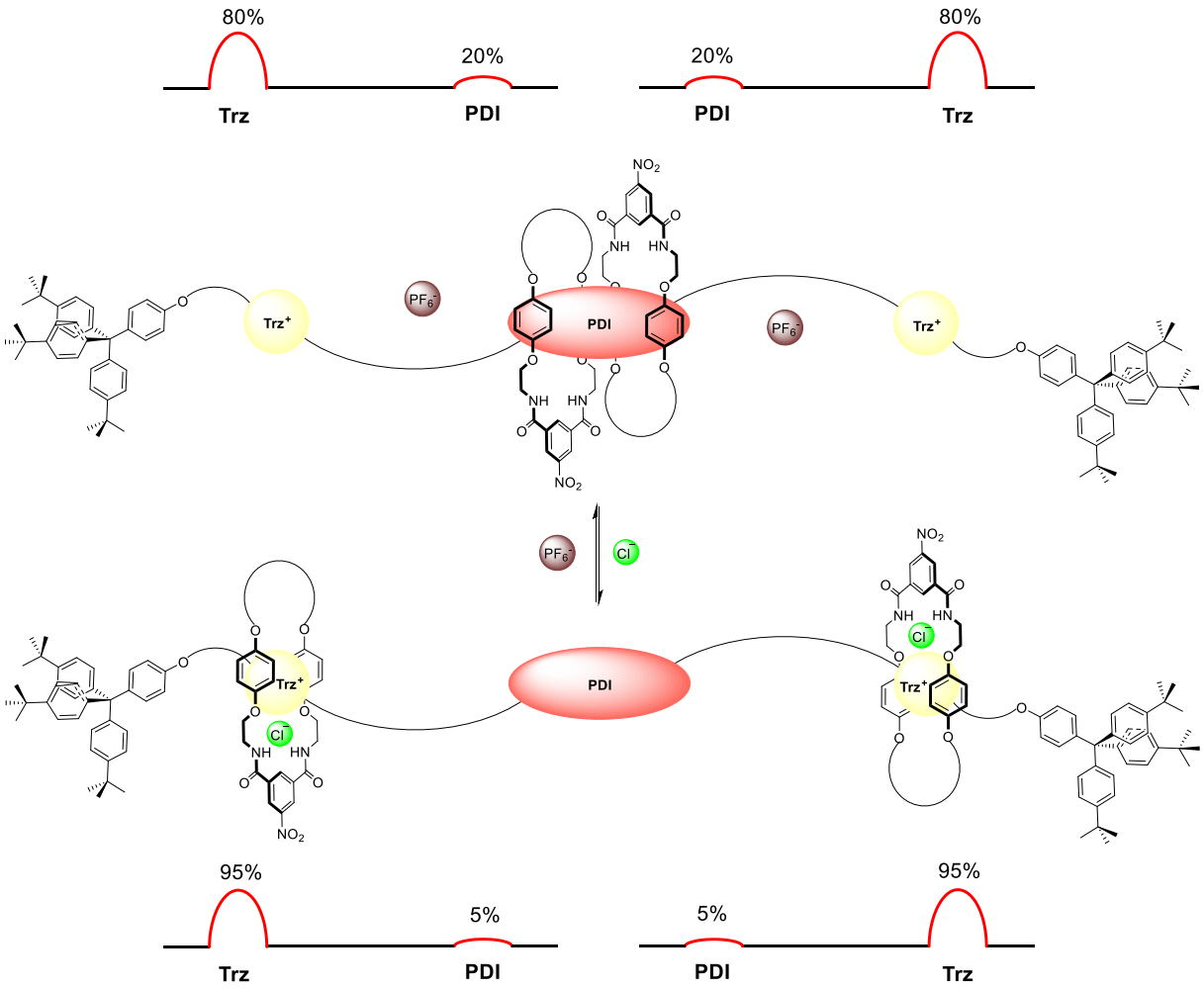


Figure 5.25. The estimated macrocycle-station occupancies of the PDI [3]rotaxanes ***90·(PF$_6$)$_2$*** *and* ***90·(Cl)$_2$*** *as determined by ^{1}H NMR spectroscopy in 3:1 $CDCl_3$:CD_3OD solution. Trz$^+$ = proto-triazolium.*

Under these solvent conditions, an occupancy swing of 15% from the PDI recognition site to the proto-triazolium stations was estimated upon exchange to the coordinating chloride salt, confirming the findings of the one and two-dimensional ^{1}H NMR experiments. However, it is thought that the lower polarity of this solvent medium is responsible for the fact this is almost half the degree of co-conformational change estimated in 1:1 $CDCl_3$:CD_3OD (Figure 5.22). This is because weaker solvophobic

[§] This peak was well resolved in the ^{1}H NMR spectrum.

effects are likely to cause the occupancy of the PDI stations in **90·$(PF_6)_2$** in 3:1 $CDCl_3$:CD_3OD to be (21%) lower (Figure 5.25).

5.2.7. UV-Vis spectroscopic studies of anion-induced shuttling behaviour in 3:1 $CHCl_3$:CH_3OH

Analogous to previous solvent-dependency studies, investigations were then carried out to ascertain if the chloride-induced shuttling exhibited by [3]rotaxane **90·$(PF_6)_2$** in 3:1 $CHCl_3$:CH_3OH could be monitored by UV-Vis spectroscopy (Figure 5.26).

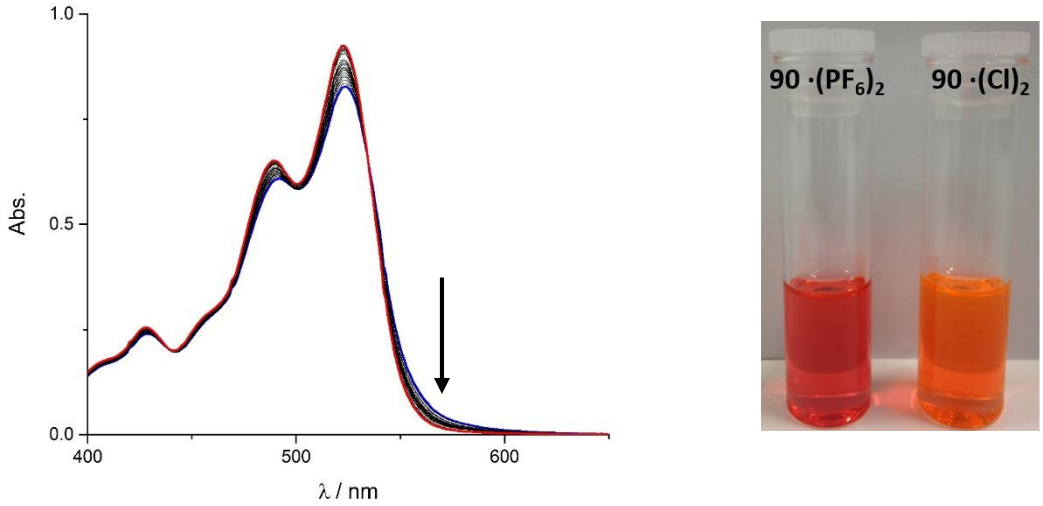


*Figure 5.26. Superimposed UV-Vis spectra of the PDI [3]rotaxane **90·$(PF_6)_2$** in 3:1 $CHCl_3$:CH_3OH (3×10^{-5} mol L^{-1}) showing the titration of up to 50 equivalents of TBA·Cl. The addition of chloride leads to a decrease in intensity of the charge–transfer absorbance bands at λ_{abs} > 550 nm leading to a naked-eye colour change of the solution from red to orange.*

The titration of **90·$(PF_6)_2$** with up to 50 equivalents of TBA·Cl resulted in an effective hypsochromic shift of the PDI absorption band owing to a decrease in intensity of the charge–transfer absorptions at higher wavelengths (λ_{abs} > 550 nm). This was ascribed to the loss of aromatic stacking interactions between the macrocycles and the PDI motif because chloride recognition facilitated an increased occupancy of the proto-triazolium stations.

The blue shift of the absorption is manifested in a colour change of the [3]rotaxane solution from red to orange upon the addition of chloride (Figure 5.26) allowing it to optically sense this anion in solution.

Notably, this is the opposite response to that caused by the addition of MeOH which produced red-shifted charge–transfer absorptions by increasing the strength of PDI macrocycle interactions.

To confirm that chloride-induced molecular shuttling was responsible for this colour change, the same titration was performed with **90·$(PF_6)_2$** in $CHCl_3$ (Figure 5.27). The perturbations of the UV-Vis spectra under these conditions were much smaller because of negligible macrocycle translocation. Therefore the [3]rotaxane solution remains orange upon the addition of chloride (Figure 5.27).

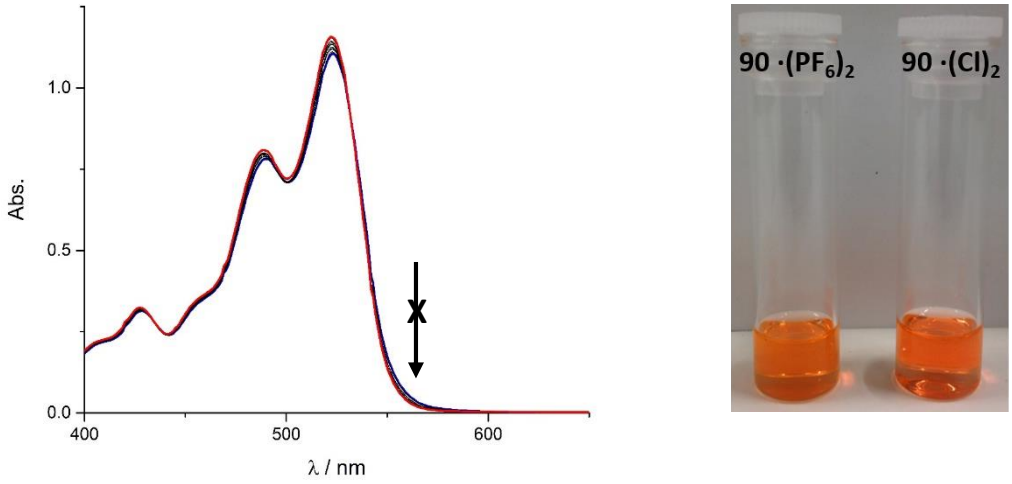


*Figure 5.27. Superimposed UV-Vis spectra of the PDI [3]rotaxane **90·$(PF_6)_2$** in $CHCl_3$ (3×10^{-5} mol L^{-1}) showing the titration of up to 50 equivalents of TBA·Cl. The addition of chloride leads to negligible changes in the absorption spectra, manifested as no observable colour change in the solution.*

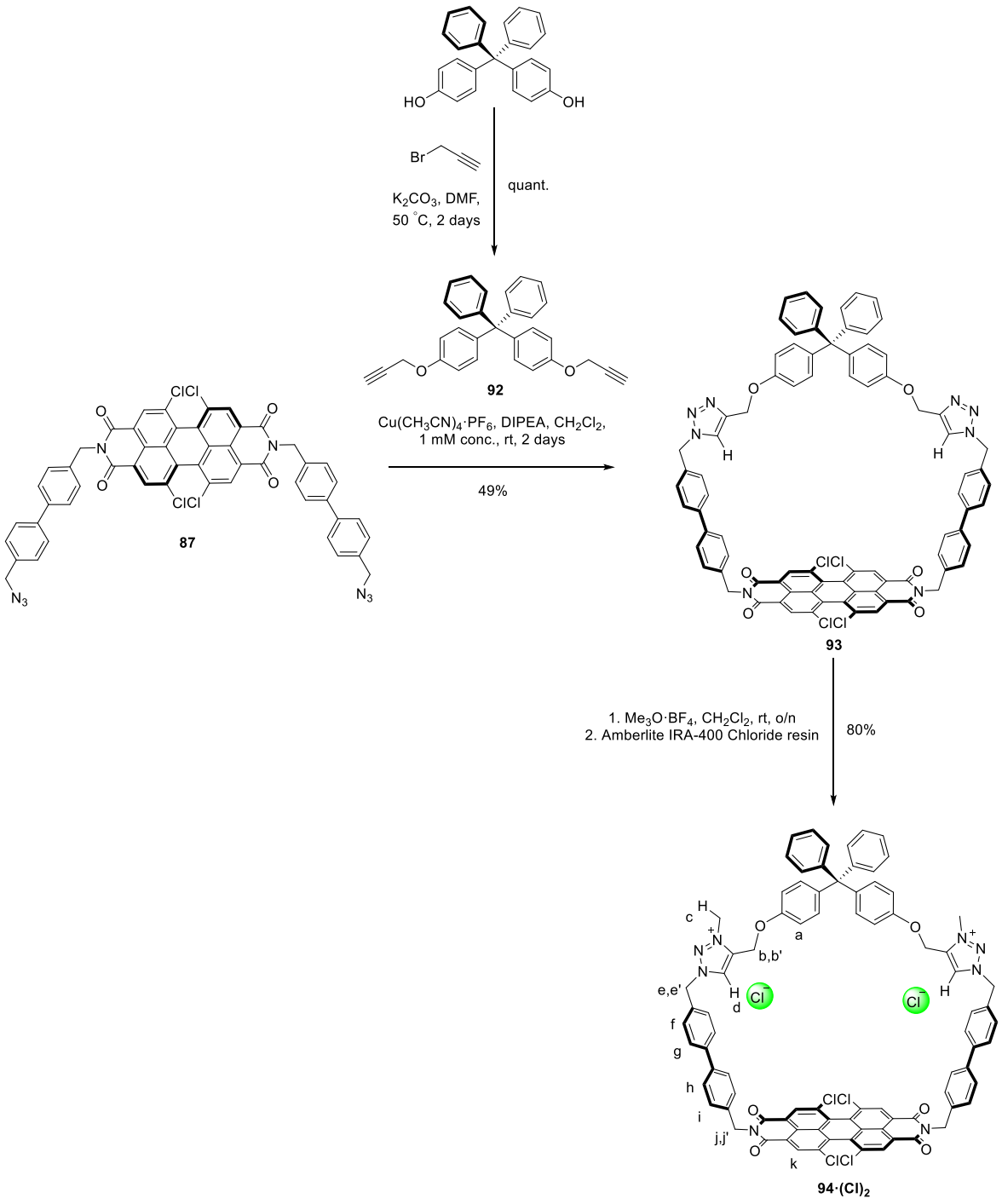
5.3. A PDI-containing [3]catenane

5.3.1. Synthesis of a four-station PDI-containing macrocycle

Having demonstrated that chloride-induced co-conformational change, involving translational motion of macrocycle components, was possible in a PDI-containing [3]rotaxane, it was decided to extend the scope of this dynamic behaviour to produce anion-mediated rotary motion in an analogous [3]catenane. Consequently, the synthetic route used to prepare the four-station axle component was

adapted to construct a symmetric macrocycle containing two proto-triazolium groups and a tetrachloro PDI unit.

Therefore, a macrocyclisation was envisaged in which a PDI bis-azide derivative was ring closed with a bis-alkyne *via* a double CuAAC 'click' reaction under high dilution conditions. This was attempted with various azide and alkyne-containing compounds, however the highest yield of a cyclised product was achieved using a rigid phenyl trityl bis-alkyne (**92**) and bis-biphenyl PDI azide **87** (Scheme 5.3).



Scheme 5.3. Synthesis of tetrachloro PDI-bis-proto-triazolium macrocycle ***94·(Cl)₂****.*

The phenyl trityl bis-alkyne **92** was prepared from the reaction of commercially available phenyl trityl bis-alcohol with two equivalents of propargyl bromide under basic conditions. Macrocycle formation was performed by reacting equimolar amounts of PDI bis-azide **87** and bis-alkyne **92** in dry CH_2Cl_2 at 1 mM concentration in the presence of Cu(I), TBTA and DIPEA. After two days, TLC analysis revealed the starting materials had been consumed and the target [1+1] bis-proto-triazole-containing macrocycle

93 was isolated using preparative silica thin-layer chromatography in 49% yield. The predominant side products of the reaction were thought to be oligomeric species that precipitate from solution over the course of the reaction. The two triazole groups of **93** were methylated using $Me_3O{\cdot}BF_4$ to give dicationic macrocycle **94·$(BF_4)_2$**. The bis-chloride salt of this bis-proto-triazolium macrocycle was prepared using Amberlite® resin for future anion templated [3]catenane synthesis. The ^{1}H NMR spectrum of macrocycle **94·$(Cl)_2$** is shown below (Figure 5.28).

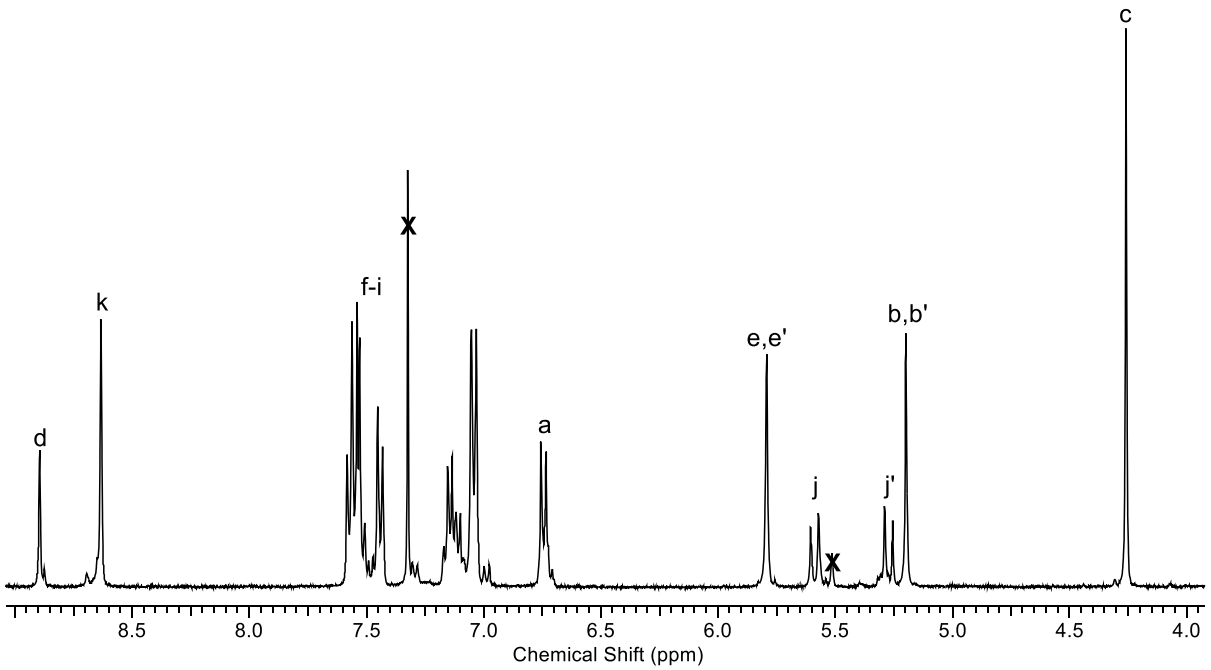


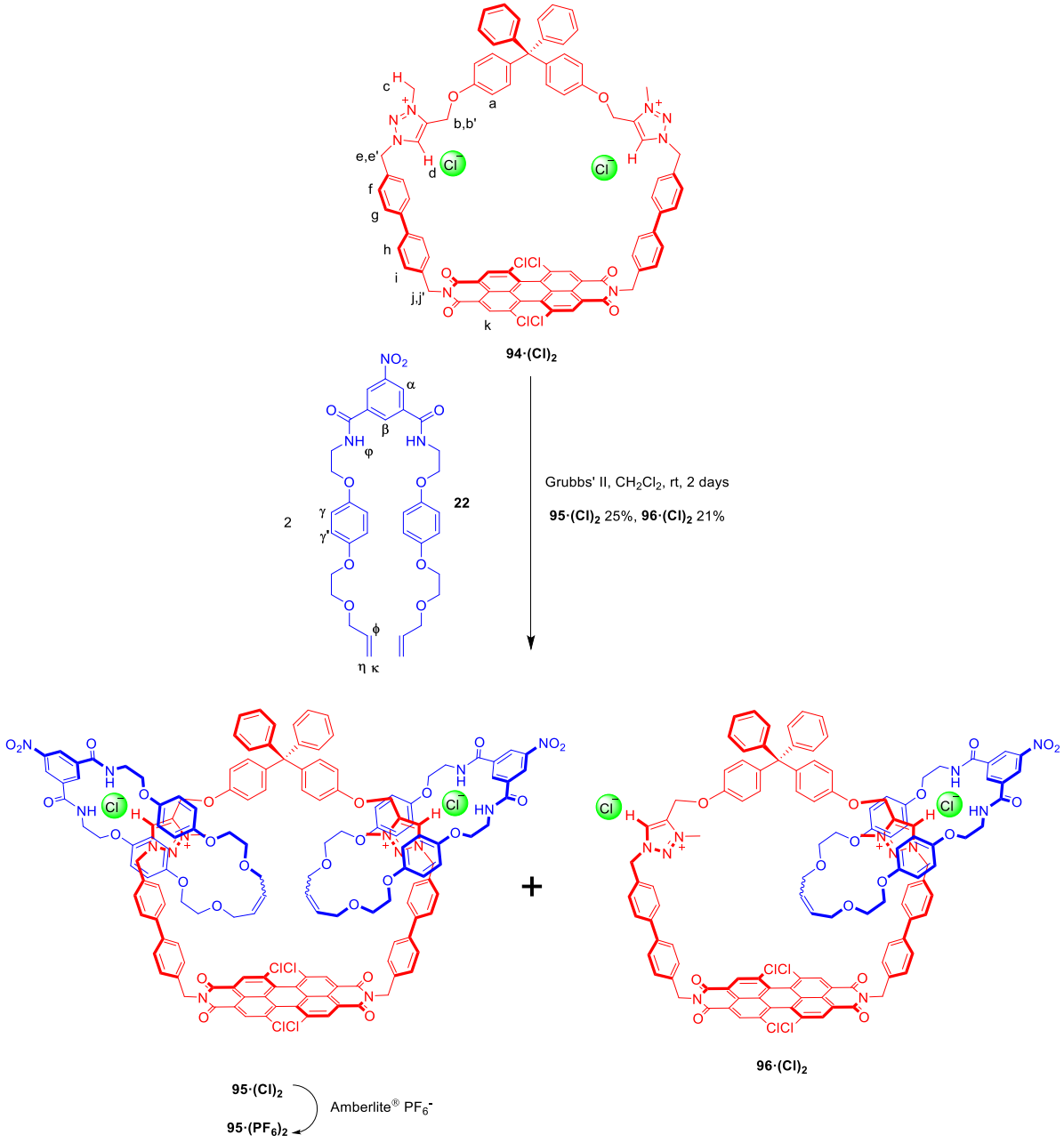
*Figure 5.28. Truncated ^{1}H NMR spectrum of PDI-containing macrocycle **94·$(Cl)_2$** ($CDCl_3$:CD_3OD, 298 K, 400 MHz).*

Analogous to the PDI-containing axle **89·$(Cl)_2$**, the macrocycle exists as a racemic mixture of two atropisomers and the ^{1}H NMR spectrum is relatively simple because protons $H_{a\text{-}i}$ and H_k are enantiotopic. However, the methylene group protons neighbouring the PDI unit (H_j and $H_{j'}$) are diastereotopic, giving two resonance signals (δ = 5.59 and 5.27 ppm) that each exhibit geminal coupling (^2J = 10 Hz). Presumably, this occurs because restricted rotation within the macrocycle framework causes H_j and $H_{j'}$ to experience different exposures to the aromatic ring currents of the PDI motif.

5.3.2. Synthesis of a four-station PDI-containing [3]catenane

Synthesis of the target PDI-containing [3]catenane was realised *via* the clipping of two bis-vinyl-appended macrocycle precursors **22** around macrocycle **94·$(Cl)_2$** in a chloride-templated RCM reaction

(Scheme 5.4). A solution of bis-proto-triazolium macrocycle **94·(Cl)$_2$** and three equivalents of isophthalamide-based macrocycle precursor **22** in dry CH_2Cl_2 was stirred for 30 minutes before Grubbs' II catalyst was added to effect a double RCM cyclisation. After two days the crude reaction mixture was subjected to preparative thin-layer chromatographic purification to afford the [3]catenane **95·(Cl)$_2$** in 25% yield. The bis-hexafluorophosphate salt was prepared by anion exchange. The analogous [2]catenane **96·(Cl)$_2$** was also isolated from the crude reaction mixture in 21% yield (Scheme 5.4).



*Scheme 5.4. Synthesis of PDI [3]catenane **95·(A)$_2$**.*

5.3.3. ^{1}H NMR spectroscopic studies of anion-induced shuttling behaviour in $CDCl_3$

^{1}H NMR spectroscopy was used to determine the predominant co-conformation of the bis-chloride salt of the [3]catenane in $CDCl_3$ by comparison of its ^{1}H NMR spectrum with that of the bis-vinyl isophthalamide-based macrocycle precursor **22** (Figure 5.29). Unfortunately, a comparison with the PDI macrocycle **94·(Cl)$_2$** was not possible because of poor solubility in $CDCl_3$ at suitable NMR concentrations.

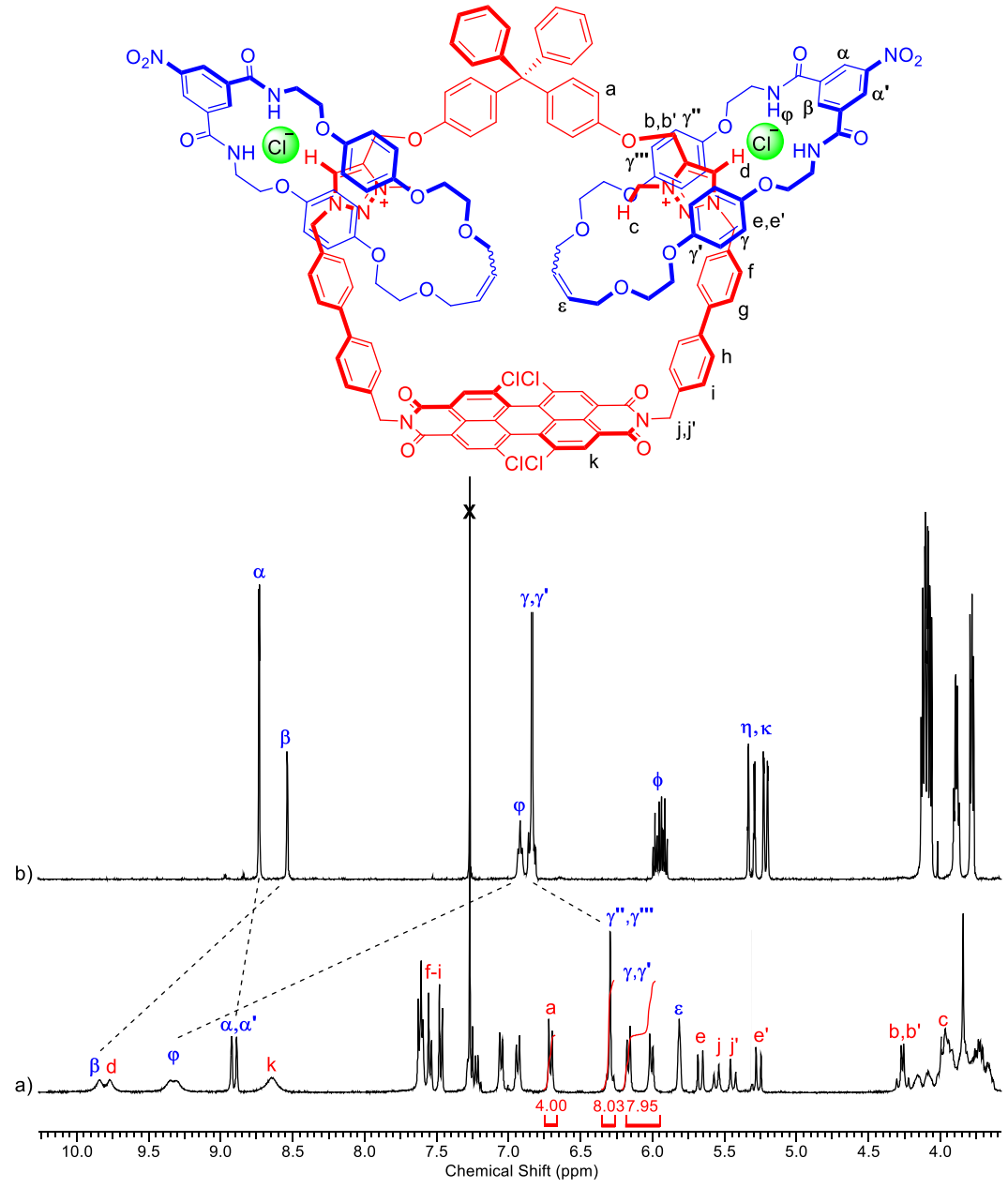


*Figure 5.29. Truncated ^{1}H NMR spectra of a) PDI [3]catenane **95·(Cl)$_2$** and b) bis-vinyl-appended macrocycle precursor **22** ($CDCl_3$, 298 K, 400 MHz).*

The resonances of protons H_β and H_φ are shifted downfield in [3]catenane **95·(Cl)$_2$** relative to the macrocycle precursor, indicating coordination of the templating chloride anion in the isophthalamide cavity. This occurs because, in identical fashion to the [3]rotaxane, each macrocycle resides at a proto-triazolium station. Interestingly, the co-conformation adopted by the [3]catenane forces the macrocycles to become de-symmetrised because a signal is seen for each of the external isophthalamide aromatic protons H_a and $H_{a'}$. This also explains why different sets of resonances are produced for each aromatic hydroquinone ring $H_{\gamma,\gamma'}$ and $H_{\gamma'',\gamma'''}$. The adoption of separate co-conformations by each isophthalamide macrocycle can be ruled out because the ^{1}H NMR spectrum of the [2]catenane also reveals de-symmetrisation of the macrocycle (*vide infra*).

While in PDI macrocycle **94·(Cl)$_2$** only the methylene protons H_j and $H_{j'}$ were diastereotopic, formation of **95·(Cl)$_2$** also causes H_e/$H_{e'}$ and H_b/$H_{b'}$ to split into separate signals, presumably because of the influence of the two interlocked isophthalamide macrocycles. Overall, this suggests a greater degree of steric constraint or crowding in the more rigid interlocked molecular architecture of the [3]catenane than the analogous [3]rotaxane.

The ^{1}H NMR spectrum of the [2]catenane in $CDCl_3$ is more complex than that of the [3]catenane (

Figure *5.30*): separate signals for the proto-triazolium protons H_b and $H_{b'}$ and the phenyl trityl aromatic protons H_a and $H_{a'}$ are observed. Therefore, the [2]catenane must adopt an asymmetric co-conformation in which the isophthalamide macrocycle cannot pass over either the phenyl trityl spacer or the tetrachloro PDI motif and so restricting its position to one half of the larger ring.

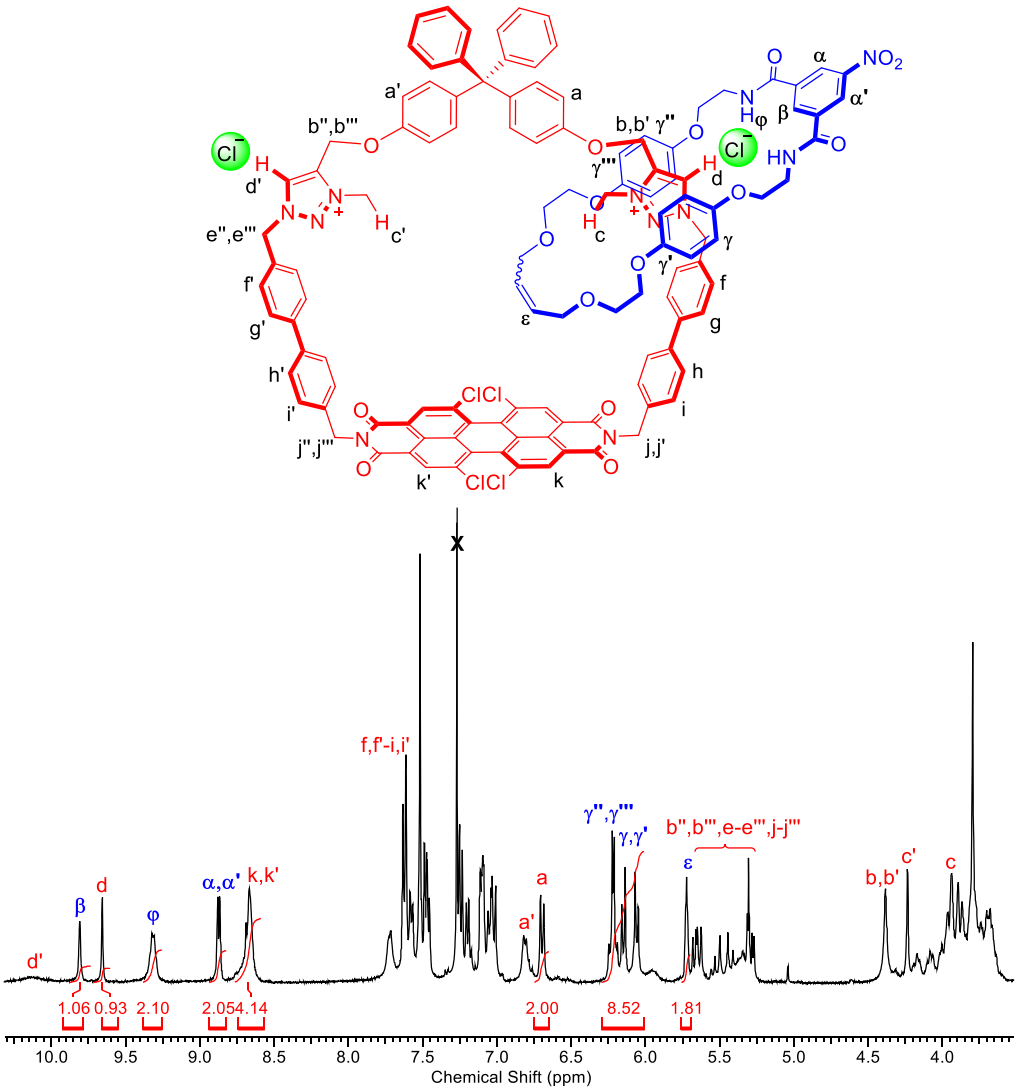


*Figure 5.30. Truncated ^{1}H NMR spectrum of PDI [2]catenane **96·(Cl)$_2$** ($CDCl_3$, 298 K, 400 MHz).*

The ^{1}H NMR spectra of **95·(Cl)$_2$** and **95·(PF$_6$)$_2$** in $CDCl_3$ were then compared to investigate if the removal of coordinating anions altered the co-conformation of the [3]catenane (Figure 5.31). In similar fashion to the [3]rotaxane the PDI proton resonances H_k were not shifted upon anion exchange, indicating negligible interactions between the two isophthalamide macrocycles and the PDI stations under these conditions. However, the equivalence of H_α and $H_{\alpha'}$ suggests that the absence of a coordinating anion enables the peripheral macrocycles to adopt a co-conformation that places the isophthalamide motifs in a more symmetric environment, while still residing at the proto-triazolium stations. As postulated for [3]rotaxane **90·(PF$_6$)$_2$**, one such arrangement might increase the strength of hydrogen bonding between the crown ether cavities of the two macrocycles and the *N*-methyl triazolium groups of the

central wheel. This would explain the downfield shift of H_c and also be responsible for the change in the splitting pattern of the hydroquinone resonances $H_{\gamma\text{-}\gamma'''}$.

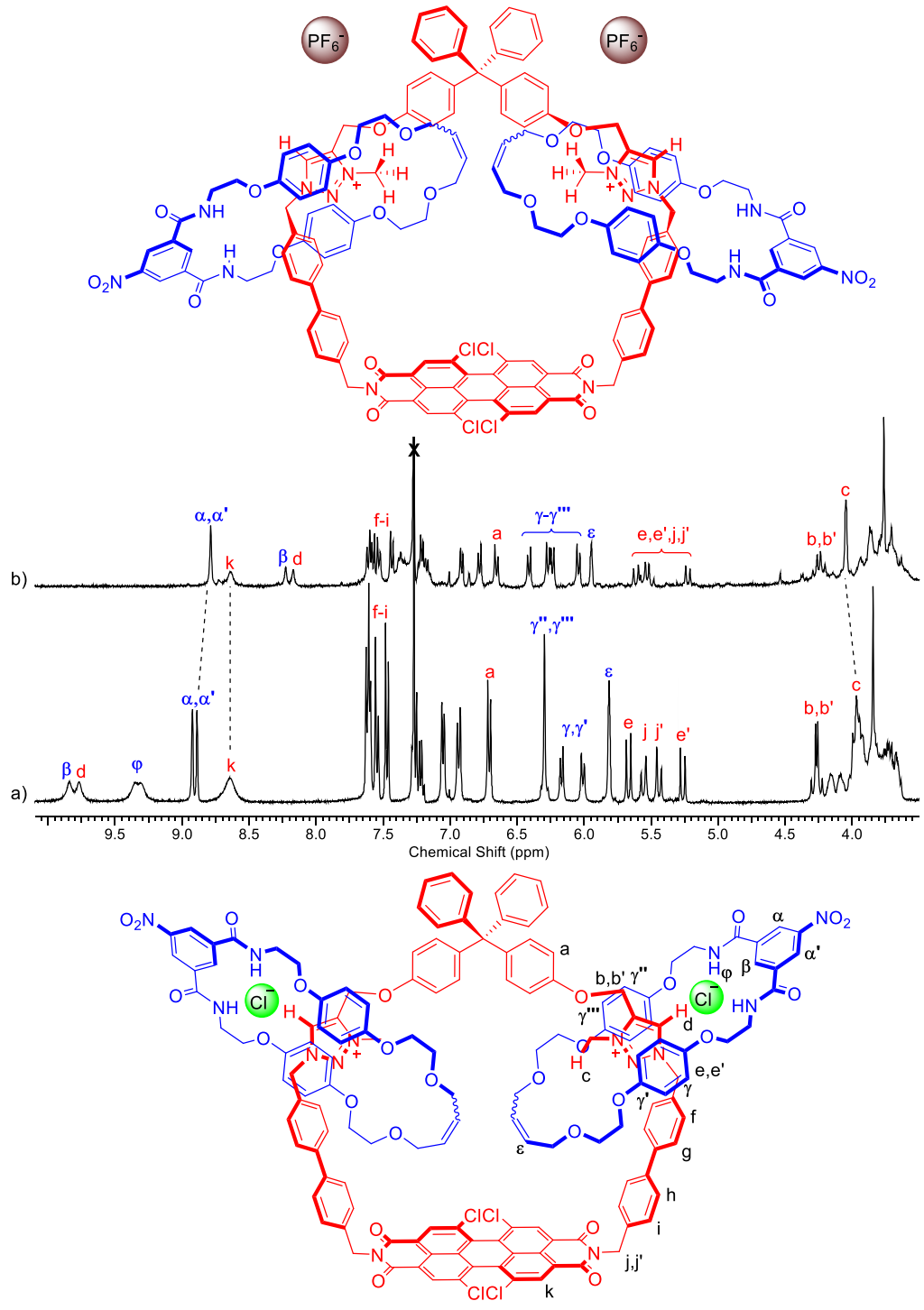


Figure 5.31. Truncated ^{1}H NMR spectra of a) bis-chloride and b) bis-hexafluorophosphate salts of [3]catenane ***95·(A)$_2$*** *($CDCl_3$, 298 K, 400 MHz). The predominant co-conformations of these [3]catenane salts are also depicted.*

5.3.4. ^{1}H NMR spectroscopic studies of anion-induced shuttling behaviour in 3:1 $CDCl_3$:CD_3OD

With the aim of inducing rotary motion of the peripheral macrocyclic wheels in [3]catenane **95·(A)$_2$** towards the PDI recognition sites of the central ring, ^{1}H NMR spectroscopy investigations of dynamic behaviour were conducted in the more polar solvent mixture of 3:1 $CDCl_3$:CD_3OD. In similar fashion to the [3]rotaxane **90·(Cl)$_2$**, CD_3OD caused the ^{1}H NMR spectrum of **95·(Cl)$_2$** to become more complex,** necessitating the use of ^{1}H–^{13}C HSQC NMR spectroscopy to assign the signals (Figure 5.32).

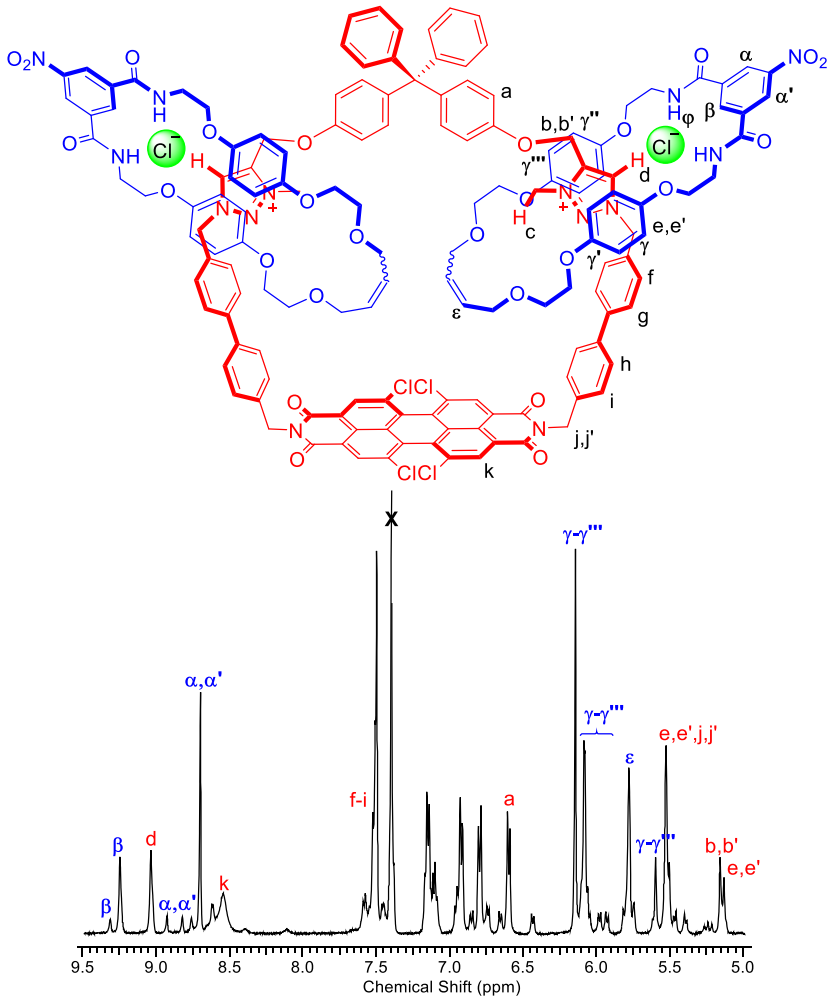


*Figure 5.32. Truncated ^{1}H NMR spectrum of [3]catenane **95·(Cl)$_2$** (3:1 $CDCl_3$:CD_3OD, 298 K, 400 MHz). The predominant co-conformation of the [3]catenane is also depicted.*

** Within this chapter the exact assignment of peaks in the ^{1}H NMR spectra of the PDI [3]catenane **95·(A)$_2$** in 3:1 $CDCl_3$:CD_3OD solution is a non-trivial task. Their complexity is most likely to be a combination of desymmetrisation and restricted motions of the macrocycle components, the latter causing co-conformations to exist in slow exchange on the NMR timescale.

The appearance of new signals suggests the peripheral rings of the [3]catenane are interacting with the PDI stations causing the formation of new co-conformations that are in slow exchange on the NMR timescale, and further de-symmetrisation of the macrocycles occurs, producing additional sets of diastereotopic protons. Importantly, the ^{1}H NMR spectrum of the central PDI-containing macrocycle is uncomplicated in 3:1 $CDCl_3$:CD_3OD, which eliminates the possibility that solvophobic-driven intermolecular aggregation of the PDI units is responsible for these changes.

Having demonstrated the potential of the PDI motif of [3]catenane **95·$(A)_2$** to act as a macrocycle recognition site by increasing the polarity of the solvent system, it was hoped that co-conformational switching of the peripheral isophthalamide macrocycles between stations might be modulated by changing the counter-anions. Therefore, the ^{1}H NMR spectra of **95·$(PF_6)_2$** and **95·$(Cl)_2$** were compared in 3:1 $CDCl_3$:CD_3OD (Figure 5.33).

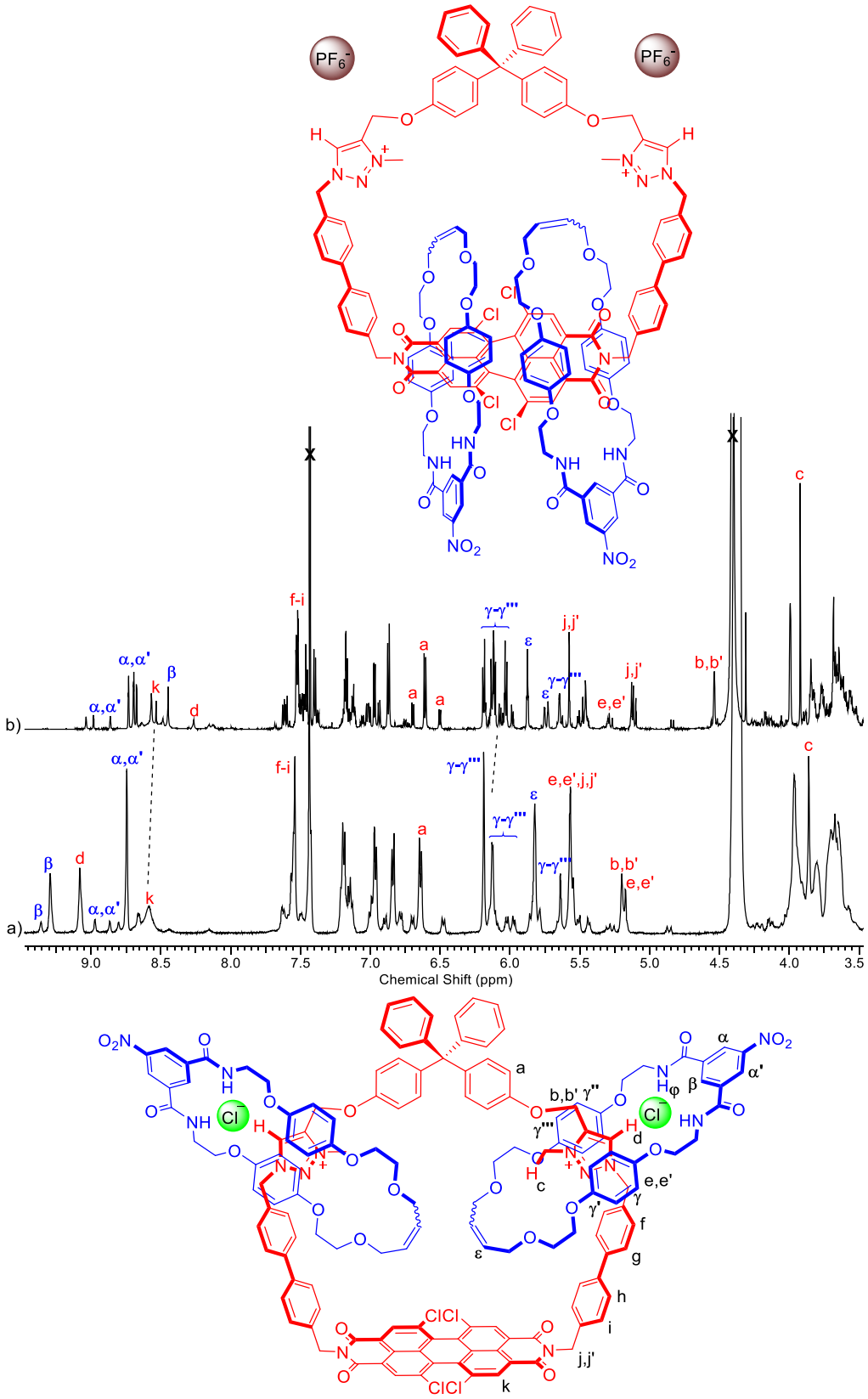


Figure 5.33. Truncated ^{1}H NMR spectra of a) bis-chloride and b) bis-hexafluorophosphate salts of [3]catenane ***95·(A)₂*** *(3:1 $CDCl_3$:CD_3OD, 298 K, 400 MHz). The predominant co-conformations of these [3]catenane salts are also depicted.*

The ^{1}H NMR spectrum of the [3]catenane **95·(PF$_6$)$_2$** exhibits further complexity upon anion exchange to the bis-hexafluorophosphate salt suggesting that, in the absence of coordinating anions, the isophthalamide-based macrocycles form stronger interactions with the PDI stations. In particular, the hydroquinone protons ($H_{\gamma\text{-}\gamma'''}$) of **95·(PF$_6$)$_2$** produce multiple signals, that overall shift upfield as a result of rotary co-conformational switching. The greater prevalence of aromatic stacking at the PDI stations is also indicated by a 0.05 ppm upfield shift of resonances associated with H_k. Importantly, this perturbation is the same magnitude as that observed upon anion exchange of the [3]rotaxane **90·(A)$_2$** in 3:1 $CDCl_3$:CD_3OD. However, the complexity of the ^{1}H NMR spectra makes it very difficult to use other diagnostic protons to track the position of the macrocyclic wheels and prevents quantitative analysis of the degree of station occupancy change.

However, two-dimensional ^{1}H ROESY NMR of **95·(Cl)$_2$** and **95·(PF$_6$)$_2$** in 3:1 $CDCl_3$:CD_3OD was used to further characterise predominant co-conformations of each salt of the [3]catenane. For the bis-chloride salt, though-space coupling interactions between macrocycle components indicated close proximity of $H_{\gamma\text{-}\gamma'''}$ to H_a and H_d suggesting a significant proportion of isophthalamide macrocycles reside at the proto-triazolium stations (Figure 5.34a). Although no couplings were observed between the macrocycle hydroquinone and PDI protons, the ^{1}H–^{1}H ROESY NMR spectrum of **95·(PF$_6$)$_2$** did reveal a new through-space interaction between H_k and H_ε (Figure 5.34b). This provided further evidence that in the absence of coordinating anions, a significant proportion of the peripheral macrocycles adopt co-conformations at the PDI stations of the [3]catenane courtesy of aromatic stacking interactions.

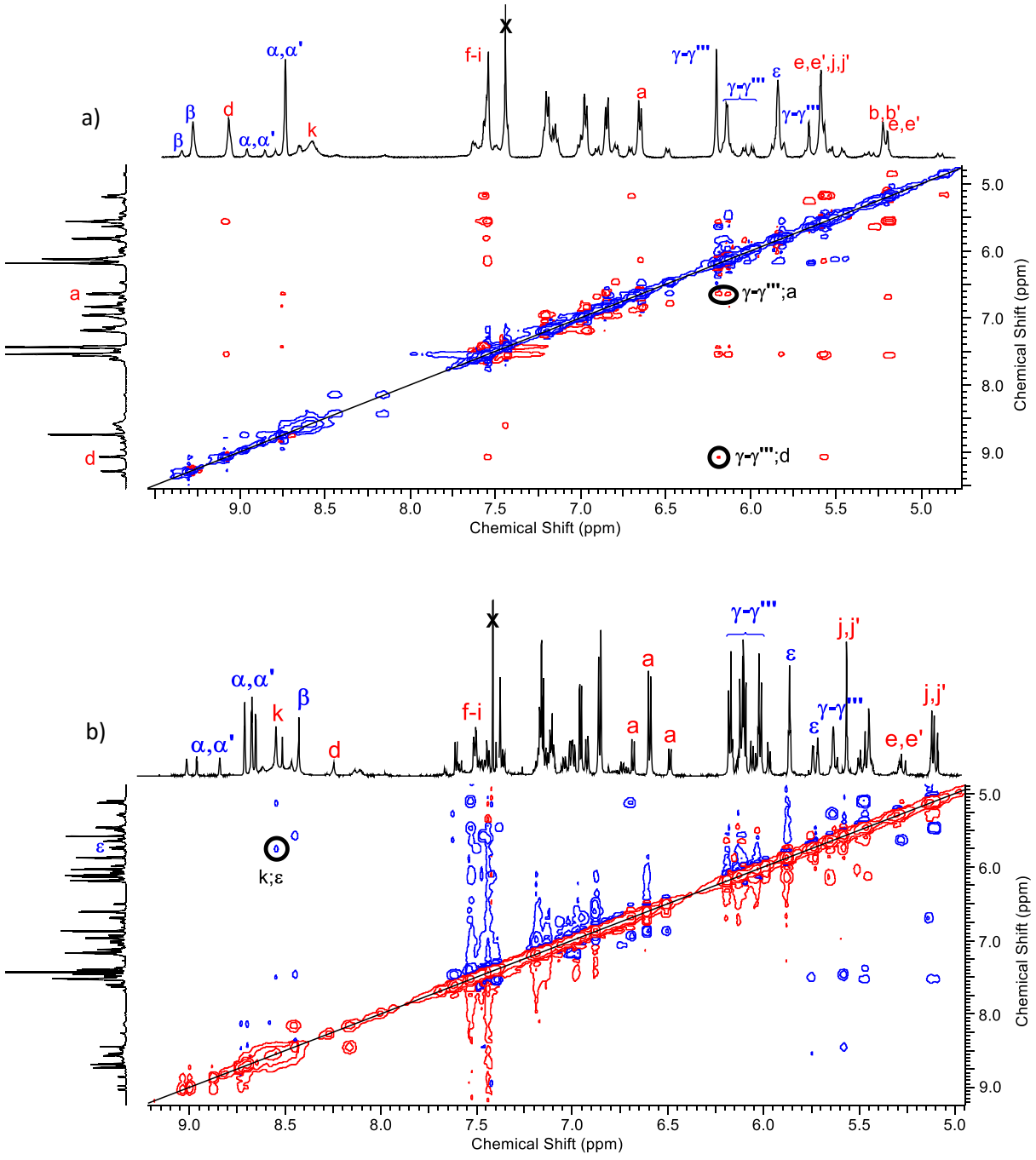


*Figure 5.34. Truncated ^{1}H–^{1}H ROESY NMR spectrum of PDI [3]catenane **95·(A)$_2$** as the a) bis-chloride and b) bis-hexafluorophosphate salts with selected coupling interactions highlighted (3:1 $CDCl_3$:CD_3OD, 298 K, 500 MHz).*

5.3.5. UV-Vis spectroscopic studies of anion-induced shuttling behaviour in 3:1 $CDCl_3$:CD_3OD

Following the ^{1}H NMR studies, UV-Vis spectroscopy was used to provide supplementary evidence that [3]catenane **95·(PF$_6$)$_2$** exhibits anion mediated rotary motion in 3:1 $CHCl_3$:CH_3OH. Analogous to the [3]rotaxane, a hypsochromic shift of the PDI absorption band occurs upon the titration of chloride into

95·$(PF_6)_2$ indicating the movement of isophthalamide macrocycles from the PDI stations to the proto-triazolium anion recognition sites upon addition of chloride (Figure 5.35). This loss of aromatic stacking interactions between hydroquinone groups and the PDI motif is manifested as a decrease in the intensity of charge–transfer absorptions at λ_{abs} > 550 nm. Therefore, colorimetric sensing of chloride by [3]catenane **95·$(PF_6)_2$** is realised *via* a vivid colour change from red to orange.

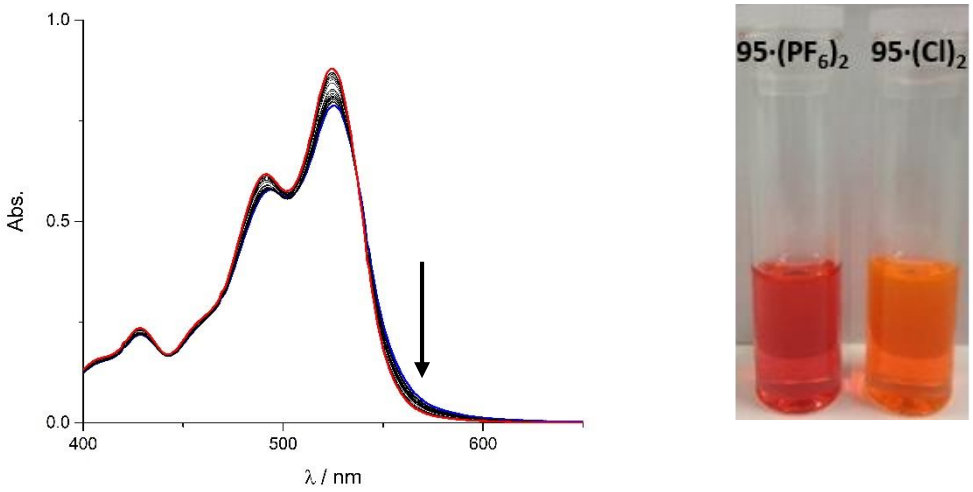


*Figure 5.35. Superimposed UV-Vis spectra of the PDI [3]catenane **95·$(PF_6)_2$** in 3:1 $CHCl_3$:CH_3OH (3×10^{-5} mol L^{-1}) showing the titration of up to 50 equivalents of tetrabutylammonium chloride. The addition of chloride leads to a decrease in intensity of the charge–transfer absorbance bands at λ_{abs} > 550 nm leading to a naked-eye colour change of the solution from red to orange.*

The same titration experiment with PDI macrocycle **94·$(BF_4)_2$** in 3:1 $CHCl_3$:CH_3OH produced negligible changes in respective absorption spectra, indicating that the changes occurring within the [3]catenane are due to chloride-induced co-conformational changes of the macrocycle components (Figure 5.36). Similarly, when the halide was added to a solution of the [3]catenane in $CHCl_3$, negligible changes in absorption were observed because, as demonstrated from the ^{1}H NMR spectroscopic analysis, rotary switching is not produced in this chlorinated solvent on account of weak aromatic solvophobic interactions between the PDI motif and the hydroquinones.

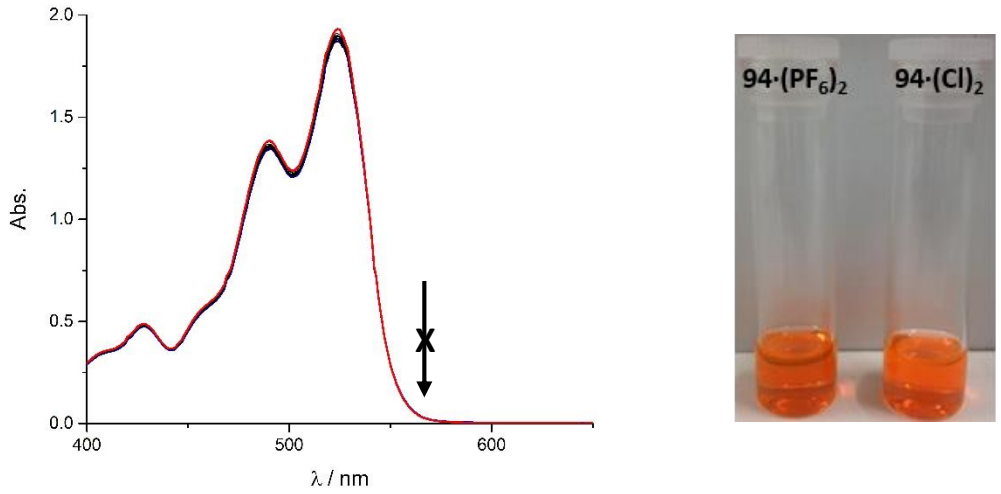


Figure 5.36. Superimposed UV-Vis spectra of the PDI macrocycle ***94·(BF4)2*** *in $CHCl_3$ (3×10^{-5} mol L^{-1}) showing the titration of up to 50 equivalents of tetrabutylammonium chloride. The addition of chloride leads to negligible changes in the absorption spectra which is manifested as no observable colour change in the solution.*

5.4. Summary and future work

The work in this chapter describes the synthesis of a perylene diimide-containing [3]rotaxane and [3]catenane containing either a four-station axle or macrocycle component respectively. The four stations comprise of two proto-triazolium anion recognition groups and an electron-deficient tetrachloro PDI motif that is twisted at the core to effectively produce two naphthalimide sub-units.

^{1}H NMR and UV-Vis spectroscopic analysis demonstrated that the PDI stations only acted as recognition sites for the hydroquinone-containing macrocycles in polar solvents such as chloroform-methanol mixtures and DMSO-d_6, indicating the facial aromatic stacking between interlocked components is primarily driven by solvophobic effects. Therefore, the macrocycle occupancies of these stations could be tuned *via* solvent-stimulated shuttling. This is the first report of aromatic stacking interactions with a PDI motif being used to control the co-conformation of a rotaxane or a catenane.

In addition, chloride anions were also demonstrated to act as stimuli to effect molecular motion in these dynamic systems in methanol-chloroform solvent mixtures. As the bis-hexafluorophosphate salts, both the [3]rotaxane and [3]catenane indicated significant macrocycle occupancy of the PDI

stations, enabling molecular shuttling to occur towards the proto-triazolium stations upon the addition of chloride, driven by halide recognition *via* hydrogen bonding. For the [3]rotaxane, this produced translational motion of the macrocycle components; however, highly novel rotary motion of the peripheral rings was exhibited in the case of the [3]catenane. This is the first example of such anion-directed dynamic behaviour in a higher-order catenane molecular architecture.

Finally, the characteristic absorption of PDI, and the unique mechanism of chloride recognition employed by the [3]rotaxane and [3]catenane, was utilised to optically sense this negatively-charged species by means of a naked-eye colour change from red to orange. It is anticipated that the introduction of ferrocenyl groups to the macrocycle components will enable these systems to elicit a turn-on fluorescence response for anions as well. Further into the future, the controlled interfacing of such systems with surfaces will generate molecular devices capable of, amongst many other applications, exquisite sensing properties.

5.5. References

1 F. Würthner, *Chem. Commun.*, 2004, 1564–1579.
2 F. Würthner, C. R. Saha-Möller, B. Fimmel, S. Ogi, P. Leowanawat and D. Schmidt, *Chem. Rev.*, 2016, **116**, 962–1052.
3 H. Langhals, *Heterocycles*, 1995, **40**, 477.
4 E. Shirman, A. Ustinov, N. Ben-Shitrit, H. Weissman, M. A. Iron, R. Cohen and B. Rybtchinski, *J. Phys. Chem. B*, 2008, **112**, 8855–8858.
5 R. O. Marcon and S. Brochsztain, *Langmuir*, 2007, **23**, 11972–11976.
6 S. K. Lee, Y. Zu, A. Herrmann, Y. Geerts, K. Müllen and A. J. Bard, *J. Am. Chem. Soc.*, 1999, **121**, 3513–3520.
7 P. Spenst and F. Würthner, *Angew. Chem. Int. Ed.*, 2015, **54**, 10165–10168.
8 F. Würthner, C. Thalacker, S. Diele and C. Tschierske, *Chem. – Eur. J.*, 2001, **7**, 2245–2253.
9 Z. Chen, B. Fimmel and F. Würthner, *Org. Biomol. Chem.*, 2012, **10**, 5845–5855.
10 M. S. Cubberley and B. L. Iverson, *J. Am. Chem. Soc.*, 2001, **123**, 7560–7563.
11 P. Osswald and F. Würthner, *J. Am. Chem. Soc.*, 2007, **129**, 14319–14326.
12 Z. Chen, M. G. Debije, T. Debaerdemaeker, P. Osswald and F. Würthner, *ChemPhysChem*, 2004, **5**, 137–140.
13 E. L. Eliel, S. H. Wilen and L. N. Mander, *Stereochemistry of organic compounds*, Wiley & Sons, 1994.
14 C. Lemouchi, S. Simonov, L. Zorina, C. Gautier, P. Hudhomme and P. Batail, *Org. Biomol. Chem.*, 2011, **9**, 8096–8101.
15 J. Baggerman, D. C. Jagesar, R. A. L. Vallée, J. Hofkens, F. C. De Schryver, F. Schelhase, F. Vögtle and A. M. Brouwer, *Chem. – Eur. J.*, 2007, **13**, 1291–1299.
16 Y. Li, H. Li, Y. Li, H. Liu, S. Wang, X. He, N. Wang and D. Zhu, *Org. Lett.*, 2005, **7**, 4835–4838.

17 B. J. Slater, E. S. Davies, S. P. Argent, H. Nowell, W. Lewis, A. J. Blake and N. R. Champness, *Chem. – Eur. J.*, 2011, **17**, 14746–14751.
18 W. Wang, L. Wang, B. J. Palmer, G. J. Exarhos and A. D. Q. Li, *J. Am. Chem. Soc.*, 2006, **128**, 11150–11159.
19 S. A. Boer, C. S. Hawes and D. R. Turner, *Chem. Commun.*, 2013, **50**, 1125–1127.
20 W. Wang, A. D. Shaller and A. D. Q. Li, *J. Am. Chem. Soc.*, 2008, **130**, 8271–8279.
21 S. Erbas-Cakmak, D. A. Leigh, C. T. McTernan and A. L. Nussbaumer, *Chem. Rev.*, 2015, **115**, 10081–10206.
22 A. Andrievsky, F. Ahuis, J. L. Sessler, F. Vögtle, D. Gudat and M. Moini, *J. Am. Chem. Soc.*, 1998, **120**, 9712–9713.
23 N. H. Evans, C. J. Serpell and P. D. Beer, *Chem. – Eur. J.*, 2011, **17**, 7734–7738.
24 B. E. Partridge, P. Leowanawat, E. Aqad, M. R. Imam, H.-J. Sun, M. Peterca, P. A. Heiney, R. Graf, H. W. Spiess, X. Zeng, G. Ungar and V. Percec, *J. Am. Chem. Soc.*, 2015, **137**, 5210–5224.
25 A. Wicklein, A. Lang, M. Muth and M. Thelakkat, *J. Am. Chem. Soc.*, 2009, **131**, 14442–14453.

Chapter Six
Experimental

6. EXPERIMENTAL

6.1. General Considerations

6.1.1. Reactants and reagents

All commercial solvents and reagents were used as purchased, unless otherwise stated. "Dry" solvents were purged with $N_{2(g)}$ and passed through an MBraun MPSP-800 column prior to use. Water was micro-filtered and de-ionised using Milli-Q Millipore equipment. For preservation, all TBA salts, $Cu(CH_3CN)_4 \cdot PF_6$ and Grubbs' II catalyst were stored in a vacuum desiccator with P_4O_{10}. Et_3N was distilled from and stored over $KOH_{(s)}$ pellets. Chromatography was undertaken using silica gel (particle size: 40-63 μm) or preparative TLC plates (20 × 20 cm, 1 cm silica thickness). Literature procedures were used to prepare known compounds, as referenced in the text. In addition, TBTA[1] was prepared by Mr. T. Mole and Dr. A. Brown, ethynyl ferrocene and the ferrocene-appended macrocycle precursor used in synthesis of rotaxanes **78·Cl** and **82·(Cl)$_2$** by Mr. J. Lim and the C_{60} fullerene bis-alkyne **79**[2] by Mr. I. Rasovic.

6.1.2. Characterisation and instrumentation

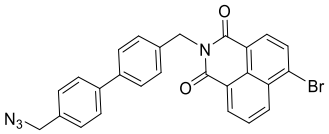
^1H, ^{13}C, ^{19}F and ^{31}P NMR spectra were recorded using Varian Mercury 300, Bruker AVIII400 and Bruker AVIII500 spectrometers at 298 K. For compounds with poor solubility or a low available mass, a Bruker AVII 500 with a $^{13}C(^1H)$ Cryoprobe was used. Spectra are all referenced to the residual solvent peak,[3] and in the cases where mixed solvents have been used, the spectra were referenced to the solvent component with the most deuterium atoms. ^1H–^1H coupling constants are reported as 3-bond (^3J) unless otherwise indicated and assignments were aided by the use of two-dimensional ROESY and COSY NMR spectroscopies. Mass spectra were recorded on Waters LCT Premier, Waters MALDI Micro MX or a Bruker μTOF instruments. A Biotage Initiator 2.0 microwave was used to perform dielectric microwave heating.

6.1.3. General procedure for anion exchange

Compounds were anion exchanged either by washing with an aqueous solution of the ammonium salt of the desired anion (as specified in the synthetic procedures), or, most commonly, using a column containing an Amberlite® ion exchange resin that had been loaded with the desired anion. Amberlite® was "loaded" by washing the resin with $NaOH_{(aq)}$ (10%), H_2O, and either $NH_4Cl_{(aq)}$ (1 M), $NH_4I_{(aq)}$ (1 M) or $NH_4PF_{6(aq)}$ (0.1 M), followed by further H_2O, and the solvent mixture to be used in the anion exchange. The compound was then dissolved in 10 - 20 mL of the solvent mixture of choice and passed through the column at least three times to achieve complete anion exchange. After this the solvent was removed *in vacuo*, the residue re-dissolved in $CHCl_3$ (5 - 10 mL) and washed with H_2O (5 - 10 mL). After drying the organic phase over anhydrous $MgSO_4$ the solvent was removed *in vacuo* to give the exchanged product.

6.2. Synthesis and characterisation of novel compounds

Biphenyl naphthalimide azide 5



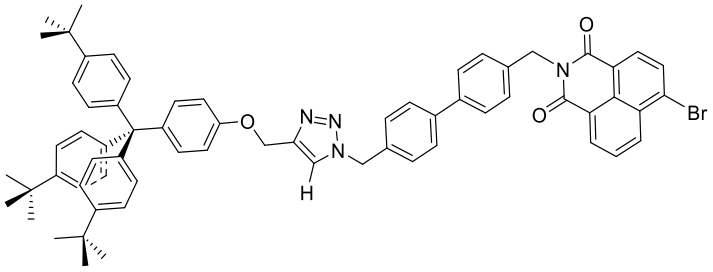
To a solution of 4-bromo-1,8-naphthalic anhydride (194 mg, 0.70 mmol, 1 eq) in degassed 1,4-dioxane (20 mL) was added biphenyl amine azide **4** (200 mg, 0.84 mmol, 1.2 eq) which was heated to 120 °C overnight under $N_{2(g)}$. On cooling, H_2O (10 mL) was added and the resulting precipitate filtered using glass wool, washed with further H_2O (10 mL) and dried *in vacuo*. Purification by silica gel column chromatography (CH_2Cl_2) gave **5** as a yellow solid (277 mg, 0.56 mmol, 80%).

^{1}H NMR (400MHz, $CDCl_3$) δ = 8.70 (1H, d, *J* = 7.3 Hz, Ar*H* nap), 8.59 (1H, d, *J* = 8.4 Hz, Ar*H* nap), 8.46 (1H, d, *J* = 7.9 Hz, Ar*H* nap), 8.06 (1H, d, *J* = 7.8 Hz, Ar*H* nap), 7.86 (1H, dd, *J* = 8.3 Hz, *J* = 7.8 Hz, Ar*H* nap), 7.63 (2H, d, *J* = 8.2 Hz, Ar*H* biphenyl), 7.56 (2H, d, *J* = 8.2 Hz, Ar*H* biphenyl), 7.54 (2H, d, *J* = 8.2 Hz, Ar*H* biphenyl), 7.36 (2H, d, *J* = 8.2 Hz, Ar*H* biphenyl), 5.43 (2H, s, CH_2), 4.37 (2H, s, CH_2)

^{13}C NMR (101 MHz, $CDCl_3$) δ = 163.72, 140.66, 139.66, 136.10, 134.20, 133.48, 132.24, 131.40, 131.05, 130.54, 129.17, 128.88, 128.47, 128.02, 127.27, 127.01, 122.74, 121.86, 54.31, 43.24.

MS (ESI): m/z calc. for $C_{26}H_{17}BrN_4O_2$ $[M+H]^+$: 497.0608; found: 497.0616.

Mono-stoppered proto-triazole biphenyl bromo-naphthalimide 7



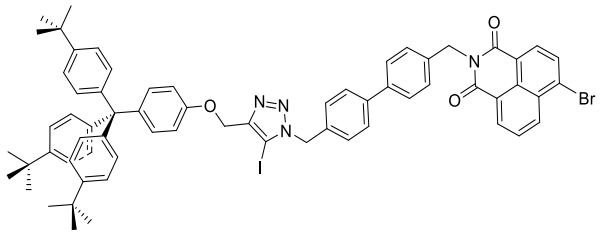
Azide **5** (100 mg, 0.20 mmol, 1 eq) and phenyl trityl stopper alkyne **6** (109 mg, 0.20 mmol, 1 eq) were dissolved in dry CH_2Cl_2 (6 mL), before TBTA (21 mg, 0.04 mmol, 0.2 eq), $Cu(CH_3CN)_4{\cdot}PF_6$ (15 mg, 0.04 mmol, 0.2 eq)and DIPEA (70 µL, 0.40 mmol, 2 eq) were added, in this order. The reaction was stirred overnight at room temperature over a flow of $N_{2(g)}$ and followed by purification of the crude mixture by silica gel chromatography without work-up to give proto-triazole naphthalimide thread **7** as an off-white solid (202 mg, 0.19 mmol, 97%).

^{1}H NMR (400MHz, $CDCl_3$) δ = 8.68 (1H, d, *J* = 7.3 Hz, Ar*H* nap), 8.58 (1H, d, *J* = 8.6 Hz, Ar*H* nap), 8.44 (1H, d, *J* = 7.8 Hz, Ar*H* nap), 8.04 (1H, d, *J* = 7.9 Hz, Ar*H* nap), 7.85 (1H, dd, *J* = 8.2 Hz, *J* = 7.3 Hz, Ar*H* nap), 7.62 (2H, d, *J* = 8.2 Hz, Ar*H* biphenyl), 7.56 (1H, s, Ar*H* triazole), 7.54 (2H, d, *J* = 8.3 Hz, Ar*H* biphenyl), 7.50 (2H, d, *J* = 8.3 Hz, Ar*H* biphenyl), 7.32 (2H, d, *J* = 8.2 Hz, Ar*H* biphenyl), 7.18 - 7.26 (6H, m, Ar*H* stopper), 7.04 - 7.13 (8H, m, Ar*H* stopper), 6.84 (2H, d, *J* = 8.3 Hz, Ar*H* stopper), 5.55 (2H, s, CH_2), 5.42 (2H, s, CH_2), 5.16 (2H, s, CH_2), 1.30 (27H, s, CH_3 stopper)

^{13}C NMR (101 MHz, $CDCl_3$) δ ppm = 164.1, 156.5, 148.9, 144.5, 144.4, 141.1, 139.6, 139.5, 138.3, 136.8, 136.1, 133.0, 132.9, 131.1, 131.0, 130.8, 130.4, 130.3, 130.2, 129.5, 129.0, 128.9, 128.1, 127.5, 126.7, 124.7, 124.5, 123.7, 122.8, 114.6, 114.6, 113.8, 113.8, 69.6, 63.6, 62.1, 44.2, 34.7, 31.7

MS (ESI): m/z calc. for $C_{66}H_{63}BrN_4O_3$ $[M+H]^+$: 1041.41; found: 1041.45.

Mono-stoppered iodo-triazole biphenyl bromo-naphthalimide 8



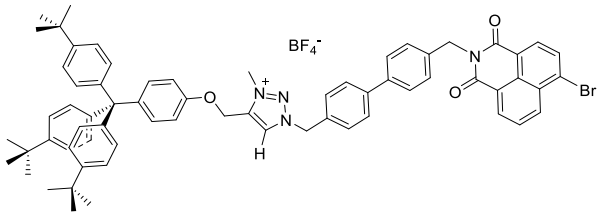
Azide **5** (50 mg, 0.10 mmol, 1 eq) was dissolved in THF (2 mL). NaI (60 mg, 0.40 mmol, 4 eq) and $Cu(ClO_4)_2{\cdot}H_2O$ (54.2 mg, 0.20 mmol, 2 eq) were added and the resulting suspension was left to stir for 5 minutes. TBTA (5.3 mg, 0.01 mmol, 0.1 eq) and DBU (15 mg, 0.1 mmol, 1 eq) were added to the mixture. Finally stopper alkyne **6** (54.2 mg, 0.10 mmol, 1 eq), CH_3CN (2 mL) and CH_2Cl_2 (10 drops) were added and the reaction was left to stir overnight. The crude mixture was then washed with 25% $NH_4OH_{(aq.)}$ and the organic phase collected, dried over anhydrous $MgSO_4$ and the solvent removed *in vacuo*. The resulting solid was purified by silica gel column chromatography (CH_2Cl_2:petroleum ether 4:1) and thread **8** isolated as an off-white solid (114 mg, 0.09 mmol, 98%).

^{1}H NMR (400MHz, $CDCl_3$) δ = 8.70 (1H, d, *J* = 7.3 Hz, Ar*H* nap), 8.59 (1H, d, *J* = 8.4 Hz, Ar*H* nap), 8.45 (1H, d, *J* = 7.9 Hz, Ar*H* nap), 8.06 (1H, d, *J* = 7.8 Hz, Ar*H* nap), 7.86 (1H, dd, *J* = 8.4 Hz, *J* = 7.3 Hz, Ar*H* nap), 7.61 (2H, d, *J* = 8.2 Hz, Ar*H* biphenyl), 7.52 (2H, d, *J* = 8.2 Hz, Ar*H* biphenyl), 7.50 (2H, d, *J* = 8.2 Hz, Ar*H* biphenyl), 7.34 (2H, d, *J* = 8.2 Hz, Ar*H* biphenyl), 7.23 (6H, d, *J* = 8.6 Hz, Ar*H* stopper), 7.04 - 7.14 (8H, m, Ar*H* stopper), 6.90 (2H, d, *J* = 8.9 Hz, Ar*H* stopper), 5.62 (2H, s, CH_2), 5.41 (2H, s, CH_2), 5.09 (2H, s, CH_2), 1.30 (27H, s, CH_3 stopper)

^{13}C NMR (101 MHz, $CDCl_3$) δ ppm = 163.66, 156.20, 148.31, 147.90, 144.05, 141.17, 140.28, 139.58, 136.46, 133.48, 132.96, 132.32, 132.25, 131.48, 131.15, 130.70, 130.51, 129.46, 129.06, 128.35, 128.12 , 127.98, 127.54, 127.18, 124.02, 123.03, 122.16, 113.55, 80.52, 63.06, 61.75, 53.98, 43.36, 34.26, 31.36.

MS (ESI): m/z calc. for $C_{66}H_{62}BrIN_4O_3$ $[M+Na]^+$: 1187.2942; found: 1187.2923

Mono-stoppered proto-triazolium biphenyl bromo-naphthalimide 9·BF_4



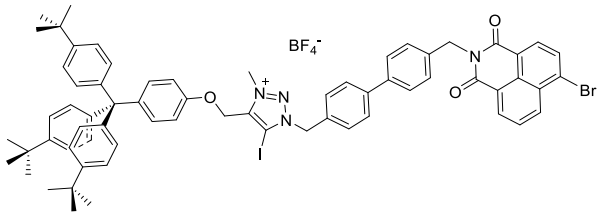
Proto-triazole compound **7** (200 mg, 0.19 mmol, 1 eq) and $Me_3O{\cdot}BF_4$ (20 mg, 0.15 mmol, 1.5 eq) were added to dry CH_2Cl_2 (10 mL). The solution was left to stir for two days at room temperature and over a flow of $N_{2(g)}$. After this time the reaction was quenched with three drops of MeOH and the solvent was subsequently removed *in vacuo*. The resulting solid was purified by silica gel column chromatography (CH_2Cl_2:MeOH 97:3) and **9·BF_4** isolated as a pale yellow solid (188 mg, 0.16 mmol, 84%).

^{1}H NMR (400MHz, $CDCl_3$) δ = 8.64 (1H, d, *J* = 7.2 Hz, Ar*H* nap), 8.56 (1H, d, *J* = 8.4 Hz, Ar*H* nap), 8.51 (1H, s, Ar*H* triazolium), 8.40 (1H, d, *J* = 7.9 Hz, Ar*H* nap), 8.02 (1H, d, *J* = 7.9 Hz, Ar*H* nap), 7.83 (1H, dd, *J* = 8.2 Hz, *J* = 7.3 Hz, Ar*H* nap), 7.42 - 7.60 (8H, m, Ar*H* biphenyl), 7.18 (6H, d, *J* = 8.6 Hz, Ar*H* stopper), 7.10 (2H, d, *J* = 8.2 Hz, Ar*H* stopper), 7.01 (6H, d, *J* = 8.6 Hz, Ar*H* stopper), 6.77 (2H, d, *J* = 8.2 Hz, Ar*H* stopper), 5.69 (2H, s, CH_2), 5.36 (2H, s, CH_2), 5.22 (2H, s, CH_2), 4.28 (3H, s, CH_3 triazolium), 1.25 (27H, s, CH_3 stopper)

^{13}C NMR (101 MHz, $CDCl_3$) δ ppm = 164.1, 156.5, 148.9, 144.5, 144.4, 141.1, 139.7, 139.5, 138.3, 136.8, 136.1, 133.0, 132.9, 132.1, 131.0, 130.8, 130.3, 130.3, 130.2, 129.5, 129.0, 128.9, 128.1, 127.5, 126.8, 124.7, 124.5, 123.7, 122.8, 114.6, 114.6, 113.8, 113.7, 69.6, 63.6, 62.1, 44.2, 34.7, 31.7

MS (ESI): m/z calc. for $C_{67}H_{66}BrN_4O_3$ $[M - BF_4]^+$: 1055.43; found: 1055.48

Mono-stoppered iodo-triazolium biphenyl bromo-naphthalimide 10·BF_4



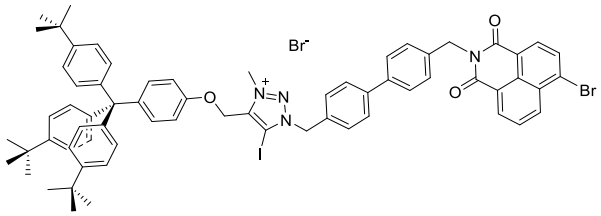
Iodo-triazole compound **8** (79 mg, 0.07 mmol, 1 eq) and $Me_3O·BF_4$ (15 mg, 0.11 mmol, 1.5 eq) were added to dry CH_2Cl_2 (5 mL). The solution was left to stir for two days at room temperature and over a flow of $N_{2(g)}$. After this time the reaction was quenched with three drops of MeOH and the solvent was subsequently removed *in vacuo*. The resulting solid was purified by silica gel column chromatography (CH_2Cl_2:MeOH 97:3) and **10·BF_4** isolated as a yellow solid (61 mg, 0.05 mmol, 76%).

^{1}H NMR (400MHz, 1:1 $CDCl_3$:MeOD) δ = 8.64 (1H, d, *J* = 6.4 Hz, Ar*H* nap), 8.57 (1H, d, *J* = 8.7 Hz, Ar*H* nap), 8.39 (1H, d, *J* = 7.9 Hz, Ar*H* nap), 8.03 (1H, d, *J* = 7.9 Hz, Ar*H* nap), 7.83 (1H, dd, *J* = 8.2 Hz, *J* = 7.6 Hz, Ar*H* nap), 7.51 - 7.57 (4H, m, Ar*H* biphenyl), 7.45 (2H, d, *J* = 8.1 Hz, Ar*H* biphenyl), 7.41 (2H, d, *J* = 8.2 Hz, Ar*H* biphenyl), 7.18 (6H, d, *J* = 8.6 Hz, Ar*H* stopper), 7.11 (2H, d, *J* = 8.0 Hz, Ar*H* stopper), 7.01 (6H, d, *J* = 8.6 Hz, Ar*H* stopper), 6.79 (2H, d, *J* = 8.1 Hz, Ar*H* stopper), 5.73 (2H, s, CH_2), 5.36 (2H, s, CH_2), 5.21 (2H, s, CH_2), 4.35 (3H, s, CH_3 triazolium), 1.23 (27H, s, CH_3 stopper)

^{13}C NMR (101 MHz, $CDCl_3$) δ ppm = 163.56, 154.76, 148.46, 147.74, 144.02, 143.75, 142.33, 142.06, 138.96, 136.83, 133.43, 132.67, 132.26, 131.42, 131.11, 130.62, 130.49, 129.47, 129.31, 128.96, 128.09, 127.93, 127.16, 124.13, 122.93, 122.05, 113.38, 89.17, 63.08, 59.22, 57.82, 53.39, 43.29, 39.48, 34.25, 31.33.

MS (ESI): m/z calc. for $C_{67}H_{65}BrIN_4O_3BF_4$ $[M - BF_4]^+$: 1179.3279; found: 1179.3312.

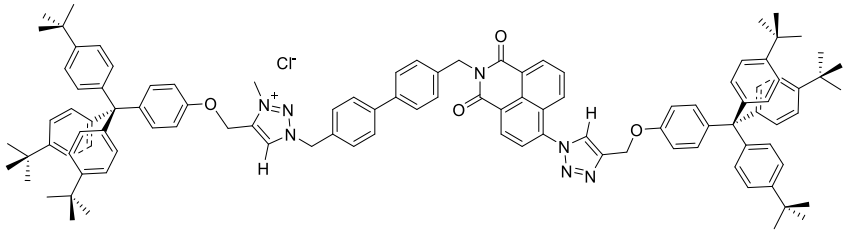
Mono-stoppered iodo-triazolium biphenyl bromo-naphthalimide 10·Br



10·BF$_4$ was anion-exchanged to the bromide salt **10·Br** using Amberlite® anion exchange resin. The solvent used was 45:45:10 $CHCl_3$:MeOH:H_2O (20 mL).

^{1}H NMR (400MHz, 1:1 $CDCl_3$:CD_3OD) δ = 8.64 (1H, dd, *J* = 7.3 Hz, ^{4}*J* = 1.0 Hz, Ar*H* nap), 8.57 (1H, dd, *J* = 8.6 Hz, ^{4}*J* = 1.0 Hz, Ar*H* nap), 8.39 (1H, d, *J* = 7.8 Hz, Ar*H* nap), 8.04 (1H, d, *J* = 7.9 Hz, Ar*H* nap), 7.84 (1H, dd, *J* = 8.5 Hz, *J* = 7.4 Hz, Ar*H* nap), 7.51 - 7.58 (4H, m, Ar*H* biphenyl), 7.41 - 7.48 (4H, m, Ar*H* biphenyl), 7.19 (6H, d, *J* = 8.6 Hz, Ar*H* stopper), 7.13 (2H, d, *J* = 8.3 Hz, Ar*H* stopper), 7.02 (6H, d, *J* = 8.6 Hz, Ar*H* stopper), 6.80 (2H, d, *J* = 8.3 Hz, Ar*H* stopper), 5.76 (2H, s, C*H*$_2$), 5.36 (2H, s, C*H*$_2$), 5.25 (2H, s, C*H*$_2$), 4.37 (3H, s, C*H*$_3$ triazolium), 1.24 (27H, s, C*H*$_3$ stopper)

Naphthalimide–proto-triazolium axle 18·Cl



To a suspension of NaN_3 (7 mg, 0.11 mmol, 1.2 eq) in degassed NMP (1 mL) in a microwave vial was added bromo-naphthalimide derivative **9·BF$_4$** (100 mg, 0.09 mmol, 1 eq). The vial was purged with $N_{2(g)}$, sealed and stirred in the absence of light for one day. After this, a solution of phenyl trityl stopper alkyne **6** (49 mg, 0.09 mmol, 1 eq) in 2:1 $CHCl_3$:EtOH (1.2 mL) was added followed by TBTA (0.01 mmol, 0.1 eq), $Cu(CH_3CN)_4{\cdot}PF_6$ (12 mg, 0.03 mmol, 0.3 eq) and DIPEA (20 µL, 0.10 mmol, 1 eq) and left to stir at room temperature, in the dark, for two days. The reaction was worked-up with 25% $NH_4OH_{(aq.)}$ (2 mL) and the organic products extracted with EtOAc (3 x 5 mL). This organic layer was washed with H_2O

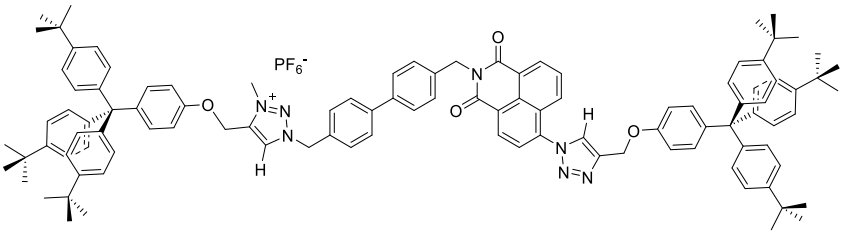
(3 x 15 mL), brine (2 x 15 mL), dried over anhydrous $MgSO_4$ and then the solvent removed *in vacuo*. The solid residue was purified using silica gel column chromatography (CH_2Cl_2:MeOH 98:2) to give **18·BF₄** (49 mg, 0.03 mmol). Anion exchange to the chloride salt was achieved by dissolving **18·BF₄** in CH_2Cl_2 (15 mL) and washing with 1 M $NH_4Cl_{(aq.)}$ (8 × 10 mL) and H_2O (2 × 10 mL). The organic layers were combined and dried over anhydrous $MgSO_4$. The solvent removed *in vacuo* to give **18·Cl** as an off-white solid (48 mg, 0.03 mmol, 30%).

^{1}H NMR (400MHz, $CDCl_3$) δ = 10.10 (1H, br. s., Ar*H* triazolium), 8.69 - 8.80 (2H, m, Ar*H* nap), 8.27 (1H, d, *J* = 8.2 Hz, Ar*H* nap), 8.10 (1H, s, Ar*H* triazole), 7.82 - 7.89 (2H, m, Ar*H* nap), 7.61 - 7.70 (4H, m, Ar*H* biphenyl), 7.59 (2H, d, *J* = 8.1 Hz, Ar*H* biphenyl), 7.51 (2H, d, *J* = 8.2 Hz, Ar*H* biphenyl), 7.20 - 7.26 (12H, m, Ar*H* stopper), 7.12 - 7.19 (4H, m, Ar*H* stopper), 7.02 - 7.12 (12H, m, Ar*H* stopper), 6.93 (2H, d, *J* = 9.0 Hz, Ar*H* stopper), 6.83 (2H, d, *J* = 8.8 Hz, Ar*H* stopper), 6.02 (2H, br. s., C*H*$_2$), 5.45 (2H, s, C*H*$_2$), 5.40 (2H, br. s., C*H*$_2$), 5.37 (2H, s, C*H*$_2$), 4.36 (3H, s, C*H*$_3$ triazolium), 1.31 (27H, s, C*H*$_3$ stopper), 1.30 (27H, s, C*H*$_3$ stopper)

^{13}C NMR (126MHz, 1:1 $CDCl_3$:CD_3OD) δ = 165.6, 165.3, 164.1, 156.5, 149.1, 149.0, 148.9, 145.3, 144.5, 144.4, 142.7, 142.4, 141.1, 139.6, 139.5, 138.3, 136.8, 136.1, 133.0, 132.9, 131.1, 131.0, 130.8, 130.4, 130.3, 130.2, 129.5, 129.0, 128.9, 128.1, 127.5, 126.7, 124.7, 124.5, 123.7, 122.8, 114.6, 114.6, 113.8, 113.8, 69.6, 67.8, 66.5, 63.6, 62.1, 44.2, 34.7, 31.7

MS (ESI): m/z calc. for $C_{107}H_{112}N_7O_4Cl$ $[M - Cl]^+$: 1559.88; found: 1559.95.

Naphthalimide–proto-triazolium axle 18·PF₆



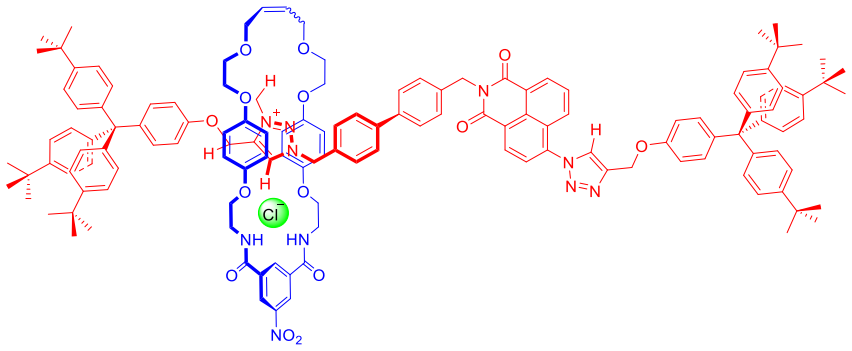
18·Cl was anion-exchanged to the hexafluorophosphate salt **18·PF₆** using Amberlite® anion exchange resin. The solvent used was 45:45:10 $CHCl_3$:MeOH:H_2O (20 mL).

^{1}H NMR (400MHz, $CDCl_3$) δ = 8.72 - 8.77 (2H, m, Ar*H* nap), 8.25 - 8.30 (2H, m, Ar*H* nap, triazolium), 8.10 (1H, s, Ar*H* triazole), 7.81 - 7.88 (2H, m, Ar*H* nap), 7.59 - 7.68 (4H, m, Ar*H* biphenyl), 7.46 - 7.55 (4H, m, Ar*H* biphenyl), 7.20 - 7.26 (12H, m, Ar*H* stopper), 7.15 (4H, dd, *J* = 8.9 Hz, *J* = 5.7 Hz, Ar*H* stopper), 7.00 - 7.12 (12H, m, Ar*H* stopper), 6.93 (2H, d, *J* = 9.0 Hz, Ar*H* stopper), 6.79 (2H, d, *J* = 8.9 Hz, Ar*H* stopper), 5.70 (2H, s, CH_2), 5.45 (2H, s, CH_2), 5.37 (2H, s, CH_2), 5.23 (2H, s, CH_2), 4.34 (3H, s, CH_3 triazolium), 1.30 (54H, s, CH_3 stopper)

^{19}F NMR (470 MHz, $CDCl_3$) δ = -72.4 (d, ^{1}J = 709 Hz, PF_6).

^{31}P NMR (202 MHz, $CDCl_3$) δ = -144.3 (sept, ^{1}J = 709 Hz, *P*F_6).

Naphthalimide–proto-triazolium [2]rotaxane 23·Cl



Axle **18·Cl** (30 mg, 19 µmol, 1 eq) and macrocycle precursor **22** (17 mg, 0.03 mmol, 1.4 eq) were dissolved in dry CH_2Cl_2 (2 mL) and stirred for 30 minutes. After this time, Grubbs' II catalyst (1.7 mg, 10 wt. %) was added and the solution stirred for a further two days at room temperature. The solvent was then removed in vacuo and the crude residue exposed to preparative silica TLC (EtOAc:MeOH 92.5:7.5) to give the [2]rotaxane **23·Cl** as an off-white solid (16 mg, 7 µmol, 38%).

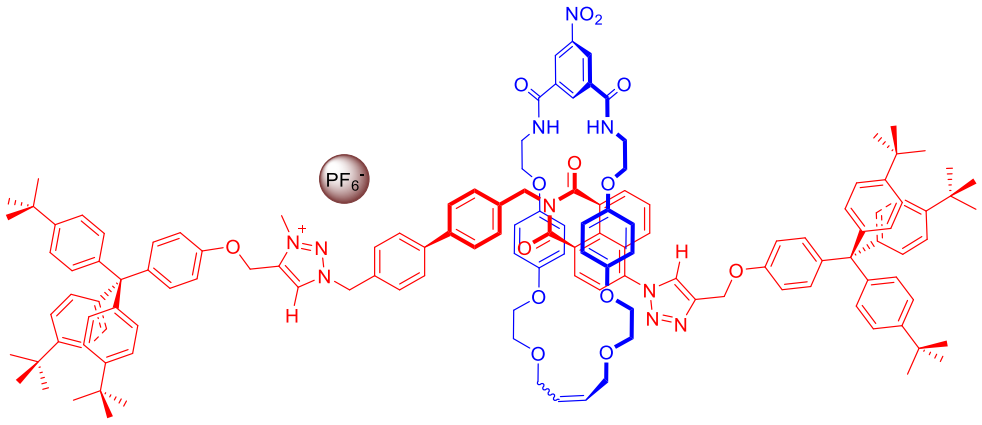
^{1}H NMR (400MHz, $CDCl_3$) δ = 9.70 (1H, br. s., Ar*H* int. macro), 9.52 (1H, s, Ar*H* triazolium), 9.34 (2H, d, *J* = 6.4 Hz, N*H* macro), 8.78 (2H, s, Ar*H* ext. macro), 8.71 - 8.77 (2H, m, Ar*H* nap), 8.26 (1H, d, *J* = 8.4 Hz, Ar*H* nap), 8.11 (1H, s, Ar*H* triazole), 7.80 - 7.90 (2H, m, Ar*H* nap), 7.67 (2H, d, *J* = 8.2 Hz, Ar*H* biphenyl), 7.50 (2H, d, *J* = 8.2 Hz, Ar*H* biphenyl), 7.38 (2H, d, *J* = 8.1 Hz, Ar*H* biphenyl), 7.31 (2H, d, *J* = 8.2 Hz, Ar*H* biphenyl), 7.20 - 7.26 (12H, m, Ar*H* stopper), 7.06 - 7.20 (16H, m, Ar*H* stopper), 7.00 (2H, d, *J* = 8.2 Hz,

Ar*H* stopper), 6.93 (2H, d, *J* = 8.9 Hz, Ar*H* stopper), 6.30 - 6.42 (8H, m, Ar*H* hydroquinone macro), 5.53 (2H, br. s., C*H* alkene macro), 5.46 (2H, s, CH_2 axle), 5.37 (2H, s, CH_2 axle), 5.25 (2H, s, CH_2 axle), 4.70 (2H, s, CH_2 axle), 4.61 (2H, t, *J* = 9.4 Hz, CH_2 macro), 4.41 - 4.54 (2H, m, CH_2 macro), 3.90 - 3.98 (2H, m, CH_2 macro), 3.88 (3H, s, CH_3 triazolium), 3.81 - 3.86 (4H, m, CH_2 macro), 3.62 - 3.81 (8H, m, CH_2 macro), 3.49 - 3.59 (2H, m, CH_2 macro), 1.31 (54H, s, CH_3 stopper)

^{13}C NMR (126MHz, 1:1 $CDCl_3$:CD_3OD) δ = 165.6, 165.3, 164.1, 156.5, 155.4, 152.6, 152.5, 149.1, 149.0, 148.9, 145.3, 144.5, 144.4, 142.7, 142.4, 141.1, 139.6, 139.5, 138.3, 136.8, 136.1, 133.0, 132.9, 131.1, 131.0, 130.8, 130.4, 130.3, 130.2, 129.5, 129.0, 128.9, 128.1, 127.5, 126.7, 126.5, 124.7, 124.5, 123.7, 122.8, 114.6, 114.6, 113.8, 113.8, 71.2, 69.6, 67.8, 66.5, 63.6, 63.5, 62.1, 58.1, 57.3, 44.2, 41.0, 39.1, 34.7, 34.7, 31.7

MS (ESI): m/z calc. for $C_{139}H_{147}N_{10}O_{14}Cl$ $[M - Cl]^+$: 2181.76; found: 2181.27.

Naphthalimide–proto-triazolium [2]rotaxane 23·PF$_6$



23·Cl was anion-exchanged to the hexafluorophosphate salt **23·PF$_6$** using Amberlite® anion exchange resin. The solvent used was 45:45:10 $CHCl_3$:MeOH:H_2O (10 mL).

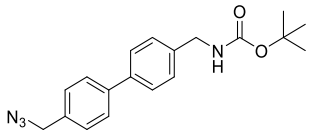
^{1}H NMR (500MHz, $CDCl_3$) δ = 8.89 - 8.96 (3H, m, Ar*H* macro), 8.45 - 8.55 (2H, m, Ar*H* nap, triazole), 8.35 (1H, d, *J* = 8.2 Hz, Ar*H* nap), 8.26 - 8.31 (2H, m, Ar*H* nap, triazolium), 7.89 (1H, d, *J* = 7.9 Hz, Ar*H* nap), 7.78 (1H, dd, *J* = 8.2 Hz, *J* = 7.9 Hz, Ar*H* nap), 7.58 (2H, d, *J* = 8.2 Hz, Ar*H* biphenyl), 7.40 - 7.50 (6H, m, Ar*H* biphenyl), 7.21 - 7.25 (8H, m, Ar*H* stopper), 7.14 - 7.21 (4H, m, Ar*H* stopper), 7.04 - 7.12 (16H, m,

Ar*H* stopper), 6.98 (2H, d, *J* = 8.9 Hz, Ar*H* stopper), 6.82 (2H, d, *J* = 8.8 Hz, Ar*H* stopper), 5.94 (8H, br. s., Ar*H* hydroquinone macro), 5.60 (2H, br. s., C*H* alkene macro), 5.41 (2H, s, CH_2 axle), 5.28 (2H, s, CH_2 axle), 5.11 (2H, s, CH_2 axle), 4.21 (2H, s, CH_2 axle), 3.90 - 3.99 (4H, m, CH_2 macro), 3.84 (2H, br. s., CH_2 macro), 3.55 - 3.70 (17H, m, CH_2 macro, CH_3 triazolium), 1.30 (54H, s, CH_3 stopper)

^{19}F NMR (470 MHz, $CDCl_3$) δ = -72.4 (d, ^1J = 708 Hz, PF_6).

^{31}P NMR (202 MHz, $CDCl_3$) δ = -144.3 (sept, ^1J = 710 Hz, *P*F_6).

Biphenyl mono azide Boc-protected amine 28



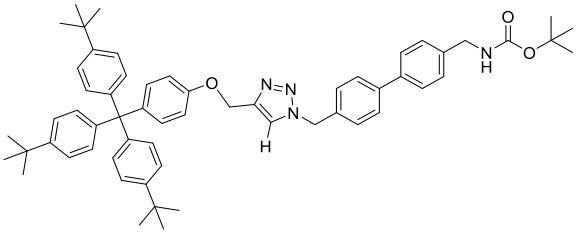
Amine **4** (2.69 g, 0.01 mol, 1 eq.) was dissolved in dry CH_2Cl_2 (125 mL) and dry Et_3N (1.57 mL, 0.01 mol, 1 eq) was added. The solution was cooled to 0 °C and Boc anhydride (4.91 g, 0.02 mol, 2 eq) in dry CH_2Cl_2 (125 mL) was added dropwise over five minutes. After addition, the reaction mixture was left to stir overnight at room temperature under a flow of $N_{2(g)}$. This solution was then diluted with CH_2Cl_2 (200 mL) and worked up by washing with a saturated $NaHCO_{3(aq)}$ solution (1 × 150 mL) and H_2O (1 × 150 mL). The organic phase was dried over anhydrous $MgSO_4$ and the solvent removed *in vacuo* to give the product **28** as an off-white solid (1.62 g, 4.80 mmol, 43%).

^{1}H NMR (400 MHz, $CDCl_3$) δ = 7.59 (4H, d, *J* = 8.07 Hz, Ar*H*), 7.35 - 7.42 (4H, m, Ar*H*), 4.40 (2H, s, CH_2), 4.38 (2H, d, *J* = 5.75 Hz, CH_2), 1.49 (9H, s, CH_3).

^{13}C NMR (101 MHz, $CDCl_3$) δ = 155.9, 140.8, 139.5, 138.3, 134.3, 128.6, 127.9, 127.4, 127.2, 79.5, 54.5, 44.3, 28.4

MS (ESI): m/z calc. for $C_{19}H_{22}N_4O_2$ $[M+Na]^+$: 361.16; found: 361.10.

Proto-triazole Boc-protected amine 29



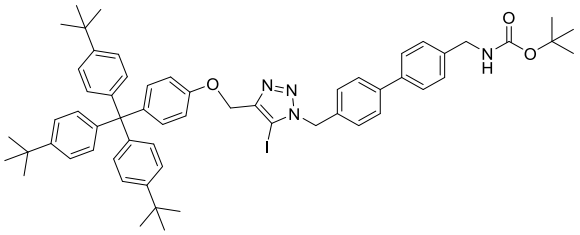
Azide **28** (19 mg, 0.06 mmol, 1 eq) was dissolved in dry CH_2Cl_2 (2 mL). Alkyne-functionalised phenyl trityl stopper compound **6** (30 mg, 0.06 mmol, 1 eq), TBTA (6 mg, 0.01 mmol, 0.2 eq), $Cu(CH_3CN)_4 \cdot PF_6$ (4 mg, 0.01 mmol, 0.2 eq) and DIPEA (19 µL, 0.12 mmol, 2 eq) were added and the resulting solution was left to stir overnight at room temperature. The reaction mixture was then washed with 25% $NH_4OH_{(aq)}$ (1 × 2 mL) and the organic phase was collected, dried over anhydrous $MgSO_4$ and the solvent removed *in vacuo*. The resulting residue was purified by silica gel column chromatography (99:1 CH_2Cl_2: MeOH) and compound **29** was isolated as a white solid (45 mg, 0.05 mmol, 85%).

^{1}H NMR (400 MHz, $CDCl_3$) δ = 7.66 (1H, s, Ar*H* triazole), 7.56 - 7.60 (2H, m, Ar*H* biphenyl), 7.53 (2H, d, *J* = 8.2 Hz, Ar*H* biphenyl), 7.33 - 7.39 (4H, m, Ar*H* biphenyl), 7.20 - 7.26 (6H, m, Ar*H* stopper), 7.04 - 7.12 (8H, m, Ar*H* stopper), 6.84 (2H, d, *J* = 8.9 Hz, Ar*H* stopper), 5.58 (2H, s, CH_2), 5.51 (2H, s, CH_2), 5.18 (2H, s, CH_2), 1.48 (9H, s, CH_3 Boc), 1.30 (27H, s, CH_3 stopper)

^{13}C NMR (101 MHz, $CDCl_3$) δ = 156.0, 148.3, 144.0, 141.3, 140.1, 139.1, 134.7, 133.4, 132.2, 130.6, 129.0, 128.6, 128.5, 127.9, 127.4, 127.2, 124.0, 123.6, 113.2, 63.0, 62.0, 54.0, 47.0, 34.2, 31.3, 30.8, 28.3

MS (ESI): m/z calc. for $C_{59}H_{69}N_4O_3$ $[M+H]^+$: 881.53; found: 881.61.

Iodo-triazole Boc-protected amine 30



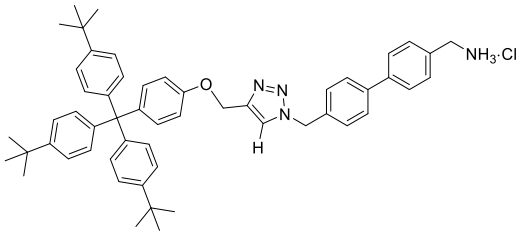
Azide **28** (100 mg, 0.30 mmol, 1 eq) was dissolved in THF (2 mL). NaI (177 mg, 1.20 mmol, 4 eq) and $Cu(ClO_4)_2 \cdot 6H_2O$ (219 mg, 0.60 mmol, 2 eq) were added and the resulting suspension was left to stir for five minutes. TBTA (16 mg, 0.03 mmol, 0.1 eq) and DBU (45 mg, 0.30 mmol, 1 eq) were then added to the mixture. Finally, alkyne-functionalised phenyl trityl stopper compound **6** (160 mg, 0.30 mmol, 1 eq), CH_3CN (2 mL) and CH_2Cl_2 (ten drops) were added and the reaction mixture was left to stir overnight in the dark. The mixture was then washed with 25% $NH_4OH_{(aq)}$ (1 × 3 mL) and the organic phase was collected, dried over anhydrous $MgSO_4$ and the solvent removed *in vacuo*. The resulting residue was purified by silica gel column chromatography (CH_2Cl_2). The iodo-triazole-containing compound **30** was isolated as an off-white solid (256 mg, 0.25 mmol, 86%).

^{1}H NMR (400 MHz, $CDCl_3$) δ = 7.54 (4H, d, *J* = 8.1 Hz, Ar*H* biphenyl), 7.33 - 7.39 (4H, m, Ar*H* biphenyl), 7.23 (6H, d, *J* = 8.7 Hz, Ar*H* stopper), 7.12 (8H, s, Ar*H* stopper), 6.91 (2H, d, *J* = 8.9 Hz, Ar*H* stopper), 5.65 (2H, s, C*H*$_2$), 5.11 (2H, s, C*H*$_2$), 4.36 (2H, d, *J* = 5.5 Hz, C*H*$_2$), 1.48 (9H, s, C*H*$_3$ Boc), 1.31 (27H, s, C*H*$_3$ stopper).

^{13}C NMR (101 MHz, $CDCl_3$) δ = 156.2, 148.3, 147.9, 144.0, 141.1, 140.3, 139.3, 138.4, 133.0, 132.3, 130.7, 129.1, 128.6, 128.4., 128.0, 127.5, 127.3, 124.0, 113.6, 68.0, 63.1, 61.8, 54.0, 34.3, 31.46, 28.4, 25.6.

MS (ESI): m/z calc. for $C_{59}H_{67}IN_4O_3$ $[M+H]^+$: 1007.43; found: 1007.43.

Proto-triazole biphenyl amine 31·Cl



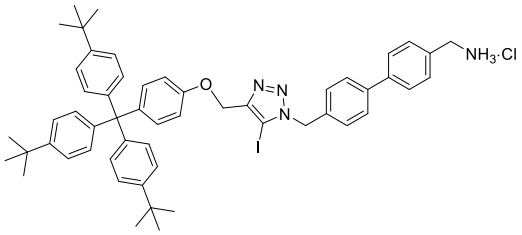
Thread **29** (45 mg, 0.05 mmol) was dissolved in dry Et_2O (5 mL). $HCl_{(g)}$ was generated *in situ* by the dropwise addition of concentrated H_2SO_4 to $NaCl_{(s)}$ and bubbled through the solution for 25 minutes. After that the solution was stirred for two hours at room temperature. The resulting precipitate was filtered and washed with Et_2O to give an off-white solid **31·Cl**, the hydrochloride salt of the free amine (41 mg, 0.05 mmol, 99%).

^{1}H NMR (400MHz, 1:1 $CDCl_3$:CD_3OD) δ = 7.94 (1H, s, triazole Ar*H*), 7.62 (4H, dd, *J* = 18.2 Hz, *J* = 8.1 Hz, biphenyl Ar*H*), 7.36 - 7.51 (4H, m, biphenyl Ar*H*), 7.18 - 7.25 (6H, m, stopper Ar*H*), 7.01 - 7.09 (8H, m, stopper Ar*H*), 6.83 (2H, d, *J* = 8.9 Hz, stopper Ar*H*), 5.58 (2H, s, CH_2), 5.13 (2H, s, CH_2), 4.06 (2H, s, CH_2), 1.23 (27H, s, stopper CH_3)

^{13}C NMR (126MHz, 1:1 $CDCl_3$:CD_3OD) δ = 155.7, 148.1, 143.8, 140.8, 140.4, 140.1, 133.6, 132.0, 130.4, 129.2, 128.5, 127.5, 127.4, 123.8, 112.9, 62.8, 61.4, 61.0, 54.1, 53.7, 44.6, 42.8, 33.9, 31.0, 29.4, 28.8, 18.1, 16.8

MS (ESI): m/z calc. for $C_{54}H_{61}N_4O$ $[M-Cl]^+$: 781.48; found: 781.51.

Iodo-triazole biphenyl amine 32.Cl



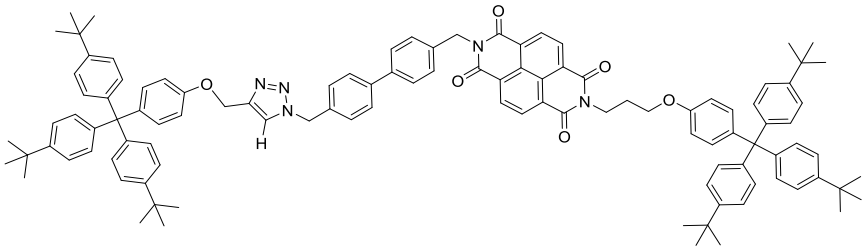
Thread **30** (298 mg, 0.30 mmol) was dissolved in dry Et_2O (25 mL). $HCl_{(g)}$ was generated *in situ* by the dropwise addition of concentrated $H_2SO_{4(aq)}$ to $NaCl_{(s)}$ and bubbled through the solution for 25 minutes. After that the solution was stirred for two hours at room temperature. The resulting precipitate was filtered and washed with Et_2O to give the hydrochloride salt of the product as a white solid **32·Cl** (280 mg, 0.30 mmol, 99%).

^{1}H NMR (400 MHz, 1:1 $CDCl_3$:CD_3OD) δ = 7.58 - 7.65 (2H, m, Ar*H* biphenyl), 7.53 - 7.58 (2H, m, Ar*H* biphenyl), 7.46 - 7.52 (2H, m, Ar*H* biphenyl), 7.28 - 7.39 (2H, m, Ar*H* biphenyl), 7.20 (6H, d, *J* = 8.7 Hz, Ar*H* stopper), 7.01 - 7.12 (8H, m, Ar*H* stopper), 6.79 - 6.91 (2H, m, Ar*H* stopper), 5.66 (2H, s, CH_2), 5.06 (2H, s, CH_2), 4.10 (2H, s, CH_2), 1.26 (27H, s, CH_3 stopper)

^{13}C NMR (101MHz, 1:1 $CDCl_3$:CD_3OD) δ = 155.8, 148.1, 143.8, 140.8, 140.2, 140.1, 133.2, 132.0, 130.4, 129.2, 128.2, 127.4, 127.2, 123.8, 113.3, 62.8, 61.3, 53.7, 49.1, 48.9, 48.7, 48.5, 48.3, 48.1, 47.8, 42.7, 33.9, 31.0

MS (MALDI): *m/z* calc. for $C_{54}H_{61}ClIN_4O$ $[M + H]^+$: 945.36; found: 945.05.

Proto-triazole NDI axle 34



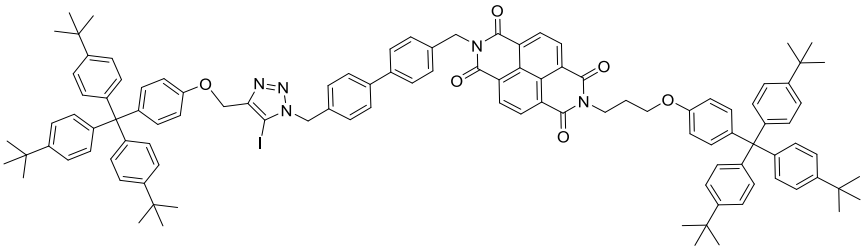
The propylamine-functionalised phenyl trityl stopper compound **27** (20 mg, 0.04 mmol, 1 eq) and commerically available 1,4,5,8-naphthalenetetracarboxylic dianhydride (10 mg, 0.04 mmol, 1 eq) were suspended in 1 mL of dry, degassed DMF with dry Et_3N (6 µL, 0.04 mmol, 1 eq) in a sealed microwave vial. The suspension was sonicated for ten minutes before heating under microwave irradiation for five minutes at 140 °C. The resulting yellow solution was allowed to cool and the vial opened to allow for the addition of amine **31·Cl** (29 mg, 0.04 mmol, 1 eq) and further dry Et_3N (6 µL, 0.04 mmol, 1 eq). The vial was resealed and the suspension sonicated for 30 minutes before heating under microwave irradiation for a further five minutes at 140 °C. Upon cooling the yellow solution was placed immediately into a round bottom flask and reduced *in vacuo* to give a golden yellow residue. This crude reaction mixture was purified by silica gel column chromatography (99:1 CH_2Cl_2:MeOH) to yield the desired neutral axle compound **34** (23 mg, 0.02 mmol, 41%).

^{1}H NMR (400MHz, $CDCl_3$) δ = 8.69 - 8.81 (4H, m, Ar*H* NDI), 7.60 - 7.68 (2H, m, Ar*H* biphenyl), 7.47 - 7.59 (5H, m, Ar*H* biphenyl, triazole), 7.33 (2H, d, *J* = 8.2 Hz, Ar*H* biphenyl), 7.19 - 7.29 (12H, m, Ar*H* stopper), 6.98 - 7.14 (16H, m, Ar*H* stopper), 6.84 (2H, d, *J* = 8.9 Hz, Ar*H* stopper), 6.64 (2H, d, *J* = 8.9 Hz, Ar*H* stopper), 5.56 (2H, s, C*H*$_2$), 5.44 (2H, s, C*H*$_2$), 5.17 (2H, s, C*H*$_2$), 4.38 - 4.47 (2H, m, C*H*$_2$), 4.04 - 4.16 (2H, m, C*H*$_2$), 2.21 - 2.32 (2H, m, C*H*$_2$), 1.31 (54H, s, C*H*$_3$ stopper)

^{13}C NMR (101MHz, $CDCl_3$) δ = 162.9, 162.8, 156.5, 156.1, 148.3, 148.3, 144.9, 144.1, 144.0, 141.2, 140.2, 139.7, 139.6, 136.0, 133.5, 132.3, 132.1, 131.2, 131.0, 130.7, 129.7, 128.5, 127.7, 127.3, 126.7, 126.7, 126.5, 124.0, 122.5, 113.2, 112.9, 65.9, 63.0, 63.0, 62.0, 53.9, 43.7, 38.6, 34.3, 31.4, 27.9

MS (ESI): m/z calc. for $C_{108}H_{112}N_5O_6$ $[M+H]^+$: 1575.86; found: 1575.98.

Iodo-triazole NDI axle 35



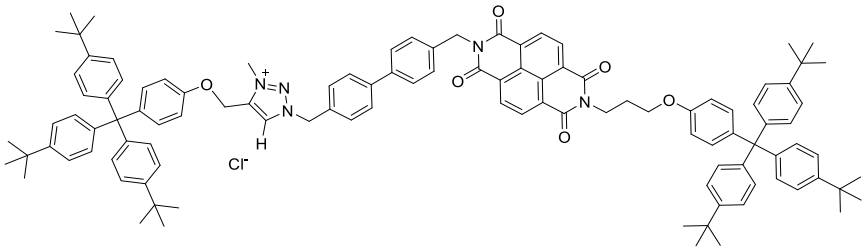
The propylamine-functionalised phenyl trityl stopper compound **27** (40 mg, 0.07 mmol, 1 eq) and commerically available 1,4,5,8-naphthalenetetracarboxylic dianhydride (19 mg, 0.07 mmol, 1 eq) were suspended in 1 mL of dry, degassed DMF with dry Et_3N (11 µL, 0.07 mmol, 1 eq) in a sealed microwave vial. The suspension was sonicated for ten minutes before heating under microwave irradiation for five minutes at 140 °C. The resulting brown solution was allowed to cool and the vial opened to allow for the addition of amine **32·Cl** (76 mg, 0.07 mmol, 1 eq) and further dry Et_3N (11 µL, 0.07 mmol, 1 eq). The vial was resealed and the suspension sonicated for 30 minutes before heating under microwave irradiation for a further five minutes at 140 °C. Upon cooling the brown solution was placed immediately into a round bottom flask and the solvent removed *in vacuo* to give a golden brown residue. This crude reaction mixture was purified by silica gel column chromatography (99:1 CH_2Cl_2:MeOH) to yield the desired neutral axle compound **35** (59 mg, 0.03 mmol, 50%).

^{1}H NMR (400MHz, $CDCl_3$) δ = 8.76 (4H, d, *J* = 7.9 Hz, Ar*H* NDI), 7.59 - 7.67 (2H, m, Ar*H* biphenyl), 7.47 - 7.56 (4H, m, Ar*H* biphenyl), 7.31 - 7.39 (2H, m, Ar*H* biphenyl), 7.23 (12H, d, *J* = 8.4 Hz, Ar*H* stopper), 6.98 - 7.13 (16H, m, Ar*H* stopper), 6.85 - 6.92 (2H, m, Ar*H* stopper), 6.64 (2H, d, *J* = 8.9 Hz, Ar*H* stopper), 5.62 (2H, s, CH_2), 5.43 (2H, s, CH_2), 5.09 (2H, s, CH_2), 4.43 (2H, t, *J* = 6.6 Hz, CH_2), 4.10 (2H, t, *J* = 6.6 Hz, CH_2), 2.26 (2H, quin, *J* = 6.2 Hz, CH_2), 1.30 (54H, s, CH_3 stopper)

^{13}C NMR (126MHz, $CDCl_3$) δ = 162.9, 162.8, 156.5, 156.2, 148.3, 148.3, 144.1, 144.0, 141.0, 140.3, 139.8, 139.6, 135.9, 133.1, 132.2, 132.1, 131.2, 131.0, 130.7, 130.7, 129.7, 128.4, 128.4, 127.6, 127.5, 127.2, 126.7, 126.7, 126.5, 124.0, 124.0, 113.5, 112.9, 65.9, 63.0, 63.0, 61.7, 53.9, 43.7, 38.6, 34.3, 31.4, 27.9

MS (ESI): m/z calc. for $C_{108}H_{111}N_5O_6I$ $[M+H]^+$: 1701.76; found: 1701.90.

Proto-triazolium NDI axle 36·Cl



Proto-triazole axle **34** (23 mg, 0.02 mmol, 1 eq) and $Me_3O{\cdot}BF_4$ (9 mg, 0.06 mmol, 3 eq) were dissolved in dry CH_2Cl_2 (2 mL). The solution was left to stir for two days at room temperature over a flow of $N_{2(g)}$. After this time the reaction was quenched with three drops of MeOH and the solvent was removed *in vacuo*. The resulting solid was purified by silica gel column chromatography (CH_2Cl_2:MeOH 95:5) and the product **36·BF$_4$** isolated as a pale yellow solid. Subsequent anion exchange to yield **36·Cl** was performed by dissolving **36·BF$_4$** in a solvent mixture of 45:45:10 $CHCl_3$:MeOH:H_2O (10 mL) and passing the solution three times through a column of Amberlite® resin loaded with chloride (23 mg, 0.02 mmol, 97%).

Axle **36·Cl** was also prepared from amine **40·(Cl)$_2$** as below.

The propylamine-functionalised phenyl trityl stopper compound **27** (20 mg, 0.04 mmol, 1 eq) and commerically available 1,4,5,8-naphthalenetetracarboxylic dianhydride (10 mg, 0.04 mmol, 1 eq) were suspended in 1 mL of dry, degassed DMF with dry Et_3N (6 µL, 0.04 mmol, 1 eq) in a sealed microwave vial. The suspension was sonicated for ten minutes before heating under microwave irradiation for five minutes at 140 °C. The resulting yellow solution was allowed to cool and the vial opened to allow for the addition of amine **40·(Cl)$_2$** (35 mg, 0.04 mmol, 1 eq) and further dry Et_3N (6 µL, 0.04 mmol, 1 eq). The vial was resealed and the suspension sonicated for 30 minutes before heating under microwave irradiation for a further five minutes at 140 °C. Upon cooling the yellow solution was placed immediately into a round bottom flask and reduced *in vacuo* to give a golden yellow residue. This crude

reaction mixture was purified by silica gel column chromatography (97:3 CH_2Cl_2:MeOH to yield the desired proto-triazolium axle compound **36·Cl** (33 mg, 0.02 mmol, 41%).

^{1}H NMR (500MHz, $CDCl_3$) δ = 9.92 (1H, br. s, Ar*H* triazolium), 8.76 (4H, d, *J* = 8.4 Hz, Ar*H* NDI), 7.67 (2H, br. d, *J* = 6.6 Hz, Ar*H* biphenyl), 7.63 (2H, d, *J* = 8.1 Hz, Ar*H* biphenyl), 7.58 (2H, d, *J* = 7.8 Hz, Ar*H* biphenyl), 7.50 (2H, d, *J* = 7.9 Hz, Ar*H* biphenyl), 7.23 (12H, d, *J* = 8.2 Hz, Ar*H* stopper), 7.14 (2H, d, *J* = 8.5 Hz, Ar*H* stopper), 6.99 - 7.10 (14H, m, Ar*H* stopper), 6.83 (2H, d, *J* = 8.4 Hz, Ar*H* stopper), 6.65 (2H, d, *J* = 8.5 Hz, Ar*H* stopper), 6.01 (2H, br. s., C*H*$_2$), 5.43 (4H, br. s., C*H*$_2$), 4.43 (2H, t, *J* = 6.2 Hz, C*H*$_2$), 4.38 (3H, s, C*H*$_3$ triazolium), 4.10 (2H, br. t, *J* = 5.6 Hz, C*H*$_2$), 2.21 - 2.30 (2H, m, C*H*$_2$), 1.24 - 1.37 (54H, m, C*H*$_3$ stopper)

^{13}C NMR (126MHz, $CDCl_3$) δ = 162.9, 162.8, 148.5, 148.3, 144.1, 143.7, 142.8, 140.0, 139.6, 136.4, 132.7, 132.2, 131.2, 131.0, 130.7, 130.6, 130.0, 129.8, 128.3, 127.3, 126.8, 126.5, 124.1, 124.0, 113.1, 112.9, 63.1, 63.0, 57.7, 57.6, 38.8, 34.3, 31.9, 31.4, 31.3, 30.9, 30.0, 29.7, 29.4, 27.9, 22.7, 14.1

MS (ESI): m/z calc. for $C_{109}H_{114}N_5O_6$ $[M-Cl]^+$: 1589.8797; found: 1589.8777.

Proto-triazolium NDI axle 36·I

36·Cl was anion-exchanged to the iodide salt **36·I** using Amberlite® anion exchange resin. The solvent used was 45:45:10 $CHCl_3$:MeOH:H_2O (20 mL).

^{1}H NMR (400MHz, 4:1 $CDCl_3$:MeOD) δ = 8.88 (1H, s, Ar*H* triazolium), 8.63 - 8.79 (4H, m, Ar*H* NDI), 7.44 - 7.62 (8H, m, Ar*H* biphenyl), 6.91 - 7.24 (28H, m, Ar*H* stopper), 6.81 (2H, d, *J* = 9.0 Hz, Ar*H* stopper), 6.56 (2H, d, *J* = 8.9 Hz, Ar*H* stopper), 5.83 (2H, s, C*H*$_2$), 5.39 (2H, s, C*H*$_2$), 5.33 (2H, s, C*H*$_2$), 4.35 (2H, s, C*H*$_2$), 4.35 (3H, s, C*H*$_3$ triazolium), 4.07 (2H, s, C*H*$_2$), 2.16 - 2.28 (2H, m, C*H*$_2$), 1.23 (54H, s, C*H*$_3$ stopper)

Proto-triazolium NDI axle 36·PF_6

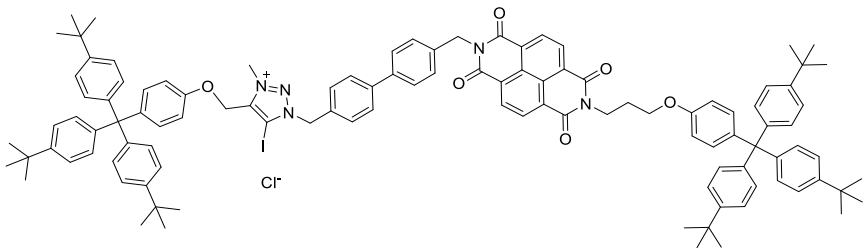
36·Cl was anion-exchanged to the hexafluorophosphate salt **36·PF_6** using Amberlite® anion exchange resin. The solvent used was 45:45:10 $CHCl_3$:MeOH:H_2O (10 mL).

^{1}H NMR (500MHz, $CDCl_3$) δ = 8.69 - 8.84 (4H, m, Ar*H* NDI), 8.35 (1H, s, Ar*H* triazolium), 7.45 - 7.68 (8H, m, Ar*H* biphenyl), 6.98 - 7.26 (28H, m, Ar*H* stopper), 6.78 (2H, d, *J* = 8.9 Hz, Ar*H* stopper), 6.65 (2H, d, *J* = 8.7 Hz, Ar*H* stopper), 5.69 (2H, s, CH_2), 5.42 (2H, s, CH_2), 5.23 (2H, s, CH_2), 4.38 - 4.48 (2H, m, CH_2), 4.33 (3H, s, CH_3 triazolium), 4.10 (2H, s, CH_2), 2.20 - 2.28 (2H, m, CH_2), 1.30 (54H, s, CH_3 stopper)

^{19}F NMR (470 MHz, $CDCl_3$) δ = -72.5 (d, ^{1}J = 707 Hz, PF_6).

^{31}P NMR (202 MHz, $CDCl_3$) δ = -144.3 (sept, ^{1}J = 709 Hz, PF_6).

Iodo-triazolium NDI axle 37·Cl



Iodo-triazole axle **35** (59 mg, 0.03 mmol, 1 eq) and $Me_3O{\cdot}BF_4$ (16 mg, 0.09 mmol, 3 eq) were dissolved in dry CH_2Cl_2 (2 mL). The solution was left to stir for two days at room temperature under a flow of $N_{2(g)}$. After this time the reaction was quenched with three drops of MeOH and the solvent was subsequently removed *in vacuo*. The resulting solid was purified by silica gel column chromatography (CH_2Cl_2:MeOH 95:5) and the product **37·BF$_4$** isolated as a pale yellow solid. Subsequent anion exchange to yield **37·Cl** was performed by dissolving **37·BF$_4$** in a solvent mixture of 45:45:10 $CHCl_3$:MeOH:H_2O (10 mL) and passing the solution three times through a column of Amberlite® resin loaded with chloride (51 mg, 0.03 mmol, 96%).

^{1}H NMR (400MHz, $CDCl_3$) δ = 8.66 - 8.83 (4H, m, Ar*H* NDI), 7.54 - 7.69 (4H, m, Ar*H* biphenyl), 7.36 - 7.54 (4H, m, Ar*H* biphenyl), 7.23 (12H, d, *J* = 8.1 Hz, Ar*H* stopper), 7.13 - 7.18 (2H, m, Ar*H* stopper), 6.97 - 7.11 (14H, m, Ar*H* stopper), 6.73 - 6.90 (2H, m, Ar*H* stopper), 6.58 - 6.70 (2H, m, Ar*H* stopper), 5.64 - 5.74 (2H, m, CH_2), 5.41 - 5.50 (2H, m, CH_2), 5.34 - 5.40 (2H, m, CH_2), 4.60 (3H, s, CH_3 triazolium), 4.39 - 4.49 (2H, m, CH_2), 4.00 - 4.16 (2H, m, CH_2), 2.19 - 2.31 (2H, m, CH_2), 1.21 - 1.37 (54H, m, CH_3 stopper)

^{13}C NMR (126MHz, $CDCl_3$) δ = 162.8, 156.5, 148.5, 148.4, 148.4, 148.3, 144.1, 143.8, 143.8, 143.7, 139.6, 132.7, 132.5, 132.1, 131.2, 131.0, 130.7, 130.6, 130.6, 129.8, 129.7, 129.5, 129.0, 128.2, 127.9, 127.3, 127.3, 127.2, 126.7, 126.7, 124.2, 124.1, 124.0, 113.2, 113.2, 112.9, 63.1, 63.0, 34.3, 31.4, 29.7, 29.6, 27.9, 14.1

MS (ESI): m/z calc. for $C_{109}H_{113}N_5O_6I$ $[M-Cl]^+$: 1715.7764; found: 1715.7697.

Iodo-triazolium NDI axle 37·I

37·Cl was anion-exchanged to the iodide salt **37·I** using Amberlite® anion exchange resin. The solvent used was 45:45:10 $CHCl_3$:MeOH:H_2O (10 mL).

^{1}H NMR (400MHz, 4:1 $CDCl_3$:MeOD) δ = 8.63 - 8.77 (4H, m, Ar*H* NDI), 7.42 - 7.60 (8H, m, Ar*H* biphenyl), 6.91 - 7.25 (28H, m, Ar*H* stopper), 6.79 - 6.86 (2H, m, Ar*H* stopper), 6.51 - 6.59 (2H, m, Ar*H* stopper), 5.83 (2H, s, CH_2), 5.38 (2H, s, CH_2), 5.28 (2H, s, CH_2), 4.38 (3H, s, CH_3 triazolium), 4.33 - 4.42 (2H, m, CH_2), 4.03 - 4.11 (2H, m, CH_2), 2.17 - 2.28 (2H, m, CH_2), 1.25 (54H, s, CH_3 stopper)

Iodo-triazolium NDI axle 37·PF_6

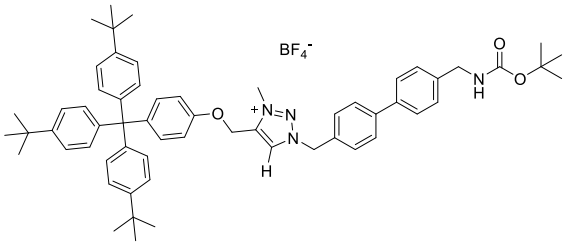
37·Cl was anion-exchanged to the hexafluorophosphate salt **37·PF_6** using Amberlite® anion exchange resin. The solvent used was 45:45:10 $CHCl_3$:MeOH:H_2O (10 mL).

^{1}H NMR (500MHz, $CDCl_3$) δ = 8.65 - 8.83 (4H, m, Ar*H* NDI), 7.38 - 7.66 (8H, m, Ar*H* biphenyl), 6.98 - 7.26 (28H, m, Ar*H* stopper), 6.74 - 6.88 (2H, m, Ar*H* stopper), 6.60 - 6.69 (2H, m, Ar*H* stopper), 5.74 (2H, s, CH_2), 5.44 (2H, s, CH_2), 5.30 (2H, s, CH_2), 4.38 - 4.48 (2H, m, CH_2), 4.34 (3H, s, CH_3 triazolium), 4.10 (2H, br. s., CH_2), 2.20 - 2.31 (2H, m, CH_2), 1.30 (54H, s, CH_3 stopper)

^{19}F NMR (470 MHz, $CDCl_3$) δ = -72.5 (d, ^1J = 708 Hz, PF_6).

^{31}P NMR (202 MHz, $CDCl_3$) δ = -144.3 (sept, ^1J = 709 Hz, *P*F_6).

Proto-triazolium Boc-protected amine 38·BF_4

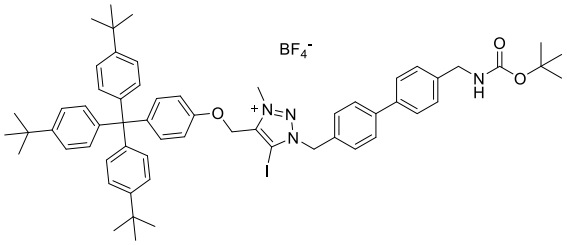


Compound **29** (100 mg, 0.11 mmol, 1 eq) and $Me_3O{\cdot}BF_4$ (84 mg, 0.57 mmol, 5 eq) were added to dry CH_2Cl_2 (5 mL). The solution was left to stir for 2 days at room temperature under a flow of $N_{2(g)}$.. The reaction was quenched with 3 drops of MeOH and the solvent was subsequently removed *in vacuo*. The resulting solid was purified by silica gel column chromatography (CH_2Cl_2:MeOH 97:3) and **38·BF_4** isolated as a sticky white solid (82 mg, 0.08 mmol, 76%).

^{1}H NMR (400MHz, $CDCl_3$) δ = 8.51 (1H, s, Ar*H* triazolium), 7.61 (2H, d, *J* = 7.9 Hz, Ar*H* biphenyl), 7.51 (2H, d, *J* = 8.4 Hz, Ar*H* biphenyl), 7.47 (2H, d, *J* = 8.4 Hz, Ar*H* biphenyl), 7.34 (2H, d, *J* = 8.1 Hz, Ar*H* biphenyl), 7.24 (6H, d, *J* = 8.4 Hz, Ar*H* stopper), 7.16 (2H, d, *J* = 8.3 Hz, Ar*H* stopper), 7.07 (6H, d, *J* = 8.6 Hz, Ar*H* stopper), 6.82 (2H, d, *J* = 8.2 Hz, Ar*H* stopper), 5.74 (2H, s, C*H*$_2$), 5.28 (2H, s, C*H*$_2$), 4.28 (3H, s, C*H*$_3$ triazolium), 1.48 (9H, s, C*H*$_3$ Boc), 1.30 (27H, s, C*H*$_3$ stopper)

MS (ESI): m/z calc. for $C_{60}H_{71}N_4O_3$ $[M - BF_4]^+$: 896.25; found: 896.20

Iodo-triazolium Boc-protected amine 39·BF_4



Compound **30** (100 mg, 0.10 mmol, 1 eq) and $Me_3O{\cdot}BF_4$ (73 mg, 0.50 mmol, 5 eq) were added to dry CH_2Cl_2 (5 mL). The solution was left to stir for 2 days at room temperature under $N_{2(g)}$.. The reaction was quenched with 3 drops of MeOH and the solvent was subsequently removed *in vacuo*. The

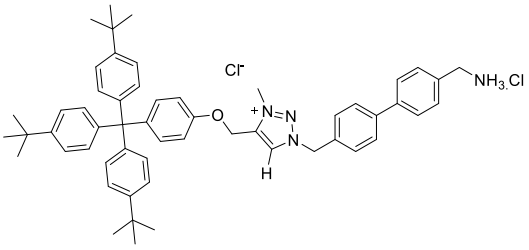
resulting solid was purified by silica gel column chromatography (CH_2Cl_2:MeOH 97:3) and **39·BF_4** isolated as a pale yellow oil (61 mg, 0.06 mmol, 55%).

^{1}H NMR (400 MHz, $CDCl_3$) δ = 7.60 (2H, d, *J* = 7.9 Hz, Ar*H* biphenyl), 7.48 (4H, d, *J* = 8.1 Hz, Ar*H* biphenyl), 7.34 (2H, d, *J* = 7.9 Hz, Ar*H* biphenyl), 7.24 (6H, d, *J* = 8.3 Hz, Ar*H* stopper), 7.16 (2H, d, *J* = 8.7 Hz, Ar*H* stopper), 7.07 (6H, d, *J* = 8.4 Hz, Ar*H* stopper), 6.82 (2H, d, *J* = 8.8 Hz, Ar*H* stopper), 5.74 (2H, s, CH_2), 5.28 (2H, s, CH_2), 4.40 (3H, s, CH_3 triazolium), 4.34 (2H, d, *J* = 5.50 Hz, CH_2), 1.48 (9H, s, CH_3 Boc), 1.30 (27H, s, CH_3 stopper)

^{13}C NMR (101 MHz, $CDCl_3$) δ = 156.33, 154.74, 148.49, 144.04, 143.75, 142.40, 142.10, 138.90, 138.78, 132.71, 130.63, 129.40, 129.33, 127.98, 127.31, 124.16, 113.35, 90.99, 63.09, 59.23, 57.87, 53.41, 44.55, 39.51, 34.28, 31.35, 28.40, 25.86.

MS (ESI): m/z calc. for $C_{60}H_{70}IN_4O_3^+$ $[M]^+$: 1021.4488; found: 1021.4454.

Proto-triazolium biphenyl amine 40·$(Cl)_2$

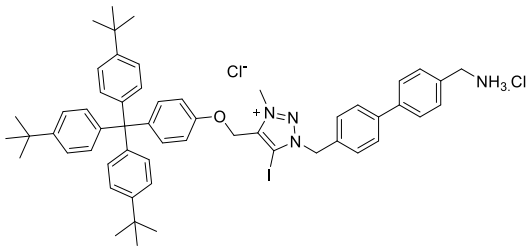


38·BF_4 (150 mg, 0.15 mmol) was dissolved in Et_2O (15 mL). $HCl_{(g)}$ was generated *in situ* by dropwise addition of concentrated H_2SO_4 to $NaCl_{(s)}$ and bubbled through the solution for 25 min. After that the solution was stirred for two hours at room temperature. The resulting precipitate was filtered and washed with Et_2O to give the product **40·$(Cl)_2$** as a white solid (128 mg, 0.15 mmol, 98%).

^{1}H NMR (400MHz, CD_3OD) δ = 8.86 (1H, s, Ar*H* triazolium), 7.58 - 7.70 (4H, m, Ar*H* biphenyl), 7.47 - 7.57 (4H, m, Ar*H* biphenyl), 7.23 (6H, d, *J* = 8.3 Hz, Ar*H* stopper), 7.17 (2H, d, *J* = 8.3 Hz, Ar*H* stopper), 7.05 (6H, d, *J* = 8.4 Hz, Ar*H* stopper), 6.89 (2H, d, *J* = 8.4 Hz, Ar*H* stopper), 5.89 (2H, s, CH_2), 5.30 (2H, s, CH_2), 4.36 (3H, s, CH_3 triazolium), 4.11 (2H, s, CH_2), 1.28 (27H, s, CH_3 stopper)

MS (ESI): m/z calc. for $C_{55}H_{63}N_4O$ $[M]^+$: 796.14; found: 796.11

Iodo-triazolium biphenyl amine 41·(Cl)$_2$

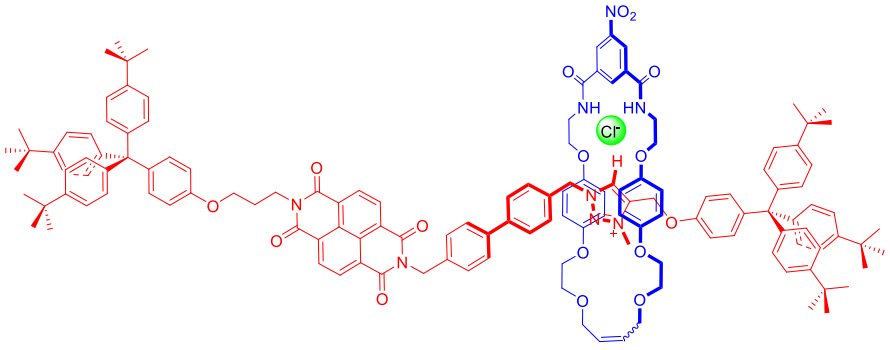


39·BF$_4$ (154 mg, 0.14 mmol) was dissolved in Et_2O (15 mL). $HCl_{(g)}$ was generated *in situ* by dropwise addition of concentrated H_2SO_4 to $NaCl_{(s)}$ and bubbled through the solution for 25 min. After that the solution was stirred for two hours at room temperature. The resulting precipitate was filtered and washed with Et_2O to give the product **41·(Cl)$_2$** as a yellow solid (138 mg, 0.14 mmol, 98%).

^{1}H NMR (400 MHz, 9:1 $CDCl_3$:CD_3OD) δ = 7.84 (4H, d, *J* = 7.9 Hz, Ar*H* biphenyl), 7.69 - 7.75 (4H, m, Ar*H* biphenyl), 7.43 (6H, d, *J* = 8.3 Hz, Ar*H* stopper), 7.37 (2H, d, *J* = 7.8 Hz, Ar*H* stopper), 7.25 (6H, d, *J* = 8.4 Hz, Ar*H* stopper), 7.09 (2H, d, *J* = 8.7 Hz, Ar*H* stopper), 6.09 (2H, s, C*H*$_2$), 5.50 (2H, s, C*H*$_2$), 4.63 (3H, s, C*H*$_3$ triazolium), 4.30 (2H, s, C*H*$_2$), 1.48 (27 H, s, C*H*$_3$ stopper).

MS (ESI): m/z calc. for $C_{55}H_{62}IN_4O$ $[M]^+$: 921.3963; found: 921.3935.

Proto-triazolium–NDI rotaxane 42·Cl



The two-station axle **36·Cl** (14 mg, 8.6 µmol, 1 eq) and bis-vinyl nitro macrocycle precursor **22** (8 mg, 12.1 µmol, 1.4 eq) were dissolved in dry CH_2Cl_2 (2 mL) and stirred for ten minutes. Grubbs' II catalyst

(1 mg, 10 wt. %) was added and the solution stirred at room temperature, monitoring by TLC and ESI mass spectrometry throughout. After one day a further addition of Grubbs' II catalyst (1 mg, 10 wt. %) was made and upon depletion of macrocycle precursor **22** (which occurred after two days) the solvent was removed *in vacuo*. The resulting crude residue was purified by iterative preparative silica TLC (CH_2Cl_2:MeOH 95:5 and EtOAc:MeOH 95:5) to give the product two station rotaxane **42·Cl** as an orange solid (16 mg, 7.1 µmol, 83%).

^{1}H NMR (500MHz, $CDCl_3$) δ = 9.62 (1H, s, Ar*H* int. macro), 9.42 (1H, s, Ar*H* triazolium), 9.14 - 9.32 (2H, m, N*H* macro), 8.76 (2H, s, Ar*H* ext. macrocycle), 8.77 (4H, m, Ar*H* NDI), 7.66 (2H, d, *J* = 8.2 Hz, Ar*H* biphenyl), 7.49 (2H, d, *J* = 8.2 Hz, Ar*H* biphenyl), 7.36 (2H, d, *J* = 8.1 Hz, Ar*H* biphenyl), 7.31 (2H, d, *J* = 8.7 Hz, Ar*H* biphenyl), 7.21 - 7.26 (12H, m, Ar*H* stopper), 7.16 (4H, d, *J* = 8.4 Hz, Ar*H* stopper), 6.97 - 7.11 (14H, m, Ar*H* stopper), 6.67 (2H, d, *J* = 8.9 Hz, Ar*H* stopper), 6.30 - 6.45 (8H, m, Ar*H* hydroquinone macro), 5.50 - 5.55 (2H, s, C*H* alkene macro), 5.45 (2H, s, CH_2 axle), 5.24 (2H, s, CH_2 axle), 4.72 (2H, s, CH_2 axle), 4.60 - 4.68 (2H, m, CH_2 macrocycle), 4.45 - 4.54 (2H, m, CH_2 macrocycle), 4.43 (2H, t, *J* = 6.6 Hz, CH_2 axle), 4.10 (2H, t, *J* = 6.6 Hz, CH_2 axle), 3.91 - 3.98 (2H, m, CH_2 macrocycle), 3.87 (3H, s, CH_3 triazolium), 3.62 - 3.86 (12H, m, CH_2 macrocycle), 3.49 - 3.58 (2H, m, CH_2 macrocycle), 2.21 - 2.30 (2H, m, CH_2 axle), 1.31 (54H, s, CH_3 stopper)

^{13}C NMR (126MHz, $CDCl_3$) δ = 164.4, 162.9, 162.9, 156.6, 152.9, 151.9, 148.5, 148.3, 144.1, 144.0, 136.3, 132.5, 132.2, 131.2, 131.1, 130.7, 130.6, 129.9, 129.8, 129.5, 127.5, 127.3, 126.8, 126.7, 126.6, 124.3, 124.0, 114.7, 114.4, 113.5, 113.0, 70.8, 69.4, 67.7, 65.9, 63.2, 63.0, 38.6, 35.6, 35.1, 34.3, 34.3, 31.9, 31.4, 30.1, 29.7, 29.7, 29.4, 28.0, 27.0, 26.9, 26.4, 26.3, 26.2, 22.7, 14.1

MS (ESI): m/z calc. for $C_{141}H_{149}N_8O_{16}$ $[M-Cl]^+$: 2211.1120; found: 2211.1052.

Proto-triazolium–NDI rotaxane 42·I

42·Cl was anion-exchanged to the iodide salt **42·I** using Amberlite® anion exchange resin. The solvent used was 45:45:10 $CHCl_3$:MeOH:H_2O (10 mL).

^{1}H NMR (400MHz, 4:1 $CDCl_3$:MeOD) δ = 9.19 (1H, s, Ar*H* int. macro), 8.74 - 8.82 (3H, m, Ar*H* triazolium, ext. macro), 8.62 - 8.71 (4H, m, Ar*H* NDI), 8.44 - 8.49 (2H, m, N*H* macro), 7.39 - 7.59 (6H, m, Ar*H* biphenyl), 7.23 - 7.28 (2H, m, Ar*H* biphenyl), 6.96 - 7.23 (28H, m, Ar*H* stopper), 6.88 - 6.93 (2H, m, Ar*H* stopper), 6.59 - 6.65 (2H, m, Ar*H* stopper), 6.03 - 6.29 (8H, m, Ar*H* hydroquinone macro), 5.78 - 5.87 (2H, s, C*H* alkene macro), 5.45 (2H, s, CH_2 axle), 5.31 (2H, s, CH_2 axle), 4.96 (2H, s, CH_2 axle), 4.30 - 4.42 (4H, m, CH_2 axle, macro), 4.00 (3H, s, CH_3 triazolium), 3.81 - 4.15 (14H, m, CH_2 axle, macro), 3.56 - 3.77 (8H, m, CH_2 macro), 2.13 - 2.28 (2H, m, CH_2 axle), 1.24 (54H, s, CH_3 stopper)

Proto-triazolium–NDI rotaxane 42·PF_6

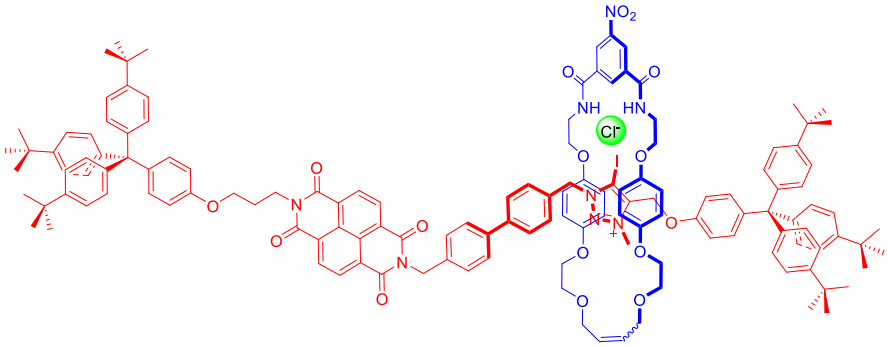
42·Cl was anion-exchanged to the hexafluorophosphate salt **42·PF_6** using Amberlite® anion exchange resin. The solvent used was 45:45:10 $CHCl_3$:MeOH:H_2O (10 mL).

^{1}H NMR (500MHz, $CDCl_3$) δ = 8.87 (2H, s, Ar*H* ext. macro), 8.67 - 8.78 (4H, m, Ar*H* NDI), 8.43 (1H, br. s, Ar*H* int. macro), 8.07 (1H, br. s, Ar*H* triazolium), 7.54 - 7.64 (2H, m, Ar*H* biphenyl), 7.40 - 7.52 (4H, m, Ar*H* biphenyl), 6.97 - 7.32 (30H, m, Ar*H* stopper, biphenyl), 6.85 - 6.94 (2H, m, Ar*H* stopper), 6.69 (2H, d, *J* = 8.9 Hz, Ar*H* stopper), 6.33 (8H, d, *J* = 8.4 Hz, Ar*H* hydroquinone macro), 5.77 - 5.92 (2H, m, C*H* alkene macro), 5.37 (2H, s, CH_2 axle), 5.30 (2H, s, CH_2 axle), 4.85 (2H, s, CH_2 axle), 4.34 - 4.47 (2H, m, CH_2 axle), 4.06 - 4.13 (2H, m, CH_2 axle), 3.92 (3H, s, CH_3 triazolium), 3.51 - 4.27 (20H, m, CH_2 macrocycle), 2.20 - 2.32 (2H, m, CH_2 axle), 1.29 (54H, s, CH_3 stopper)

^{19}F NMR (470 MHz, $CDCl_3$) δ = -72.4 (d, ^{1}J = 709 Hz, PF_6).

^{31}P NMR (202 MHz, $CDCl_3$) δ = -144.3 (sept, ^{1}J = 709 Hz, *P*F_6).

Iodo-triazolium–NDI rotaxane 43·Cl



The two-station axle **37·Cl** (25 mg, 14.2 µmol, 1 eq) and bis-vinyl nitro macrocycle precursor **22** (13 mg, 19.9 µmol, 1.4 eq) were dissolved in dry CH_2Cl_2 (2 mL) and stirred for ten minutes. Grubbs' II catalyst (1 mg, 10 wt. %) was added and the solution stirred at room temperature, monitoring by TLC and ESI mass spectrometry throughout. After one day another addition of Grubbs' II (1 mg, 10 wt. %) was made and after a further 24 hours the solvent was removed *in vacuo*. The resulting crude residue was purified by iterative preparative silica TLC (CH_2Cl_2:MeOH 95:5 and EtOAc:MeOH 95:5) to give the product two station rotaxane **43·Cl** as an orange solid (5 mg, 2.1 µmol, 21%).

^{1}H NMR (400MHz, $CDCl_3$) δ = 9.69 (1H, s, Ar*H* int. macro), 9.05 (2H, d, ^4J = 1.1 Hz, Ar*H* ext. macro), 8.83 - 8.92 (2H, m, N*H* macro), 8.76 (4H, d, *J* = 8.1 Hz, Ar*H* NDI), 7.64 - 7.71 (2H, m, Ar*H* biphenyl), 7.54 - 7.63 (2H, m, Ar*H* biphenyl), 7.41 - 7.48 (2H, m, Ar*H* biphenyl), 7.29 - 7.34 (2H, m, Ar*H* biphenyl), 7.14 - 7.25 (14H, m, Ar*H* stopper), 7.00 - 7.10 (14H, m, Ar*H* stopper), 6.95 (2H, d, *J* = 8.6 Hz, Ar*H* stopper), 6.67 (2H, d, *J* = 8.9 Hz, Ar*H* stopper), 6.16 - 6.30 (8H, m, Ar*H* hydroquinone macro), 5.50 - 5.54 (2H, m, C*H* alkene macro), 5.44 (2H, s, CH_2 axle), 4.88 (2H, s, CH_2 axle), 4.63 - 4.77 (2H, m, CH_2 macro), 4.41 (2H, s, CH_2 axle), 4.37 - 4.46 (4H, m, CH_2 axle, macrocycle), 4.18 (3H, s, CH_3 triazolium), 4.06 - 4.14 (2H, m, CH_2 axle), 3.59 - 3.99 (14H, m, CH_2 macro), 3.41 - 3.52 (2H, m, CH_2 macro), 2.21 - 2.31 (2H, m, CH_2 axle), 1.31 (54H, s, CH_3 stopper)

^{13}C NMR (126MHz, $CDCl_3$) δ = 164.4, 162.8, 156.5, 151.9, 148.5, 148.4, 148.4, 148.3, 144.1, 143.8, 143.8, 143.7, 139.6, 136.3, 132.7, 132.5, 132.1, 131.2, 131.0, 130.7, 130.6, 130.6, 129.8, 129.7, 129.5, 129.0, 128.2, 127.9, 127.3, 127.3, 127.2, 126.7, 126.7, 124.2, 124.1, 124.0, 114.7, 114.4, 113.2, 113.2,

112.9, 70.8, 69.4, 67.7, 65.9, 63.1, 63.0, 38.6, 35.6, 34.3, 31.4, 29.7, 29.6, 27.9, 26.4, 26.3, 26.2, 22.7, 14.1

MS (ESI): m/z calc. for $C_{141}H_{148}N_8O_{16}INa$ $[M-Cl+Na]^{2+}$: 1179.99891; found: 1179.99781

Iodo-triazolium–NDI rotaxane 43·I

43·Cl was anion-exchanged to the iodide salt **43·I** using Amberlite® anion exchange resin. The solvent used was 45:45:10 $CHCl_3$:MeOH:H_2O (10 mL).

^{1}H NMR (400MHz, 4:1 $CDCl_3$:MeOD) δ = 9.25 (1H, s, Ar*H* int. macro), 8.85 (2H, s, Ar*H* ext. macro), 8.63 - 8.77 (4H, m, Ar*H* NDI), 8.38 - 8.46 (2H, m, N*H* macro), 7.38 - 7.64 (8H, m, Ar*H* biphenyl), 6.90 - 7.30 (30H, m, Ar*H* stopper), 6.56 - 6.64 (2H, m, Ar*H* stopper), 6.19 - 6.29 (8H, m, Ar*H* hydroquinone macro), 5.43 - 5.52 (2H, m, C*H* alkene macro), 5.37 (2H, s, CH_2 axle), 4.99 (2H, s, CH_2 axle), 4.57 (2H, s, CH_2 axle), 4.31 - 4.49 (6H, m, CH_2 macro, axle), 4.15 (3H, s, CH_3 triazolium), 4.02 - 4.11 (2H, m, CH_2 axle), 3.44 - 3.97 (16H, m, CH_2 macro), 2.16 - 2.27 (2H, m, CH_2 axle), 1.25 (54H, s, CH_3 stopper)

Iodo-triazolium–NDI rotaxane 43·PF_6

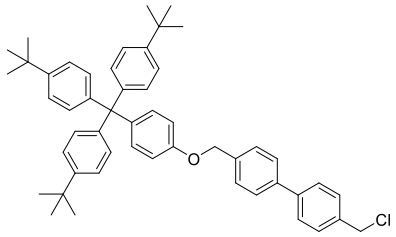
43·Cl was anion-exchanged to the hexafluorophosphate salt **43·PF_6** using Amberlite® anion exchange resin. The solvent used was 45:45:10 $CHCl_3$:MeOH:H_2O (10 mL).

^{1}H NMR (500MHz, $CDCl_3$) δ = 8.97 (3H, br. s, Ar*H* ext., int. macro), 8.57 - 8.74 (4H, m, Ar*H* NDI), 7.43 - 7.62 (8H, m, Ar*H* biphenyl), 7.01 - 7.32 (28H, m, Ar*H* stopper), 6.84 - 6.94 (2H, m, Ar*H* stopper), 6.72 (2H, d, *J* = 8.9 Hz, Ar*H* stopper), 5.98 (10H, br. s., Ar*H* hydroquinone macro, C*H* alkene macro), 5.43 (2H, br. s, CH_2 axle), 5.30 (2H, br. s., CH_2 axle), 5.00 (2H, br. s, CH_2 axle), 4.34 - 4.43 (2H, m, CH_2 axle), 4.31 (3H, s, CH_3 triazolium), 3.57 - 4.13 (22H, m, CH_2 axle, macro), 2.21 - 2.29 (2H, m, CH_2 axle), 1.29 (54H, s, CH_3 stopper)

^{19}F NMR (470 MHz, $CDCl_3$) δ = -72.5 (d, ^1J = 707 Hz, PF_6).

^{31}P NMR (202 MHz, $CDCl_3$) δ = -144.3 (sept, ^1J = 709 Hz, *P*F_6).

Chloromethyl biphenyl mono stoppered axle pre-cursor 44



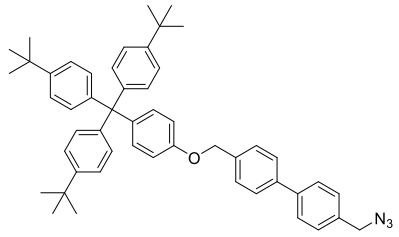
Commercially available 4,4'-bis(chloromethyl)-1,1'-biphenyl (186 mg, 0.75 mmol, 1.5 eq) was dissolved in degassed acetone (30 mL) and to this solution was added dried K_2CO_3 (207 mg, 1.5 mmol, 3 eq). A solution of alcohol-functionalised phenyl trityl stopper **2** (250 mg, 0.50 mmol, 1 eq) in acetone (10 mL) was added dropwise before heating the reaction for one day under reflux. After this time the solvent was removed *in vacuo* and the crude solid re-dissolved in CH_2Cl_2 (50 mL). This was washed with H_2O (3 × 50 mL) and the organic layer isolated and dried over anhydrous $MgSO_4$. Removal of the solvent *in vacuo* was followed by purification by silica gel column chromatography (4:1 petroleum ether:CH_2Cl_2) giving the mono stoppered axle pre cursor **44** (182 mg, 0.25 mmol, 51%).

^{1}H NMR (400MHz, $CDCl_3$) δ = 7.56 - 7.69 (4H, m, Ar*H* biphenyl), 7.43 - 7.56 (4H, m, Ar*H* biphenyl), 7.19 - 7.32 (6H, m, Ar*H* stopper), 7.04 - 7.16 (8H, m, Ar*H* stopper), 6.88 (2H, d, *J* = 7.9 Hz, Ar*H* stopper), 5.09 (2H, s, CH_2), 4.65 (2H, s, CH_2), 1.31 (27H, s, CH_3 stopper)

^{13}C NMR (101MHz, $CDCl_3$) δ = 156.6, 148.3, 144.1, 141.0, 140.1, 139.9, 136.5, 136.5, 132.3, 130.7, 129.1, 128.1, 127.5, 127.3, 124.0, 113.3, 69.6, 63.1, 46.0, 34.3, 31.4

MS (ESI): m/z calc. for $C_{51}H_{55}OClK$ $[M+K]^+$: 758.36; found: 758.25

Biphenyl azide mono stoppered axle precursor 45



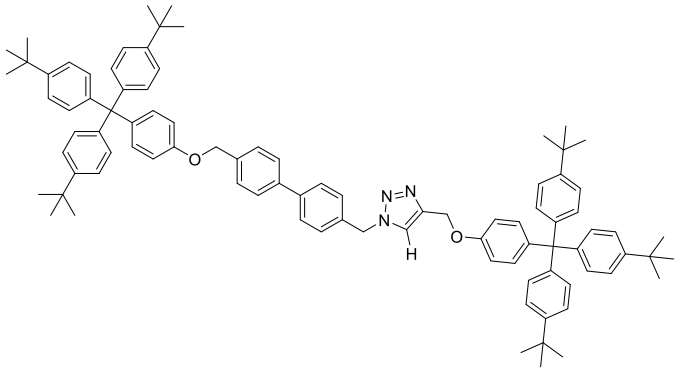
Compound **44** (114 mg, 0.16 mmol, 1 eq) and NaN_3 (100 mg, 1.55 mmol, 10 eq) were suspended in DMSO (40 mL) and heated at 105 °C overnight. After cooling H_2O (50 mL) was added to the solution and the resulting precipitate was collected by filtration and dried under vacuum giving the desired axle pre cursor **45** (109 mg, 0.15 mmol, 94%).

^{1}H NMR (400MHz, $CDCl_3$) δ = 7.61 (4H, dd, *J* = 8.3 Hz, ^4J = 2.4 Hz, Ar*H* biphenyl), 7.51 (2H, d, *J* = 7.6 Hz, Ar*H* biphenyl), 7.39 (2H, d, *J* = 8.2 Hz, Ar*H* biphenyl), 7.23 (6H, d, *J* = 8.6 Hz, Ar*H* stopper), 7.04 - 7.15 (8H, m, Ar*H* stopper), 6.87 (2H, d, *J* = 8.9 Hz, Ar*H* stopper), 5.08 (2H, s, CH_2), 4.39 (2H, s, CH_2), 1.30 (27H, s, CH_3 stopper)

^{13}C NMR (101MHz, $CDCl_3$) δ = 156.6, 148.3, 144.1, 140.8, 140.1, 139.9, 136.5, 134.4, 132.3, 130.7, 128.7, 128.1, 127.5, 127.3, 124.0, 113.3, 69.6, 63.1, 54.5, 34.3, 31.4

MS (ESI): m/z calc. for $C_{51}H_{55}ON_3Na$ $[M+Na]^+$: 749.43; found: 749.34

Proto-triazole axle 46



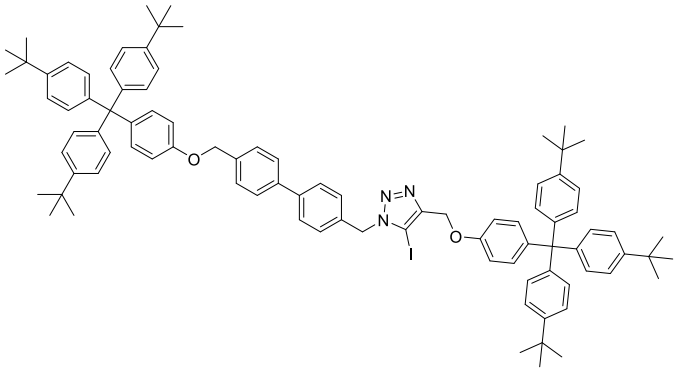
Azide **45** (50 mg, 0.07 mmol, 1 eq) and the alkyne-functionalised phenyl trityl stopper compound **6** (37 mg, 0.07 mmol, 1 eq) were dissolved in dry CH_2Cl_2 (3 mL). To this solution were added in order TBTA (7 mg, 0.01 mmol, 0.2 eq), $Cu(CH_3CN)_4{\cdot}PF_6$ (5 mg, 0.01 mmol, 0.2 eq) and DIPEA (13 µL, 0.14 mmol, 2 eq) and the reaction was left to stir overnight at room temperature. After this time the reaction mixture was washed with 25% $NH_4OH_{(aq)}$ (1 × 3 mL) and the organic phase was collected, dried over anhydrous $MgSO_4$ and the solvent removed *in vacuo*. The resulting residue was purified by silica gel column chromatography (CH_2Cl_2) and the proto-triazole-containing compound **46** was isolated as a white solid (58 mg, 0.05 mmol, 66%).

^{1}H NMR (400MHz, $CDCl_3$) δ = 7.61 (1H, s, Ar*H* triazole), 7.55 - 7.60 (4H, m, Ar*H* biphenyl), 7.51 (2H, d, *J* = 7.7 Hz, Ar*H* biphenyl), 7.36 (2H, d, *J* = 7.6 Hz, Ar*H* biphenyl), 7.20 - 7.26 (12H, m, Ar*H* stopper), 7.02 - 7.15 (16H, m, Ar*H* stopper), 6.86 (4H, t, *J* = 9.1 Hz, Ar*H* stopper), 5.59 (2H, s, C*H*$_2$), 5.19 (2H, s, C*H*$_2$), 5.08 (2H, s, C*H*$_2$), 1.31 (54H, s, C*H*$_3$ stopper)

^{13}C NMR (101MHz, $CDCl_3$) δ = 156.0, 148.3, 148.3, 144.8, 144.1, 144.0, 139.8, 136.7, 133.5, 132.3, 130.7, 129.0, 128.6, 128.6, 128.0, 127.9, 127.8, 127.2, 124.0, 123.7, 122.6, 113.2, 113.2, 69.5, 63.0, 63.0, 62.0, 54.0, 53.9, 53.4, 34.2, 31.4, 20.5

MS (ESI): m/z calc. for $C_{91}H_{102}N_3O_2$ $[M+H]^+$: 1269.80; found: 1269.89.

Iodo-triazole axle 47



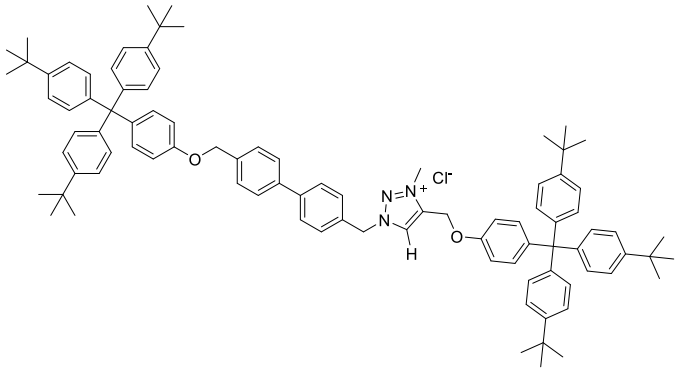
Azide **45** (66 mg, 0.07 mmol, 1 eq) was dissolved in THF (1 mL). NaI (54 mg, 0.28 mmol, 4 eq) and $Cu(ClO_4)_2{\cdot}6H_2O$ (67 mg, 0.14 mmol, 2 eq) were added and the resulting suspension was left to stir for five minutes. TBTA (5 mg, 0.01 mmol, 0.1 eq) and DBU (15 mg, 0.07 mmol, 1 eq) were then added to the mixture. Finally, alkyne-functionalised phenyl trityl stopper compound **6** (49 mg, 0.07 mmol, 1 eq), and CH_3CN (1 mL) were added and the reaction was left to stir overnight in the dark. The crude mixture was then washed with 25% $NH_4OH_{(aq)}$ (1 × 2 mL) and the organic phase was collected, dried over anhydrous $MgSO_4$ and the solvent removed *in vacuo*. The resulting residue was purified by silica gel column chromatography (CH_2Cl_2). The iodo-triazole-containing compound **47** was isolated as a white solid (59 mg, 0.04 mmol, 60%).

^{1}H NMR (400MHz, $CDCl_3$) δ = 7.57 (4H, dd, *J* = 8.3 Hz, ^4J = 1.6 Hz, Ar*H* biphenyl), 7.49 (2H, d, *J* = 7.8 Hz, Ar*H* biphenyl), 7.37 (2H, d, *J* = 7.7 Hz, Ar*H* biphenyl), 7.19 - 7.26 (12H, m, Ar*H* stopper), 7.04 - 7.15 (16H, m, Ar*H* stopper), 6.82 - 6.93 (4H, m, Ar*H* stopper), 5.65 (2H, s, CH_2), 5.11 (2H, s, CH_2), 5.08 (2H, s, CH_2), 1.30 (54H, s, CH_3 stopper)

^{13}C NMR (101MHz, $CDCl_3$) δ = 148.3, 148.3, 144.3, 144.1, 144.0, 144.0, 134.7, 132.3, 130.7, 130.5, 129.1, 128.6, 128.4, 128.0, 128.0, 127.6, 127.5, 127.3, 124.4, 124.0, 123.7, 113.6, 113.3, 68.4, 63.1, 54.1, 53.4, 47.1, 34.3, 31.4, 30.9, 27.8, 22.2

MS (ESI): m/z calc. for $C_{91}H_{101}N_3O_2I$ $[M+H]^+$: 1395.70; found: 1395.81.

Proto-triazolium axle 48·Cl



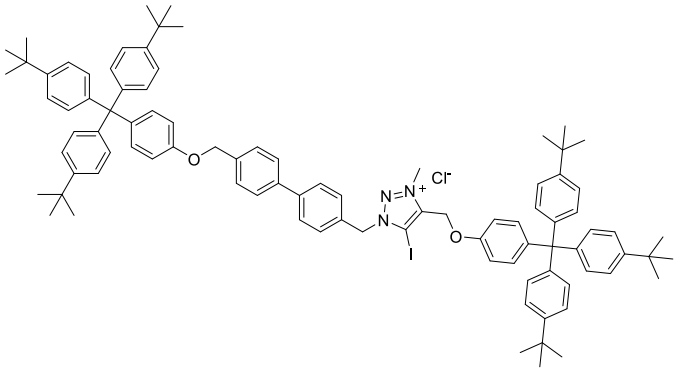
Proto-triazole axle **46** (58 mg, 0.05 mmol, 1 eq) and $Me_3O{\cdot}BF_4$ (10 mg, 0.07 mmol, 1.5 eq) were dissolved in dry CH_2Cl_2 (4 mL). The solution was left to stir for two days at room temperature under a flow of $N_{2(g)}$. After this time the reaction was quenched with three drops of MeOH and the solvent was removed *in vacuo*. The resulting solid was purified by silica gel column chromatography (CH_2Cl_2:MeOH 95:5) and the product **48·BF$_4$** isolated as a pale yellow solid. Subsequent anion exchange to yield **48·Cl** was performed by dissolving **48·BF$_4$** in a solvent mixture of 45:45:10 $CHCl_3$:MeOH:H_2O (10 mL) and passing the solution three times through a column of Amberlite® resin loaded with chloride (46 mg, 0.04 mmol, 69%).

^{1}H NMR (400MHz, $CDCl_3$) δ = 8.46 (1H, s, Ar*H* triazolium), 7.62 - 7.66 (2H, m, Ar*H* biphenyl), 7.47 - 7.58 (6H, m, Ar*H* biphenyl), 7.19 - 7.26 (12H, m, Ar*H* stopper), 7.01 - 7.17 (16H, m, Ar*H* stopper), 6.77 - 6.89 (4H, m, Ar*H* stopper), 5.74 (2H, s, C*H*$_2$), 5.27 (2H, s, C*H*$_2$), 5.07 (2H, s, C*H*$_2$), 4.32 (3H, s, C*H*$_3$ triazolium), 1.30 (54H, s, C*H*$_3$ stopper)

^{13}C NMR (126MHz, $CDCl_3$) δ = 156.6, 148.4, 148.3, 148.2, 144.3, 144.1, 143.7, 140.0, 139.5, 139.4, 136.9, 132.7, 132.3, 130.7, 130.6, 130.1, 129.7, 129.2, 128.1, 128.0, 127.4, 127.3, 126.6, 124.1, 124.0, 124.0, 113.2, 113.2, 72.3, 69.5, 63.1, 63.0, 38.9, 34.3, 34.2, 31.3

MS (MALDI): *m/z* calc. for $C_{92}H_{104}N_3O_2$ $[M - Cl]^+$: 1284.82; found: 1284.69.

Iodo-triazolium axle 49·Cl



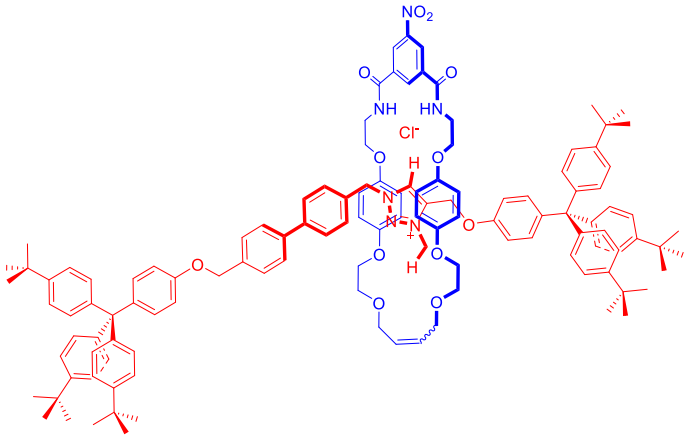
Iodo triazole axle **47** (59 mg, 0.04 mmol, 1 eq) and $Me_3O{\cdot}BF_4$ (10 mg, 0.07 mmol, 1.5 eq) were dissolved in dry CH_2Cl_2 (30 mL). The solution was left to stir for two days at room temperature under $N_{2(g)}$. After this time the reaction was quenched with three drops of MeOH and the solvent was removed *in vacuo*. The resulting solid was purified by silica gel column chromatography (CH_2Cl_2:MeOH 95:5) and the product **49·BF$_4$** isolated as a white solid. Subsequent anion exchange to yield **49·Cl** was performed by dissolving **49·BF$_4$** in a solvent mixture of 45:45:10 $CHCl_3$:MeOH:H_2O (10 mL) and passing the solution three times through a column of Amberlite® resin loaded with chloride (56 mg, 0.04 mmol, 97%).

^{1}H NMR (400MHz, $CDCl_3$) δ = 7.46 - 7.56 (2H, m, Ar*H* biphenyl), 7.31 - 7.46 (6H, m, Ar*H* biphenyl), 7.15 - 7.25 (12H, m, Ar*H* stopper), 6.95 - 7.15 (16H, m, Ar*H* stopper), 6.65 - 6.86 (4H, m, Ar*H* stopper), 5.70 (2H, s, C*H*$_2$), 5.36 (2H, s, C*H*$_2$), 4.99 (2H, s, C*H*$_2$), 4.42 (3H, s, C*H*$_3$ triazolium), 1.27 (54H, s, C*H*$_3$ stopper)

^{13}C NMR (126MHz, $CDCl_3$) δ = 156.5, 154.5, 148.4, 148.3, 144.1, 143.8, 143.3, 142.1, 141.8, 139.9, 139.2, 136.8, 132.6, 132.3, 130.7, 130.6, 128.9, 128.0, 128.0, 127.2, 124.2, 124.1, 124.0, 113.3, 113.2, 104.6, 69.4, 63.1, 63.0, 59.5, 57.1, 39.7, 34.3, 34.3, 31.4, 29.7

MS (MALDI): *m/z* calc. for $C_{92}H_{103}IN_3O_2$ $[M - Cl]^+$: 1410.72; found: 1410.97.

Proto-triazolium [2]rotaxane 50·Cl



The one-station axle **48·Cl** (30 mg, 22.7 µmol, 1 eq) and bis-vinyl nitro macrocycle precursor **22** (18 mg, 27.2 µmol, 1.2 eq) were dissolved in dry CH_2Cl_2 (2 mL) and stirred for ten minutes. Grubbs' II catalyst (2 mg, 10 wt. %) was added and the solution stirred at room temperature, monitoring by TLC and ESI mass spectrometry throughout. After one day a further addition of Grubbs' II catalyst (2 mg, 10 wt. %) was made and upon depletion of macrocycle precursor **22** (which occurred after two days) the solvent was removed *in vacuo*. The resulting crude residue was purified by preparative silica TLC (EtOAc:MeOH 99:1 and CH_2Cl_2:MeOH 98:2) to give the product one station rotaxane **50·Cl** as an off-white solid (9 mg, 4.6 µmol, 20%).

^{1}H NMR (500MHz, $CDCl_3$) δ = 9.69 (1H, br. s, Ar*H* int. macro), 9.49 (1H, br. s, Ar*H* triazolium), 9.26 - 9.42 (2H, m, N*H* macro), 8.80 (2H, s, Ar*H* ext. macro), 7.55 (4H, d, *J* = 8.2 Hz, Ar*H* biphenyl), 7.42 (2H, d, *J* = 8.1 Hz, Ar*H* biphenyl), 7.32 (2H, d, *J* = 8.7 Hz, Ar*H* biphenyl), 7.20 - 7.27 (12H, m, Ar*H* stopper), 7.06 - 7.20 (16H, m, Ar*H* stopper), 7.01 (2H, d, *J* = 8.7 Hz, Ar*H* stopper), 6.88 (2H, d, *J* = 8.9 Hz, Ar*H* stopper), 6.32 - 6.49 (8H, m, Ar*H* hydroquinone macro), 5.54 (2H, br. s., C*H* alkene macro), 5.27 (2H, s, CH_2 axle), 5.09 (2H, s, CH_2 axle), 4.72 (2H, s, CH_2 axle), 4.56 - 4.68 (2H, m, CH_2 macro), 4.45 - 4.56 (2H, m, CH_2 macro), 3.94 - 4.00 (2H, m, CH_2 macro), 3.88 (3H, s, CH_3 triazolium), 3.63 - 3.92 (12H, m, CH_2 macro), 3.52 - 3.62 (2H, m, CH_2 macro), 1.31 (54H, s, CH_3 stopper)

^{13}C NMR (126MHz, $CDCl_3$) δ = 164.1, 153.0, 151.9, 148.5, 148.3, 144.1, 144.0, 132.5, 132.3, 130.9, 130.7, 130.6, 129.8, 129.6, 128.8, 128.2, 127.5, 127.2, 126.6, 124.3, 124.0, 115.0, 114.4, 113.8, 113.3, 70.8, 69.4, 68.1, 67.6, 66.5, 63.1, 39.9, 38.9, 38.7, 34.3, 34.3, 31.9, 31.4, 30.3, 29.7, 29.7, 29.4, 28.9, 23.7, 23.0, 22.7, 14.1, 14.0, 10.9

MS (ESI): m/z calc. for $C_{124}H_{139}N_6O_{12}$ $[M-Cl]^+$: 1905.0524; found: 1905.0453.

Proto-triazolium [2]rotaxane 50·I

50·Cl was anion-exchanged to the iodide salt **50·I** using Amberlite® anion exchange resin. The solvent used was 45:45:10 $CHCl_3$:MeOH:H_2O (10 mL).

^{1}H NMR (400MHz, 4:1 $CDCl_3$:MeOD) δ = 9.22 (1H, s, Ar*H* int. macro), 8.73 (3H, s, Ar*H* triazolium, ext. macro), 8.62 - 8.70 (2H, m, N*H* macrocycle), 7.36 - 7.53 (8H, m, Ar*H* biphenyl), 6.94 - 7.29 (30H, m, Ar*H* stopper), 6.84 (2H, d, *J* = 8.9 Hz, Ar*H* stopper), 6.24 - 6.60 (8H, m, Ar*H* hydroquinone macro), 5.60 - 5.70 (2H, m, C*H* alkene macro), 5.31 (2H, s, CH_2 axle), 5.04 (2H, s, CH_2 axle), 4.80 (2H, s, CH_2 axle), 4.67 - 4.78 (2H, m, CH_2 macro), 4.29 - 4.39 (2H, m, CH_2 macro), 3.85 (3H, s, CH_3 triazolium), 3.54 - 4.07 (16H, m, CH_2 macro), 1.24 (54H, s, CH_3 stopper)

Proto-triazolium [2]rotaxane 50·PF_6

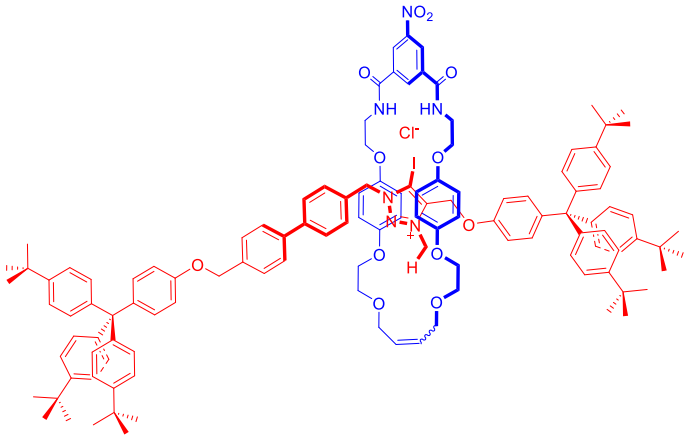
50·Cl was anion-exchanged to the hexafluorophosphate salt **50·PF_6** using Amberlite® anion exchange resin. The solvent used was 45:45:10 $CHCl_3$:MeOH:H_2O (10 mL).

^{1}H NMR (500MHz, $CDCl_3$) δ = 8.87 (2H, s, Ar*H* ext. macro), 8.50 (1H, br. s, Ar*H* int. macro), 8.25 (1H, br. s, Ar*H* triazolium), 7.43 - 7.60 (8H, m, Ar*H* biphenyl), 7.03 - 7.29 (28H, m, Ar*H* stopper), 6.95 (2H, d, *J* = 8.5 Hz, Ar*H* stopper), 6.88 (2H, d, *J* = 8.7 Hz, Ar*H* stopper), 6.26 - 6.58 (8H, m, Ar*H* hydroquinone macro), 5.64 - 5.73 (2H, m, C*H* alkene macro), 5.21 (2H, s, CH_2 axle), 5.07 (2H, s, CH_2 axle), 4.73 (2H, s, CH_2 axle), 4.33 - 4.51 (4H, m, CH_2 macro), 3.79 (3H, s, CH_3 triazolium), 3.52 - 4.15 (16H, m, CH_2 macro), 1.31 (54H, s, CH_3 stopper)

^{19}F NMR (470 MHz, $CDCl_3$) δ = -72.7 (d, ^{1}J = 706 Hz, PF_6).

^{31}P NMR (202 MHz, $CDCl_3$) δ = -144.3 (sept, ^1J = 709 Hz, PF_6).

Iodo-triazolium [2]rotaxane 51·Cl



The one-station axle **49·Cl** (33 mg, 22.8 µmol, 1 eq) and bis-vinyl nitro macrocycle precursor **22** (18 mg, 27.4 µmol, 1.4 eq) were dissolved in dry CH_2Cl_2 (2 mL) and stirred for ten minutes. Grubbs' II catalyst (2 mg, 10 wt. %) was added and the solution stirred at room temperature, monitoring by TLC and ESI mass spectrometry throughout. After one day a further addition of Grubbs' II catalyst (2 mg, 10 wt. %) was made and after three days the solvent was removed *in vacuo*. The resulting crude residue was purified by iterative preparative silica TLC (CH_2Cl_2:MeOH 97:3) to give the product one-station rotaxane **51·Cl** as a white solid (5 mg, 2.4 µmol, 11%).

^{1}H NMR (400MHz, $CDCl_3$) δ = 9.35 (1H, br. s, Ar*H* int. macro), 9.01 (2H, s, Ar*H* ext. macro), 8.38 - 8.54 (2H, m, N*H* macro), 7.63 - 7.68 (2H, m, Ar*H* biphenyl), 7.53 - 7.58 (2H, m, Ar*H* biphenyl), 7.48 - 7.52 (2H, m, Ar*H* biphenyl), 7.30 - 7.35 (2H, m, Ar*H* biphenyl), 7.15 - 7.26 (12H, m, Ar*H* stopper), 7.06 - 7.14 (16H, m, Ar*H* stopper), 6.97 (2H, d, *J* = 8.4 Hz, Ar*H* stopper), 6.88 (2H, d, *J* = 8.9 Hz, Ar*H* stopper), 6.29 - 6.39 (8H, m, Ar*H* hydroquinone macro), 5.40 - 5.51 (2H, m, C*H* alkene macro), 5.09 (2H, s, CH_2 axle), 4.88 (2H, s, CH_2 axle), 4.67 - 4.80 (2H, m, CH_2 macro), 4.51 - 4.60 (2H, m, CH_2 macro), 4.49 (2H, s, CH_2 axle), 4.15 (3H, s, CH_3 triazolium), 3.97 - 4.06 (2H, m, CH_2 macro), 3.85 - 3.95 (2H, m, CH_2 macro), 3.59 - 3.83 (10H, m, CH_2 macro), 3.45 - 3.56 (2H, m, CH_2 macro), 1.32 (54H, s, CH_3 stopper)

^{13}C NMR (126MHz, $CDCl_3$) δ = 164.4, 155.1, 153.0, 151.6, 148.5, 148.3, 144.1, 143.9, 142.8, 139.9, 135.9, 132.5, 132.3, 130.7, 130.7, 130.6, 130.2, 129.2, 128.2, 127.9, 127.4, 126.7, 124.3, 124.0, 115.8, 115.4, 114.7, 114.1, 113.2, 70.7, 69.6, 69.4, 67.6, 66.9, 63.2, 63.1, 39.8, 39.5, 37.1, 34.3, 34.3, 32.7, 31.9, 31.4, 30.0, 29.7, 29.7, 29.4, 27.1, 22.7, 19.7, 14.1

MS (ESI): *m/z* calc. for $C_{124}H_{138}IN_6O_{12}$ $[M - Cl]^+$: 2031.9524; found: 2031.9476.

Iodo-triazolium [2]rotaxane 51·I

51·Cl was anion-exchanged to the iodide salt **51·I** using Amberlite® anion exchange resin. The solvent used was 45:45:10 $CHCl_3$:MeOH:H_2O (10 mL).

^{1}H NMR (400MHz, 4:1 $CDCl_3$:MeOD) δ = 9.28 (1H, s, Ar*H* int. macro), 8.88 (2H, d, ^4J = 1.3 Hz, Ar*H* ext. macro), 7.42 - 7.66 (8H, m, Ar*H* biphenyl), 6.90 - 7.32 (30H, m, Ar*H* stopper), 6.80 - 6.87 (2H, m, Ar*H* stopper), 6.29 - 6.43 (8H, m, Ar*H* hydroquinone macro), 5.34 - 5.42 (2H, m, C*H* alkene macro), 5.06 (2H, s, CH_2 axle), 4.92 (2H, s, CH_2 axle), 4.50 (2H, s, CH_2 axle), 4.43 - 4.62 (4H, m, CH_2 macro), 4.13 (3H, s, CH_3 triazolium), 3.94 - 4.16 (4H, m, CH_2 macro), 3.45 - 3.90 (12H, m, CH_2 macro), 1.25 (54H, s, CH_3 stopper)

Iodo-triazolium [2]rotaxane 51·PF_6

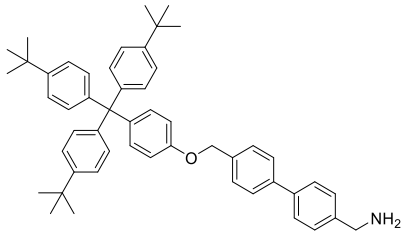
51·Cl was anion-exchanged to the hexafluorophosphate salt **51·PF_6** using Amberlite® anion exchange resin. The solvent used was 45:45:10 $CHCl_3$:MeOH:H_2O (10 mL).

^{1}H NMR (400MHz, $CDCl_3$) δ = 8.83 - 8.92 (3H, m, Ar*H* int., ext. macro), 7.38 - 7.59 (8H, m, Ar*H* biphenyl), 7.01 - 7.32 (28H, m, Ar*H* stopper), 6.90 - 6.98 (2H, m, Ar*H* stopper), 6.80 - 6.90 (2H, m, Ar*H* stopper), 6.31 - 6.56 (8H, m, Ar*H* hydroquinone macro), 5.49 - 5.58 (2H, m, C*H* alkene macro), 5.03 (4H, s, CH_2 axle), 4.72 (2H, br. s, CH_2 axle), 4.34 - 4.52 (2H, m, CH_2 macro), 4.18 - 4.32 (2H, m, CH_2 macro), 4.15 (3H, s, CH_3 triazolium), 3.52 - 4.12 (16H, m, CH_2 macro), 1.30 (54H, s, CH_3 stopper)

^{19}F NMR (470 MHz, $CDCl_3$) δ = -72.5 (d, ^1J = 706 Hz, PF_6).

^{31}P NMR (202 MHz, $CDCl_3$) δ = -144.3 (sept, ^1J = 708 Hz, *P*F_6)

Biphenyl amine mono stoppered axle pre-cursor 52



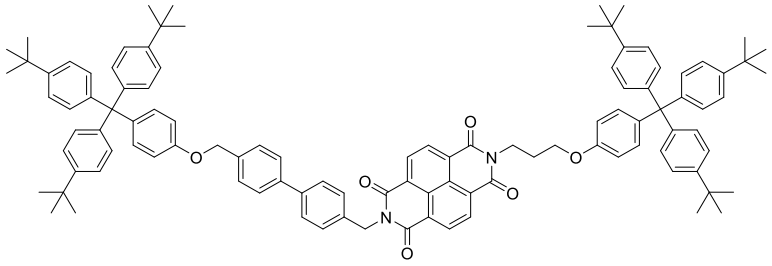
Azide **45** (200 mg, 0.28 mmol) was dissolved in $CHCl_3$ (10 mL) and Pd/C (40 mg, 20 wt. %) was added to the solution followed by MeOH (10 mL). The reaction was stirred under an atmosphere of $H_{2(g)}$ for two days after which the crude mixture was filtered through a plug of Celite, which was rinsed with a further 50 mL of 1:1 $CHCl_3$:MeOH to give a clear solution. The solvent was then removed *in vacuo* and the free amine **52** isolated by silica gel column chromatography (CH_2Cl_2:MeOH 95:5) as a white solid (180 mg, 0.26 mmol, 92%).

^{1}H NMR (500MHz, 1:1 $CDCl_3$:CD_3OD) δ = 7.55 - 7.62 (4H, m, Ar*H* biphenyl), 7.44 - 7.51 (2H, m, Ar*H* biphenyl), 7.34 - 7.42 (2H, m, Ar*H* biphenyl), 7.17 - 7.26 (6H, m, Ar*H* stopper), 7.01 - 7.12 (8H, m, Ar*H* stopper), 6.82 - 6.89 (2H, m, Ar*H* stopper), 5.07 (2H, s, CH_2), 4.17 (2H, br. s, NH_2), 3.86 (2H, s, CH_2), 1.27 (27H, s, CH_3 stopper)

^{13}C NMR (126MHz, MeOD) δ = 156.3, 148.1, 143.9, 140.1, 139.7, 136.1, 132.0, 130.5, 127.8, 127.7, 127.1, 126.9, 123.8, 113.1, 69.5, 62.8, 44.8, 34.0, 31.0

MS (ESI): *m/z* calc. for $C_{51}H_{58}NO$ $[M + H]^+$: 700.45; found: 700.41.

NDI axle 53



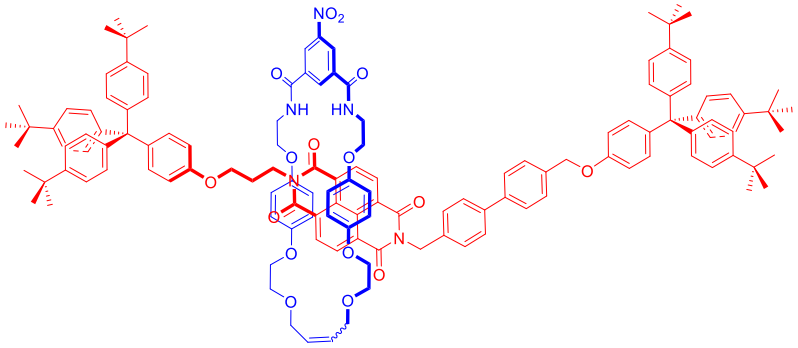
The propylamine-functionalised phenyl trityl stopper compound **27** (40 mg, 0.07 mmol, 1 eq) and commerically available 1,4,5,8-naphthalenetetracarboxylic dianhydride (19 mg, 0.07 mmol, 1 eq) were suspended in 1 mL of dry, degassed DMF with dry Et_3N (6 µL, 0.07 mmol, 1 eq) in a sealed microwave vial. The suspension was sonicated for ten minutes before heating under microwave irradiation for five minutes at 140 °C. The resulting brown solution was allowed to cool and the vial opened to allow for the addition of amine **52** (50 mg, 0.07 mmol, 1 eq) and further dry Et_3N (6 µL, 0.07 mmol, 1 eq). The vial was resealed and the suspension sonicated for 30 minutes before heating under microwave irradiation for a further five minutes at 140 °C. Upon cooling the brown solution was placed immediately into a round bottom flask and reduced *in vacuo* to give a golden brown residue. This crude reaction mixture was purified by silica gel column chromatography (CH_2Cl_2) to yield the desired one station axle compound **53** (89 mg, 0.06 mmol, 83%).

^{1}H NMR (400MHz, $CDCl_3$) δ = 8.71 - 8.83 (4H, m, Ar*H* NDI), 7.63 (2H, m, Ar*H* biphenyl), 7.61 - 7.68 (2H, m, Ar*H* biphenyl), 7.52 - 7.59 (4H, m, Ar*H* biphenyl), 7.45 - 7.50 (2H, m, Ar*H* biphenyl), 7.19 - 7.26 (12H, m, Ar*H* stopper), 6.96 - 7.14 (16H, m, Ar*H* stopper), 6.80 - 6.91 (2H, m, Ar*H* stopper), 6.57 - 6.69 (2H, m, Ar*H* stopper), 5.45 (2H, s, CH_2), 5.06 (2H, s, CH_2), 4.44 (2H, t, *J* = 7.0 Hz, CH_2), 4.11 (2H, t, *J* = 6.1 Hz, CH_2), 2.21 - 2.33 (2H, m, CH_2), 1.30 (54H, s, CH_3 stopper)

^{13}C NMR (126MHz, $CDCl_3$) δ = 162.9, 162.8, 162.8, 156.6, 156.5, 148.3, 144.1, 140.4, 140.3, 139.9, 139.6, 136.3, 135.6, 132.3, 132.1, 131.2, 131.0, 130.7, 130.7, 129.7, 129.6, 128.0, 127.3, 127.2, 126.7, 126.7, 126.6, 124.0, 113.2, 112.9, 69.6, 65.9, 63.0, 63.0, 43.7, 38.6, 34.3, 31.4, 27.9

MS (MALDI): *m/z* calc. for $C_{105}H_{109}N_2O_6$ $[M + H]^+$: 1495.83; found: 1495.66.

NDI [2]rotaxane 54



The one-station axle **53** (45 mg, 30.1 µmol, 1 eq) and bis-vinyl nitro macrocycle precursor **22** (30 mg, 45.2 µmol, 1.5 eq.) were dissolved in dry CH_2Cl_2 (2 mL) and stirred for ten minutes. Grubbs' II catalyst (3 mg, 10 wt. %) was added and the solution stirred at room temperature, monitoring by TLC throughout. After one day a further addition of Grubbs' II (3 mg, 10 wt. %) was made and upon depletion of macrocycle precursor **22** (which occurred after four days) the solvent was removed *in vacuo*. The resulting crude residue was purified by preparative silica TLC (CH_2Cl_2:MeOH 99:1) to give the product one station rotaxane **54** as an orange solid (1 mg, 0.47 µmol, 2%).

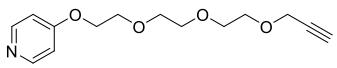
^{1}H NMR (500MHz, $CDCl_3$) δ = 9.19 (1H, s, Ar*H* int. macro), 9.10 (2H, s, Ar*H* ext. macro), 8.50 - 8.61 (4H, m, Ar*H* NDI), 7.53 - 7.63 (6H, m, Ar*H* biphenyl), 7.46 - 7.51 (2H, m, Ar*H* biphenyl), 7.18 - 7.25 (12H, m, Ar*H* stopper), 7.03 - 7.13 (16H, m, Ar*H* stopper), 6.83 - 6.89 (2H, m, Ar*H* stopper), 6.71 - 6.77 (2H, m, Ar*H* stopper), 6.24 - 6.33 (2H, m, C*H* alkene macro), 5.63 - 5.80 (8H, m, Ar*H* hydroquinone macro), 5.27 (2H, s, CH_2 axle), 5.05 (2H, s, CH_2 axle), 4.31 (2H, t, *J* = 7.0 Hz, CH_2 axle), 4.17 - 4.26 (4H, m, CH_2 macro), 3.98 - 4.17 (6H, m, CH_2 macro, axle), 3.37 - 3.81 (12H, m, CH_2 macro), 2.20 - 2.29 (2H, m, CH_2 axle), 1.30 (54H, s, CH_3 stopper)

^{13}C NMR (126MHz, $CDCl_3$) δ = 164.9, 163.5, 163.1, 156.6, 156.5, 152.4, 151.3, 149.2, 148.3, 148.3, 144.1, 144.0, 140.8, 140.1, 139.9, 136.6, 136.2, 135.3, 132.3, 131.1, 131.0, 130.7, 130.6, 130.2, 130.0,

129.7, 128.6, 128.2, 128.2, 127.2, 126.7, 126.0, 125.9, 125.6, 124.0, 114.1, 114.0, 113.9, 113.2, 113.1, 71.1, 69.6, 68.8, 67.2, 66.9, 65.9, 63.0, 63.0, 44.0, 40.7, 38.5, 34.3, 31.4, 29.7, 28.1

MS (MALDI): *m/z* calc. for $C_{137}H_{143}N_5O_{16}Na$ $[M + Na]^+$: 2139.05; found: 2139.54

Pyridine polyether alkyne 56



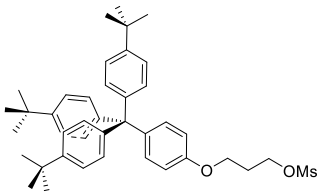
A solution of 4-hydroxypyridine (1.26 g, 13.3 mmol, 1.25 eq), PPh_3 (3.49 g, 13.3 mmol, 1.25 eq) and diethyl azodicarboxylate (DEAD) (2.09 mL, 13.3 mmol, 1.25 eq) in dry THF (100 mL) was stirred at room temperature for 30 minutes under a flow of $N_{2(g)}$ before triethylene glycol mono-alkyne **55** (2.00 g, 10.6 mmol, 1 eq) was added. The reaction was stirred for two days at room temperature before the solvent was removed *in vacuo* and the resulting residue purified using silica gel column chromatography (5 - 10% MeOH:CH_2Cl_2) to afford **56** (1.4 g, 5.3 mmol, 50%).

^{1}H NMR (300MHz, $CDCl_3$) δ = 7.37 (2H, d, *J* = 7.6 Hz, Ar*H*), 6.32 (2H, d, *J* = 7.6 Hz, Ar*H*), 4.15 (2H, d, ^4J = 2.3 Hz, CH_2), 3.91 (2H, t, *J* = 5.1 Hz, CH_2), 3.72 (2H, t, *J* = 5.1 Hz, CH_2), 3.49 - 3.67 (8H, m, CH_2), 2.42 (1H, t, ^4J = 2.3 Hz, C*H* alkyne)

^{13}C NMR (76MHz, $CDCl_3$) δ = 178.8, 140.4, 118.3, 79.4, 74.6, 70.6, 70.5, 70.3, 70.0, 68.9, 58.3, 56.6

MS (ESI): *m/z* calc. for $C_{14}H_{19}NO_4K$ $[M + K]^+$: 305.10; found: 305.05

Phenyl trityl stopper propyl mesylate 58



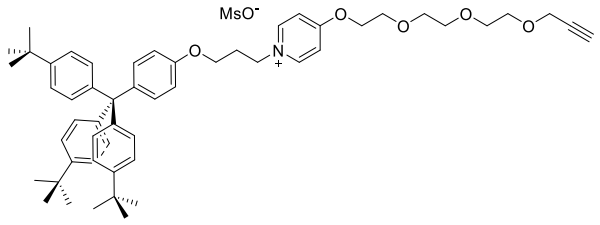
Phenyl trityl stopper propyl alcohol **57** (475 mg, 0.84 mmol, 1 eq) was dissolved in dry THF (20 mL) and dry Et_3N (0.23 mL, 1.68 mmol, 2 eq) and methanesulfonyl chloride (0.10 mL, 1.27 mmol, 1.5 eq) were

added. The reaction was stirred overnight at room temperature before the solvent was removed under reduced pressure. The crude reaction mixture was then re-dissolved in CH_2Cl_2 (50 mL) and washed with H_2O (3 x 50 mL) and 5% $NaHCO_{3(aq)}$ (3 x 50 mL) and dried over anhydrous $MgSO_4$. Removing the solvent *in vacuo* gave the desired phenyl trityl stopper propyl mesylate **58** (508 mg, 0.79 mmol, 94%).

^{1}H NMR (300MHz, $CDCl_3$) δ = 7.20 - 7.27 (6H, m, Ar*H* stopper), 7.02 - 7.14 (8H, m, Ar*H* stopper), 6.77 (2H, d, *J* = 8.2 Hz, Ar*H* stopper), 4.45 (2H, t, *J* = 6.2 Hz, CH_2), 4.08 (2H, t, *J* = 5.9 Hz, CH_2), 3.00 (3H, s, CH_3 Ms), 2.22 (2H, quin, *J* = 5.9 Hz, CH_2), 1.26 - 1.34 (27H, m, CH_3 stopper)

^{13}C NMR (76MHz, $CDCl_3$) δ = 156.4, 148.3, 144.1, 139.7, 132.4, 130.7, 124.1, 113.5, 65.1, 58.3, 37.9, 34.3, 32.6, 31.4, 30.2,

Mono-stoppered pyridinium polyether alkyne 59·MsO



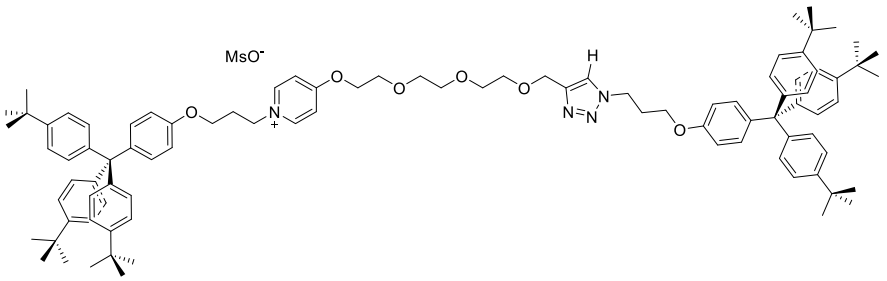
Pyridine derivative **56** (106 mg, 0.40 mmol, 1 eq) and phenyl trityl stopper propyl mesylate **58** (307 mg, 0.50 mmol, 1.2 eq) were suspended in dry MeCN (5 mL) and heated under microwave irradiation for 2 hours at 160 °C. Following this the solvent was removed from the crude reaction mixture and purified using silica gel column chromatography (10 - 20% MeOH:CH_2Cl_2) to give **59·MsO** (138 mg, 0.15 mmol, 38%).

^{1}H NMR (300MHz, $CDCl_3$) δ = 9.02 (2H, d, *J* = 7.6 Hz, Ar*H* py), 7.37 (2H, d, *J* = 7.6 Hz, Ar*H* py), 7.20 - 7.26 (6H, m, Ar*H* stopper), 7.01 - 7.17 (8H, m, Ar*H* stopper), 6.76 (2H, d, *J* = 9.4 Hz, Ar*H* stopper), 4.78 (2H, t, *J* = 5.5 Hz, CH_2), 4.50 (2H, t, *J* = 6.2 Hz, CH_2), 4.17 (2H, d, ^4J = 2.3 Hz, CH_2), 4.13 (2H, t, *J* = 5.6 Hz, CH_2), 3.96 (2H, t, *J* = 5.5 Hz, CH_2), 3.53 - 3.72 (8H, m, CH_2), 2.45 (1H, t, ^4J = 2.3 Hz, C*H* alkyne), 2.35 (2H, quin, *J* = 5.9 Hz, CH_2), 1.30 (27H, s, CH_3 stopper)

^{13}C NMR (76MHz, $CDCl_3$) δ = 170.2, 156.1, 148.3, 147.2, 144.0, 140.1, 132.3, 130.6, 124.0, 113.4, 112.8, 110.0, 75.0, 70.3, 70.1, 69.4, 69.2, 67.8, 63.0, 58.4, 53.4, 34.3, 31.4, 28.5

MS (ESI): *m/z* calc. for $C_{54}H_{68}NO_5$ $[M - MsO]^+$: 810.51; found: 810.55

Pyridinium proto-triazole axle 60·MsO



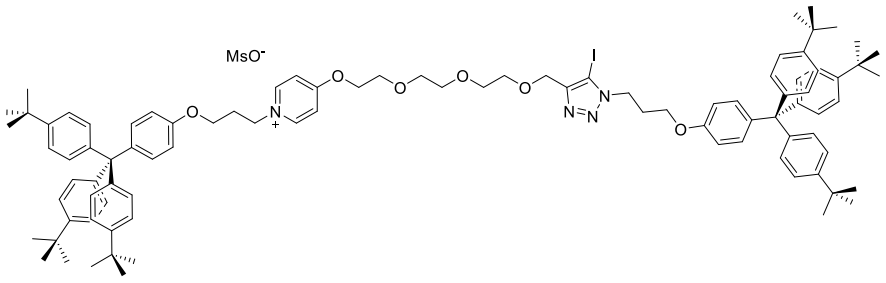
Azide **26** (47 mg, 0.08 mmol, 1 eq) and the mono-stoppered alkyne-functionalised pyridinium **59·MsO** (66 mg, 0.08 mmol, 1 eq) were dissolved in dry CH_2Cl_2 (2 mL). To this solution were added in order TBTA (8 mg, 0.02 mmol, 0.2 eq), $Cu(CH_3CN)_4{\cdot}PF_6$ (6 mg, 0.02 mmol, 0.2 eq) and DIPEA (28 μL, 0.16 mmol, 2 eq) and the reaction was left to stir overnight at room temperature. After this time the reaction mixture was washed with 25% $NH_4OH_{(aq)}$ (1 × 3 mL) and the organic phase was collected, dried over anhydrous $MgSO_4$ and the solvent removed *in vacuo*. The resulting residue was purified by silica gel column chromatography (1:9 MeOH:CH_2Cl_2) and the proto-triazole-containing compound **60·MsO** was isolated as a white solid (64 mg, 0.04 mmol, 55%).

^{1}H NMR (300MHz, $CDCl_3$) δ = 8.79 (2H, br. s., Ar*H* py), 7.70 (1H, br. s., Ar*H* triazole), 7.17 - 7.26 (14H, m, Ar*H* stopper, py), 7.03 - 7.13 (16H, m, Ar*H* stopper), 6.70 (2H, d, *J* = 8.8 Hz, Ar*H* stopper), 6.74 (2H, d, *J* = 8.8 Hz, Ar*H* stopper), 4.59 - 4.76 (4H, m, C*H*$_2$), 4.41 - 4.57 (4H, m, C*H*$_2$), 4.10 (2H, t, *J* = 5.3 Hz, C*H*$_2$), 3.84 - 3.99 (4H, m, C*H*$_2$), 3.69 (2H, br. s., C*H*$_2$), 3.61 (4H, br. s., C*H*$_2$), 3.53 (2H, br. s., C*H*$_2$), 2.31 (4H, br. s., C*H*$_2$), 1.29 (54H, s, C*H*$_3$ stopper)

^{13}C NMR (126MHz, $CDCl_3$) δ = 170.1, 156.1, 148.2, 146.7, 143.9, 143.9, 139.8, 139.8, 132.2, 132.2, 130.6, 124.0, 113.2, 112.8, 112.7, 70.3, 70.2, 70.2, 69.5, 69.4, 67.7, 64.1, 63.8, 62.9, 59.4, 47.1, 34.2, 31.4, 31.3, 29.9, 28.4

MS (ESI): *m/z* calc. for $C_{94}H_{117}N_4O_6$ [M - MsO]$^+$: 1399.90; found: 1399.86

Pyridinium iodo-triazole axle 61·MsO



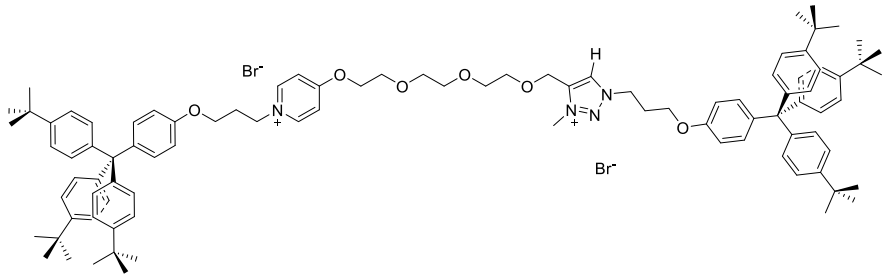
Azide **26** (76 mg, 0.13 mmol, 1.5 eq) was dissolved in THF (1 mL). NaI (52 mg, 0.34 mmol, 4 eq) and $Cu(ClO_4)_2{\cdot}6H_2O$ (64 mg, 0.17 mmol, 2 eq) were added and the resulting suspension was left to stir for five minutes. TBTA (5 mg, 0.01 mmol, 0.1 eq) and DBU (13 mg, 0.09 mmol, 1 eq) were added to the mixture. Finally, alkyne-functionalised pyridinium **59·MsO** (75 mg, 0.09 mmol, 1 eq), and CH_3CN (1 mL) were added and the reaction mixture was left to stir overnight in the dark. The crude mixture was then washed with 25% $NH_4OH_{(aq)}$ (1 × 2 mL) and the organic phase was collected, dried over anhydrous $MgSO_4$ and the solvent removed *in vacuo*. The resulting residue was purified by silica gel column chromatography (1:9 MeOH:CH_2Cl_2). The iodo-triazole-containing compound **61·MsO** was isolated as an off-white solid (139 mg, 0.09 mmol, 95%).

^{1}H NMR (300MHz, $CDCl_3$) δ = 9.05 (2H, d, *J* = 7.0 Hz, Ar*H* py), 7.32 (2H, d, *J* = 7.0 Hz, Ar*H* py), 7.22 (12H, d, *J* = 8.5 Hz, Ar*H* stopper), 7.04 - 7.11 (16H, m, Ar*H* stopper), 6.65 - 6.80 (4H, m, Ar*H* stopper), 4.87 (2H, br. s., C*H*$_2$), 4.58 (2H, s, C*H*$_2$), 4.42 - 4.56 (4H, m, C*H*$_2$), 4.11 (2H, t, *J* = 5.9 Hz, C*H*$_2$), 4.00 (2H, br. s., C*H*$_2$), 3.94 (2H, t, *J* = 5.9 Hz, C*H*$_2$), 3.48 - 3.73 (8H, m, C*H*$_2$), 2.24 - 2.42 (4H, m, C*H*$_2$), 1.30 (54H, s, C*H*$_3$ stopper)

^{13}C NMR (126MHz, $CDCl_3$) δ = 170.3, 156.1, 156.0, 148.2, 148.0, 146.8, 146.7, 140.0, 139.9, 132.3, 132.2, 130.8, 130.6, 124.2, 124.0, 113.5, 112.9, 112.8, 90.2, 79.4, 75.0, 70.4, 70.3, 70.2, 70.1, 69.7, 69.3, 69.2, 69.1, 67.8, 64.1, 63.7, 62.9, 60.0, 59.6, 58.4, 53.5, 47.9, 33.9, 31.3

MS (ESI): *m/z* calc. for $C_{94}H_{116}IN_4O_6$ [M - MsO]$^+$: 1523.79; found: 1523.77

Pyridinium proto-triazolium axle 62·(Br)$_2$



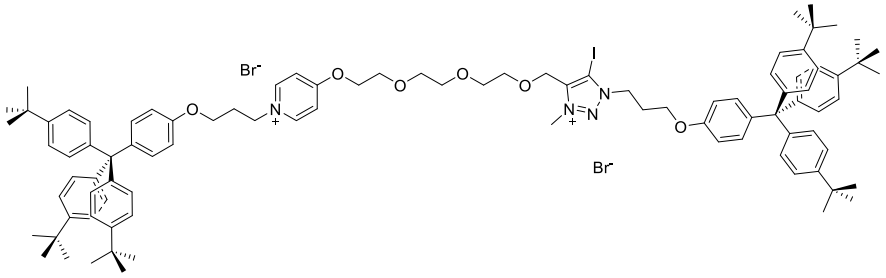
Proto-triazole axle **60·MsO** (64 mg, 0.04 mmol, 1 eq) and $Me_3O{\cdot}BF_4$ (19 mg, 0.13 mmol, 3 eq) were dissolved in dry CH_2Cl_2 (20 mL). The solution was left to stir for two days at room temperature under $N_{2(g)}$. After this time the reaction was quenched with three drops of MeOH and the solvent was removed *in vacuo*. The resulting solid was purified by silica gel column chromatography (CH_2Cl_2:MeOH 90:10) and the product **62·(BF$_4$)$_2$** isolated as a pale yellow solid. Subsequent anion exchange was performed by washing a solution of **62·(BF$_4$)$_2$** in CH_2Cl_2 (10 mL) with 1 M $NH_4Br_{(aq)}$ (8 x 10 mL) and then H_2O (2 x 10 mL). The organic layer was then dried over anhydrous $MgSO_4$ and removal of the solvent gave the bis-bromide salt **62·(Br)$_2$** (50 mg, 0.03 mmol, 80%).

^{1}H NMR (300MHz, $CDCl_3$) δ = 9.00 (1H, br. s., Ar*H* triazolium), 8.72 (1H, br. s., Ar*H* py), 7.34 (2H, br. s., Ar*H* py), 7.21 (12H, d, *J* = 8.2 Hz, Ar*H* stopper), 7.06 (16H, d, *J* = 8.2 Hz, Ar*H* stopper), 6.72 (2H, d, *J* = 8.2 Hz, Ar*H* stopper), 6.64 (2H, d, *J* = 8.8 Hz, Ar*H* stopper), 4.94 (2H, br. s., C*H*$_2$), 4.83 (2H, br. s., C*H*$_2$), 4.61 - 4.75 (2H, m, C*H*$_2$), 4.46 (2H, br. s., C*H*$_2$), 4.21 (3H, br. s., C*H*$_3$ triazolium), 3.89 - 4.12 (6H, m, C*H*$_2$), 3.73 (2H, br. s., C*H*$_2$), 3.50 - 3.66 (6H, m, C*H*$_2$), 2.45 (2H, br. s., C*H*$_2$), 2.27 (2H, br. s., C*H*$_2$), 1.31 (54H, s, C*H*$_3$ stopper)

^{13}C NMR (126MHz, $CDCl_3$) δ = 170.3, 156.1, 156.0, 146.8, 146.7, 140.0, 139.9, 132.3, 132.2, 130.8, 130.6, 124.2, 124.0, 113.5, 112.9, 112.8, 90.2, 79.4, 75.0, 70.4, 70.3, 70.2, 70.1, 69.7, 69.3, 69.2, 69.1, 67.8, 64.1, 63.7, 62.9, 60.0, 59.6, 58.4, 53.5, 47.9, 33.9, 31.3

MS (ESI): *m/z* calc. for $C_{95}H_{120}N_4O_6$ $[M - 2Br]^{2+}$: 706.96; found: 707.00

Pyridinium iodo-triazolium axle 63·(Br)$_2$



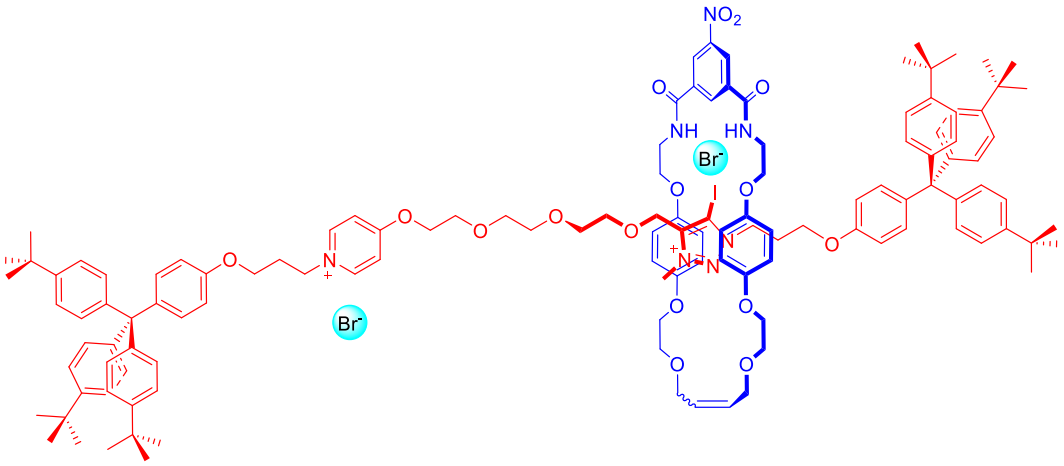
Iodo-triazole axle **61·MsO** (32 mg, 0.02 mmol, 1 eq) and $Me_3O{\cdot}BF_4$ (9 mg, 0.06 mmol, 3 eq) were dissolved in dry CH_2Cl_2 (15 mL). The solution was left to stir for two days at room temperature under $N_{2(g)}$. After this time the reaction was quenched with three drops of MeOH and the solvent was removed *in vacuo*. The resulting solid was purified by silica gel column chromatography (CH_2Cl_2:MeOH 90:10) and the product **63·(BF$_4$)$_2$** isolated as a pale yellow solid. Subsequent anion exchange was performed by washing a solution of **63·(BF$_4$)$_2$** in CH_2Cl_2 (10 mL) with 1 M $NH_4Br_{(aq)}$ (8 x 10 mL) and then H_2O (2 x 10 mL). The organic layer was then dried over anhydrous $MgSO_4$ and removal of the solvent gave the bis-bromide salt **63·(Br)$_2$** (22 mg, 0.01 mmol, 66%).

^{1}H NMR (300MHz, $CDCl_3$) δ = 8.81 (2H, d, *J* = 7.0 Hz, Ar*H* py), 7.41 (2H, d, *J* = 6.5 Hz, Ar*H* py), 7.18 - 7.26 (12H, m, Ar*H* stopper), 7.00 - 7.13 (16H, m, Ar*H* stopper), 6.74 (2H, d, *J* = 8.8 Hz, Ar*H* stopper), 6.68 (2H, d, *J* = 8.8 Hz, Ar*H* stopper), 4.92 (2H, s, C*H*$_2$), 4.80 (2H, br. s., C*H*$_2$), 4.72 (2H, t, *J* = 6.7 Hz, C*H*$_2$), 4.51 (2H, t, *J* = 5.9 Hz, C*H*$_2$), 4.22 (3H, s, C*H*$_3$ triazolium), 3.95 - 4.14 (6H, m, C*H*$_2$), 3.76 (2H, br. s., C*H*$_2$), 3.55 - 3.72 (6H, m, C*H*$_2$), 2.43 (2H, br. s., C*H*$_2$), 2.31 (2H, quin, *J* = 5.9 Hz, C*H*$_2$), 1.25 (54H, s, C*H*$_3$ stopper)

^{13}C NMR (126MHz, $CDCl_3$) δ = 206.3, 170.5, 156.1, 155.7, 154.7, 148.3, 148.2, 146.3, 144.4, 144.0, 144.0, 140.2, 139.9, 137.4, 132.3, 132.3, 130.6, 130.6, 129.1, 124.3, 124.1, 124.0, 122.6, 122.2, 113.9, 112.8, 96.1, 71.3, 71.0, 70.9, 70.7, 69.6, 68.1, 68.0, 65.9, 63.3, 63.0, 62.9, 61.9, 60.4, 58.9, 52.2, 50.9, 39.6, 36.1, 34.3, 33.3, 31.9, 31.3, 29.7, 29.4, 29.4, 29.2, 29.0, 28.6, 28.4, 26.9, 25.6, 24.7, 23.9, 22.7, 19.7, 15.3, 14.1, 13.7

MS (ESI): *m/z* calc. for $C_{95}H_{119}IN_4O_6$ $[M - 2Br]^{2+}$: 769.40; found: 769.40

Pyridinium iodo-triazolium [2]rotaxane 64·$(Br)_2$



Axle **63·$(Br)_2$** (96 mg, 56.5 µmol, 1 eq) and bis-vinyl nitro macrocycle precursor **22** (51 mg, 78.5 µmol, 1.4 eq) were dissolved in dry CH_2Cl_2 (5 mL) and stirred for ten minutes. Grubbs' II catalyst (5mg, 10 wt. %) was added and the solution stirred at room temperature, monitoring by TLC and ESI mass spectrometry throughout. After one day a further addition of Grubbs' II catalyst (5 mg, 10 wt. %) was made and after three days the solvent was removed *in vacuo*. The resulting crude residue was purified by iterative preparative silica TLC (CH_2Cl_2:MeOH 96:4) to give the [2]rotaxane **64·$(Br)_2$** as an off-white solid (3 mg, 1.1 µmol, 2%).

^{1}H NMR (300MHz, $CDCl_3$) δ = 9.73 (1H, s, Ar*H* int. macro), 9.05 (2H, s, Ar*H* ext. macro), 8.62 (2H, br. s., Ar*H* py), 7.17 - 7.26 (14H, m, Ar*H* stopper, py), 6.99 - 7.16 (16H, m, Ar*H* stopper), 6.78 (2H, d, *J* = 8.8 Hz, Ar*H* stopper), 6.71 (2H, d, *J* = 8.8 Hz, Ar*H* stopper), 6.48 (4H, d, *J* = 8.2 Hz, Ar*H* hydroquinone macro), 6.37 (4H, d, *J* = 8.2 Hz, Ar*H* hydroquinone macro), 5.90 (2H, br. s., C*H* alkene macro), 4.66 (2H, br. s., CH_2), 4.42 - 4.60 (6H, m, CH_2), 4.25 (6H, br. s., CH_2), 4.03 - 4.18 (8H, m, CH_2), 3.99 (3H, br. s., CH_3 triazolium), 3.84 (8H, d, *J* = 5.3 Hz, CH_2), 3.75 (4H, br. s., CH_2), 3.67 (4H, br. s., CH_2), 3.58 (4H, d, *J* = 7.6 Hz, CH_2), 2.36 - 2.46 (2H, m, CH_2), 2.26 - 2.36 (2H, m, CH_2), 1.28 (54H, s, CH_3 stopper)

^{13}C NMR (126MHz, $CDCl_3$) δ = 206.3, 170.5, 164.6, 156.1, 155.7, 154.7, 153.3, 152.5, 148.3, 148.2, 146.3, 144.4, 144.0, 144.0, 140.2, 139.9, 137.4, 136.3, 132.3, 132.3, 131.2, 130.6, 130.6, 129.1, 124.6, 124.3, 124.1, 124.0, 122.6, 122.2, 117.5, 115.6, 113.9, 112.8, 96.1, 72.4, 71.3, 71.0, 70.9, 70.7, 69.6,

68.1, 68.0, 67.9, 66.8, 65.9, 63.3, 63.0, 62.9, 61.9, 60.4, 58.9, 52.2, 50.9, 40.1, 39.6, 36.1, 34.3, 33.3, 31.9, 31.3, 29.7, 29.4, 29.4, 29.2, 29.0, 28.6, 28.4, 26.9, 25.6, 24.7, 23.9, 22.7, 19.7, 15.3, 14.1, 13.7

MS (ESI): *m/z* calc. for $C_{127}H_{154}IN_7O_{16}$ $[M - 2Br]^{2+}$: 1080.5259; found: 1080.5287

Pyridinium iodo-triazolium [2]rotaxane 64·$(PF_6)_2$

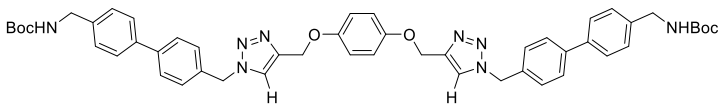
64·$(Cl)_2$ was anion-exchanged to the bis-hexafluorophosphate salt **64·$(PF_6)_2$** using Amberlite® anion exchange resin. The solvent used was 45:45:10 $CHCl_3$:MeOH:H_2O (10 mL).

^{1}H NMR (500MHz, 1:1 $CDCl_3$:CD_3OD) δ = 8.89 (1H, t, ^4J = 1.5 Hz, Ar*H* int. macro), 8.87 (2H, d, ^4J = 1.6 Hz, Ar*H* ext. macro), 8.29 (2H, d, *J* = 7.6 Hz, Ar*H* py), 7.13 - 7.26 (14H, m, Ar*H* stopper, py), 6.95 - 7.12 (16H, m, Ar*H* stopper), 6.72 (2H, d, *J* = 8.6 Hz, Ar*H* stopper), 6.67 (2H, d, *J* = 8.4 Hz, Ar*H* stopper), 6.52 (4H, d, *J* = 8.9 Hz, Ar*H* hydroquinone macro), 6.35 (4H, d, *J* = 8.9 Hz, Ar*H* hydroquinone macro), 5.87 (2H, s, C*H* alkene), 4.52 (2H, s, CH_2), 4.41 - 4.46 (4H, m, CH_2), 4.36 - 4.40 (2H, m, CH_2), 4.18 (3H, s, CH_3 triazolium), 4.13 - 4.17 (2H, m, CH_2), 3.48 - 4.11 (32H, m, CH_2), 2.21 - 2.28 (2H, m, CH_2), 2.10 (2H, t, *J* = 5.8 Hz, CH_2), 1.25 (54H, s, CH_3 stopper)

^{19}F NMR (470 MHz, $CDCl_3$) δ = -72.7 (d, ^1J = 706 Hz, PF_6).

^{31}P NMR (202 MHz, $CDCl_3$) δ = -144.3 (sept, ^1J = 709 Hz, *P*F_6).

Bis-proto-triazole Boc-protected bis-amine 66



Azide **28** (317 mg, 0.94 mmol, 2 eq) and bis-alkyne **65** (87 mg, 0.47 mmol, 1 eq) were dissolved in dry CH_2Cl_2 (20 mL). To this solution were added in order TBTA (101 mg, 0.19 mmol, 0.4 eq), $Cu(CH_3CN)_4$·PF_6 (70 mg, 0.19 mmol, 0.4 eq) and DIPEA (330 µL, 1.88 mmol, 4 eq) and the reaction was left to stir overnight at room temperature. During this time, the bis-proto-triazole product precipitated from

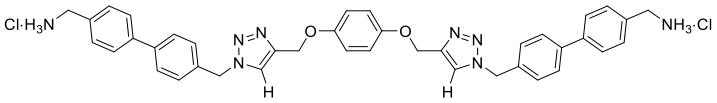
solution and was collected *via* filtration and dried *in vacuo* to give a white solid **66** (329 mg, 0.38 mmol, 81%).

R_f = 0.3 (95:5 CH_2Cl_2/MeOH)

^{1}H NMR (400MHz, DMSO-d_6) δ = 8.28 (2H, s, Ar*H* triazole), 7.65 (4H, d, *J* = 8.1 Hz, Ar*H* biphenyl), 7.60 (4H, d, *J* = 8.1 Hz, Ar*H* biphenyl), 7.34 - 7.44 (6H, m, Ar*H* biphenyl, N*H*), 7.31 (4H, d, *J* = 8.2 Hz, Ar*H* biphenyl), 6.95 (4H, s, Ar*H* hydroquinone), 5.64 (4H, s, CH_2), 5.06 (4H, s, CH_2), 4.15 (4H, d, ^4J = 5.7 Hz, CH_2), 1.40 (18H, s, CH_3 Boc)

MS (ESI): *m/z* calc. for $C_{50}H_{55}N_8O_6$ $[M + H]^+$: 863.42; found: 863.48

Bis-proto-triazole Boc-protected bis-amine 67·(Cl)$_2$

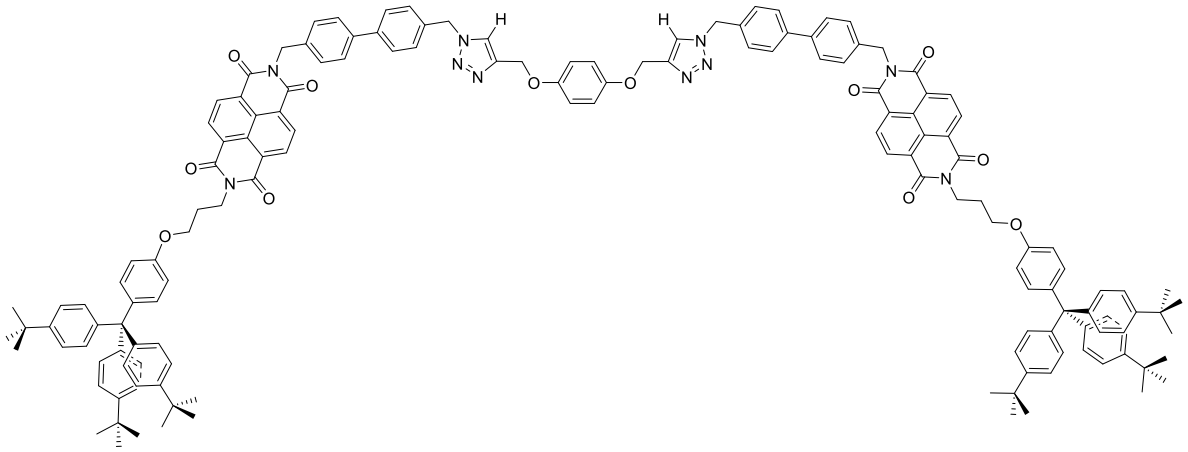


The bis-Boc derivative **66** (50 mg, 0.06 mmol) was suspended in dry DMF (10 mL) and concentrated HCl (1 mL, 11 M) was added causing formation of a partial solution. The reaction was stirred for two hours before the solvent was removed *in vacuo* to give an off-white powder **67·(Cl)$_2$**, which was used without further purification (42 mg, 0.06 mmol, assumed quant.).

R_f = baseline (95:5 CH_2Cl_2/MeOH)

MS (ESI): *m/z* calc. for $C_{40}H_{39}N_8O_2$ $[M + H]^+$: 663.32; found: 662.48

Bis-proto-triazole bis-NDI axle 68



Azide **69** (150 mg, 0.15 mmol, 2 eq) and bis-alkyne **65** (11 mg, 0.06 mmol, 1 eq) were dissolved in dry CH_2Cl_2 (25 ml). Then TBTA (12 mg, 0.02 mmol, 0.4 eq), $Cu(MeCN)_4 \cdot PF_6$ (9 mg, 0.02 mmol, 0.4 eq) and *N,N*-diisopropylethylamine (41 µl, 0.24 mmol, 4 eq) were added to the mixture and left to stir at room temperature for 2 days, monitoring by thin layer chromatography (CH_2Cl_2:MeOH 99:1). The mixture was diluted with CH_2Cl_2 and washed with a 0.02 M EDTA/0.1 M $NH_4OH_{(aq)}$ solution, the organic layer was dried over $MgSO_4$, and the solvent was removed *in vacuo*. The resultant crude was purified by silica gel column chromatography (CH_2Cl_2:MeOH 99:1) to give **68** (100 mg, 0.04 mmol, 81%)

68 was also prepared from bis-amine **67·(Cl)$_2$**.

The propylamine-functionalised phenyl trityl stopper compound **27** (66 mg, 0.12 mmol, 2 eq) and commerically available 1,4,5,8-naphthalenetetracarboxylic dianhydride (32 mg, 0.12 mmol, 2 eq) were suspended in 1 mL of dry, degassed DMF with dry Et_3N (18 µL, 0.12 mmol, 2 eq) in a sealed microwave vial. The suspension was sonicated for ten minutes before heating under microwave irradiation for five minutes at 140 °C. The resulting brown solution was allowed to cool and the vial opened to allow for the addition of bis-amine **67** (43 mg, 0.06 mmol, 1 eq) and further dry Et_3N (18 µL, 0.12 mmol, 2 eq). The vial was resealed and the suspension sonicated for 30 minutes before heating under microwave irradiation for a further five minutes at 140 °C. Upon cooling the brown solution was placed immediately into a round bottom flask and reduced *in vacuo* to give a golden brown residue. This crude

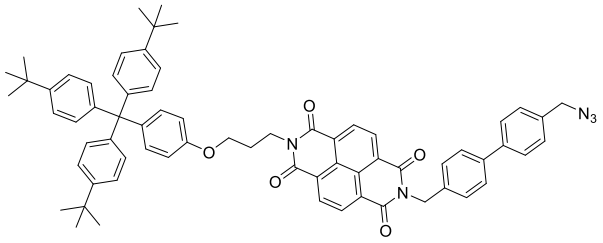
reaction mixture was purified by silica gel column chromatography (CH_2Cl_2:MeOH 97:3) to yield the desired axle compound **68** (16 mg, 0.01 mmol, 12%).

^{1}H NMR (400 MHz, $CDCl_3$) δ = 1.31 (s, 54H, stopper C*H*$_3$) 2.20 - 2.34 (m, 4H, axle C*H*$_2$) 4.10 (br. s., 4H, axle C*H*$_2$) 4.43 (br. s., 4H, axle C*H*$_2$) 5.10 (s, 4H, axle C*H*$_2$) 5.42 (s, 4H, axle C*H*$_2$) 5.53 (s, 4H, axle C*H*$_2$) 6.64 (d, *J* = 8.68 Hz, 4H, hydroquinone Ar*H*) 6.85 (s, 2H, triazole Ar*H*) 7.01 - 7.12 (m, 16H, stopper Ar*H*) 7.24 (d, *J* = 8.31 Hz, 12H, stopper Ar*H*) 7.30 (d, *J* = 7.95 Hz, 4H, biphenyl Ar*H*) 7.46 - 7.56 (m, 8H, biphenyl Ar*H*) 7.63 (d, *J* = 8.07 Hz, 4H, biphenyl Ar*H*) 8.73 (d, *J* = 7.58 Hz, 8H, NDI Ar*H*)

^{13}C NMR (101 MHz, $CDCl_3$) δ = 27.97, 31.41, 34.31, 38.67, 43.71, 53.88, 62.71, 63.06, 65.99, 112.95, 115.84, 122.60, 124.06, 126.53, 126.72, 127.26, 127.72, 128.56, 129.74, 130.72, 131.02, 131.19, 132.19, 133.55, 136.08, 139.71,141.21, 144.14, 144.78, 148.32, 152.76, 156.52, 162.85

MS (ESI): m/z calc. for $C_{148}H_{142}N_{10}NaO_{12}$ $[M + Na + H + H]^{3+}$:759.36 found; 759.31

Mono-stoppered NDI biphenyl azide 69



The propylamine-functionalised phenyl trityl stopper compound **27** (110 mg, 0.20 mmol, 1 eq) and commerically available 1,4,5,8-naphthalenetetracarboxylic dianhydride (52 mg, 0.20 mmol, 1 eq) were suspended in 2 mL of dry, degassed DMF with dry Et_3N (28 µL, 0.20 mmol, 1 eq) in a sealed microwave vial. The suspension was sonicated for ten minutes before heating under microwave irradiation for five minutes at 140 °C. The resulting brown solution was allowed to cool and the vial opened to allow for the addition of amine **4** (47 mg, 0.20 mmol, 1 eq) and further dry Et_3N (28 µL, 0.20 mmol, 1 eq). The vial was resealed and the suspension sonicated for 30 minutes before heating under microwave irradiation for a further five minutes at 140 °C. Upon cooling the brown solution was placed

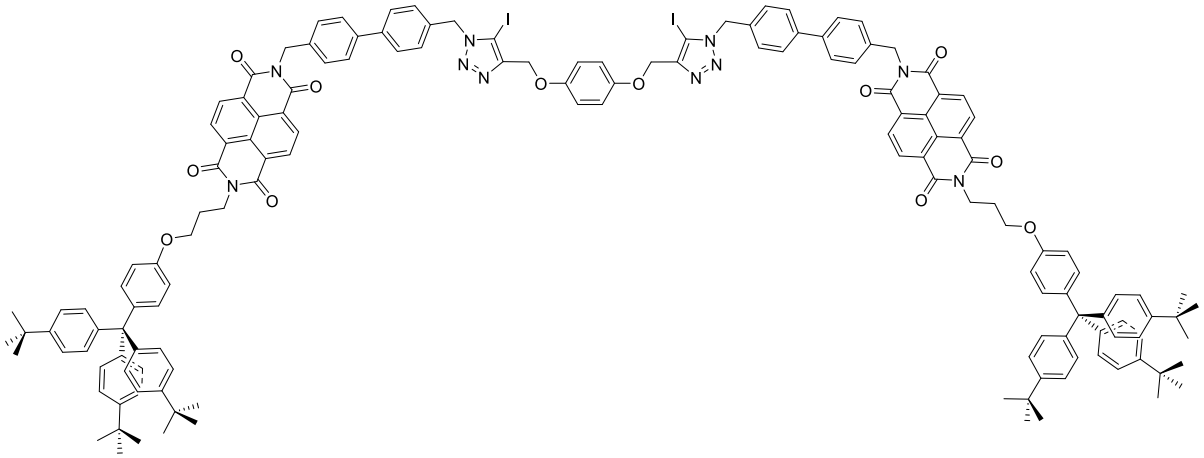
immediately into a round bottom flask and reduced *in vacuo* to give a golden brown residue. This crude reaction mixture was purified by silica gel column chromatography (CH_2Cl_2) to yield the desired mono-stoppered biphenyl NDI azide-containing compound **69** (160 mg, 0.16 mmol, 80%).

^{1}H NMR (400 MHz, $CDCl_3$) δ = 1.30 (s, 27H, stopper C*H*$_3$) 2.21 - 2.31 (m, 2H, axle C*H*$_2$) 4.10 (s, 2H, axle C*H*$_2$) 4.38 (s, 2H, axle C*H*$_2$) 4.41 - 4.49 (m, 2H, axle C*H*$_2$) 5.45 (s, 2H, axle C*H*$_2$) 6.99 - 7.09 (m, 8H, stopper Ar*H*) 7.23 (m, 6H, stopper Ar*H*) 7.37 (d, *J* = 8.07 Hz, 2H, biphenyl Ar*H*) 7.52 - 7.60 (m, 4H, biphenyl Ar*H*) 7.64 (s, 4H, biphenyl Ar*H*) 8.70 - 8.81 (m, 4H, NDI Ar*H*)

^{13}C NMR (101MHz, $CDCl_3$) δ = 162.9, 148.3, 144.1, 140.0, 135.8, 134.5, 132.1, 131.1, 130.7, 129.7, 128.6, 127.4, 126.6, 124.0, 112.9, 108.0, 98.4, 67.6, 66.0, 63.0, 54.5, 43.7, 38.6, 34.3, 33.2, 31.4, 28.5, 23.6

MS (MALDI): m/z calc. for $C_{68}H_{66}N_3O_5$ $[M - N_2 + H]^+$: 1005.50; found: 1005.35

Bis-iodo-triazole bis-NDI axle 70



Azide **69** (100 mg, 0.10 mmol, 2.5 eq) was dissolved in dry, degassed THF (2 ml), NaI (46 mg, 0.31 mmol, 8 eq) was added followed by $Cu(ClO_4)\cdot 6H_2O$ (57 mg, 0.16 mmol, 4 eq), which was left stirring for 5 minutes. TBTA (4 mg, 0.01 mmol, 0.2 eq) and DBU (12 mg, 0.08 mmol, 2 eq) were added followed by **65** (7 mg, 0.04 mmol, 1 eq). The mixture was left to stir at room temperature for 2 days, avoiding exposure to light. The mixture was diluted with CH_2Cl_2 then washed with a 0.02 M EDTA/0.1 M

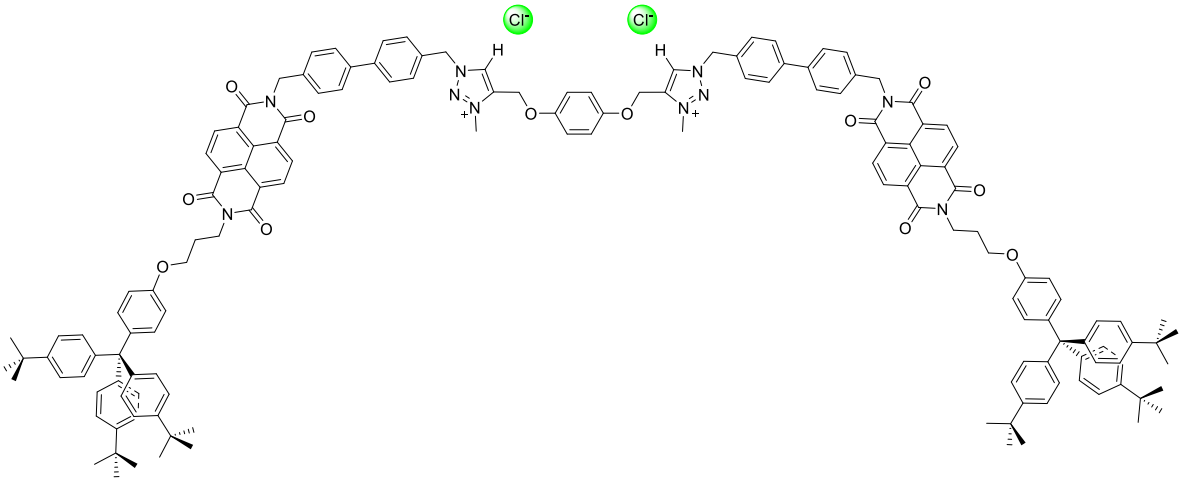
$NH_4OH_{(aq)}$ solution, the organic layer was dried over $MgSO_4$, and the solvent was removed *in vacuo*. The resultant solid was purified by silica gel column chromatography (99:1 CH_2Cl_2:MeOH) giving bis-iodo-triazole-containing compound **70** (83 mg, 0.03 mmol, 87%).

^{1}H NMR (400 MHz, $CDCl_3$) δ = 1.21 - 1.38 (m, 54H, stopper C*H*$_3$) 2.26 (d, *J* = 7.34 Hz, 4H, axle C*H*$_2$) 4.10 (s, 4H, axle C*H*$_2$) 4.43 (s, 4H, axle C*H*$_2$) 5.05 (s, 4H, axle C*H*$_2$) 5.42 (s, 4H, axle C*H*$_2$) 5.60 (s, 4H, axle C*H*$_2$) 6.64 (d, *J* = 8.80 Hz, 4H, hydroquinone Ar*H*) 6.94 (s, 4H, stopper Ar*H*) 6.98 - 7.10 (m, 16H, stopper Ar*H*) 7.23 (d, *J* = 8.44 Hz, 12H, stopper Ar*H*) 7.31 (d, *J* = 8.19 Hz, 4H, biphenyl Ar*H*) 7.51 (d, *J* = 7.82 Hz, 8H, biphenyl Ar*H*) 7.62 (d, *J* = 8.19 Hz, 4H, biphenyl Ar*H*) 8.69 - 8.79 (m, 8H, NDI Ar*H*)

^{13}C NMR (101MHz, $CDCl_3$) δ = 162.8, 156.5, 152.9, 148.1, 144.1, 140.1, 135.9, 133.1, 132.1, 131.1, 130.7, 129.7, 128.3, 127.5, 127.2, 126.7, 126.5, 124.0, 116.3, 112.9, 98.4, 80.5, 68.4, 67.4, 65.9, 63.0, 62.5, 53.9, 53.4, 43.7, 38.6, 34.3, 33.2, 31.4, 27.8, 23.3

MS (ESI): m/z calc. $C_{148}H_{138}I_2N_{10}O_{12}Na$ $[M + Na]^+$: 2525.85; found: 2525.09

Bis-proto-triazolium bis-NDI axle 71·(Cl)$_2$



Axle **68** (100 mg, 0.04 mmol, 1 eq) was dissolved in CH_2Cl_2 (40 ml) with $Me_3O{\cdot}BF_4$ (15 mg, 0.10 mmol, 2.5 eq) and the mixture was left stirring overnight at room temperature. The reaction was quenched with three drops of MeOH and the solvent was removed *in vacuo*. The resultant solid was purified by preparative silica TLC (CH_2Cl_2:MeOH 97:3) and isolated as **71·(BF$_4$)$_2$**. Subsequent anion exchange was

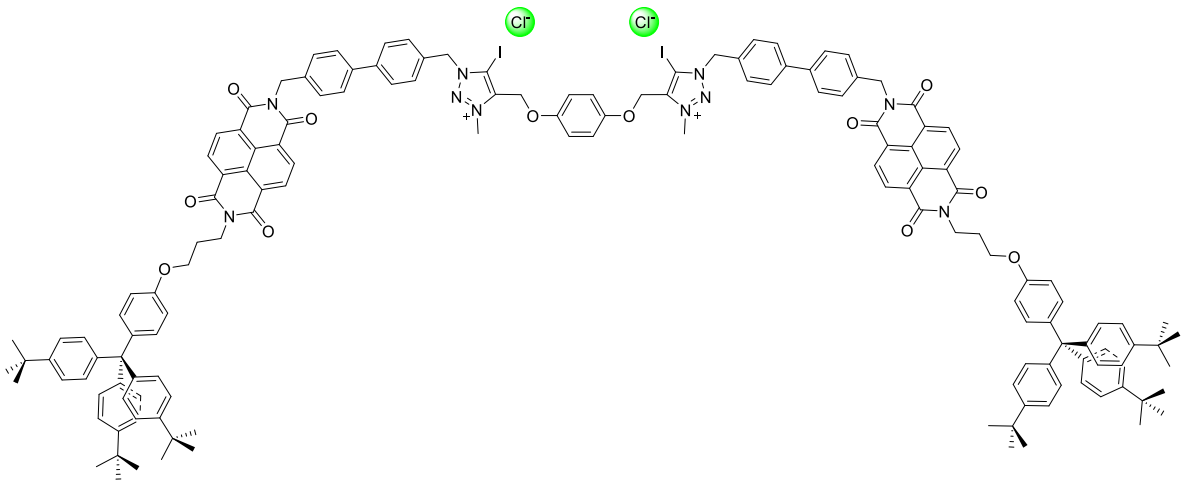
achieved by dissolving **71·$(BF_4)_2$** in (45:45:10 $CHCl_3$:MeOH:H_2O) and passing the solution three times through a column of Amberlite® resin loaded with chloride to yield **71·$(Cl)_2$** (96 mg, 0.04 mmol, 92%).

^{1}H NMR (400 MHz, $CDCl_3$) δ = 1.30 (s, 54H, stopper C*H*$_3$) 2.16 - 2.27 (m, 4H, axle C*H*$_2$) 4.03 - 4.12 (m, 4H, axle C*H*$_2$) 4.36 (br. s., 10H, axle C*H*$_2$, triazolium C*H*$_3$) 5.35 (s, 4H, Axle C*H*$_2$) 5.46 - 5.54 (m, 4H, axle C*H*$_2$) 5.88 - 5.97 (m, 4H, axle C*H*$_2$) 6.64 (d, *J* = 8.93 Hz, 4H, hydroquinone Ar*H*) 6.94 - 6.99 (m, 2H, triazolium Ar*H*) 6.99 - 7.09 (m, 18H, stopper Ar*H*) 7.22 (d, *J* = 8.56 Hz, 12H, stopper Ar*H*) 7.41 - 7.51 (m, 8H, biphenyl, Ar*H*) 7.57 (d, *J* = 8.31 Hz, 8H, biphenyl Ar*H*) 8.69 (d, *J* = 6.85 Hz, 8H, NDI Ar*H*)

^{13}C NMR (101 MHz, $CDCl_3$) δ = 31.37, 34.27, 63.02, 65.31, 66.45, 112.92, 124.01 126.04, 126.61, 126.97, 127.17, 127.28, 128.06, 129.67, 130.23, 131.37, 132.16, 138.83, 141.26, 144.12, 148.27, 156.50, 162.72

MS (ESI): m/z calc. for $C_{150}H_{146}N_{10}O_{12}$ $[M - 2Cl]^{2+}$ = 1140.0572 found 1140.0522

Bis-iodo-triazolium bis-NDI axle 72·$(Cl)_2$



Axle **70** (83 mg, 0.04 mmol, 1 eq) was dissolved in CH_2Cl_2 (33 ml) with $Me_3O{\cdot}BF_4$ (15 mg, 0.10 mmol, 2.5 eq) and the mixture was left stirring overnight at room temperature. The reaction was quenched with three drops of MeOH and the solvent was removed *in vacuo*. The resultant solid was purified by preparative silica TLC (CH_2Cl_2:MeOH 97:3) and isolated as **72·$(BF_4)_2$**. Subsequent anion exchange was

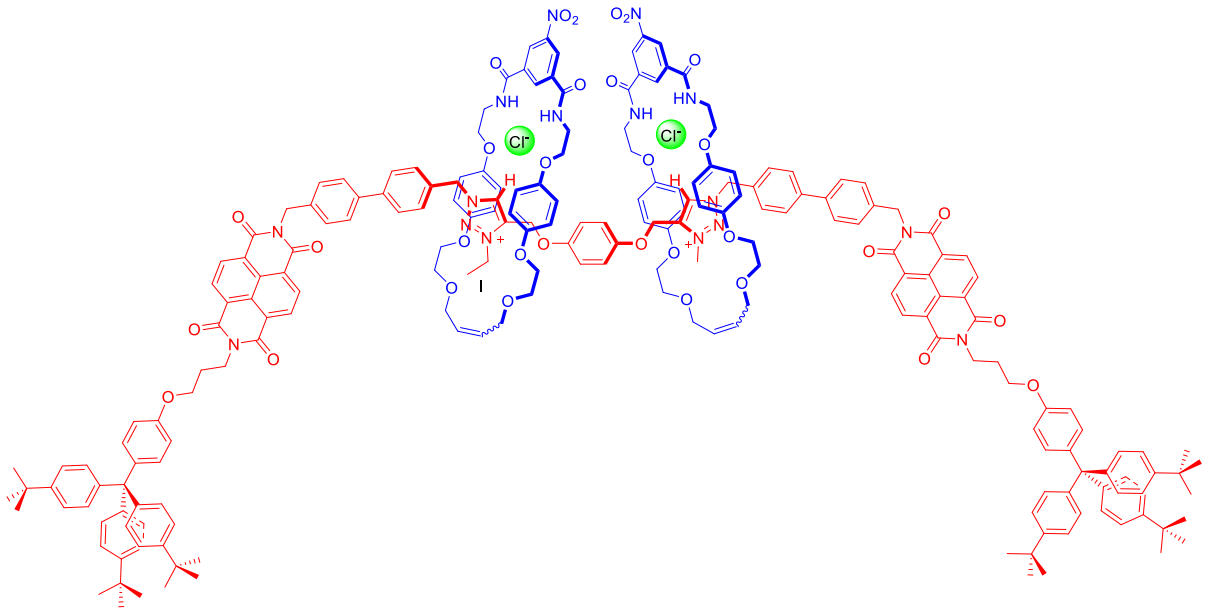
achieved by dissolving **72·$(BF_4)_2$** in (45:45:10 $CHCl_3$:MeOH:H_2O) and passing the solution three times through a column of Amberlite® resin loaded with chloride to yield **72·$(Cl)_2$**, (86 mg, 0.03 mmol, 90%).

^{1}H NMR (400 MHz, $CDCl_3$) δ = 1.30 (s, 54H, stopper C*H*$_3$) 2.16 - 2.29 (m, 4H, axle C*H*$_2$) 4.04 - 4.12 (m, 4H, axle C*H*$_2$) 4.37 - 4.50 (m, 10H, axle C*H*$_2$, triazolium C*H*$_3$) 5.32 - 5.38 (m, 4H, axle C*H*$_2$) 5.42 - 5.48 (m, 4H, axle C*H*$_2$) 5.58 - 5.63 (m, 4H, axle C*H*$_2$) 6.61 - 6.69 (m, 4H, hydroquinone Ar*H*) 6.91 - 6.96 (m, 4H, stopper Ar*H*) 7.06 (d, *J* = 8.68 Hz, 14H, stopper Ar*H*) 7.21 (s, 14H, biphenyl, stopper Ar*H*) 7.37 - 7.62 (m, 14H, biphenyl, stopper Ar*H*) 8.60 - 8.76 (m, 8H, NDI Ar*H*)

^{13}C NMR (101 MHz, $CDCl_3$) δ = 31.35, 34.26, 112.90, 124.00, 126.61, 127.14,127.56, 129.07, 129.75, 130.68, 130.79, 132.15, 139.17, 144.09, 148.27, 155.98, 162.73

MS (ESI): *m/z* calc. for $C_{150}H_{144}I_2N_{16}O_{12}$ $[M - 2BF_4]^{2+}$ = 1265.9538 found 1265.9501

Bis-proto-triazolium bis-NDI [3]rotaxane 73·$(Cl)_2$



Axle **71·$(Cl)_2$** (21 mg, 9.0 µmol, 1 eq) and **22** (16 mg, 27.0 µmol, 3 eq) were dissolved in dry CH_2Cl_2 (5 ml), the mixture was left to stir for 30 minutes. Grubbs' II catalyst (2 mg, 10 wt. %) was added and the solution stirred at room temperature, monitoring by TLC (CH_2Cl_2:MeOH 95:5) and ESI mass spectrometry throughout. After one day a further addition of Grubbs' II catalyst (2 mg, 10 wt. %) was

made and after a further day the solvent was removed *in vacuo*. The crude was purified by iterative preparative silica TLC using the solvent mixtures (EtOAc:MeOH 95:5 then CH_2Cl_2:MeOH 95:5) to yield [3]rotaxane **73·(Cl)$_2$** (9 mg, 2.0 µmol, 25%)

^{1}H NMR (500MHz, $CDCl_3$) δ = 10.04 (2H, br. s., Ar*H* int. macro), 9.88 (2H, br. s., Ar*H* triazolium), 9.38 (4H, br. s., N*H* macro), 8.63 - 8.83 (12H, m, Ar*H* NDI, ext. macro), 7.90 (4H, d, *J* = 7.5 Hz, Ar*H* biphenyl), 7.65 (4H, d, *J* = 8.1 Hz, Ar*H* biphenyl), 7.68 (4H, d, *J* = 7.9 Hz, Ar*H* biphenyl), 7.54 (4H, d, *J* = 7.8 Hz, Ar*H* biphenyl), 7.23 (12H, d, *J* = 8.2 Hz, Ar*H* stopper), 6.99 - 7.13 (16H, m, Ar*H* stopper), 6.65 (4H, d, *J* = 8.5 Hz, Ar*H* stopper), 6.41 (8H, d, *J* = 8.2 Hz, Ar*H* hydroquinone macro), 6.32 (4H, br. s., Ar*H* hydroquinone axle), 6.24 (8H, d, *J* = 8.1 Hz, Ar*H* hydroquinone macro), 5.87 (4H, br. s., C*H* alkene macro), 5.62 (4H, br. s., CH_2 axle), 5.44 (4H, s, CH_2 axle), 4.42 (4H, t, *J* = 6.6 Hz, CH_2 axle), 4.24 (4H, br. s., CH_2 axle), 4.09 (8H, d, *J* = 5.5 Hz, CH_2 macro, axle), 4.05 (10H, br. s., CH_2 macro, CH_3 triazolium), 3.98 (4H, br. s., CH_2 macro), 3.90 (4H, br. s., CH_2 macro), 3.71 - 3.86 (16H, m, CH_2 macro), 3.64 (4H, d, *J* = 11.4 Hz, CH_2 macro), 2.19 - 2.27 (4H, m, CH_2 axle), 1.30 (54H, s, CH_3 stopper)

^{13}C NMR (101 MHz, $CDCl_3$) δ = 17.66, 20.81, 31.38, 34.30, 62.76, 65.78, 66.06, 67.79 - 69.03, 70.75, 112.93, 114.43, 115.02, 115.44, 124.03, 125.84, 126.36, 126.77, 127.35, 127.65 128.91, 129.84, 130.14, 130.71, 130.92, 131.12, 132.18, 134.29, 136.08, 137.17, 139.29, 140.53, 144.12, 148.31, 151.99, 153.08, 156.72, 164.21

MS (ESI): *m/z* calc. for $C_{214}H_{216}N_{16}O_{32}$ $[M - 2Cl]^{2+}$ = 1761.7941 found 1761.7911

Bis-proto-triazolium bis-NDI [3]rotaxane 73·(PF$_6$)$_2$

73·(Cl)$_2$ was anion-exchanged to the bis-hexafluorophosphate salt **73·(PF$_6$)$_2$** using Amberlite® anion exchange resin. The solvent used was 45:45:10 $CHCl_3$:MeOH:H_2O (10 mL).

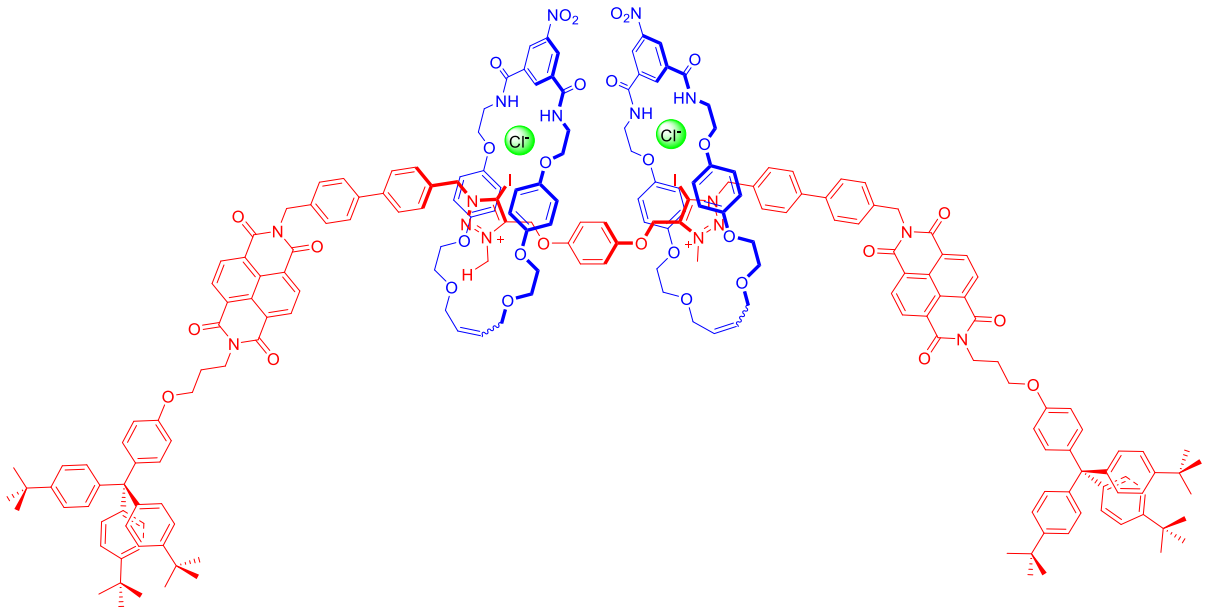
^{1}H NMR (400MHz, $CDCl_3$) δ = 8.73 (4H, br. s., Ar*H* ext. macro), 8.55 - 8.70 (8H, m, Ar*H* NDI), 8.26 (2H, br. s., Ar*H* int. macro), 7.89 (2H, s, Ar*H* triazolium), 7.37 - 7.59 (16H, m, Ar*H* biphenyl), 7.22 (12H, d, *J* = 8.6 Hz, Ar*H* stopper), 6.99 - 7.12 (16H, m, Ar*H* stopper), 6.71 (4H, d, *J* = 8.8 Hz, Ar*H* stopper), 6.62 (4H,

br. s., Ar*H* hydroquinone axle), 6.08 (4H, br. s., C*H* alkene macro), 6.00 (8H, br. s., Ar*H* hydroquinone macro), 5.88 - 5.98 (8H, m, Ar*H* hydroquinone macro), 5.55 (4H, br. s., CH_2 axle), 5.22 (4H, br. s., CH_2 axle), 4.70 (4H, br. s., CH_2 axle), 4.48 (4H, s, CH_2 axle), 4.36 (4H, br. s., CH_2 axle), 4.03 - 4.14 (12H, m, CH_2 macro, CH_3 triazolium), 4.00 (8H, br. s., CH_2 macro), 3.69 (26H, br. s., CH_2 macro), 2.19 (4H, br. s., CH_2 axle), 1.30 (54H, s, CH_3 stopper)

^{19}F NMR (470 MHz, $CDCl_3$) δ = -72.7 (d, ^1J = 706 Hz, PF_6).

^{31}P NMR (202 MHz, $CDCl_3$) δ = -144.3 (sept, ^1J = 709 Hz, *P*F_6).

Bis-iodo-triazolium bis-NDI [3]rotaxane 74·$(Cl)_2$



Axle **72·$(Cl)_2$** (21.3 mg, 8 µmol) and **22** (16 mg, 24 µmol) were dissolved in dry CH_2Cl_2 (5 ml) and were left to stir for 30 minutes**.** Grubbs' II catalyst (2 mg, 10 wt. %) was added and the solution stirred at room temperature, monitoring by TLC (CH_2Cl_2:MeOH 95:5) and ESI mass spectrometry throughout. After one day a further addition of Grubbs' II catalyst (2 mg, 10 wt. %) was made and the following day the solvent was removed *in vacuo*. The crude mixture was purified by iterative preparative silica TLC (EtOAC:MeOH 95:5 then CH_2Cl_2:MeOH 95:5) to give [3]rotaxane **74·$(Cl)_2$** (3 mg, 1 µmol 12%)

^{1}H NMR (500MHz, $CDCl_3$) δ = 9.51 (2H, br. s., Ar*H* int. macro), 8.94 (4H, s, Ar*H* ext. macro), 8.84 (4H, br. s., N*H* macro), 8.71 - 8.80 (8H, m, Ar*H* NDI), 7.67 (4H, d, *J* = 8.1 Hz, Ar*H* biphenyl), 7.57 (4H, d, *J* = 7.9 Hz, Ar*H* biphenyl), 7.61 (4H, d, *J* = 7.9 Hz, Ar*H* biphenyl), 7.44 (4H, d, *J* = 7.6 Hz, Ar*H* biphenyl), 7.23 (12H, d, *J* = 8.4 Hz, Ar*H* stopper), 7.00 - 7.12 (16H, m, Ar*H* stopper), 6.66 (4H, d, *J* = 8.7 Hz, Ar*H* stopper), 6.60 (4H, br. s., Ar*H* hydroquinone axle), 6.36 (8H, d, *J* = 8.2 Hz, Ar*H* hydroquinone macro), 6.24 (8H, d, *J* = 8.2 Hz, Ar*H* hydroquinone macro), 5.98 (4H, br. s., C*H* alkene macro), 5.45 (4H, s, CH_2 axle), 5.09 (4H, br. s., CH_2 axle), 4.43 (4H, t, *J* = 6.6 Hz, CH_2 axle), 4.28 (4H, br. s., CH_2 axle), 4.00 - 4.23 (30H, m, CH_2 macro, axle, CH_3 triazolium), 3.90 (8H, d, *J* = 7.9 Hz, CH_2 macro), 3.78 (12H, br. s., CH_2 macro), 2.20 - 2.32 (4H, m, CH_2 axle), 1.31 (54H, s, CH_3 stopper)

^{13}C NMR (101 MHz, $CDCl_3$) δ = 18.01, 31.38, 34.30, 62.94, 65.88, 67.88, 69.16, 70.82, 112.93, 114.43, 115.01, 115.44, 124.03, 126.44, 126.77, 127.35, 128.91, 129.84, 130.14, 130.29, 132.18, 134.80, 136.42, 137.02, 139.13, 140.27, 144.12, 148.31, 147.62, 151.87, 155.88, 156.89, 162.82, 163.36

MS (ESI): *m/z* calc. for $C_{214}H_{214}I_2N_{16}O_{32}$ $[M - 2Cl]^{2+}$ = 1887.6877 found 1887.6868

Bis-iodo-triazolium bis-NDI [3]rotaxane 74·$(PF_6)_2$

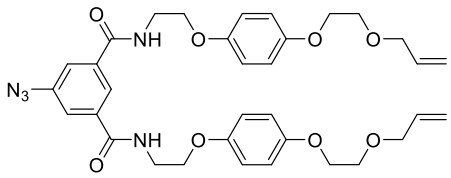
74·$(Cl)_2$ was anion-exchanged to the bis-hexafluorophosphate salt **74·$(PF_6)_2$** using Amberlite® anion exchange resin. The solvent used was 45:45:10 $CHCl_3$:MeOH:H_2O (10 mL).

^{1}H NMR (500MHz, $CDCl_3$) δ = 8.76 - 8.86 (6H, m, Ar*H* ext., int. macro), 8.59 - 8.72 (8H, m, Ar*H* NDI), 7.41 - 7.60 (16H, m, Ar*H* biphenyl), 7.22 (12H, d, *J* = 8.4 Hz, Ar*H* stopper), 7.06 (16H, d, *J* = 8.4 Hz, Ar*H* stopper), 6.72 (8H, d, *J* = 8.1 Hz, Ar*H* stopper, hydroquinone axle), 6.10 (4H, br. s., C*H* alkene macro), 5.96 (16H, br. s., Ar*H* hydroquinone macro), 5.55 (4H, br. s., CH_2 axle), 5.23 (4H, br. s., CH_2 axle), 4.80 (4H, br. s., CH_2 axle), 4.36 (4H, br. s., CH_2 axle), 4.25 (8H, br. s., CH_2 axle, macro), 4.01 - 4.14 (16H, m, CH_2 macro, CH_3 triazolium), 3.71 (26H, br. s., CH_2 macro), 2.24 (4H, br. s., CH_2 axle), 1.28 (54H, s, CH_3 stopper)

^{19}F NMR (470 MHz, $CDCl_3$) δ = -72.7 (d, ^{1}J = 706 Hz, PF_6).

^{31}P NMR (202 MHz, $CDCl_3$) δ = -144.3 (sept, ^1J = 709 Hz, PF_6).

Azido bis-vinyl-appended macrocycle precursor 76



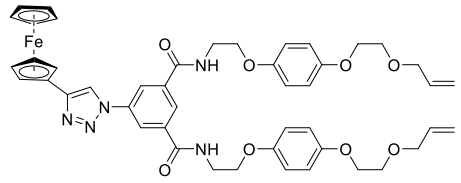
5-Azidoisophthalic acid **75** (1.05 g, 5.08 mmol, 1 eq) was suspended in dry CH_2Cl_2 (80 mL) and oxalyl chloride (4.36 mL, 50.8 mmol, 10 eq) was slowly added, followed by one drop of DMF. This was stirred at 40 °C until a homogenous solution was formed (~ 1 hour) and then the solvent was removed *in vacuo*. This residue was re-dissolved in dry CH_2Cl_2 (20 mL) and added dropwise to a solution of amine **21** (2.08 g, 10.2 mmol, 2 eq), with Et_3N (4.26 mL, 30 mmol, 6 eq) in dry CH_2Cl_2 (80 mL). The reaction was stirred at room temperature overnight and worked-up by washing with 1 M $HCl_{(aq)}$ (2 x 50 mL), H_2O (2 x 50 mL) and the organic layer then dried over anhydrous $MgSO_4$ and the solvent removed under reduced pressure. The crude mixture was then purified using silica gel column chromatography (CH_2Cl_2:MeOH 95:5) and the target macrocycle precursor **76** isolated as a colourless oil that solidified on standing (2.5 g, 3.86 mmol, 76%).

^{1}H NMR (400MHz, $CDCl_3$) δ = 7.89 (1H, s, Ar*H* int. isophthalamide), 7.58 (2H, d, ^4J = 1.5 Hz, Ar*H* ext. isophthalamide), 6.80 - 6.93 (8H, m, Ar*H* hydroquinone), 6.64 - 6.71 (2H, m, N*H*), 5.88 - 6.02 (2H, m, C*H* alkene), 5.26 - 5.36 (2H, m, C*H* alkene), 5.22 (2H, dd, ^2J = 10.5 Hz, J = 1.5 Hz, C*H* alkene), 4.04 - 4.16 (12H, m, CH_2), 3.86 (4H, q, J = 5.5 Hz, CH_2), 3.79 (4*H*, d, J = 5.4 Hz, CH_2)

^{13}C NMR (101MHz, $CDCl_3$) δ = 166.0, 153.3, 152.6, 141.4, 136.3, 134.5, 121.4, 120.6, 117.4, 115.6, 115.3, 72.3, 68.5, 68.0, 67.0, 39.9

MS (ESI): *m/z* calc. for $C_{34}H_{40}N_5O_8$ $[M + H]^+$ = 646.29 found 646.37

Ferrocene-triazole-appended bis-vinyl-appended macrocycle precursor 77



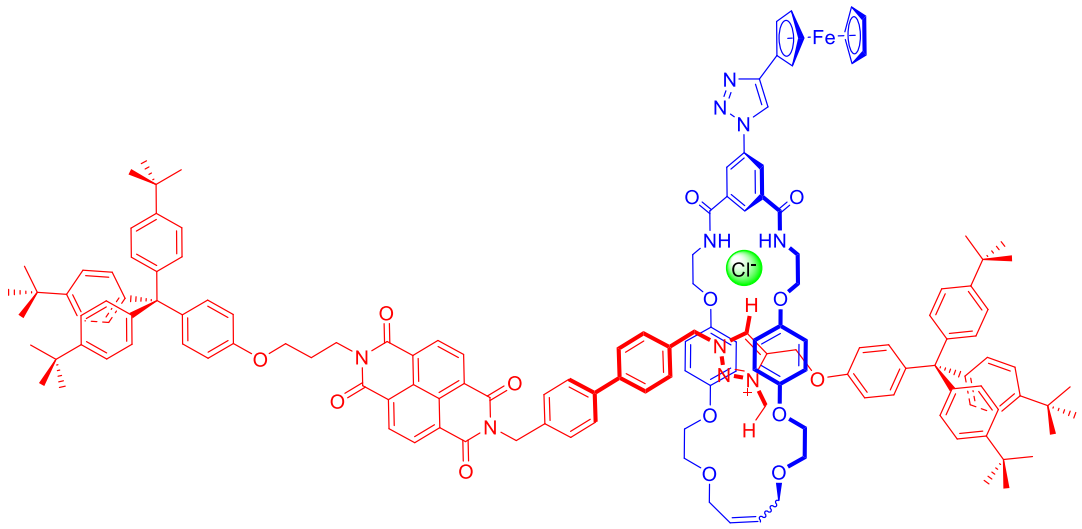
Azide **76** (100 mg, 0.15 mmol, 1 eq) and ethynyl ferrocene (35 mg, 0.17 mmol, 1.1 eq) were dissolved in dry CH_2Cl_2 (25 mL). To this solution were added in order TBTA (16 mg, 0.03 mmol, 0.2 eq), $Cu(CH_3CN)_4 \cdot PF_6$ (12 mg, 0.03 mmol, 0.2 eq) and DIPEA (54 μL, 0.30 mmol, 2 eq) and the reaction was left to stir overnight at room temperature. After this time the reaction mixture was washed with 25% $NH_4OH_{(aq)}$ (1 × 10 mL) and the organic phase was collected, dried over anhydrous $MgSO_4$ and the solvent removed *in vacuo*. The resulting residue was purified by silica gel column chromatography (6:4 EtOAc:CH_2Cl_2) and the ferrocene-appended macrocycle precursor **77** was isolated as an orange solid (122 mg, 0.14 mmol, 95%).

^{1}H NMR (400MHz, $CDCl_3$) δ = 8.41 (2H, d, ^4J = 1.5 Hz, Ar*H* ext. isophthalamide), 8.25 (1H, t, ^4J = 1.5 Hz, Ar*H* int. isophthalamide), 8.06 (1H, s, Ar*H* triazole), 6.81 - 6.94 (10H, m, Ar*H* hydroquinone, N*H*), 5.86 - 6.01 (2H, m, C*H* alkene), 5.31 (2H, dd, ^2J = 17.2 Hz, J = 1.6 Hz, C*H* alkene), 5.13 - 5.26 (2H, m, C*H* alkene), 4.81 (2H, t, J = 1.8 Hz, Ar*H* ferrocene), 4.37 (2H, t, J = 1.7 Hz, Ar*H* ferrocene), 4.04 - 4.19 (17H, m, Ar*H* ferrocene, CH_2), 3.92 (4H, q, J = 5.3 Hz, CH_2), 3.73 - 3.82 (4H, m, CH_2)

^{13}C NMR (101MHz, $CDCl_3$) δ = 165.7, 153.2, 152.5, 148.1, 137.1, 136.3, 134.4, 125.1, 121.3, 117.3, 116.6, 115.5, 115.3, 74.2, 72.2, 69.6, 69.0, 68.5, 67.9, 66.9, 66.7, 40.0

MS (ESI): *m/z* calc. for $C_{46}H_{50}FeN_5O_8$ $[M + H]^+$ = 857.30 found 857.20

Ferrocene-macrocycle-containing proto-triazolium NDI [2]rotaxane 78·Cl



Axle **36·Cl** (13 mg, 8.0 µmol, 1 eq) and bis-vinyl ferrocene macrocycle precursor **77** (10 mg, 11.7 µmol, 1.5 eq) were dissolved in dry CH_2Cl_2 (3 mL) and stirred for ten minutes. Grubbs' II catalyst (1 mg, 10 wt. %) was added and the solution stirred at room temperature, monitoring by TLC and ESI mass spectrometry throughout. After one day a further addition of Grubbs' II catalyst (1 mg, 10 wt. %) was made and upon depletion of macrocycle precursor **77** (which occurred after two days) the solvent was removed *in vacuo*. The resulting crude residue was purified by preparative silica TLC (EtOAc and CH_2Cl_2:MeOH 97:3) to give rotaxane **78·Cl** as an orange solid (15 mg, 5.5 µmol, 69%).

^{1}H NMR (400MHz, $CDCl_3$) δ = 9.63 (1H, br. s., Ar*H* int. macro), 9.38 (1H, br. s., Ar*H* triazolium), 9.28 (2H, d, *J* = 6.6 Hz, N*H* macro), 8.75 (4H, d, *J* = 7.6 Hz, Ar*H* NDI), 8.36 (2H, s, Ar*H* ext. macro), 7.67 (1H, s, Ar*H* triazole), 7.58 (2H, d, *J* = 8.2 Hz, Ar*H* biphenyl), 7.43 (2H, d, *J* = 8.2 Hz, Ar*H* biphenyl), 7.31 (4H, d, *J* = 7.9 Hz, Ar*H* biphenyl), 7.20 - 7.26 (14H, m, Ar*H* stopper, biphenyl), 7.17 (6H, d, *J* = 8.6 Hz, Ar*H* stopper), 7.00 - 7.11 (12H, m, Ar*H* stopper), 6.67 (2H, d, *J* = 8.9 Hz, Ar*H* stopper), 6.31 - 6.44 (8H, m, Ar*H* hydroquinone macro), 5.50 (2H, br. s., C*H* alkene macro), 5.38 (2H, s, CH_2 axle), 5.26 (2H, s, CH_2 axle), 4.73 (2H, s, CH_2 axle), 4.62 - 4.71 (4H, m, ArH ferrocene, CH_2 axle), 4.48 - 4.61 (2H, m, CH_2 macro), 4.43 (2H, t, *J* = 7.0 Hz, CH_2 axle), 4.32 (2H, t, *J* = 1.8 Hz, Ar*H* ferrocene), 4.11 (2H, t, *J* = 6.1 Hz, CH_2 macro), 4.02 - 4.06 (5H, m, Ar*H* ferrocene), 3.93 (2H, d, *J* = 9.0 Hz, CH_2 macro), 3.63 - 3.89 (13H, m, CH_2 macro,

C*H*$_3$ triazolium), 3.47 - 3.58 (4H, m, C*H*$_2$ macro), 2.26 (2H, quin, *J* = 6.6 Hz, C*H*$_2$ axle), 1.28 - 1.34 (54H, s, C*H*$_3$ stopper)

^{13}C NMR (101MHz, $CDCl_3$) δ = 165.7, 162.9, 162.8, 153.2, 152.5, 148.5, 148.3, 148.1, 144.1, 143.7, 142.8, 140.0, 139.6, 137.1, 136.3, 134.4, 132.7, 132.2, 131.2, 131.0, 130.7, 130.6, 130.0, 129.8, 128.3, 127.3, 126.8, 126.5, 125.1, 124.1, 121.3, 117.3, 116.6, 115.5, 115.3, 113.1, 112.9, 74.2, 72.2, 69.6, 69.0, 68.5, 67.9, 66.9, 66.7, 63.1, 63.0, 57.7, 57.6, 40.0, 38.8, 34.3, 31.9, 31.4, 31.3, 30.9, 30.0, 29.7, 29.4, 27.9, 22.7, 14.1

MS (ESI): *m/z* calc. for $C_{153}H_{159}FeN_{10}O_{14}$ $[M - Cl]^+$ = 2417.14147 found 2417.13894

Ferrocene-macrocycle-containing proto-triazolium NDI [2]rotaxane 78·PF$_6$

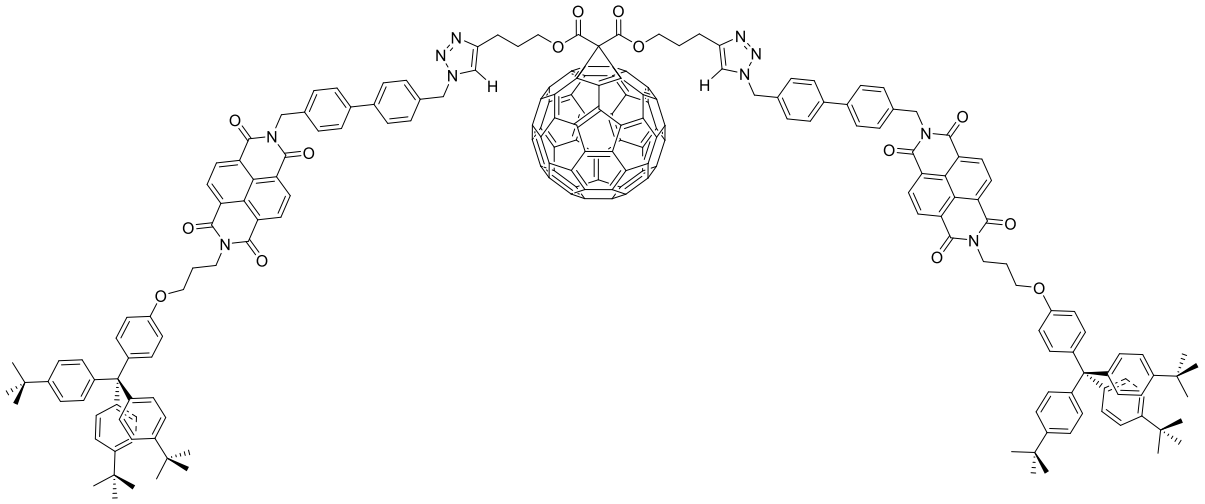
78·Cl was anion-exchanged to the hexafluorophosphate salt **78·PF$_6$** using Amberlite® anion exchange resin. The solvent used was 45:45:10 $CHCl_3$:MeOH:H_2O (10 mL).

^{1}H NMR (400MHz, $CDCl_3$) δ = 8.62 - 8.76 (4H, m, Ar*H* NDI), 8.41 (2H, br. s., Ar*H* ext. macro), 8.25 (1H, br. s., Ar*H* int.macro), 8.06 (1H, br. s., Ar*H* triazolium), 7.39 - 7.55 (9H, m, Ar*H* biphenyl, triazole), 7.17 - 7.26 (12H, m, Ar*H* stopper), 7.02 - 7.16 (16H, m, Ar*H* stopper), 6.86 (2H, d, *J* = 8.8 Hz, Ar*H* stopper), 6.72 (2H, d, *J* = 8.9 Hz, Ar*H* stopper), 6.17 (4H, d, *J* = 7.9 Hz, Ar*H* hydroquinone), 6.03 (4H, d, *J* = 8.7 Hz, Ar*H* hydroquinone), 5.94 (2H, br. s., C*H* alkene), 5.34 (2H, br. s., C*H*$_2$ axle), 5.27 (2H, br. s., C*H*$_2$ axle), 4.90 (2H, s, C*H*$_2$ axle), 4.41 (2H, t, *J* = 7.0 Hz, C*H*$_2$ axle), 4.11 (2H, t, *J* = 6.0 Hz, C*H*$_2$ axle), 3.87 - 4.07 (11H, m, Ar*H*, ferrocene, C*H*$_3$ triazolium, C*H*$_2$ macro), 3.51 - 3.80 (21H, m, Ar*H* ferrocene, C*H*$_2$ macro), 2.27 (2H, quin, *J* = 6.5 Hz, C*H*$_2$ axle), 1.29 (54H, s, C*H*$_3$ stopper)

^{19}F NMR (470 MHz, $CDCl_3$) δ = -72.7 (d, ^1J = 706 Hz, P*F*$_6$).

^{31}P NMR (202 MHz, $CDCl_3$) δ = -144.3 (sept, ^1J = 709 Hz, *P*F$_6$).

Bis-proto-triazole bis-NDI C_{60} fullerene axle 80

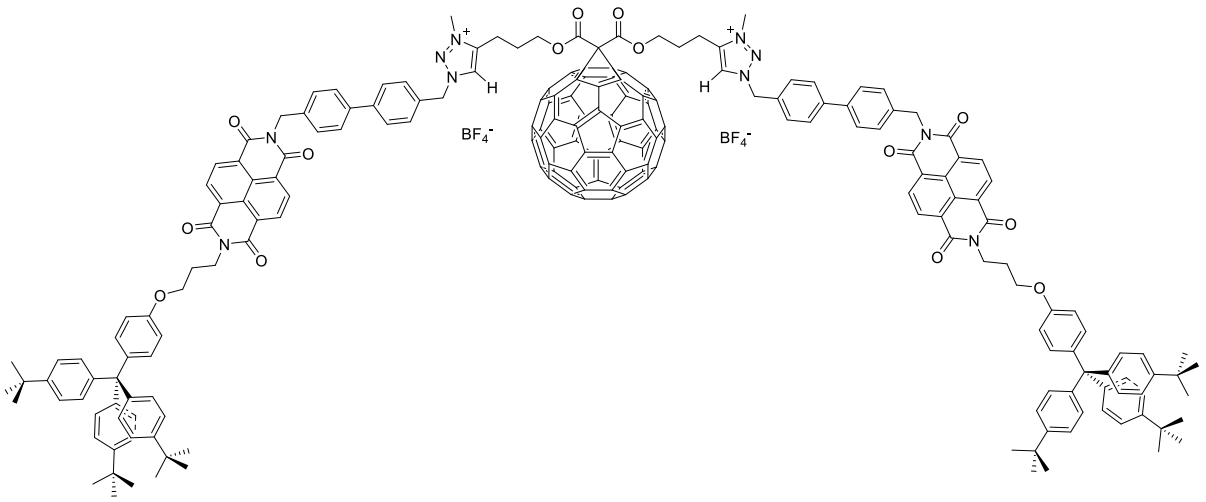


Azide **69** (43 mg, 0.04 mmol, 2 eq) and C_{60} fullerene bis-alkyne **79** (20 mg, 0.02 mmol, 1 eq) were dissolved in dry CH_2Cl_2 (3 ml). Then TBTA (5 mg, 0.01 mmol, 0.4 eq), $Cu(MeCN)_4 \cdot PF_6$ (3 mg, 0.01 mmol, 0.4 eq) and *N,N*-diisopropylethylamine (15 µl, 0.08 mmol, 4 eq) were added to the mixture and left to stir at room temperature for 2 days, monitoring by thin layer chromatography (CH_2Cl_2:MeOH 99:1). The mixture was diluted with CH_2Cl_2 and washed with a 0.02 M EDTA/0.1 M $NH_4OH_{(aq)}$ solution, the organic layer was dried over anhydrous $MgSO_4$, and the solvent was removed *in vacuo*. The resultant crude was purified by silica gel column chromatography (CH_2Cl_2:MeOH 99:1) to give **80** as a brown solid (46 mg, 0.02 mmol, 73%).

^{1}H NMR (400MHz, $CDCl_3$) δ = 8.69 - 8.82 (8H, m, Ar*H* NDI), 7.63 (4H, d, *J* = 8.2 Hz, Ar*H* biphenyl), 7.45 - 7.56 (10H, m, Ar*H* biphenyl, triazole), 7.18 - 7.26 (16H, m, Ar*H* stopper, biphenyl), 6.98 - 7.13 (16H, m, Ar*H* stopper), 6.66 (4H, d, *J* = 8.7 Hz, Ar*H* stopper), 5.50 (4H, s, CH_2), 5.42 (4H, s, CH_2), 4.50 (4H, t, *J* = 6.1 Hz, CH_2), 4.43 (4H, t, *J* = 6.8 Hz, CH_2), 4.10 (4H, t, *J* = 5.9 Hz, CH_2), 2.84 (4H, t, *J* = 7.5 Hz, CH_2), 2.14 - 2.30 (8H, m, CH_2), 1.28 (54H, s, CH_3 stopper)

^{13}C NMR (101 MHz, $CDCl_3$) δ = 15.2, 23.6, 27.3, 28.5, 31.4, 33.2, 34.3, 52.0, 54.5, 63.0, 65.8, 66.0, 67.6, 69.7, 71.5, 82.4, 98.4, 108.0, 112.9, 124.0, 126.6, 127.4, 128.6, 130.7, 131.1, 139.0, 134.5, 135.8, 141.0, 141.9, 142.2, 143.0, 143.0, 143.1, 143.9, 144.6, 144.7, 144.9, 145.1, 145.2, 145.3, 148.3, 162.9, 163.5.

Bis-proto-triazolium bis-NDI C_{60} fullerene axle 81·$(BF_4)_2$



Axle **80** (46 mg, 0.02 mmol, 1 eq) was dissolved in CH_2Cl_2 (4 ml) with $Me_3O{\cdot}BF_4$ (7 mg, 0.06 mmol, 3 eq) and the mixture was left stirring overnight at room temperature. The reaction was quenched with three drops of MeOH and the solvent was removed *in vacuo*. The resultant solid was purified by preparative silica TLC (CH_2Cl_2:MeOH 97:3) to give **81·$(BF_4)_2$** as a brown solid (45 mg, 0.01 mmol, 92%).

^{1}H NMR (400MHz, $CDCl_3$) δ = 8.67 - 8.79 (8H, m, Ar*H* NDI), 8.56 (2H, br. s., Ar*H* triazolium), 7.60 (4H, d, *J* = 8.1 Hz, Ar*H* biphenyl), 7.53 (8H, s, Ar*H* biphenyl), 7.48 (4H, d, *J* = 8.1 Hz, Ar*H* biphenyl), 7.23 (12H, d, *J* = 8.6 Hz, Ar*H* stopper), 6.97 - 7.10 (16H, m, Ar*H* stopper), 6.65 (4H, d, *J* = 8.8 Hz, Ar*H* stopper), 5.67 (4H, br. s., CH_2), 5.38 (4H, s, CH_2), 4.63 (4H, br. s., CH_2), 4.42 (4H, t, *J* = 7.0 Hz, CH_2), 4.18 - 4.26 (6H, m, CH_3 triazolium), 4.10 (4H, t, *J* = 5.9 Hz, CH_2), 3.04 (4H, br. s., CH_2), 2.34 (4H, br. s., CH_2), 2.19 - 2.30 (4H, m, CH_2), 1.28 (54H, s, CH_3 stopper)

^{13}C NMR (101 MHz, $CDCl_3$) δ = 15.2, 23.6, 27.3, 28.5, 31.4, 31.7, 33.2, 34.2, 37.8, 52.0, 54.5, 63.0, 65.8, 66.0, 67.6, 69.9, 71.5, 82.4, 98.6, 108.0, 112.9, 124.0, 126.6, 127.6, 128.6, 130.7, 130.8, 131.1, 139.0, 134.6, 135.8, 141.0, 141.9, 142.2, 143.0, 143.4, 143.6, 143.9, 144.6, 144.7, 144.9, 145.1, 145.2, 145.3, 148.8, 162.9, 163.5.

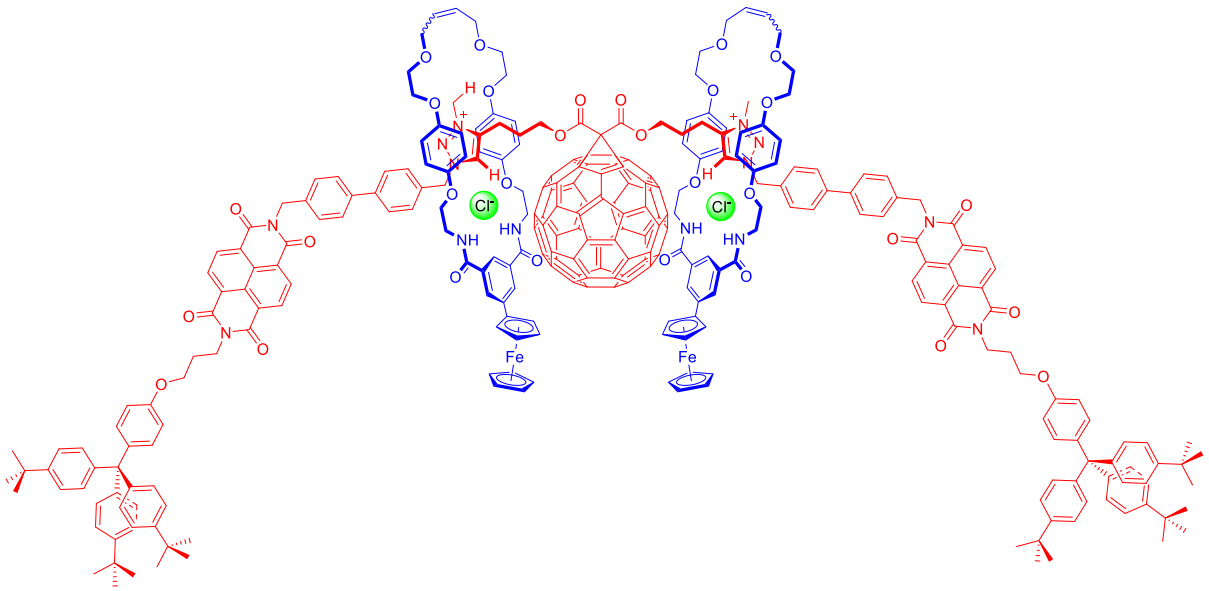
Bis-proto-triazolium bis-NDI C_{60} fullerene axle 81·$(Cl)_2$

Subsequent anion exchange was achieved by dissolving **81·$(BF_4)_2$** in (CH_2Cl_2:MeOH 90:10) and passing the solution three times through a column of Amberlite® resin loaded with chloride to yield **81·$(Cl)_2$** (44 mg, 0.01 mmol, quant.).

^{1}H NMR (400MHz, $CDCl_3$) δ = 9.98 (2H, s, Ar*H* triazolium), 8.63 - 8.80 (8H, m, Ar*H* NDI), 7.67 (4H, d, *J* = 8.2 Hz, Ar*H* biphenyl), 7.61 (4H, d, *J* = 8.3 Hz, Ar*H* biphenyl), 7.52 (4H, d, *J* = 8.2 Hz, Ar*H* biphenyl), 7.48 (4H, d, *J* = 8.2 Hz, Ar*H* biphenyl), 7.22 (12H, d, *J* = 8.6 Hz, Ar*H* stopper), 6.96 - 7.13 (16H, m, Ar*H* stopper), 6.65 (4H, d, *J* = 8.9 Hz, Ar*H* stopper), 5.95 (4H, s, CH_2), 5.40 (4H, s, CH_2), 4.73 (4H, s, CH_2), 4.42 (4H, t, *J* = 7.0 Hz, CH_2), 4.37 (6H, s, CH_3 triazolium), 4.10 (4H, t, *J* = 5.9 Hz, CH_2), 3.30 (4H, br. s., CH_2), 2.25 (4H, quint., *J* = 6.5 Hz, CH_2), 1.29 (54H, s, CH_3 stopper)

MS (MALDI): m/z calc. for $C_{211}H_{150}ClN_{10}O_{14}$ $[M - Cl]^+$: 3084.108; found: 3084.109.

Ferrocene-macrocycle-containing C_{60} fullerene [3]rotaxane 82·$(Cl)_2$



Axle **81·$(Cl)_2$** (67 mg, 20.8 µmol, 1 eq) and a ferrocenyl-containing macrocycle precursor (49 mg, 62.1 µmol, 3 eq) were dissolved in dry CH_2Cl_2 (15 ml), the mixture was left to stir for 30 minutes. Grubbs' II catalyst (5 mg, 10 wt. %) was added and the solution stirred at room temperature, monitoring by TLC (CH_2Cl_2:MeOH 95:5) and ESI mass spectrometry throughout. After one day a further addition of

Grubbs' II catalyst (5 mg, 10 wt. %) was made and after a further day the solvent was removed *in vacuo*. The crude was purified by iterative preparative silica TLC (EtOAc:MeOH 95:5 then CH_2Cl_2:MeOH 95:5) to yield [3]rotaxane **82·(Cl)$_2$** as a brown solid (11 mg, 2.3 μmol, 11%).

^{1}H NMR (400MHz, $CDCl_3$) δ = 9.96 (2H, br. s., Ar*H* int. macro), 9.29 (2H, br. s., Ar*H* triazolium), 9.11 (4H, br. s., N*H* macro), 8.65 - 8.84 (8H, m, Ar*H* NDI), 8.30 (4H, s, Ar*H* ext. macro), 7.67 (4H, d, *J* = 7.8 Hz, Ar*H* biphenyl), 7.61 (4H, d, *J* = 8.3 Hz, Ar*H* biphenyl), 7.55 (4H, m, Ar*H* biphenyl), 7.48 (4H, d, *J* = 8.1 Hz, Ar*H* biphenyl), 7.23 (12H, d, *J* = 8.6 Hz, Ar*H* stopper), 6.97 - 7.13 (16H, m, Ar*H* stopper), 6.66 (4H, d, *J* = 9.0 Hz, Ar*H* stopper), 6.30 (8H, d, *J* = 8.8 Hz, Ar*H* hydroquinone macro), 6.22 (8H, d, *J* = 8.8 Hz, Ar*H* hydroquinone macro), 5.85 (4H, br. s., C*H* alkene macro), 5.48 (4H, br. s., CH_2 axle), 5.42 (4H, s, CH_2 axle), 4.72 (4H, s, Ar*H* ferrocene), 4.42 (4H, t, *J* = 7.0 Hz, CH_2 axle), 4.21 - 4.33 (8H, m, ArH ferrocene, CH_2 axle), 4.05 - 4.19 (16H, m, CH_2 axle, macro), 3.83 - 4.04 (23H, m, Ar*H* ferrocene, CH_3 triazolium, CH_2 axle, macro), 3.60 - 3.83 (20H, m, CH_2 macro), 2.19 - 2.31 (4H, m, CH_2 axle), 2.05 (4H, br. s., CH_2 axle), 1.30 (54H, s, CH_3 stopper)

^{13}C NMR (101 MHz, $CDCl_3$) δ = 15.2, 23.4, 27.3, 28.5, 31.4, 31.7, 33.2, 34.2, 37.8, 39.9, 52.0, 54.5, 63.0, 65.8, 66.0, 66.7, 67.0, 67.6, 68.0, 68.5, 69.7, 69.9, 71.5, 72.3, 74.2, 82.4, 98.6, 108.0, 112.9, 115.3, 115.6, 116.6, 117.2, 120.6, 121.4, 124.0, 126.6, 127.6, 128.6, 130.7, 130.8, 131.1, 139.0, 134.5, 134.6, 135.8, 136.3, 141.0, 141.4, 141.9, 142.2, 143.2, 143.4, 143.6, 143.9, 144.6, 144.7, 144.9, 145.1, 145.2, 145.3, 148.1, 148.8, 152.6, 153.3, 162.9, 163.5, 165.7, 166.0.

Ferrocene-macrocycle-containing C_{60} fullerene [3]rotaxane 82·(PF_6)$_2$

82·(Cl)$_2$ was anion-exchanged to the bis-hexafluorophosphate salt **82·(PF_6)$_2$** using Amberlite® anion exchange resin. The solvent used was 45:45:10 $CHCl_3$:MeOH:H_2O (10 mL).

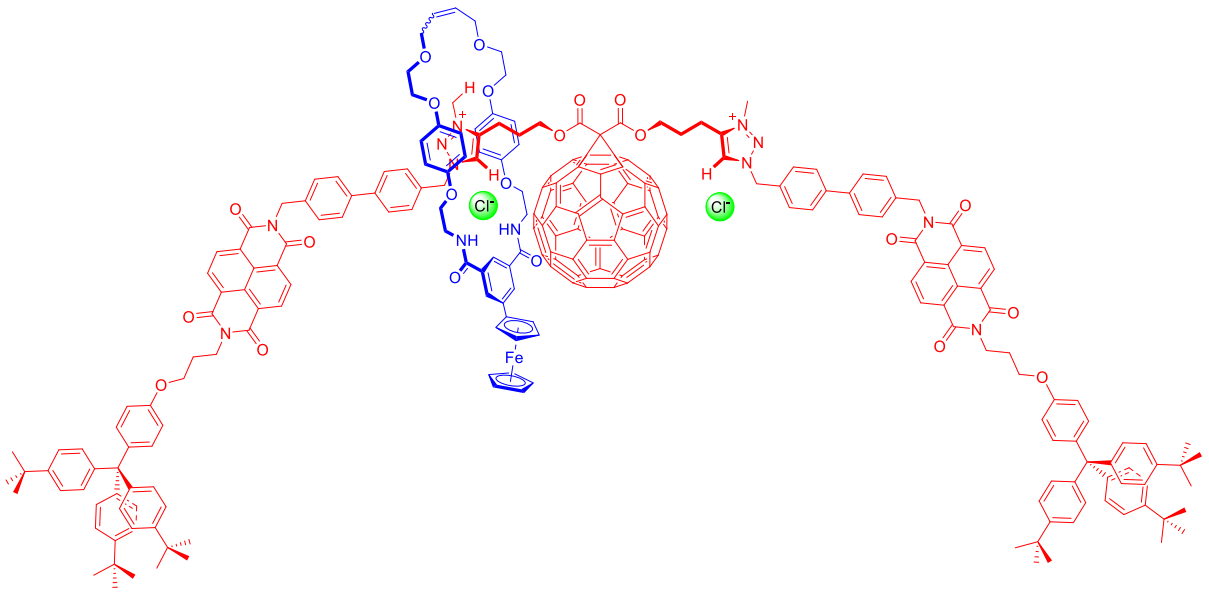
^{1}H NMR (400MHz, $CDCl_3$) δ = 8.53 - 8.65 (8H, m, Ar*H* NDI), 8.43 (2H, br. s., Ar*H* int. macro), 8.19 (4H, br. s., Ar*H* ext. macro, triazolium), 7.44 - 7.68 (16H, m, Ar*H* biphenyl), 7.22 (12H, d, *J* = 8.6 Hz, Ar*H* stopper), 7.00 - 7.12 (16H, m, Ar*H* stopper), 6.71 (4H, d, *J* = 8.8 Hz, Ar*H* stopper), 6.20 (3H, br. s., C*H* alkene macro), 5.71 - 5.87 (16H, m, Ar*H* hydroquinone macro), 5.58 (4H, br. s., CH_2 axle), 5.28 (4H, br.

s., CH_2 axle), 4.52 (4H, br. s., CH_2 axle), 4.25 - 4.35 (8H, m, CH_2 axle), 4.17 (8H, br. s., Ar*H* ferrocene), 3.93 - 4.09 (20H, m, Ar*H* ferrocene, CH_3 triazolium, CH_2 axle), 3.50 - 3.80 (40H, m, CH_2 macro), 2.12 - 2.28 (8H, m, CH_2 axle), 1.33 (54H, s, CH_3 stopper)

^{19}F NMR (470 MHz, $CDCl_3$) δ = -72.7 (d, ^1J = 707 Hz, PF_6).

^{31}P NMR (202 MHz, $CDCl_3$) δ = -144.3 (sept, ^1J = 709 Hz, *P*F_6).

Ferrocene-macrocycle-containing C_{60} fullerene [2]rotaxane 83·(Cl)$_2$

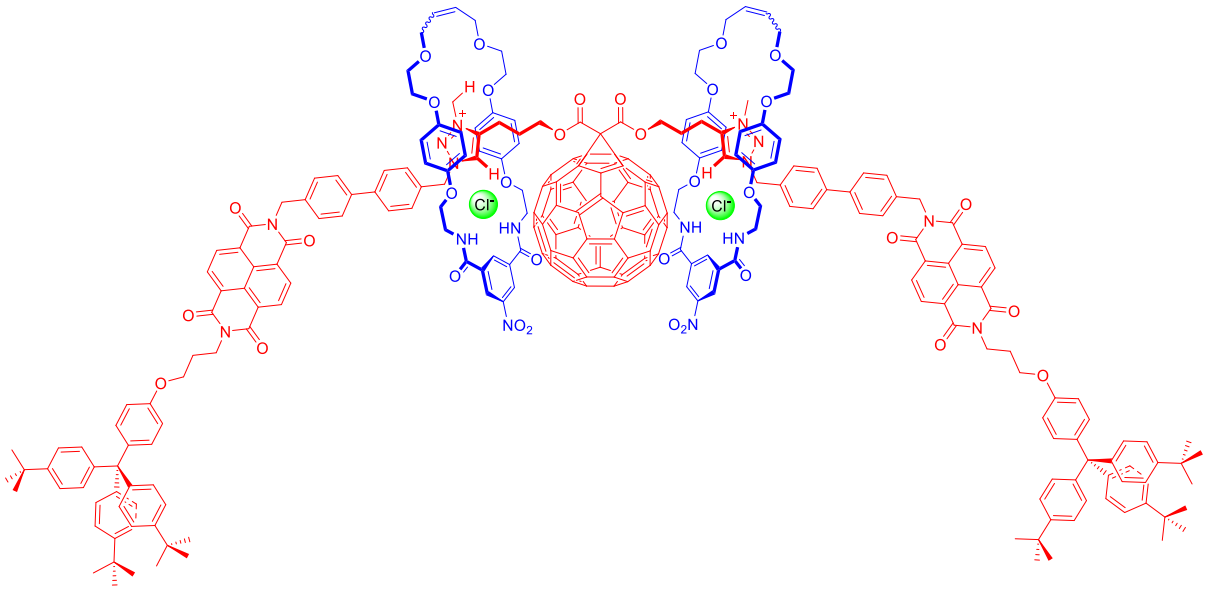


[2]rotaxane **83·(Cl)$_2$** was isolated from the crude reaction mixture of **82·(Cl)$_2$** by iterative preparative silica TLC (EtOAc:MeOH 95:5 then CH_2Cl_2:MeOH 95:5) as a brown solid (12 mg, 3.1 µmol, 15%).

^{1}H NMR (400MHz, $CDCl_3$) δ = 9.98 (1H, br. s., Ar*H* int. macro), 9.29 (1H, br. s., Ar*H* triazolium), 9.08 (2H, br. s., N*H* macro), 8.65 - 8.84 (8H, m, Ar*H* NDI), 8.31 (2H, s, Ar*H* ext. macro), 7.89 (2H, d, *J* = 7.9 Hz, Ar*H* biphenyl), 7.58 - 7.74 (8H, m, Ar*H* biphenyl), 7.43 - 7.57 (6H, m, Ar*H* biphenyl), 7.25 (12H, d, *J* = 8.6 Hz, Ar*H* stopper), 6.96 - 7.12 (16H, m, Ar*H* stopper), 6.65 (4H, d, *J* = 8.8 Hz, Ar*H* stopper), 6.29 (4H, d, *J* = 8.7 Hz, Ar*H* hydroquinone macro), 6.17 (4H, d, *J* = 8.6 Hz, Ar*H* hydroquinone macro), 5.85 (2H, br. s., C*H* alkene macro), 5.61 (2H, s, CH_2 axle), 5.45 (4H, s, CH_2 axle), 4.70 (4H, s., CH_2 axle, Ar*H* ferrocene), 4.32 - 4.48 (6H, m, CH_2 axle), 4.27 (2H, br. s., CH_2 axle), 4.19 (4H, m, CH_2 axle, Ar*H* ferrocene), 3.91 - 4.15 (12H, m, CH_2 axle, CH_3 triazolium, Ar*H* ferrocene), 3.60 - 3.89 (19H, m, CH_2 macro, CH_3 triazolium),

3.58 (4H, s, CH_2 macro), 3.24 (2H, br. s., CH_2 axle), 2.39 - 2.54 (2H, m, CH_2 axle), 2.20 - 2.32 (4H, m, CH_2 axle), 1.30 (54H, s, CH_3 stopper)

Nitro-macrocycle-containing C_{60} fullerene [3]rotaxane 84·(Cl)$_2$



Axle **81·(Cl)$_2$** (24 mg, 7.7 µmol, 1 eq) and **22** (15 mg, 23 µmol, 3 eq) were dissolved in dry CH_2Cl_2 (5 ml), the mixture was left to stir for 30 minutes. Grubbs' II catalyst (1.5 mg, 10 wt. %) was added and the solution stirred at room temperature, monitoring by TLC (CH_2Cl_2:MeOH 95:5) and ESI mass spectrometry throughout. After one day a further addition of Grubbs' II catalyst (1.5 mg, 10 wt. %) was made and after a further day the solvent was removed *in vacuo*. The crude was purified by iterative preparative silica TLC (EtOAc:MeOH 95:5 then CH_2Cl_2:MeOH 92.5:7.5) to yield [3]rotaxane **84·(Cl)$_2$** (6 mg, 1.4 µmol, 18%).

^{1}H NMR (400MHz, $CDCl_3$) δ = 9.95 (2H, br. s., Ar*H* int. macro), 9.32 (2H, br. s., Ar*H* triazolium), 8.99 (4H, s, Ar*H* ext. macro), 8.68 - 8.83 (8H, m, Ar*H* NDI), 7.89 (4H, d, *J* = 7.3 Hz, Ar*H* biphenyl), 7.59 - 7.72 (8H, m, Ar*H* biphenyl), 7.53 (4H, d, *J* = 8.3 Hz, Ar*H* biphenyl), 7.23 (12H, d, *J* = 8.6 Hz, Ar*H* stopper), 7.00 - 7.12 (16H, m, Ar*H* stopper), 6.66 (4H, d, *J* = 8.8 Hz, Ar*H* stopper), 6.29 (8H, d, *J* = 8.8 Hz, Ar*H* hydroquinone macro), 6.16 (6H, d, *J* = 8.3 Hz, Ar*H* hydroquinone macro), 5.86 (4H, br. s., C*H* alkene), 5.57 (4H, br. s., CH_2 axle), 5.43 (4H, s, CH_2 axle), 4.42 (4H, t, *J* = 7.0 Hz, CH_2 axle), 4.14 - 4.33 (8H, m, CH_2

axle, macro), 3.95 - 4.14 (16H, m, C*H*$_2$ axle, macro), 3.63 - 3.93 (34H, m, C*H*$_2$ macro, C*H*$_3$ triazolium), 2.41 (4H, br. s., C*H*$_2$ axle), 2.21 - 2.28 (4H, m, C*H*$_2$ axle), 1.28 (54H, s, C*H*$_3$ stopper)

^{13}C NMR (101 MHz, $CDCl_3$) δ = 15.2, 23.6, 27.3, 28.5, 31.4, 31.7, 33.2, 34.2, 37.8, 40.1, 52.0, 54.5, 63.0, 65.8, 66.0, 66.8, 67.6, 67.9, 68.6, 69.9, 71.5, 72.4, 82.4, 98.6, 108.0, 112.9, 115.6, 117.5, 124.0, 124.6, 126.6, 127.6, 128.6, 130.7, 130.8, 131.1, 131.2, 139.0, 134.4, 134.6, 135.8, 136.3, 141.0, 141.9, 142.2, 143.0, 143.4, 143.6, 143.9, 144.6, 144.7, 144.9, 145.1, 145.2, 145.3, 148.2, 148.8, 152.5, 153.3, 162.9, 163.5, 164.6

MS (MALDI): m/z calc. for $C_{275}H_{220}N_{16}O_{34}$ $[M - 2Cl]^{2+}$: 2145.802; found: 2145.813

Nitro-macrocycle-containing C_{60} fullerene [3]rotaxane 84·$(PF_6)_2$

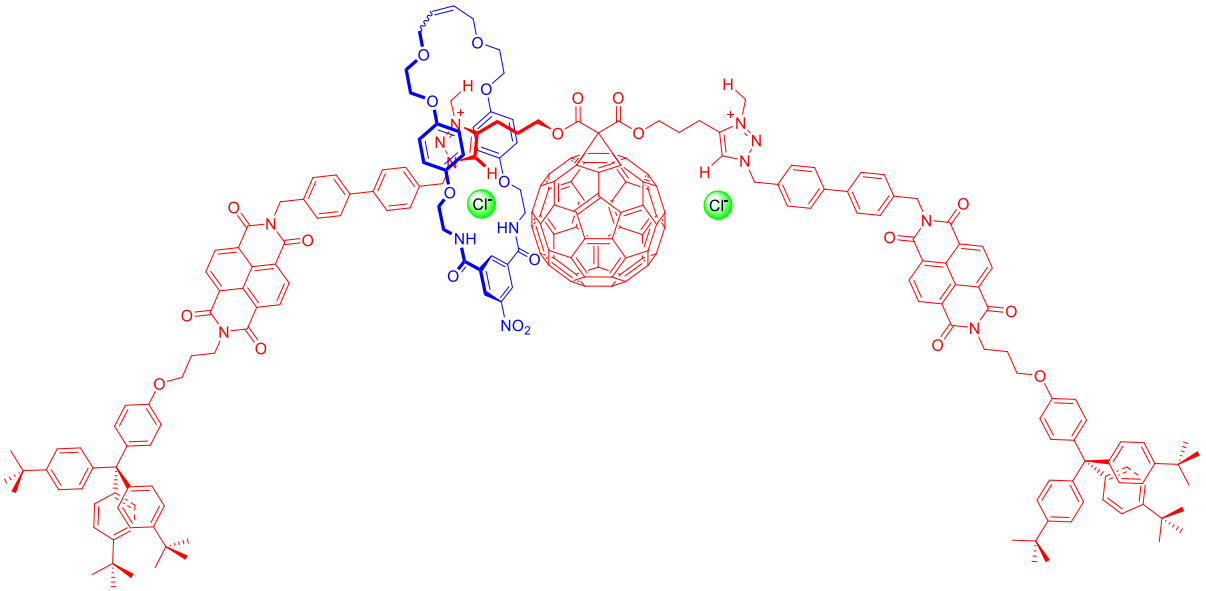
84·$(Cl)_2$ was anion-exchanged to the bis-hexafluorophosphate salt **84·$(PF_6)_2$** using Amberlite® anion exchange resin. The solvent used was 45:45:10 $CHCl_3$:MeOH:H_2O (10 mL).

^{1}H NMR (500MHz, $CDCl_3$) δ = 8.91 (6H, s, Ar*H* int., ext. macro), 8.66 (4H, d, *J* = 7.5 Hz, Ar*H* NDI), 8.60 (4H, d, *J* = 7.5 Hz, Ar*H* NDI), 8.19 (2H, s, Ar*H* triazolium), 7.39 - 7.62 (16H, m, Ar*H* biphenyl), 7.22 (12H, d, *J* = 8.4 Hz, Ar*H* stopper), 7.06 (16H, d, *J* = 8.4 Hz, Ar*H* stopper), 6.73 (4H, d, *J* = 8.7 Hz, Ar*H* stopper), 6.16 (4H, br. s., C*H* alkene), 5.90 (16H, d, *J* = 5.3 Hz, Ar*H* hydroquinone), 5.58 (4H, br. s., C*H*$_2$ axle), 5.23 (4H, br. s., C*H*$_2$ axle), 4.46 - 4.56 (4H, m, C*H*$_2$ axle), 4.36 (4H, br. s., C*H*$_2$ axle), 4.14 (6H, br. s., C*H*$_3$ triazolium), 4.00 - 4.12 (12H, m, C*H*$_2$ macro, axle), 3.56 - 3.80 (36H, m, C*H*$_2$ macro), 2.21 - 2.27 (4H, m, C*H*$_2$ axle), 2.18 (4H, quin, *J* = 2.9 Hz, C*H*$_2$ axle), 1.28 (54H, s, C*H*$_3$ stopper)

^{19}F NMR (470 MHz, $CDCl_3$) δ = -72.7 (d, ^1J = 706 Hz, P*F*$_6$).

^{31}P NMR (202 MHz, $CDCl_3$) δ = -144.3 (sept, ^1J = 710 Hz, *P*F$_6$).

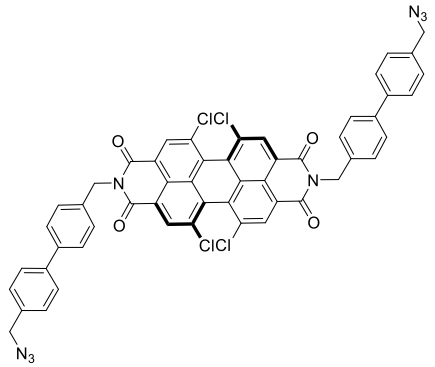
Nitro-macrocycle-containing C_{60} fullerene [2]rotaxane 85·$(Cl)_2$



[2]rotaxane **85·$(Cl)_2$** was isolated from the crude reaction mixture of **84·$(Cl)_2$** by iterative preparative silica TLC using the solvent mixtures (EtOAc:MeOH 95:5 then CH_2Cl_2:MeOH 92.5:7.5) as a brown solid (7 mg, 1.6 µmol, 24%).

^{1}H NMR (400MHz, $CDCl_3$) δ = 9.94 (1H, br. s., Ar*H* int. macro), 9.31 (1H, br. s., Ar*H* triazolium), 8.98 (2H, s, Ar*H* ext. macro), 8.66 - 8.82 (8H, m, Ar*H* NDI), 7.89 (2H, d, *J* = 7.9 Hz, Ar*H* biphenyl), 7.58 - 7.72 (8H, m, Ar*H* biphenyl), 7.43 - 7.57 (6H, m, Ar*H* biphenyl), 7.23 (12H, d, *J* = 8.6 Hz, Ar*H* stopper), 6.96 - 7.11 (16H, m, Ar*H* stopper), 6.66 (4H, d, *J* = 8.8 Hz, Ar*H* stopper), 6.28 (4H, d, *J* = 8.7 Hz, Ar*H* hydroquinone macro), 6.15 (4H, d, *J* = 8.6 Hz, Ar*H* hydroquinone macro), 5.96 (2H, br. s., CH_2 axle), 5.87 (2H, br. s., C*H* alkene macro), 5.60 (2H, s, CH_2 axle), 5.42 (4H, s, CH_2 axle), 4.70 (2H, br. s., CH_2 axle), 4.32 - 4.48 (6H, m, CH_2 axle), 4.27 (2H, br. s., CH_2 axle), 4.19 (2H, d, *J* = 8.7 Hz, CH_2 axle), 3.91 - 4.15 (7H, m, CH_2 axle, CH_3 triazolium), 3.60 - 3.89 (19H, m, CH_2 macro, CH_3 triazolium), 3.58 (4H, s, CH_2 macro), 3.22 (2H, br. s., CH_2 axle), 2.39 - 2.54 (2H, m, CH_2 axle), 2.20 - 2.33 (4H, m, CH_2 axle), 1.30 (54H, s, CH_3 stopper)

Tetra-chloro PDI bis-biphenyl azide 87

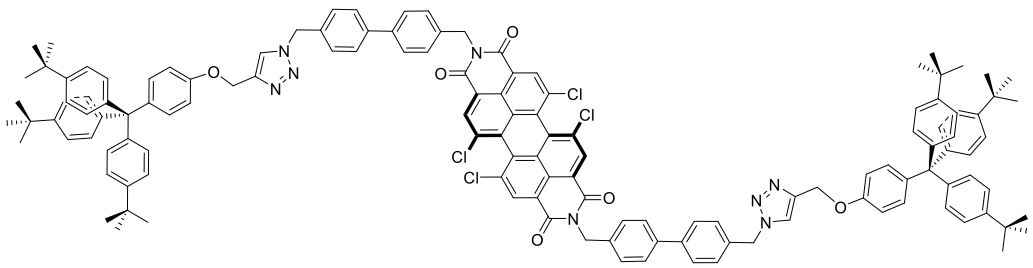


Tetrachloro perylene-3,4,9,10-tetracarboxylic dianhydride **86** (500 mg, 0.95 mmol, 1 eq), biphenyl amine azide **4** (494 mg, 2.08 mmol, 2.2 eq) and $Zn(OAc)_2{\cdot}2H_2O$ (312 mg, 1.42 mmol, 1.5 eq) were heated in molten imidazole (3 g) for four hours at 140 °C. On cooling to room temperature the reaction mixture was poured onto 1 M $HCl_{(aq)}$ (50 mL) and the resulting precipitate collected by suction filtration. The orange solid was washed with H_2O (~ 200 mL) until neutral pH and dried *under vacuo*. This crude solid was purified by silica gel column chromatography (CH_2Cl_2) to give the PDI biphenyl bis azide as a red solid **87** (400 mg, 0.42 mmol, 44%).

^{1}H NMR (400MHz, $CDCl_3$) δ = 8.72 (4H, s, Ar*H* PDI), 7.65 (4H, d, *J* = 7.9 Hz, Ar*H* biphenyl), 7.50 - 7.61 (8H, m, Ar*H* biphenyl), 7.37 (4H, d, *J* = 7.3 Hz, Ar*H* biphenyl), 5.46 (4H, s, CH_2), 4.37 (4H, s, CH_2)

MS (ESI): m/z calc. for $C_{104}H_{56}Cl_8N_{16}NaO_8$ $[2M + Na]^+$: 1961.19; found: 1961.72

Bis-proto-triazole PDI axle 88



PDI bis-azide **87** (41 mg, 0.04 mmol, 1 eq) and phenyl trityl stopper alkyne **6** (51 mg, 0.09 mmol, 2.2 eq) were dissolved in dry CH_2Cl_2 (60 mL). Then TBTA (9 mg, 0.01 mmol, 0.4 eq), $Cu(MeCN)_4{\cdot}PF_6$ (6 mg,

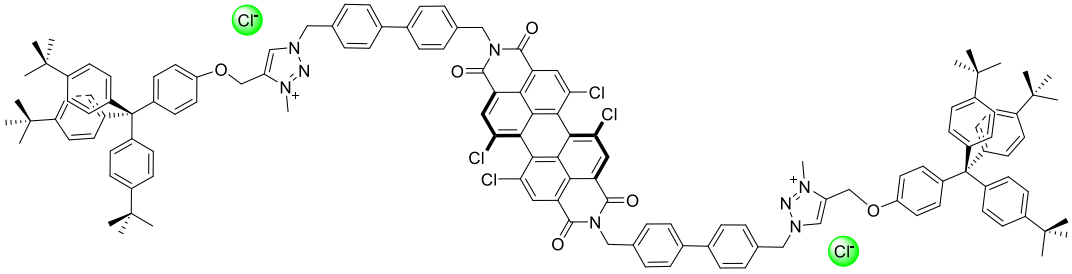
0.01 mmol, 0.4 eq) and *N,N*-diisopropylethylamine (18 µl, 0.1 mmol, 2.5 eq) were added to the mixture and left to stir at room temperature for 2 days, monitoring by thin layer chromatography (CH_2Cl_2:MeOH 99:1). The mixture was washed with a 0.02 M EDTA/0.1 M $NH_4OH_{(aq)}$ solution, the organic layer was dried over $MgSO_4$, and the solvent was removed *in vacuo*. The resultant crude was purified by silica gel column chromatography (CH_2Cl_2:MeOH 99:1) to give **88** as an red/orange solid (66 mg, 0.03 mmol, 66%).

^{1}H NMR (400MHz, $CDCl_3$) δ = 8.71 (4H, s, Ar*H* PDI), 7.64 (4H, d, *J* = 8.2 Hz, Ar*H* biphenyl), 7.53 - 7.60 (6H, m, Ar*H* biphenyl , triazole), 7.52 (4H, d, *J* = 8.2 Hz, Ar*H* biphenyl), 7.33 (4H, d, *J* = 8.2 Hz, Ar*H* biphenyl), 7.22 (12H, d, *J* = 8.6 Hz, Ar*H* stopper), 6.98 - 7.13 (16H, m, Ar*H* stopper), 6.83 (4H, d, *J* = 8.9 Hz, Ar*H* stopper), 5.56 (4H, s, C*H*$_2$), 5.45 (4H, s, C*H*$_2$), 5.17 (4H, s, C*H*$_2$), 1.30 (54H, s, C*H*$_3$ stopper)

^{13}C NMR (101MHz, $CDCl_3$) δ = 162.2, 156.0, 148.3, 144.8, 144.0, 141.2, 140.2, 139.8, 136.0, 135.4, 133.5, 133.2, 132.3, 131.4, 130.7, 129.7, 128.7, 128.5, 127.7, 127.3, 124.0, 123.3, 123.1, 122.5, 113.2, 63.0, 62.0, 53.9, 43.6, 34.2, 31.3

MS (ESI): m/z calc. for $C_{132}H_{121}Cl_4N_8O_6$ $[M + H]^+$: 2057.27; found: 2057.23

Bis-proto-triazolium PDI axle 89·(Cl)$_2$



Axle **88** (66 mg, 0.03 mmol, 1 eq) was dissolved in CH_2Cl_2 (25 ml) with $Me_3O{\cdot}BF_4$ (11 mg, 0.07 mmol, 2.2 eq) and the mixture was left stirring overnight at room temperature. The reaction was quenched with three drops of MeOH and the solvent was removed *in vacuo*. The resultant solid was purified by preparative silica TLC (CH_2Cl_2:MeOH 98:2) to give **89·(BF$_4$)$_2$** as an orange/red solid (64 mg, 0.03 mmol, 88%). Subsequent anion exchange was achieved by dissolving **89·(BF$_4$)$_2$** in (CH_2Cl_2:MeOH 90:10) and

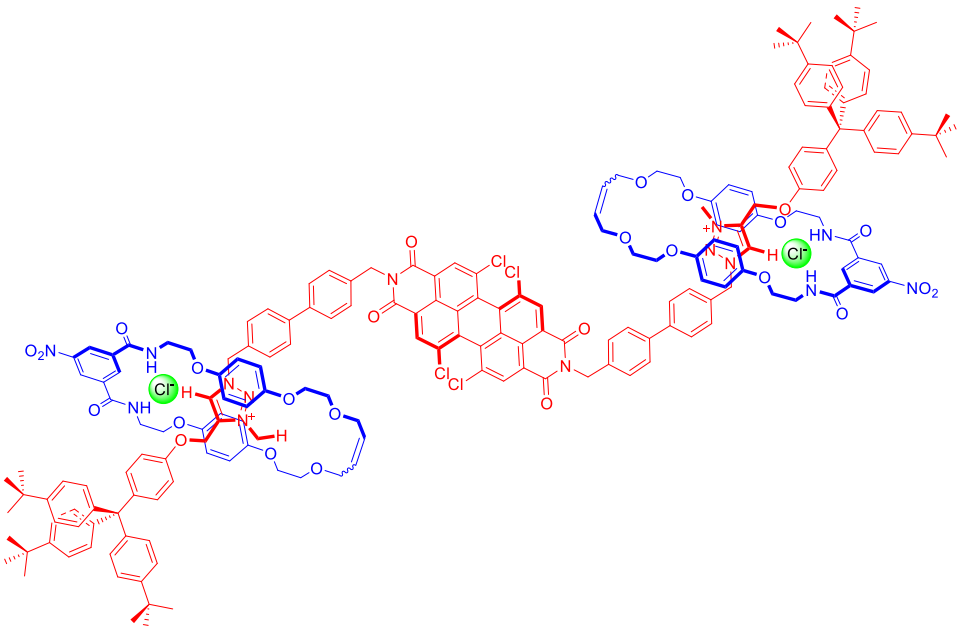
passing the solution three times through a column of Amberlite® resin loaded with chloride to yield **89·(Cl)$_2$** (61 mg, 0.03 mmol, quant.).

^{1}H NMR (400MHz, $CDCl_3$) δ = 10.14 (2H, br. s., Ar*H* triazolium), 8.68 (4H, s, Ar*H* PDI), 7.67 (4H, d, *J* = 7.5 Hz, Ar*H* biphenyl), 7.61 (4H, d, *J* = 8.1 Hz, Ar*H* biphenyl), 7.55 (4H, d, *J* = 7.9 Hz, Ar*H* biphenyl), 7.48 (4H, d, *J* = 7.9 Hz, Ar*H* biphenyl), 7.22 (8H, d, *J* = 8.4 Hz, Ar*H* stopper), 7.13 (4H, d, *J* = 8.4 Hz, Ar*H* stopper), 7.04 (16H, d, *J* = 8.4 Hz, Ar*H* stopper), 6.83 (4H, d, *J* = 8.7 Hz, Ar*H* stopper), 6.03 (4H, br. s., C*H*$_2$), 5.42 (8H, s, C*H*$_2$), 4.36 (6H, s, C*H*$_3$ triazolium), 1.28 (54H, s, C*H*$_3$ stopper)

^{13}C NMR (101MHz, $CDCl_3$) δ = 162.2, 156.1, 148.3, 144.8, 144.0, 142.4, 141.2, 140.2, 139.8, 136.0, 135.4, 133.4, 133.2, 132.3, 131.4, 130.8, 129.7, 128.7, 128.5, 127.7, 127.3, 124.0, 123.3, 123.0, 122.5, 113.2, 63.0, 62.0, 53.9, 43.6, 37.8, 34.2, 31.3

MS (ESI): m/z calc. for $C_{134}H_{126}Cl_4N_8O_6$ $[M - 2Cl]^{2+}$: 1042.93; found: 1043.00

Bis-proto-triazolium PDI [3]rotaxane 90·(Cl)$_2$



Axle **89·(Cl)$_2$** (45 mg, 20.9 µmol, 1 eq) and **22** (41 mg, 63.1 µmol, 3 eq) were dissolved in dry CH_2Cl_2 (5 ml), the mixture was left to stir for 30 minutes. Grubbs' II catalyst (4 mg, 10 wt. %) was added and the solution stirred at room temperature, monitoring by TLC (CH_2Cl_2:MeOH 97:3) and ESI mass

spectrometry throughout. After one day a further addition of Grubbs' II catalyst (4 mg, 10 wt. %) was made and after a further day the solvent was removed *in vacuo*. The crude was purified by iterative preparative silica TLC (EtOAc:MeOH 95:5 then CH_2Cl_2:MeOH 97:3) to yield [3]rotaxane **90·(Cl)$_2$** as a red solid (12 mg, 3.6 µmol, 17%).

^{1}H NMR (400MHz, $CDCl_3$) δ = 9.67 (2H, br. s., Ar*H* int. macro), 9.49 (2H, br. s., Ar*H* triazolium), 9.33 (4H, br. s., N*H* macro), 8.75 (4H, s, Ar*H* ext. macro), 8.72 (4H, s, Ar*H* PDI), 7.66 (4H, d, *J* = 8.2 Hz, Ar*H* biphenyl), 7.48 (4H, d, *J* = 8.2 Hz, Ar*H* biphenyl), 7.36 (4H, d, *J* = 7.8 Hz, Ar*H* biphenyl), 7.31 (4H, d, *J* = 8.8 Hz, Ar*H* biphenyl), 7.25 (12H, s, Ar*H* stopper), 7.16 (12H, d, *J* = 8.4 Hz, Ar*H* stopper), 7.09 (4H, d, *J* = 8.1 Hz, Ar*H* stopper), 7.00 (4H, d, *J* = 8.6 Hz, Ar*H* stopper), 6.40 (8H, d, *J* = 9.0 Hz, Ar*H* hydroquinone macro), 6.34 (8H, d, *J* = 9.0 Hz, Ar*H* hydroquinone macro), 5.51 (4H, br. s., C*H* alkene), 5.46 (4H, s, C*H*$_2$ axle), 5.23 (4H, br. s., C*H*$_2$ axle), 4.70 (4H, s, C*H*$_2$ axle), 4.57 - 4.65 (4H, m, C*H*$_2$ macro), 4.47 (4H, t, *J* = 9.9 Hz, C*H*$_2$ macro), 3.90 - 3.97 (4H, m, C*H*$_2$ macro), 3.83 - 3.90 (14H, m, C*H*$_3$ triazolium, C*H*$_2$ macro), 3.61 - 3.81 (16H, m, C*H*$_2$ macro), 3.48 - 3.61 (4H, m, C*H*$_2$ macro), 1.31 (54H, s, C*H*$_3$ stopper)

^{13}C NMR (126MHz, $CDCl_3$) δ = 164.2, 162.3, 154.9, 153.0, 151.9, 148.6, 148.5, 143.9, 142.4, 142.0, 139.0, 136.4, 135.8, 135.4, 133.2, 132.5, 132.1, 132.0, 131.4, 130.7, 130.6, 130.6, 130.0, 129.9, 129.8, 129.7, 129.6, 129.1, 128.7, 128.6, 128.5, 127.6, 127.2, 126.3, 124.2, 124.1, 123.3, 123.1, 114.9, 114.3, 113.5, 70.8, 69.4, 67.6, 66.1, 63.2, 57.4, 54.8, 43.6, 42.9, 40.1, 38.5, 35.9, 34.3, 31.9, 31.9, 31.4, 29.7, 29.7, 29.6, 29.6, 29.5, 29.4, 29.3, 29.3, 29.2, 29.2, 29.1, 27.2, 27.1, 25.5, 22.7, 18.6, 17.3, 14.1, 12.3

MS (ESI): m/z calc. for $C_{198}H_{196}Cl_4N_{14}O_{26}$ $[M - 2Cl]^{2+}$: 1664.66; found: 1664.27

Bis-proto-triazolium PDI [3]rotaxane 90·(PF$_6$)$_2$

90·(Cl)$_2$ was anion-exchanged to the bis-hexafluorophosphate salt **90·(PF$_6$)$_2$** using Amberlite® anion exchange resin. The solvent used was 45:45:10 $CHCl_3$:MeOH:H_2O (10 mL).

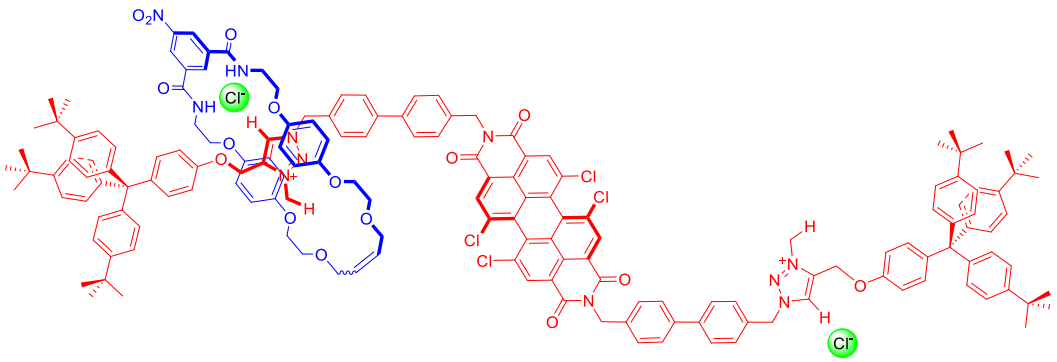
^{1}H NMR (400MHz, $CDCl_3$) δ = 8.85 (4H, s, Ar*H* ext. macro), 8.71 (4H, s, Ar*H* PDI), 8.22 (2H, br. s., Ar*H* int. macro), 7.97 (2H, s, Ar*H* triazolium), 7.62 (8H, d, *J* = 8.2 Hz, Ar*H* biphenyl), 7.45 (8H, d, *J* = 7.7 Hz,

Ar*H* biphenyl), 7.25 (12H, s, Ar*H* stopper), 7.10 - 7.19 (16H, m, Ar*H* stopper), 6.92 (4H, d, *J* = 8.9 Hz, Ar*H* stopper), 6.46 - 6.56 (8H, m, Ar*H* hydroquinone macro), 6.24 (8H, dd, *J* = 8.9 Hz, ^{4}J = 2.4 Hz, Ar*H* hydroquinone macro), 5.73 (4H, br. s., C*H* alkene axle), 5.42 (4H, s, CH_2 axle), 5.18 (4H, s, CH_2 axle), 4.73 (4H, s, CH_2 axle), 4.25 - 4.41 (8H, m, CH_2 macro), 3.80 - 4.00 (16H, m, CH_2 macro), 3.77 (6H, s, CH_3 triazolium), 3.61 - 3.74 (16H, m, CH_2 macro), 1.30 (54H, s, CH_3 stopper)

^{19}F NMR (470 MHz, $CDCl_3$) δ = -72.7 (d, ^{1}J = 705 Hz, PF_6).

^{31}P NMR (202 MHz, $CDCl_3$) δ = -144.3 (sept, ^{1}J = 711 Hz, *P*F_6).

Bis-proto-triazolium PDI [2]rotaxane 91·$(Cl)_2$

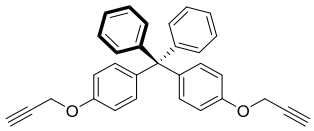


[2]rotaxane **91·$(Cl)_2$** was isolated from the crude reaction mixture of **90·$(Cl)_2$** by iterative preparative silica TLC (EtOAc:MeOH 95:5 then CH_2Cl_2:MeOH 92.5:7.5) as a red solid (11 mg, 4 µmol, 20%).

^{1}H NMR (400MHz, $CDCl_3$) δ = 10.05 (1H, s, Ar*H* triazolium), 9.67 (1H, s, Ar*H* int. macro), 9.51 (1H, s, Ar*H* triazolium), 9.30 - 9.40 (2H, m, N*H* macro), 8.66 - 8.82 (6H, m, Ar*H* PDI, ext. macro), 7.40 - 7.82 (16H, m, Ar*H* biphenyl), 7.11 - 7.39 (12H, m, Ar*H* stopper), 6.90 - 7.11 (18H, m, Ar*H* stopper), 6.83 (2H, br. s., Ar*H* stopper), 6.28 - 6.45 (8H, m, Ar*H* hydroquinone macro), 5.42 - 5.57 (6H, m, C*H* alkene macro, CH_2 axle), 5.23 (2H, s, CH_2 axle), 4.70 (2H, s, CH_2 axle), 4.55 - 4.68 (4H, m, CH_2 macro), 4.49 (2H, d, *J* = 10.0 Hz, CH_2 macro), 4.35 (4H, br. s., CH_2 axle), 3.91 - 3.95 (2H, m, CH_2 macro), 3.65 - 3.89 (16H, m, CH_3 triazolium, CH_2 macro), 3.43 - 3.61 (2H, m, CH_2 macro), 1.29 (54H, s, CH_3 stopper)

MS (ESI): m/z calc. for $C_{166}H_{161}Cl_4N_{11}O_{16}$ $[M - 2Cl]^{2+}$: 1352.54; found: 1352.64

Phenyl trityl bis-alkyne 92



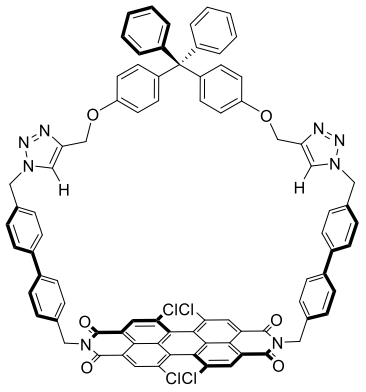
Commercial phenyl trityl bis-alcohol (750 mg, 2.13 mmol, 1 eq) was dissolved in dry, degassed DMF (10 mL) with $KCO_{3(s)}$ (1.8 g, 12.8 mmol, 6 eq) and propargyl bromide (80 wt. % in toluene, 0.71 mL, 6.39 mmol, 3 eq). The solution was heated to 50 °C for two days and upon cooling H_2O (20 mL) was added and the organic products extracted with EtOAc (3 x 30 mL). The organic layers were combined and washed with further H_2O (100 mL) and brine (100 mL) before the solvent was removed *in vacuo*. The crude residue was then purified using a silica plug (CH_2Cl_2) to give bis-alkyne **92** as a white solid (914 mg, 2.13 mmol, quant.).

^{1}H NMR (400MHz, $CDCl_3$) δ = 7.24 (4H, d, *J* = 6.8 Hz, Ar*H*), 7.16 - 7.22 (6H, m, Ar*H*), 7.12 (4H, d, *J* = 9.0 Hz, Ar*H*), 6.82 - 6.91 (4H, m, Ar*H*), 4.67 (4H, d, ^4J = 2.4 Hz, CH_2), 2.53 (2H, t, ^4J = 2.4 Hz, C*H* alkyne)

^{13}C NMR (101MHz, DMSO-d_6) δ = 154.9, 146.4, 139.2, 131.3, 130.2, 126.9, 125.3, 113.1, 78.2, 76.0, 62.9, 55.1

MS (ESI): m/z calc. for $C_{31}H_{25}O_2$ $[M + H]^+$: 429.54; found: 429.34

Bis-proto-triazole PDI macrocycle 93



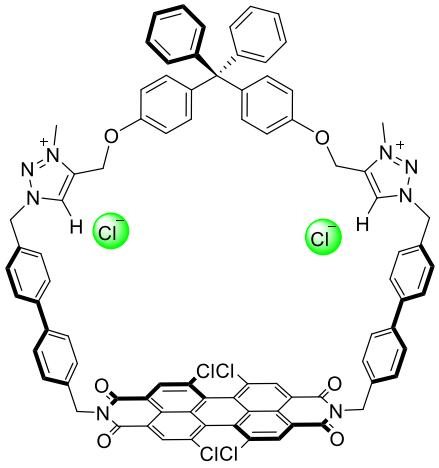
PDI bis-azide **87** (50 mg, 0.05 mmol, 1 eq) and phenyl trityl bis-alkyne **92** (22 mg, 0.05 mmol, 1 eq) were dissolved in dry CH_2Cl_2 (75 mL). Then TBTA (11 mg, 0.02 mmol, 0.4 eq), $Cu(MeCN)_4{\cdot}PF_6$ (8 mg, 0.02 mmol, 0.4 eq) and *N,N*-diisopropylethylamine (22 µl, 0.13 mmol, 2.5 eq) were added to the mixture and left to stir at room temperature for two days, monitoring by thin layer chromatography (CH_2Cl_2:MeOH 97:3). The mixture was washed with a 0.02 M EDTA/0.1 M $NH_4OH_{(aq)}$ solution, the organic layer was dried over $MgSO_4$, and the solvent was removed *in vacuo*. The resultant crude was purified by silica gel column chromatography (CH_2Cl_2:MeOH 97:3) to give macrocycle **93** as a red solid (35 mg, 0.02 mmol, 49%).

^{1}H NMR (400MHz, $CDCl_3$) δ = 8.69 (4H, s, Ar*H* PDI), 7.63 (4H, d, *J* = 8.2 Hz, Ar*H* biphenyl), 7.46 - 7.56 (10H, m, Ar*H* biphenyl, triazole), 7.34 (4H, d, *J* = 8.2 Hz, Ar*H* biphenyl), 7.01 - 7.23 (14H, m, Ar*H* stopper), 6.77 (4H, d, *J* = 8.8 Hz, Ar*H* stopper), 5.65 (2H, d, ^2J = 13.6 Hz, CH_2), 5.56 (4H, s, CH_2), 5.33 (2H, d, ^2J = 13.6 Hz, CH_2), 5.05 (4H, s, CH_2)

^{13}C NMR (101MHz, DMSO-d_6) δ = 156.1, 146.9, 142.9, 139.7, 138.7, 138.7, 136.3, 135.2, 131.5, 130.3, 128.7, 128.7, 127.9, 127.5, 127.0, 126.8, 125.8, 124.3, 113.4, 63.1, 61.2, 52.5, 42.4, 30.7

MS (ESI): m/z calc. for $C_{83}H_{53}Cl_4N_8O_6$ $[M + H]^+$: 1397.28; found: 1397.47

Bis-proto-triazolium PDI macrocycle 94·(Cl)$_2$



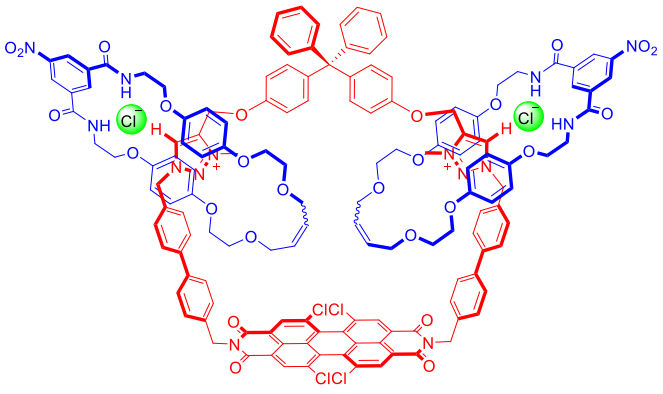
Macrocycle **93** (35 mg, 0.03 mmol, 1 eq) was dissolved in CH_2Cl_2 (20 ml) with $Me_3O{\cdot}BF_4$ (8 mg, 0.07 mmol, 2.2 eq) and the mixture was left stirring overnight at room temperature. The reaction was quenched with three drops of MeOH and the solvent was removed *in vacuo*. The resultant solid was purified by preparative silica TLC (CH_2Cl_2:MeOH 95:5) to give **94·(BF$_4$)$_2$** as an orange solid. Subsequent anion exchange was achieved by dissolving **94·(BF$_4$)$_2$** in (CH_2Cl_2:MeOH 90:10) and passing the solution three times through a column of Amberlite® resin loaded with chloride to yield **94·(Cl)$_2$** as a red solid (36 mg, 0.02 mmol, 80%).

^{1}H NMR (400MHz, 1:1 $CDCl_3$:CD_3OD) δ = 8.89 (2H, s, Ar*H* triazolium), 8.63 (4H, s, Ar*H* PDI), 7.39 - 7.64 (16H, m, Ar*H* biphenyl), 6.99 - 7.20 (14H, m, Ar*H* stopper), 6.74 (4H, d, *J* = 8.9 Hz, Ar*H* stopper), 5.79 (4H, s, CH_2), 5.59 (2H, d, ^2J = 13.7 Hz, CH_2), 5.27 (2H, d, ^2J = 13.6 Hz, CH_2), 5.20 (4H, s, CH_2), 4.26 (6H, s, CH_3 triazolium)

^{13}C NMR (101MHz, DMSO-d_6) δ = 156.2, 146.9, 142.4, 139.7, 138.7, 138.7, 136.3, 135.2, 131.5, 130.3, 128.7, 128.7, 127.9, 127.5, 127.0, 126.8, 125.8, 123.0, 113.4, 63.1, 61.2, 52.4, 42.4, 37.8, 30.7

MS (ESI): m/z calc. for $C_{85}H_{58}Cl_4N_8O_6$ $[M - 2Cl]^{2+}$: 714.16; found: 714.22

Bis-proto-triazolium PDI [3]catenane 95·(Cl)$_2$



Macrocycle **94·(Cl)$_2$** (44 mg, 29.3 µmol, 1 eq) and **22** (57 mg, 87.7 µmol, 3 eq) were dissolved in dry CH_2Cl_2 (10 ml), the mixture was left to stir for 30 minutes. Grubbs' II catalyst (6 mg, 10 wt. %) was added and the solution stirred at room temperature, monitoring by TLC (CH_2Cl_2:MeOH 95:5) and ESI mass spectrometry throughout. After one day a further addition of Grubbs' II catalyst (5 mg, 10 wt. %) was made and after a further day the solvent was removed *in vacuo*. The crude was purified by iterative preparative silica TLC using the solvent mixtures (EtOAc:MeOH 95:5 then CH_2Cl_2:MeOH 95:5) to yield [3]catenane **95·(Cl)$_2$** as a red solid (20 mg, 7.3 µmol, 25%).

^{1}H NMR (400MHz, $CDCl_3$) δ = 9.84 (2H, br. s., Ar*H* int. iso. macro), 9.77 (2H, br. s., Ar*H* triazolium), 9.35 (2H, s, N*H* iso. macro), 9.31 (2H, s, N*H* iso. macro), 8.92 (2H, s, Ar*H* ext. iso. macro), 8.89 (2H, s, Ar*H* ext. iso. macro), 8.65 (4H, br. s., Ar*H* PDI), 7.51 - 7.66 (12H, m, Ar*H* biphenyl), 7.47 (4H, d, *J* = 8.3 Hz, Ar*H* biphenyl), 7.17 - 7.26 (6H, m, Ar*H* stopper), 7.05 (4H, d, *J* = 7.3 Hz, Ar*H* stopper), 6.94 (4H, d, *J* = 8.8 Hz, Ar*H* stopper), 6.71 (4H, d, *J* = 9.0 Hz, Ar*H* stopper), 6.23 - 6.37 (8H, m, Ar*H* hydroquinone iso. macro), 6.17 (4H, d, *J* = 8.8 Hz, Ar*H* hydroquinone iso. macro), 6.01 (4H, d, *J* = 8.8 Hz, Ar*H* hydroquinone iso. macro), 5.81 (4H, br. s., C*H* alkene iso. macro), 5.67 (2H, d, ^2J = 13.4 Hz, CH_2 PDI macro), 5.56 (2H, d, ^2J = 13.7 Hz, CH_2 PDI macro), 5.44 (2H, d, ^2J = 13.7 Hz, CH_2 PDI macro), 5.26 (2H, d, ^2J = 13.4 Hz, CH_2 PDI macro), 4.20 - 4.32 (4H, m, CH_2 PDI macro), 4.16 (4H, br. s., CH_2 iso. macro), 4.09 (4H, d, *J* = 4.4 Hz, CH_2 iso. macro), 3.90 - 4.00 (12H, m, CH_2 iso. macro), 3.70 - 3.88 (22H, m, CH_3 triazolium, CH_2 iso. macro), 3.66 - 3.68 (4H, m, CH_2 iso. macro)

^{13}C NMR (126MHz, $CDCl_3$) δ = 164.3, 164.2, 162.1, 154.9, 153.0, 152.8, 152.1, 152.0, 148.6, 146.4, 142.6, 141.1, 138.9, 136.8, 135.7, 135.4, 133.2, 132.2, 131.3, 130.8, 130.5, 130.2, 129.4, 129.3, 128.6, 127.7, 127.6, 127.1, 126.2, 126.1, 123.3, 123.0, 115.0, 114.9, 114.1, 114.0, 113.4, 70.8, 69.3, 67.9, 67.8, 66.7, 63.6, 57.6, 56.5, 43.1, 39.9, 38.5, 29.7, 22.7, 14.1

MS (ESI): m/z calc. for $C_{149}H_{128}Cl_4N_{14}O_{26}$ $[M - 2Cl]^{2+}$: 1335.89; found: 1335.52

Bis-proto-triazolium PDI [3]catenane 95·$(PF_6)_2$

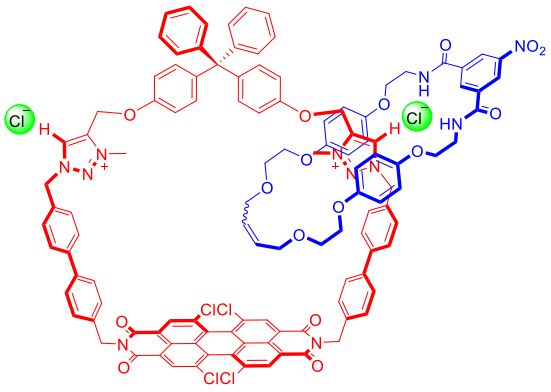
95·$(Cl)_2$ was anion-exchanged to the bis-hexafluorophosphate salt **95·$(PF_6)_2$** using Amberlite® anion exchange resin. The solvent used was 45:45:10 $CHCl_3$:MeOH:H_2O (10 mL).

^{1}H NMR (500MHz, $CDCl_3$) δ = 8.78 (4H, br. s., Ar*H* ext. iso. macro), 8.64 (4H, br. s., Ar*H* PDI), 8.20 (2H, br. s., Ar*H* int. iso. macro), 8.15 (2H, br. s., Ar*H* triazolium), 7.49 - 7.70 (14H, m, Ar*H* biphenyl), 7.44 (4H, d, *J* = 7.6 Hz, Ar*H* biphenyl), 7.02 - 7.25 (6H, m, Ar*H* stopper), 6.91 (4H, d, *J* = 7.5 Hz, Ar*H* stopper), 6.77 (4H, d, *J* = 7.8 Hz, Ar*H* stopper), 6.65 (4H, d, *J* = 8.2 Hz, Ar*H* stopper), 6.41 (4H, d, *J* = 8.4 Hz, Ar*H* hydroquinone iso. macro), 6.27 (4H, d, *J* = 8.5 Hz, Ar*H* hydroquinone iso. macro), 6.24 (4H, d, *J* = 8.2 Hz, Ar*H* hydroquinone iso. macro), 6.04 (4H, d, *J* = 8.4 Hz, Ar*H* hydroquinone iso. macro), 5.95 (4H, br. s., C*H* alkene iso. macro), 5.61 (2H, d, ^2J = 13.7 Hz, CH_2 PDI macro), 5.53 (4H, d, ^2J = 17.7 Hz, CH_2 PDI macro), 5.23 (2H, d, ^2J = 13.3 Hz, CH_2 PDI macro), 4.14 - 4.33 (4H, m, CH_2 PDI macro), 3.50 - 4.10 (46H, m, CH_3 triazolium, CH_2 iso. macro)

^{19}F NMR (470 MHz, $CDCl_3$) δ = -72.7 (d, ^1J = 706 Hz, PF_6).

^{31}P NMR (202 MHz, $CDCl_3$) δ = -144.3 (sept, ^1J = 708 Hz, *P*F_6).

Bis-proto-triazolium PDI [2]catenane 96·(Cl)$_2$



[2]catenane **96·(Cl)$_2$** was isolated from the crude reaction mixture of **95·(Cl)$_2$** by iterative preparative silica TLC using the solvent mixtures (EtOAc:MeOH 95:5 then CH_2Cl_2:MeOH 95:5) as a red solid (9 mg, 4 µmol, 21%).

^{1}H NMR (400MHz, $CDCl_3$) δ = 10.14 (1H, br. s., Ar*H* triazolium), 9.81 (1H, s, Ar*H* int. iso. macro), 9.66 (1H, s, Ar*H* triazolium), 9.32 (2H, d, *J* = 7.1 Hz, N*H* iso. macro), 8.87 (2H, d, *J* = 5.1 Hz, Ar*H* ext. iso. macro), 8.67 (4H, s, Ar*H* PDI), 7.39 - 7.81 (16H, m, Ar*H* biphenyl), 6.92 - 7.25 (14H, m, Ar*H* stopper), 6.81 (2H, d, *J* = 8.2 Hz, Ar*H* stopper), 6.69 (2H, d, *J* = 8.2 Hz, Ar*H* stopper), 6.17 - 6.27 (4H, m, Ar*H* hydroquinone iso. macro), 6.15 (2H, d, *J* = 9.0 Hz, Ar*H* hydroquinone iso. macro), 6.06 (2H, d, *J* = 8.8 Hz, Ar*H* hydroquinone iso. macro), 5.70 - 5.75 (2H, m, C*H* alkene), 5.18 - 5.70 (8H, m, CH_2 PDI macro), 4.38 (2H, br. s., CH_2 PDI macro), 4.27 (2H, br. s., CH_2 PDI macro), 3.57 - 4.31 (26H, m, CH_3 triazolium, CH_2 iso. macro)

MS (ESI): m/z calc. for $C_{117}H_{93}Cl_4N_{11}O_{16}$ $[M - 2Cl]^{2+}$: 1024.78; found: 1024.87

6.3. References

1 B.-Y. Lee, S. R. Park, H. B. Jeon and K. S. Kim, *Tetrahedron Lett.*, 2006, **47**, 5105–5109.

2 R. Pereira de Freitas, J. Iehl, B. Delavaux-Nicot and J.-F. Nierengarten, *Tetrahedron*, 2008, **64**, 11409–11419.

3 H. E. Gottlieb, V. Kotlyar and A. Nudelman, *J. Org. Chem.*, 1997, **62**, 7512–7515.

Chapter 7
Conclusions

7. CONCLUSIONS

The aim of the work described in this thesis was to realise anion-induced molecular motion in mechanically interlocked molecular architectures. This began in Chapter Two with the construction of a series of bistable [2]rotaxanes that exhibited large-amplitude translational motion of the macrocyclic wheel from an electron-deficient aromatic motif (namely NI or NDI) to a proto/iodo-triazolium site upon the stimulus of halide recognition (Figure 7.1). Importantly, quantitative analysis of positional integrities revealed the XB NDI-containing [2]rotaxane to exhibit superior positional switching relative to the HB analogue in competitive solvent media courtesy of strong halide binding.

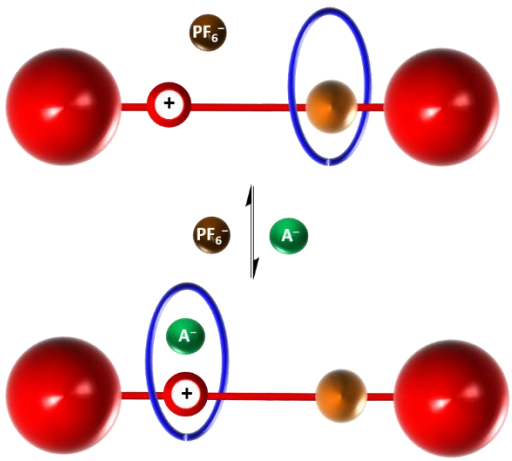


Figure 7.1. Schematic of anion-induced translational molecular motion within a bistable [2]rotaxane. Yellow sphere = electron-deficient aromatic motif e.g. NI, NDI, red sphere = triazolium-based anion recognition site and A^- = halide anion.

The success of this bistable [2]rotaxane design was to be the blueprint for future dynamic systems, including the exotic four-station [3]rotaxanes described in Chapter Three. The higher-order of these interlocked architectures facilitated recognition of oxoanions *via* novel pincer-like shuttling of the macrocycle components towards the core bis-triazolium recognition sites to form a unique 1:1 stoichiometric sandwich complex (Figure 7.2). In agreement with the findings of Chapter Two, the XB [3]rotaxane was found to be a superior host to the HB analogue, permitting the strong recognition of

multidentate oxoanion guests, in particular, the selective binding of the environmentally important anion nitrate.

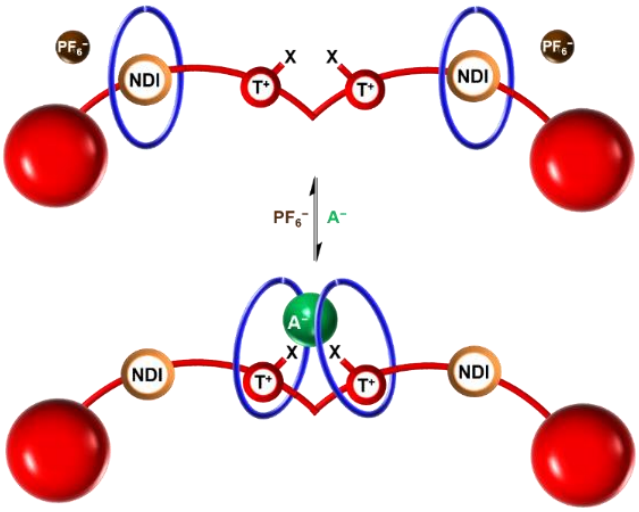


Figure 7.2. Schematic of a [3]rotaxane capable of the recognition of oxoanions (A^-) via a dynamic pincer-like shuttling mechanism. NDI = naphthalene diimide, T^+ = triazolium and X = I or H.

Whilst the dynamic behaviour of the interlocked systems in Chapter Three was utilised for colorimetric anion sensing, the work in Chapter Four extended this to a four-station [3]rotaxane capable of chloride sensing *via* a dual fluorescence response. This was possible because the mechanism of anion-induced molecular motion resulted in the simultaneous switching-on of fluorescence at the NDI station and quenching of the C_{60} fullerene fluorescence by proximal ferrocene-decorated macrocycle components (Figure 7.3).

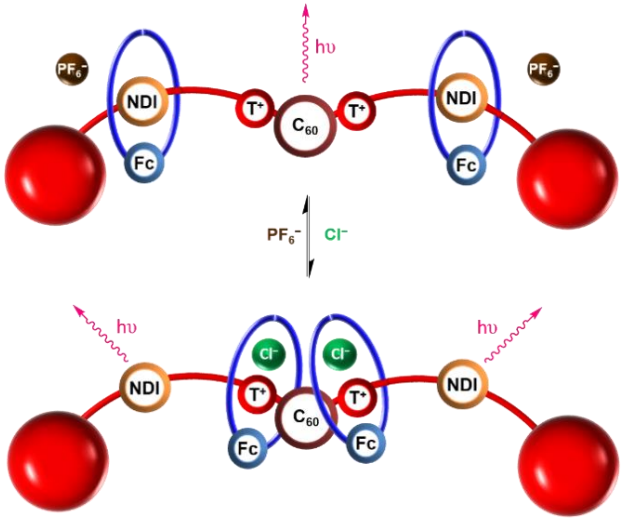


Figure 7.3. Schematic of the four-station C_{60} fullerene-containing [3]rotaxane capable of chloride sensing via a dual fluorescence response. NDI = naphthalene diimide, T^+ = proto-triazolium and Fc = ferrocene.

The work in Chapter Five also demonstrates the ability of carefully-designed mechanically interlocked molecular switches to produce effective chemical sensing by means of their inherent dynamic properties and for the first time this was achieved in a [3]catenane. In this system, chloride stimulated rotary motion of macrocycles from the PDI-based stations to triazolium sites is manifested in a naked-eye colour change (Figure 7.4).

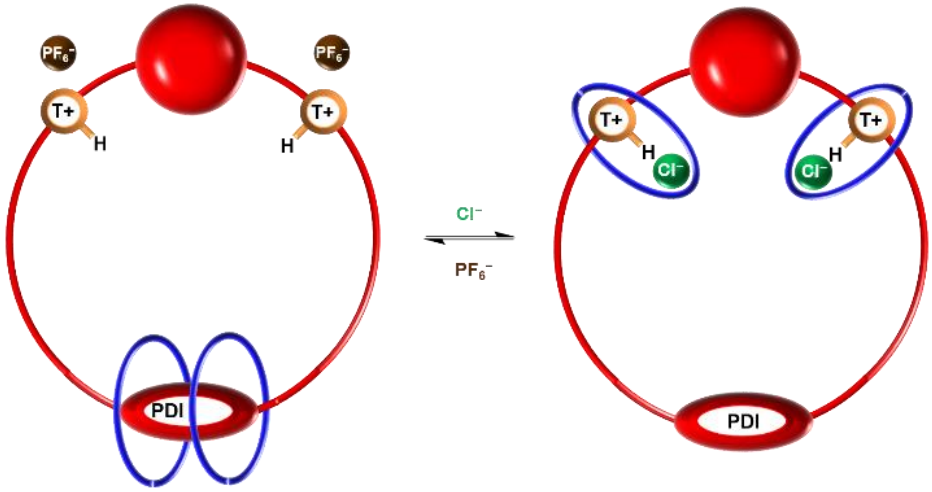


Figure 7.4. Schematic of chloride-induced rotary molecular motion in a four-station PDI-bis-triazolium [3]catenane. PDI = perylene diimide, T^+ = proto-triazolium.

In summary, these results explicitly demonstrate how it is possible to tame the inherent dynamics of mechanically interlocked molecules using negatively charges species as chemical stimuli, allowing the controlled translational and rotational motions of rotaxane and catenane components to be exploited for the purpose of anion recognition and sensing. In the future, the concepts outlined throughout this thesis could be extended toward the construction of new molecular machines with applications in other areas of nanotechnology such as synthetic electronic devices, drug delivery systems and catalysis.

Appendices

APPENDICES

1. ^{1}H NMR anion binding titration protocol

The ^{1}H NMR spectra for anion titration experiments were obtained on a Bruker AVIII500 spectrometer at 298 K with ^{1}H operating at 500 MHz. The host concentration was 1.0 mM and the initial sample volume 0.50 mL. Solutions (100 mM) of guest anions were prepared from their tetrabutylammonium salts and added in aliquots of 0, 0.2, 0.4, 0.6, 0.8, 1.0, 1.2, 1.4, 1.6, 1.8, 2.0, 2.5, 3.0, 4.0, 5.0, 7.0 and 10 equivalents after each of which the sample was shaken in the NMR tube and a spectrum recorded. Integrations of ^{1}H NMR spectra at the end of the titration procedure were performed to ensure the concentrations added were correct. In all cases the bound and unbound species were found to be on fast exchange on the NMR timescale permitting stability constants to be calculated using the WinEQNMR2[1] computer programme.

The stoichiometry of binding was investigated by visual analysis of the titration data, approximations of Job plots and by analysis of the residual distributions of fitted titration data[2] (*vide infra*). An estimation of the association constant and the limiting chemical shifts were required as input parameters for WinEQNMR2. These were refined by non-linear least-squares analysis to achieve the best fit between observed and calculated chemical shifts and comparisons of these calculated and experimental binding isotherms are always shown in the text. Importantly, visual comparison of these curves and the residual distribution of the fitted titration data also served to demonstrate that an appropriate model of appropriate stoichiometry had been used.[2] This is because residuals will be distributed randomly when they arise from random experimental errors.

WinEQNMR2 provides an estimate of the standard error of the measurement, and in the vast majority of cases these were < 10% (and always < 20%) of the absolute value of the association constant that is quoted. These errors were taken into account when comparing similarities and differences between K_a values. However, it is possible that the magnitude of these errors are underestimated because they

only account for the fitting of a binding isotherm to the titration data and do not consider elements of systematic error in the experimental procedure.

2. Fluorescence experiments

Fluorescence emission spectra were recorded on a Horiba Fluorolog 3 or a Varian Cary-Eclipse fluorescence spectrophotometer using a Hellma Quartz cuvette of pathlength 10 mm at 298 K. For all the qualitative data displayed in Chapter Four samples were prepared by careful dilution to a concentration of 1×10^{-5} mol L^{-1}. For titration experiments, a starting volume of 1 mL was used at a concentration of 1×10^{-4} mol L^{-1} and up to 50 equivalents of TBA·Cl were added. Importantly, the concentration of the host was maintained throughout the experiments by preparing the chloride stock solution using the host stock solution. In all cases, λ_{ex} is given in the main text.

The percentage fluorescence emission intensity changes (ΔI %) (λ_{ex} = 300 nm) were calculated by integrating spectra between the same λ_{em} limits and calculating the percentage increase or decrease. Importantly, the spectra were plotted on axes of the same scale to ensure the integrals could be compared. The measurement of a global change over the spectrum is more accurate than measurement at a single wavelength because it accounts for chromatic shifting. The same methodology was also used to measure the percentage change in absorption spectra.

As an example, the integrated fluorescence emission spectra of **82·$(PF_6)_2$** and **82·$(Cl)_2$** from the NDI fluorophore (where ΔI = 526%) are shown below (Figure A.1).

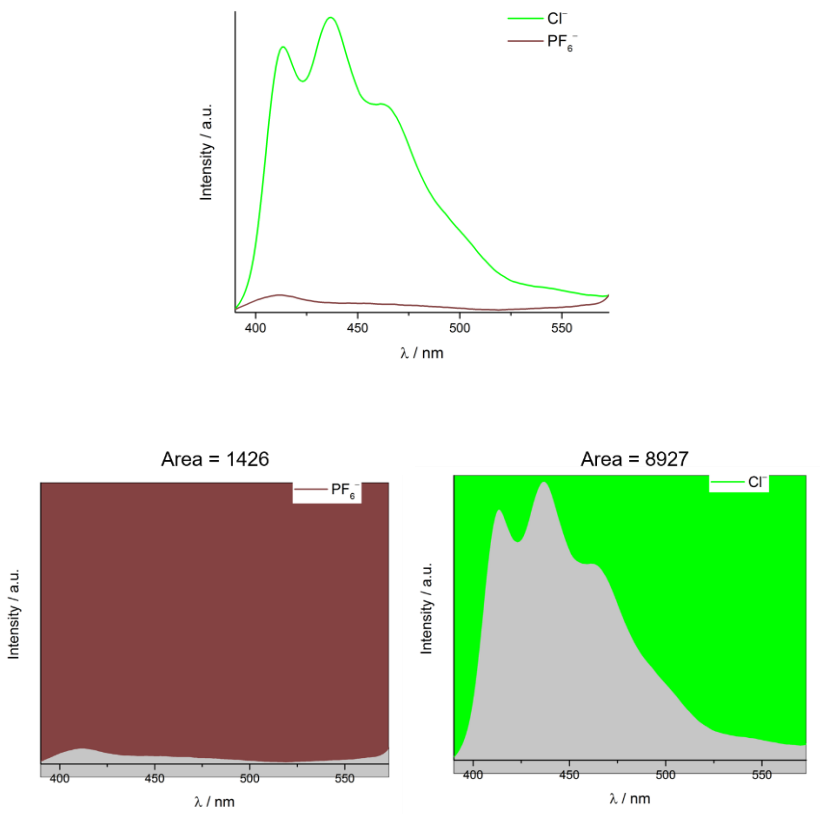


Figure A.1. Fluorescence emission spectra (λ_{ex} = 300 nm) of the bis-hexafluorophosphate and bis-chloride salts of the ferrocene-macrocycle-containing [3]rotaxane ***82·(A)₂*** *in $CHCl_3$ (1×10^{-5} mol L^{-1}) showing emission from the NDI fluorophore. Each emission spectrum is then integrated from λ_{em} = 390-570 nm.*

3. UV-Vis experiments

The electronic absorption spectra were recorded on a PGT60 U spectrophotometer using a Hellma Quartz cuvette of pathlength 10 mm at 298 K.

The concentrations of the qualitative UV-Vis spectra recorded in Chapters Two and Four are stated in the main text.

For the UV-Vis oxoanion titration experiments performed with **73·$(PF_6)_2$** in Chapter Three, a starting volume of 0.35 mL of the host at a concentration of 1.4×10^{-3} mol L^{-1} was used. Spectra were recorded for each 0.2 equivalent of the oxoanion guest (as its tetrabutylammonium salt) added up to 2 equivalents (20 µL total). The concentration of the host was always kept constant.

For the UV-Vis MeOH "titration" experiments detailed in Chapter Five, samples of compounds **89·$(BF_4)_2$** and **90·$(PF_6)_2$** were prepared at the same concentration (1×10^{-4} mol L^{-1}) and volume (1 mL) in a variety of methanol-chloroform solvent mixtures.

For the UV-Vis chloride titration experiments performed with the systems in Chapter Five, a starting volume of 0.7 mL of the host at a concentration of 3×10^{-5} mol L^{-1} was used. Spectra were recorded for each aliquot of the chloride guest (as its tetrabutylammonium salt) added up to 50 equivalents (500 µL total). The concentration of the host was always kept constant.

4. Estimations of station occupancies

The method used for estimating the station occupancies of the interlocked molecules described throughout this thesis, is described below. Particular details are included for the [2]rotaxane systems in Chapter Two from which this methodology originated.

A Δδ scale in each anionic state of the system (counter anion) for each station (NDI and triazolium) was constructed using the δ values of the station's diagnostic protons, $H_{e,e'}$ and H_I respectively, obtained from the appropriate ^{1}H NMR spectra. The following equation was then used to estimate the occupancy of a station:

Occ.(station) = Δδ(rotaxane)/Δδ(model)

Where,

Δδ(rotaxane) = δ(0% occ.) – δ(rotaxane)

Δδ(model) = δ(0% occ.) − δ(100% occ.)

And,

δ(100% occ.) = δ of the station's diagnostic protons in the model one station rotaxane

δ(0% occ.) = δ of the station's diagnostic protons in the two station axle

δ(rotaxane) = δ of the station's diagnostic protons in the multi-station rotaxane

The estimation of the percentage occupancies of each station in the XB two station rotaxane **43·PF$_6$** in $CDCl_3$ from Chapter Two is used as an example to demonstrate this.

For the triazolium station (Figure A.2 to A.5):

δ(0% occ.) = δ(H_I) (**37·PF$_6$**) = 4.41 ppm

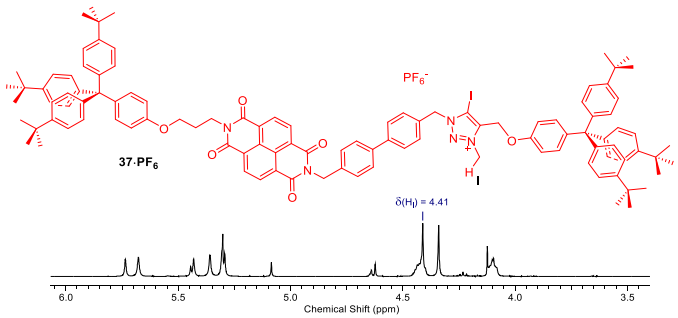


*Figure A.2. Truncated ^{1}H NMR spectrum of two-station axle **37·PF$_6$** ($CDCl_3$, 298 K, 400 MHz).*

δ(100% occ.) = δ(H_I) (**51·PF$_6$**) = 4.15 ppm

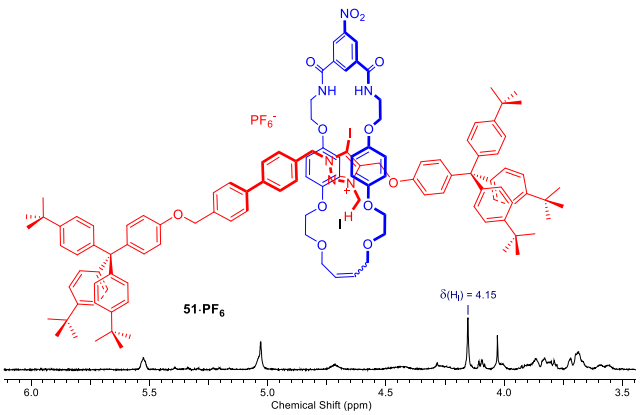


*Figure A.3. Truncated ^{1}H NMR spectrum of one-station [2]rotaxane **51·PF$_6$** ($CDCl_3$, 298 K, 400 MHz).*

δ(rotaxane) = δ(H_I) (**43·PF$_6$**) = 4.31 ppm

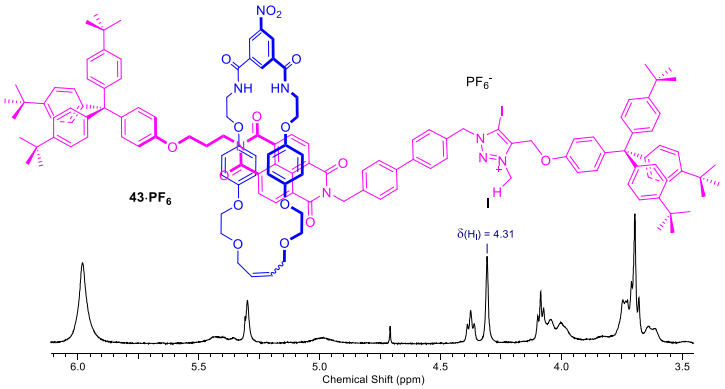


*Figure A.4. Truncated ^{1}H NMR spectrum of two-station [2]rotaxane **43·PF$_6$** ($CDCl_3$, 298 K, 400 MHz).*

Therefore: Occ.(triazolium) = (4.41 – 4.31) / (4.41 – 4.15) = 0.38 = 38%

And this implies: Occ.(NDI) = 1 – 0.38 = 0.62 = 62%

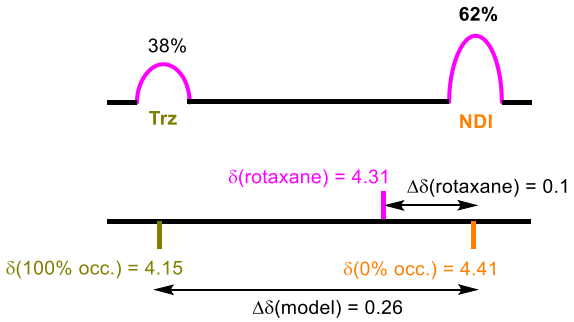


Figure A.5. Δδ scale for the triazolium station as the hexafluorophosphate salt in $CDCl_3$.

For the NDI station (Figures A.6 – A.9):

δ(0% occ.) = δ($H_{e,e'}$) (**37·PF$_6$**) = 8.76 ppm

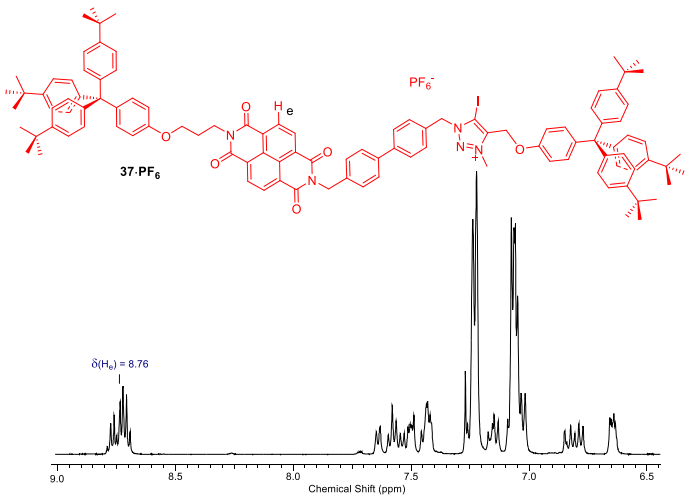


*Figure A.6. Truncated ^{1}H NMR spectrum of two-station axle **37·PF$_6$** ($CDCl_3$, 298 K, 400 MHz).*

δ(100% occ.) = δ($H_{e,e'}$) (**54**) = 8.56 ppm

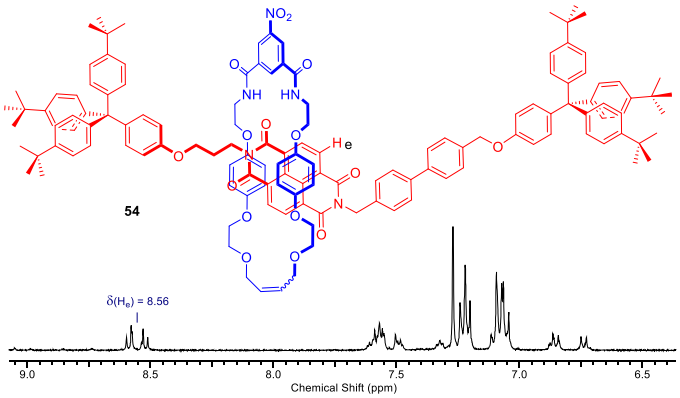


*Figure A.7. Truncated ^{1}H NMR spectrum of one-station [2]rotaxane **54** ($CDCl_3$, 298 K, 400 MHz).*

δ(rotaxane) = δ($H_{e,e'}$) (**43·PF$_6$**) = 8.65 ppm

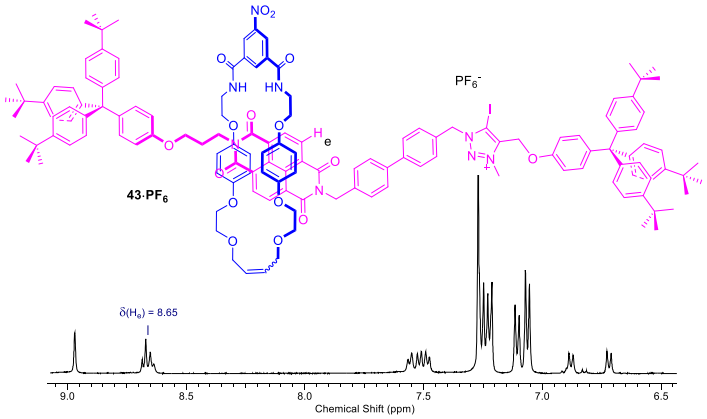


*Figure A.8. Truncated ^{1}H NMR spectrum of two-station [2]rotaxane **43·PF$_6$** ($CDCl_3$, 298 K, 400 MHz).*

Occ.(NDI) = (8.76 – 8.65) / (8.76 – 8.56) = 0.55 = 55%

And this implies: Occ.(triazolium) = 1 – 0.55 = 0.45 = 45%

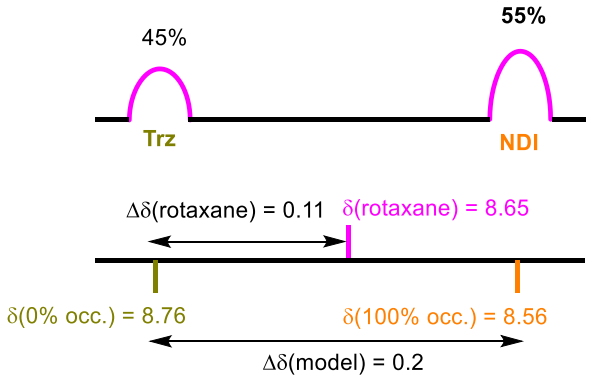


Figure A.9. Δδ scale for the NDI station in $CDCl_3$.

Definition data used to estimate the % occupancies reported in Chapter Two (Figures 2.32, 2.33 and 2.34) were taken only from the triazolium shifts, $\delta(H_I)$, since the NDI protons $H_{e,e'}$ often produced a complex multiplet (see **37·PF$_6$**) and were frequently found to overlap with the peak from the macrocycle protons H_α (see **42·Cl**), both of which made the diagnostic shift of $\delta(H_{e,e'})$ more difficult to determine. In addition Δδ(model) for NDI was always found to be smaller than Δδ(model) for the triazolium station.

^{1}H NMR spectra of the compounds **36·Cl**, **36·I**, **36·PF$_6$**, **37·Cl**, **37·I**, **37·PF$_6$**, **42·Cl**, **42·I**, **42·PF$_6$**, **43·Cl**, **43·I**, **43·PF$_6$**, **50·Cl**, **50·I**, **50·PF$_6$**, **51·Cl**, **51·I**, **51·PF$_6$** and **54** in $CDCl_3$ gave $\delta(H_I)$ and $\delta(H_{e,e'})$ values that were then used to estimate the percentage occupancies of the two station [2]rotaxanes **42·A** and **43·A** shown in Figure 2.32 (Table A.1 and A.2).

*Table A.1. Tabulated $\delta(H_I)$ and $\delta(H_{e,e'})$ values that were used to estimate the percentage occupancies of the two-station HB [2]rotaxane **42·A** in $CDCl_3$.*

Station	Anion	δ(rotaxane)	δ(0% occ.)	δ(100% occ.)	% Occ.(triazolium)	% Occ.(NDI)
	Cl^-	3.88	4.38	3.88	100	0
Triazolium	I^-	3.87	4.41	3.87	100	0
$\delta(H_I)$	PF_6^-	3.92	4.33	3.79	76	24
	Cl^-	8.76			100	0
NDI	I^-	8.76	8.76	8.56	100	0
$\delta(H_{e,e'})$	PF_6^-	8.73			85	15

*Table A.2. Tabulated δ(H_I) and δ($H_{e,e'}$) values that were used to estimate the percentage occupancies of the two-station XB [2]rotaxane **43·A** in $CDCl_3$.*

Station	Anion	δ(rotaxane)	δ(0% occ.)	δ(100% occ.)	% Occ. (triazolium)	% Occ. (NDI)
	Cl^-	4.18	4.40	4.16	92	8
Triazolium	I^-	4.16	4.37	4.15	95	5
δ(H_I)	PF_6^-	4.31	4.41	4.15	38	62
	Cl^-	8.76			100	0
NDI	I^-	8.76	8.76	8.56	100	0
δ($H_{e,e'}$)	PF_6^-	8.65			45	55

^{1}H NMR spectra of the compounds **36·Cl**, **36·I**, **36·PF_6**, **37·Cl**, **37·I**, **37·PF_6**, **42·Cl**, **42·I**, **42·PF_6**, **43·Cl**, **43·I**, **43·PF_6**, **50·Cl**, **50·I**, **50·PF_6**, **51·Cl**, **51·I**, **51·PF_6** and **54** in 4:1 $CDCl_3$:MeOD gave δ(H_I) and δ($H_{e,e'}$) values that were then used to estimate the percentage occupancies of the two station rotaxanes **42·A** and **43·A** shown in Figure 2.33 (Table A.3 and A.4).

*Table A.3. Tabulated δ(H_I) and δ($H_{e,e'}$) values that were used to estimate the percentage occupancies of the two-station HB [2]rotaxane **42·A** in 4:1 $CDCl_3$:MeOD.*

Station	Anion	δ(rotaxane)	δ(0% occ.)	δ(100% occ.)	% Occ.(triazolium)	% Occ.(NDI)
	Cl^-	3.92	4.33	3.86	87	13
Triazolium	I^-	4.00	4.35	3.85	70	30
δ(H_I)	PF_6^-	4.01	4.31	3.86	67	33
	Cl^-	8.69			95	5
NDI	I^-	8.67	8.70	8.51	84	16
δ($H_{e,e'}$)	PF_6^-	8.65			74	26

*Table A.4. Tabulated δ(H_I) and δ($H_{e,e'}$) values that were used to estimate the percentage occupancies of the two-station XB [2]rotaxane **43·A** in 4:1 $CDCl_3$:MeOD.*

Station	Anion	δ(rotaxane)	δ(0% occ.)	δ(100% occ.)	% Occ.(triazolium)	% Occ.(NDI)
	Cl^-	4.17	4.42	4.17	100	0
Triazolium	I^-	4.15	4.39	4.13	92	8
δ(H_I)	PF_6^-	4.25	4.37	4.14	52	48
	Cl^-	8.70			100	0
NDI	I^-	8.70	8.70	8.51	100	0
δ($H_{e,e'}$)	PF_6^-	8.63			63	37

^{1}H NMR spectra of the compounds **36·I**, **36·PF_6**, **37·I**, **37·PF_6**, **42·I**, **42·PF_6**, **43·I**, **43·PF_6**, **50·I**, **50·PF_6**, **51·I**, **51·PF_6** and **54** in 1:1 $CDCl_3$:MeOD gave δ(H_I) and δ($H_{e,e'}$) values that were then used to estimate the

percentage occupancies of the two station rotaxanes **42·A** and **43·A** shown in Figure 2.34 (Table A.5 and A.6).

*Table A.5. Tabulated δ(H_I) and δ($H_{e,e'}$) values that were used to estimate the percentage occupancies of the two-station HB [2]rotaxane **42·A** in 1:1 $CDCl_3$:MeOD.*

Station	Anion	δ(rotaxane)	δ(0% occ.)	δ(100% occ.)	% Occ.(triazolium)	% Occ.(NDI)
Triazolium	I^-	4.21	4.36	3.94	36	64
δ(H_I)	PF_6^-	4.21	4.34	3.95	33	67
NDI	I^-	8.63	8.71	8.55	50	50
δ($H_{e,e'}$)	PF_6^-	8.61			37	63

*Table A.6. Tabulated δ(H_I) and δ($H_{e,e'}$) values that were used to estimate the percentage occupancies of the two-station XB [2]rotaxane **43·A** in 1:1 $CDCl_3$:MeOD.*

Station	Anion	δ(rotaxane)	δ(0% occ.)	δ(100% occ.)	% Occ.(triazolium)	% Occ.(NDI)
Triazolium	I^-	4.26	4.43	4.16	63	37
δ(H_I)	PF_6^-	4.33	4.40	4.19	33	67
NDI	I^-	8.65	8.71	8.55	60	40
δ($H_{e,e'}$)	PF_6^-	8.61			37	63

An identical methodology was used to estimate station occupancies in the various systems reported in Chapters Three, Four and Five. In all cases, δ(0% occ.) and δ(100% occ.) were given by the ^{1}H NMR spectra of the axle component and appropriate model one-station [2]rotaxane respectively.

The value of δ(100% occ.) was deemed to be accurate and so the one-station [2]rotaxane an appropriate model for the system under investigation because of almost identical chemical environments of the stations, and most importantly, identical chemical shifts of the station's diagnostic protons δ(H_I/$H_{e,e'}$) in the absence of a macrocycle. Where appropriate, these observations are confirmed in the main text. For reasons stated above, occupancies were always initially estimated using the triazolium shifts, δ(H_I), however, the differing chemical environments of the triazolium stations in the [3]rotaxanes reported in Chapters Three and Four necessitated the use of chemical shift changes of the NDI protons δ($H_{e/e'}$). These estimations were always supported with two-dimensional ^{1}H ROESY NMR spectroscopy data.

As a final point, since the chemical shift scales (Δδ) are solvent specific, ^{1}H NMR spectra were required of four-station axle **71·(A)$_2$** and model one-station NDI [2]rotaxane **54** in DMSO-d_6 to ascertain δ(0% occ.) and δ(100% occ.) respectively in this solvent.

5. Characterisation data for C_{60} fullerene bis-alkyne

The ^{1}H and ^{13}C NMR spectra of methanofullerene **79**[3] recorded in $CDCl_3$ are shown in Figure A.10. An abundance of signals in the characteristic fullerene region between δ = 130-150 ppm indicates symmetry of the C_{60} cage has been broken upon mono-functionalisation.

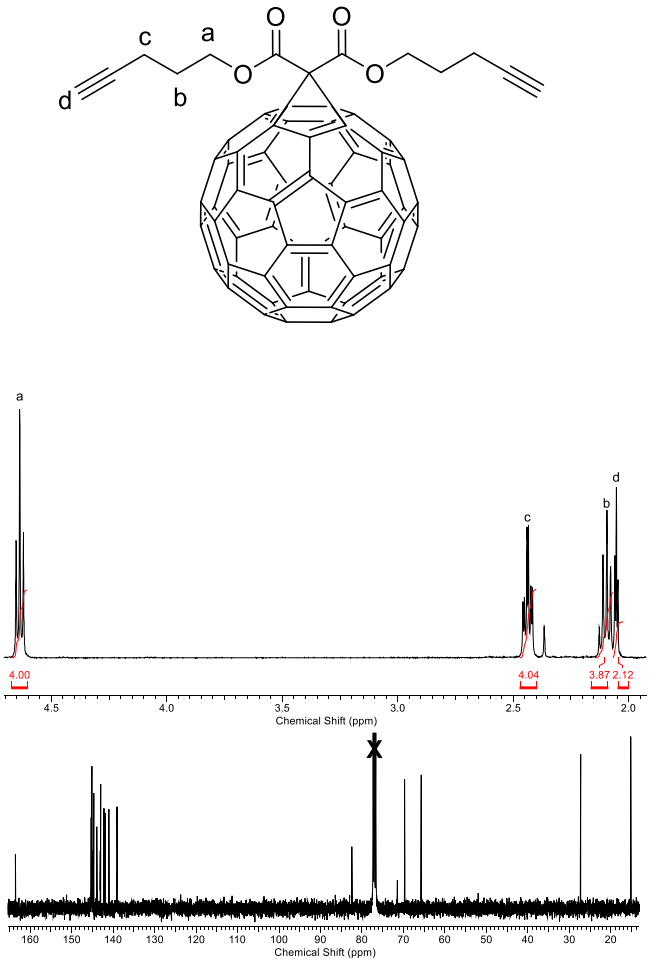


*Figure A.10. ^{1}H (top) and ^{13}C (bottom) NMR spectra of methanofullerene **79** ($CDCl_3$, 298 K).*

MS (MALDI): m/z calc. for $C_{73}H_{15}O_4$ $[M+H]^+$: 955; found: 955

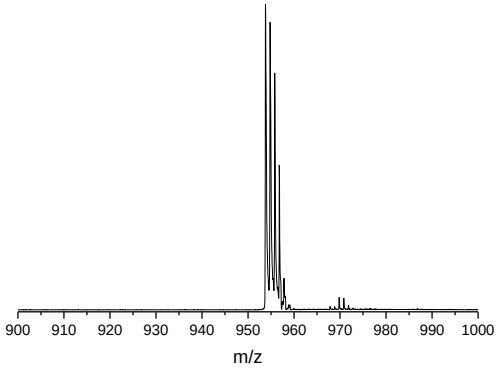


*Figure A.11. MALDI mass spectrum showing peak for [**79**+H]⁺.*

6. Crystal structure data

X-ray diffraction

Single crystal X-ray diffraction data for **43·Cl** were collected using synchrotron radiation on Beamline I19 at Diamond Lightsource[4] The diffractometer was equipped with a Cryostream N2 open-flow cooling device,[5] and the data were collected at 100(2) K. Cell parameters and intensity data (including inter-frame scaling) were processed using CrysAlis Pro.[6]

All structures were solved by charge-flipping methods using SUPERFLIP.[7] All structures were refined using full-matrix least-squares on F^2 within the CRYSTALS suite.[8,9] All non-hydrogen atoms were refined with anisotropic displacement parameters. Hydrogen atoms were generally visible in the difference map and their positions and displacement parameters were refined using restraints prior to inclusion into the model using riding constraints.[10]

Discussion of structures

Crystals suitable for X-ray diffraction structural analysis were obtained for the chloride salt of the XB rotaxane **43·Cl** by slow evaporation of a solution of the rotaxane in 1:1 $CDCl_3$:CD_3OD. All crystals were small and very weakly diffracting; despite the use of synchrotron radiation, diffraction was relatively weak and data were of relatively low quality. Despite this, the structure of the rotaxane, the location

of the macrocycle along the two station axle, and the locations of the anion, chloroform and water molecules can be determined unambiguously. The macrocycle can be clearly seen, situated at the iodotriazolium station with the coordinating chloride anion encapsulated within the rotaxane's three-dimensional binding cavity. Short contacts between the I···Cl^- (2.987(6) Å) and N–H···Cl^- (2.626(14) Å) indicate strong halogen and hydrogen bonds, respectively, with distances shorter than the sum of the van der Waals' radii (XB: 80%, HB: 93%), which contribute to the stabilisation of the rotaxane–anion complex.

Areas of diffuse electron density, which appear to result from disordered solvent molecules was present. While one molecule of chloroform and one molecule of water were apparent from the difference map, the remaining diffuse electron density could not be modelled sensibly. Therefore PLATON-SQUEEZE[11,12] was used to include this electron density in the refinement.

Thermal motion of the stopper-^{t}Bu groups and the macrocycle polyether part are evident. It was possible to model this motion as positional disorder over two sites. However, in some cases, the ellipsoids for the stopper-^{t}Bu groups are quite large as a result of relatively low quality data. It was necessary to apply restraints to bond lengths and angles, as well as thermal and vibrational ellipsoid parameters of the affected atoms to ensure a chemically sensible refinement.

Accommodating the chloride anion within the rotaxane cavity appears to be quite sterically demanding, causing the polyether-alkene part of the macrocycle to adopt a relatively strained geometry. This appears to force a hydrogen atom from the alkene group and a hydrogen atom from the iodotriazolium-methyl group close together.

Hydrogen atoms were located from the difference map but those attached to carbon atoms were repositioned geometrically. The H atoms were initially refined with soft restraints on the bond lengths and angles to regularise their geometry and U_{iso}(H), after which the positions were refined with riding constraints.[10] Water treatment: the H atoms were located in the difference map near the oxygen atom and refined with soft restraints, whereafter the positions were refined with riding constraints.

7. References

1 M. J. Hynes, J. Chem. Soc. *Dalton Trans.*, 1993, 311–312.
2 F. Ulatowski, K. Dąbrowa, T. Bałakier and J. Jurczak, *J. Org. Chem*., 2016, **81**, 1746–1756.
3 R. Pereira de Freitas, J. Iehl, B. Delavaux-Nicot and J.-F. Nierengarten, *Tetrahedron*, 2008, **64**, 11409–11419.
4 Nowell, H., Barnett, S. A., Christensen, K. E., Teat, S. J., Allan, D. R., *J. Synchrotron Rad*., 2012, **19**, 435- 441.
5 Cosier, J., Glazer, A. M., *J. Appl. Crystallogr*., 1986, **19**, 105-107.
6 CrysAlis Pro, Agilent Technologies, 2010.
7 Palatinus, L.; Chapuis, G., *J. Appl. Crystallogr*., 2007, **40**, 786-790.
8 Betteridge, P. W., Carruthers, J. R., Cooper, R. I., Prout, K., Watkin, D. J., *J. Appl. Crystallogr*., 2003, **36**, 1487.
9 Parois, P., Cooper, R. I., Thompson, A. L. *Chem. Cent. J*., 2015, **9**, 30.
10 Cooper, R. I., Thompson, A. L., Watkin, D. J., *J. Appl. Crystallogr*., 2010, **43**, 1100-1107.
11 Spek, A., *J. Appl. Crystallogr*. 2003, **36**, 7-13.
12 van der Sluis, P., Spek, A. L., *Acta Crystallogr., Sect. A: Found. Crystallogr*., 1990, **46**, 194-201.